BULLETIN OF THE EARTHQUAKE RESEARCH INSTITUTE,
TOKYO UNIVERSITY. Vol. XXX, Part 1. March, 1952.

東京大學
地震研究所彙報

第 30 號　第 1 册

昭和 27 年 3 月

目　次

論文及報告

			頁
1.	表面波の研究 V. 不均質媒質を傳はるラブ波 (英文)	佐藤泰夫	1
2.	地球内の電氣傳導度と温度 (英文)	力武常次	13
3.	各種の地質境界線の近くの地電位差 (英文)	佐久間修三	25
4.	地表層の性質と地震動振幅との關係 (英文)	金井清	31
5.	地震計記象による發震機構の假定の吟味 (英文)	金井清	39
6.	電磁制振式新低域濾波器について (英文)	秋間哲夫	53
7.	軟弱地盤の上に落された物体によつて起された土地の振動 (英文)	岸上冬彦	59
8.	應力がかゝつた狀態に於ける岩石彈性率の動力學的研究		
	1. 軸壓のかゝつた狀態に於けるヤング率の測定 (英文)	下鶴大輔	63
9.	火山の帶磁 (英文)	力武常次	71
10.	筑波山斑糲岩の帶磁と地磁氣異常 (英文)	横山泉	83
11.	物の倒れた方向から震央を求めること	佐藤泰夫	93

(The titles in occidental languages are given on the back cover.)

本彙報ハ年4回 (但シ第1號ヨリ第6號マデハ不定期ニ，第7號ハ3冊トシテ發行セリ)，彙報別冊ハ不定期ニ發行ス．

本彙報掲載ノ論文及ビ報告ノ内容ニ關シテハ著者ノミニ其責任アルモノトス．

本彙報ニ關スル照會通信ハ東京大學地震研究所長ヘ宛テラレタシ．

The Bulletin is published quarterly. (Vols. I–VI were published at irregular intervals and Vol. VII consisted of three parts.)
Supplementary Volume is published at irregular interval.

The authors of the papers alone are responsible for the statements and opinions contained in their respective papers.

All communications relating to this Bulletin should be addressed to the Director of the Earthquake Research Institute, Tokyo University.

1. *Study on Surface Waves V.*
Love-Waves Propagated upon Heterogeneous Medium.

By Yasuo SATÔ,

Earthquake Research Institute.

(Read March 14, 1940.—Received Dec. 20, 1951.)

1. Introduction.

The existence of long waves with large horizontal transverse component of displacement in actual seismograms led A.E.H. Love[1] to the discovery of the possibility of waves with such characteristics when there is a layered structure. An alternative condition which may give rise to the waves of the same characteristics was found by E. Meissner[2] and also independently by K. Sezawa[3], and the lack of Meissner's theory was supplemented by K. Aichi[4]. The Progress in our knowledge concerning the crustal structure of the earth resulted in the refinement of the theory in various points[5].

The effect of the double superficial layer on the velocity of propagation of Love-waves was examined independently by R. Stoneley[6] and T. Matuzawa[7] in 1927, and the effect of the heterogeneity in the lower layer was also examined independently by H. Jeffreys[8] and T. Matuzawa[9].

1) A.E.H. LOVE, *Some Problems of Geodynamics.* (1911), 176.

2) E. MEISSNER, *Vieljahr. Nat. Forsch. Ges., Zurich,* **67** (1921), 181. Verh. 2. Int. Kongr. f. Tech. Mech., Zurich, (1926), 137.

3) K. SEZAWA, "A Kind of Waves transmitted over a Semi-infinite Solid Body of Varying Elasticity." *Bull. Earthq. Res. Inst.,* **9** (1931), 310.

4) K. AICHI, "On the Transversal Seismic Waves travelling upon the Surface of Heterogeneous Medium." *Proc. Phys.-Math. Soc. Japan,* [iii], **4** (1922), 137.

5) S. HOMMA also published a paper concerning this problem. *Journ. Meteor. Soc. Jap.,* [ii], **18** (1940), 8. (In Japanese).

6) R. STONELEY and E. TILOTSON, "The Effect of a Double Surface Layer on Love Waves." *M.N.R.A.S. Geo. Sup.,* **1** (1927), 521. "The Dispersion of Waves in a Double Superficial Layer." do., 527.

7) T. MATUZAWA, "Propagation of Love Waves along a doubly Stratified Layer." *Proc. Phys.-Math. Soc. Japan,* [iii], **10** (1927), 25.

8) H. JEFFREYS, "The Effect on Love Waves of Heterogeneity in the Lower Layer." *M.N.R.A.S. Geo. Sup.,* **2** (1928), 101.

9) T. MATUZAWA, "Observation of Some Recent Earthquakes and their Time Distance Curves" *Bull. Earthq. Res. Inst.,* **6** (1929), 211.

The propagation in two dimensions and over the surface of sphere, and the problems of the generation of Love-waves were treated by K. Sezawa[10] and H. Nakano[11] and others from various points of view. R. Yosiyama[12] in general solved rigorously the waves of Love-type over the heterogeneous sphere.

In order to elucidate the nature of surface waves we meet with the neccesity of the theory of waves propagated along double superficial layer upon the heterogeneous substratum as ascertained in various parts of the world.

The theory of waves of Love type propagated in heterogeneous medium was treated by Meissner[13] Sezawa[14], Jeffreys[15], Matuzawa[16], Yosiyama[17], Homma[18] and others. The assumed heterogeneity of the medium in these studies were roughly classified into three groups; in the first group the velocity increases linearly with the depth from the surface, and in the second group the rigidity varies linearly, while in the third the rigidity varies with the n-th power of the distance from the centre[19]. The first case was fully treated by H. Jeffreys, the second case by Sezawa and Matuzawa, and the last case rigorously by R. Yosiyama. In the present analysis, the results of these authorities could of course be utilized, but in view of the refinement in mathematics, we have treated the second case and obtained the solution in Whittaker's confluent hypergeometric function, $W_{k,m}(z)$[20].

2. Waves of Love type propagated over semi-infinite solid in which rigidity increases linearly with the depth z from the surface.

We shall take Cartesian coordinates x and z, whose origin lies on the surface, and take x-axis horizontally and z vertically upward, so

10) K. SEZAWA, "Propagation of Love-waves on a Spherical Surface and Allied Problems." *Bull. Earthq. Res. Inst.*, **7** (1929), 437. "Love waves Generated from a Source of a certain Depth." *Bull. Earthq. Res. Inst.*, **13** (1929), 1.

11) H. NAKANO, "Love-wave in Cylindrical Coordinates." *Geophys. Mag.*, **8** (1929).

12) R. YOSIYAMA, *Zisin*, **10** (1938), 272 (in Japanese).

13) *loc. cit.*, 2).

14) *loc. cit.*, 3).

15) *loc. cit.*, 8).

16) *loc. cit.*, 9).

17) *loc. cit.*, 12), and *Zisin* **11** (1939), 57, 145, 247.

18) *loc. cit.*, 5), and also see *Kensin-Ziho*, **10** (1938), 459 and **12** (1942), 37.

19) S. Homma, investigated a problem assuming some other kind of heterogeneity, but has not yet published it.

20) WHITTAKER and WATSON, *Modern Analysis*, *p.* 337.

that $\mu = \mu_0 - \beta z$. We shall confine our study, for the present, to the case of plane waves propagated in the direction of x-axis. However this is by no means an essential limitation, for the nature of the general cylindrical wave is exactly the same so far as the variation of the amplitude with z and the velocity of propagation are concerned.

Now in our problem the displacement has only transverse horizontal component, so $u = w = 0$.

Then the equation of motion in such medium is, as usual,

$$\rho \frac{\partial^2 v}{\partial t^2} = \mu \nabla^2 v + \frac{\partial \mu}{\partial z} \frac{\partial v}{\partial z}, \qquad \nabla^2 = \frac{\partial^2}{\partial x^2} + \frac{\partial^2}{\partial z^2} \quad \cdots\cdots\cdots (2.1)$$

where ρ and μ are the density and rigidity of the medium, and μ is assumed to be the function of z alone.

Putting V for

$$V \equiv \sqrt{\mu}\, v$$

we have $$\rho \frac{\partial^2 V}{\partial t^2} = \mu \nabla^2 V - \frac{1}{2} V \frac{d^2 \mu}{dz^2} + \frac{1}{4\mu} V \left(\frac{d\mu}{dz} \right)^2 \quad \cdots\cdots\cdots (2.2)$$

Assuming now $V = Z \exp(ipt - ifx)$
and changing the independent variable z into μ, we have

$$\frac{d^2 Z}{d\mu^2} + \left\{ \frac{\rho p^2}{\mu} - f^2 - \frac{1}{2\mu} \frac{d^2 \mu}{dz^2} + \frac{1}{4\mu^2} \left(\frac{d\mu}{dz} \right)^2 \right\} Z = 0$$

which now reduces itself in our problem to

$$\frac{d^2 Z}{d\mu^2} + \left\{ \frac{1/4}{\mu^2} + \frac{\rho p^2/\beta^2}{\mu} - \frac{f^2}{\beta^2} \right\} Z = 0 \quad \cdots\cdots\cdots (2.3)$$

because $\dfrac{d\mu}{dz} = -\beta$, $\dfrac{d^2 \mu}{dz^2} = 0$ from the assumption.

Substituting again

$$\kappa = \rho p^2 / 2f\beta, \qquad \zeta = 2f\mu / \beta \quad \cdots\cdots\cdots (2.4)$$

and $$W = \frac{4f^2}{\beta^2} Z$$

we get $$\frac{d^2 W}{d\zeta^2} + \left\{ \frac{1/4}{\zeta^2} + \frac{\kappa}{\zeta} - \frac{1}{4} \right\} W = 0. \quad \cdots\cdots\cdots (2.5)$$

The solution of the last equation is the Whittaker's[21] confluent hyper-

21) *loc. cit.*, 20).

geometric function $W_{\kappa,0}(\zeta)$

$$W = W_{\kappa,0}(\zeta) = e^{-\zeta/2}\zeta^{\kappa} S$$

in which $$S = 1 + \sum_{n=1}\left\{(-)^n \prod_{m=1}^{n}\left(\frac{(\kappa - m + 1/2)^2}{m\zeta}\right)\right\}$$

or
$$W = M_{\kappa,0}(\zeta) = \zeta^{1/2} e^{-\zeta/2}\left\{1 + \sum_{n=1}^{\infty}\left(\prod_{m=1}^{n}\frac{(1/2 - \kappa + m - 1)}{m^2}\right)\zeta^n\right\}$$

$$= \zeta^{1/2} e^{-\zeta/2} {}_1F_1\left(\frac{1}{2} - \kappa,\ 1,\ \zeta\right) \quad \ldots\ldots\ldots\ldots\ldots (2.6)$$

of which the former is utilized in this problem.

We have thus obtained the solution v of the equation (2.1) which is now written

$$v = A(\beta / 2f)^{3/2} \Phi(\zeta)\, e^{i(pt - fx)} \quad \ldots\ldots\ldots\ldots\ldots (2.7)$$

where $$\Phi(\zeta) = \zeta^{\kappa - 1/2} e^{-\zeta/2} S.$$

Although we have hitherto confined ourselves to the solution of the two dimensional problem, the restriction is a matter of no essential necessity, because the solution of the three dimensional problem is obtained following the line skilfully opened by K. Sezawa provided the present $\Phi(\zeta)$ function is substituted for his $\Phi(z)$ into his solution by replacing ζ above by $2kz$ of Sezawa's notation[22].

3. Love waves propagated along stratified surface.

As first proved by Meissner[23], the boundary condition of zero surface traction can be satisfied without surface layers provided the medium is heterogeneous.

Thus $$\frac{dv}{dz} = 0$$

or
$$\frac{d\Phi}{d\zeta} = 0 \quad \ldots\ldots\ldots\ldots\ldots (3.1)$$

If there are surface layers, the free surface wave can exist as discovered by Love and Stoneley and Matuzawa.

We shall, for simplicity's sake, also assume that the medium is homogeneous and isotropic in each crustal layer while in the substratum the rigidity increases linearly with the depth from the boundary surface.

22) *loc. cit.*, 3).

23) *loc. cit.*, 2).

It is well-known that the relevant solution of the waves in the crustal layers is

$$v_i = \{A_i e^{is_i z} + B_i e^{-is_i z}\} e^{i(pt-fx)}$$

where $s_i^2 = -f^2 + k_i^2, \quad k_i^2 = \rho_i p^2/\mu_i, \quad i=1, 2 \ldots\ldots$ (3.2)

while the solution in the substratum is given by (2.7) in the previous section.

The boundary conditions to be satisfied by these waves are the vanishing of surface traction at the uppermost surface and the continuity of displacement and traction on the boundary surfaces of two media; i.e.,

$$\begin{cases} \text{at the free surface} & \dfrac{\partial v_1}{\partial z} = 0 \\ \text{at the boundary surfaces} & v_i = v_{i+1} \text{ and } \mu_i \dfrac{\partial v_i}{\partial z} = \mu_{i+1} \dfrac{\partial v_{i+1}}{\partial z} \end{cases} \quad (3.3)$$

When there is a superficial layer with thickness H_1, (the origin of coordinate being taken on the lower boundary of this layer) and the intermediate layer with thickness H_2, the boundary conditions gives the relations (cf. Fig. 1)

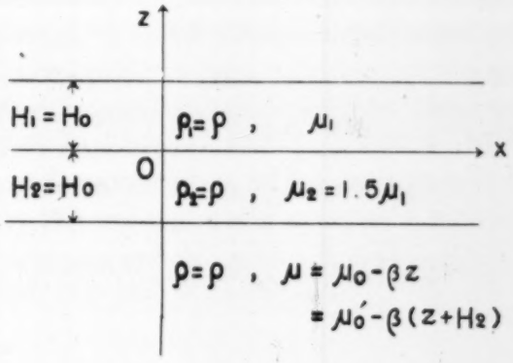

Fig. 1.

$$\begin{aligned} &A_1 \exp(is_1H_1) - B_1 \exp(-is_1H_1) = 0 \\ &A_1 + B_1 = A_2 + B_2 \\ &\mu_1 s_1 A_1 - \mu_1 s_1 B_1 = \mu_2 s_2 A_2 - \mu_2 s_2 B_2 \qquad \ldots\ldots\ldots\ldots (3.4) \\ &A_2 \exp(-is_2H_2) + B_2 \exp(is_2H_2) = A_3 \left(\frac{\beta}{2f}\right)^{3/2} \Phi(\zeta_0) \\ &i\mu_2 s_2 A_2 \exp(-is_2H_2) - i\mu_2 s_2 B_2 \exp(is_2H_2) = (-2f\mu_0') A_3 \left(\frac{\beta}{2f}\right)^{3/2} \Phi'(\zeta_0) \end{aligned}$$

which give

$$\begin{vmatrix} \exp(is_1H_1) & -\exp(-is_1H_1) & 0 & 0 & 0 \\ 1 & 1 & -1 & -1 & 0 \\ \mu s_1 s_1 & -\mu_1 s_1 & -\mu_2 s_2 & \mu_2 s_2 & 0 \\ 0 & 0 & \exp(-is_2H_2) & \exp(is_2H_2) & -\left(\frac{\beta}{2f}\right)^{3/2} \Phi(\zeta_0) \\ 0 & 0 & i\mu_2 s_2 \exp(-is_2H_2) & -i\mu_2 s_2 \exp(is_2H_2) & 2f\mu_0' \left(\frac{\beta}{2f}\right)^{3/2} \Phi'(\zeta_0) \end{vmatrix} = 0 \quad (3.5)$$

where μ_0' implies the value of rigidity of heterogeneous medium at the boundary surface $z=-H_2$, i.e., $\mu=\mu_0-\beta z=\mu_0'-\beta(z+H_2)$.

Developing the above determinant we have

$$\begin{aligned}\Delta_0 \equiv &\left\{1-\frac{\mu_1}{\mu_2}\frac{s_1}{s_2}\tan s_1H_1 \tan s_2H_2\right\}\left\{2f\frac{1}{s_2}\frac{\Phi'(\zeta_0)}{\Phi(\zeta_0)}\right\}\\ &+\left\{\frac{\mu_2}{\mu_0'}\tan s_2H_2+\frac{\mu_1}{\mu_0'}\frac{s_1}{s_2}\tan s_1H_1\right\} \qquad =0\end{aligned} \qquad \cdots\cdots(3.6)$$

If we put

$$\begin{aligned}&k^2\equiv\rho p^2/\mu_0', \quad k_j^2\equiv\rho_j p^2/\mu_j \quad (j=1,\ 2)\\ &s_j^2=k_j^2-f^2 \qquad\qquad (\ ,,\ )\\ &\frac{k_j^2}{k^2}=\frac{\rho_j}{\rho}\frac{\mu_0'}{\mu_j}\equiv r_j'^2 \qquad (\ ,,\ ) \qquad \cdots\cdots\cdots(3.7)\\ &\omega_j\equiv kH_j \qquad\qquad (\ ,,\ )\\ &v\equiv k/f\end{aligned}$$

then $$s_jH_j=\omega_j\sqrt{(r_j'^2-v^{-2})} \qquad (j=1,\ 2)$$

Here, v is the phase velocity of surface waves, and ω is the frequency of the waves. The expression (3.6) becomes

$$\begin{aligned}\Delta_0=&\left\{1-\frac{\mu_1}{\mu_2}\frac{\sqrt{r_1'^2-v^{-2}}}{\sqrt{r_2'^2-v^{-2}}}\tan\omega_1\sqrt{r_1'^2-v^{-2}}\cdot\tan\omega_2\sqrt{r_2'^2-v^{-2}}\right\}\\ &\cdot\left\{2\frac{v^{-1}}{\sqrt{r_2'^2-v^{-2}}}\frac{\Phi'(\zeta_0)}{\Phi(\zeta_0)}\right\}\\ &+\left\{\frac{\mu_2}{\mu_0'}\tan\omega_2\sqrt{r_2'^2-v^{-2}}+\frac{\mu_1}{\mu_0'}\frac{\sqrt{r_1'^2-v^{-2}}}{\sqrt{r_2'^2-v^{-2}}}\tan\omega_1\sqrt{r_1'^2-v^{-2}}\right\}=0\end{aligned}$$

$$\frac{\Phi'(\zeta_0)}{\Phi(\zeta_0)}=\frac{\kappa-1/2}{\zeta}-\frac{1}{2}+\frac{S'}{S},$$

$$S=1+\sum_{n=1}\left\{(-)^n\prod_{r=1}^{n}\frac{(\kappa-r+1/2)^2}{r\zeta}\right\},\quad S'=\sum_{n=1}\left[\left(-\frac{n}{\zeta}\right)\left\{(-)^n\prod_{r}\frac{(\kappa-r+1/2)^2}{r\zeta}\right\}\right]$$

$$\cdots\cdots\cdots(3.8)$$

4. Numerical calculations.

4.1 Determination of velocity.

In this article we will give the results of numerical calculations performed under the assumptions shown in the following lines (cf. Fig. 1).

$$H_1 = H_2 \equiv H_0$$
$$\rho_1 = \rho_2 \equiv \rho \qquad \cdots\cdots\cdots(4.1)$$
$$\frac{\mu_1}{\mu_2} = \frac{\mu_2}{\mu_0'} = \frac{1}{1.50}$$

from which we obtain

$$r_1'^2 = 2.25, \qquad r_2'^2 = 1.50$$
$$\omega_1 = \omega_2 \equiv \omega.$$

Further we assume

$$\theta_0 \equiv D_0/H_0 = 40 \qquad \cdots\cdots\cdots(4.2)$$

where $D_0 \equiv \mu_0'/\beta$ implies the depth where the rigidity is twice that of the boundary surface.

Then

$$\kappa \equiv \rho p^2/2f\beta$$
$$= \theta_0 \omega v/2 = 20\omega v \qquad \cdots\cdots\cdots(4.3)$$
$$\zeta_0 = 2f\mu_0'\beta$$
$$= 2\theta_0\omega/v = 80\,\omega/v$$

Although the process of computation is very much complicated, its principle is simple.

At first we assume a pair of the values of ω and v; then we calculate Δ_0 in (3.8) by means of the expressions (2.6) and (2.7). If it does not vanish, we assume another value of ω (v remains unaltered) and again calculate the value Δ_0. We repeat such processes and by interpolation determine the pair of the values of ω and v which satisfy $\Delta_0 = 0$. Thus we obtain the following results. (Table I and Fig. 2)

Table I.

$1/v$	ω	v (phase vel.)	$1/\omega$	group vel.
0.90	0.161	1.111	6.21	1.012
0.95	0.2300	1.053	4.348	0.932
0.97	0.272	1.031	3.68	—
1.00	0.3295	1	3.035	0.871
1.05	0.4360	0.952	2.294	0.814
1.10	0.5510	0.909	1.815	0.750
1.15	0.6726	0.870	1.485	0.707
1.20	0.8094	0.833	1.236	0.679
1.25	0.9746	0.800	1.026	0.659
1.30	1.1870	0.769	0.8425	0.652
1.35	1.5098	0.741	0.6623	0.648
1.40	2.0475	0.714	0.4884	0.646
1.45	3.2635	0.690	0.3064	0.653
1.475	—	—	—	0.658
1.50	∞	0.667	0	0.667

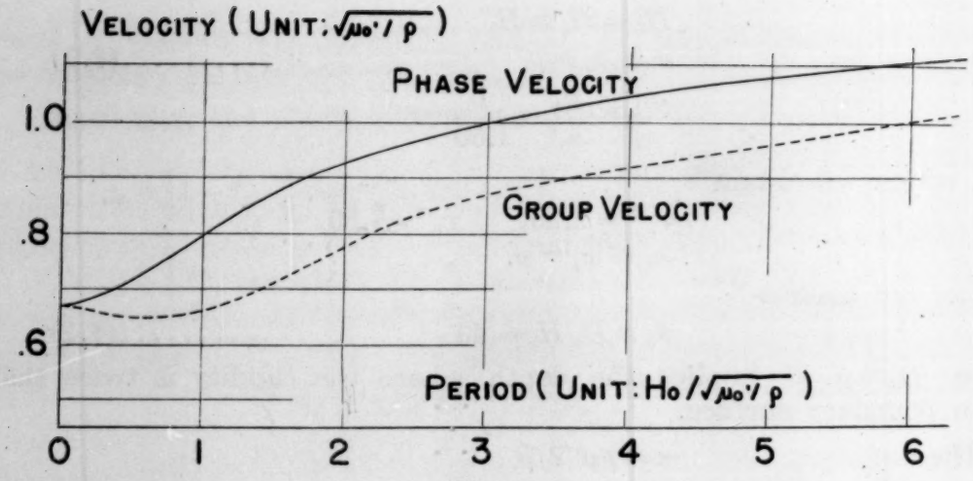

Fig. 3.

The last column of the same table gives the value of group velocity, which is determined by using the method of numerical differentiation (we adopted Stirling's formula), and graphical differentiation (in this case Askania's apparatus was used).

In this calculation, the determination of ω, when the wave length is not so small, is extremely troublesome. For, in this case, κ and ζ_0 are both large, and the convergency of the series S and S' are not good. Thus the asymptotic expansion in such a case is desirable, which, however, is not obtained yet.

4.2. Vertical distribution of amplitude.

Now that the velocity has been determined in the previous chapter, we will obtain the vertical distribution of amplitude here.

The necessary formulae are obtained utilizing the above four expressions in (3.4) and developing the five determinants of 4th degree. The result is as follows,

$$\begin{cases} A_1: & \{(\beta/2f)^{3/2}\,\mu_2 s_2\,\Phi(\zeta_0)\cdot(\cos s_1H_1 - i\sin s_1H_1)\} \\ =B_1: & \{(\beta/2f)^{3/2}\,\mu_2 s_2\,\Phi(\zeta_0)\cdot(\cos s_1H_1 + i\sin s_1H_1)\} \\ =A_2: & \{(\beta/2f)^{3/2}\,\Phi(\zeta_0)\cdot(\mu_2 s_2\cos s_1H_1 - i\mu_1 s_1\sin s_1H_1)\} \\ =B_2: & \{(\beta/2f)^{3/2}\,\Phi(\zeta_0)\cdot(\mu_2 s_2\cos s_1H_1 + i\mu_1 s_1\sin s_1H_1)\} \\ =A_3: & \{2(\mu_2 s_2\cos s_1H_1 - \mu_1 s_1\sin s_1H_1\sin s_2H_2)\} \end{cases}$$

We introduce these expressions into (3.2) and (2.7), and get the following three expressions which are sufficient to show the vertical distribution of the amplitude of the waves in question.

$$\begin{cases} v_1 = C\,\Phi(\zeta_0)\,\{\mu_2 s_2 \cos s_1 H_1 \cos s_1 z + \mu_2 s_2 \sin s_1 H_1 \sin s_1 z\} \exp(ipt - ifx) \\ v_2 = C\,\Phi(\zeta_0)\,\{\mu_2 s_2 \cos s_1 H_1 \cos s_2 z + \mu_1 s_1 \sin s_1 H_1 \sin s_2 z\} \exp(ipt - ifx) \\ v_3 = C\,\Phi(\zeta)\ \{\mu_2 s_2 \cos s_1 H_1 \cos s_2 H_2 - \mu_1 s_1 \sin s_1 H_1 \sin s_2 H_2\} \exp(ipt - ifx) \end{cases} \quad \ldots (4.5)$$

If we introduce the numerical values which we have adopted in § 4.1, and further modify them in order to obtain the expressions more convenient for numerical calculations, we arrive at the following expressions,

$$\begin{cases} v_1 = C'\left\{\cos\left(\omega\sqrt{2.25-v^{-2}}\,\frac{z}{H_0}\right) \right. \\ \qquad\qquad \left. + \tan(\omega\sqrt{2.25-v^{-2}})\,\sin\left(\omega\sqrt{2.25-v^{-2}}\,\frac{z}{H_0}\right)\right\} \\ v_2 = C'\left\{\cos\left(\omega\sqrt{1.50-v^{-2}}\,\frac{z}{H_0}\right) + \frac{1}{1.50}\,\frac{\sqrt{2.25-v^{-2}}}{\sqrt{1.50-v^{-2}}} \right. \\ \qquad\qquad \left. \cdot \tan(\omega\sqrt{2.25-v^{-2}})\,\sin\left(\omega\sqrt{1.50-v^{-2}}\,\frac{z}{H_0}\right)\right\} \\ v_3 = C'\left(\frac{\zeta}{\zeta_0}\right)^{\kappa-\frac{1}{2}} \exp\{(\zeta_0-\zeta)/2\}\,\frac{S(\zeta)}{S(\zeta_0)}\,\cos(\omega\sqrt{1.50-v^{-2}}) \\ \quad \cdot\left\{1 - \frac{1}{1.50}\,\frac{\sqrt{2.25-v^{-2}}}{\sqrt{1.50-v^{-2}}}\tan(\omega\sqrt{2.25-v^{-2}})\tan(\omega\sqrt{1.50-v^{-2}})\right\} \end{cases} \quad \ldots (4.6)$$

Table II.

Case	A	B	C
$1/v$	0.997	1.10	1.40
ω	0.324025	0.55	2.044
κ	6.5	10.0	29.2
ζ_0	25.7645	48.40	228.93
ζ/ζ_0	$\left(\frac{\zeta}{\zeta_0}\right)^{\kappa-\frac{1}{2}} \exp\{-(\zeta-\zeta_0)/2\}\,\frac{S(\zeta)}{S(\zeta_0)}$		
1.00	1.000	1.000	1.000
1.02	0.918	—	—
1.04	0.836	—	—
1.05	—	0.546	0.0168
1.06	0.761	—	—
1.08	0.688	—	—
1.10	—	0.292	0.00027
1.12	0.554	—	—
1.20	0.344	0.0786	—
1.30	0.1769	0.01677	—
1.50	0.0395	0.00068	—

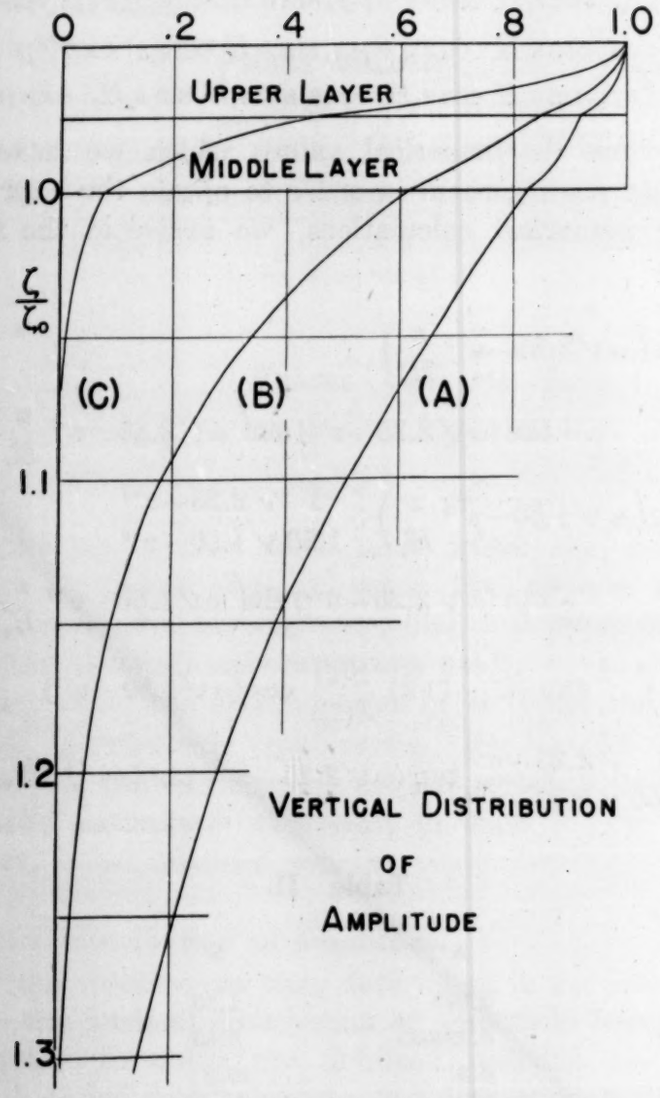

Fig. 3.

Since the waves show dispersive property in this problem, the vertical distribution of amplitude is not invariant with regard to period. Therefore we have performed numerical calculations corresponding to some typical values of velocity ($v=0.997$, 1.10, 1.40) or period. The results are shown in Table II and in Fig. 3.

This paper was completed under the kind guidance of Prof. H. Kawasumi. The author offers heartiest thanks to his incessant instruction.

1. 表面波の研究 V.
不均質媒質を傳はるラブ波

地震研究所　佐藤泰夫

今日までに我我に知られた所によれば，地球の表面近くの構造は，極めて複雑なものであるが，簡單なモデルとしては，一様な二つの層を表面におき，その下の彈性率を，深さの 1 次式でかはるものと假定して，大きなあやまりはないやうである．猶，密度はこの三つの部分で大したちがひはない．

そこで我々は，第 1 圖に示すやうな物質の配置を考へて，この中をつたはるラブ型の表面波についてしらべたが，これは今日の所では，實際に觀測するものに，もつともよく適合する可能性を持つた解の一つと思ふ．

問題は 2 次元的な扱ひをしたが，3 次元としても，本質的な變化があるわけではない．

彈性率が 1 次式でかはる媒質内の解としては，變數を適當に變換して confluent hypergeometric の形にみちびき，Whittaker の $W_{k,m}(z)$ 函數の形に解を求めた．

上の式を用ゐて速度方程式をかきあらはし，更に $\mu_0'=1.50\,\mu_2$, $\mu_2=1.50\,\mu_1$, $\theta_0\equiv D_0/H_0\equiv\mu_0'/H_0\beta=40$ (D_0 は μ の値が，境界面の値 μ_0' の 2 倍になる深さ) と假定してこの方程式を數値的にといた．結果は第 I 表及び第 2 圖に示す．なほ，このやうにして得られた位相速度を，數値的 (Stirling の公式によつた) もしくは圖的に (Askania の微分器を用ゐた) 微分して，群速度をも求めたが，これも同じ表と圖に示してある．

一度速度が定まるならば，媒質内の振幅の分布も決定する．もつとも，現在の問題では波が分散性であり (正分散)，速度は周期によつて異るから，振幅の分布も當然周期に依存する．我我は代表的な三つの場合をえらんで數値計算を行ひ，その結果を第 II 表と第 3 圖とに掲げた．

本研究は河角教授のねんごろな御指導によるものであり，日頃からの絶える事ない御教示にあはせて心からの感謝をささげたい．

2. *Electrical Conductivity and Temperature in the Earth.*

By Tsuneji RIKITAKE,

Earthquake Research Institute.

(Read Oct. 16 and Nov. 20, 1951.—Received Dec. 20, 1951.)

Introduction.

In his former paper, the writer[1] attempted to determine the temperature-distribution within the earth from the distribution of the electrical conductivity and the theory of ionic crystals. The conductivity-distribution was obtained by the writer[2] from the standpoint of electromagnetic induction theory which has been developed by S. Chapman[3),4)], A. T. Price[4),5)], B. N. Lahiri, K. Terada[6)] and the writer. Since the main part of the electric conduction in rocks at high temperature is due to the motion of ions as experimentally proved by T. Nagata[7)] and H. P. Coster[8)], the influence of pressure on the conductivity can be approximately estimated from the viewpoint of theoretical physics of solids. The writer's preliminary work was made under the assumptions that the compressibility does not depend on pressure and that the temperature in the earth increases proportionally to depth as was critically reviewed by B. Gutenberg[9)]. These assumptions will be eliminated in the present paper. The pressure-effect on the activation energy of the motion of ions will be also examined more accurately. In short, the purpose of this paper is to revise the treatment in the previous study as accurately as possible.

---

1) T. RIKITAKE, *Bull. Earthq. Res. Inst.*, **27** (1949), 17.

2) T. RIKITAKE, *Trans. Oslo Meeting, I. U. G. G. A. T. M. E.*, (1950), 435. *Bull. Earthq. Res. Inst.*, **28** (1950), 45, **29** (1951) 219 and 263.

3) S. CHAPMAN, *Phil. Trans. Roy. Soc. London A*, **218** (1919), 1.

4) S. CHAPMAN and A. T. PRICE, *Phil. Trans. Roy. Soc. London A*, **229** (1930), 427.

5) B. N. LAHIRI and A. T. PRICE, *Phil. Trans. Roy. Soc. London A*, **237** (1939), 509.

6) K. TERADA, *Geophys. Mag.*, **13** (1939), 63 and **16** (1948), 5.

7) T. NAGATA, *Bull. Earthq. Res. Inst.*, **15** (1937), 663.

8) H. P. COSTER, *M. N. R. A. S. Geophys. Suppl.*, **5** (1949), 193.

9) B. GUTENBERG, *Appl, Mec. Rev.*, **4** (1951), Rev. 3427.

In Part I of this paper, the effect of pressure on the ionic conductivity is estimated in detail. Then, after taking into account the pressure-effect, the temperature-distribution in the earth's mantle that is compatible with the conductivity-distribution is obtained while the crystal structure is assumed to be the same throughout the mantle. The temperature-distribution thus determined has a discontinuous increase at the depth of 400 *km* corresponding to the discontinuity of the electrical conductivity. Since we have no evidence for a particular source of heat at this depth, the discontinuity might be due to the fact that we assume the same crystal structure in both up- and down-side of this level. From this viewpoint, the temperature below this level is recalculated in Part II under the assumption that the substance takes another phase below the depth of 400 *km*, the activation energy for the motion of ions being taken so as to avoid the discontinuity of temperature. As believed by a number of geophysicists, the substance might have a different phase below the depth of about 400 *km* which is called the "20° discontinuity" by seismologists. Hence it will be logical to assume another constant for the ionic mobility below this level though it will be impossible to prove experimentally.

Part I. The mantle having only one phase.

1. Ionic conductivity in the earth's mantle.

In the earth's mantle, which is believed to be composed largely of olivine and pyroxene, the motion of ions would be the main cause of electric conduction as proved in case of igneous rocks at high temperature. As was also shown experimentally, the conductivity of rocks at low temperature is electronic as is the case in most semi-conductors. In order to study the earth's mantle, then, we will consider only the ionic conduction.

As has been suggested first by J. Frenkel[10], the ionic conductivity in crystals is closely connected with the lattice defect. Since a very large field is required to remove an ion from its normal site in crystals, we suspect that there already exists lattice defect in crystals. In that case, ions may move by jumping into vacant sites or may move through interstitial positions. Since it is beyond the scope of this paper to mention the theory of lattice defect in detail, only the results of the

10) J. FRENKEL, *Z. Physik*, **35** (1926), 652.

theory will be dealt with. The electrical conductivity σ is expressed by[11]

$$\sigma = \sigma_0 e^{-\epsilon_0/kT}, \quad \ldots\ldots\ldots\ldots\ldots\ldots\ldots\ldots\ldots\ldots (1)$$

where

$$\sigma_0 = (Ne^2\nu r^2/kT)e^{-\frac{\alpha r_0}{k}\left(\frac{d\epsilon}{dV}\right)_0}, \quad \ldots\ldots\ldots\ldots\ldots\ldots (2)$$

$$\epsilon = \frac{1}{2}W + U, \quad \ldots\ldots\ldots\ldots\ldots\ldots\ldots\ldots\ldots\ldots (3)$$

and where T, W and U denote respectively absolute temperature, energy required to make a lattice defect, and activation energy. k, N, e, ν, r, α and V denote respectively Boltzamann's constant, number of ion in unit volume, charge of electron, vibration frequency of ion at lattice point, interionic distance, thermal expansion coefficient, and volume per pair of ions. The suffix 0 means the quantity at zero temperature.

Strictly speaking, different conductivities of the type shown in (1) are responsible for respective ions and the total conductivity should be given by summing up all these conductivities. But it is assumed here that only a type of conductivity is effective in the earth's interior as approximately proved by the experiments of rocks at high temperature.

2. The effect of pressure on ϵ_0 and σ_0.

In order to estimate the conductivity at any pressure, $(\partial\epsilon_0/\partial p)_T$ and $(\partial \log \sigma_0/\partial p)_T$ are calculated in the following.

The energy required to make a lattice defect in ionic crystals is given by

$$W = U^+ + U^- - E, \quad \ldots\ldots\ldots\ldots\ldots\ldots\ldots (4)$$

in which U^+, U^- and E denote respectively the energy required to take off a positive ion, that required to take off a negative one and that required to make a pair of ions. According to the classical theory of ionic crystals, E is given by the sum of electrostatic interaction energy, repulsive interaction energy, van der Waals interaction energy and zero point energy. On neglecting the last two, we have

$$E = Ar^{-1} - Br^{-n}, \quad \ldots\ldots\ldots\ldots\ldots\ldots (5)$$

in which A and B are both constants determined later, the first and

11) N. F. MOTT and R. W. GURNEY, *Electronic processes in ionic crystals.* Oxford, (1940).

second terms corresponding to electrostatic and repulsive interaction respectively.

To get the activation energy U, we should take into account the polarization energy due to the electric field in ion vacancies. Hence we have for positive ion

$$U^+=E-\frac{e^2}{2q^+r}(1-1/\kappa), \quad \cdots\cdots\cdots\cdots\cdots\cdots(6)$$

and for negative ion

$$U^-=E-\frac{e^2}{2q^-r}(1-1/\kappa), \quad \cdots\cdots\cdots\cdots\cdots\cdots(7)$$

in which κ denotes the dielectric constant, while q^+r or q^-r denote the effective radii of the respective vacancies. According to a more rigorous estimate, it is known that $q^+ \simeq 0.6$ and $q^- \simeq 0.9$.

Since positive ions seem likely to contribute in the main to the conductivity of rocks as experimentally shown by Coster[8], it would be allowed to take the next expression as ϵ;

$$\epsilon=\frac{3}{2}E-\left(\frac{3}{q^+}+\frac{1}{q^-}\right)\frac{e^2}{4r}(1-1/\kappa). \quad \cdots\cdots\cdots\cdots(8)$$

Now we are in a position to determine A and B in (5) from the condition of equilibrium. At zero temperature, there exist thermodynamical relations

$$\left(\frac{\partial E}{\partial V}\right)_{V=V_0}=-P, \quad \left(\frac{\partial^2 E}{\partial V^2}\right)_{V=V_0}=\frac{1}{\chi_0 V_0}, \quad \cdots\cdots\cdots(9)$$

where P and χ denote respectively pressure and compressibility.

On introducing the relation

$$V=c^3r^3 \quad \cdots\cdots\cdots\cdots\cdots\cdots\cdots(10)$$

where c denotes a constant peculiar to the crystal structure, we get

$$A=\frac{9-3(n+3)\chi_0 P}{(n-1)\chi_0}cV_0^{4/3}, \quad B=\frac{9-12\chi_0 P}{n(n-1)\chi_0}cV_0^{\frac{n+3}{3}}. \quad \cdots\cdots(11)$$

Putting (11) in (5), the internal energy of the crystal becomes as follows;

$$E=\frac{3V_0}{(n-1)\chi_0}\left\{(3-\overline{n+3}\chi_0 P)(V_0/P)^{1/3}-\frac{3-4\chi_0 P}{n}(V_0/V)^{n/3}\right\}. \quad \cdots(12)$$

At zero temperature or $V=V_0$, we have

$$E_0=\frac{9V_0}{n\chi_0}\left(1-\frac{\chi_0 P}{3}\right), \quad \cdots\cdots\cdots\cdots\cdots\cdots(13)$$

and, with the aid of the relation $-\left(\frac{d^3E}{dV^3}\right)_{V=V_0}=\frac{1}{\chi_0 V_0^2}\left\{1+\frac{d}{dP}\left(\frac{1}{\chi_0}\right)\right\}$, the differential equation

$$\frac{1}{\chi_0^2}\frac{d}{dP}\left(\frac{1}{\chi_0}\right)=K-M\chi_0 P, \quad \cdots\cdots\cdots\cdots\cdots\cdots(14)$$

where

$$K=\frac{(n+3)^2-16}{3(n-1)}, \qquad M=\frac{4}{9}(n+3).$$

Meanwhile we find $\chi_0 P<0.1$ at depths shallower than about 1000 km in the earth's mantle. Hence the second terms in the righthand-side of (13) and (14) can be neglected, the pressure-effect on the compressibility being then shown by

$$\frac{1}{\chi_0}=\frac{1}{\chi_{00}}+KP, \quad \cdots\cdots\cdots\cdots\cdots\cdots(15)$$

in which χ_{00} denotes the compressibility at zero temperature and pressure.

In the next place, we find

$$\frac{d\epsilon_0}{dP}=-\chi_0 V_0\frac{d\epsilon_0}{dV_0}$$

or

$$\epsilon_0=\epsilon_{00}e^{-\int_0^P\frac{\chi_0\nu_0}{\epsilon_0}\frac{d\epsilon_0}{dV_0}dP} \quad \cdots\cdots\cdots\cdots\cdots\cdots(16)$$

The quantity $\frac{V_0}{\epsilon_0}\frac{d\epsilon_0}{Vd_0}$ or $\frac{d\log\epsilon_0}{d\log V_0}$ is supposed to be -2 in the preliminary study. In this article, however, it will be accurately obtained through (8) and (13), while χ_0 is also calculated by (15). The pressure-distribution obtained by K. E. Bullen[12] is adopted. As to the value of n which amounts to 6 for light material such as lithium fluoride and to 12 for crystals with only very heavy ions such as caesium iodide, W. H. Ramsey[13] proved that it takes a value between 6 and 9 in the earth's mantle from the studies on the relation between compressibility and pressure as also expected by the fact that the heaviest element which is abundant in the earth is iron. The writter adopted $n=8$

12) K. E. Bullen, *Bull. Seism. Soc. Amer.*, **30** (1940), 235 and **32** (1942), 19.
13) W. H. Ramsey, *M. N. R. A. S. Geophys. Suppl.*, **6** (1950), 42.

from this view, the influence of slight difference of n on K in (15) being fairly small.

ϵ_{00} is taken to be $2.3\,eV$ as obtained from the experiments of various rocks such as basalt, gabbro, andesite, granite and peridotite. χ_{00} is assumed to be $0.90\times10^{-12}\,cgs$ which corresponds to the reduced value to zero temperature and pressure of the substance in the upper part of the earth's mantle. The change in the volume is estimated from the relation

$$V_0=V_{00}(\chi_0/\chi_{00})^{1/K}, \quad \text{.....(17)}$$

which is readily obtained from the definition of compressibility. Taking into consideration the fact that the density amounts to $3.3\,gr./cm^3$, V_{00} is estimated at $7.7\times10^{-23}\,cm^3$ for olivine whose molecular weight amounts to about 150. We further assume $r_{00}=3\times10^{-8}\,cm$ and $n=5$ as obtained for most ionic crystals. Looking at the expression (16), we find that ϵ_0 is most seriously affected by the change in χ_0, while the change of the polarization energy or that in the second term of the righthand-side of (8), which includes rather ambiguous quantities as stated above, will have scarcely any great influence on ϵ_0, the effect of the polarization energy being only a few percent as revealed in the numerical calculation.

On executing the integral in (16) numerically, the value thus obtained are shown in Table I for various depths.

Next, we must investigate the effect of pressure on σ_0. On logarithmically differentiating, we get

$$\frac{d\log\sigma_0}{dP}=\frac{d\log N}{dP}+\frac{d\log\nu}{dP}+\frac{2}{3}\frac{d\log V_0}{dP}-\frac{d}{dP}\left\{\frac{\alpha V_0}{k}\left(\frac{d\epsilon}{dV}\right)_{V=V_0}\right\} \quad (18)$$

Meanwhile, the frequency of small vibration of ion at its normal site may be given by

$$\nu=\frac{1}{r}\sqrt{\frac{E}{m}}, \quad \text{.....(19)}$$

where m denotes mass of the ion, the relation being derived from the equation of small motion of ions under the action of periodic field.

Taking into account further the relation

$$\frac{\alpha V_0}{\chi_0}=-3k\frac{d\log\nu}{d\log V_0}, \quad \text{.....(20)}$$

which is obtained from the equilibrium condition of the Einstein-model

Table I.

Depth (*km*)	ϵ_0 (*eV*)	σ_0 T (*emu. deg.*)
0	2.3	0.10
33	2.3	0.10
100	2.5	0.11
200	2.8	0.12
300	3.1	0.13
400	3.3	0.13
500	3.7	0.14
600	4.0	0.15
700	4.2	0.16
800	4.7	0.17
900	5.0	0.18
1000	5.3	0.19
1200	6.1	0.21
1400	6.7	0.23
1600	7.4	0.25

of solids, the righthand-side of (18) can be estimated. Thus we have

$$\frac{d\log\sigma_0}{dP}=\left(\frac{K}{2}+\frac{2}{3}P\right)\chi_0, \quad \cdots\cdots\cdots\cdots\cdots\cdots(21)$$

and then

$$\sigma_0=\sigma_{00}e^{\int_0^P\left(\frac{d\log\sigma_0}{dP}\right)dP}. \quad \cdots\cdots\cdots\cdots\cdots\cdots(22)$$

According to the experiments of igneous rocks, $\sigma_{00}kT$ is estimated at 10^{-4} *emu* at about 1000° *K*. Adopting then $k\sigma_{00}=0.1$, $\sigma_0 T$ is calculated for various depths as also shown in Table I.

3. The temperature-distribution that is compatible with the conductivity-distribution.

As studied in section 3, ϵ_0 and σ_0 for any pressure can be estimated from their values at zero pressure, so we may readily determine the temperature in the earth's mantle that is compatible with the conductivity-distribution obtained from the electromagnetic induction theory by the writer himself. The change in the conductivity with the increase of depth are reproduced in Fig. 1. The temperature fit for the conductivity at various depths are determined as shown in Table II and Fig. 2.

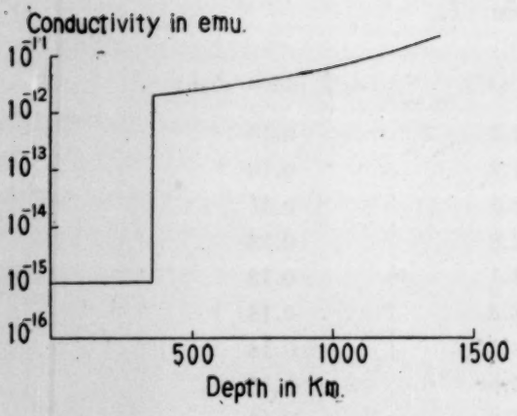

Fig. 1. The distribution of electrical conductivity in the earth as obtained from the electromagnetic induction theory.

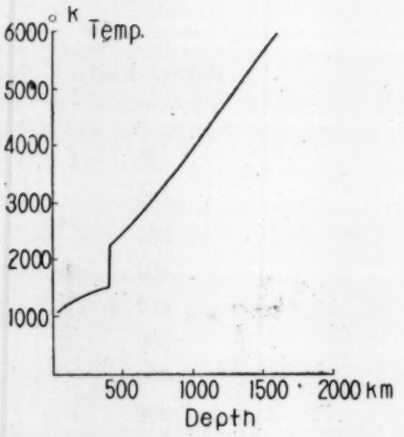

Fig. 2. The temperature in the earth's mantle having only one phase.

As also studied by the writer, the conductivity deeper than about 1500 *km* is ambiguous because the induced electric currents do not penetrate into such a great depth. Hence the temperature deeper than this level is also indeterminable.

Corresponding to the discontinuous increase in the conductivity at a depth of 400 *km*, there occurs a jump of the temperature. But it is doubtful that such a discontinuity of temperature really exists because we have no particular evidence for the source of heat at this depth. The discontinuity should be due to the fact that we assume only one phase of substance throughout the mantle.

Table II.

Depth (*km*)	T (°*K*)
33	1080
100	1180
200	1370
300	1460
400	1540
400	2260
600	2750
800	3340
1000	3940
1200	4620
1400	5320
1600	6020

Part II. The Mantle having another phase below the depth of 400 km.

1. The temperature-distribution which has no discontinuity and is also compatible with the conductivity-distribution.

The behavior of the bulk modulus and density seems anomalous from just below the depth of 400 *km* to 1000 *km*. Some geophysicists

believed that this anomaly is due to a transition to a crystal structure which is more stable at high pressure. As was shown in Part I of this paper, there occurs a discontinuous increase in temperature at the depth of 400 *km* in case of the mantle having only one phase, the existence of such a discontinuity being implausible from physical consideration. Hence it will be natural to take into account the change in physical conditions in the deeper part of the mantle. For the sake of simplicity, the writer assumes here that the bulk modulus and density at zero temperature and pressure become respectively 2.1×10^{12} *cgs* and 4.2 *gr./cm*^{3} in the region deeper than 400 *km* as obtained from extrapolation of Bullen's distribution, while the same values are adopted in the upper part of the mantle. The pressure-effect is estimated in a similar way with Part I. Though we have no experimental value for ϵ_0 and σ_0 in this region, ϵ_0 should be chosen so as to avoid the discontinuity of temperature at the depth of 400 *km*, while $k\sigma_0$ at zero temperature and pressure is assumed to amount to 0.1 as before. It it easily found out that the temperature becomes continuous by assuming $\epsilon_{00}=1.8\,eV$ below the depth of 400 *km*. Adopting these values, the temperature-distribution in the deeper part of the mantle is determined as done in Part I. The results are shown in Table III and Fig. 3 together with the results of the upper region as determined in Part I.

Table III.

Depth (*km*)	T (°*K*)
33	1080
100	1180
200	1370
300	1460
400	1540
600	1730
800	1950
1000	2240
1200	2530
1400	2850
1600	3170

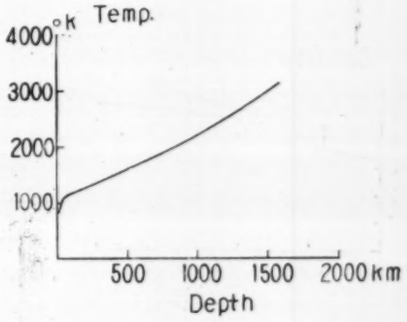

Fig. 3. The temperature in the earth's mantle having a different phase below the depth of 400 *km*.

2. Some considerations on the changes in density and compressibility in the earth's mantle.

With the aid of the temperature-distribution thus obtained, we

shall examine here the distribution of density and compressibility in the earth's mantle.

The effect of pressure and temperature can be written as follows;

$$\frac{1}{\chi(T,P)}=\frac{1}{\chi_{00}}+P\left[\frac{\partial}{\partial P}\left(\frac{1}{\chi}\right)\right]_{00}+T\left[\frac{\partial}{\partial T}\left(\frac{1}{\chi}\right)\right]_{00}+\frac{1}{2}P^2\left[\frac{\partial^2}{\partial P^2}\left(\frac{1}{\chi}\right)\right]_{00}+\cdots\cdots,$$

$$V(T,P)=V_{00}+P\left(\frac{\partial V}{\partial P}\right)_{00}+T\left(\frac{\partial V}{\partial T}\right)_{00}+\frac{1}{2}P^2\left(\frac{\partial^2 V}{\partial P^2}\right)_{00}+\cdots\cdots.$$

Neglecting higher order terms we have

$$\frac{1}{x}=\frac{1}{\chi_{00}}+K\left(P-\frac{\alpha_{00}}{\chi_{00}}T\right)+\cdots\cdots, \tag{23}$$

$$\frac{\rho_{00}}{\rho}=\frac{V}{V_{00}}=1-\chi_{00}P+\alpha_{00}T+\cdots\cdots \tag{24}$$

α_{00}, which is estimated from (20), amounts to 1.7×10^{-5} and 1.2×10^{-5} per *degree*, respectively for upper and lower side of the mantle, the values being reasonable judging from the experimental results of rocks. The results calculated from (23) and (24) are graphically shown in Figs. 4 and 5, where the density and bulk modulus due to Bullen's investigation are also shown. Though some discrepancies are found between

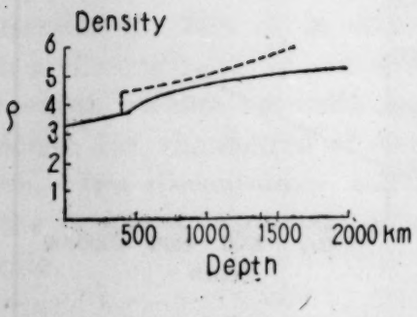

Fig. 4. Bullen's distribution of density (full line) and the calculated one (broken line).

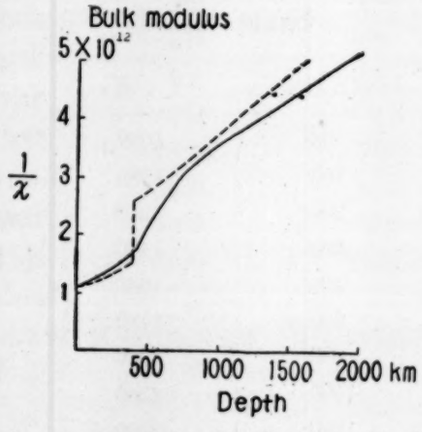

Fig. 5. Bullen's distribution of bulk modulus (full line) and the calculated one (broken line).

Bullen's and the calculated distribution, it might be said that the general aspects are roughly agreeing. Hence the temperature-distribution obtained in this paper seems to be approximately consistent with the distribution of density and bulk modulus in the earth's mantle.

Summary and Conclusion.

The theory of ionic crystals is applied to study the electrical conductivity in the earth's mantle in a manner improving that of the writer's previous study. The constants included are estimated as accurately as possible. The changes in physical conditions in up- and down-sides of the "20° discontinuity" is also taken into acconnt.

After taking into account the pressure-effect on the conductivity, it is found that the temperature likely amounts to 1000° K just below the earth's crust and then increases almost proportionally to depth, the rate of increase being estimated at 1.4° K per km. The distribution is roughly consistent with the distribution of density and bulk modulus in the earth's mantle which is determined by Bullen.

The earth's internal temperature has been hitherto studied from standpoints quite different from the one considered here, such as from the studies in the cooling of the earth and the pressure-effect on melting point. In order to compare the present result with those obtained before, the distribution obtained by H. Jeffreys[14], E. C. Bullard[15] and B. Gutenberg[16] are shown in Fig. 6 together with the writers'. However, all these distribution are by no means conclusive. Much more experiments for various quantities, especially under high pressure and temperature, are necessary before a more concrete knowledge on the earth's internal temperature is to be obtained. The writer is grateful to Dr. T. Nagata for his helpful advice.

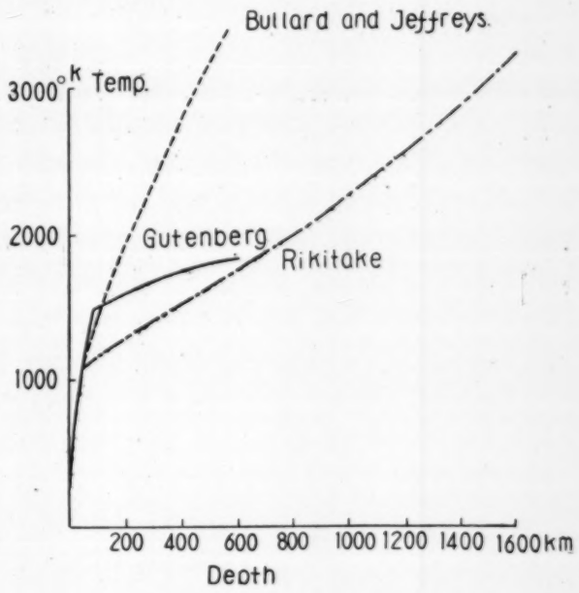

Fig. 6. The temperature-distribution within the earth obtained by Bullard, Jeffreys, Gutenberg and the writer.

14) H. JEFFREYS, *The Earth*. Cambridge (1924), p. 79.
15) E. C. BULLARD, *M. N. R. A. S. Geophys. Suppl.*, **4** (1939), 534.
16) B. GUTENBERG, *Physics of the Earth, VII. Internal Constitution of the Earth*. 1st ed., p. 153.

2. 地球内の電氣傳導度と溫度

地震研究所　力　武　常　次

筆者はかつて地球内の電氣傳導度の分布より，イオン結晶の理論にもとずいて，地球内の溫度の分布を求めることを試みた．その際壓縮率が一定であること，溫度が深さとともに直線的に變化すること等の假定のもとに計算を行つた．本論文に於いては，それ等の假定を捨て，出來得る限りの正確な議論を行う．高溫に於ける岩石の實驗より，電氣傳導度は主としてイオンにより

$$\sigma = Ae^{-B/T}$$

(T は絶對溫度) が成立つことがしられているが，この式中の常數 A および B の壓力による變化は，イオン結晶中の格子缺陷理論を應用することにより，かなり正確に見つもることが出來る．したがつて K.E. Bullen によつて求められている地球内の壓力分布を使用し，A および B の壓力零の値より出發して，地球磁氣學的に求めた σ に對して T を決定出來る．地球の mantle が一定の結晶構造をもつているとすると岩石の實驗値より推定した溫度は 400 km の深さに於て不連續をもつことになり，物理的に不合理であるから，この深さの下では物質は異つた相をとるとし，溫度の不連續がないという條件のもとに活性化エネルギーを見つもる．かくして決定した溫度分布は地殼の下で 1000°K, 1600 km の深さで 3000°K という値となり，その間は 1.4°K/km の增溫率でほとんど直線的に增加する．

このようにして求めた溫度の影響を壓力とともに考慮すると，密度および壓縮率の分布を求めることが出來るが，Bullen の得た分布と大體に於いて調和することがわかつた．

3. *Earth-current Potentials near Boundaries of Various Geological Formations.*

By Shūzō SAKUMA,

Earthquake Research Institute.

(Read Sept. 20, 1949.—Received Dec. 20, 1951.)

1. Introduction.

Since the natural potential method came into use in the field of the geophysical exploration for ores, the nature of the earth-current potential was brought to light to some extent. The factors which affect the earth-current, such as topographies and kinds of rocks, have been also studied from the viewpoint of application to explorations. In fact, the method of the natural potential well-logs, which is based on the knowledge of natural potential among different kind of sedimentary rocks, is now adopted in the exploration for oil.

Some geophysicists had already expected[1] and pointed out the existence of anomalous earth-current near the boundaries of formations. Though their remarks were keen and suggesting, most of them were based only on observations at some scattered points near the boundary-lines aimed at and not on those at sufficient networks all over the area in question, as usually done nowadays in electrical prospectings.

The purpose of the present study is to make up for this imperfectness in those past observations, to find out the relations between geological structures and earth-current potentials if any and to throw some light upon the nature of earth-current.

2. Method and Results of the Observations.

Two Cu-$CuSO_4$ electrodes in the unglazed porcelain pots each 5 cm in diametre and 13 cm in length, were adopted to minimize the polarization effects. The electromotive force between the electrodes was measured by a potentiometer constructed for this purpose. The elect-

1) S. ONO, *Nippon Gakuzyutu-Kyōkai Hōkoku*, **14** (1939), 530. (In Japanese).
M. NAMBA, *Mem. Coll. Sci. Kyoto*, A. **21** (1938), 203.
G. PETRUCCI, *Rivista Geomineraria*, **9** (1943).

rodes were buried in the ground, and after the electromotive force was read, the electrodes were exchanged and the second reading was taken. The average of the two readings gives the natural earth-current potential in the section. All of the sections in the network was occupied in this way.

A) Natural potential near an active fault. (The Tanna Fault at the Ikenoyama-Pass).

The Tanna Fault, which is one of the most remarkable geological faults in the Idu Peninsula, runs nearly in the N–S direction over the Ikenoyama-Pass. At the time of the Idu Earthquake in 1930, the western side of the fault subsided and slided to the south about 1 m,

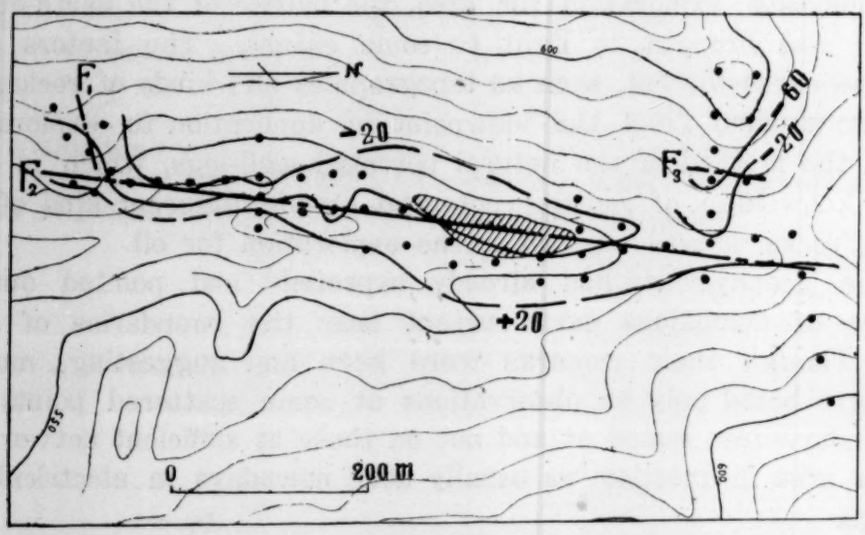

Fig. 1. Topographies and the earth-current at the Ikenoyama-Pass. (in mV) hatched area: pond, F_1, F_2, and F_3: faults in the 1930 earthquake, black circle: position of electrode.

in the same way as those which had occurred in geological ages.[2] Slight traces of the activities of the fault at that time was noticed on the Ikenoyama-Pass. A shallow pond exists along the fault-line. The route of the present survey traversed several times across the fault-line. As will be seen in Fig. 1, a remarkable zone of negative potential runs on and along the fault-line itself, superposed by general earth-current which flows from east to west. Rocks which compose the mountain in this area are all quarternary andesite lavas and no

2) Y. OTUKA, *Bull. Earthq. Res. Inst.*, **11** (1933), 530.
H. KUNO, *Bull. Earthq. Res. Inst.*, **14** (1936), 92; 619.

decisive difference was found between the rocks from the eastern and western side of the fault in the detailed petrological studies by H. Kuno.

Soon after the Idu Earthquake, Y. Kato[3] measured earth-current at several points in this area. Though his survey did not cover the whole of the present area, the direction of earth-current agrees with the present results. Persistency of this kind of anomaly can be inferred from the fact.

B) Difference in the natural potential among various formations. (Akane-saki).

The Miocene tuffs and the pyroxene-dacite lavas are sharply bordered by a nearly vertical distinct fault which runs E–W near the Akane-saki at the eastern coast of the Idu Peninsula. The slope towards the sea is so steep that the potential survey was confined to only one route along the coast highway. Results are shown in Fig. 2. Besides the

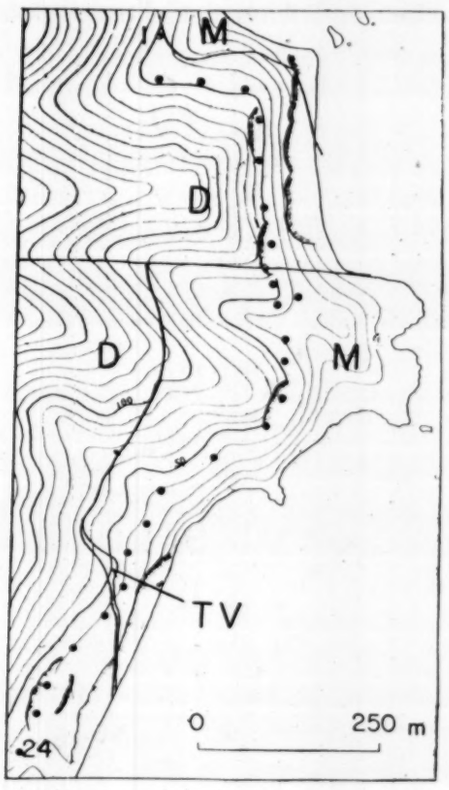

Fig. 2 (a). Geology and the route of the survey near Akane-saki.

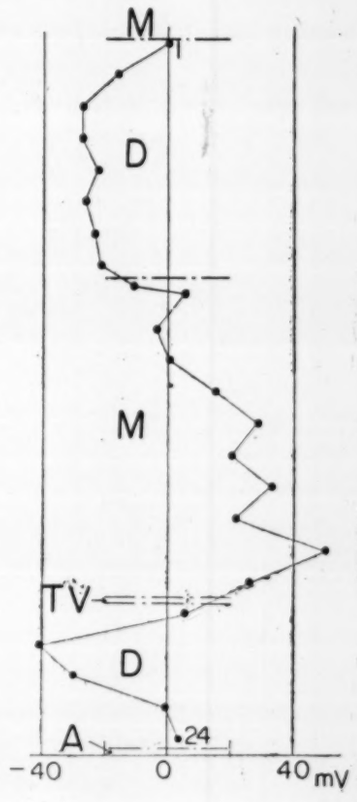

Fig. 2 (b). Earth-current potential along the route.

M: Miocene tuff, D: Dacite, TV: andesite, A: alluvium.

3) Y. KATO, personal communication.

effect of the distinct fault as seen in the former example of the Tanna Fault, the dacites have negative potential in comparison with the adjacent tuffs. These systematic potential differences among various formations which amounted to 20–60 mV are quite similar to the phenomena which are utilized in the electrical-logs in oil wells, though they differ greatly both in the scale of dimension of structures and in the kind of rocks.

C) An example of natural potential across a geological fault, (Usami).

As will be seen in Fig. 3, the steep slope, which consists of layers of lavas and pyroclastic materials, has suffered erosion much along the fault. Rocks on both sides of the fault are the so-called Aziro-basalts, olivine-twopyroxene-basalts and andesites at the northern side and olivine-augite-basalts at the southern side[4]. Earth-current potential is greatly disturbed near the fault, but any simple tendency in the type of anomaly such as at the Ikenoyama-Pass and Akane-saki could hardly

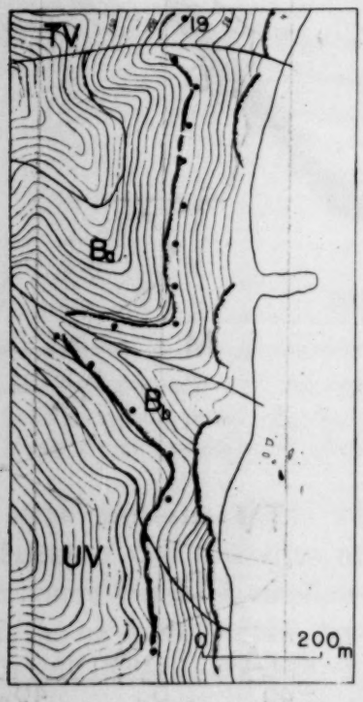

Fig. 3 (a). Geology, topography and the route of survey near Usami.

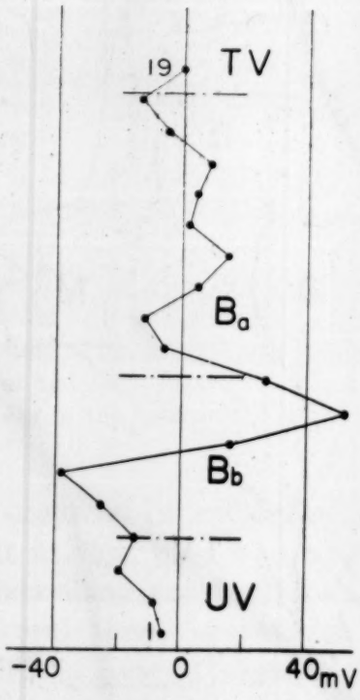

Fig. 3 (b). Earth-current potential along the route.

B_a and B_b : Aziro-basalts, TV : andesite of the Taga volcano, UV : andesite of the Usami volcano.

4) H. TSUYA, *Bull. Earthq. Res. Inst.*, **8** (1930), 409 ; **15** (1937), 215.

be pointed out. No remarkable anomaly was found at the less distinct boundary-line between the Aziro-basalt and the andesite lavas of the Usami volcano.

Summarizing these three cases, we can infer the following nature of the earth-current.

(1) Earth-current potentials always differ obviously among those formations the rocks of which differ greatly from one another in physical and chemical properties. In contrast to that, no remarkable anomaly in earth-current is observed on or along comparatively level ground, when there is no distinct difference among the rocks.

(2) Even on similar kind of formations, however, remarkable anomalies in natural potential are observed across distinct faults. Though the types and the causes of the anomaly could not yet be clarified, the negative potential zone along the Tanna Fault seems to be one of the representative cases.

D) Earth-current in the old atrio of Volcano Asama.

On the basis of the above mentioned results, the writer examined the results of the earth-current survey at Yunotaira, the atrio of

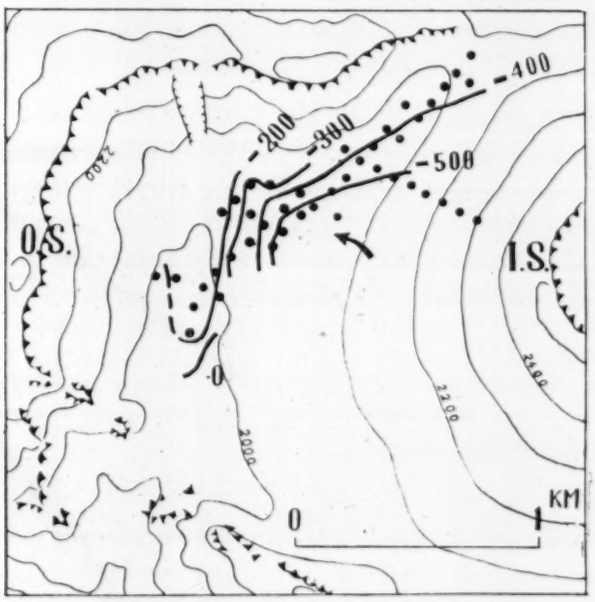

Fig. 4. Earth-current potential at Yunotaira. (in mV).
I.S.: inner somma, O.S.: outer somma, arrow: sink-line.

Volcano Asama, which was carried out by him in 1947. The inner somma lava-flows and other volcanic materials occupy the surveyed area. On Fig. 4, however, a line of sink of earth-current seems to

exist along the nearly E–W line across the crater, if we eliminate the topographical effects, such as the upward earth-current. When we consider the geological history of the Asama volcano, it must not be out of description that the centre of volcanic activities shifted from west to east as if a weak zone existed beneath the atrio in the E–W direction. It is not too unreasonable to infer that the distribution of the earth-current potential may be in connection, to some extent, with the above presumed weak zone.

On the mechanism of causation of earth-current, especially on the anomalies near the boundaries of formations, various interpretations may be given from both chemical and physical standpoints. However, the present writer restricts himself here to point out the existence of some relations of earth-current with structures of the earth's surface.

In concluding, the writer expresses his sincere thanks to Dr. H. Kuno, Dr. T. Nagata and Dr. T. Minakami for their valuable advices and criticisms given in the course of this work. The expense for the research was defrayed from the Funds for the Scientific Research from the Ministry of Education.

---

3. 各種の地質境界線の近くの地電位差

地震研究所　佐久間修三

かつて小野澄之助博士等によつて，地質の不連續線附近で地電位差異常があることが指摘されているが，その後電氣探鑛法としても，岩質の相異に伴ふ地電位差の現象が用いられる様になつた．筆者は，なるべく簡單な條件と考えられる地質境界線の二三の例について詳しく地電位差を測つた．

(A) 明瞭な斷層を境として，岩質の略同一な岩石が接している例として丹那斷層をしらべた．斷層線に沿ひ，明かに帶狀の負電位の地域がある．

(B) 岩質の明にちがう例として，凝灰岩と石英安山岩が斷層で接する赤根崎附近の地電位差分布をみると，地質境界線で 20～60 mV の電位の相異があらわれ，凝灰岩が高電位となる．

(C) 宇佐美北方の網代玄武岩中の斷層線の附近にも著しい地電位の變化があるが，前二者ほど簡單でない．

(D) 淺間火山の火口原の地電位差分布を檢討すると，山地の上向電流と重なつて略東西に走る負電位帶があるかに思われる．上述の知見から，これを既に地學的見地から想像されている東西方向の弱線とむすびつけて考えることも出來よう．

---

4. *Relation between the Nature of Surface Layer and the Amplitudes of Earthquake Motions.*

By Kiyoshi KANAI,

Earthquake Research Institute.

(Read Dec. 18, 1951.—Received Dec. 20, 1951.)

1. The present paper is the continuation of my research work[1] on the effect of solid viscosity of surface layer on the earthquake motion. In the previous paper, I investigated mathematically the case of a layer, and carried out the numerical calculations for some special cases. It was found that the diagramatical features of the results of the previous investigation closely resemble the features of the spectrogramic diagrams of earthquake motions of the ground which were obtained by the accelerometer at several places in Tokyo and Yokohama.

It is a well-known fact that the earthquake damage done to Japanese style wooden buildings at the past earthquakes were closely related with the thickness of alluvium. Recently, it seems that the problem of the relation between the earthquake damage to Japanese style wooden buildings and the thickness, the velocity of seismic waves, the damping coefficient and etc. of superficial soil layer recieved the attention of many seismologists.

In connection with these problems, in the first part of this paper, the oscillations of doubly stratified visco-elastic layers excited by seismic waves will be dealt with mathematically. Next, the numerical calculation of the problem of a stratified visco-elastic layer excited by seismic waves will be carried out again more elaborately because of its increasing importance in connection with the problem of earthquake-proof constructions.

2. In the present chapter, we will investigate the case in which primary distortional waves propagated vertically upwards through the doubly stratified visco-elastic layers residing on the semi-infinite visco-elastic body.

Let, ρ, μ, v, ξ and H be the density, elastic constant, velocity, coefficient of solid viscosity and thickness of layer, and u the displace-

1) K. KANAI, "The Effect of Solid Viscosity of Surface Layer on the Earthquake Movements", *Bull. Earthq. Res. Inst.*, **28** (1950), 31.

ment. Suffix 1, 2, 3 represent the first layer, the second layer and the bottom medium respectively. Then the equation of the motion of each medium may be written as follows:

$$\rho_n \frac{\partial^2 u_n}{\partial t^2} = \left(\mu_n + \xi_n \frac{\partial}{\partial t}\right) \frac{\partial^2 u_n}{\partial z^2} \cdot [n=1, 2, 3] \quad (1)$$

If the incident waves in the lowest medium be of the type

$$u_0 = a\, e^{i(pt+f_3 z)}, \quad \ldots\ldots\ldots\ldots\ldots(2)$$

the resulting displacements of the lowest medium, the second layer and the first layer are expressed by

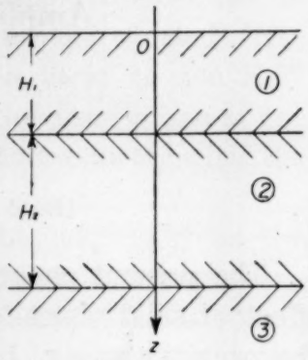

Fig. 1.

$$\left.\begin{aligned} u_3 &= a\, e^{i(pt+f_3 z)} + A\, e^{i(pt-f_3 z)}, \\ u_2 &= B\, e^{i(pt+f_2 z)} + C\, e^{i(pt-f_2 z)}, \\ u_1 &= D\, e^{i(pt+f_1 z)} + E\, e^{i(pt-f_1 z)}, \end{aligned}\right\} \ldots\ldots\ldots\ldots(3)$$

where A, B, C, D, E are arbitrary constants determined by boundary conditions and f_1, f_2, f_3 have the meaning such that

$$f_1^2 = \frac{\rho_1 p^2}{\mu_1 + i\xi_1 p}, \quad f_2^2 = \frac{\rho_2 p^2}{\mu_2 + i\xi_2 p}, \quad f_3^2 = \frac{\rho_3 p^2}{\mu_3 + i\xi_3 p}, \quad \ldots(4)$$

in which $2\pi/p$ is the period of waves.

The boundary conditions at the plane, $z=0$, $z=H_1$, $z=H_1+H_2$ are as follows:

$z=0$;
$$\left(\mu_1 + \xi_1 \frac{\partial}{\partial t}\right) \frac{\partial u_1}{\partial z} = 0, \quad \ldots\ldots\ldots\ldots\ldots(5)$$

$z=H_1$;
$$u_1 = u_2, \quad \ldots\ldots\ldots\ldots\ldots\ldots\ldots(6)$$
$$\left(\mu_1 + \xi_1 \frac{\partial}{\partial t}\right) \frac{\partial u_1}{\partial z} = \left(\mu_2 + \xi_2 \frac{\partial}{\partial t}\right) \frac{\partial u_2}{\partial z}, \quad \ldots\ldots\ldots(7)$$

$z=H_1+H_2$;
$$u_2 = u_3, \quad \ldots\ldots\ldots\ldots\ldots\ldots\ldots(8)$$
$$\left(\mu_2 + \xi_2 \frac{\partial}{\partial t}\right) \frac{\partial u_2}{\partial z} = \left(\mu_3 + \xi_3 \frac{\partial}{\partial t}\right) \frac{\partial u_3}{\partial z}. \quad \ldots\ldots\ldots(9)$$

Introducing (3) in (5)–(9) by means of (4), we find finally

$$\frac{|u_{1_{z=0}}|}{2|u_0|} = \frac{2}{\sqrt{\Phi_1^2 + \Phi_2^2}}, \quad \ldots\ldots\ldots\ldots\ldots(10)$$

where

$$\left.\begin{matrix}\Phi_1\\ \Phi_2\end{matrix}\right\} = \{1+\alpha\cos(N_2-N_1)\}\left.\begin{matrix}\cos\\ \sin\end{matrix}\right\}(P_2+P_1)\left.\begin{matrix}\cosh\\ \sinh\end{matrix}\right\}(Q_2+Q_1)$$

$$\pm\}\alpha\sin(N_2-N_1)\left.\begin{matrix}\sin\\ \cos\end{matrix}\right\}(P_2+P_1)\left.\begin{matrix}\sinh\\ \cosh\end{matrix}\right\}(Q_2+Q_1)$$

$$+\{\beta\cos(N_3-N_1)+\gamma\cos(N_3-N_2)\}\left.\begin{matrix}\cos\\ \sin\end{matrix}\right\}(P_2+P_1)\left.\begin{matrix}\sinh\\ \cosh\end{matrix}\right\}(Q_2+Q_1)$$

$$\pm\{\beta\sin(N_3-N_1)+\gamma\sin(N_3-N_2)\}\left.\begin{matrix}\sin\\ \cos\end{matrix}\right\}(P_2+P_1)\left.\begin{matrix}\cosh\\ \sinh\end{matrix}\right\}(Q_2+Q_1)$$

$$+\{1-\alpha\cos(N_2-N_1)\}\left.\begin{matrix}\cos\\ \sin\end{matrix}\right\}(P_2-P_1)\left.\begin{matrix}\cosh\\ \sinh\end{matrix}\right\}(Q_2-Q_1)$$

$$\mp\alpha\sin(N_2-N_1)\left.\begin{matrix}\sin\\ \cos\end{matrix}\right\}(P_2-P_1)\left.\begin{matrix}\sinh\\ \cosh\end{matrix}\right\}(Q_2-Q_1)$$

$$-\{\beta\cos(N_3-N_1)-\gamma\cos(N_3-N_2)\}\left.\begin{matrix}\cos\\ \sin\end{matrix}\right\}(P_2-P_1)\left.\begin{matrix}\sinh\\ \cosh\end{matrix}\right\}(Q_2-Q_1)$$

$$\mp\}\{\beta\sin(N_3-N_1)-\gamma\sin(N_3-N_2)\}\left.\begin{matrix}\sin\\ \cos\end{matrix}\right\}(P_2-P_1)\left.\begin{matrix}\sinh\\ \cosh\end{matrix}\right\}(Q_2-Q_1), \quad (11)$$

$$\left.\begin{aligned}&\alpha=\frac{\rho_1v_1M_1}{\rho_2v_2M_2}, \quad \beta=\frac{\rho_1v_1M_1}{\rho_3v_3M_3}, \quad \gamma=\frac{\rho_2v_2M_2}{\rho_3v_3M_3},\\ &M_n=\left\{1+\left(\frac{\xi_np}{\mu_n}\right)^2\right\}^{1/4}, \quad N_n=\frac{1}{2}\tan^{-1}\frac{\xi_np}{\mu_n}, \quad [n=1,2,3]\\ &P_n=\frac{pH_n}{v_n}\cdot\frac{\cos N_n}{M_n}, \quad Q_n=\frac{pH_n}{v_n}\cdot\frac{\sin N_n}{M_n}. \quad [n=1,2]\end{aligned}\right\}\ldots\ldots(12)$$

The numerical calculations are now being worked out.

In the case of dilatational waves, it is necessary to replace μ by $\lambda+2\mu$ and ξ by $\eta+2\xi$.

3. In this chapter, we will examine the special case of the previous chapter in which $H_1=0$, that is, $P_1=Q_1=0$, in (10)–(12). It means the case of a stratified visco-elastic layer. Then from (10)–(12) we find

$$\frac{|u_{z=0}|}{2|u_0|}=\frac{1}{\sqrt{\Phi_1'^2+\Phi_2'^2}}, \quad \ldots\ldots\ldots\ldots\ldots\ldots(10')$$

$$\left.\begin{aligned}\Phi_1'&=\cos P_2\cosh Q_2+\gamma\{\cos(N_3-N_2)\cos P_2\sinh Q_2\\ &\qquad+\sin(N_3-N_2)\sin P_2\cosh Q_2\},\\ \Phi_2'&=\sin P_2\sinh Q_2+\gamma\{\cos(N_3-N_2)\sin P_2\cosh Q_2\\ &\qquad-\sin(N_3-N_2)\cos P_2\sinh Q_2\},\end{aligned}\right\}\ldots\ldots(11')$$

$$\left.\begin{aligned} \gamma &= \frac{\rho_2 v_2 M_2}{\rho_3 v_3 M_3}, \quad N_n = \frac{1}{2}\tan^{-1}\frac{\xi_n p}{\mu_n} \quad [n=2,\ 3], \\ P_2 &= \frac{pH_2}{v_2}\frac{\cos N_2}{M_2}, \quad Q_2 = \frac{pH_2}{v_2}\frac{\sin N_2}{M_2}. \end{aligned}\right\} \quad \cdots\cdots\cdots(12')$$

If $\xi_3 \to 0$, that is to say, $N_3 \to 0$ in equation (11′), these are coincident with the result obtained previously. The form of equation (11′) is somewhat simplified for carrying out numerical calculations easily compared with the previous one[2].

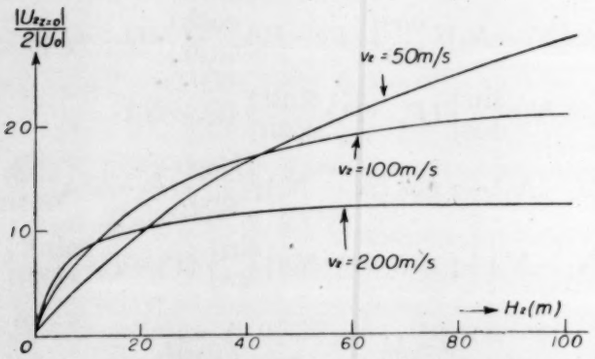

Fig. 2. The case of $\xi_2=10^6$ C.G.S., $\rho_2=1.5$, $\rho_3=2.25$, $v_3=1.7$ km/sec, $p=2\pi/T=2\pi/(4H_2/v_2)$.

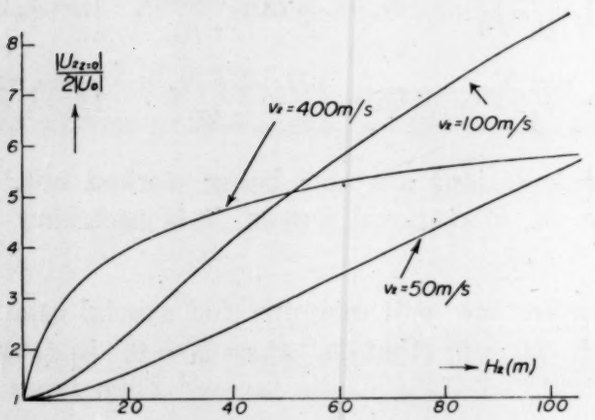

Fig. 3. The case of $\xi_2=10^7$ C.G.S., $\rho_2=1.5$, $\rho_3=2.25$, $v_3=1.7$ km/sec, $p=2\pi/T=2\pi/(4H_2/v_2)$.

Using (10′)-(12′), we calculated the ratio of the displacements at the free surface of a layer to twice the displacements of incident waves for six cases, namely $v_2=50$ m/sec, 100 m/sec, 200 m/sec when $\xi_2=10^6$

2) *loc. cit.*, 1), equation (14).

C.G.S. and $v_2=50$ m/sec, 100 m/sec, 400 m/sec when $\xi_2=10^7$ C.G.S., besides under the conditions of $\xi_3 \to 0$, $\rho_2=1.5$, $\rho_3=2.25$, $v_3=1.7$ km/sec and $p=2\pi/T_0=2\pi/(4H_2/v_2)$ for different values of the thickness of layer. Here, twice the displacements of incident waves means the displacements at the free surface when bed rocks are disclosed, and $T_0(=4H_2/v_2)$ is the period of synchronous vibration of a layer. The results are shown in Figs. 2 and 3.

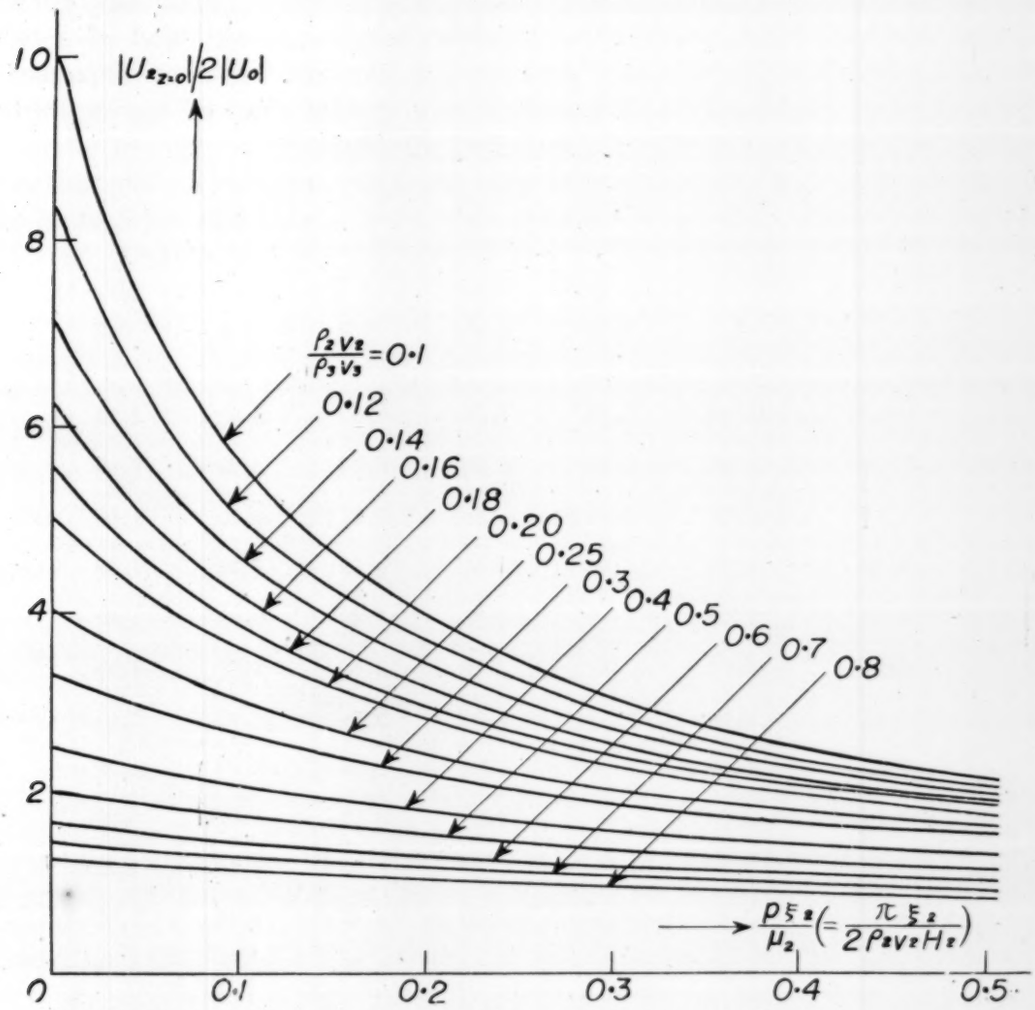

Fig. 4. Relation among the amplitude at the surface, impedance ratio of two medium, coefficient of viscosity and thickness of surface layer.

From these figures, it will be seen that, when the thickness of weak layer is fairly large, as the velocity of weak layer decreases, the amplitudes of the earthquake motions at free surface increases. While,

when the thickness of weak layer is small, this relation is not so simple. In all cases, as the thickness of weak layer increases, the amplitudes mentioned above increases.

The diagrammatical feature of the case of small velocity of layer and large solid viscosity as when $\xi_2=10^7$ and $v_2=50$ m/s, 100 m/s resemble the relation[3] between the damage ratio of Japanese-style wooden buildings in the former Tokyo city at the time of the Kwanto earthquake of 1923 and the thickness of alluvium. On the other hand, the curve of the case of large velocity of layer at large viscosity and of small viscosity resemble the relation between the damage ratio of Japanese-style wooden buildings in Yokohama city at the time of the Kwanto earthquake of 1923 and the thickness of alluvium[4].

Table I.

$\frac{\rho_2 v_2}{\rho_3 v_3}$ \ $\frac{\pi\xi_2}{2\rho_2 v_2 H_2}$	0	0.01	0.05	0.1	0.3	0.5
0.1	10.00	9.27	7.18	5.60	3.03	2.14
0.12	8.34	7.82	6.28	5.04	2.85	2.05
0.14	7.15	6.76	5.58	4.57	2.70	1.96
0.16	6.25	5.96	5.01	4.19	2.56	1.89
0.18	5.55	—	4.55	3.86	2.43	1.82
0.20	5.00	—	4.18	3.58	2.31	1.75
0.25	4.00	—	3.46	3.04	2.07	1.61
0.30	3.33	—	2.95	2.64	1.87	1.48
0.40	2.50	—	2.28	2.09	1.57	1.28
0.50	2.00	—	1.85	1.72	1.35	1.12
0.60	1.67	—	1.56	1.47	1.18	1.00
0.70	1.43	—	1.35	1.28	1.05	0.89
0.80	1.25	—	1.19	1.14	0.95	0.82

3) H. KAWASUMI, *Journal Architect. Inst. Japan*, Vol. **66**, No. 773 (1951), 12, (in Japanese).

4) S. OMOTE, "Earthquake Damage in Yokohama City Due to the Great Kwanto Earthquake of September 1, 1923", *Bull Earthq. Res. Inst.*, **27** (1949), 57.

Since it seems that very few observations have been made in regard to the velocity of transmission of distortional waves through the ground and the coefficient of solid viscosity, I do not doubt that this result will be confirmed more closely as soon as such observations are made.

Finally, systematical relations among the ratio of the amplitudes of earthquake motion at the free surface of a weak layer and those of bed rocks disclosed, coefficient of solid viscosity, velocities and densities of weak layer and bed rocks, and the thickness of weak layer, were obtained. The results are shown in Fig. 4 and Table I. This chart will be of use in estimating the practical degree of ground against earthquake, when the requisite constants are examined by such means as seismic prospecting.

In conclusion, the author wishes to express his thanks to Miss S. Yoshizawa for her help in preparing this paper.

---

4. 地表層の性質と地震動振幅との關係

地震研究所　金　井　　清

舊式日本家屋の震害と冲積層の厚さとの間に密接な關係があることは，數多くの地震について指摘されて來たところであるが，近年になつて，どく地表近くの軟弱層の厚さとか，その中での地震波の速度，減衰係數などが大分問題にされ出して來た．

本論文の初めの部分では，これらの問題を究明する意味で，地表近くに 2 つの層があり，各層ともに粘性の影響を入れた場合についての彈性波の問題の解式を導いた．

今回は，その特別な場合の地表層が 1 つある場合についてのみ數値計算を行つた．

數値計算例を見ると，關東地震の際の舊東京市における木造家屋の被害と冲積層の厚さとの關係，即ち，冲積層の厚さが 30 m 以上になると被害が急激に增す傾向に似た曲線がある．又，同じ地震の横濱市の被害のように冲積層の厚さが 40 m 位を越すと餘り被害が增さない傾向に似た曲線も見られる．

冲積層及び基盤の常數のはつきりわかつたものが少いので，これらの關係について，これ以上の吟味をすることは現在のところできない．

最後に，地盤に耐震上の良否の階級をつける 1 つの指數とする意味で，地震地下探査法などで得られる地盤の諸常數を使つて，軟弱層の表面での振幅と基盤が露出したところでの振幅との比を見出す圖表を作つておいた．

5. *Examinations of the Assumption concerning Mechanism of Earthquake Origin through Seismograms.*

By Kiyoshi KANAI,

Earthquake Research Institute.

(Read Sep. 18, 1951.—Received Dec. 20, 1951.)

1. Introduction.

We have performed the earthquake observation at four points of different depth in Hitachi Mine (Ibaraki prefecture) these three years. The seismograms obtained here, even when they are of ground surface, are far simpler than those obtained in other places. The reason for this may be that as Hitachi Mine, belonging to the paleozoic system, has no remarkable discontinuity surfaces concerning the property of ground and has little begolith near its surface, there are few chances to cause such phenomena as reflection and refraction of seismic waves resulting in complex wave form.

This fact gives many advantages to the study in the mechanism of earthquake origin through seismograms.

We will begin this paper with the calculation of the pendulum motion generated by the seismic waves according to the mechanism of earthquake origin assumed in the previous paper[1], that is the pendulum motion caused by P- and S-waves in time of the sudden and rectangular pressure-change in earthquake origin. Then, taking one of the earthquakes observed in Hitachi Mine as an example and comparing the seismograms of P- and S-waves in both horizontal and vertical directions with the pendulum motion calculated here, we will examine the mechanism of earthquake origin assumed in the previous paper.

2. The initial movement of a seismograph subjected to an arbitrary earthquake motion, is solved by operational calculus.

The expressions for ground movements[2] generated by rectangular

1) K. KANAI, "Possibility of the Period of P-waves becoming smaller than those of S-waves", *Bull. Earthq. Res. Inst.*, **29** (1951), 529.

2) *loc. cit.*, 1), 531.

type of pressure change beginning with a quiescent state of spherical source, are reduced to the following form:

u_{f1} (Radial component of P-waves)

$$\begin{aligned}&=-0.05684\sin(1.0406\,t_1)\,e^{-0.8033\,t_1}-0.03124\cos(1.0406\,t_1)\,e^{-0.8033\,t_1}\\&\quad-0.00576\sin(4.1852\,t_1)\,e^{-1.8015\,t_1}-0.06905\cos(4.1852\,t_1)\,e^{-1.8015\,t_1}\\&\quad-0.1924\sin(1.4410\,t_1)\,e^{-3.648\,t_1}+0.1003\cos(1.4410\,t_1)\,e^{-3.648\,t_1},\end{aligned}$$

$$\left[\,t_1=\frac{t-c_1(r-a)}{a\,c_2}\,\right]$$

v_{f2} (Transversal component of S-waves)

$$\begin{aligned}&=-0.2312\sin(1.0406\,t_2)\,e^{-0.8033\,t_2}+0.01180\cos(1.0406\,t_2)\,e^{-0.8033\,t_2}\\&\quad+0.02339\sin(4.1852\,t_2)\,e^{-1.8015\,t_2}+0.02119\cos(4.1852\,t_2)\,e^{-1.8015\,t_2}\\&\quad+0.04844\sin(1.4410\,t_2)\,e^{-3.648\,t_2}-0.03310\cos(1.4410\,t_2)\,e^{-3.648\,t_2}.\end{aligned}$$

$$\left[\,t_2=\frac{t-c_2(r-a)}{a\,c_2}\,\right] \quad ..(1)$$

Let ξ be the ground movement and x the displacement of the pendulum relative to the moving ground, then, the equation of motion of the pendulum will be expressed as

$$\ddot{x}+2k\dot{x}+n^2x=-\ddot{\xi}. \quad \text{.....(2)}$$

The operational form of x becomes

$$x>p\int_0^\infty e^{-pt}x\,dt=\frac{-p^3\int_0^\infty e^{-pt}\xi\,dt}{p^2+2kp+n^2}\,, \quad \text{.....(3)}$$

from which the interpretation of (3) becomes

$$x=\frac{1}{2\pi i}\int_{c-i\infty}^{c+i\infty}\frac{-z\phi(z)e^{zt}dz}{z^2+2kz+n^2}\,. \quad \text{.....(4)}$$

In the present case, the type of earth movements takes $\xi=e^{-at}\sin bt$ and $\xi=e^{-at}\cos bt$.

Then

$$\left.\begin{aligned}x&=\frac{-b}{2\pi i}\int_{c-i\infty}^{c+i\infty}\frac{z^2e^{zt}dz}{\{(z+a)^2+b\}(z^2+2kz+n^2)}\,, && t>0\\&=0\,, && t<0\end{aligned}\right\} \quad \text{.....(5)}$$

for $\xi=e^{-at}\sin bt$ and

$$\left.\begin{aligned} x&=\frac{-1}{2\pi i}\int_{c-i\infty}^{c+i\infty}\frac{z^2(z+a)e^{zt}dz}{\{(z+a)^2+b^2\}(z^2+2kz+n^2)}, && t>0\\ &=0, && t<0\end{aligned}\right\} \quad \cdots\cdots(6)$$

for $\xi=e^{-at}\cos bt$.

The integration of (5) has been solved by the same method as in the previous paper[3]. Rewriting the expression to simplify numerical calculations, we get

$$\left.\begin{aligned} x=\frac{-1}{\sqrt{\Phi}}\Bigg[&\{(a/n)^2+(b/n)^2\}e^{-at}\sin\left\{bt-\tan^{-1}\left(\frac{2(b/a)}{1-(b/a)^2}\right)-\eta-\zeta\right\}\\ &+\frac{(b/n)e^{-kt}}{\sqrt{1-(k/n)^2}}\sin\left\{nt\sqrt{1-(k/n)^2}\right.\\ &\left.-\tan^{-1}\left(\frac{2(k/n)\sqrt{1-(k/n)^2}}{2(k/n)^2-1}\right)-\eta+\zeta\right\}\Bigg], && t>0\\ =0, && t<0\end{aligned}\right\} \quad \cdots(7)$$

where

$$\left.\begin{aligned} \Phi=&\{(k/n-a/n)^2+(b/n-\sqrt{1-(k/n)^2})^2\}\{(k/n-a/n)^2\\ &+(b/n+\sqrt{1-(k/n)^2})^2\},\\ \eta=\tan^{-1}&\left(\frac{b/n-\sqrt{1-(k/n)^2}}{k/n-a/n}\right),\quad \zeta=\tan^{-1}\left(\frac{b/n+\sqrt{1-(k/n)^2}}{k/n-a/n}\right).\end{aligned}\right\} \quad \cdots(8)$$

Evaluating the integral of equation (6), we get

$$\left.\begin{aligned} x=\frac{-1}{\sqrt{\Phi}}\Bigg[&\{(a/n)^2+(b/n)^2\}e^{-at}\cos\left\{bt-\tan^{-1}\left(\frac{2(b/a)}{1-(b/a)^2}\right)-\eta-\zeta\right\}\\ &+e^{-kt}\sqrt{\frac{(a/n-b/n)^2}{1-(k/n)^2}+1}\sin\left\{nt\sqrt{1-(k/n)^2}+\tan^{-1}\left(\frac{\sqrt{1-(k/n)^2}}{a/n-k/n}\right)\right.\\ &\left.-\tan^{-1}\left(\frac{2(k/n)\sqrt{1-(k/n)^2}}{2(k/n)^2-1}\right)-\eta+\zeta\right\}\Bigg], && t>0\\ =0, && t<0\end{aligned}\right\} \quad (9)$$

where Φ, η and ζ are the same as in (8).

Using (7)–(9), the initial movement of a seismograph subjected to the earthquake motion expressed by (1) may be calculated.

The results of numerical calculation for the three cases of seismo-

3) K. SEZAWA and K. KANAI, "On the Initial Movement of a Seismograph subjected to an Arbitrary Earthquake Motion, Solved with Operational Calculus. I", *Bull. Earthq. Res. Inst.*, **19** (1941), 170.

graphical constants (i) $T_0=2\pi/n=0.25$ $k^2/n^2=0.4$, (ii) $T_0=2\pi/n=1$ sec, $k^2/n^2=0.4$, (iii) $T_0=10$ sec, $k^2/n^2=0.4$ shown in Figs. 1~12. In these cases, the period of S-waves is assumed to be about 1.5 sec, that is to say, $1.0406(t/ac_2)=(2\pi/1.5)t$ or $ac_2=(1.0406\times1.5)/2\pi$ was assumed in

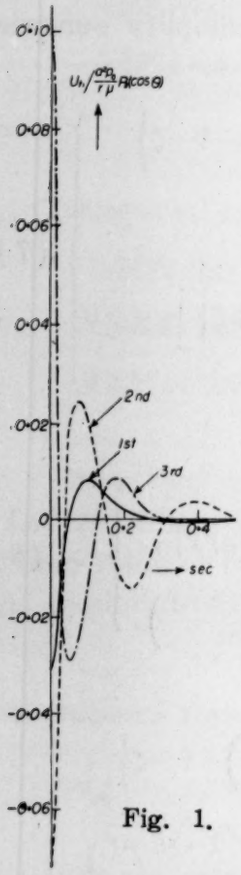

Fig. 1.

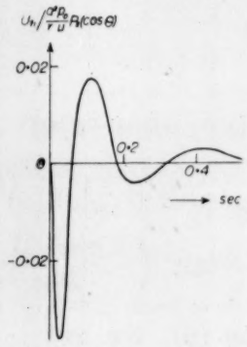

Fig. 2.

Fig. 1. The case of P-waves. Constants of seismograph are 0.25 sec in period, 13 : 1 in damping ratio.

Fig. 2. Resultant of the three curves of Fig. 1.

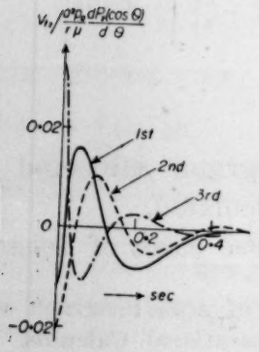

Fig. 3.

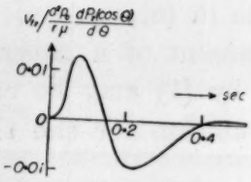

Fig. 4.

Fig. 3. The case of S-waves. Constants of seismograph are 0.25 sec in period, 13 : 1 in damping ratio.

Fig. 4. Resultant of the three curves of Fig. 3.

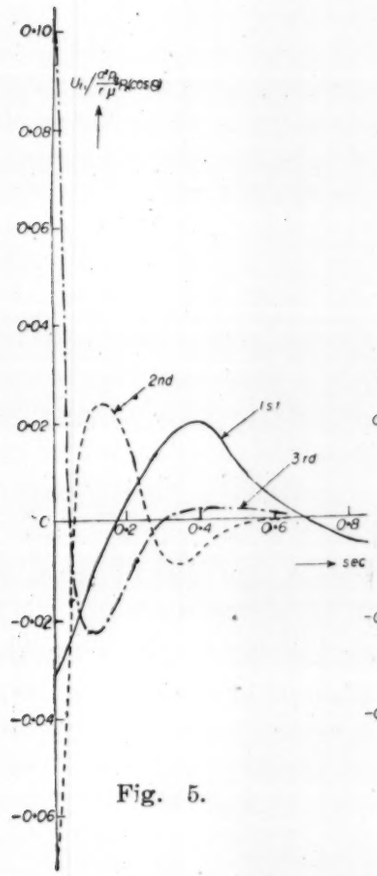

Fig. 5.

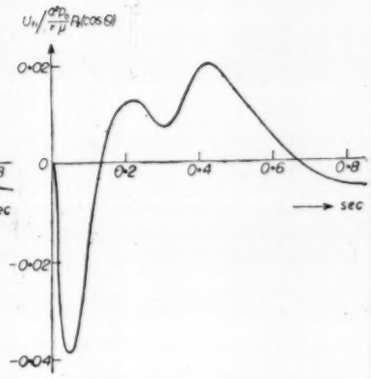

Fig. 6.

Fig. 5. The case of P-waves. Constants of seismograph are 1 sec in period, 13 : 1 in damping ratio.
Fig. 6. Resultant of the three curves of Fig. 5.

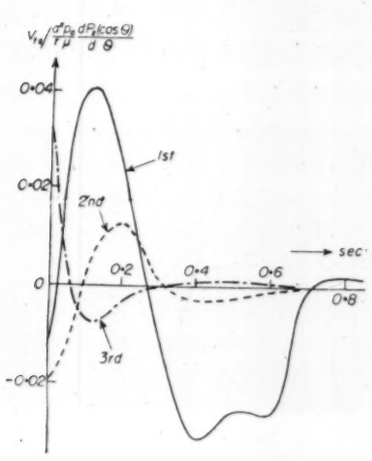

Fig. 7.

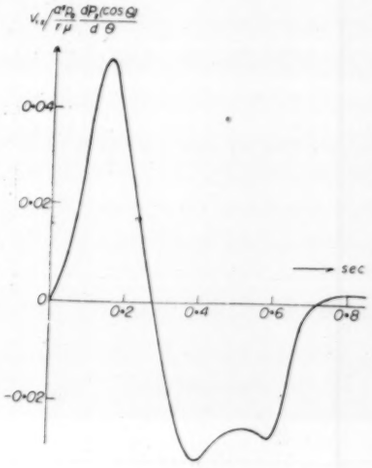

Fig. 8.

Fig. 7. The case of S-waves. Constants of seismograph are 1 sec in period, 13 : 1 in damping ratio.
Fig. 8. Resultant of the three curves of Fig. 7.

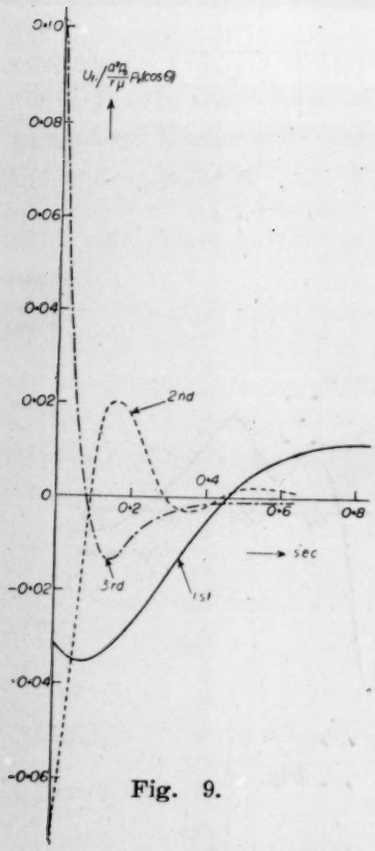

Fig. 9.

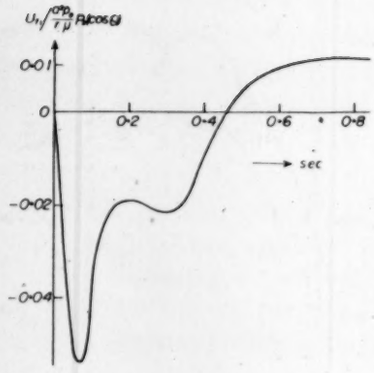

Fig. 10.

Fig. 9. The case of P-waves. Constants of seismograph are 10 sec in period, 13 : 1 in damping ratio.
Fig. 10. Resultant of the three curves of Fig. 9.

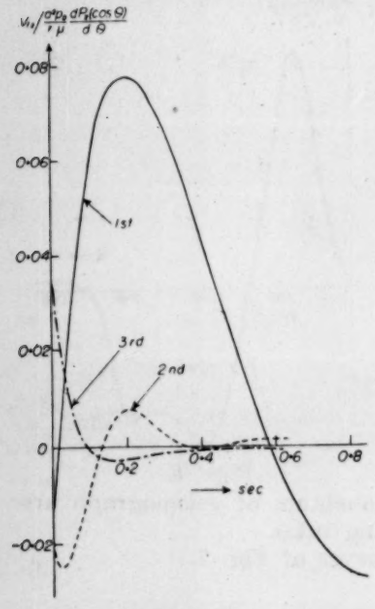

Fig. 11.

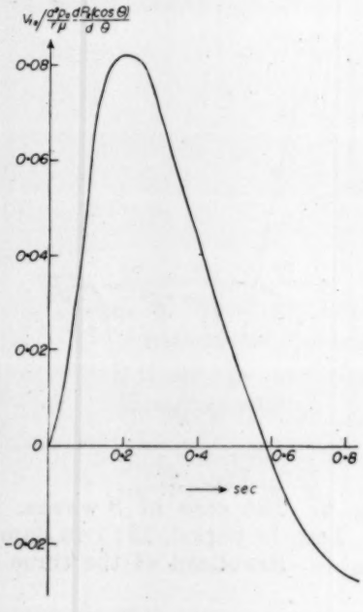

Fig. 12.

Fig. 11. The case of S-waves. Constants of seismograph are 10 sec in period, 13 : 1 in damping ratio.
Fig. 12. Resultant of the three curves of Fig. 11.

equation (1). The case (i) and (ii) correspond to the vertical seismograph and horizontal one installed at Hitachi Mine respectively.

3. Examination of the assumption concerning the mechanism of earthquake origin.

(i) Observation value.

Let us examine the mechanism of earthquake origin assumed in the previous paper, using the seismograms of Kashi (Fukushima prefecture) earthquake of Jan. 26, 1951.

The horizontal and vertical seismograms used here in this discussion are shown in Fig. 13 and 14 respectively. After studying these seismograms in comparison with the results obtained in the previous chapter, we find that Figs. 2, 4, 6, 8 resemble considerably the first impulsion of P- and S-waves in Figs. 13 and 14.

Then we examine precisely the initial movements of P-and S-waves by comparing them with the calculated results. Table I shows the constants of seismographs used in this case.

Table I. Constants of seismographs.

Seismograph	Period (sec)	Damp. ratio	Magnif.
Vertical	0.25	13 : 1	150
Horiz. (EW)	1.0	13 : 1	150

Considering the actual amplitude of the pendulum (recorded amplitude/magnification) and the fact that the earthquake origin is approximately to the NW-direction from the observation point, we infer the amplitude of pendulum motion caused by horizontal motion of earthquake, and they are given in Table II.

Table II. Actual amplitudes of pendulum (μ).

Wave	Vertical	Horizontal	
		EW	Result
P	2.0	1.0	1.5
S	0.9?	10.6	15.0

(ii) Incident angle.

The actual amplitude of the ground surface is composed of the amplitude of incident wave and those of the reflected P- and S-waves, and the ratio of the horizontal amplitude of ground surface to the vertical one depends on the incident angle. Fig. 15 indicates these relations.

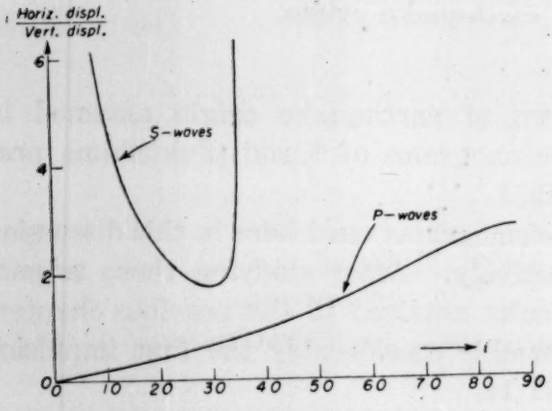

Fig. 15. Relation between the ratio of horizontal amplitude of ground surface to the vertical one and the incident angle.

From Table II, we obtain R_1, the ratio of the amplitude of horizontal seismograph pendulum to that of vertical one, and from Figs. 2, 4, 6 and 8, we obtain R_2, the ratio of horizontal amplitude to vertical one which derives from the characteristics of seismograph, in other words, the ratio of the amplitude of the pendulum of 1 sec period (horizontal seismograph) under the influence of the seismic waves generated at the assumed origin to the amplitude of the pendulum of 0.25 sec period (vertical seismograph) under the same condition. R_1/R_2 is to represent the ratio of horizontal displacement to vertical one of the actual ground movement at the surface. These values are shown in Table III.

Table III. Ratio of horizontal displacement to vertical one.

Wave	Pendulum		Actual ground
	Observed $[R_1]$	Calculated $[R_2]$	$[R_1/R_2]$
P	$\frac{1.5}{2.0}=0.75$	$\frac{0.038}{0.036}=1.1$	0.7
S	$\frac{15.0}{0.9}=17$	$\frac{0.048}{0.013}=3.7$	4.6

Therefore, if R_1/R_2 is found, the incident angle will be determined by referring to Fig. 15. In this case it becomes about 34° (exactly speaking, the incident angle of P-waves is different from that of S-waves, but the present observation cannot be expected to be so accurate).

Assuming the structure of earth crust as shown in Fig. 16[4], and considering the incident angle to be 34° and the duration of preliminary tremour to be 12 sec, we get the hypocenter at the epicentral distance of 80 km and the depth of 80 km. This position coincides approximately with the result observed by the Central Meteorological Observatory, Japan, which is epicenter: 37.2° N, 140.1° E, depth; shallow.

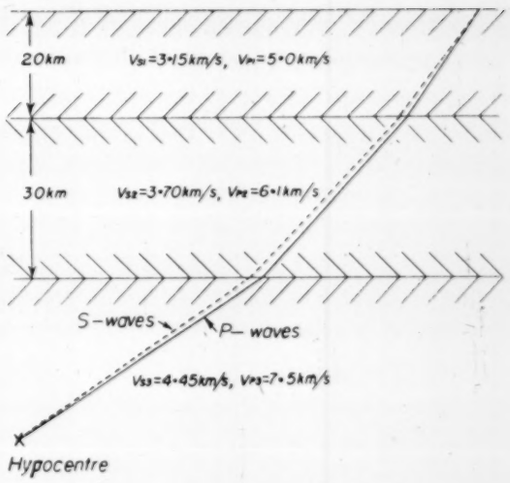

Fig. 16. Assumed structure of earth crust and the paths of P- and S-waves of this earthquake.

(iii) Relation between the amplitudes of P-waves and S-waves.

Since the incident angle was known to be 34° in the previous chapter, the ratio of the amplitude of ground surface to that of incident wave concerning each of the vertical and horizontal components of both P- and S-waves can be calculated[5]. Using these values and those of Table II, the amplitude of seismograph pendulum considering only the incident wave is estimated. This relation is shown in Table IV.

Table IV.

Wave	Component	Amplitude	
		Ground motion / Incident Wave (Calculated)	Incident wave (μ) (Seismograph)
P	Vertical	1.60	$\frac{2.0}{1.60}=1.25$
	Horizontal	1.25	$\frac{1.5}{1.25}=1.20$
S	Vertical	0.8	$\frac{0.9}{0.8}=1.1$
	Horizontal	3.7	$\frac{15.0}{3.7}=4.1$

4) T. MATUZAWA, K. YAMADA and T. SUZUKI, "On the Forerunners of Earthquake-motions (The Second Paper)", *Bull. Earthq. Res. Inst.*, **7** (1929), 241.

5) T. MATUZAWA, *Zishin (Earthquake)*, **4** (1932), 125 (in Japanese).

Table V shows the ratio of the amplitude of S-waves to that of P-waves concerning each of the horizontal and vertical components.

Table V. Ratio of the amplitude of S-waves to that of P-waves.

Component	Actual $[R_3]$	Calculated $[R_4]$	$\frac{dP_2(\cos\theta)}{d\theta} / P_2(\cos\theta)$ $[R_3/R_4]$
Vertical	0.88	$\frac{0.013}{0.036}=0.36$	2.5
Horizontal	3.7	$\frac{0.048}{0.038}=1.26$	2.9

We have (R_3), the second column of Table V by using the fourth column of Table IV, which is the presumed value of the case where the actual incident wave is recorded by our seismograph. The values in the third column, (R_4), represent the ratio among ordinates of the first impulsion shown Figs. 2, 4, 6 and 8. Accordingly the ratio of (R_3) to (R_4) corresponds to the ratio of $dP_2(\cos\theta)/d\theta$ to $P_2(\cos\theta)$. (In this path the refraction coefficient in two discontinuities is almost equal to 1.[6] Namely it may be considered that there is no difference between the displacement of the wave generated at the earthquake origin and that of incident wave).

Assuming the mechanism to be such, the distributions of the amplitudes of P- and S-waves against the deviation from the axis line coincide respectively to the distributions of $P_2(\cos\theta)$ and $dP_2(\cos\theta)/d\theta$ against θ, and the relation above is shown in Fig. 17. From Fig. 17 and the values in the fourth column of Table V, it is known that the waves which reached the observation point came from the direction which deviates by 35° or 75° from the axis line of spherical origin. Then as the

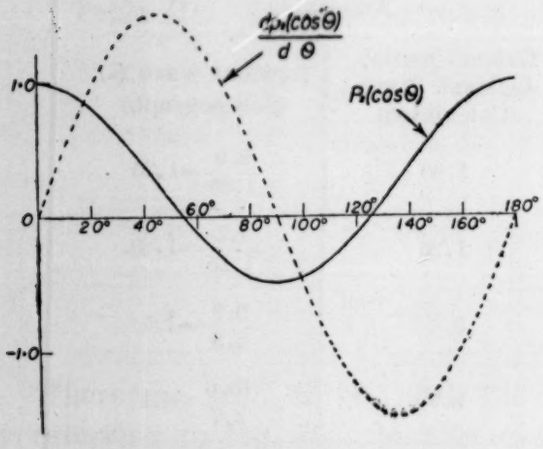

Fig. 17. Distribution of $P_2(\cos\theta)$ and $dP_2(\cos\theta)/d\theta$ against θ.

6) H. KAWASUMI, T. SUZUKI, *Zishin (Earthquake)*, **4** (1932), 277 (in Japanese).

preliminary movement of P-wave was of the push-type, we may be sure that the waves which reached the observation point came from the direction of 35° to the axis line. Consequently it is found that the observation point is very near to the nodal line in the distributions of the pull-type and the push-type concerning the initial movement of P-waves. Fig. 18 shows the distributions of the up- and the down-type concerning the initial movement of this earthquake. This coincides fairly well with the analyzed results.

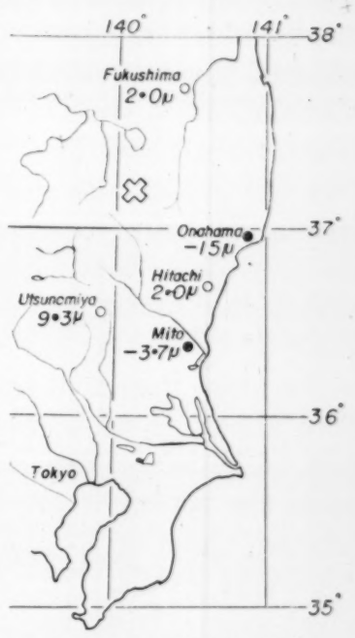

Fig. 18. Distribution of the up- and the down-type concerning the initial movement of this earthquake. Marks ○ and ● indicate the up- and the down-type respectively.

(iv) The period of earthquake and dimensions of earthquake origin.

The ratio between the period of initial movement of S-waves and that of P-waves becomes 2 from the seismograms as well as from the calculated results.

The examinations mentioned above give no contradiction even if we conclude that the earthquake is caused according to the mechanism of earthquake origin assumed here. Then we obtain the dimensions of earthquake origin using the constants which were used in the calculations, and we have

$$a=\frac{T_0}{2\pi c_2}=\frac{T_0 v_2}{2\pi}=\frac{1.5\times 4.45}{2\pi}\fallingdotseq 1\,\mathrm{km}$$

which seems to be quite acceptable.

4. Conclusion.

In this paper, we first solved the problem of seismograph pendulum stimulated by earthquake waves in the case when the rectangular type of pressure-change occurred suddenly in the spherical source. Then taking the constants of the seismograph used in the observation of earthquake in Hitachi Mine, we performed numerical calculation.

Next, from the actual seismogram and the pendulum motion obtained from numerical calculations, it was proved that there are cases

where the assumed mechanism of earthquake origin can be applied to an actual earthquake. To explain more concretely, in the first place, taking the effect of surface reflection and the characteristics of seismographs into consideration, the incident angle was determined from the ratios of the horizontal seismograms of P- and S-waves to the vertical seismograms of them. When the earthquake origin was given by this incident angle and the duration of preliminary tremour, it coincided with the observation made by the Central Meteorological Observatory, Japan. Secondly, considering the facts mentioned above, we required the amplitude ratios between P- and S-waves of incident waves concerning horizontal and vertical components, and both of them became about 3. Moreover the observation point was found to be very near to the nodal line of P-waves of the push- and pull-type. These results were almost equal to the distribution diagrams of the push- and pull-type of initial motions of this earthquake. In the third place, as regards the period of the initial movement of this earthquake, the ratio between those of P- and S-waves became 2, which was equal to the calculated result. For the radius of spherical origin, we had 1.0 km which was a fairly acceptable value.

Thus it was proved to be possible that such phenomenon as the period of P-waves which is shorter than that of S-waves as seen in the seismogram was due to the difference of combinations among the free oscillations of different modes generated at the spherical origin which was discussed in the previous paper[7].

In conclusion, the author wishes to express his thanks to Motoyama Office, Hitachi Mine for the kind assistance offered and to Messrs. T. Tanaka, T. Suzuki and K. Osada who took part in the observation, as well as to Miss S. Yoshizawa for her help in preparing this paper.

---

7) *loc. cit.*, 1).

Fig. 13. Horizontal seismogram of Kashi earthquake

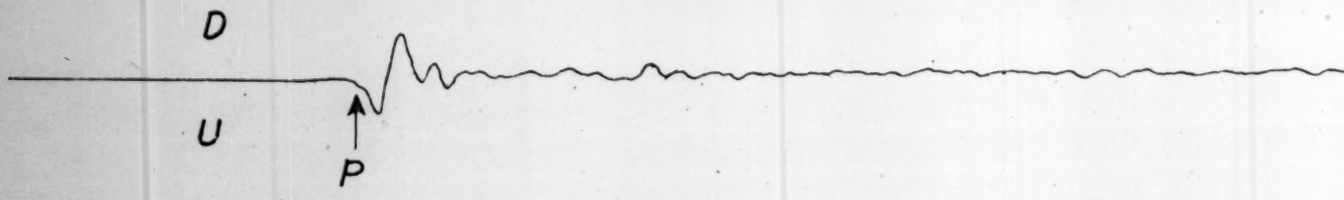

Fig. 14. Vertical seismogram of Kashi earthquake of

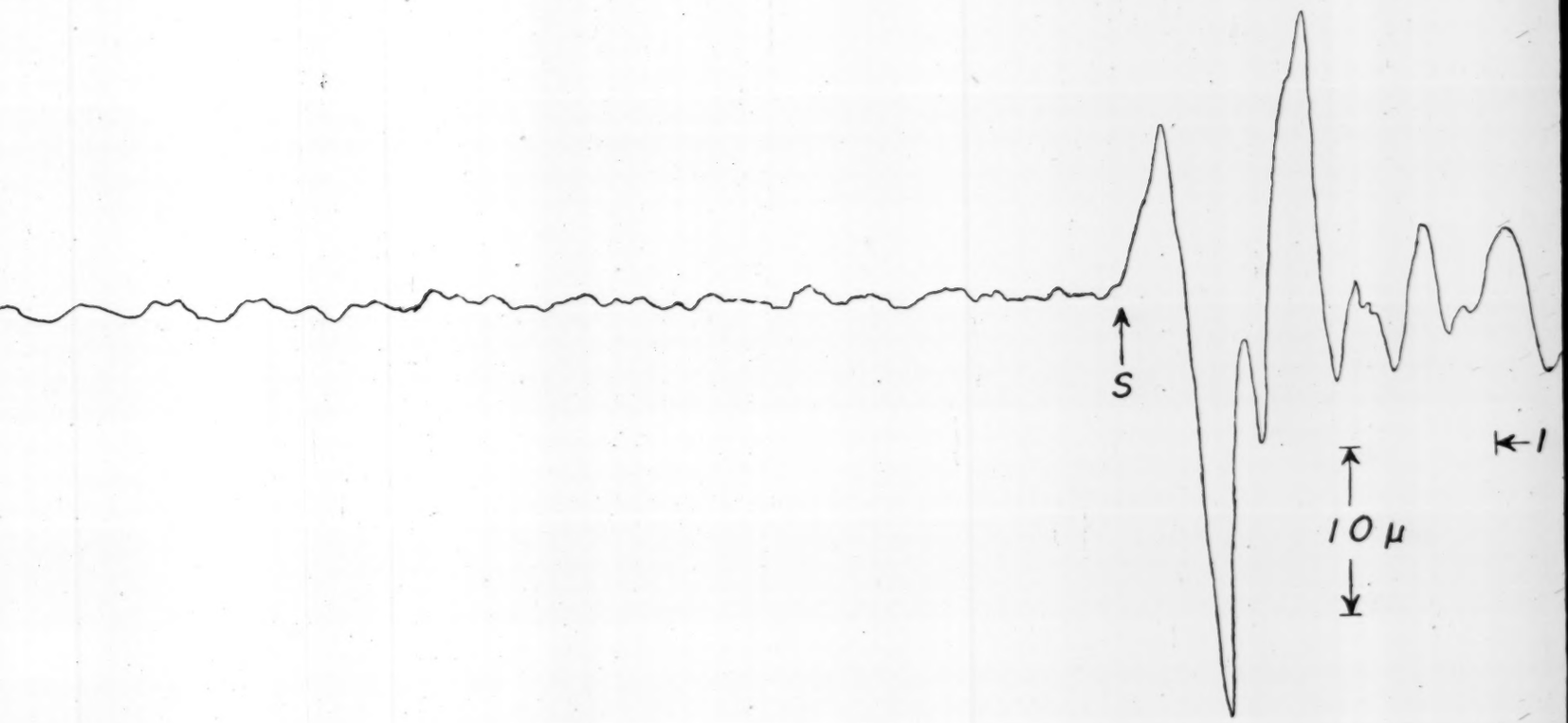

uake of Jan. 26, 1951 observed at Hitachi Mine. Constants of seismograph are 1 sec in period, 13 : 1 in damping ratio, 150 in magnification. Origin

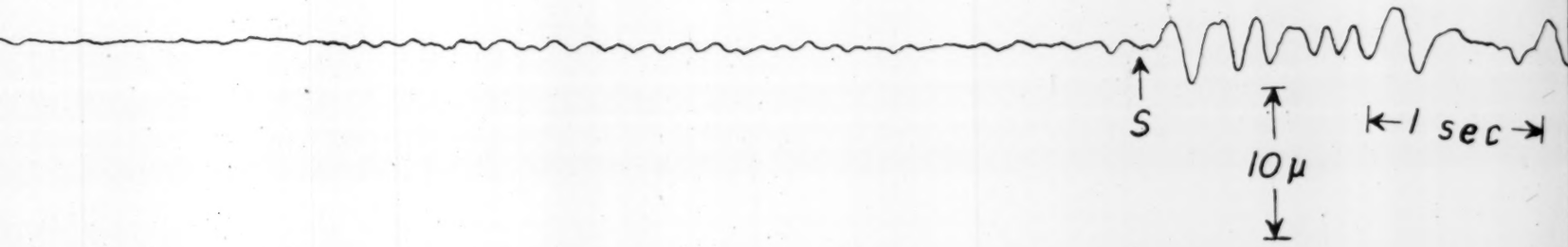

of Jan. 26, 1951 observed at Hitachi Mine. Constants of seismograph are 0.25 sec in period, 13 : 1 in damping ratio, 150 in magnification. Origina

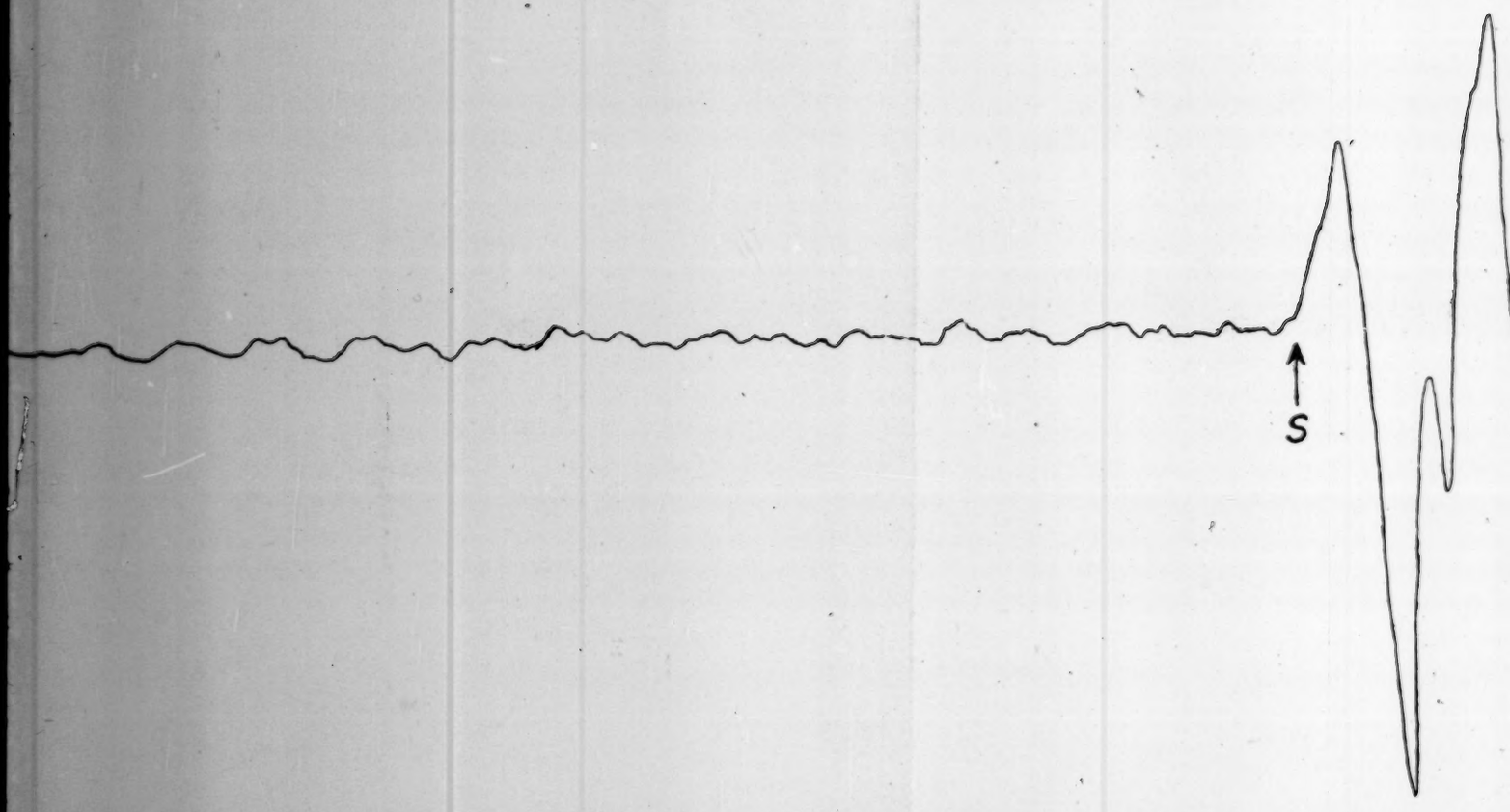

earthquake of Jan. 26, 1951 observed at Hitachi Mine. Constants of seismograph are 1 sec in period, 13 : 1 in damping ratio, 150 i

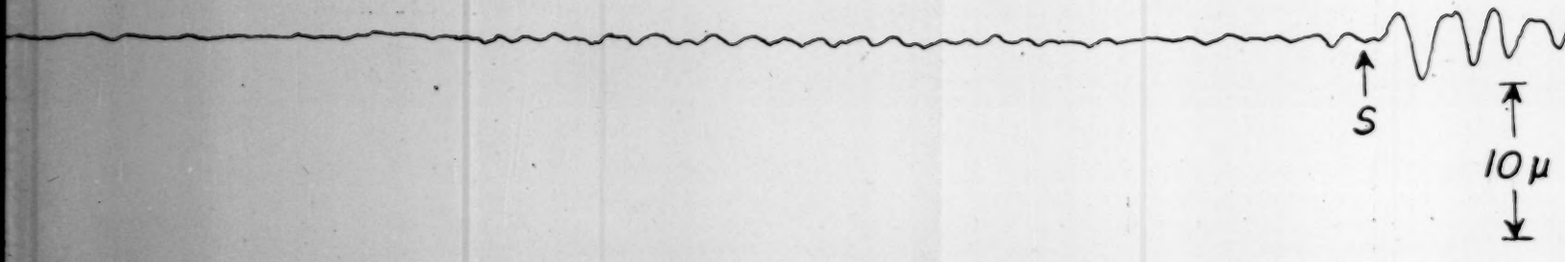

thquake of Jan. 26, 1951 observed at Hitachi Mine. Constants of seismograph are 0.25 sec in period, 13 : 1 in damping ratio, 150 i

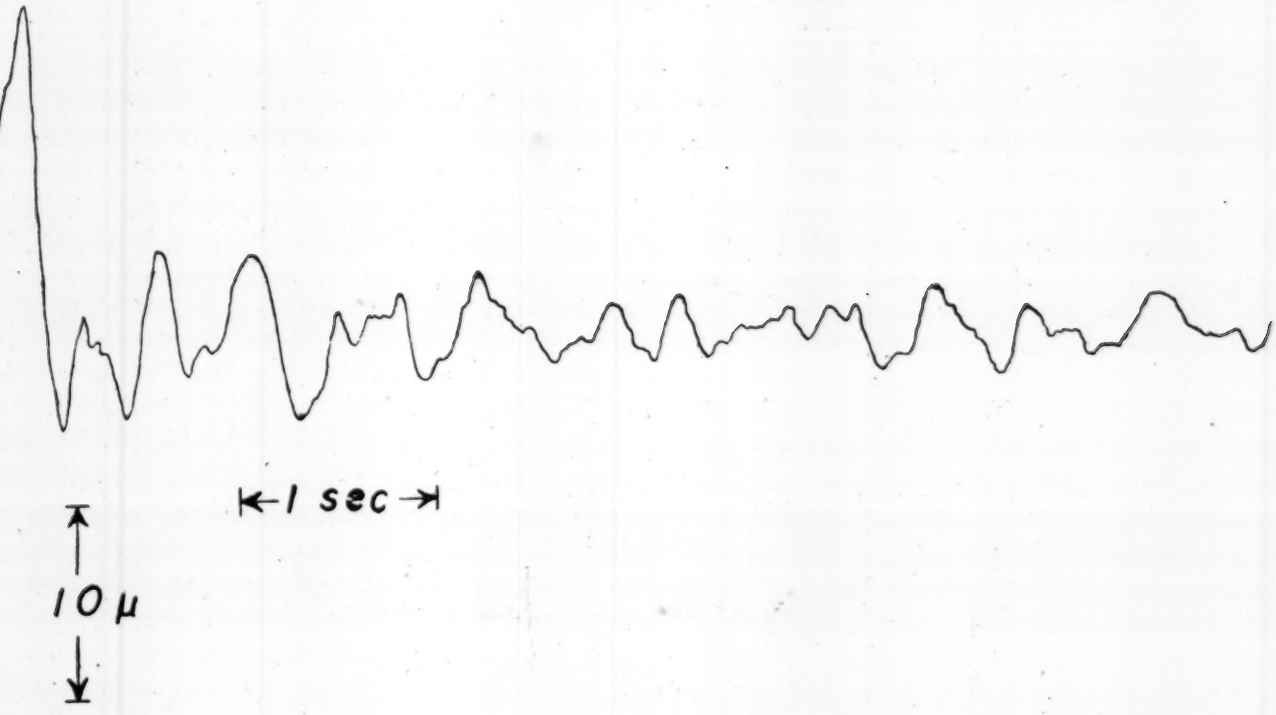

50 in magnification. Original ×9.4.

50 in magnification. Original ×9.3.

5. 地震計記象による發震機構の假定の吟味

地震研究所 金 井 清

この研究では，先づ，球源で急激な短形的壓力變化が起つて發生した地震波を受けたときの地震計振子の運動をしらべ，日立鑛山における地震觀測に使用している地震計の常數を入れて數値計算を行つた．

次に，實際の地震記象と，數値計算で出した振子の運動とから，こゝで假定した發震機構が實際の地震にあてはまつている場合があることを證明した．

卽ち，第 1 に入射波形による地震計振子の特性と表面反射の影響とを考慮に入れて，P 波 S 波の水平と上下成分記錄の比から入射角をきめた．この入射角と初期微動繼續時間から震源をきめると中央氣象臺の結果と大體一致した．

第 2 に上記の考慮を拂つた上で，水平，上下成分の各々について，入射波の P, S 波の振幅比を求めたところ，水平，上下兩成分についての價がほとんど等しく，約 3 となり，觀測點は P 波の押し引きの節圍に近いことになつた．この結果は，この地震の押し引き分布圖とかなりよく合う．

第 3 に，この地震の P, S 波の初動の周期の比は計算結果と等しく，2 になつた．又，球源の半徑を計算すると 1 km となり，常識的な値となつた．

從つて，この地震の記象に見られるような，P 波の周期が S 波のそれに比べて短いという現象が，球源で發生した型の違う自由振動の重ね合せの相違によつて起る場合があり得るという，前論文の議論に 1 つの證據が與えられたことになる．

6. A New Mechanical Low-pass Filter for Seismogram Analyses.

By Tetsuo AKIMA,

Earthquake Research Institute.

(Read March 20, 1951.—Received Nov. 20, 1951.)

1. Introduction: The writer has already studied the behavior of a torsion pendulum as applied as a low-pass filter for seismogram analyses and described some of the interesting results obtained by using this filter for a certain near earthquake.[1)]

As was mentioned previously, the damping of the filter pendulum of the apparatus was effected by oil into which a part of the pendulum is dipped. This arrangement has an inconvenient point, for the temperature of oil must be kept constant by a thermostat in order to get a reliable low-pass filter. The apparatus had some further inconveniences, e.g., the manupulation had to be done in a dark room; the tracing of the original wave forms of mechanically recorded seismograms was difficult on account of their being arc shaped, etc.

In order to improve the apparatus into a more convenient one by eliminating the several points mentioned above, the writer has constructed a new apparatus with an electro-magnetic damper. The design, construction and working of the new apparatus will be described in the following pages.

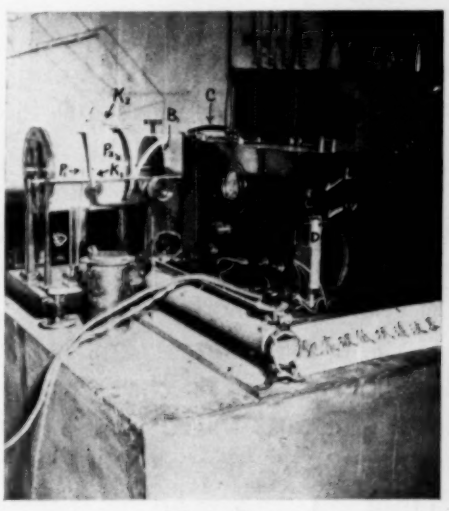

Fig. 1.

2. The apparatus: The appearance of this new apparatus may be seen on the photographs of Fig. 1. It is shown schematically in Fig. 2. The pendulum w in Fig. 2 is a brass rod approximately 6 mm in diameter. 4 such pendulums with length of 5 cm, 7 cm, 10 cm and 14 cm are prepared. The moment of inertia of each pendulums can be changed by the aid of two brass cylinders w_1 and w_2 which are slided along the pendulum w.

1) T. AKIMA, *Bull. Earthq. Res. Inst.*, **26**, (1948), 95, and **27**, (1949), 69.

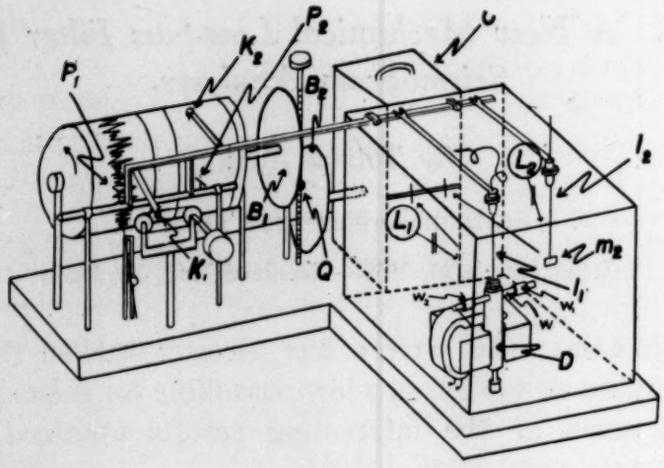

Fig. 2.

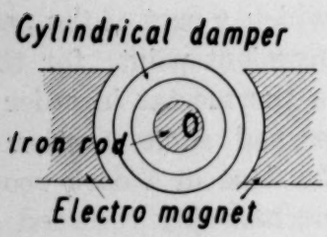

Fig. 3.

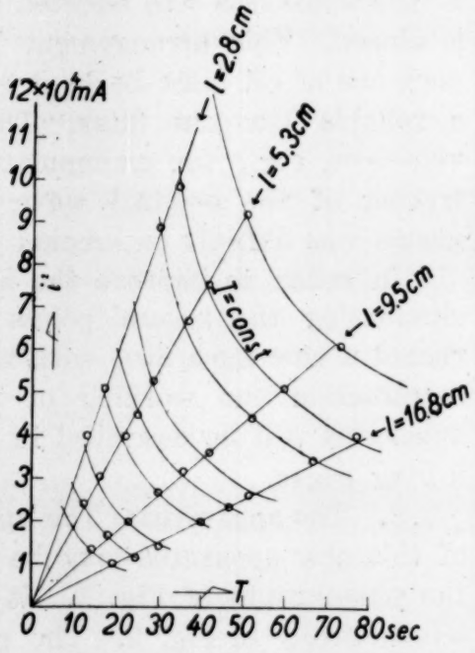

Fig. 4.

The natural period of the pendulum ranged approximately from 5.5 sec to 60 sec.

The damper D is an aluminium cylinder approximately 3 mm thick with an external diameter of 2.5 cm. The horizontal section of the damper at the section of the electro-magnet is shown in Fig. 3, in which 0 is an iron rod and stands vertically along the central axis of the cylindrical damper.

The most important point for the pendulum to work as a reliable low-pass filter is that its constant of damping $h\,(=\varepsilon/n)$ must be kept at a constant value of 0.64 for all values of $u\,(=n/p)$. This point must be tested at first of the apparatus. Fig. 4 shows the result of experiments on the relation between the natural period T of the torsion pendulum and the square of the current i which must be fed to the coil of the magnet in order to keep the value of h at 0.64 for all

values of T. As T is in our case determined by the length of the suspension wire l, and by the moment of inertia of the torsion pendulum I, the experiments were performed under the condition l=constant and I=constant separately. As is seen in these results, the relation between i^2 and T is linear under the former condition and hyperbolic under the latter condition. These relations agree well with the results of the following theoretical considerations.

In our present case, the resistant constant R and the restitutive constant E of the vibrational system are expressed respectively as follows;

$$R=\frac{C_0\sigma D}{S}\phi^2=C_1i^2, \qquad E=\frac{\pi\mu r^4}{2l}=\frac{C_2}{2l}$$

where C_0 is a constant determined by the ratio of length and breadth of the section of magnetic flux which pass perpendicularly through the surface of the damper, S the area of the section of magnetic flux given above, ϕ the total magnetic flux, σ and D the electric conductivity and the thickness of the aluminium damper and μ, r and l the rigidity, radius and length of the suspension wire respectively.

From these two equations we get

$$\varepsilon=\frac{R}{2I}=C_1i^2/2I, \quad n=\sqrt{\frac{E}{I}}=\frac{C_3}{\sqrt{Il}}, \quad T=\frac{2\pi}{n}=C_4\sqrt{Il} \quad \text{.....(1),}$$

and, therefore,

$$h=\frac{\varepsilon}{n}=\frac{C_1i^2}{2I}\Big/\frac{C_3}{\sqrt{Il}}=C_5\sqrt{\frac{l}{I}}i^2 \quad \text{.....(2).}$$

Then, under the condition of l=constant,

$$(1)\times(2) \qquad Th=C_6i^2 \quad \text{.....(3),}$$

and under the condition of I=constant,

$$(1)/(2) \qquad T/h=C_7/i^2 \quad \text{.....(4).}$$

The equations (3) and (4) express the relations between T and i^2 which the writer obtained experimentally.

Using the results of Fig. 4, we can easily keep the value of h constant for each value of T by controlling the electric current flowing through the coil of the magnet.

As is seen in equation (3), the gradients of the straight lines in case of l=constant are inversely proportional to the values of h. Using

this property, we can draw other straight lines for other values of h starting with the standard straight line experimentally determined for $h=0.64$. Fig. 5 was constructed from the two standard lines determined for two suspension wires with the same length but with different diameters of 1.04 mm and 0.074 mm.

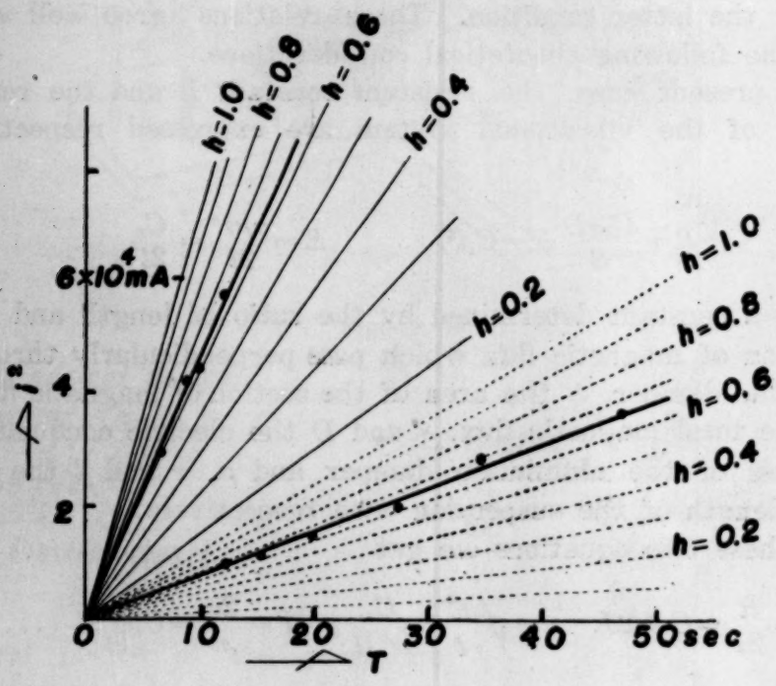

Fig. 5.

In the new apparatus, a rigid rod l_2 is attached vertically beside the torsion pendulum. The light reflected from a small mirror m_2 attached at the lowest end of this rigid rod draws the original wave form in parallel with the filtered wave forms on the oscillograph paper which is moving downward with a velocity of approximately 1 mm/sec in the camera C in Fig. 2. It is easy therefore, to observe time correspondence between the filtered and the original waves, or to investigate the time lag of the filtered waves behind the original waves.

The rotation of the drum on which the original seismograms are wound is transmitted from the recording camera C by means of a small friction roller Q which is placed between the two circular plates B_1 and B_2. The ratio of the rotating velocities can be varied continuously by moving this small roller Q downward or upward. The range of the working natural periods of the filter pendulum can be enlarged to approximately 2.5 sec~300 sec. The uniformity of the drum rota-

tion was tested by a chronometer and was satisfactorily high for our purpose.

For the tracing of wave forms of mechanically recorded seismograms to be studied, a pen p_1, beside a pen p_2, was added in this apparatus. The length of the arm of the pen p_1 can be changed according to the curvature of the arced shape of seismograms which is to be filtered. Two pens K_1 and K_2 are moved as the pen p_2 and are used for checking the accuracy of the tracing.

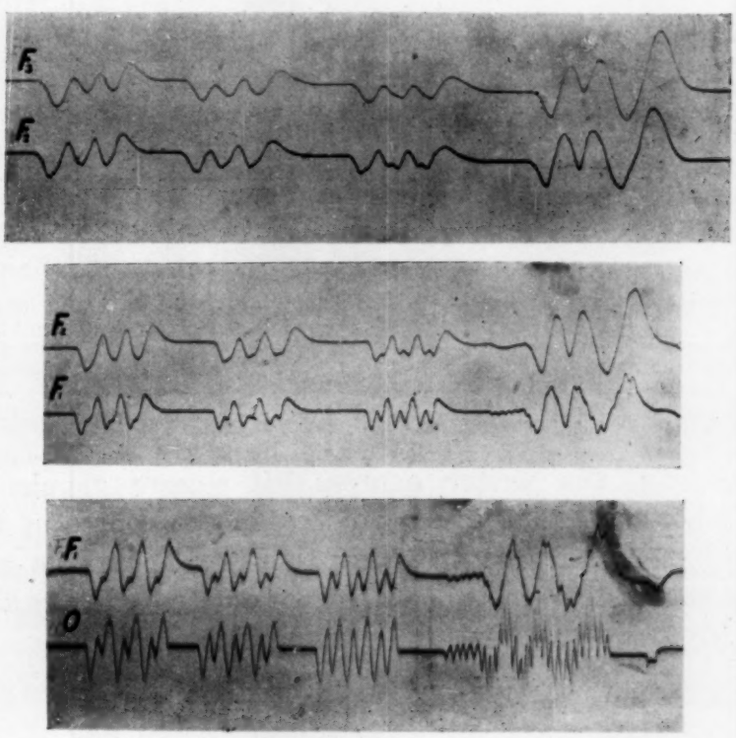

Fig. 6.

3. Some preliminary tests: Several preliminary tests were performed in order to see how the new apparatus works. An example of the results of these tests is shown in Fig. 6. The wave forms marked 0 are the original ones composed of two sinsoidal waves with different periods and amplitudes such as 1) a sine pt + a sine $2pt$, 2) a sine pt + $2a$ sine $2pt$, 3) a sine pt + $4a$ sine $2pt$, and the wave forms marked F_1, F_2, F_3 are the once-, twice- and thrice-filtered ones respectively. These results are quantitatively satisfactory.

The last example shown in this figure is a result of the filteration on an artificial wave form.

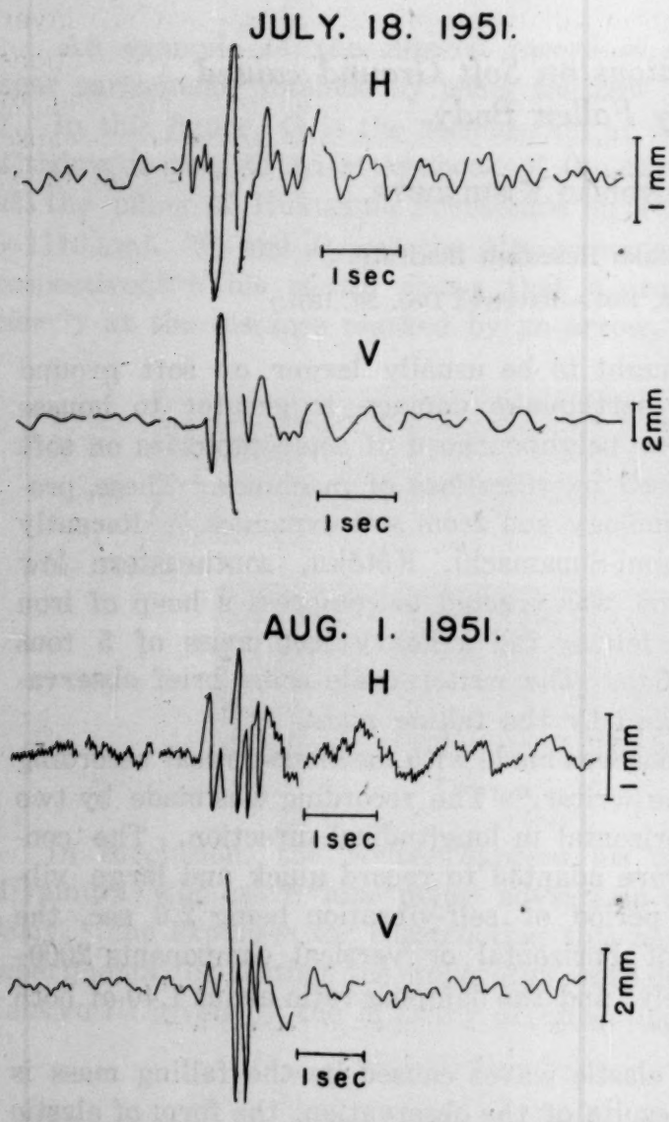

Fig. 1. Upper two records observed at the northern mill (67 m), lower at the southern mill (55 m).

servation was not sufficient.)

The acceleration of the maximum amplitude in vertical component was greater than that in horizontal. But at about 200 m distant, the values of acceleration in the two components became near, and probably at far off stations the horizontal component will be greater than the vertical. The difference of acceleration would be mainly due to that of the vibration-period as seen in Table I and Fig. 2.

To compare earth-vibrations at different places, an iron ball about 2.3 tons in weight was dropped from 7m height to the ground at the southern mill of the factory about 800 m south of the former place. The results are shown in Table II and Fig. 2. Although the energy of the falling of the mass was about 16/30 of the former case, the acceleration of the ground motions was larger than that in the former case. The 2.3 ton ball fell directly to the ground, but the 5 ton mass stroke the ground moderately for it fell to a heap of iron scraps. The writer considers the difference to be due to the condition of the ground.

The vibration-periods at the southern mill were smaller than those at the northern, so the writer thinks the ground accelerations at the two places mainly depend upon the difference in the vibration-period

of the ground. The difference will be made only at the surface layer of about 2 m thick. But at 67 m in the northern mill, accelerations were comparatively small. The small acceleration would be due to the hardness of the ground where the tromometers were set because the instruments were set near an office house and the foundation of the house was made firm.

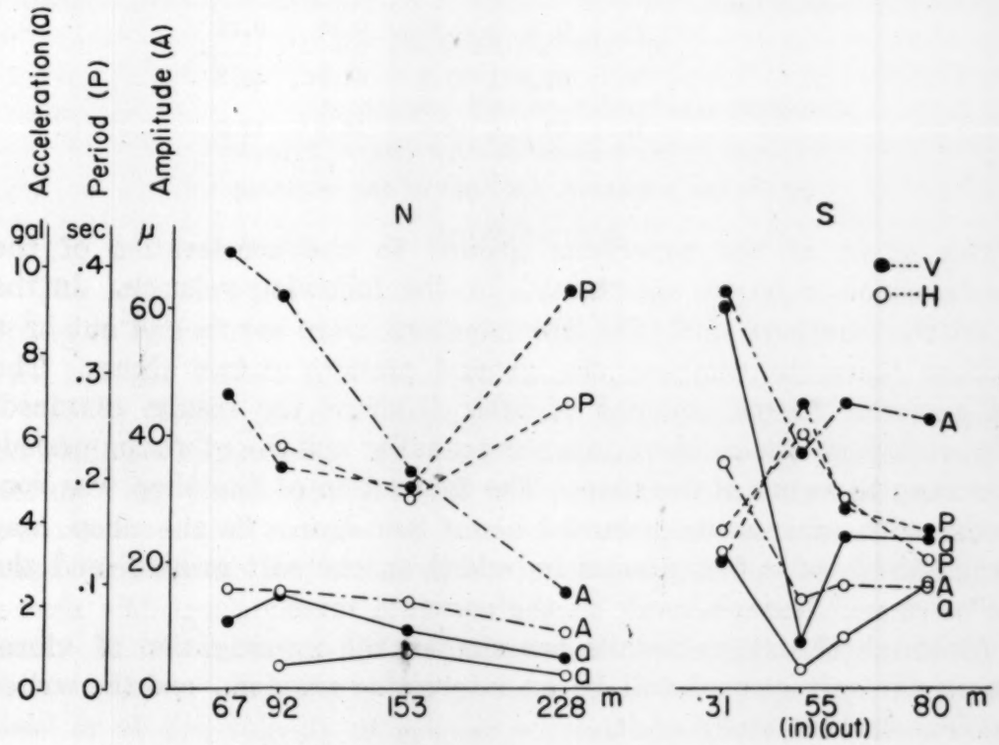

Fig. 2. N, S=Observations in the grounds of the northern or southern mill respectively.

Table I.

Distance (m)		67	92	153	228
Acceleration (gal.)	V	1.61	2.26	1.40	0.73
	H		0.54	0.89	0.32
Period (sec.)	V	0.28	0.21	0.19	0.38
	H		0.23	0.18	0.27
Amplitude (μ)	V	69.0	62.2	34.2	15.3
	H	15.9<	15.9	13.7	9.0

V : vertical component, H : horizontal component

An example of the filtered record of an actual seismogram of a near earthquake obtained by using the new apparatus is shown in Fig. 7. In this figure, O is the seismogram of *N-S* component recorded at Titizima in case of an after-shock of the earthquake which took place at the offing of Hukusima Prefecture on Nov. 11, 1938 (Mag.=III, Δ =1110 km). F_1 and F_2 are the filtered waves once- and twice-filtered respectively. This record shows that a group of long waves appears clearly at the instance marked by an arrow.

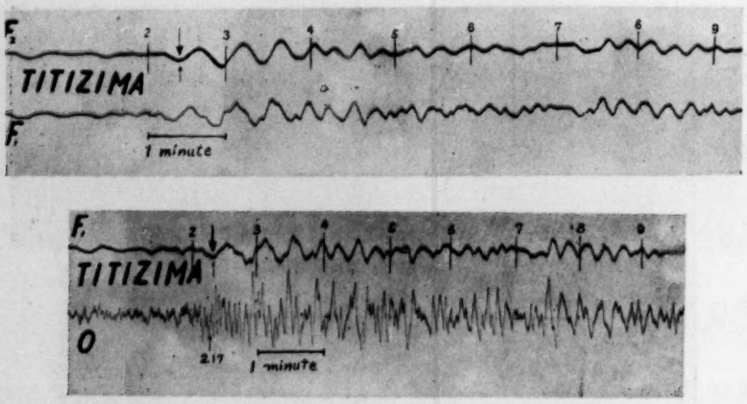

Fig. 7.

In conclusion, the writer express his sincere thanks to Mr. S. Miyamura who gave him many advices in the course of the present study. The expenses for constructing this new apparatus and for the experiments for testing the apparatus were defrayed from the Kagaku-Kenkyu-Hi given by the Ministry of Education.

---

6. 電磁制振式新低域濾波器について

地震研究所　秋　間　哲　夫

曾つて震研彙報 26, 27 號で發表した捩り振子を應用した低域濾波器には，實用上いくつかの缺點があるので，之を今度新しく改良した．本論は，この新裝置が十分滿足すべき機能を有することを述べたものである．

---

7. *Earth-vibrations on Soft Ground caused by Fallen Body.*

By Fuyuhiko KISHINOUYE,

Earthquake Research Institute.

(Read Sept. 18, 1951.—Received Dec. 20, 1951.)

Earth-vibrations are thought to be usually larger on soft ground than on hard ground, and earthquake damage is greater to houses elected on soft ground. The neighbourhood of some factories on soft ground is frequently disturbed by vibrations of machines. These problems are studied from seismology and from soil dynamics.[1] Recently at a steel factory in Minami-Sunamachi, Kōtōku, southeastern low ground of Tokyo, a machine was erected to compress a heep of iron scraps into small volume by letting fall a heavy iron mass of 5 tons in weight from the height 6 m. The writer made some brief observations of earth-vibrations caused by the falling mass.

Recording of the vibrations was made with mechano-optical recording tromometers designed by the writer.[2] The recording was made by two components, vertical and horizontal in longitudinal direction. The constants of the instruments were adapted to record quick and large vibrations for this case: the period of self-vibration being 2.6 sec, the geometrical magnification of horizontal or vertical components 2000–1000 and 840–420 respectively, and the damping ratio about 1.40 of both components.

Portions of record of elastic waves caused by the falling mass is shown in Fig. 1. As the results of the observation, the form of elastic waves was almost equal in every case if the position of the observation was the same. The periods of vibrations increased with the distance of observing station. The velocity of propagation of waves were obtained as 380 m/sec for the initial phase and 140 m/sec or 100 m/sec for maximum amplitudes. (But the writer considers that the values mentioned above have to be examined again, for the accuracy of the ob-

1) RUDORF K. BERNHARD, *Trans Amer. Min. Metal. Engg.*, **138** (1940), 326–349. G. ANGENHEISTER, *Ergebn. exakt. Naturwiss.*, **15**, Berlin, (1936), &c.

2) F. KISHINOUYE, *Bull. Earthq. Res. Inst.*, **20** (1942), 215.
The vertical component tromometer was reported at the monthly meeting of Earthq. Res. Inst. on July 6, 1943.

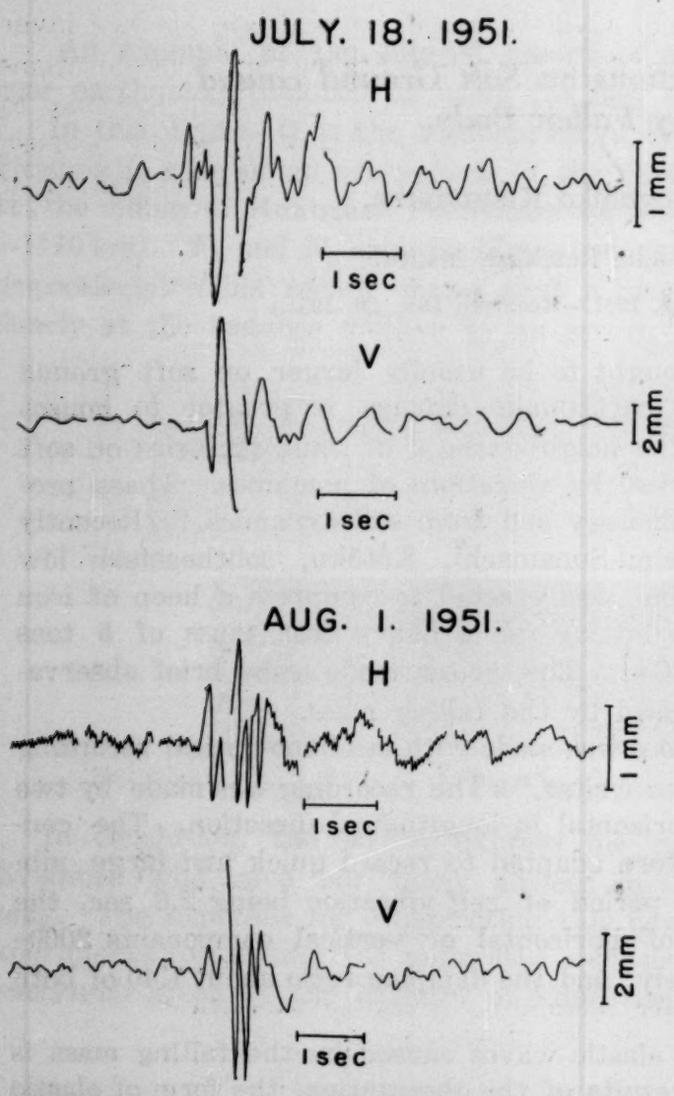

Fig. 1. Upper two records observed at the northern mill (67 m), lower at the southern mill (55 m).

servation was not sufficient.)

The acceleration of the maximum amplitude in vertical component was greater than that in horizontal. But at about 200 m distant, the values of acceleration in the two components became near, and probably at far off stations the horizontal component will be greater than the vertical. The difference of acceleration would be mainly due to that of the vibration-period as seen in Table I and Fig. 2.

To compare earth-vibrations at different places, an iron ball about 2.3 tons in weight was dropped from 7m height to the ground at the southern mill of the factory about 800 m south of the former place. The results are shown in Table II and Fig. 2. Although the energy of the falling of the mass was about 16/30 of the former case, the acceleration of the ground motions was larger than that in the former case. The 2.3 ton ball fell directly to the ground, but the 5 ton mass stroke the ground moderately for it fell to a heap of iron scraps. The writer considers the difference to be due to the condition of the ground.

The vibration-periods at the southern mill were smaller than those at the northern, so the writer thinks the ground accelerations at the two places mainly depend upon the difference in the vibration-period

of the ground. The difference will be made only at the surface layer of about 2 m thick. But at 67 m in the northern mill, accelerations were comparatively small. The small acceleration would be due to the hardness of the ground where the tromometers were set because the instruments were set near an office house and the foundation of the house was made firm.

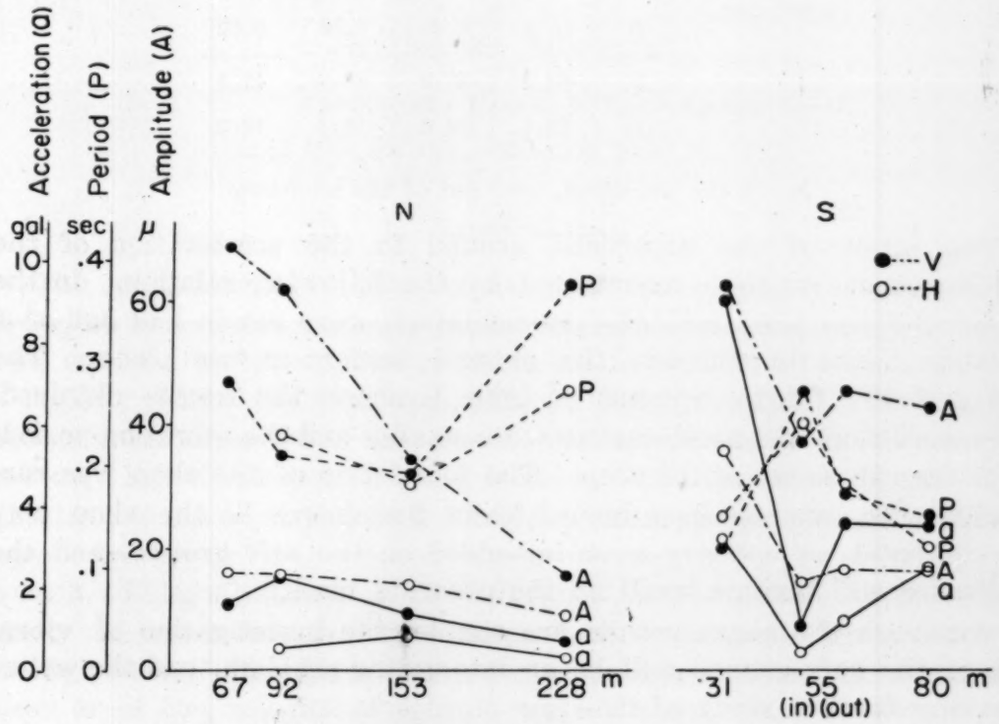

Fig. 2. N, S=Observations in the grounds of the northern or southern mill respectively.

Table I.

Distance (m)		67	92	153	228
Acceleration (gal.)	V	1.61	2.26	1.40	0.73
	H		0.54	0.89	0.32
Period (sec.)	V	0.28	0.21	0.19	0.38
	H		0.23	0.18	0.27
Amplitude (μ)	V	69.0	62.2	34.2	15.3
	H	15.9<	15.9	13.7	9.0

V: vertical component, H: horizontal component

Table II.

Distance (m)		31	55(in)	55(out)	80
Acceleration (gal.)	V	9.04	1.13	3.58	3.52
	H	3.23	0.49	1.20	2.41
Period (sec.)	V	0.12	0.27	0.17	0.15
	H	0.15	0.24	0.18	0.12
Amplitude (μ)	V	62.3	37.3	44.9<	42.3
	H	35.5	14.0	16.4	16.2

in: in the workshop, out: out of the workshop

The effect of the superficial ground to the acceleration of the ground motion may be ascertained by the following relation. In the site of the southern mill the tromometers were set in and out of a workshop house to compare the ground motions at two places. The third and the fourth columns of table II shows the results obtained. In the workshop, the accelerations were smaller and the vibration-periods longer than those out of the shop. The foundation of the shop was constructed with concrete base buried about 2 m deep. So the shop may be considered as a heavy mass imbedded on the soft ground, and the amplitudes will become small on the concrete mass.

Although the above results are simple; the investigation of vibrations on the soft ground will be an interesting problem, and the writer is making further study of it.

Lastly the writer express his thanks to Mr. R. Ikegami, Mr. J. Moroga and Mr. H. Yoshioka for their help in the observations, and to Miss M. Kotaka for her assitance in preparing this paper. The cost of this study was defrayed from the Grant in Aid for Developmental Scientific Research of the Department of Education.

---

7. 軟弱地盤の上に落された物體によつて起された土地の振動

地震研究所　岸　上　冬　彦

東京都江東區南砂町の軟弱地盤といわれる土地に重い物體が落された時の土地の振動を微動計によつて記錄し，距離・振動の振幅及び加速度の關係を調べた．互に 800 m 離れた 2 個所で觀測して比較し，又基礎の硬い工作場の內と外とに微動計を据えて比較した．その結果，地表から 2 m 位の地質の差が振動周期とそれに關連して振動加速度に影響すると考えた．

8. *Dynamical Measurements of the Elastic Constants of Rocks subjected to Initial Stresses.* 1. *Measurement of Young's Modulus under Uniaxial Compression.*

By Daisuke SHIMOZURU,

Earthquake Research Institute.

(Read Nov. 21, 1950.—Received Nov. 20, 1951.)

1. Introduction.

The experimental studies concerning the elastic and plastic properties of rocks have recently made remarkable developments. Among these studies, measurements of cubic compressibility, Young's modulus or rigidity under elevated temperature and hydrostatic pressure have extended our knowledge on the behaviour of rocks in the earth's interior. But if the earth's crust is subjected, in addition to hydrostatic pressure, to such stresses as simple tension, compression or shearing stress, the elastic properties of the crust may differ from those with no such additional stress. This difference in the elastic constants and density of the crust will in turn produce a change in the velocity of seismic waves. In effect, some Japanese observations of the earth tides[1] or of the velocity of seismic waves[2] seem to show the change in elasticity of the earth's crust with time. They seem also to have some relations with the occurrence of earthquakes.

The author intends to study experimentally (1) the variation of the elastic constants of rocks due to the change in type or amount of the initial stress, and (2) the relations of these elastic behaviours of rocks to their fine structures. For geophysical applications, rock samples must be subjected to a differential force under the confining hydrostatic pressure. As the first step of the study, however, igneous rock bars were simply kept compressed parallel to the axis, and the flexural vibrations of the bars were observed in this condition. Young's modulus was calculated from the resonance frequency of the flexural vibrations. Relations among the rate of change in Young's modulus, the amount

1) NISHIMURA, E., *Trans. Amer. Geophys. Union*, v. 31, no. 3, 1950.
2) HAYAKAWA, M., *Rep. Geol. Surv., Japan*, special number, 1950.

of stress and the fine structures of rocks are also discussed in this paper.

2 Method of Experiment.

A rock specimen, cut into a rectangular form, was compressed between the upper and lower shafts of a testing machine through a pair of knife-edge so as to admit pure flexural vibrations of the specimen. If the ends of specimen are cramped or simply supported, the mode of the actual vibration becomes sometimes complicated owing to the mechanical imperfectness of the end conditions. The dimensions and densities of the rock specimen were as follows;

Specimen	Locality	Dimension (cm)	Density
Augite-basalt	Ajiro, Izu	1.75×1.90×24.55	3.00
Biotite-granite	Inada	1.95×2.45×19.93	2.69
Augite-hypersthene-andesite	Suwa	2.00×2.50×19.96	2.66
Pitchstone	Wadatoge	2.00×2.50×19.98	2.36

The method adopted here is to calculate Young's modulus from the measured natural frequency of the flexural vibration of the specimen. Therefore, it was necessary that the shape of the specimen should be accurately known, otherwise the value of Young's modulus calculated from the resonance frequency would be incorrect. The driving force was applied at the middle of the specimen by means of a light aluminium rod cemented to the voice coil of a dynamic speaker and contacted with the specimen. The voice coil was drived by a variable frequency vacuum tube oscillator. Both of the mass and electric reactance of the driving system were so small that they did not affect the vibration frequency of the specimen. Thus the specimen was forced into the flexural vibration of variable frequency. At the opposite side of the driving system, a rochelle salt pick-up of twister bimorph type touched the specimen at the middle. (cf. Fig. 4). When the natural frequency of the specimen coincides with the driving frequency, the resonance is observed by means of a pick-up and an amplifier. As the natural frequency of the pick-up is 1,2000 cps when cramped at the middle, and that of the specimen several thousands cps, we could easily distinguish the resonance frequency of the specimen from that of the pick-up.

Thus at each stage of the increasing compression, the respective resonance frequency was measured.

3. Method of Calculation of Young's Modulus.

From the natural frequency of the specimen, we must calculate Young's modulus or the velocity of longitudinal wave as the function of the applied stress. As the mass and stiffness of the testing machine are very large compared with the vibrating specimen, the natural frequency of the specimen would not be affected. Strictly speaking, the finite strain theory must be adopted in calculating the natural frequency, but for the present case, the common theory was used as a first approximation.

The equation of the motion of the flexural vibration of the bar subjected to the axial compression, neglecting the rotatory inertia and the internal friction, is

$$E\kappa^2 \frac{\partial^4 y}{\partial x^4} + \frac{T}{a} \frac{\partial^2 y}{\partial x^2} + \rho \frac{\partial^2 y}{\partial t^2} = 0$$

End conditions are

$$x = \pm \frac{l}{2}: \quad y = 0, \quad Ei \frac{\partial^2 y}{\partial x^2} = I_0 \frac{\partial^2}{\partial t^2} \left(\frac{\partial y}{\partial x} \right),$$

where E: Young's modulus,
y: lateral displacement,
a: sectional area,
κ: radius of giration,
ρ: density,
l: length,
i: moment of inertia of the specimen,
I_0; 〃 of the end masses (knife-edge),
T: compressional force per cm².

The general solution of the equation of motion is

$$y = e^{ipt} \{ A \cos mx + B \cosh nx + C \sin mx + D \sinh nx \},$$

in which

$$m = \frac{\sqrt{\sqrt{\alpha^2 + \beta^2} - \alpha}}{l}, \qquad n = \frac{\sqrt{\sqrt{\alpha^2 + \beta^2} + \alpha}}{l},$$

$$\alpha = -\frac{Tl^2}{2aE\kappa^2}, \qquad \beta^2 = \frac{\rho l^4 p^2}{E\kappa^2}.$$

By eliminating A, B, C, D by means of the above end conditions,

we obtain the following equation finally,

$$(m^2-n^2)^2 \sinh\frac{nl}{2}\cosh\frac{nl}{2} - \left(\frac{I_0}{Ei}\right)p^4\left(-m\cosh\frac{nl}{2}\tan\frac{ml}{2}+n\sinh\frac{nl}{2}\right)\left(m\sinh\frac{nl}{2}\cot\frac{ml}{2}-n\cosh\frac{nl}{2}\right)=0$$

From this equation, by trial-and-error method, E was decided graphically for each value of T.

4. Discussion.

Fig. 1a shows an example of the resonance curve of granite, and Fig. 1b that of basalt. Exciting frequency is plotted against amplified current. The former curve is a typical resonance curve, but the latter is abnormally rugged. As basalt has usually many remarkable cracks along its flow structure, the zig-zags in the resonance curve are attributed to these cracks. Smooth resonance curves were obtained in the case of other specimens.

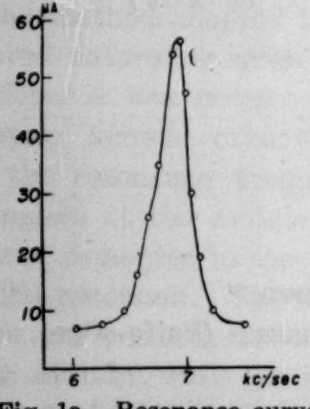

Fig. 1a. Resonance curve of Granite.

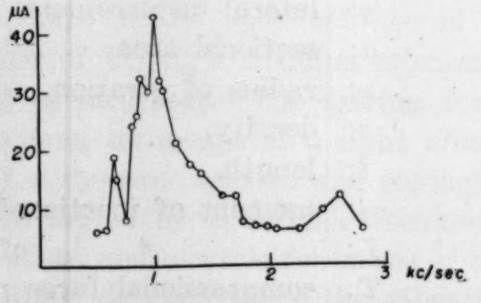

Fig. 1b. Resonance curve of Basalt.

In Fig. 2 Young's modulus E, as calculated from the resonance frequency, was plotted against the applied compressional stress. When the specimen is free from stress, Young's modulus of basalt is the smallest, and that of pitchstone the largest.

Next, let us consider the rate of change of Young's modulus with the increase in stress. At small compression, the rate of increase in E with stress $(\partial E/\partial T)$ has, to E itself, the greatest value in the case of basalt, and the smallest value for pitchstone. This is just contrary to that of Young's modulus when specimens are free from stress. The

fact leads to the conclusion that a rock which has a large initial value of E shows little change in E with stress.

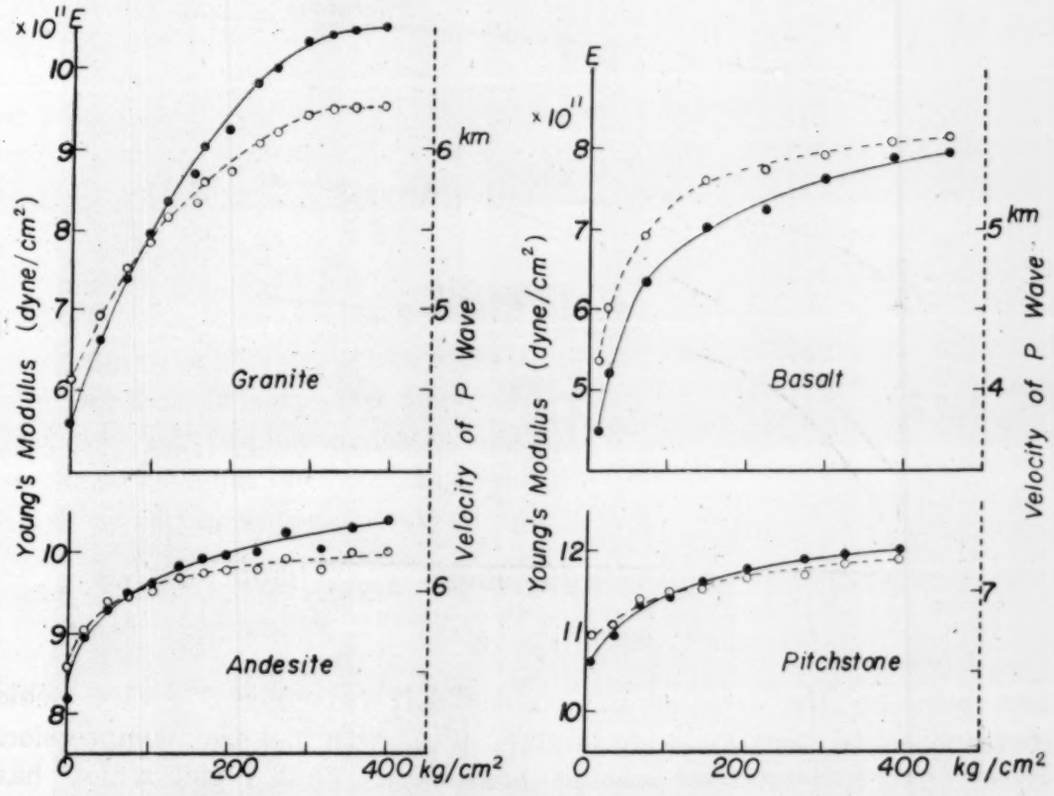

Fig. 2. Young's modulus vs stress. Solid line is Young's modulus. Broken line is the velocity of longitudinal wave.

Fig. 5 shows the photomicrographs of these four rocks. In granite, there are many small cleavages in or between the crystals, and there is no ground-mass. Basalt shows a notable flow structure and has a holocrystalline ground-mass rich in augite. Andesite has a glassy groundmass, and pitchstone is glass including feldspar. Even when the applied force is small, cavities or cracks in basalt would be compressed and the rock will become relatively compact as a whole. The conspicuous rate of increase of E in the case of basalt may thus be explained. On the contrary, pitchstone which has no cracks or cavities, exhibits little change of E with stress. Thus the considerable steepness of the initial slope in E-T diagram in the case of basalt and granite is not due to the compression of rock-forming minerals, but depends largely on the diminishing of many cracks in the rocks. At considerably large stress, $\partial E/\partial T$ becomes small in basalt, andesite and pitchstone with the

exception of granite. This tendency may probably be due to the existence of a torelably compact ground-mass. Fig. 3 represents the rela-

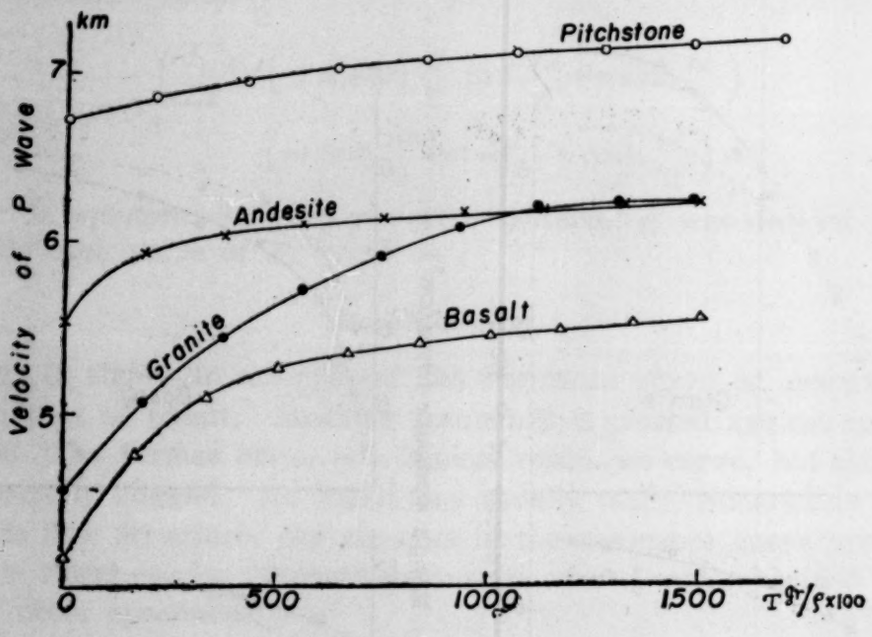

Fig. 3.

tion between the velocity of longitudinal wave and $T/\rho \times 100$ (which corresponds to the depth in meter, if T was not the compressional stress, but hydrostatic confining pressure.). Thus rocks which have compact ground-mass and no cracks should exhibit little change of E with stress.

5. Acknowledgment.

The author wishes to express his gratitude to Professor R. Takahasi for his kind advice and criticism. He is also thankful to Dr. T. Hayasi, Institute of Applied Mathematics, who kindly accommodated the author with a testing machine for a long period. The author's thanks are also due to Assist. Prof. R. Morimoto who gave him valuable petrological informations.

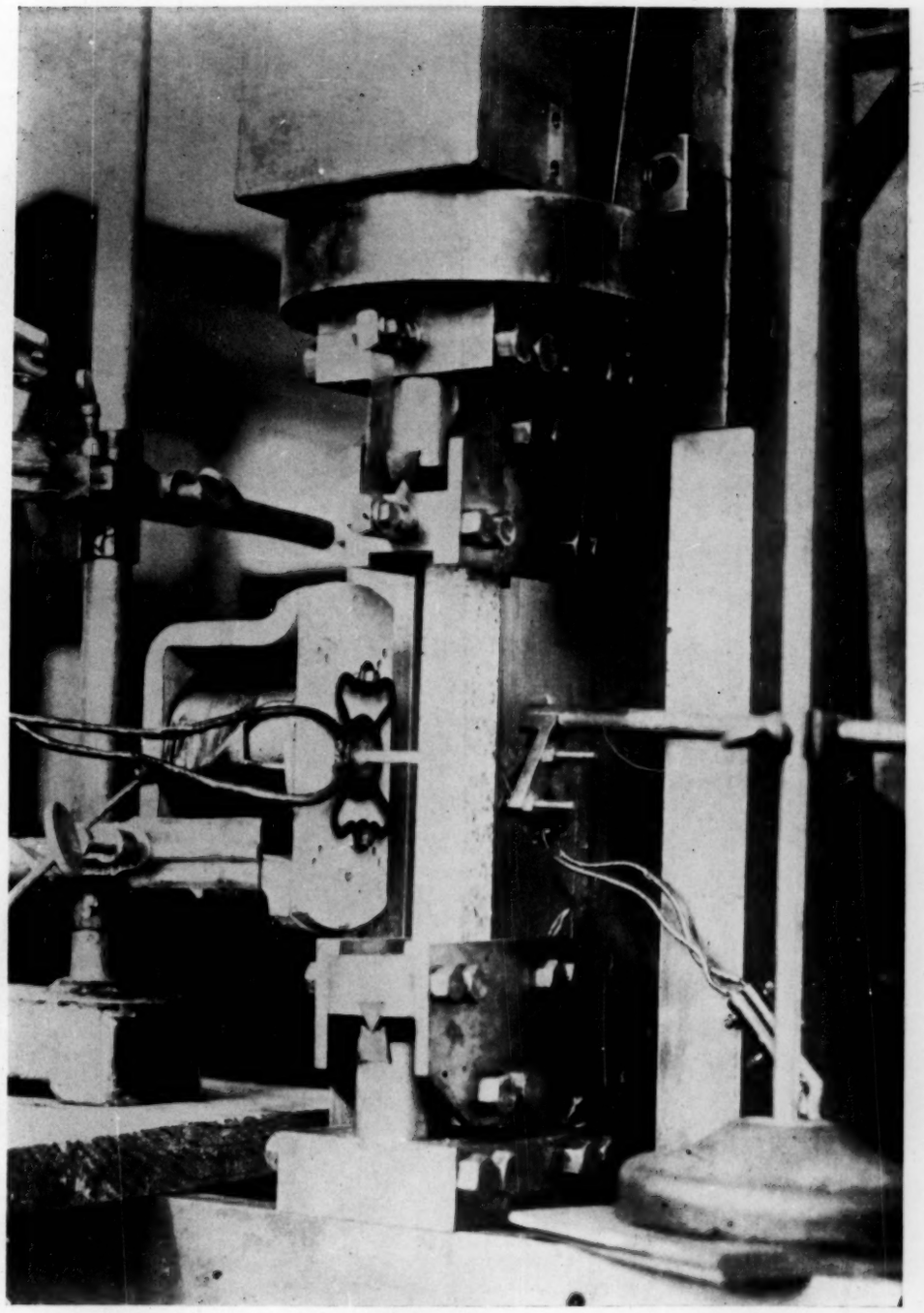

Fig. 4.

（震研彙報　第三十号　圖版　下鶴）

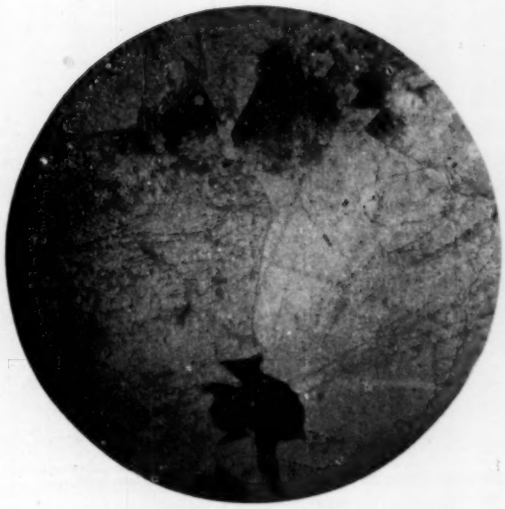

Granite

Andesite

Basalt

Pitchstone

Fig. 5.

8. 應力がかゝつた狀態に於ける岩石彈性率の動力學的研究

1. 軸壓のかゝつた狀態に於けるヤング率の測定

地震研究所 下 鶴 大 輔

最近十年間に於ける岩石の彈性に關する實驗的研究は多くの成果をもたらし,地球內部の岩石の模樣の記述に或る程度成功したと云へる. 然し,我々の地殼に,破壞限界內に於て應力が作用してゐる時,彈性が變化し,從つて,歪んだ領域を通過する地震波の速度が變化する. 卽ち,地殼の或る深さに於て,どの樣な種類のどの位の應力が作用した時に,その場所の彈性率はどれだけ變化するであらうかといふ事を研究する事は興味ある事である. その爲めには,岩石の試片に高溫のもとで,靜水壓をかけて,その狀態で,應力を作用させ,動力學的にその岩石の彈性率又は P 波, S 波の速度を測定すれば良い譯であるが,先づ豫備的實驗として,四種類の代表的火山岩をとり,室溫,一氣壓のもとで,軸方向の壓力をかけた狀態で,電氣的方法に依り,撓み振動を勵起させ,その固有振動數からヤング率を計算し,壓力に依るヤング率の變化の模樣をしらべた. その結果,明らかになつた事は, 1) ヤング率—應力曲線 (第二圖) を見ると判る樣に,應力が小なる時に,玄武岩と,花崗岩のヤング率の割合が他に比して,大きい. この理由として造岩鑛物が壓縮されるよりはむしろ,結晶中の割れ目が先づ壓縮される事が考へられる事と, 2) 又,全體として,應力零の時のヤング率の大きいものは,應力に依るヤング率の變化の割合が小さい. 3) 更に,應力が增加すると,非常に緻密な石基を持つた岩石程,ヤング率の增加する割合は少ないと云ふ事である. 將來は他の電氣的方式に依つて,成るべく地球內部の狀態に近い條件のもとに,應力の形を色々變へて,彈性率を測定しようと思ふ.

9. *On Magnetization of Volcanoes.*

By Tsuneji RIKITAKE,

Earthquake Research Institute.

(Read Oct. 16, 1951.—Received Dec. 20, 1951.)

1. Introduction.

It is a well known fact that geomagnetic anomalies of particular distribution are found out in the neighborhood of volcanoes as clarified, for examples, by the magnetic surveys of Volcano Mihara[1),2)], Volcano Stromboli[3)], Volcano Miyake-sima[4),5)] Volcano Omuro[6)], Volcano Usu[7)], Volcano Asama[8)], Volcano Fuji (Huji or Fuzi)[9)] Volcano Sakura-jima[10),11)] and others. These anomalies are all interpreted as due to the magnetization of the volcanoes, the direction of the magnetization being roughly the same with the geomagnetic force there. In order to determine the intensity of magnetization, for example, we take, as T. Minakami[8),10)] did, one or two rotational ellipsoids of suitable dimension having uniform magnetization in the direction of the present geomagnetic force. Then, by comparing the magnetic field caused by the ellipsoids with the observed anomaly, the intensity of magnetization is determined. Thoug the intensity thus determined is thought to be reasonable from the results of the experimental study[12)] on the intensity of natural remanent magnetization and induced one, we should pay attention to the fact that the dimension of the magnetic mass is chosen rather arbitrarily. From the theoretical standpoint, it is desirable to determine simultaneously both

1) R. TAKAHASI and T. NAGATA, *Bull. Earthq. Res. Inst.*, **15** (1937), 441.

2) T. RIKITAKE, I. YOKOYAMA, A. OKADA, and Y. HISHIYAMA, *Bull. Earthq. Res. Inst.*, **29** (1951), 583.

3) M. BOSSOLASCO, *Geofisica pura e applicata*, **5** (1943), 11.

4) T. MINAKAMI, *Bull. Earthq. Res, Inst.*, **19** (1941), 356.

5) R. TAKAHASI and K. HIRANO, *Bull. Earthq. Res. Inst.*, **19** (1951), 82 and 373.

6) T. NAGATA, *I.U.G.G.A.T.M.E. Trans. Oslo Meeting*, (1950).

7) T. NAGATA, *I.U.G.G. Assoc. Volcanology, Brussel Meeting*, (1951).

8) T. MINAKAMI, *Bull. Earthq. Res. Inst.*, **16** (1938), 100 and **18** (1940) 178.

9) T. MINAKAMI, not published.

10) H. TSUYA and T. MINAKAMI, *Bull. Earthq. Res. Inst.*, **18** (1940), 318.

11) Y. HARADA, T. HATAKEYAMA and T. OBAYASHI, *Bull. Earthq. Res. Inst.*, **24** (1946), 207.

12) T. NAGATA, *Bull. Earthq. Res. Inst.*, **21** (1943), 1.

the intensity of magnetization and the extent of magnetic mass that is effective to the anomaly. The effective region of volcano thus determined may have some geophysical significances for the structure of volcano. The writer will attempt here to analyse the anomalies near volcanoes from the standpoint stated above.

2. Theory.

As studied by T. Terada[13], a volcano is more or less a conical heap of rocky mass, the essential tendency of the geometrical form of it being expressible by a mean profile curve. For the sake of mathematical simplicity, the writer also deals with the mean topography of a volcano which is obtained after Terada's method.

As already studied in the writer's earlier paper[14], the components of the magnetic field due to a uniformly magnetized circular cone having the radius a_0 at the bottom and the height h is obtained as follows;

$$\left.\begin{aligned} \Delta X &= J\left\{\cos\theta\left(\frac{F}{r}\cos 2\phi - G\cos^2\phi\right) - H\sin\theta\cos\phi\right\}, \\ \Delta Y &= J\left\{\cos\theta\sin 2\phi\left(\frac{F}{r} - \frac{G}{2}\right) - H\sin\theta\sin\phi\right\}, \\ \Delta Z &= J\{H\cos\theta\cos\phi + G\sin\phi\}, \end{aligned}\right\} \quad (1)$$

where

$$\left.\begin{aligned} F &= \int_z^h aI_1 dz_1 + \int_0^z aI_1' dz_1, \\ G &= \int_z^h aI_2 dz_1 + \int_0^z aI_2' dz_1, \\ H &= \int_z^h aI_3 dz_1 - \int_0^z aI_3' dz_1, \end{aligned}\right\} \quad (2)$$

and

$$\left.\begin{aligned} \left.\begin{matrix} I_1 \\ I_1' \end{matrix}\right\} &= \int_0^\infty e^{\mp a(z_1 - z)} J_1(ar) J_1(aa)\, da, \\ \left.\begin{matrix} I_2 \\ I_2' \end{matrix}\right\} &= \int_0^\infty a e^{\mp a(z_1 - z)} J_0(ar) J_1(aa)\, da, \\ \left.\begin{matrix} I_3 \\ I_3' \end{matrix}\right\} &= \int_0^\infty a e^{\mp a(z_1 - z)} J_1(ar) J_1(aa)\, da. \end{aligned}\right\} \quad (3)$$

13) T. TERADA, *Bull. Earthq. Res. Inst.*, **7** (1929), 207.
14) T. RIKITAKE, *Bull. Earthq. Res. Inst.*, **29** (1951), 161.

Here, we assume that the cone is magnetized in a direction in xz-plane with inclination θ. J and a denote respectively the intensity of magnetization and the radius at $z=z_1$. The origin of the cylindrical coordinate r, ϕ and z is taken at the centre of the base plane of the cone.

At a point on the central axis of the cone where $r=0$ and $z=h+d$, we have

$$\frac{2F}{r}=G=\int_0^h \frac{(a_0-kz_1)^2}{\{(a_0-kz_1)^2+(h+d-z_1)\}^{3/2}}\,dz_1\,,\quad H=0\,, \tag{4}$$

where

$$k=\cot\lambda\,, \tag{5}$$

λ denoting the slope of the cone. In that case, it becomes simply that

$$\left.\begin{aligned} \Delta X&=-\pi JG\cos\theta\,,\\ \Delta Y&=0\quad\ \ ,\\ \Delta Z&=2\pi JG\sin\theta\ \ ,\end{aligned}\right\} \tag{6}$$

where, after integrating (4), G is given by

$$G=\frac{m}{(m^2+1)^{3/2}}\log\frac{\alpha+m\beta+m^2+1+\sqrt{m^2+1}\,\sqrt{(1+\alpha)^2+(m+\beta)^2}}{\alpha+m\beta+\sqrt{m^2+1}\,\sqrt{\alpha^2+\beta^2}}$$
$$+\frac{m}{m^2+1}\left\{\frac{m^2-1-(\alpha-m\beta)}{\sqrt{(1+\alpha)^2+(m+\beta)^2}}+\frac{\alpha-m\beta}{\sqrt{\alpha^2+\beta^2}}\right\}, \tag{7}$$

and where

$$m=1/k\,,\quad \alpha=c_0m/h\,,\quad \beta=dm/h\,. \tag{8}$$

c_0 denotes the radius of the top plane of the cone.

With (6) and (7), it is possible to calculate the magnetic anomaly on the central axis due to the cone if the form of the cone and J are given. Corresponding to dip anomaly ΔI, if ΔI is small, we define a function $f(\Delta I)$ which is given by

$$\begin{aligned} f(\Delta I)&=\{\tan(I_0+\Delta I)-\tan I_0\}/\tan I_0\\ &=\Delta Z/Z_0-\Delta X/X_0\\ &=\pi JG\left(\frac{2\sin\theta}{Z_0}+\frac{\cos\theta}{X_0}\right), \end{aligned} \tag{10}$$

where I_0, Z_0 and X_0 denote respectively the normal value of I, Z and X there.

Since we have a good number of geomagnetic dip surveys in the neighborhood of various volcanoes, the writer would like to deal with the dip anomaly in the main.

Theoretically speaking, we can calculate G just on the top of the cone from the shape of the cone for any h. Hence, it is possible to determine h by comparing the observed f on the top with the one calculated from (10) where we take certain value of J from the experiment of rocks composing the volcano. According to the experimental results, however, J is considerably scattered even in case of samples taken from the same lava flow. And, moreover, a volcano is not composed of a sort of lava but is usually composed of lava and pyroclastic ejecta whose magnetic properties are by no means the same. Thus it is impossible in practice to determine the effective height of the cone by taking a value of J from experiment.

In order to avoid this difficulty, the writer calculates f for various heights on the central axis of the cone from the distribution of dip anomaly. By taking the ratio of f to that just on the top, the effect of J will be almost approximately eliminated. From the potential theory, the components of the anomaly on a plane can be expressed by

$$\left.\begin{aligned} \Delta X &= \sum_k \sum_n e^{-kz} (A_{kn} \cos n\phi + B_{kn} \sin n\phi) J_n(kr), \\ \Delta Z &= \sum_k \sum_n e^{-kz} (C_{kn} \cos n\phi + D_{kn} \sin n\phi) J_n(kr), \end{aligned}\right\} \tag{11}$$

where the anomaly is assumed to occur from the source beneath $z=0$. $f(\Delta I)$ at $z=d$ is calculated from (11) as follows;

$$f(\Delta I) = \sum_k \sum_n e^{-kd} \left\{ \left(\frac{C_{kn}}{Z_0} - \frac{A_{kn}}{X_0} \right) \cos n\phi + \left(\frac{D_{kn}}{Z_0} - \frac{B_{kn}}{X_0} \right) \sin n\phi \right\} J_n(kr). \tag{12}$$

Thus it is easily obtained from (12) that

$$f_{z=d} = \sum_k \alpha_{k0} e^{-kd} \tag{13}$$

at $r=0$ and $z=d$, while we have on $z=0$

$$f_{z=0} = \sum_k \sum_n (\alpha_{kn} \cos n\phi + \beta_{kn} \sin n\phi) J_n(kr). \tag{14}$$

Since the distribution of dip anomaly on a conical volcano is roughly circular symmetric, we can, to a fair degree of approximation, express the distribution by

$$f_{z=0} = \sum_k \alpha_{k0} J_0(kr), \tag{15}$$

where the terms for $n>0$ are all ignored. Hence, we can obtain f at a height $z=d$ through (13). However, it should be borne in mind that

we assume that the dip anomaly is given on a plane notwithstanding the fact that we measure the anomaly on the slope of the volcano. The influence of this treatment will be discussed in the following section.

In the next place, we compare $\frac{f_{z=d}}{f_{z=0}}$ thus obtained from the observation with the calculated one or $\frac{G_{z=d}}{G_{z=0}}$ that is readily given by (10). As $\frac{G_{z=d}}{G_{z=0}}$ is of course a function of h, we easily determine h from the curve $\frac{G_{z=d}}{G_{z=0}}$ *vs* h so as to make $\frac{f_{z=d}}{f_{z=0}}$ equal to $\frac{G_{z=d}}{G_{z=0}}$. Since the effective height of the volcano is thus obtained, the mean intensity of magnetization J is readily determined from (10) where θ is assumed to agree with the inclination of the present geomagnetic force as approximately proved in the previous investigations.

As mentioned above, it is possible to determine simultaneously both the effective height and mean intensity of magnetization while the shape of volcano is idealized by preferring its mean topography.

3. Examination of the method.

In order to examine and test the method described in the former section, the dip anomaly near Volcano Mihara in Ooshima Island will b analysed in the following. According to the writter's survey[11] in 1950, the dip-angle increases with the height above sea level as reproduced in Fig. 1, the general tendency of increase being expressed by the curve in the figure where the curve being determined as a quadratic expression of the height by means of the least square method. On the other hand, the height above sea level is read off at every 500 m on the map of 1/50,000 scale along the eight azimuthal lines radiating from the centre of the volcano. By averaging the height thus read off, we get the mean profile as shown in Fig. 2. As seen in the figure, the idealized form of Volcano Mihara is fairly expressed by a circular cone, the slope of

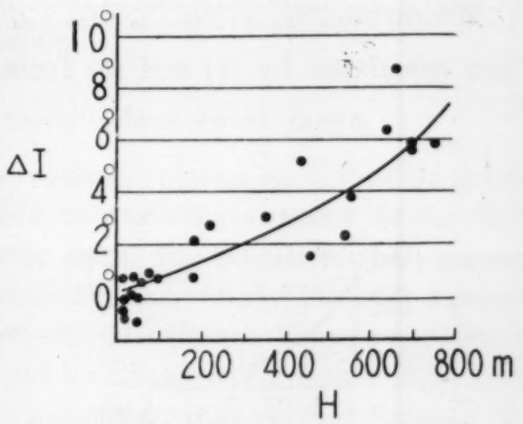

Fig. 1. The relation between dip-anomaly and height on Volcano Mihara.

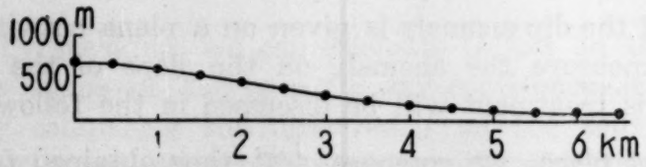

Fig. 2. Mean profile of Volcano Mihara. Ordinate: Height above sea level, abscissa: Distance from the centre of the volcano.

which amounts to about 9°, while the radius of the top plane amounts to almost 500 m. Combining, then, the relation between the dip anomaly and height with the mean topography, the relation between $f(\Delta I)$ and the horizontal distance from the centre is obtained as shown in Fig. 3.

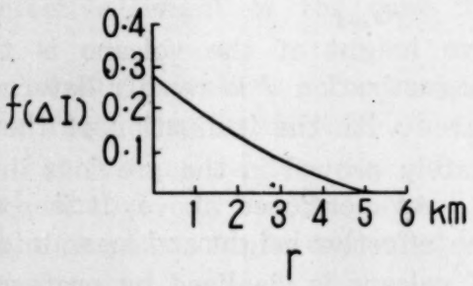

Fig. 3. The relation between $f(\Delta I)$ and the horizontal distance from the centre of the volcano.

From the relation shown in Fig. 3, the coefficients a_{10}, a_{20}, ... in (5) are determined by solving certain simultaneous equations. As fully studied by E. H. Vestine and H. Davids[15], we select a value $r = r_1$ sufficiently large so that f becomes negligibly small. From f at $r = 0$, $\frac{1}{6}r_1$, $\frac{2}{6}r_1$, ..., $\frac{5}{6}r_1$, it is possible to determine a_{10}, a_{20}, ..., a_{60}. With these coefficients, f at any height on the central axis of the cone is obtained from (13) as shown in Fig. 4.

Meanwhile, $G_{d=0}$, $G_{d=1\,km}$, $G_{d=4\,km}$ and $G_{d=5\,km}$ for the various value of h are calculated by (7) and (8) from which $\frac{f_{d=1\,km}}{f_{d=0}}$, $\frac{f_{d=4\,km}}{f_{d=0}}$, and $\frac{f_{d=5\,km}}{f_{d=0}}$

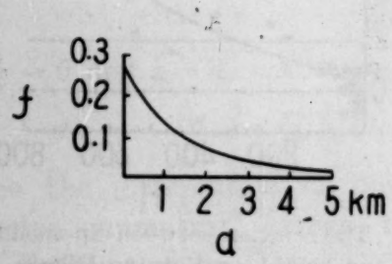

Fig. 4.

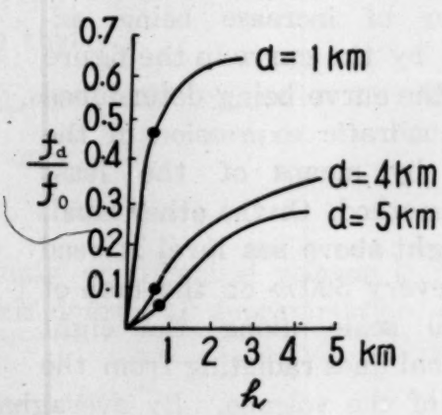

Fig. 5.

15) E. H. VESTINE and N. DAVIDS, *Terr. Magn.*, **50** (1945), 1.

are obtained as shown in Fig. 5. On the curves in the figure, the actually determined value of $\frac{f_{d=1\,km}}{f_{d=0}}$, $\frac{f_{d=4\,km}}{f_{d=0}}$, and $\frac{f_{d=5\,km}}{f_{d=0}}$ are respectively shown with small circles. Thus we graphically get, as the effective height of the volcano, $h=0.58$, 0.73 and $0.75\,km$ respectively for $d=1$, 4, and $5\,km$.

Now we must examine to what extent the determination of h is affected by the assumption that the anomaly is treated as a distribution on a plane. Since the height above sea level of Volcano Mihara reaches as high as $750\,m$, it would be seriously influenced by the fact that the anomaly is given on the slope if we should adopt a small value of d such as $1\,km$. The effect, however, would become small as d increases. As obtained above, h for $d=1\,km$ seems rather small, while the values for $d=4$ and $5\,km$ nearly agree with each other. Hence, it may be said that the said effect is almost avoided by adopting d several times larger than the topographical height of the volcano. It is not possible, however, to take a very large d because f at such great height becomes practically zero.

Next, we calculate $G_{d=0}$ for $h=750\,m$ by (7) and, taking $\theta=47.°9$, $X_0=0.305$ and $Z_0=0.337\,emu$, J is determined to be $0.037\,emu$.

After all, it is concluded here that the magnetization of a conical body, from the summit to just the sea level, is responsible for the dip anomaly in the neighborhood of Volcano Mihara, while the mean intensity obtained is $0.037\,emu$. The conclusion is just the same with the one obtained in the writer's previous paper[14].

4. Magnetization of various volcanoes in Japan.

Since the method is applicable to conical volcano as tested in section 3, we will examine the magnetization of various volcanoes here. In so far as the writer collect the magnetic data, the results of the magnetic surveys in the neighborhood of Volcano Miyake-sima[4], Volcano Asama[8], and Volcano Sakura-jima[10] surveyed by Minakami, Volcano Omuro by Nagata[6], and Volcano Akagi surveyed by the writer are available, these volcanoes being famous because of their beautiful conical forms. The changes in geomagnetic dip on these volcanoes with the height above sea level or base plane[16] are respectively shown in Figs. 6–10 where

16) The base plane of a volcano is defined from the mean profile curve. It is taken at the height where topography becomes almost flat. As to the volcanic island, the height above sea level is adopted as did in section 3.

the general tendency of increase in dip angle is also shown by the curves in the figures, the curves being determined as quadratic expressions of height as in section 3. The mean profiles of topography are also calculated by the same method as in section 3. The relations

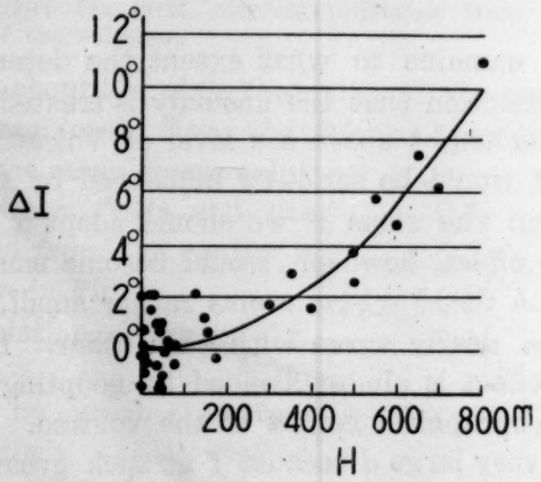

Fig. 6. The relation between dip-anomaly and height on Volcano Miyake-sima.

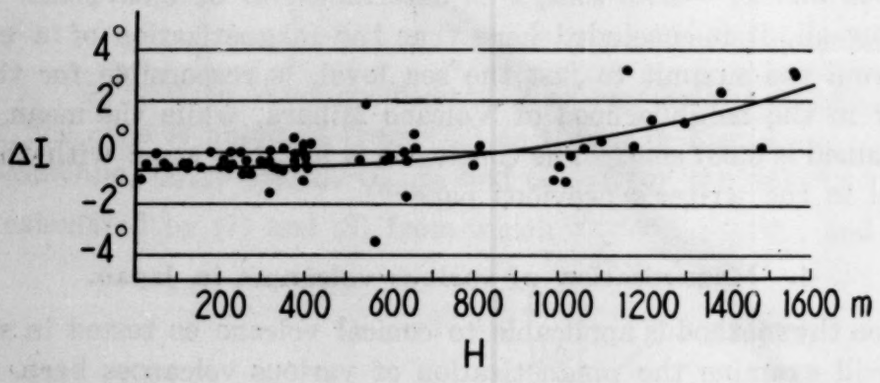

Fig. 7. The relation between dip-anomaly and height on Volcano Asama.

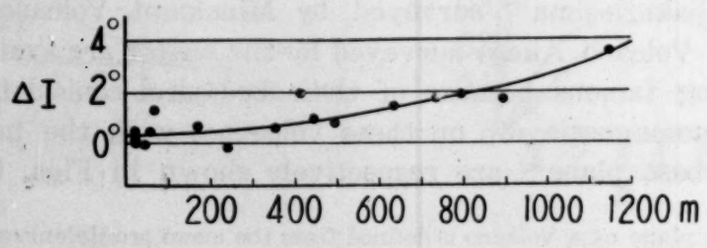

Fig. 8. The relation between dip-anomaly and height on Volcano Sakura-jima.

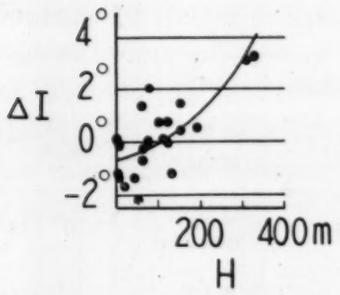

Fig. 9. The relation between dip-anomaly and height on Volcano Omuro.

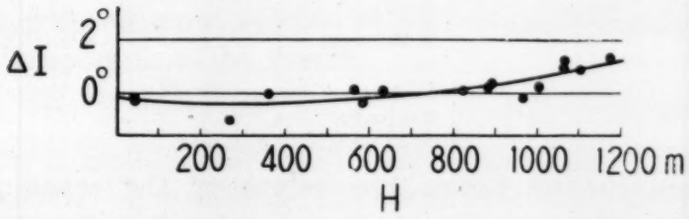

Fig. 10. The relation between dip-anomaly and height on Volcano Akagi.

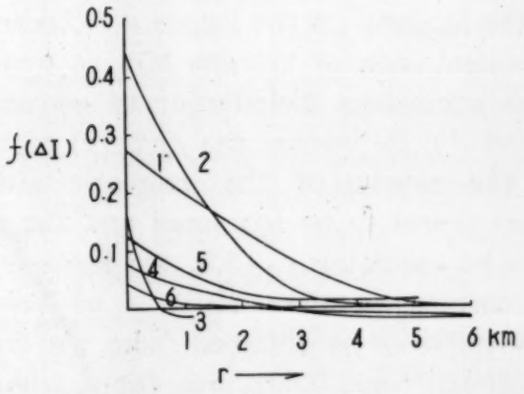

Fig. 11. The relations between and horizontal distance on various volcanoes. 1 Mihara, 2 Miyake-sima, 3 Omuro, 4 Asama, 5 Sakura-jima, 6 Akagi.

between $f(\Delta I)$ and horizontal distance from the centre of the volcano are shown in Fig. 11. From these data the height h of the conical mass that is effective to the dip anomaly and the mean intensity of magnetization J are both determined for respective volcanoes as tabulated in Table I where the specific intensity of natural remanent magnetization J_n experimentally measured and J previously obtained by another investigator are also shown.

Table I. The magnetization of various volcanoes.[17]

Volcano	Rock	Max. height	Survey	h	J	J_n	J by another author
Mihara	basalt	755 *m*	1950 by Rikitake	750*m*	0.037 *emu*	0.016 ~0.036 *emu*	0.068 *emu* by Nagata
Miyake-sima	basalt	813	1940 by Minakami	520	0.052	0.0047 ~0.0224	0.015~0.020 by Minakami
Omuro	basalt	581	1942 by Nagata	270	0.0050	0.0012 ~0.0032	—
Asama	andesite	2532	1937 by Minakami	600	0.0012	0.0013 ~0.0025	0.0022 by Minakami
Sakura-jima	andesite	1230	1939 by Minakami	1250	0.0009	0.0015 ~0.0073	0.0018 by Minakami
Akagi	andesite	1828	1951 by Rikitake	400	0.001	—	—

As revealed in the table, the values of the mean intensity of magnetization J differ considerably from each other for the respectiv volcanoes, while, taking into account the specific intensity of natural remanent magnetization J_n of the rocks composing the volcanoes, we see in general that the larger J_n is the larger J. According to Nagata[12], however, J of the central cone of Volcano Mihara was determined to be 0.0058 *emu* from the anomalous distribution of geomagnetic declination around the crater and J/ρ (ρ denotes the density) of the whole volcano to be 0.027 from the results of the magnetic and torsion balance surveys. The former seems to be too small and the latter, from which we get $J = 0.068$ *emu* by assuming $\rho = 2.5$, too large compared with the writer's value. According to Minakami[4], J of Volcano Miyake-sima amounted to 0.015~0.020 *emu* as obtained from his dip survey. As to Volcano Asama, Minakami[8] got 0.0022 *emu* for J where the anomaly is replaced by the field caused by a rotational ellipsoid of suitable dimension. He[10] also obtained $J = 0.0018$ *emu* for Volcano Sakura-jima. Summing up these earlier studies, we may say that the writer's values of J agree roughly in their order with the ones previously obtained.

As has been pointed out by Nagata[12], the order of J obtained here cannot be explained by the induced magnetism of volcano in geomagnetic field as clarified by the measurements of the magnetic susceptibility of rocks composing these volcanoes.

17) Volcano Mihara, Miyake-sima, Asama and Sakura-jima were active at the time of the surveys, while Omuro and Akagi are Quarternary volcanoes and now are dormant.

The scales of effective mass of volcano as expressed by the values of h are different for respective volcanoes, especially h of Asama is as small as $600\,m$ while, on the contrary, h amounts to more than $1200\,m$ in the case of Sakura-jima. As seen in Figs. 8 and 9, there spreads an extensive area of negative anomaly in dip-angle at the foot of Mt. Asama while we find only the positive anomaly on Volcano Sakura-jima though we cannot measure the anomaly in the sea that surrounds the volcano. The difference in the distribution of anomaly may probably correspond to that in the scale of effective mass determined. However, it is not clear why these differences occur. Since we do not expect, as tested in section 3, any great error of determination, the difference should be ascribed to the structure of volcano though no marked geological evidence for such differences is to be found.

5. Conclusion.

A method of determining simultaneously the mean intensity of magnetization and effective scale of magnetic mass of a volcano from the distribution of anomaly in the earth's magnetic field observed at the place. Applying the method to the results of the magnetic surveys of various volcanoes in Japan, the mean intensity of magnetization is determined, the values agreeing roughly with the experiments on the natural remanent magnetization of rocks composing the volcanoes and the results previously obtained by the analyses of magnetic survey. The effective scales of magnetic mass are also found to differ markedly for respective volcanoes, the difference being probably due to the one in the structure of the volcanoes though we find no marked geological evidences for such differences.

In conclusion, the writer wishes to express his sincere thanks to Miss Y. Hishiyama for her kind assistance. The study was done with the financial aid of the research grant from the Department of Education, and the writer wishes to express his cordial thanks for the grant received.

9. 火山の帶磁

地震研究所 力武常次

從來多くの火山について磁氣測量が實施され，火山附近の地磁氣異常は山體の帶磁に基ずくことが明らかにされた．またその帶磁はほゞ現在の地球磁場と一致していることも知られてきた．そして，磁氣測量の結果より火山の平均の帶磁の强さが求められている．

しかしながら，火山の山體のどの範圍が地磁氣異常に對して有效であるかという點については，山體の規模の定め方がやゝ任意的であるように思われる．本論文に於いては，山體の有效範圍と帶磁の强さを同時に求める方法を考案し，三原山，三宅島火山，大室山，淺間山，櫻島火山および赤城山等の圓錐形の諸火山に應用した結果をのべてある．

まず山體を圓錐で近似し，その圓錐の一樣な帶磁を考える時は，火山頂上の地磁氣要素は直ちに帶磁の强さ J および有效な高さ h の函數として求められる．もし J が岩石試料についての實驗値より知られているとすれば，h は直ちに求められるわけであるが，J の實驗値は多くの場合相當のばらつきを示すので，全體の平均を求めるには別の方法を考えねばならない．

そこで，火山直上のある高さの地磁氣要素と山頂の値との比をとることによつて J を消去する．前者は磁氣測量の結果をつかつて，ポテンシヤル論により求めることが出來る．實際には，測量は同一平面上に於いて行われているのではないから，山體の數倍の高さに於ける値を採用してその影響をさける．このような比は，有效高度とともに變化するが，その曲線を計算によりえがいておいて，その上に實測より計算された値をプロットすることにより，有效高度 h が定められ，從つて J が求まる．

この方法によつて求められた J は從來の研究者の求めた値および岩石の自然殘留磁氣の强さと大體に於いて調和する．h としては，各火山について異つた値が得られたが，その意味については，現在のところ明確でない．なお上記の考察は伏角の測定結果について行われたものである．

10. *Magnetization of the Gabbro from Mt. Tsukuba with Special Relation to the Geomagnetic Anomalies*.*

By Izumi YOKOYAMA,

Earthquake Research Institute.

(Read Nov. 20, 1951.—Received Dec. 20, 1951.)

1. Introduciton.

In August, 1951, a magnetic dip survey was carried out at Mt. Tsukuba by the Earthquake Research Institute with a miniature earth-inductor [1]. The number of surveyed sites reached 20, while the error of each measurment was about ±1 *minute* of arc. The observed values are shown in Table I and plotted in Fig. 2 with an altitude abscissa.

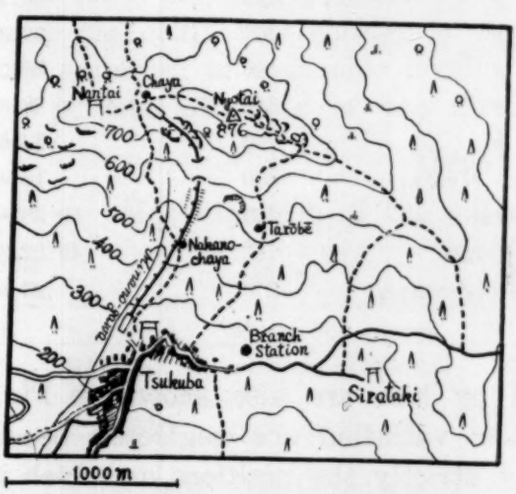

Fig. 1. Topographical map of Mt. Tsukuba.

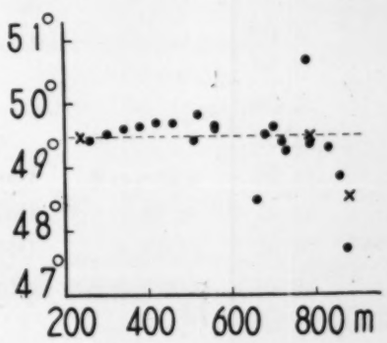

Fig. 2. The distribution of the dip at Mt. Tsukuba. The mark × denotes the values obtained by A. Tanakadate in Dec., 1906.

Looking at the general aspect of the distribution, one notices a conspicuous decrease in the dip-angle above the height of 500 *meters*. Taking into consideration the fact that the dip-angle usually increases with the increase in height on volcanoes, the geomagnetic anomaly found on Mt. Tsukuba, which is not a volcano, appears curious and interesting. As early as in Dec., 1906, A. Tanakadate suggested the unusual magnetization of the rocks near the summits of Mt. Tsukuba performing a survey with

* Communicated by T. RIKITAKE.

1) T. RIKITAKE, *Bull. Earthq. Res. Inst.*, **29** (1951), 147.

Table I.

The observed values of magnetic dip.

Time		Locality		Approximate Altitude	Dip
Aug. 8	10*h*02*m*	ケーブル斜面	slope of the cable way	300 *meters*	49°29.′3
	10 48	仲の茶屋	Naka-no-chaya	520	47.0
	11 32	トンネルと鞍部との中間	between the tunnel and the saddle-point	700	36.1
	11 59	鞍　部	saddle-point	790	20.7
	13 04	男體頂上	summit of Nantai	860	48 49.8
	13 44	女體頂上	summit of Nyotai	875	47 41.7
	14 34	辨慶茶屋	Benkei-chaya	660	48 28.5
	15 04	ハイキング・コース岐路	fork of the hiking-course	560	49 34.2
	15 54	白　瀧	Sirataki	260	24.3
Aug. 9	09 18	ケーブル斜面	slope of the cable-way	340	34.9
	09 32	〃	〃	380	36.9
	09 48	〃	〃	420	40.1
	10 00	〃	〃	460	39.8
	10 20	〃	〃	560	37.2
	10 54	〃	〃	680	28.8
	11 22	〃	〃	730	14.6
	13 32	女體への道	the way to Nyotai	830	16.4
	14 41	大黒岩	Daikoku-iwa	780	50 38.8
	15 01	出舟入舟	Debune-iribune	720	49 22.8
	16 40	太郎兵衞茶屋跡	site of Tarobē-chaya	510	23.6

a dip-circle. The values observed by him are also shown in Fig. 2 where the corrections for the secular variation are neglected because it is almost impossible to identify strictly the positions on which the observations were made. But these old measurements seem to agree with the results of our present survey.

From the standpoint of geology, Mt. Tsukuba is composed of various gabbroic rocks surrounded with granitic ones and the relation between them is not distinct because the outcrop has not been found about the boundary. According to H. Tsuya[2] who made a field survey at the time of the land-slide of July, 1938, the boundary is thought to coincide approximately with the contour line of 500 *meters*. Referring to these facts, samples of rocks were taken at eight localities from the

2) H. TSUYA, *Bull. Earthq. Res. Inst.*, **17** (1939), 517.

midway up to the top of the mountain in order to study the magnetization of the rocks which may furnish some clues to the interpretation of the geomagnetic anomaly.

2. Magnetization of the gabbro.

A 2-*cm* cube was cut from each oriented sample and its magnetization was measured with an induction-type magnetometer[3] which was lent for use by the Geophysical Institute of Tokyo University. It operates on the principle that the faint residual magnetism of a rock is sufficient to induce an alternating voltage in a signal pick-up coil when the specimen is rotated close to the coil. This voltage is electronically amplified to a usuable level. The errors in determinations of the direction

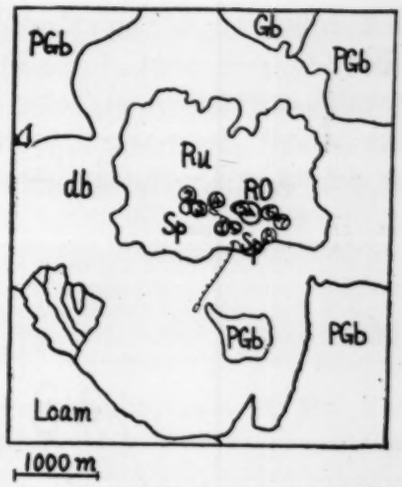

Fig. 3. Geological map of Mt. Tsukuba.

Legend

db: Detritus
Gb: Biotite-granite
PGb: Porphyritic biotite-granite
RO: Olivine-gabbro
Sp: Spessartite
Ru: Uralite-gabbro

Table II.

Magnetization of the gabbro from Mt. Tsukuba.

Sample No.	Locality		Decli.	Dip.	Intensity in 10^{-4} *c.g.s.* per *cc*	Rock
1	トンネル上	above the tunnel	241°E	− 3°	12.0	Uralite-gabbro
2	男體頂上	summit of Nantai	46	11	6.3	Norite
3	立身石附近	near Rissin-seki	135	−10	34.0	Amphibolite (so-called spessartite)
4	五軒茶屋附近	near Gokenjaya			order of 10^{-6}	〃
5	女體頂上	summit of Nyotai	253	−12	7.4	Leucoratic part of olivine-gabbro
6	大黒岩	Daikoku-iwa	321	−40	120.0	Amphibolite (so-called spessartite)
7	出舟入舟	Debune-iribune	54	− 8	0.7	Leucocratic part of the uralite-gabbro
8	辨慶七戻	Benkei-nanamodori	25	65	18.0	〃

3) T. NAGATA, K. AKASI and T. RIKITAKE, *Bull. Earthq. Res. Inst.*, **21** (1943), 276.

and intensity of polarization of the samples are respectively $\pm 5°$ and about 5 per cent depending on the intensity of magnetization. The results are shown in Table II. In nomenclature of the rock specimens, the writer owes much to R. Morimoto. The directions are represented as points in the lower hemisphere of the Schmidt equal-area projection[4]

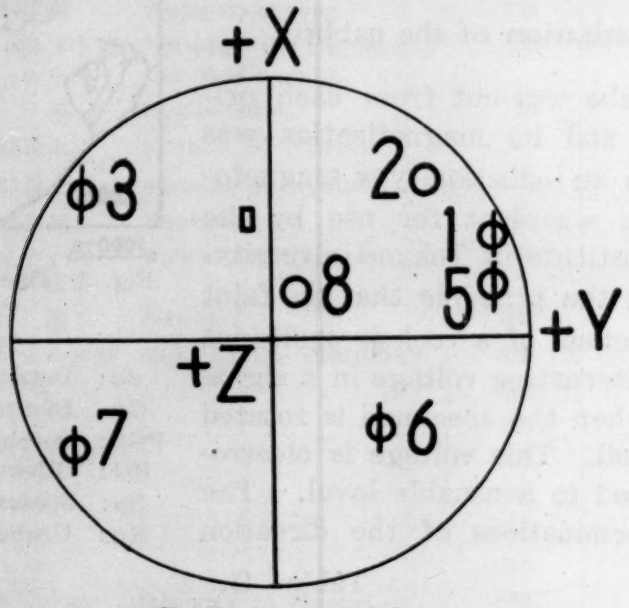

□: Earth's present field
○: North seeking magnetization
Φ: South seeking magnetization

Fig. 4. Equal area plot of magnetization of rock samples.

(Fig. 4). The anomalously intense magnetization of sample No. 6 (Table II) seems to correspond to the large value of the dip-angle at Daikoku-iwa (780 *meters* altitude).

Taking into account the fact that Mt. Tsukuba stands at the edge of Kwanto-plain, we may surmize that the summits have been struck by lightnings and the rocks there have locally magnetized very abnormally against the earth's magnetic field. Therefore, samples No. 2 (the summit of Nantai), No. 6 (Daikoku-iwa) and No. 7 (Debune-iribune) do not necessarily agree with the general aspect of magnetization of the mountain-body. Moreover, we cannot assert that the gabbroic rocks of Mt. Tsukuba have not been influenced by any thermal action of the surrounding granitic rocks. Geological age of the granitic rocks, host rock of the gabbro, is post-Permo-Carboniferous and perhaps, pre-

4) J. W. GRAHAM, *Journ. Geophys. Res.*, **54** (1949), 162.

Miocene. Thus it is rather difficult to touch on the Palaeomagnetism directly from the above data. Though it will be of great interest to study the Palaeomagnetism of such an old geological age, a good number of samples will be needed for that purpose, so the discussion concerning the subject will be made after we measure the magnetization of much more samples from Mt. Tsukuba.

3. Interpretation of the anomalous distribution of magnetic dip-angle.

For studying the distribution of the magnetic dip-angle at Mt. Tsukuba, we have luckily a slope in approximately the NS-direction where formerly the rails of cable-way were laid. The results of the observations along this slope are shown in Fig. 5. The normal value for this district (49°25.'0) is decided from the values at the Branch Station of Earthquake Research Institute at Tsukuba village and the Kakioka Magnetic Observatory. Though observations were impossible to carry out because of a tunnel at about 600 *meters* altitude, a decrease above the height of 500 *meters* is remarkable as already mentioned.

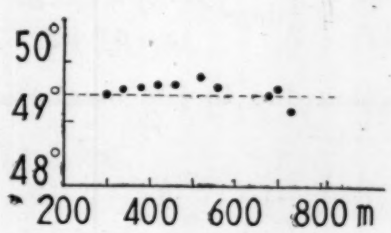

Fig. 5. The distribution of the dip along the slope of the disused cable-way.

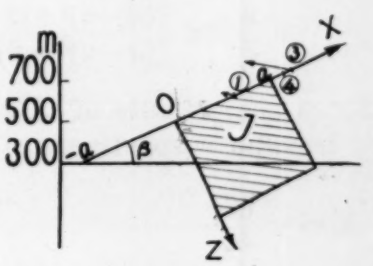

Fig. 6. The schematic model of the slope of the disused cable-way.

In order to interpret the anomaly, we assume a two-dimensional model as shown in Fig. 6. The slope of the disused cable-way is represented schematically cut by the plane in NS-direction. Reflecting the geological knowledge, the contact plane of gabbro and granite is assumed to be situated at 500 *meters* altitude and to be perpendicular to the slope. And the depth of the block of gabbro is assumed to be half of the length of the slope for conveniences' sake. To decide the direction of magnetization J, the writer referred to those of sample No. 1, 3 and 4 which are regarded to be on the NS-direction plane and

to keep clear of lightnings effects. Thus the block of gabbroic rocks is assumed to be uniformly magnetized (its intensity J) upwards about 7° contrariwise to the present geomagnetic field.

The magnetic potential due to the uniform magnetization of the said mass is given by

$$\phi=2J_z\int_0^a\int_0^b\frac{z-\zeta}{(x-\xi)^2+(z-\zeta)^2}d\xi d\zeta+2J_x\int_0^a\int_0^b\frac{x-\xi}{(x-\xi)^2+(z-\zeta)^2}d\xi d\zeta. \quad (1)$$

where J_x and J_z denote the components of the magnetization respectively in X and Z-direction.

The first term of the righthand side of (1) becomes

$$\begin{aligned}\phi_1&=2J_z\int_0^a\int_0^b\frac{z-\zeta}{(x-\xi)^2+(z-\zeta)^2}d\xi d\zeta\\&=-2J_z\int_0^b(z-\zeta)d\xi\int_x^{x-a}\frac{d\xi'}{\xi'^2+(z-\zeta)^2}\\&=2J_z\int_0^b\left(\cot^{-1}\frac{z-\zeta}{x}-\cot^{-1}\frac{z-\zeta}{x-a}\right)d\zeta\\&=2J_z\left[(z-b)\left(\tan^{-1}\frac{x-a}{z-b}-\tan^{-1}\frac{x}{z-b}\right)-z\left(\tan^{-1}\frac{x-a}{z}-\tan^{-1}\frac{x}{z}\right)\right.\\&\quad\left.+\frac{x}{2}\log\frac{\{(x-a)^2+(z-b)^2\}(x^2+z^2)}{\{(x-a)^2+z^2\}\{x^2+(z-b)^2\}}-\frac{a}{2}\log\frac{(x-a)^2+(z-b)^2}{(x-a)^2+z^2}\right]. \quad (2)\end{aligned}$$

The force components of X and Z-direction due to the magnetic potential ϕ_1 become respectively

$$\begin{aligned}X_1&=-\frac{\partial\phi_1}{\partial x}\\&=J_z\log\frac{\{(x-a)^2+z^2\}\{x^2+(z-b)^2\}}{(x^2+z^2)\{(x-a)^2+(z-b)^2\}}. \quad \cdots\cdots\cdots\cdots\cdots\cdots\cdots\cdots(3)\end{aligned}$$

$$\begin{aligned}Z_1&=-\frac{\partial\phi_1}{\partial z}\\&=2J_z\left(\tan^{-1}\frac{x}{z-b}-\tan^{-1}\frac{x-a}{z-b}+\tan^{-1}\frac{x-a}{z}-\tan^{-1}\frac{x}{z}\right). \quad \cdots\cdots\cdots(4)\end{aligned}$$

Similarly, we have

$$\begin{aligned}\phi_2&=2J_x\int_0^a\int_0^b\frac{x-\xi}{(x-\xi)^2+(z-\zeta)^2}d\xi d\zeta\\&=2J_x\left[(x-a)\left(\tan^{-1}\frac{z-b}{x-a}-\tan^{-1}\frac{z}{x-a}\right)-x\left(\tan^{-1}\frac{z-b}{x}-\tan^{-1}\frac{z}{x}\right)\right.\end{aligned}$$

$$+\frac{z}{2}\log\frac{\{(z-b)^2+(x-a)^2\}(x^2+z^2)}{\{(z-b)^2+x^2\}\{z^2+(x-a)^2\}}-\frac{b}{2}\log\frac{(z-b)^2+(x-a)^2}{(z-b)^2+x^2}\Bigg] \quad ..(5)$$

$$X_2=2J_x\left(\tan^{-1}\frac{z-b}{x}-\tan^{-1}\frac{z-b}{x-a}+\tan^{-1}\frac{z}{x-a}-\tan^{-1}\frac{z}{x}\right). \quad .....(6)$$

$$Z_2=J_x\log\frac{\{(x-a)^2+z^2\}\{x^2+(z-b)^2\}}{(x^2+z^2)\{(x-a)^2+(z-b)^2\}}. \quad .....(7)$$

Taking $a=b$ and neglecting z compared to a and b, we get

$$X_1=J_z\log\frac{\left\{\left(\frac{x}{a}-1\right)^2+\left(\frac{z}{a}\right)^2\right\}\left\{\left(\frac{x}{a}\right)^2+1\right\}}{\left\{\left(\frac{x}{a}\right)^2+\left(\frac{z}{a}\right)^2\right\}\left\{\left(\frac{x}{a}-1\right)^2+1\right\}}. \quad .....(8)$$

$$Z_1=2J_z\left\{\tan^{-1}\frac{-x}{a}-\tan^{-1}\left(1-\frac{x}{a}\right)+\tan^{-1}\left(\frac{\frac{x}{a}-1}{\frac{z}{a}}\right)-\tan^{-1}\frac{x}{z}\right\} \quad ....(9)$$

$$X_2=2J_x\left\{\cot^{-1}\frac{-x}{a}-\cot^{-1}\left(1-\frac{x}{a}\right)+\cot^{-1}\left(\frac{\frac{x}{a}-1}{\frac{z}{a}}\right)-\cot^{-1}\frac{x}{z}\right\} \quad .....(10)$$

$$Z_2=J_x\log\frac{\left\{\left(\frac{x}{a}-1\right)^2+\left(\frac{z}{a}\right)^2\right\}\left\{\left(\frac{x}{a}\right)^2+1\right\}}{\left\{\left(\frac{x}{a}\right)^2+\left(\frac{z}{a}\right)^2\right\}\left\{\left(\frac{x}{a}-1\right)^2+1\right.} \quad .....(11)$$

and

$$J_x=-J\cos\alpha\,, \qquad J_z=-J\sin\alpha.$$

where α denotes the direction of the magnetization J measuring from the slope. The magnetic field caused by the magnetization is obtained as follows;

$$\Delta H=(X_1+X_2)\cos\beta+(Z_1+Z_2)\sin\beta. \quad .....(12)$$

$$\Delta Z=-(X_1+X_2)\sin\beta+(Z_1+Z_2)\cos\beta. \quad .....(13)$$

where β denotes the inclination of the slope to the level. Now, we consider the following function

$$f(\Delta I)=\frac{\tan(I_0+\Delta I)-\tan I_0}{\tan I_0}\cdot\frac{\Delta Z}{Z_0}-\frac{\Delta H}{H_0}. \quad \cdots\cdots\cdots\cdots(14)$$

For simplicity's sake, we take

$$Z_0 = H_0 = 0.3\,\Gamma$$

and taking $\alpha=32°$ and $\beta=25°$, the function $f(\Delta I)$ becomes

$$f=\frac{J}{0.3}\Bigg[0.29\log\frac{\left\{\left(\frac{x}{a}-1\right)^2+\left(\frac{z}{a}\right)^2\right\}\left\{\left(\frac{x}{a}\right)^2+1\right\}}{\left\{\left(\frac{x}{a}-1\right)^2+1\right\}\left\{\left(\frac{x}{a}\right)^2+\left(\frac{z}{a}\right)^2\right\}}$$

$$+2.26\left\{\tan^{-1}\frac{\frac{z}{a}}{1-\frac{x}{a}}-\tan^{-1}\frac{1}{1-\frac{x}{a}}+\tan^{-1}\frac{a}{x}-\tan^{-1}\frac{z}{x}\right\}$$

$$-0.52\left\{\cot^{-1}\frac{\frac{z}{a}}{1-\frac{x}{a}}-\cot^{-1}\frac{1}{1-\frac{x}{a}}+\cot^{-1}\frac{a}{x}-\cot^{-1}\frac{z}{x}\right\}\Bigg]. \quad (15)$$

in the end. Their numerical values for $a=1\,km$, $z=-1\,m$ and $x=-1\sim$

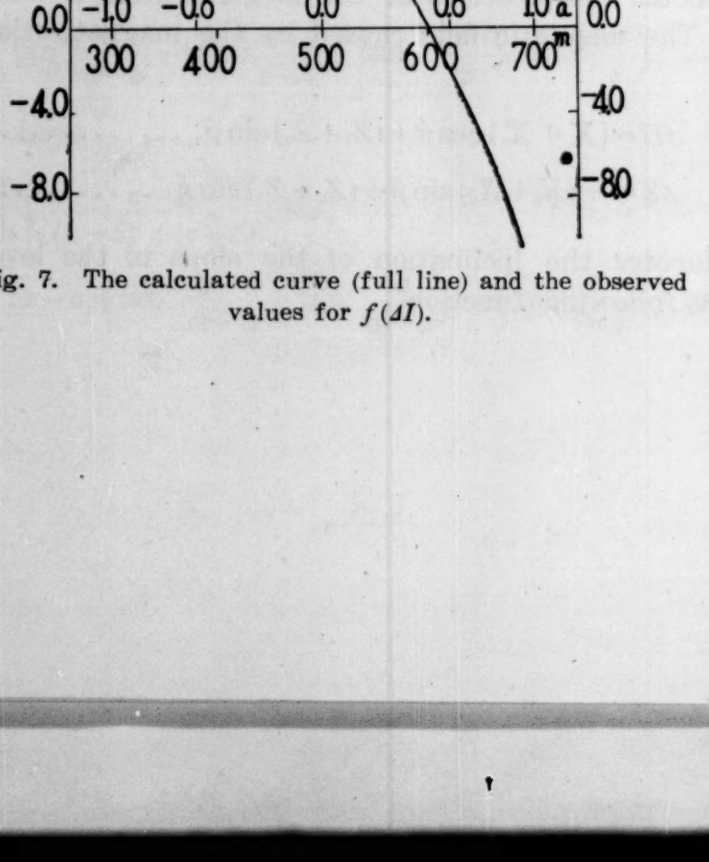

Fig. 7. The calculated curve (full line) and the observed values for $f(\Delta I)$.

$+1\,km$ are represented in Fig. 7. As seen in the figure, the decrease at about 500 meters altitude seems to be explained roughly, and the curve theoretically obtained covers approximately the points plotted as the results of the observations if J is assumed to be of the order of 10^{-3} *c.g.s.* per *cc.*

4. Conclusion.

The anomalous distribution of the magnetic dip at Mt. Tsukuba seems to be interpreted roughly with assumptions reasonable from the view-points of geology and geophysics. The discussion concerning the Palaeomagnetism at Mt. Tsukuba will be made after we measure the magnetization of a number of rocks.

In the end, the writer wishes to express his sincere appreciation to Dr. T. Rikitake for his helpful advices. The induction-type magnetometer became available through the courtesy of the Geophysical Institute of Tokyo University and the writer's hearty thanks are especially due to Dr. T. Nagata. The writer owes the geological knowledge about Mt. Tsukuba to Prof. H. Tsuya, Prof. T. Ichimura, and Ass. Prof. R. Morimoto, to whom the writer's cordial thanks are also due.

---

10. 筑波山斑糲岩の帶磁と地磁氣異常

地震研究所 横 山 泉

1951 年 8 月，小型地磁氣感應儀を用いて筑波山の地磁氣伏角測定が實施された．その高度分布を調べると，大體 500 m を境として伏角が減少するという著しい異常を示す．これを說明する鍵として，8 ケの岩石試料を採取して來て，その帶磁の强さと方向とを電磁誘導型磁力計で測定した．その結果および地質學的資料を參考として妥當と思われる模型を考え，それによる伏角異常を求めると，上記觀測結果を定性的にも定量的にも大體說明出來るようである．筑波山斑糲岩を古地磁氣學的に論ずることは，岩石試料の數が少ないので，より多くの試料の採取および測定をまつて行う豫定である．

---

11. 物の倒れた方向から震央を求めること

地震研究所　佐　藤　泰　夫

(昭和26年6月19日発表——昭和26年12月20日受理)

1. 序　言

震央を求める方法は，現在迄数多く考案されてゐるけれども，これを大きくわける時は二つに区分することができると思ふ．その第一は観測点からの距離を用ゐるもので，走時曲線をはじめてして，$P\sim S$ 時間，更に又震度分布によつて震央を求めるもの迄，いづれもこの中に入れることができよう[1]．これに対して，他の一つは，震央の在る方向をもととして定めるものである．すでに古くからこの方法もしばしば用ゐられ，かべに出来たわれ目から震源を推定したり[2]，物の倒れた方向から震央を求めること[3]などがこころみられて来た．これらは古い教科書にはいづれものせられてゐるが[4]，今日では，前者に比して，もはや実用的価値は乏しいと言はねばならない．しかし，地震動の起された，といふ意味の震源ではなく，地震に伴ふ地なりの中心を求めたり，或は光りものの源をしらべようとする場合などには，依然としてこの方法も多小の意味をもつてゐると思はれる．現に長野地震に際して岸上，永田，宮村三氏によつて行はれた調査にも[5]，鳥取地震の場合の発光源の調査にも[6]，更に最近の数多くの大地震に伴つた地鳴りの音源を求める通信調査にも[7]，この原理は適用されて一応の効果をあげてゐるようである．

---

1) 大森房吉　地震学講話　第8章．
松沢武雄　地震　第4章
A. IMAMURA *Theoretical and Applied Seismology*, (1937), Chap. XI. 等

2) この考へは Mallet によるものである
W. H. HOBBS, *Earthquakes* (1907), p. 16.
C. DAVISON, *A Manual of Seismology*, Cambridge (1921), §133.
このやうな古典的方法の解説は Davison の本にくわしい

3) 大森房吉「煉瓦柱破壊及び柱状物体転倒に関する調査」震災予防調査会報告 **28** (1899), 4.「明治27年6月20日　東京地震の調査」，同上 71.「明治24年10月28日濃尾大地震に関する調査」，同上 79.　猶，前掲 Davison の書物 §127 参照

4) 前掲 1), 2).　猶，J. MILNE, *Seismology* (1898), p. 40 を参照

5) 岸上多彦・永田武・宮村攝三　「昭和16年7月15日長野地震の統計的調査」地震研究所彙報 **19** (1941), 628.

6) 表俊一郎「昭和18年3月4日鳥取地震調査報告」地震研究所彙報 **21** (1943), 435.
西毛晶夫・高木聖・山之上昭和「昭和18年3月4日及5日の鳥取地震に伴ふ発光現象」験震時報 **14** (1948), 4.

7) 佐藤泰夫「地なりの方向性について」音響 **2** (1948), 16.　地震，[ii], **1** (1948), 4.

2. 従来の方法

そこで，従来とられて来たこの方法をふりかへつてみると，あまり古いものは別として，これ又二種類が在るように思はれる．一つは岸上ら三氏の考へられたもので，震央（音源，発光源等の場合もあるが，簡単に震央とかくことにする）をむくと考へられる矢を延長した時，交点が密に分布する場所を以て求める地点となすものである．これは巧みな方法であつて，実際上の手つづきからみても興味ふかいものであるが，確率論的な基礎を与へたり，誤差の計算を行はうとすると，極度の困難にうちあたるのである．もう一つの方法は増山氏の創案にかかるものであつて[8]，ほぼ次のやうな原理にもとづく．

今3本の直線

$$a_k x+b_k y+1=0 \quad (k=1,\ 2,\ 3) \qquad \cdots\cdots (2.1)$$

があつた時，これらが1点に会する条件

$$\begin{vmatrix} a_1 b_1\ 1 \\ a_2 b_2\ 1 \\ a_3 b_3\ 1 \end{vmatrix} =0 \qquad \cdots\cdots (2.2)$$

は，(2.1) 式の中の x, y の係数 (a_k, b_k) を坐標としてもつ3点 $P_k(k=1, 2, 3)$ が1直線上にある条件と全く同等である．従つて多数の直線

$$a_k x+b_k y+1=0 \quad (k=1,\ 2,\ \cdots\cdots n)$$

が1点——この点こそまさに震央とみなされる——に会する条件は，多数の点 (a_k, b_k) $(k=1,\ 2,\ \cdots\cdots n)$ が1直線上にある条件でおきかへて考へることができる．この方法は，射影幾何学の“対応の原理”を思ひ起す時，ごく自然に考へられる方法であり，極めて巧妙なやり方であるけれども，このようにしてきめられた震央の位置は，坐標変換に対して，不変量ではないといふ欠陥をもつてゐる[9]．猶その他にも我々がこれを実際に適用しようとすると，不便を感ずる点がないわけではない[10]．

そこで我々は，実際に使ひやすい公式を以下に導いてみようと思ふ．

---

8) 気象学会において発表された．

9) n 個の直線の方程式を

$$a_k x+b_k y+1=0 \quad (k=1,\ 2,\ 3,\ \cdots\cdots n) \qquad \cdots\cdots (2.1)'$$

で表はす．この係数を坐標にもつ点を $P_k(a_k, b_k)$ とする時，これらにもつともよく適合する直線

$$Ax+y+B=0 \qquad \cdots\cdots (2.3)$$

は，最小二乗法によれば次のやうに定められる。第1図において

$$H_k=b_k-Y_k, \quad Y_k=-Aa_k-B$$

従つて

$$\sum H_k^2 \ ; \ min.$$

とする直線は

$$\frac{\partial}{\partial A}\sum H_k^2=0 \qquad \frac{\partial}{\partial B}\sum H_k^2=0 \qquad \cdots\cdots (2.4)$$

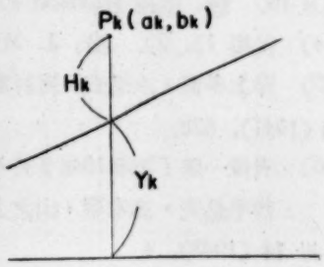

第 1 図

3. 新しい方法

我々に最初与へられる材料は，初動分布のやうに，観測点の位置と，直角に交る二方向のベクトルの成分（もしくは物の倒れた場合のやうに倒れた方向を示す矢印）である．今観測点の坐標を $P_k(x_k, y_k)$，その点で観測されたベクトルを $r_k(u_k, v_k)$ とする．r_k を含む直線 L_k の方程式は（第3図参照）

即ち

$$\begin{cases} A\sum a_k^2+B\sum a_k+\sum a_kb_k=0 \\ A\sum a_k+B\cdot n+\sum b_k=0 \end{cases}$$

これから定まる A, B は

$$A=\begin{vmatrix}[a1] & [ab]\\ n & [b1]\end{vmatrix}\Big/\begin{vmatrix}[aa] & [a1]\\ [a1] & n\end{vmatrix}$$
$$B=\begin{vmatrix}[ab] & [aa]\\ [b1] & [a1]\end{vmatrix}\Big/\begin{vmatrix}[aa] & [a1]\\ [a1] & n\end{vmatrix} \qquad \cdots\cdots(2.5)$$

但し $[ab]\equiv\sum a_kb_k$ 等．

これによつて直線と点とを交換した場合の直線が定められたわけである．

一般に，点(a_k, b_k) は直線 $a_kx+b_ky+1=0$ に対応するのであるから，逆に直線 $Ax+y+B=0$ は点 $x=A/B$, $y=1/B$ に対応するはづである．従つて (2.5) の A, B を代入すれば，震央の坐標 (X_0, Y_0) は

$$\begin{cases} X_0=\begin{vmatrix}[a1] & [ab]\\ n & [b1]\end{vmatrix}\Big/\begin{vmatrix}[ab] & [aa]\\ [b1] & [a1]\end{vmatrix} \\ Y_0=\begin{vmatrix}[aa] & [a1]\\ [a1] & n\end{vmatrix}\Big/\begin{vmatrix}[ab] & [aa]\\ [b1] & [a1]\end{vmatrix} \end{cases} \qquad \cdots\cdots(2.6)$$

で与へられる．

かうして定められた X_0, Y_0 が不変量かどうかは一目ではわからないから，一つの例をとつて考へてみる．第2図に示す3直線

$$x=1,\quad y=1,\quad x+y=1$$

があつた時，これから定められる点を求めてみよう．標準の形に方程式をかけば

$$\begin{cases} -x+1=0 \\ -y+1=0 \\ -x-y+1=0 \end{cases} \qquad \cdots\cdots(2.7)$$

であるから，公式 (2.4) によつて，$[aa]$, $[a1]$, $[ab]$, $[b1]$, n 等の値を求めて (2.6) に代入すれば

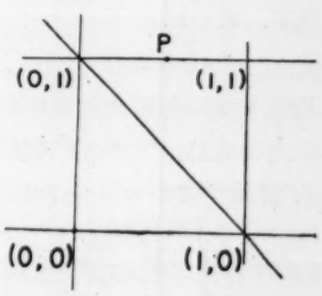

第 2 図

$$\begin{cases} X_0=1/2 \\ Y_0=1 \end{cases} \qquad \cdots\cdots(2.8)$$

従つて求める点は図の P となる．これが不変量でないことはあきらかであらう．

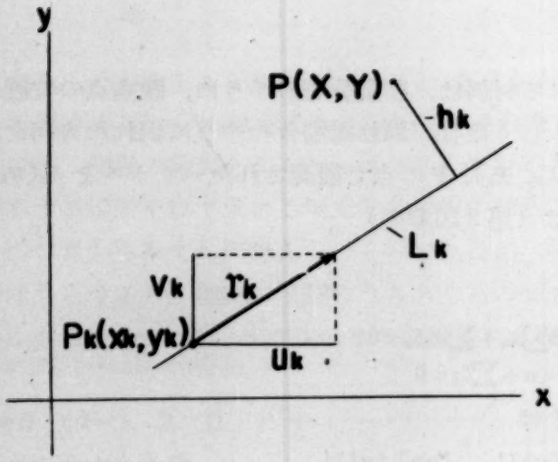

第 3 図

$$\begin{vmatrix} x & y & 1 \\ x_k & y_k & 1 \\ x_k+u_k, & y_k+v_k & 1 \end{vmatrix}=0 \quad \cdots\cdots(3.1)$$

この直線に点 $P(X, Y)$ からひいた垂線の長さ h_k は

$$h_k^2=\left\{\left(Y-X\frac{v_k}{u_k}\right)-\left(y_k-x_k\frac{v_k}{u_k}\right)\right\}^2\Big/\left\{1+\left(\frac{v_k}{u_k}\right)^2\right\} \quad \cdots\cdots(3.2)$$

従つて L_k に到る距離の二乗の和を極小にするやうな一点 $P(X, Y)$ の坐標は

$$\frac{\partial}{\partial X}\sum h_k^2=0, \quad \frac{\partial}{\partial Y}\sum h_k^2=0 \quad \cdots\cdots(3.3)$$

によつて与へられる．これは又かきかへれば

$$\begin{cases} -X\left[\frac{vv}{r^2}\right]+Y\left[\frac{uv}{r^2}\right]=-\left[x\frac{vv}{r^2}\right]+\left[y\frac{uv}{r^2}\right] \\ -X\left[\frac{uv}{r^2}\right]+Y\left[\frac{uu}{r^2}\right]=-\left[x\frac{uv}{r^2}\right]+\left[y\frac{uu}{r^2}\right] \end{cases} \quad \cdots\cdots(3.4)$$

となる．ここに

$$r_k=|\mathfrak{r}_k|$$

このやうにしてきめられた点 P が坐標変換に対して不変であることはいふ迄もない．

又上の式は，すべての観測が等しいウエイトをもつとしたが，各観測にベクトルの長さ r_k に比例するウエイトをつければ，

$$\begin{cases} -X\left[\frac{vv}{r}\right]+Y\left[\frac{uv}{r}\right]=-\left[x\frac{vv}{r}\right]+\left[y\frac{uv}{r}\right] \\ -X\left[\frac{uv}{r}\right]+Y\left[\frac{uu}{r}\right]=-\left[x\frac{uv}{r}\right]+\left[y\frac{uu}{r}\right] \end{cases} \quad \cdots\cdots(3.4)$$

又 r_k^2 に比例するウエイトをつければ

$$\begin{cases} -X[vv]+Y[uv]=-[xvv]+[yuv] \\ -X[uv]+Y[uu]=-[xuv]+[yvv] \end{cases} \quad \cdots\cdots(3.5)$$

となる.

どのやうなウエイトをつけて計算すべきかは，個々の問題について考へるべきことであるかもしれないが，一般に，震央からへだたつた場所の観測は，震央決定に関して非常に大きな影響をもつが[11]，これに反して震央附近の観測はその影響が極めて小さい．所が，方向決定の精度はどちらかといふと後者の方がよい場合が多い．従つて近くの観測を有効につかふためには近くのものに大きなウエイトを与へるのがよいことになり，それには r_k 又は r_k^2 に比例したウエイトを与へるのなどは一つの方法と思はれる[12]．しかも式(3.5)は形ももつとも簡単で便利であろう[13].

4. 應 用 例

以上の所論を実際に応用した例を次に一つ示す.

岸上，永田，宮村三氏によつて行はれた長野地震の統計的調査については，前にもふれたが[14]，これは，此の種の調査として極めて完全なものであつて，今日まで殆んど匹敵しうるものを見ない程であるから，その中にあげられてゐる，墓石の倒れた方向に関する資料を例にとつて，計算を行つてみる.

くわしい数値も（上記論文第Ⅲ表第一調和項の欄にある a_1, b_1 をわれわれの u_k, v_k としてそのまま採用した），説明図も（下記第4図は同論文の第3図である，従つて図中の矢印は墓石の倒れた方向を示すとみてよい）原論文にあるから，ここでは単に得られた結果の点を記入することにとどめる.

第4図において

A 点： すべての測定点のウエイトを等しくとつて得られた結果

B 点： ベクトルの大きさに比例するウエイトをつけて得られた結果

C 点： ベクトルの大きさの二乗に比例するウエイトをつけて得られた結果

を示す．なほ参考までに，中央気象台発表の震央[15](D 点)，および，さきに筆者が地なりのきこえて来た方向を用ゐてきめたもの[16](E 点)——不完全ではあるが——を示す.

---

10) もう一つの具合のわるい点あをげるなら，一般に原点を通る直線は $ax+by+1=0$ の形にかくことが出来ないので，もしこのような直線が一つでもあると解を求めることは不可能となる.

11) このことは最初にあげた震央距離を用ゐる方法と事情が逆になつてゐる.

12) 初動方向を資料としてつかふ時などは，震央附近のベクトルは大きいのが普通であるから，以上のことがなりたつが，物の倒れた場合のやうにウエイトをつけることが困難な現象も少くない.

13) 我我と類似の問題として，平面上に点 $Q_k(k=1, 2, \cdots\cdots n)$ が存在する時，一直線 L をひいて，Q_k より L に至る距離 η_k の二乗の和を最小ならしめる，という問題がある.

14) 前掲 5).

15) 138°14′E, 36°42′N.

16) 前掲 7).

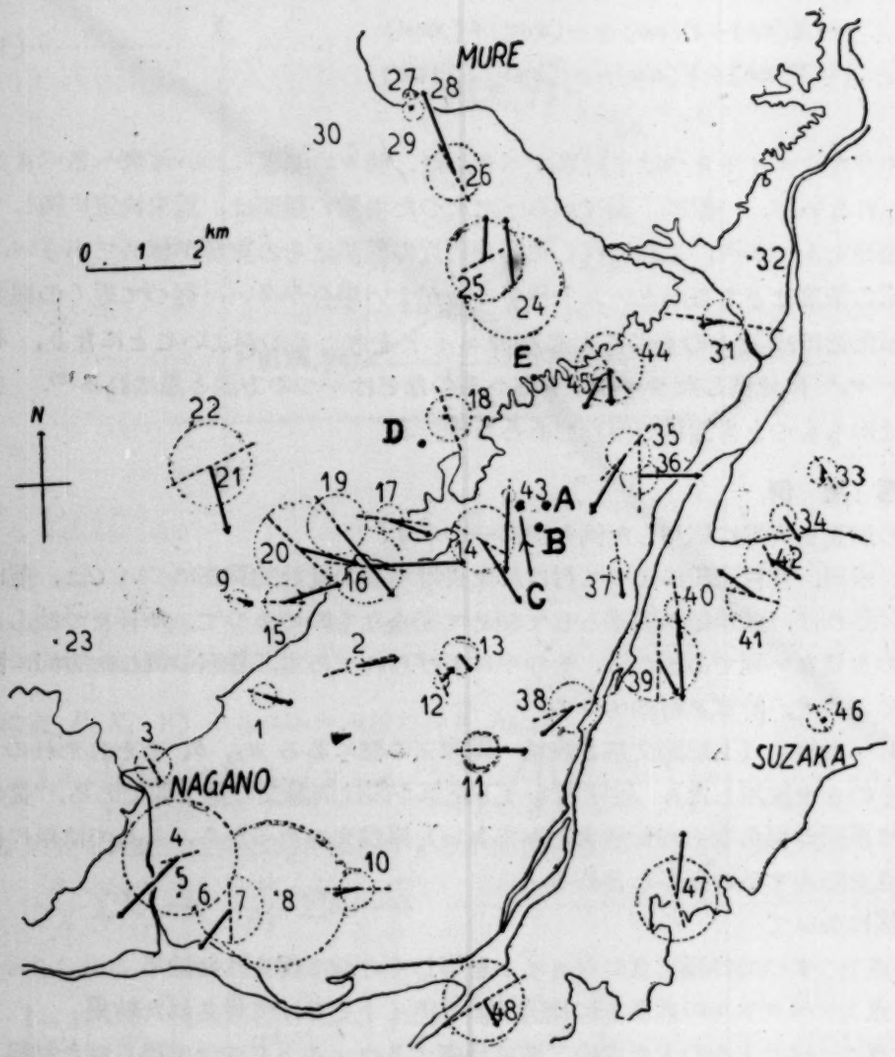

第 4 図

最後に，A. B. C 3 点の決定にあたつてえられた標準偏差をしめせば次のとほりである．

$$\text{A 点：}\begin{cases}\sigma_x=0.56\ km\\ \sigma_y=0.56\ km\end{cases}$$

$$\text{B 点：}\begin{cases}\sigma_x=0.53\ km\\ \sigma_y=0.59\ km\end{cases}\qquad\cdots\cdots(4.1)$$

$$\text{C 点：}\begin{cases}\sigma_x=0.39\ km\\ \sigma_y=0.50\ km\end{cases}$$

x は東西方向，y は南北方向をあらはす．

資料をつかはせていただき，御指導をたまはつた岸上・永田・宮村三先生に厚く御礼申上げる．

11. *Determination of Epicentre by means of the Directions of Overturning.*

By Yasuo Satô,
Earthquake Research Institute.

In order to determine the position of an epicentre, we can employ a number of methods, which may be briefly classified in two groups. One uses the distance between the epicentre and observation points, and the other utilizes the bearings which are expected to show the direction of the epicentre[2), 3), 4)].

First, assume a vector $\mathfrak{r}_k$ at a point $P_k(x_k, y_k)\,(k=1, 2, \ldots, n)$, then the equation of a straight line L_k which is determined by $\mathfrak{r}_k$ is

$$\begin{vmatrix} x & y & 1 \\ x_k & y_k & 1 \\ x_k+u_k, & y_k+v_k & 1 \end{vmatrix} = 0 \quad \ldots\ldots\ldots\ldots (3.1)$$

If we assume a point $P(X, Y)$, then the distance h_k between P and L_k is

$$h_k^2 = \left\{\left(Y - X\frac{v_k}{u_k}\right) - \left(y_k - x_k\frac{v_k}{u_k}\right)\right\}^2 \Big/ \left\{1+\left(\frac{v_k}{u_k}\right)^2\right\} \quad \ldots\ldots\ldots (3.2)$$

Now, we will determine a point P which statisfies the condition

$$\sum_k h_k^2 : \text{ minimum},$$

then the point may be regarded as the centre of the said vectors $\mathfrak{r}_k$.

The equations to determine X, Y are

$$\begin{cases} -X\left[\frac{vv}{r^2}\right] + Y\left[\frac{uv}{r^2}\right] = -\left[x\frac{vv}{r^2}\right] + \left[y\frac{uv}{r^2}\right] \\ -X\left[\frac{uv}{r^2}\right] + Y\left[\frac{uu}{r^2}\right] = -\left[x\frac{uv}{r^2}\right] + \left[y\frac{uu}{r^2}\right] \end{cases} \quad \ldots\ldots\ldots (3.3)$$

in which $r_k \equiv |\mathfrak{r}_k|$.

If the reliability of every observation is weighted according to the absolute value of observed vector $\mathfrak{r}_k$, then the equation becomes

$$\begin{cases} -X\left[\frac{vv}{r}\right] + Y\left[\frac{uv}{r}\right] = -\left[x\frac{vv}{r}\right] + \left[y\frac{uv}{r}\right] \\ -X\left[\frac{uv}{r}\right] + Y\left[\frac{uu}{r}\right] = -\left[x\frac{uv}{r}\right] + \left[y\frac{uu}{r}\right] \end{cases} \quad \ldots\ldots\ldots (3.4)$$

and if the above weight r_k is replaced by the square of r_k,

$$\begin{cases} -X[vv] + Y[uv] = -[xvv] + [yuv] \\ -X[uv] + Y[uu] = -[xuv] + [yuu] \end{cases} \quad \ldots\ldots\ldots\ldots (3.5)$$

The above theory was successfully applied to the determination of the epicentre of Nagano earthquake of July 15, 1941, using the data published by F. Kishinouye, T. Nagata and S. Miyamura[17]. The result is illustrated in Fig. 4. A, B and C are the obtained position of the epicentre using the equations (3.3), (3.4) and (3.5) respectively. The central deviation of x (eastward) and y (northward) coordinates of the points A, B, and C are the order of half a kilometer (cf. (4.1)). The point D indicates the seismometrical determination of Central Meteorological Observatory of Japan (138°14′ E, 36°42′ N).

17) *Bull. Earthq. Res. Inst.*, **19**, (1941) 628.

昭和27年3月10日印刷
昭和27年3月15日發行

東京都文京區本富士町一番地
東京大學構内
編纂發行者 東京大學地震研究所

東京都千代田區富士見町一丁目十番地
印刷者 笠井康賴

東京都千代田區富士見町一丁目十番地
印刷所 株式會社國際文献印刷社

東京都千代田區神田一ツ橋通
賣捌所 岩波書店

東京都中央區日本橋通二丁目六番地
丸善株式會社

Sold by
Iwanami Shoten,
Hitotsubashi dôri, Chiyoda-ku, Tôkyô,
and
Maruzen Co., Ltd.,
Nihonbashi dôri, Chûô-ku, Tôkyô.
Price of this copy: 430 Yen. (Postage exclusive.)

BULLETIN OF

THE EARTHQUAKE RESEARCH INSTITUTE

TOKYO UNIVERSITY

Vol. XXX, Part 1. March, 1952.

Contents.

Papers and Reports.

Page

1. Y. Satô, Study on Surface Waves V. Love-Waves Propagated upon Heterogeneous Medium. (in English) 1
2. T. Rikitake, Electrical Conductivity and Temperature in the Earth. (in English) 13
3. S. Sakuma, Earth-current Potentials near Boundaries of Various Geological Formations. (in English) 25
4. K. Kanai, Relation between the Nature of Surface Layer and the Amplitudes of Earthquake Motions. (in English) 31
5. K. Kanai, Examinations of the Assumption concerning Mechanism of Earthquake Origin through Seismograms. (in English) 39
6. T. Akima, A New Mechanical Low-pass Filter for Seismogram Analyses. (in English) 53
7. F. Kishinouye, Earth-vibrations on Soft Ground caused by Fallen Body. (in English) 59
8. D. Shimozuru, Dynamical Measurements of the Elastic Constants of Rocks subjected to Initial Stresses. 1. Measurement of Young's Modulus under Uniaxial Compression. (in English) 63
9. T. Rikitake, On Magnetization of Volcanoes. (in English) 71
10. I. Yokoyama, Magnetization of the Gabbro from Mt. Tsukuba with Special Relation to the Geomagnetic Anomalies. (in English) 83
11. Y. Satô, Determination of Epicentre by means of the Directions of Overturning. (in Japanese) 93

(For the papers written in Japanese or in occidental languages, the abstracts are given in occidental languages or in Japanese respectively.)

BULLETIN OF THE EARTHQUAKE RESEARCH INSTITUTE,
TOKYO UNIVERSITY. Vol. XXX, Part 2. June, 1952.

東京大學
地震研究所彙報

第 30 號　第 2 冊

昭和 27 年 6 月

目　次

論文及報告

頁

12. 表面波の研究 VI ラブ波及びその他の SH 波の發生 (英文)..... 佐藤泰夫 101

13. 實在建物の振動減衰性について 第1報 (英文)..... 金井清・吉澤靜代 121

14. 水準改測の結果から見た日本の陸地變動 (英文)..... 宮部直巳 127

15. 褶曲運動による地表の變形について (邦文)..... 杉村新 163

所報

(The titles in occidental languages are given on the back cover.)

本彙報ハ年4回 (但シ第1號ヨリ第6號マデハ不定期ニ，第7號ハ3冊トシテ發行セリ)，彙報別冊ハ不定期ニ發行ス．

本彙報掲載ノ論文及ビ報告ノ内容ニ關シテハ著者ノミニ其責任アルモノトス．

本彙報ニ關スル照會通信ハ東京大學地震研究所長ヘ宛テラレタシ．

The Bulletin is published quarterly. (Vols. I–VI were published at irregular intervals and Vol. VII consisted of three parts.)
Supplementary Volume is published at irregular interval.

The authors of the papers alone are responsible for the statements and opinions contained in their respective papers.

All communications relating to this Bulletin should be addressed to the Director of the Earthquake Research Institute, Tokyo University.

12. *Study on Surface Waves VI. Generation of Love- and Other Type of SH-Waves.*

By Yasuo SATÔ,

Earthquake Research Institute.

(Read June 20, 1950.—Received March 18, 1952.)

1. Introduction.

Since the celebrated study of H. Lamb[1], the problem of the generation of elastic waves in semi-infinite elastic medium has become not unusual. Even if we restrict our attention to the problem of SH-waves, we can give the papers of K. Sezawa[2], of H. Jeffreys[3], and of many others. Thus our knowledge in this field of seismology is by no means meagre, yet we must pay much more effort to make perfectly clear the hidden nature of the generation of Love- and other type of SH-waves propagated in the layered medium. We will begin with the proof of reciprocal relation in this kind of problems.

2. Reciprocal formula.

In this paragraph we will show the reciprocal relation in the problem of generation of SH-waves in the medium with a superficial layer.

The well-known Green's theorem in two-dimensional space is

$$\int\phi\frac{\partial\psi}{\partial n}ds-\iint\phi\nabla^2\psi dS=\int\psi\frac{\partial\phi}{\partial n}ds-\iint\psi\nabla^2\phi dS \quad \cdots\cdots\cdots(2.1)$$

where ϕ and ψ are wave-functions that satisfy

$$\nabla^2\phi=b^2\frac{\partial^2\phi}{\partial t^2}, \qquad \nabla^2\psi=b^2\frac{\partial^2\psi}{\partial t^2} \quad \cdots\cdots\cdots\cdots(2.2)$$

excluding singular points. In these expressions, n implies the outward normal of closed boundary curves, ds the line element of the same curve, dS the surface element of the area surrounded by the above curve, and

1) H. LAMB, *Phil. Trans.*, **A 203** (1904), 1-42.

2) K. SEZAWA, "Propagation of Love-waves on a Spherical Surface and Allied Problems", *Bull. Earthq. Res. Inst.*, **7** (1929), 437. "Love-waves Generated from a Source of a certain Depth", *ibid*, **13** (1935), 1.

3) H. JEFFREYS, "Generation of Love Wave and Others", *Beitr. z. Geophys.*, **30** (1931), 336.

b the reciprocal of the propagation velocity of waves in this medium.

If we assume that the motion is proportional to $\exp(ipt)$, then the expressions (2.2) is transformed as follows

$$(\nabla^2+k^2)\phi=0, \qquad (\nabla^2+k^2)\psi=0, \qquad k=bp \quad \ldots\ldots(2.3)$$

Further, if we define the functions Φ and Ψ by the expressions

$$\mu(\nabla^2\phi+k^2\phi)+\Phi=0, \qquad \mu(\nabla^2\psi+k^2\psi)+\Psi=0 \quad \ldots\ldots(2.4)$$

then Φ and Ψ are the "source functions" and have the next property

1) $\Phi=\Psi=0$ at every point except singular points.

2) $$\iint \Phi dS = -\mu\iint(\nabla^2\phi+k^2\phi)dS$$
$$\iint \Psi dS = -\mu\iint(\nabla^2\psi+k^2\psi)dS \quad \ldots\ldots\ldots\ldots\ldots\ldots\ldots\ldots(2.5)$$

which show the intensity of source.

So far, the functions ϕ and ψ are arbitrary while they satisfy some conditions which ordinary analytic functions can satisfy easily. Now, we will confine ourselves to the problem of the generation of SH-waves in layered medium. We will assume, when the source lies at the point P, the displacement in the surface layer to be ϕ and that in the substratum ϕ', and, when the source is at Q, the displacement in the part of layer and substratum to be ψ and ψ' respectively. Then Φ and Ψ will vanish except at the source points P and Q. (See Fig. 1).

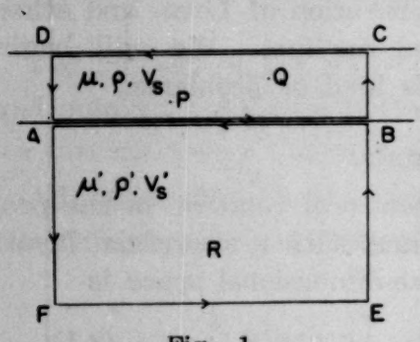

Fig. 1.

Adding $-\iint k^2\phi\psi dS$ to both members of (2.1) we have

$$\int\phi\frac{\partial\psi}{\partial n}ds+\frac{1}{\mu}\iint\phi\Psi dS=\int\psi\frac{\partial\phi}{\partial n}ds+\frac{1}{\mu}\iint\psi\Phi dS \quad \ldots\ldots(2.6)$$

Introducing (2.5) into the above formula we can obtain

in the surface layer
$$\int\phi\frac{\partial\psi}{\partial n}ds+\frac{1}{\mu}\phi_Q\iint\Psi dS$$
$$=\int\psi\frac{\partial\phi}{\partial n}ds+\frac{1}{\mu}\psi_P\iint\Phi dS \quad \ldots\ldots\ldots(2.7\,a)$$

in the substratum
$$\int\phi'\frac{\partial\psi'}{\partial n}ds=\int\psi'\frac{\partial\phi'}{\partial n}dS \quad \ldots\ldots\ldots(2.7\,b)$$

in which we have adopted the notations ϕ_Q and ψ_P, which are defined by

$$\begin{cases} \iint \phi \Psi dS = \phi_Q \iint \Psi dS \\ \iint \psi \Phi dS = \psi_P \iint \Phi dS \end{cases} \quad \cdots\cdots\cdots\cdots\cdots\cdots (2.8)$$

for Φ and Ψ do not vanish only at the points Q and P respectively.

Now, in our problem of generation of SH-waves, ϕ and ψ can be written at very distant places as

$$\begin{cases} \phi = \sum \phi_m r^{-m} \\ \psi = \sum \psi_n r^{-n} \end{cases} \quad \cdots\cdots\cdots\cdots\cdots\cdots\cdots (2.9)$$

where m and n are non-negative, though they may take fractional values.

Now, we will consider the integral $\int_{ABCDA} \phi \frac{\partial \psi}{\partial n} ds$, (cf. Fig. 1)

on CD; $\quad \frac{\partial \psi}{\partial n} = \frac{\partial \psi}{\partial z} = 0, \qquad \therefore \int_{CD} = 0$

on BC and DA; $\quad \phi \frac{\partial \psi}{\partial n} = \pm \phi \frac{\partial \psi}{\partial x} = \pm \sum \sum (-n) \phi_m \psi_n x^{-m-n-1}$

$$\therefore \int \phi \frac{\partial \psi}{\partial n} ds = \pm \sum \sum (-n) x^{-m-n-1} \int \phi_m \psi_n dz \to 0 \quad (x \to \pm \infty)$$

on AB; $\quad \int_{AB} \phi \frac{\partial \psi}{\partial n} ds = -\int_{AB} \phi \frac{\partial \psi}{\partial z} dx$

thus we have

$$\int_{ABCDA} = -\int_{AB} \phi \frac{\partial \psi}{\partial z} dx \quad \cdots\cdots\cdots\cdots (2.10)$$

In a similar way, we will consider the integral $\int_{AFEBA} \phi' \frac{\partial \psi'}{\partial n} ds$, in which ϕ', ψ' imply the displacements in the part of semi-infinite elastic body. The following equations are obtained without difficulty

$$\int_{AF} = \int_{FE} = \int_{EB} = 0.$$

Since, on the boundary surface AB, $\phi = \phi'$ and $\mu \frac{\partial \psi}{\partial z} = \mu' \frac{\partial \psi}{\partial z}$ must hold, we have

$$\int_{AFEBA} = \int_{BA} \phi' \frac{\partial \psi'}{\partial n} ds = \int_{AB} \phi' \frac{\partial \psi'}{\partial z} dx = \frac{\mu}{\mu'} \int_{AB} \phi \frac{\partial \psi}{\partial z} dx \quad \ldots (2.11)$$

Adding the two expressions (2.7 a) and (2.7b)$\times \frac{\mu'}{\mu}$, and utilizing the above relations (2.10) and (2.11), we obtain at once the next formula

$$\phi_Q \iint \Psi dS = \psi_P \iint \Phi dS \quad \cdots\cdots\cdots\cdots\cdots (2.12)$$

This is a reciprocal formula showing the relation between the displacement of the point Q when a focus lies at P, and the displacement of P when a focus lies at the point Q.

Now, what kind of a formula will hold if the focus lies at a point in the semi-infinite part? In this case, we will denote the displacement in the layer as ϑ, and that in the part of semi-infinite body as ϑ'. Further, we assume a function Θ which corresponds to the previously defined function Φ; then we have the next equations similar to (2.7 a) and (2.7 b),

$$\begin{cases} \int \phi \frac{\partial \vartheta}{\partial n} ds = \int \vartheta \frac{\partial \phi}{\partial n} ds + \frac{1}{\mu} \vartheta_P \iint \Phi dS \quad \cdots\cdots (2.13\,a) \\ \int \phi' \frac{\partial \vartheta'}{\partial n} ds + \frac{1}{\mu'} \phi_R \iint \Theta dS = \int \vartheta' \frac{\partial \phi'}{\partial n} ds \quad \cdots\cdots\cdots\cdots (2.13\,b) \end{cases}$$

Making an expression (2.13 a)$\times \mu$+(2.13 b)$\times \mu'$,

$$\phi_R' \iint \Theta dS = \vartheta_P \iint \Phi dS \quad \cdots\cdots\cdots\cdots (2.14)$$

Thus we have obtained the reciprocal formula connecting the amount of displacement and the strength of source when one is situated in the superficial layer and the other in the substratum. Later, we will show an application of the above theorem.

3. Integral representation of displacements when a periodic point source is in the layer.

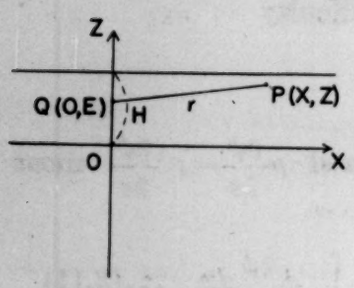

Fig. 2.

Let us first assume a periodic point origin lying at $Q\,(O, E)$ (cf. Fig. 2), then the displacement v_0 at $P\,(x, z)$ in the layer due to this origin is expressed by,

$$v_0 = H_0^{(2)}(kr) \exp(ipt)$$

$$= \frac{i}{\pi} \int_{-\infty}^{\infty} \exp\{ifx \pm \beta(z-E)+ipt\} \frac{df}{\beta}^{4)} \quad (3.1)$$

in which $\pm$ corresponds to $z \lessgtr E$,

$$\beta=\sqrt{(f^2-k^2)}, \qquad k=p/V_s$$

$$r=\overline{QP}.$$

In order to satisfy the boundary conditions, we must assume another type of waves such as

in the layer; $$v_1=\{A\cosh\beta z+B\sinh\beta z\}\exp(ifx) \quad \ldots\ldots\ldots(3.2)$$

in the semi-infinite body; $v'=C\exp(\beta' z)\exp(ifx)$

$$\beta'=\sqrt{(f^2-k'^2)}, \qquad k'=p/V_s'$$

($\exp(ipt)$ is abridged for brevity.)

The boundary conditions are the vanishing of stress at the free surface $z=H$, and the continuity of displacement and stress at the plane of interface $z=0$. Therefore we have

$$\begin{cases} A\sinh\beta H+B\cosh\beta H & =\dfrac{i}{\pi}\exp\{-\beta(H-E)\}df \\ A & -C & =-\dfrac{i}{\pi}\exp\{-\beta E\}\dfrac{df}{\beta} \\ & B\beta & -\dfrac{\mu'}{\mu}C\beta'=-\dfrac{i}{\pi}\exp\{-\beta E\}df \end{cases} \quad \ldots\ldots(3.3)$$

Solving this equation with respect to A, B, and C, and substituting the obtained result into the expressions of (3.2), we have

$$\begin{cases} v=v_0+v_1=\dfrac{i}{\pi}\dfrac{(\beta+\chi\beta')e^{\beta H}+(\beta-\chi\beta')e^{-\beta H}}{(\beta+\chi\beta')e^{\beta H}-(\beta-\chi\beta')e^{-\beta H}}\{e^{\beta(H-z)}+e^{-\beta(H-z)}\}\dfrac{1}{\beta}\exp(ifx)df \\ \qquad\qquad \ldots\ldots z>E \\ v=v_0+v_1=\dfrac{i}{\pi}\dfrac{(\beta+\chi\beta')e^{\beta z}+(\beta-\chi\beta')e^{-\beta z}}{(\beta+\chi\beta')e^{\beta H}-(\beta-\chi\beta')e^{-\beta H}}\{e^{\beta(H-E)}+e^{-\beta(H-E)}\}\dfrac{1}{\beta}\exp(ifx)df \\ \qquad\qquad \ldots\ldots z<E \\ v'=\dfrac{i}{\pi}\dfrac{2e^{\beta' z}}{(\beta+\chi\beta')e^{\beta H}-(\beta-\chi\beta')e^{-\beta H}}\{e^{\beta(H-E)}+e^{-\beta(H-E)}\}\exp(ifx)df \\ \qquad\qquad \ldots\ldots z<0 \end{cases}$$

in which $\chi=\mu'/\mu$ $\quad\ldots\ldots\ldots\ldots\ldots(3.4)$

The denominator of the above three expressions is a well-known form as the characteristic equation of Love-waves.

4) Notation of definite integral $\int_{-\infty}^{\infty}$ will be omitted hereafter so long as no confusion occurs.

4. Refracted Waves.

In this section we will calculate the surface displacement due to the refracted wave at a very distant place.

By following H. Nakano's procedure[5], the integration path can be transformed into the path of steepest descent, namely *AJLMNS'RSB* illustrated in Fig. 4; and the refracted waves are expressed, as is well

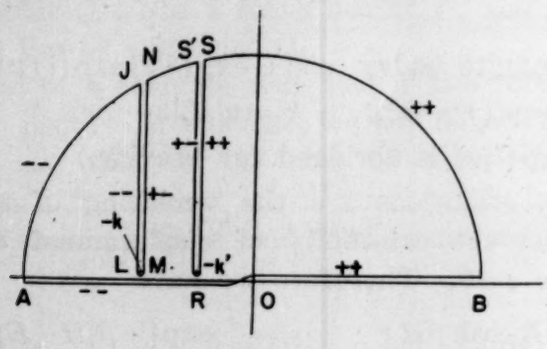

Fig. 3. One cut is taken so as to connect $-k$ and k; and the other to connect $-k'$ and k'.

known, by the integral $\int_{S'RS}$. Although the paths *JLMN* and *S'RS* must take special curved figure while the epicentral distance is not so large compared with the wave-length, we may adopt simple straight line parallel to longitudinal axis when the distance becomes extremely great. (cf. Fig. 3. This is the path used by H. Lamb[6], K. Sezawa[7] and others. Two signs beside the integration path in Figs. 3 and 4

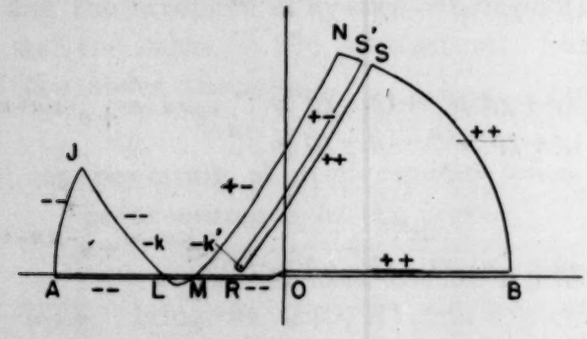

Fig. 4. One cut is taken so as to connect $-k$ and k; and the other to connect $-k'$ and k'.

5) H. NAKANO, "On Rayleigh Wave", *Jap, Journ. Astro. and Geophys.*, **2** (1925), 1-94. Especially Fig. 7.

6) *loc. cit.*, 1). Fig. 3.

7) *loc. cit.*, 2). Latter paper. Fig. 2.

specify on which one of the four sheets of Riemann surface the point resides. The former sign is related to the branch points $\beta=0$, and the latter to $\beta'=0$.) Thus the refracted waves at the place $z>E$ takes the following form.

$$v[S']=\frac{i}{\pi}\int_{-k'}^{-k'+i\infty}\frac{2\chi\beta'\cosh\beta(H-E)}{\beta^2\sinh^2\beta H-\chi^2\beta'^2\cosh^2\beta H}\{e^{\beta(H-z)}+e^{-\beta(H-z)}\}\cdot\exp(ifx)df$$

$$\beta=\sqrt{(f^2-k^2)},\quad \beta'=\sqrt{(f^2-k'^2)},\quad z>E \quad \ldots.(4.1)$$

This expression is identical with that obtained by K. Sezawa[8]. He, however, simply neglects the second term of denominator assuming that this term is small compared with the first one.

Of course, such a treatment is allowed so long as $\sinh\beta H$ does not vanish. But if it happens to vanish such a simple calculation is not to be allowed. We will, therefore, show a way of calculating the above integral more strictly.

Changing the integration variable from f to ζ defined by

$$f=-k+i\zeta^2$$

we have

$$v[S']=\frac{i}{\pi}2\int_0^\infty\frac{2\chi\sqrt{(-i2k')}\cdot\zeta\cos\sqrt{(k^2-k'^2)}\cdot(H-E)}{(k^2-k'^2)\sin^2\sqrt{(k^2-k'^2+i2k'\zeta^2)}\cdot H-\chi^2(-i2k'\zeta^2)\cos^2\sqrt{(k^2-k'^2)}H}$$
$$\cdot\{\exp(i\sqrt{(k^2-k'^2)}\cdot(H-z))+\exp(-i\sqrt{(k^2-k'^2)}\cdot(H-z))\}$$
$$\cdot\exp(-ik'x-\zeta^2x)\cdot i2\zeta d\zeta \qquad \ldots..(4.2)$$
$$\propto\int_0^\infty\frac{\zeta^2\exp(-\zeta^2x)d\zeta}{(k^2-k'^2)\sin^2\sqrt{(k^2-k'^2+i2k'\zeta^2)}\cdot H+i2\chi^2k'\zeta^2\cos^2\sqrt{(k^2-k'^2)}\cdot H}$$

From the last expression we will pick up the term $\sin^2\sqrt{\{(k^2-k'^2)+i2k'\zeta^2\}}\cdot H$ and consider it more precisely. As the factor $\exp(-\zeta^2x)$ is involved in the numerator, the integrand takes extremely small value except when ζ is very small; therefore we can assume ζ in the above term $\sin\sqrt{\{(k^2-k'^2)+ik'\zeta^2\}}\cdot H$ to be very small. Consequently, if $\sqrt{(k^2-k'^2)}\cdot H$ differs a little from $n\pi$ we can neglect $i2k'\zeta^2$ compared with $k^2-k'^2$. If, however, $\sqrt{(k^2-k'^2)}\cdot H$ is equal to $n\pi$, then

$$\sin^2\sqrt{\{(k^2-k'^2)+i2k'\zeta^2\}}\cdot H=\sin^2\left\{n\pi\left(1+i\frac{2k'\zeta^2H^2}{n^2\pi^2}\right)^{\frac{1}{2}}\right\}$$
$$\fallingdotseq\{(-)^n\cdot(ik'\zeta^2H^2/n\pi)\}^2=0(\zeta^4) \qquad \ldots..(4.3)$$

8) *do.*, expression (23).

Therefore in this case also, we can neglect $i2k'\zeta^2$ compared with the second term in the denominator. Thus the integral in the last line of (4.2) takes the form of

$$\int_0^\infty \frac{\zeta^2 \exp(-x\zeta^2)}{B^2+iA^2\zeta^2}d\zeta$$

in which

$$A^2=2\chi^2k'\cos^2\sqrt{(k^2-k'^2)}\cdot H$$

$$B^2=(k^2-k'^2)\sin^2\sqrt{(k^2-k'^2)}\cdot H \quad \ldots\ldots\ldots(4.4)$$

4.1

$$\int_0^\infty \exp(-xz^2)\frac{z^2}{z^2+a^2}dz \quad (x>0).$$

We employ the following notations:

$$I(x, a^2) \equiv \int_0^\infty \exp(-xz^2)\frac{z^2}{z^2+a^2}dz \quad \ldots\ldots\ldots\ldots\ldots\ldots(4.5)$$

$$E(x) \equiv \int_0^\infty \exp(-xz^2)dz = I(x, 0) \quad \ldots\ldots\ldots\ldots\ldots\ldots(4.6)$$

$$J(x, a^2) \equiv \int_0^\infty \exp(-xz^2)\frac{1}{z^2+a^2}dz \quad \ldots\ldots\ldots\ldots\ldots\ldots(4.7)$$

Now, the following expressions are obtained easily,

$$I(x, a^2) = \int_0^\infty \exp(-xz^2)\left(1-\frac{a^2}{z^2+a^2}\right)dz$$

$$= E(x)-a^2J(x, a^2) \quad \ldots\ldots\ldots\ldots\ldots\ldots(4.8)$$

$$\frac{\partial}{\partial x}J(x,a^2) = -I(x, a)$$

$$= -E(x)+a^2J(x, a^2) \quad \ldots\ldots\ldots\ldots\ldots\ldots(4.9)$$

Since (4.9) is a linear differencial equation of $J(x, a)$, we can solve and obtain the next expression

$$J(x, a^2)=\exp(a^2x)\cdot\left\{\int^x \exp(-a^2t)\cdot(-E(t))dt + A\right\} \quad \ldots(4.10)$$

When x tends to ∞, $J(x, a^2)$ and $I(x, a^2)$ both tends to 0 obviously. Therefore, $J(x, a^2)$ is expressed by

$$J(x, a^2)=\exp(a^2x)\cdot\int_x^\infty \exp(-a^2t)\cdot E(t)dt \quad \ldots\ldots\ldots(4.11)$$

Introducing (4.8) we have

$$I(x, a^2)=E(x)-a^2\exp(a^2x)\int_x^\infty \exp(-a^2t)\cdot E(t)dt \quad \ldots.(4.12)$$

Now, $E(x)$ is, putting $xz^2=\zeta^2$.

$$E(x)=x^{-1/2}\int_0^\infty \exp(-\zeta^2)d\zeta$$

$$=\frac{\sqrt{\pi}}{2}x^{-1/2},$$

therefore

$$I(x,a^2)=\frac{\sqrt{\pi}}{2}\left[x^{-1/2}-a^2\exp(a^2x)\int_x^\infty \frac{\exp(-a^2t)}{\sqrt{t}}dt\right]. \quad \ldots(4.14)$$

If a^2 is imaginary we put $a^2\to ib^2$

$$I(x,ib^2)=\frac{\sqrt{\pi}}{2}\left[x^{-1/2}-ib^2\exp(ib^2x)\int_x^\infty \frac{\exp(-ib^2t)}{\sqrt{t}}dt\right] \quad \ldots(4.15)$$

and

$$\int_x^\infty \frac{\exp(-ib^2t)}{\sqrt{t}}dt=\frac{1}{b}\left\{\int_{b^2x}^\infty \frac{\cos\tau}{\sqrt{\tau}}d\tau-i\int_{b^2x}^\infty \frac{\sin\tau}{\sqrt{\tau}}dt\right\} \quad \ldots.(4.16)$$

Using Fresnel's integral[9] defined by

$$\begin{cases} S(x)=\dfrac{1}{\sqrt{(2\pi)}}\displaystyle\int_0^x \frac{\sin x}{\sqrt{x}}dx \\ C(x)=\dfrac{1}{\sqrt{(2\pi)}}\displaystyle\int_0^x \frac{\cos x}{\sqrt{x}}dx \end{cases} \quad \ldots\ldots\ldots(4.17)$$

we obtain

$$\int_x^\infty \frac{\exp(ib^2t)}{\sqrt{t}}dt=\frac{1}{b}\sqrt{(2\pi)}\left\{\left(\frac{1}{2}-C(b^2x)\right)-i\left(\frac{1}{2}-S(b^2x)\right)\right\} \quad ..(4.18)$$

or, introducing it into (4.15), we have

$$I(x,ib^2)=\frac{\sqrt{\pi}}{2}x^{-1/2}-\frac{\pi}{\sqrt{2}}ib\exp(ib^2x)\cdot\left\{\left(\frac{1}{2}-C(b^2x)\right)-i\left(\frac{1}{2}-S(b^2x)\right)\right\}$$

$\ldots\ldots(4.19)$

The integral (4.4) in § 4 is expressed by the function $I(x,a^2)$ as

$$\int_0^\infty \frac{\zeta^2\exp(-x\zeta^2)}{B^2+iA^2\zeta^2}d\zeta=\frac{1}{iA^2}I\left(x,-i\frac{B^2}{A^2}\right),$$

therefore, it is equal to

---

9) BROMWICH, *Infinite Series* (1926), p. 336.
TERAZAWA, *Sûgaku-Gairon*, p. 189. (In Japanese).
JAHNKE-EMDE, *Tables of Functions* (1933), p. 108. Notations of this book is different with those adopted by others.

10) *ibid.*

$$=\frac{1}{iA^2}\left[\frac{\sqrt{\pi}}{2}x^{-1/2}+i\frac{\pi}{\sqrt{2}}\frac{B}{A}\exp\left(-i\frac{B^2}{A^2}x\right)\right.$$
$$\left.\cdot\left\{\left(\frac{1}{2}-C\left(\frac{B^2}{A^2}x\right)\right)+i\left(\frac{1}{2}-S\left(\frac{B^2}{A^2}x\right)\right)\right\}\right] \quad \ldots(4.20)$$

Now, we will examine the last expression.

If B takes a finite value it is easily deduced by the asymptotic formula

$$\begin{cases} S(x)=\frac{1}{2}-\sqrt{\left(\frac{2x}{\pi}\right)}\cdot\{M\cos x+N\sin x\}, \\ \qquad M=\frac{1}{2x}-\frac{1\cdot3}{(2x)^3}+\frac{1\cdot3\cdot5\cdot7}{(2x)^5}-\cdots\cdot \\ C(x)=\frac{1}{2}-\sqrt{\left(\frac{2x}{\pi}\right)}\cdot\{M\sin x-N\cos x\}, \\ \qquad N=\frac{1}{(2x)^2}-\frac{1\cdot3\cdot5}{(2x)^4}+\frac{1\cdot3\cdot5\cdot7\cdot9}{(2x)^6}-\cdots\cdot \end{cases} \quad \ldots\ldots\ldots(4.21)$$

that the terms of $x^{-1/2}$ cancel each other and only the next term remains, so that (4.20) is proportional to $x^{-3/2}$ [11], while if B vanishes the same expression at once becomes

$$\frac{1}{iA^2}\frac{\sqrt{\pi}}{2}x^{-1/2}. \quad \ldots\ldots\ldots\ldots\ldots(4.22)$$

The physical meaning of the above fact may be interpreted as follows.

Generally, the refracted waves propagated on the medium under the layer decrease their amplitude by the function $x^{-3/2}$, however, if the condition

$$\sqrt{(k^2-k'^2)}H=n\pi \quad \ldots\ldots\ldots\ldots\ldots(4.23)$$

is satisfied the defference of the optical path (— we are using terms of optics here —) *ABCDEFG*, *ABDEFG*, *ABDFG*,.....in Fig. 5 is the integer multiple of the wave-length;

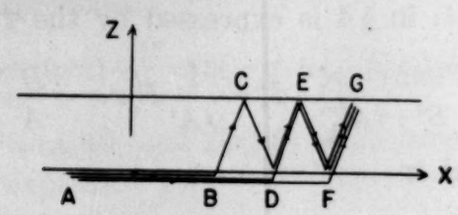

Fig 5.

consequently such waves predominate over the ordinary ones, and the rate of decrease of amplitude becomes smaller.

11) *loc. cit.*, 2). Latter paper, expression (27).

The above condition, of course can be expressed in other words; namely, if the travel time of the wave path *BD*, *BCD* and so on differs by the integer multiple of their period, then such waves predominate and the amplitude becomes far larger than the waves with other period.

This reminds us of the explanation offered for the formation of Love-waves. Indeed Fig. 5 is just the same with the figure used for the illustration of Love-waves in the former paper[12].

Summing up the above discussion we can make a table of the following form.

Table I

	Distance factor	Condition
Love-waves	x^0	$-\arctan(\chi\beta'/\tilde{\beta})+\tilde{\beta}H=n\pi$
Predominant SH-waves	$x^{-1/2}$	$\sqrt{(k^2-k'^2)}\cdot H=n\pi$
Ordinary SH-waves	$x^{-3/2}$	———

5. Reflected waves.

Just as we have obtained the refracted waves from the contour integration of (3.4), we can expect the generation of reflected waves by a similar treatment.

To our astonishment, however, we cannot find any term which represents the nature of refection. For the integrand of (3.4) (upper and middle expression) has no branch point at $f=k$; namely $f=k$ is not the singular point of the integrand of

$$v_0+v_1=2\frac{i}{\pi}\frac{\beta\cosh\beta E+\chi\beta'\sinh\beta E}{\beta\sinh\beta H+\chi\beta'\cosh\beta H}\cosh\beta(H-z)\cdot\frac{1}{\beta}\exp(ifx)df \quad \cdots\cdots\ z>E$$

$$v_0+v_1=2\frac{i}{\pi}\frac{\beta\cosh\beta z+\chi\beta'\sinh\beta z}{\beta\sinh\beta H+\chi\beta'\cosh\beta H}\cosh\beta(H-E)\cdot\frac{1}{\beta}\exp(ifx)df \quad \cdots\cdots\ z<E \qquad (5.1)$$

Thus, from a harmonic origin, we cannot expect reflected waves.

12) Y. SATÔ, "Study on Surface Waves I, Velocity of Love-Waves." *Bull. Earthq. Res. Inst.*, **29** (1951), 1. Fig. 2. See also Fig. 1.

This is we think, due to the interference of the direct and reflected waves; that is to say, when direct and reflected waves are superposed they cancel each other leaving no resultant waves. To obtain the effect of reflection we must strictly calculate the case of impulsive origin. Hitherto, no one has noticed clearly this fact.

6. Amplitude distribution of Love-waves.

We all know that velocity of Love-waves is determined by the characteristic equation

$$(\beta+\chi\beta')\exp(\beta H)-(\beta-\chi\beta')\exp(-\beta H)=0 \quad \ldots\ldots(6.1)$$

and once this condition is satisfied the vertical distribution of amplitude is also determined. Therefore, if the amplitude is given at any point, the whole distribution of it is determined immediately. This is a very convenient property, for we do not have to calculate the motion of all points, and we have merely to obtain the amplitude of any one point, of the free surface, for instance.

Further we can apply the reciprocal theorem, which we have obtained in § 2, and make matters more simple. The amplitude at the point Q when the focus is situated at P is expressed by the amplitude at P when the focus is at the point Q. Therefore, if the motion is determined when the focus lies at a special point, we can at once obtain the motion when the focus lies at any point. Thus we can assume, without losing generality, that the focus lies very near the free surface.

From the first equation of (3.4), we can easily obtain the displacement due to Love-phase as follows,

$$v[L_n]=4\exp\{ipt-iK_nx\}\cdot\cos\tilde{\beta}(H-E) \div\left[fH\left\{\frac{1}{\beta' H}\frac{1}{\beta^2-\chi^2\beta'^2}\chi(k^2-k'^2)-1\right\}\right]_{f=-K_n} \quad \ldots(6.2)$$

in which $\tilde{\beta}=\beta/i$

$f=-K_n$ is the root of the equation (6.1),

and n implies the number of nodes in the layer.

In the above expression, $\exp(ipt-iK_nx)$ is the factor that expresses the time-distance relation of the L_n-branch of Love-waves, and the factor $\cos\tilde{\beta}(H-E)$ represents the effect of the depth of focus.

At first, we assumed that the focus is situated at the point $Q(O,E)$. However, the focus may not be such a concentrated point, but may be distributed on the Z-axis with an intensity $I(E)$, then the displacement

due to this origin is roughly proportional to

$$\int\left[I(E)\cos\tilde{\beta}(H-E)\right]_{f=-K_n}dE \quad \cdots\cdots\cdots(6.3)$$

Therefore, if n is not small, $\cos\tilde{\beta}(H-E)$ oscillates rapidly and the probability of the absolute value of the integral taking a small value becomes large. Consequently we can expect no large amplitude of Love-waves with nodes in the stratum.

Now we will proceed to obtain the displacement $v[L_n]$. However, from the preparatory consideration in this article, we may put $E=H$ to make the factor $\cos\tilde{\beta}(H-E)$ a unity.

Thus we can find that the amplitude of Love-waves is determined by the function

$$A_n=\left[1/fH\left\{\frac{1}{\beta' H}\frac{1}{\beta^2-\chi^2\beta'^2}\chi(k^2-k'^2)-1\right\}\right]_{f=-K_n} \quad \cdots\cdots(6.4)$$

6.1 Amplitude function A_n.

In this section we will perform the numerical calculation of the amplitude function.

If we put a new notation

$$K_n=-k\sin\vartheta_n \quad \cdots\cdots\cdots\cdots\cdots(6.5)$$

then the above expression (6.4) takes the following form

$$A_n=\operatorname{cosec}\vartheta_n\Big/\left\{\frac{1}{\sqrt{(\cos^2\theta_0-\cos^2\vartheta_n)}}\cdot\frac{\chi\cos^2\theta_0}{\cos^2\vartheta_n+\chi^2(\cos^2\theta_0-\cos^2\vartheta_n)}+\omega_n\right\} \quad (6.6)$$

where $k'=k\sin\theta_0$ and $\operatorname{cosec}\vartheta_n$ is the phase velocity.

Since A_n is a real function, the phase angle of every branch of Love-waves is altogether equal.

We assumed two cases;

[I]: $\chi=\mu'/\mu=4$, $\rho=\rho'$, consequently $\sin\theta_0=V_s/V_s'=1/2$,

[II]: $\chi=\mu'/\mu=8$, $\rho=\rho'$, consequently $\sin\theta_0=1/2\sqrt{2}$,

and calculated the value of A_n corresponding to some given values of ϑ_n, where n was assumed to be 0, 1, 2, 3, 4.

The result is found in Tables II (case [I]), III (case [II]) and Figs. 6 (case [I]), 7 (case [II]), which make clear the relation between ϑ and A_n, or the velocity and amplitude. For our practical purposes, however, it is preferable for us to get the relation between period and amplitude or wave-length and amplitude. Therefore using the

relation of period and velocity (Figs. 8 (case [I]) and 10 (case [II]), which is the dispersion curve), we eliminate velocity (or ϑ) and obtain the curves connecting the amplitude and period.

Table II

Case [I]. $\chi=4$, $\sin\theta_0=1/2$, $\rho=\rho'$.

$$A_n=\operatorname{cosec}\vartheta_n\Big/\left\{\frac{1}{\sqrt{(\cos^2\theta_0-\cos^2\vartheta_n)}}\cdot\frac{\chi\cos^2\theta_0}{-(\chi^2-1)\cos^2\vartheta_n+\chi^2\cos^2\theta_0}+\omega_n\right\}.$$

ϑ	Velocity (V_{Love}/V_s)	Amplitude function A_n				
		A_0	A_1	A_2	A_3	A_4
30°	2.000	0	0	0	0	0
30.5	1.970	.0489	.0449	.0414	.0385	.0366
31	1.942	.0766	.0669	.0594	.0534	.0485
32	1.887	.1265	.1015	.0846	.0725	.0635
33	1.836	.1740	.1285	.1019	.0844	.0720
34	1.788	.2181	.1492	.1134	.0915	.0765
35	1.743	.262	.166	.1216	.0960	.0792
36	1.701	.301	.178	.1268	.0984	.0804
37	1.662	.334	.186	.1293	.0993	.0803
38	1.624	.362	.192	.1305	.0989	.0796
39	1.589	.388	.195	.1305	.0980	.0784
40	1.556	.410	.197	.1297	.0967	.0771
41	1.524	.426	.197	.1281	.0950	.0754
42	1.494	.440	.196	.1260	.0929	.0736
43	1.466	.450	.194	.1236	.0908	.0718
44	1.440	.456	.191	.1210	.0886	.0698
45	1.414	.460	.188	.1184	.0864	.0679
46	1.390	.461	.184	.1152	.0839	.0658
47	1.367	.460	.180	.1122	.0813	.0638
48	1.346	.458	.176	.1091	.0791	.0620
49	1.325	.454	.172	.1060	.0766	.0600
50	1.305	.448	.1674	.1031	.0743	.0582
55	1.221	.406	.1437	.0873	.0627	.0490
60	1.155	.349	.1207	.0728	.0521	.0406
65	1.103	.289	.0980	.0590	.0422	.0328
70	1.064	.228	.0769	.0462	.0330	.0256
75	1.035	.1695	.0567	.0340	.0243	.0189
80	1.015	.1118	.0374	.0224	.0160	.01245
85	1.0038	.0558	.0186	.01115	.00797	.00620
90	1	0	0	0	0	0

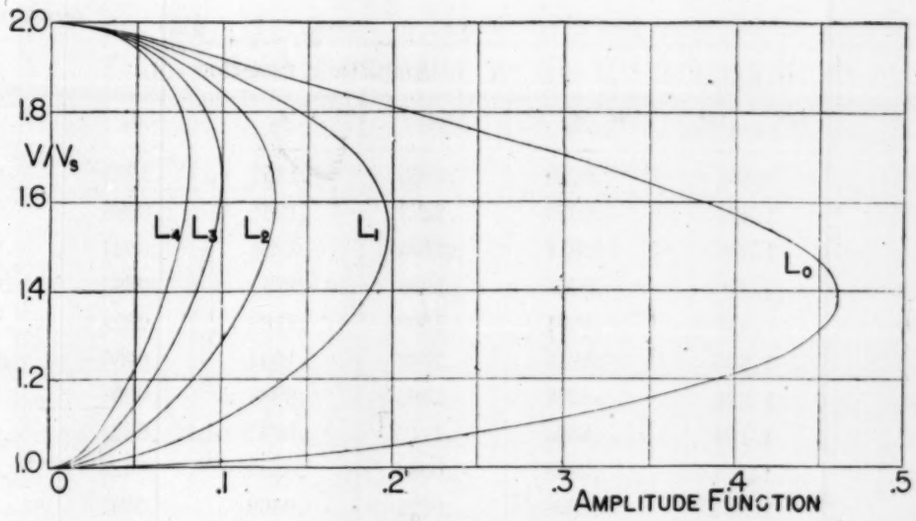

Fig. 6.

Case [I]. $\chi=\mu'/\mu=4$, $\rho=\rho'$, $\sin\theta_0=V_s/V_s'=1/2$.

Abscissa is the amplitude function $A_n=\left[1/fH\left\{\frac{1}{\beta' H}\frac{1}{\beta^2-\chi^2\beta'^2}\chi(k^2-k^2)-1\right\}\right]_{f=-K_n}$.

L_0, L_1...implies the 0-th, 1st...branch of the dispersion curves of Love-waves.

Table III

Case [II]. $\chi=8$, $\sin\theta_0=1/2\sqrt{2}$, $\rho=\rho'$.

$$A_n=\operatorname{cosec}\vartheta_n\Big/\left\{\frac{1}{\sqrt{(\cos^2\theta_0-\cos^2\vartheta_n)}}\cdot\frac{\chi\cos^2\theta_0}{-(\chi^2-1)\cos^2\vartheta_n+\chi^2\cos^2\theta_0}+\omega_n\right\}.$$

ϑ	Velocity (V_{Love}/V_s)	Amplitude function A_n				
		A_0	A_1	A_2	A_3	A_4
20°42′20″	2.8284	0	0	0	0	0
21	2.790	.0254	.0246	.0239	.0232	.0226
22	2.670	.0854	.0763	.0696	.0639	.0591
23	2.559	.1495	.1247	.1069	.0936	.0832
24	2.459	.2172	.1666	.1351	.1136	.0980
25	2.366	.2836	.2004	.1550	.1263	.1065
26	2.281	.3468	.2265	.1681	.1337	.1109
28	2.130	.4551	.2586	.1805	.1388	.1126
30	2.000	.5358	.2717	.1820	.1368	.1096
32	1.887	.5895	.2733	.1779	.1318	.1047
34	1.788	.6203	.2680	.1710	.1255	.0991
36	1.701	.6327	.2589	.1626	.1186	.0934
38	1.624	.6318	.2477	.1541	.1118	.0877

(to be continued.)

(continued.)

ϑ	Velocity (V_{Love}/V_s)	Amplitude function A_n				
		A_0	A_1	A_2	A_3	A_4
40	1.556	.6210	.2365	.1457	.1053	.0824
42	1.494	.6026	.2229	.1367	.0986	.0771
44	1.440	.5814	.2104	.1284	.0924	.0722
46	1.390	.5563	.1980	.1204	.0865	.0675
48	1.346	.5291	.1860	.1128	.0809	.0631
50	1.305	.5013	.1742	.1054	.0756	.0589
55	1.221	.4300	.1468	.0885	.0634	.0493
60	1.155	.3604	.1217	.0732	.0524	.0407
65	1.103	.2938	.0986	.0593	.0423	.0330
70	1.064	.2306	.0771	.0463	.0331	.0257
75	1.035	.1703	.0568	.0341	.0244	.0190
80	1.015	.1122	.0374	.0224	.0160	.0125
85	1.0038	.0557	.01856	.01114	.00795	.00619
90	1	0	0	0	0	0

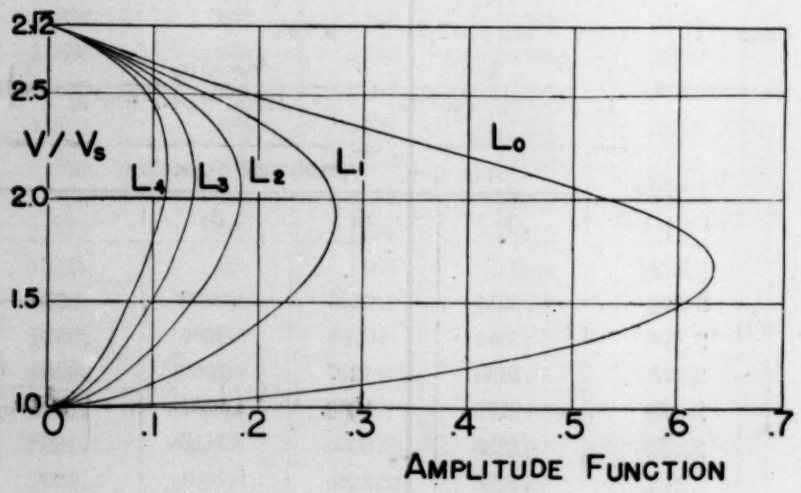

Fig. 7.

Case [II]. $\chi=\mu'/\mu=8$, $\rho=\rho$, $\sin\theta_0=V_s/V_s'=1/2\sqrt{2}$.

Abscissa is the amplitude function $A_n=\left[1/fH\left\{\frac{1}{\beta' H}\frac{1}{\beta^2-\chi^2\beta'^2}\chi(k^2-k'^2)-1\right\}\right]_{f=-K_n}$.

L_0, L_1...implies the 0-th, 1st...branch of the dispersion curves of Love-waves.

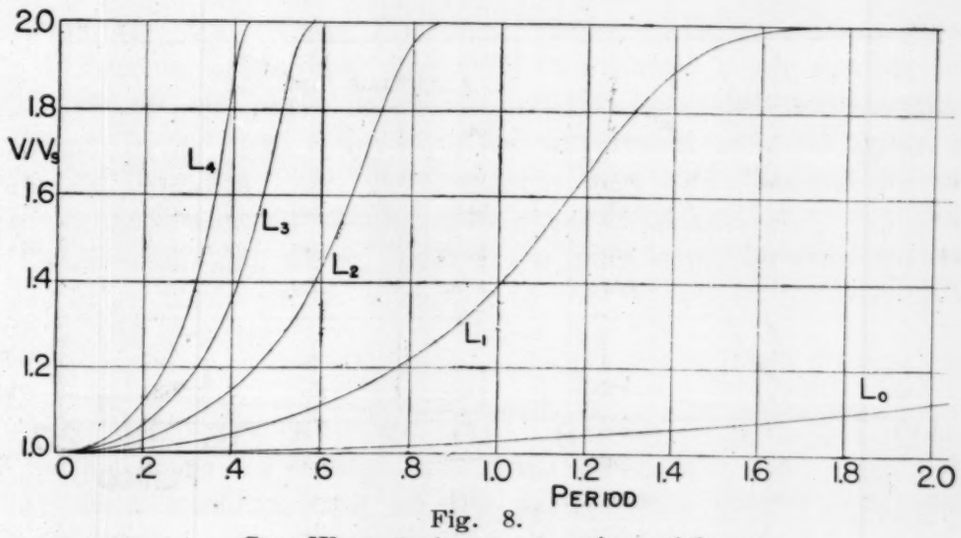

Fig. 8.

Case [I]. $\chi=4$, $\rho=\rho'$, $\sin\theta_0=1/2$.

Relation between the velocity of Love-waves and the period, the unit of which is H/V_s, or the time necessary to travel the superficial layer from the bottom to the surface.

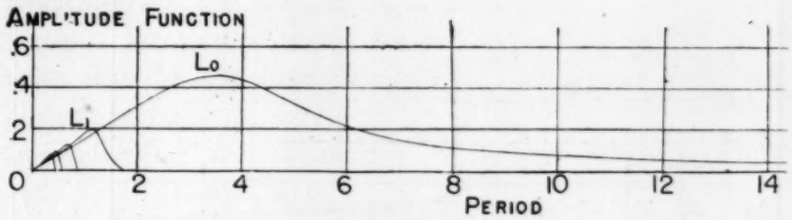

Fig. 9 a.

Case [I]. $\chi=4$, $\rho=\rho'$, $\sin\theta_0=1/2$.

Time unit ; H/V_s.

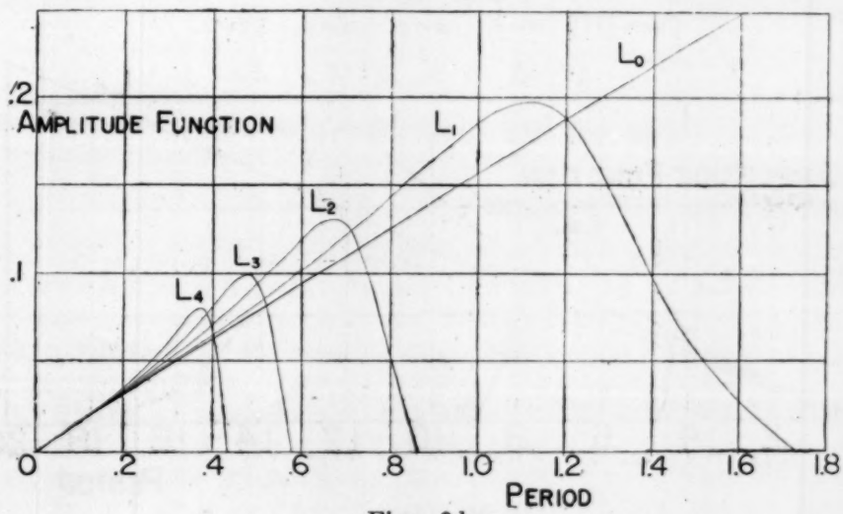

Fig. 9 b.

Case [I]. $\chi=4$, $\rho=\rho$, $\sin\theta=1/2$.

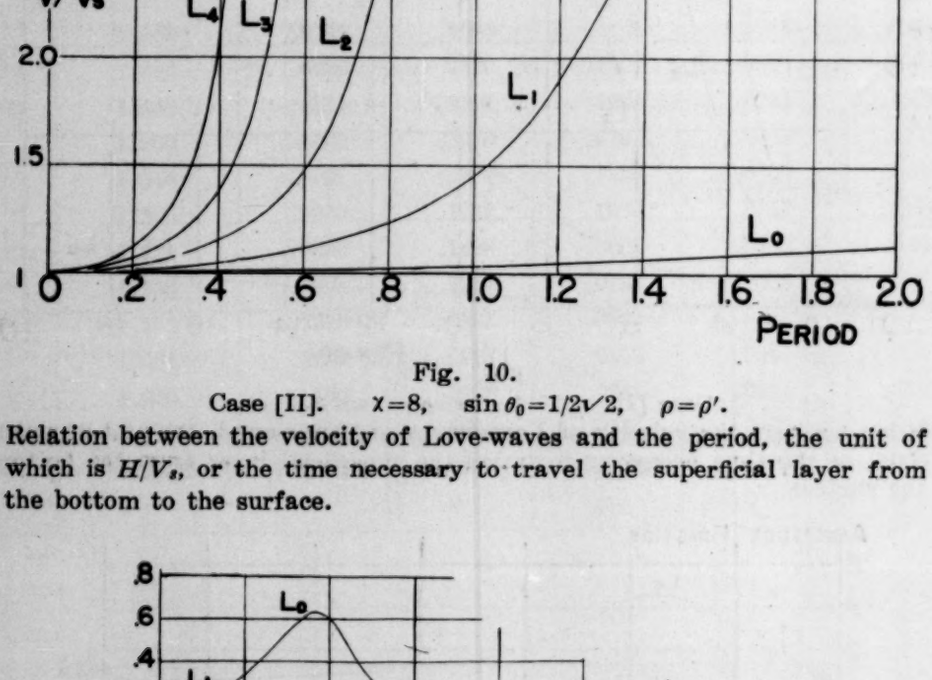

Fig. 10.
Case [II]. $\chi=8$, $\sin\theta_0=1/2\sqrt{2}$, $\rho=\rho'$.
Relation between the velocity of Love-waves and the period, the unit of which is H/V_s, or the time necessary to travel the superficial layer from the bottom to the surface.

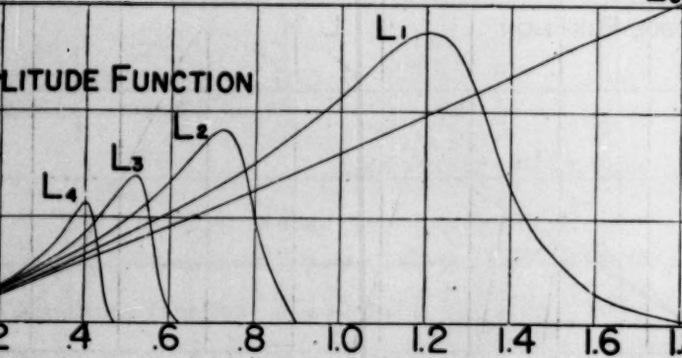

Fig. 11 a.
Case [II]. $\chi=8$, $\rho=\rho$, $\sin\theta_0=1/2\sqrt{2}$.

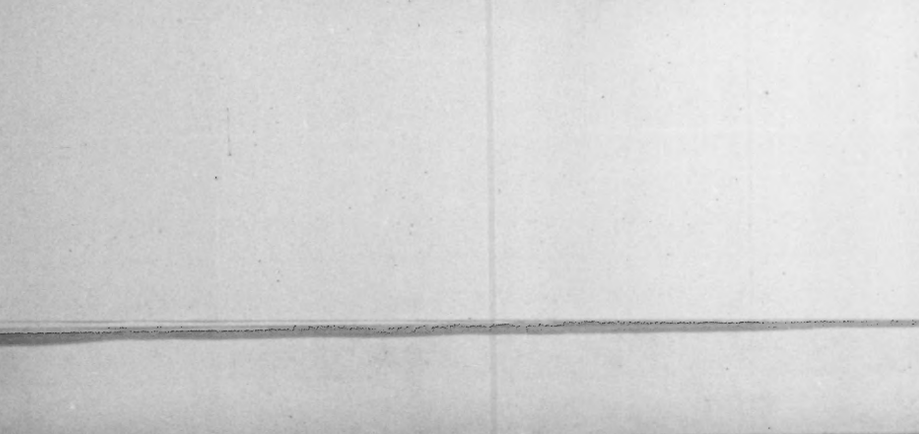

Fig. 11 b.
Case [II]. $\chi=8$, $\rho=\rho'$, $\sin\theta_0=1/2\sqrt{2}$.

From the final results Figs. 9a, 9b (case [I]) and 11a, 11b (case [II]), it becomes clear how the amplitude varies with respect to the period. While the period is short, displacements with more nodes are sometimes larger than those with less or without node; however, when the period becomes long, displacements due to L_0 become far larger than the displacements belonging to other branches.

Considering the above reasons we may conclude that we cannot expect large displacement belonging to the branch of Love-waves with nodes in the stratum.

Résumé

In this paper we treated four main subjects.

1) In a medium such as the semi-infinite elastic body with a superficial layer, one sort of reciprocal theorem holds.

2) The refracted waves may predominate if the period satisfies some condition (4.23). This property may give us a clue for determining the thickness of the superficial layer.

3) From a harmonic origin we can expect no reflected waves. This is, we think, due to the interference of direct and reflected waves.

4) The amplitude of Love-waves is determined as the function of the period, including the branches with one or several nodes in the layer. (Figs. 6, 7, 10 and 11)

---

12. 表面波の研究 VI

ラブ波及びその他の SH 波の發生

地震研究所　佐藤泰夫

ラブ波に關する研究は，今日その數が少いわけでは決してないが，しかもなほ，その本性が完全に理解しつくされた，といふ事は困難である．そこで，新しい問題ではないけれども，ラブ波その他の SH 波の發生の問題を，もう一度とり上げて，二三の性質をしらべてみたいと考へる．

本論文において扱つた問題は，ほぼ次にしめす四つにまとめることができる．

第一は相反定理である．半無限體表面に，他の物質からなる層がのつてゐるやうな媒質でも，やはり一種の相反定理が成立つが，この事を §2 において証明した．

第二に屈折波である．屈折波を表はす式は，既に積分表示がえられてゐるのであるが，從來はその計算が完全に行はれてゐなかつた．§4 においてはこの問題をとり上げ，今までよりは，いくらかくわしい積分の仕方を示した．その結果によれば，表面層のあつさ，速度，周期の間に，條件

$$\sqrt{(k^2-k'^2)}\cdot H=\sqrt{\left(\frac{1}{V_s^2}-\frac{1}{V_s'^2}\right)}\cdot pH=n\pi \quad \text{.....(4.23)}$$

がみたされる時には，その屈折波は特に卓越し，一般の屈折波では，$x^{-3/2}$ に比例して振幅が減少するのに比し，$x^{-1/2}$ に比例することとなる．この事から，我々は屈折波の卓越周期によつて，表面層の厚さを知る可能性があるのではないか，と考へる．(Table I 参照)

第三に反射波がある．反射波に相当して，当然 $f^2=k^2$ が 變位の積分表示式の分岐点となることが豫想されたが，意外にも，この点は特異点とはならない．從つて反射波は存在しない．これは，我々が最初 $\exp(ipt)$ に比例する震源を假定した結果，直接波と反射波が干渉して，互に消し合つた爲と考へられる．從つて，反射波を求めるためには，非周期的な振動源を考へて正確に計算を行はなくてはなるまい．(このことは從來注意されてゐなかつた．)

第四にラブ波を扱つた．ラブ波については，一個所で振巾を決定すれば，その縱方向の振巾分布は，完全にきまつてしまふといふ，都合の良い性質があるので，上記の相反定理もあはせ用ゐれば，震源も觀測点も，表面近くにあるとして一般性を失はない．定量的な結果は第 10, 11 圖にみられるが，一般的にいつて，周期があまり短くなければ，層内に節をもつ波の振巾は，さほど大きくならないであらう．

13. *On the Damping of Vibration of Actual Buildings. I.*

By Kiyoshi KANAI and Shizuyo YOSHIZAWA,

Earthquake Research Institute.

(Read March 18, 1952.—Received March 20, 1952.)

1. Introduction.

If there were no movements of damping or dissipation in the vibrations of a structure, it is probable that almost any structure would suffer damage in an earthquake owing to resonance, as actual earthquake movements consist generally of a large range of vibrational periods.

Fortunately, however, we have many kinds of damping and dissipation in a structure on land, so that a structure may be free from resonance even in synchronous vibrations. The question of air resistance and damping in the material used in the structure as well as in the foundation has been studied by some investigators[1]. The problem of the dissipation of vibrational energy of building in the form of elastic waves transmitted into the ground have been studied theoretically by us. The statistical studies concerning the damage of non-wooden buildings due to earthquake were explained considerably by the results of the theoretical studies based upon the idea of dissipation.

In this investigation, we examined the damping coefficient of many kinds of actual buildings, using the results of vibration experiments by means of vibrator in order to obtain a better insight into the aseismic properties of a structure.

---

1) K. SEZAWA, "On the Decay of Waves in Visco-Elastic Solid Bodies", *Bull. Earthq. Res. Inst.*, **3** (1927), 43.

K. SUYEHIRO, "On the Upper Limit of the Frequency of Transverse Vibration of Prismatic Bars", *Proc. Imp. Acad. Japan*, **4** (1928), 286.

K. SUYEHIRO, "On the Damped Transversal Vibration of Prismatic Bars", *Bull. Earthq. Res. Inst.*, **6** (1929), 63.

K. MUTO, "Biegungschwingungen mit Berücksichtigung der Stabmasse und der äusseren und inneren Dämpfung, *ZAMM*, **10** (1930), 346.

J. L. ALFORD and G. W. HOUSNER, "A dynamic test of a four story reinforced concrete building", *Publ. Earthq. Eng. Res. Inst.*, Aug., 1951.

2. Damping ratio of the actual buildings.

Firstly, the following process was used in examining the damping ratio of the actual buildings by means of resonance curves. When a constant force is applied to one mass system, the damping coefficient will be evaluated from the following formula.

$$h=\frac{1}{\sqrt{2}}\sqrt{1-\left\{1+\left(\frac{p_2^2-p_1^2}{2n_0^2}\right)^2\right\}^{-1/2}}, \quad \cdots\cdots\cdots\cdots(1)$$

where, $h=\varepsilon/n$, $\varepsilon=\xi/M$, $n=\sqrt{K/M}$, and ξ, K, M are damping coefficient, stiffness, mass respectively. p_2, p_1 and n_0 are frequencies of resonance curve at $1/\sqrt{2}$ times resonance amplitude and resonance freqnency. Generally speaking, for actual buildings, the value of $|p_2-p_1|/n_0$ is much less than 1, so equation (1) may be transformed as follows;

$$h=(p_2^2-p_1^2)/4n_0^2. \quad \cdots\cdots\cdots\cdots\cdots(2)$$

Damping ratio $v(=e^{\varepsilon T})$ will then be calculated easily by means of equation (2) using the results of vibration experiments, the results are shown in Fig. 1.

It will be seen that, for actual ferro-concrete buildings, the damping ratio increases with the decrease in natural period. This feature

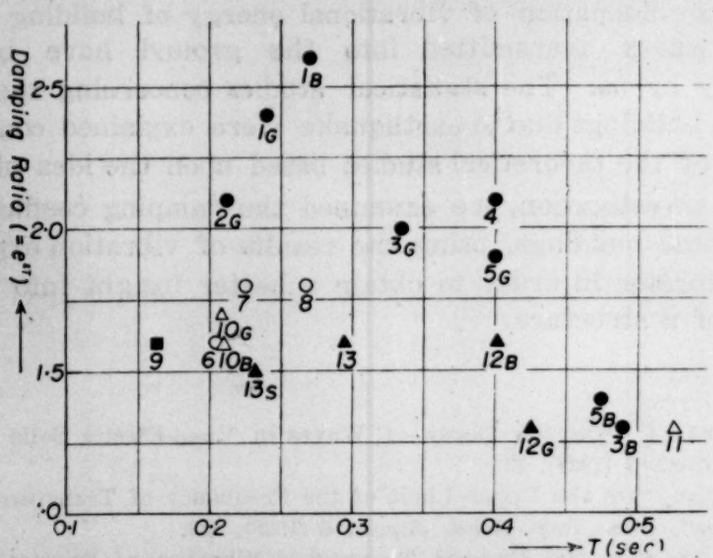

Fig. 1. Relation between the damping ratio and the natural period of actual buildings. Marks ●, ○, △, ▲, ■ and B, G represent ferro-concrete, non-column ferro-concrete, precast ferro-concrete, wooden, concrete block building and beam, girder direction respectively. Mark S reperesents the condition fixed brace-strut.

tells us that the rigid construction in ferro-concrete building is very desirable in preventing earthquake damage. On the other hand, for actual precast ferro-concrete, wooden and brick building, the damping ratio in question scarcely increases with the decrease in natural period, and takes very small value.

3. Damping coefficient of the actual buildings.

Secondly, the following method was used in examining the damping coefficient of the actual buildings. It can be shown that, in a one mass system with damping, the resonance amplitude is given by

$$y_0 = \frac{rmn_0^2}{M}\left(\frac{1}{2\varepsilon n_0}\right), \quad \cdots\cdots\cdots\cdots\cdots\cdots(3)$$

where m and r are the eccentric mass and eccentricity of vibrator. From equation (3), we obtain

$$\xi = \frac{\pi rm}{T_0 y_0}. \quad \cdots\cdots\cdots\cdots\cdots\cdots(4)$$

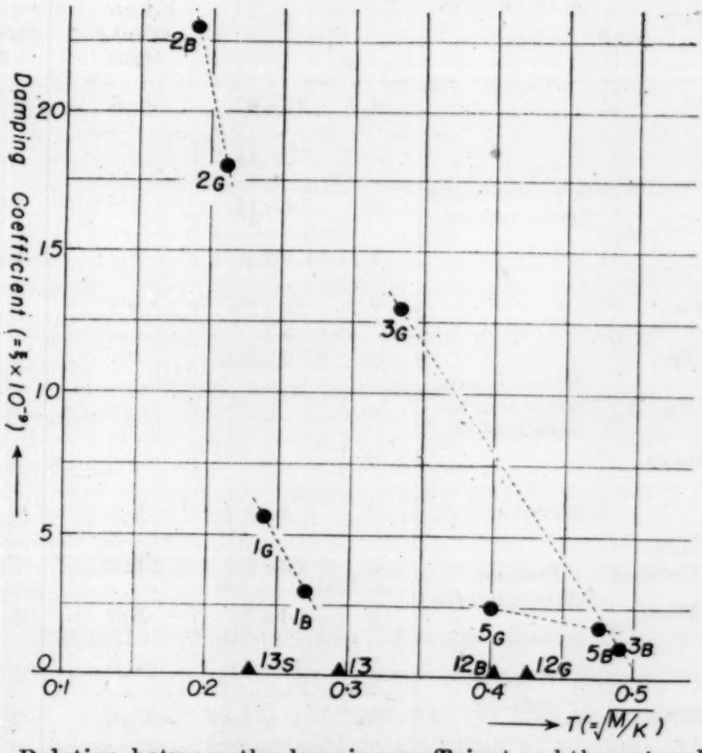

Fig. 2. Relation between the damping coefficient and the natural period of actual buildings. Marks ●, ▲ and B, G represent ferro-concrete, wooden building and beam, girder direction respectively.

Damping coefficient was then calculated by means of equation (4), and the results are given in Fig. 2. In Fig. 2, the relation between the two points connected by broken lines shows that the damping coefficient for the direction of short period is larger than the damping coefficient for long period of the same building. In other words, as the value of mass is constant for two directions of the same building, the damping coefficient of actual building increases with the increase in the vibrational stiffness.

This fact can be explained by the results[2] of theoretical studies, based upon the idea that the vibration energy of buildings dissipates to the ground as elastic waves originating from the foundation.

The constants of the buildings as well as the vibrator and the results of experiments are shown in Table I and Table II.

Table I.

No.	Name of Building	Construction	Stories	Plan (m)	Vibrator		
					Eccentricity (cm)	Eccentric mass (kg)	Location (floor)
1	Sanno A	Ferro-concrete fire-damaged	4	12×8	21.5	65	Roof
2	Sanno B		4	20×11.4	〃	〃	〃
3	Aoyama		3	54×11	〃	80	2nd
4	Mampei		4	44.4×21.0	〃	65	4th
5	Nonomiya		7	33×19	〃	〃	7th
6	Takaba No. 6	Non-column ferro-concrete apartment	4	37.9×6.6	〃	〃	Roof
7	Takaba No. 2		4	〃	〃	〃	〃
8	Nishinomiya		4	〃	〃	〃	〃
9	Matsui	Concrete block	2	4.3×3.5	9.0	45.7	2nd
10	Women's Medical College	Precast ferro-concrete	2	28×12	22.5	7.5	〃
11	Examination		2	4×3	5.0	45.7	〃
12	Chitose	Wooden school	2	10×8	11.0	〃	〃
13	Kamakura		1	11×4.6	23.0	1.63	Beam

2) K. SEZAWA and K. KANAI, "Improved Theory of Energy Dissipation in Seismic Vibrations of a Structure", *Bull. Earthq. Res. Inst.*, **14** (1936), 164.

Table II. Results of vibration experiment. G; girder direction, B; beam direction, (S); the condition fixed brace struts.

No.	Name of Build.	Direction	Resonance			Damping		
			Force (ton)	Period (sec)	Ampl. (mm)	$h(=\varepsilon/n)$	$v(=e^{\varepsilon T})$	$\xi\times10^{-9}$
1	Sanno A	G	0.96	0.24	0.0494	0.14	2.4	5.7
		B	0.76	0.27	0.0748	0.15	2.6	3.0
2	Sanno B	G	1.23	0.212	0.0252	0.11	2.1	18
3	Aoyama	G	0.61	0.334	0.025	0.11	2.0	13
		B	0.28	0.49	0.15	0.042	1.3	1.1
4	Mampei	G	0.35	0.40	0.034	0.12	2.1	2.7
5	Nonomiya	G	0.35	0.40	0.047	0.10	1.9	2.5
		B	0.24	0.475	0.097	0.052	1.4	1.8
6	Takaba No. 6	B	1.33	0.204	0.095	0.070	1.6	4.5
7	Takaba No. 2	B	1.09	0.225	0.160	0.091	1.8	2.2
8	Nishinomiya	B	0.77	0.268	0.155	0.090	1.8	1.8
9	Matsui	G	0.61	0.163	0.76	0.071	1.6	0.16
10	Women's Medical College	G	0.15	0.208	0.100	0.084	1.7	0.48
		B	0.15	0.210	0.167	0.078	1.6	0.33
11	Examination.	G	0.033	0.526	2.6	0.039	1.3	0.081
12	Chitose School	G	0.11	0.426	19.0	0,045	1.3	0.002
		B	0.12	0.402	14.0	0.074	1.6	0.003
13	Kamakura School	(S)	0.027	0.232	0.366	0.068	1.5	0.014
			0.017	0.295	0.920	0.073	1.6	0.004

4. Conclusion.

From the present investigations, it was found that the damping due to air resistance and the inner friction due to visco-elastic property of the materials composing the structure do not appear to dominate the damping in usual cases. But the dissipation of energy of vibrations into the ground seems to play an important part in the prevention of the vibrations of a building.

In conclusion, it must be added that the above is a research work done as a member of the Committee for Seismic Tests of Structures, undertaken under the grant from the Scientific Research Expenditure of Department of Education to whom the authors wish to express their gratitude. The authors also wish to express their hearty thanks to Mr. K. Nakagawa of the Architectual Research Institute, Messrs. T. Tanaka, T. Suzuki who has aided the authors in preparing the present paper.

13. 實在建物の振動減衰性について 第1報

地震研究所 { 金井 清
吉澤靜代

實在建物の振動減衰性については，空氣抵抗，材料の粘性抵抗，基礎のプラスチック性，振動勢力の地下逸散などが考えられる．實在建物の振動試驗結果から振動減衰係數を算出してみたところ，同じ建物でも，周期の短い振動方向については，減衰係數が大きいことが見られる．この事實は，振動勢力の地下逸散による減衰性で定性的には說明できるが，その他の原因とすると說明は容易でない．一般に，建物の周期が短くなると振動減衰性が增す傾向を示し，特に鐵筋コンクリート造の場合には著しい．このことは，短周期の建物は耐震的に剛性と減衰性の二重の意味で有利なことを敎えるものであろう．

又，鐵筋コンクリート造建物に比べると，組立鐵筋コンクリート造，木造，その他の構造の建物の減衰性は小さい．特に木造の減衰係數の小さいことは（Fig. 2 參照）輕い建物の地下逸散性が小さいという數理的結果に一致するものである．

14. *Vertical Earth Movements in Japan as Deduced from the Results of Rerunning the Precise Levels.*

By Naomi MIYABE,

Geographical Survey Institute.

(Read Sept. 16, 1947.—Received March 20, 1952.)

1. There are many lines of levels in Japan on which precise levels were rerun. By rerunning precise levels, the vertical displacements, relative to some reference marks, of bench-marks distributed along these lines are worked out, revealing the vertical earth movements in the regions concerned. The vertical earth movements in various regions thus obtained however refer to different reference marks, since the dates of the earlier and the later runs of levels are not the same for different lines, while the earth's surface is considered to be moving up- or downwards during the time intervals between the date of the precise levels along one line and that along another. Consequently, the vertical earth movement in a certain region cannot be compared, as it is, with those of other regions where precise levels were run at a different date.

In the present paper, the writer has tried to deduce from the vertical displacements of bench-marks in various regions at various epochs those which refer to the level of same data and which are due to the same epoch. For this purpose, the time interval from which the deduced vertical displacements are obtained must be carefully selected.

The distribution of lines of levels shown in Fig. 1 are those along which precise levels were run more than two times and the results of rerunning the precise levels along these lines are made use of in the present deduction of vertical earth movements. The dates of levelling surveys carried out along these lines are shown schematically in fig. 2.

The epoch and the time-interval from which the deduced vertical displacements of bench-marks are obtained were selected so as to satisfy the following two conditions, i.e., (1) the time-interval from which the vertical displacements of bench-marks distributed along each separate line of levels are obtained, must be common with each of the intervals for various lines and (2) the time-interval must be taken as long as possible. Thus the time-interval is taken as 1900–1928, as designated by the shaded part in Fig. 2.

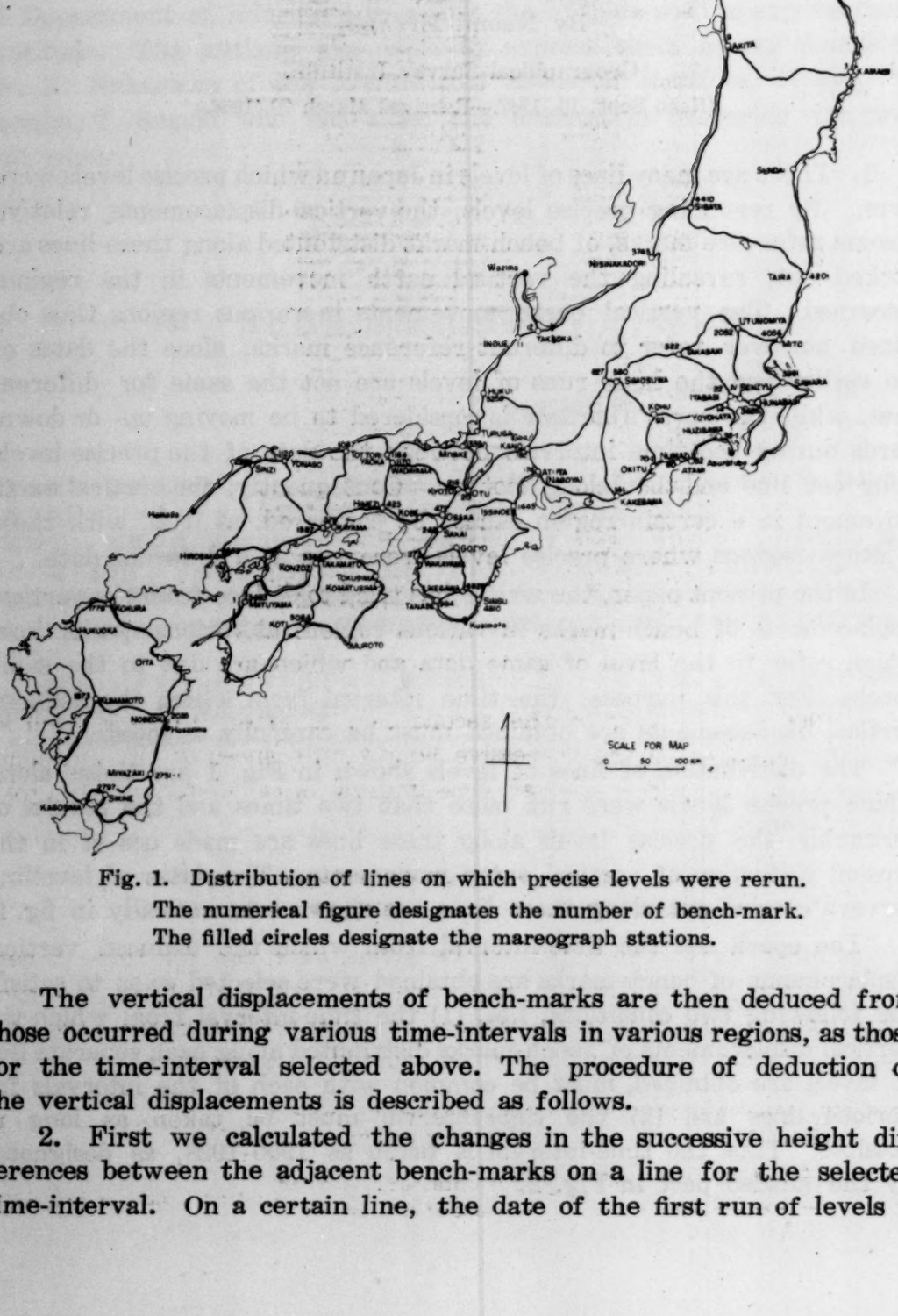

Fig. 1. Distribution of lines on which precise levels were rerun. The numerical figure designates the number of bench-mark. The filled circles designate the mareograph stations.

The vertical displacements of bench-marks are then deduced from those occurred during various time-intervals in various regions, as those for the time-interval selected above. The procedure of deduction of the vertical displacements is described as follows.

2. First we calculated the changes in the successive height differences between the adjacent bench-marks on a line for the selected time-interval. On a certain line, the date of the first run of levels is

Fig. 2a. Dates of Surveys for Lines of Levels.
(Circles designate the epochs of surveys)

before 1900, while that of the second run is after 1928. In such a case, the changes in the successive height differences of the adjacent bench-marks during the selected time-interval is calculated by the following formula:

$$\frac{(\text{hgt. diff, obtained by 2nd run})-(\text{hgt. diff. obtained by 1st run})}{(\text{date of 2nd run}) \quad - \quad (\text{date of 1st run})} \times 28.$$

On other lines, where the precise levels were run for three times and the date of the 1st run is before 1900 and that of the 3rd run after 1928, the changes in the successive height differences of the adjacent bench-marks are calculated by the following formula:

$$\frac{(\text{hgt. diff. obtained by 2nd run})-(\text{hgt. diff. obtained by 1st run})}{(\text{date of 2nd run}) \quad - \quad (\text{date of 1st run})} \times \{(\text{date of 2nd run})-1900\}$$

$$+\frac{(\text{hgt. diff. obtained by 3rd run})-(\text{hgt. diff. obtained by 2nd run})}{(\text{date of 3rd run}) \quad - \quad (\text{date of 2nd run})} \times \{1928-(\text{date of 2nd run})\}$$

Fig. 2b. Dates of Surveys for Lines of Levels.
(Circles designate the epochs of surveys)

For the calculation of the values of changes in the successive height differences of the adjacent bench-marks on the line along which the precise levels were run more than three times, a similar formula is applied. The values of changes in the successive height differences between the adjacent bench-marks thus calculated may however be quite erroneous owing to following reasons (a), although in the above calculation the earth's surface is regarded as moving under a constant

speed at the point where the bench-mark is situated during the time-interval of the successive surveys, the earth's surface may not exactly move under a constant speed, but move sometimes acutely and sometimes chronicly, (b) the precise levels were not rerun frequently so the movements of the earth's surface cannot be traced from time to time with sufficient accuracy, and (c) there are many lines of levels on which the dates of surveys differ very much from the selected time-interval, i.e., the dates of the first run of levels along several lines are long before 1900 and those of the last run of levels along several lines become long after 1928.

The writer thought that these errors could be corrected by adjusting the values of changes in the successive height differences between the adjacent bench-marks as calculated above so as the sums of these values over the lines of levels, forming circuits, would be always zero. In this case, of course it is assumed that the value of gravity remains the same during the above mentioned time-interval in the area under consideration, in association with the observed changes in the heights of the earth's surface.

Under this assumption, the values of changes in the successive height differences of the adjacent bench-marks distributed along the lines shown above in Fig. 1 are deduced. Then the vertical displacements of these bench-marks are worked out assuming that, (I) for the displacements of the bench-marks distributed on lines in Honsyu, the vertical displacement of B. M. 3 situated at Kusimoto is −188.0 mm. during 1900–1928, as estimated from the secular variation in the height of sea-level observed at the Kusimoto mareograph station; (II) for the displacements of the bench-marks in Kyusyu, the vertical displacement of B.M. 2635 at Nobeoka is 93.3 mm during the selected time-interval, as estimated from the mareogram data taken at Hosozima near Nobeoka; and, (III) for the displacements of the bench-marks in Sikoku, the height of B. M. 5078 situated near Komatusima has not changed during the time-interval under consideration.

The results of the present deduction are given in the annexed table.

The vertical displacements thus deduced of the bench-marks situated in Southern Kwanto include those due to acute crustal deformation associated with the 1923 earthquake, and the vertical displacements thus deduced of the bench-marks situated in the region of the Tango peninsula include those due to the crustal deformation associated with the 1927 earthquake.

Table. Deduced Vertical Displacements of Bench-marks.

(J denotes the junction point, and B the local base point.)

Locality	B.M.	Displace.	Locality	B.M.	Displace.	Locality	B.M.	Displace.
		mm			mm			mm
Kusi-	3	−188.0		4912	− 24.1		4977	−119.8
moto	9221	−188.8		4911	− 39.6		4976	−113.4
	9220	−168.4		4910	− 43.9		4975	−114.5
	9219	−177.1		4909	− 43.8		4974	−103.3
	9218	−161.7		4908	− 41.1		4973	−108.1
	9217	−161.2		4907	− 93.6		4972	− 93.6
	9216	−152.7		4906	−106.0		4971	−102.4
	9215	−159.5		4905	− 24.9		4970	− 97.2
	9214	−158.1		4904	− 31.2		4969	− 92.1
	9213	−150.1		4903	− 50.8		4968	− 92.6
	9212	−142.5		4902	− 48.4		4967	− 89.8
	9211	−135.7		4901	− 39.8		4966	− 90.2
	9210	−130.9		4900	− 37.0	Singu	J 4810	− 89.7
	9209	−130.1		4899	− 40.2			
	9208	−120.3		4898	− 40.1			
	9207	−120.4		4897	− 45.1	Waka-	J 271	− 8.5
	9206	−116.7		4896	− 41.8	yama	1586	− 25.6
	9205	−116.3		4895	− 38.6		1585	− 42.6
	9204	−116.5		4894	− 34.8		1584	− 7.5
	9203	−110.1		4893	− 32.7		1583	− 5.3
	9202	−107.0		4892	−192.1		1582	− 3.2
	9201	−105.3		4891	−105.6		1581	− 4.2
	9200	− 98.6		4890	− 18.6		1580	− 3.1
	9199	− 99.8		4889	8.7		1579	− 4.7
	9198	−100.3		4888	− 3.9		1578	− 16.0
	9197	− 99.7		4887	− 16.4		1577	− 20.2
	9196	− 78.1		4886	− 12.1		1576	− 3.0
	9195	− 77.9		4885	− 7.8		1575	− 17.5
	9194	− 67.5		4884	− 19.9		1574	− 24.1
	9193	− 62.4		4883	14.4		1573	− 26.8
	9192	− 61.0		4882	27.2		1572	− 29.6
	9191	− 64.7		4881	46.4		1571	− 30.3
	9190	− 56.7		4880	35.4		1570	− 30.1
	9189	−114.9		4879	30.9		1569	− 26.6
	9188	− 51.8		4878	10.1		1568	− 30.6
	9187	− 48.3		4877	− 14.9		1567	− 42.8
	9186	− 46.8		J 273	− 24.8		1566	− 39.6
	9185	− 46.2		272	− 19.6		1565	− 32.7
Tanabe	J 9184	− 45.0	Waka-	J 271	− 8.5		1564	− 39.0
	4928	− 45.7	yama				1563	− 32.1
	4927	− 38.9				Gozyo	J 1562	− 34.8
	4926	− 44.6	Kusi-	3	−188.0		4876	−127.1
	4925	− 27.1	moto	9221	−188.8		4875	− 45.4
	4924	− 27.5		4989	−186.5		4874	− 40.5
	4923	− 45.5		4988	−217.6		4873	− 34.7
	4922	− 31.5		4987	−165.3		4872	− 38.8
	4921	− 26.2		4986	−160.3		4871	− 46.8
	4920	− 26.2		4985	−158.9		4870	− 42.7
	4919	− 16.5		4984	−156.7		4869	− 41.2
	4918	− 14.9		4983	−146.1		4868	−103.7
	4917	− 20.9		4982	−152.0		4867	− 32.7
	4916	− 17.9		4981	−139.1		4866	− 39.9
	4915	− 43.1		4980	−130.4		4865	− 38.8
	4914	− 38.4		4979	−127.3		4864	− 37.7
	4913	− 26.2		4978	−124.8		4863	− 36.5

(to be continued.)

(continued.)

Locality	B.M.	Displace.	Locality	B.M.	Displace.	Locality	B.M.	Displace.
		mm			mm			mm
	4862	– 38.1		4961	– 69.4		4786	– 52.0
	4861	– 39.4		4960	– 64.3		4785	– 70.0
	4860	– 40.0		4959	– 57.0		4784	– 57.2
	4859	– 40.7		4958	– 57.5		4783	– 58.7
	4858	– 41.4		4957	– 54.2		4782	– 60.7
	4857	– 42.1		4956	– 55.8		4781	– 68.9
	4856	– 42.8		4955	– 52.1		4780	– 70.6
	4855	– 34.5		4954	– 48.2		4779	– 61.7
	4854	– 55.1		4953	– 51.0		4778	– 55.1
	4853	– 48.4		4952	– 44.2		4777	– 65.2
	4852	– 58.4		4951	– 46.2		4776	– 55.7
	4851	– 94.4		4950	– 43.6		4775	– 44.6
	4850	– 64.2		4949	– 42.2		4774	– 44.0
	4849	– 48.7		4948	– 44.1		4773	– 42.1
	4848	– 45.1		4947	– 50.6		4772	– 52.8
	4847	– 47.8		4946	– 37.4		4771	– 68.8
	4846	– 49.6		4945	– 41.1		4770	– 49.5
	4845	– 42.7		4944	– 69.9		4769	– 44.0
	4844	– 33.1		4943	– 53.4		4768	– 38.7
	4843	– 39.3		4942	– 30.6		4767	– 61.4
	4842	– 31.9		4941	– 73.5		4766	– 33.2
	4841	– 44.1		4940	– 32.8		4765	– 32.5
	4840	– 33.8		4939	3.0		4764	– 52.7
	4839	– 36.5		4938	– 37.5		4763	– 40.0
	4838	– 36.4		4937	– 33.0		4762	– 32.5
	4837	– 39.8		4936	– 34.6		4761	– 32.0
	4836	– 57.0		4935	– 35.2		4760	– 34.6
	4835	– 44.5		4934	– 37.6		4759	– 30.5
	4834	– 39.5		4933	– 38.5		4758	– 29.4
	4833	– 51.7		4932	– 47.9		4757	– 19.9
	4832	– 88.3		4931	– 49.9		4756	– 25.0
	4831	– 60.2		4930	– 43.4		4755	– 28.1
	4830	– 53.8		4929	– 51.0		4754	– 24.8
	4829	– 87.8	Tanabe	J 9184	– 45.0		4753	– 32.7
	4828	– 74.9					4752	– 21.0
	4827	– 61.0					4751	– 19.7
Uke-	J 4826	– 92.2	Singu	J 4810	– 89.7		4750	– 24.5
gawa	4825	– 70.5		4809	– 91.2		4749	– 16.5
	4824	– 66.3		4808	–103.6		4748	– 19.6
	4823	– 81.8		4807	– 87.0		4747	– 13.8
	4822	– 81.6		4806	– 87.3		4746	– 76.0
	4821	– 80.6		4805	– 85.7		4745	– 13.3
	4820	– 81.9		4804	– 81.8		4744	– 19.5
	4819	– 83.3		4803	– 81.9		4743	– 12.6
	4818	–112.2		4802	– 77.8		4742	– 18.8
	4817	– 83.5		4801	– 77.0		4741	– 15.8
	4816	– 84.1		4800	– 82.9		4740	– 12.5
	4815	–110.3		4799	– 83.8		4739	– 15.6
	4814	– 85.4		4798	–100.4		4738	– 10.3
	4813	– 80.8	Kino-	4797	– 83.9		4737	– 12.9
	4812	– 85.3	moto	4796	– 78.9		4736	– 14.4
	4811	– 84.9		4795	– 70.0		J 1510	– 20.9
Singu	J 4810	– 89.7		4794	– 78.2		1509	– 11.3
				4793	– 64.4		1508	– 17.2
				4792	– 60.3	Sana	1507	– 17.8
Uke-	4826	– 92.2		4791	– 62.6		1506	– 20.9
gawa	4865	– 75.1		4790	– 71.1		1505	– 17.9
	4964	– 71.7		4798	–190.7		1504	– 25.0
	4963	– 67.5		4788	– 57.8		1503	– 20.3
	4962	– 78.3		4787	– 57.5		1502	– 24.3

(to be continued.)

(continued.)

Locality	B.M.	Displace.	Locality	B.M.	Displace.	Locality	B.M.	Displace.
		mm			mm			mm
	1501	− 22.1		228	− 37.2		1432	17.3
Uzi-	1500	− 25.2	Suita	J 472	− 32.9		1433	15.1
yamada	1499	− 19.1					1434	14.4
	1498	− 15.0					1435	13.9
	1497	− 15.1	Sakai	J 246	−107.9		1436	− 80.9
	1496	− 16.0		1377	− 67.3		1437	16.3
	1495	− 13.0		1378	− 74.9		1438	14.8
	1494	− 12.8		1379	− 64.2		1439	13.5
	1493	− 12.0		1380	− 73.8		1440	13.5
	1492	− 14.3		1381	− 79.3		1441	8.2
	1491	− 17.7		1382	− 73.3		1442	3.7
	1490	− 18.0		1383	− 59.5		1443	0.2
	1489	− 10.5		1384	− 41.0		1444	− 8.1
	1488	− 11.7		1385	− 35.7	Issin-	J 1445	− 16.1
	1487	− 16.0		1386	− 30.1	den		
	1486	− 13.0		1387	− 38.2			
	1485	− 12.4		1388	− 33.1	Suita	J 472	− 32.9
	1484	− 13.0		1389	− 27.8		227	− 23.7
	1483	− 14.2		1390	− 34.6		226.1	− 14.5
	1482	− 15.7		1391	− 33.1		226	− 15.9
	1581	− 15.8		1392	− 38.8		225.1	− 5.6
Issin-	J 1445	− 16.1		1393	− 71.2		225	− 9.5
den				1394	− 55.0		224.1	− 6.3
				1395	− 45.2		224	2.5
Waka-	J 271	− 8.5		1396	− 35.4		223.1	− 5.8
yama	270	− 9.3		1397	− 37.4		223	− 9.0
	269	− 10.2		1398	− 23.4		222.1	8.2
	268	− 9.3		1399	− 22.2		222	2.0
	267	− 22.6		1400	− 37.2		221.1	− 4.2
	266	− 21.7		1401	− 39.4		221	− 20.7
	265	− 25.6		1402	−225.7		220	−134.5
	264	− 27.6		1403	− 22.3		219.1	−248.3
	263	− 31.7		1404	− 29.3		219	−134.3
	262	− 35.7		1405	− 29.9		218.1	− 96.1
	261	− 44.0		1406	− 24.0		218	− 63.3
	260	− 39.2		1407	− 22.5		217.1	− 59.5
	259	− 45.7		1408	− 21.1		217	− 43.5
	258	− 51.4		1409	− 19.6		216.1	− 27.8
	257	− 57.2		1410	− 31.1	Kyoto	J 216	− 22.1
	256	− 74.8		1411	− 26.4		215.1	− 20.3
	255	− 78.8		1412	− 13.8		215	− 7.7
	254	− 80.2		1413	− 6.8		214.1	− 4.5
	253	− 71.7		1414	− 6.4		214	9.8
	252	− 77.6		1415	− 5.9		213.1	− 19.5
	251	− 70.8		1416	− 11.1	Otu	J 213	− 29.9
	250	− 87.8		1417	11.4			
	249	− 73.0		1418	6.8			
	248	− 79.4		1419	− 7.4	Otu	J 213	− 29.9
	247	− 85.3		1420	− 15.3		212.1	− 63.7
Sakai	J 246	−107.9		1421	− 14.8		212	− 31.4
	245	− 79.6		1422	− 16.2		211.1	− 47.0
	244	− 94.7		1423	− 18.9		211	− 21.4
	243	− 84.7		1424	− 21.6		210.1	− 13.1
	235	−113.2		1425	− 32.4		210	− 12.5
	234	− 80.1		1426	− 27.2		209.1	− 22.2
	233	− 63.5		1427	− 21.5		209	− 5.0
	232	−200.4		1428	− 8.4		208.1	− 9.4
	229.1	−127.2		1429	13.4		208	− 14.5
	J 229	− 45.4		1430	117.0		207.1	− 10.5
	228.1	− 41.3		1431	19.8		207	− 7.3

(to be continued.)

(continued.)

Locality	B.M.	Displace.	Locality	B.M.	Displace.	Locality	B.M.	Displace.
		mm			mm			mm
	206.1	− 8.3		5189	− 15.9		5249	− 99.4
	206	− 12.1		5190	− 17.2		5250	− 96.7
	205.1	− 21.7		5191	− 20.7		5251	− 94.0
	205	− 21.1		5192	− 20.3		5252	− 97.0
	204.1	− 29.7		5193	− 24.2		5253	− 93.8
	204	− 31.6		5194	− 23.8		5254	− 90.5
	203.1	− 49.7		5195	− 31.5		5255	− 91.0
	203	− 31.3		5196	− 31.1		5256	− 94.5
	202.1	− 36.0		5197	− 27.9		5257	− 93.0
	202	− 34.5		5198	− 30.2	Hukui	J 5258	− 87.4
	201.1	− 30.2		5199	− 32.6			
	201	− 30.7		5200	− 34.8			
	200.1	− 28.8		5201	− 35.3	Hukui	J 5258	− 87.4
	200	− 33.8		5202	− 39.7		903	− 90.4
	199.1	− 32.0		5203	− 29.2		904	− 89.9
	199	− 36.1		5204	− 44.6		905	− 89.6
	198.1	− 50.0		5205	− 57.1		906	− 96.9
	198	− 37.5		5206	− 52.5		907	− 78.4
	197.1	− 46.9		5207	− 60.2		908	− 66.8
	197	− 53.8		5208	− 58.0		909	− 45.8
	196.1	− 64.4		5209	− 66.4		910	− 50.0
	196	− 64.6		5210	− 65.2		911	− 48.0
	195.1	− 64.5		5211	− 65.4		912	− 63.0
	195	− 61.6		5212	− 69.5		913	− 44.2
	194.1	−148.6		5213	− 73.1		914	− 38.8
	194	− 18.9		5214	− 75.5		915	− 35.3
	193.1	− 36.7		5215	− 64.2		916	− 25.6
	193	− 31.2		5216	− 66.9		917	− 16.0
	192.1	− 19.6		5217	− 75.8		918	− 15.7
	192	− 20.0		5218	− 80.2		919	− 13.7
	191.1	− 28.0		5219	− 84.5		920	− 13.6
	191	− 45.8		5220	− 85.2		921	− 26.5
	190.1	− 53.7		5221	− 89.0		922	− 46.0
	190	− 70.7		5222	− 91.1		923	− 17.6
	189.1	− 69.8		5223	− 91.5		924	− 32.4
	189	−190.4		5224	− 91.8		925	− 27.9
	188.1	− 82.0		5225	− 92.5		926	− 29.4
	188	− 80.1		5226	−105.6		927	− 13.9
	187.1	− 63.5		5227	−107.5		928	− 19.5
	187	− 70.7		5228	−105.1		929	− 14.1
	186.1	−203.6		5229	−116.4		930	− 17.6
	186	− 43.9		5230	−107.3		931	− 2.7
	185.1	− 36.4		5231	−113.4		932	− 5.8
Kano	J 185	− 41.4		5232	−114.1		933	− 9.9
	716	− 25.7		5233	−113.5		934	− 42.4
	717	− 23.9		5234	−110.9		935	− 20.8
	718	− 20.7		5235	−109.4		936	− 17.5
	719	− 12.8		5236	−109.9		937	− 19.4
	720	7.5		5237	−106.7		938	− 12.7
	721	1.3		5238	−112.6		939	− 9.0
	722	2.7		5239	−110.4		940	− 7.4
	723	1.4		5240	−107.8		941	− 5.9
	724	− 16.1		5241	−106.9		942	− 22.4
	J 725	− 9.3		5242	−105.9		943	− 8.0
	5183	− 14.3		5243	−105.1		944	− 9.7
	5184	− 15.6		5244	−103.9		945	− 8.3
	5185	− 18.3		5245	−102.7		946	− 14.6
	5186	− 24.1		5246	−102.9		947	− 14.5
	5187	− 20.4		5247	−101.4		948	− 17.3
	5188	− 19.8		5248	−102.0		949	− 16.6

(to be continued.)

(continued.)

Locality	B.M.	Displace.	Locality	B.M.	Displace.	Locality	B.M.	Displace.
		mm			mm			mm
	950	– 13.3		460	– 37.0		1179	– 57.4
	951	– 23.0		459	– 40.3		1178	– 50.6
	952	– 12.6		458	– 48.4		1177	– 52.4
	953	– 9.4		457	– 59.3		1176	– 48.7
	954	– 10.5		456	– 18.5		1175	– 51.8
Miyake	J 1339	– 5.2		455	– 51.1		1174	– 52.2
	1338	– 10.1		454	– 47.7		1173	– 52·5
	1337	– 7.2		453	– 51.3		1172	– 58.3
	1336	– 9.2		452	– 46.5		1171	– 53.1
	1335	– 8.0		451	– 41.8	Wada-	J 1170	– 55.3
	1334	– 11.2		450	– 44.0	yama	1169	– 55.7
	1333	– 10.8		449	– 48.5		1168	– 53.8
	1332	– 11.1		448	– 38.7		1167	– 66.1
	1331	– 12.4		447	– 43.7		1166	– 58.4
	1330	– 20.6		446	– 43.4		1165	– 57.0
	1329	– 24.4		445	– 43.1	Yaoka	J 1164	– 57.3
	1323	– 30.3		444	– 39.3			
	1327	– 30.3		443	– 35.5			
	1326	– 39·6		442	– 33.3	Kyoto	J 216	– 22.1
	1325	– 41.2		441	– 35.0		J 239	– 21.0
	1324	– 38.1		440	– 40.0		1299	– 20.5
	1323	– 34.1		439	– 44.2		1298	– 33.2
	1322	– 40.9		438	– 43.1		1297	– 31.1
	1321	– 44.4		437	– 47.3		1296	– 23.7
	1320	– 40.8		436	– 43.7		1295	– 9.9
	1319	– 43.2		435	– 38.0		1294	4.0
	1318	– 31.8		434	– 42.2		1293	6.0
	1317	– 37.3		433	– 40.1		1292	1.0
	1316	– 33.9		432	– 43.2		1291	– 5.8
	1315	– 33.2		431	– 51.3		1290	2.0
	1314	– 35.5		430	– 49.8		1289	– 1.1
	1313	– 34.8		429	– 45.4		1288	– 10.8
	1312	– 31.7		428	– 41.1		1287	– 4.4
	1311	– 33.8		427	– 45.2		1286	– 4.2
	1310	– 33.6		426	– 54.2		1285	– 12.9
	1309	– 32.7		425	– 53.9		1284	– 0.9
	1308	– 28.8		424	– 58.9		1283	– 5.7
	1307	– 37.9	Himezi	J 423	– 59.2		1282	– 3.4
	1306	– 27.4		1201	– 64.4		1281	– 2.8
	1305	– 31.2		1200	– 60.7		1280	2.0
	1304	– 28.1		1199	– 56.2		1279	1.4
	1303	– 31.9		1198	– 57.0		1278	0.8
	1302	– 33.7		1197	– 56.8		1277	– 4.2
	1301	– 31.4		1196	– 55.6		1276	– 8.3
	1300	– 33.6		1195	– 54.6		1275	– 8.1
Otu	J 213	– 29.9		1194	– 54.9		1274	– 11.5
				1193	– 55.5		1273	– 11.8
				1192	– 56.3		1272	– 18.5
Suita	J 472	– 32.9		1191	– 56.7		1271	– 16.8
	471	– 32.2		1190	– 60.3		1270	– 18.7
	470	– 31.5		1189	– 62.9		1269	– 21.5
	469	– 26.7		1188	– 60.0		1268	– 23.7
	468	– 19.7		1187	– 56.1		1267	– 28.5
	467	– 12.7		1186	– 56.9		1266	– 25.4
	466	– 25.3		1185	– 58.1		1265	– 31.0
	465	– 25.2		1184	– 58.2		1264	– 31.0
	464	– 29.1		1183	– 54.7		1263	– 32.7
	463	– 29.8		1182	– 50.4		1262	– 32.4
	462	– 30.5		1181	– 57.7		1261	– 35.8
	461	– 33.8		1180	– 48.9		1260	– 40.6

(to be continued.)

(continued.)

Locality	B.M.	Displace.	Locality	B.M.	Displace.	Locality	B.M.	Displace.
		mm			mm			mm
	1259	− 49.0		1240	6.4		405	− 47.3
	1258	− 48.8		1239	7.0		404	− 36.0
	1257	− 48.7		1238	−103.9		403	− 35.3
	1256	− 40.3		1237	−152.0		402	− 37.2
	1255	− 41.1		1236	654.4		401	− 36.8
	1254	− 42.8		J 1235	542.8		400	− 31.4
	1253	− 58.2		1234	431.3		399	− 34.0
	1252	− 68.7		1233	285.7		398	− 36.5
	1251	− 55.3		J 1232	102.9		397	− 38.5
	1250	− 72.9		1231	43.8		396	− 40.9
	1249	− 59.5		1230	− 82.2		395	− 40.2
	1248	− 60.9		J 1229	174.0		394	− 39.6
	1247	− 68.2		1228	325.2		393	− 35.2
	1246	− 68.4		1227	199.0		392	− 39.9
	1245	− 78.5		1226	170.4		391	− 42.3
	1244	− 72.1		1225	120.6		390	− 40.5
	1243	− 62.0		1224	100.5		389	− 64.7
	1242	− 59.8		1223	63.8		388	− 59.6
Wada-yama	J 1170	− 55.3		1222	42.2		387	− 54.5
				1221	38.1		386	− 42.6
				1220	5.0		385	− 44.4
Miyake	1339	− 5.2		1219	− 0.3		384	− 39.0
	1340	− 3.0		1218	− 22.9		383	− 41.7
	1341	− 4.4		1217	− 8.6		382	− 33.5
	1342	− 11.1		1216	− 11.7		381	− 33.6
	1343	− 0.5		1215	− 10.2		380	− 31.7
	1344	6.6		1214	− 19.4	Oka-yama	J 379	− 29.8
	1345	5.8		1213	− 56.1		1001	− 20.2
	1346	5.0		1212	−497.5		1002	− 10.6
	1347	6.8		1211	−241.0		1003	− 19.4
	1348	10.9		1210	−171.9		1004	− 18.4
	1349	6.4		1209	− 96.8		1005	− 10.6
	1350	6.8		1208	− 89.5		1006	− 10.5
	1351	4.8		1207	− 49.7		1007	− 12.7
	1352	0.0		1206	− 49.3		1008	− 15.4
	1353	0.8		1205	− 52.4		1009	− 18.2
	1354	− 1.6		1204	− 48.5		1010	− 20.8
	1355	2.3		1203	− 53.4		1011	− 12.1
	1356	3.7		1202	− 56.8		1012	− 3.3
	1357	11.6	Yaoka	J 1164	− 57.3		1013	0.5
	1358	12.9					1014	− 1.2
	1359	11.2					1015	− 16.4
	1360	9.6	Himezi	J 423	− 59.2		1016	0.6
	1361	10.6		422	− 56.7		1017	3.3
	1362	11.6		421	− 54.6		1018	2.7
	1363	19.3		420	− 54.9		1019	3.7
	1364	16.2		419	− 26.7		1020	− 4.5
	1365	16.2		418	− 39.6		1021	0.8
	1366	16.2		417	− 52.4		1022	3.8
	1367	17.6		416	− 51.8		1023	6.8
	1368	17.2		415	− 51.5		1024	8.7
	1369	19.3		414	− 53.6		1025	7.6
	1370	22.1		413	− 52.8		1026	7.5
	1371	11.7		412	− 52.3		1027	12.2
	1372	6.2		411	− 60.8		1028	− 7.1
	1373	21.9		410	− 48.5		1029	11.6
	1374	7.9		409	− 44.4		1030	5.6
	1375	16.4		408	− 50.2		B 32	5.4
	1376	− 18.3		407	− 44.5		1031	5.2
	1241	− 12.4		406	− 51.1		1032	3.5

(to be continued.)

(continued.)

Locality	B.M.	Displace.	Locality	B.M.	Displace.	Locality	B.M.	Displace.
		mm			mm			mm
	1033	1.7		1141	− 19.6		1106	− 5.4
	1034	4.2		1140	− 18.8		1107	− 5.7
	1035	4.7		1139	− 18.6		1108	− 2.3
	1036	− 1.3		1138	− 21.2		1109	− 1.6
	1037	− 24.6		1137	− 34.0		1110	0.8
	1038	− 47.9		1136	− 30.5		1111	9.1
	1039	3.8		1135	− 28.6		1112	9.9
	1040	8.2		1134	− 44.7		1113	9.4
	1041	− 1.6		1133	− 42.7		1114	8.4
	1042	4.5		1132	− 42.6		1115	9.3
	1043	0.5		1131	− 37.9		1116	8.6
	1044	2.9		1130	− 43.0		1117	7.0
	1045	10.4		1129	− 40.0		1118	10.2
	1046	22.1		1128	− 34.6		1119	19.5
	1047	− 7.9		1127	− 36.7	Yonago	J 1120	15.6
	1048	− 10.4		1126	− 44.0		2253	18.0
	1049	− 14.1		1125	− 89.7		2254	13.3
	1050	− 20.9		1124	− 41.5		2255	− 36.6
	1051	− 35.0		1123	− 45.8		2256	24.6
	1052	− 29.4		1122	− 48.7		2257	22.5
	1053	− 23.7		1121	− 69.0		2258	13.7
	1054	− 26.9	Tottori	J 1067	− 59.1		2259	10.1
	1055	− 28.0		1068	− 34.3		2260	18.7
	1056	− 30.9		1069	− 31.5		2261	14.4
	1057	− 33.8		1070	− 25.1		2262	20.7
	1058	− 24.1		1071	− 13.4		2263	20.0
	1059	− 16.9		1072	− 14.8		2264	− 0.1
	1060	− 25.7		1073	− 5.9		2265	11.6
	1061	− 31.9		1074	5.9		2266	8.4
	1062	− 58.5		1075	1.2		2267	11.9
	1063	− 32.0		1076	− 7.0		2268	9.0
	1064	− 19.8		1077	−128.1		2272	15.8
	1065	− 28.3		1078	− 9.2		2273	1.1
	1066	− 50.5		1079	− 6.8		2274	− 2.6
Tottori	J 1067	− 59.1		1080	1.4		2275	6.2
				1081	− 9.3		2276	− 0.6
				1082	2.6		2277	3.4
Yaoka	J 1164	− 57.3		1083	5.1		2278	16.5
	1163	− 56.1		1084	− 0.4		2279	18.9
	1162	− 52.3		1085	3.9		2280	16.8
	1161	− 56.2		1086	3.2	Sinzi	J 2269	14.0
	1160	− 50.7		1087	0.1			
	1159	− 51.7		1088	− 0.7			
	1158	− 42.8		1089	− 5.7	Oka-	J 379	− 29.8
	1157	− 37.6		1090	− 6.5	yama	378	− 24.4
	1156	− 31.0		1091	− 1.4		377	− 19.0
	1155	− 20.0		1092	0.4		376	− 19.8
	1154	− 21.2		1093	− 6.4		375	− 23.9
	1153	− 24.7		1094	0.1		J 1587	− 18.5
	1152	− 24.1		1095	− 1.3		1588	− 20.5
	1151	− 29.7		1096	− 2.9		1589	− 38.2
	1150	− 34.0		1097	− 6.4		1590	− 22.6
	1149	− 26.2		1098	− 4.1		1591	− 25.2
	1148	− 27.4		1099	− 3.4		1592	− 38.7
	1147	− 24.9		1100	− 2.4		1593	− 31.0
	1146	− 19.1		1101	− 6.6		1594	− 34.5
	1145	− 18.5		1102	− 9.7		1595	− 17.2
	1144	− 14.4		1103	− 7.6		1596	− 24.9
	1143	− 15.4		1104	− 2.7		1597	− 16.0
	1142	− 16.3		1105	− 6.8		1598	− 9.9

(to be continued.)

(continued.)

Locality	B.M.	Displace.	Locality	B.M.	Displace.	Locality	B.M.	Displace.
		mm			mm			mm
	1599	– 11.5		1659	– 32.5		2315	21.1
Yakake	1600	– 13.6		1660	– 33.7		2314	3.7
	1601	– 15.6		1661	– 33.1		2313	10.8
	1602	– 15.3		1662	– 39.5		2312	36.1
	1603	– 15.5		1663	– 41.8		2311	48.6
	1604	– 13.2		1664	– 43.2	Ton-	2310	47.1
	1605	– 10.9		1665	– 35.5	bara	2309	49.8
	1606	– 16.2		1666	– 74.2		2308	29.0
	1607	– 9.3		1667	– 66.4		2307	45.8
Takaya	1608	– 14.9		1668	– 65.0		2306	48.5
	1609	– 15.1	Hiro-	J 1669	– 65.3		2305	44.1
	1610	– 13.8	sima	2364	– 44.2		2304	48.0
	1611	– 14.4		2363	– 41.7		2303	49.8
Kamibe	1612	– 25.5		2362	– 52.0		2302	45.2
	1613	– 8.8		2361	– 34.0		2301	43.5
	1614	– 8.7		2360	– 24.8		2300	33.3
	1615	8.3		2359	– 25.0	Kakeai	2299	33.0
	1616	13.8		2358	– 71.5		2298	38.3
	1617	10.2	Kabe	J 2357	– 34.9		2297	27.0
	1618	15.5		2356	– 32.3		2296	11.4
	1616	10.6		2355	– 29.6		2295	12.1
Imazu	1920	10.7		2354	– 28.6		2294	29.8
	1621	5.6		2353	– 27.3		2293	23.6
	1622	4.2		2352	– 26.7		2292	35.9
	1623	0.6		2351	– 29.8		2291	29.8
	1624	5.8		2350	– 26.2		2290	14.8
Onomiti	1625	4.9		2349	– 19.1		2289	25.0
	1626	6.6		2348	– 14.7		2288	– 33.5
	1627	6.3		2347	– 10.0	Ii	2287	– 58.3
	1628	6.1		2346	– 12.0		2286	12.0
	1629	6.7		2345	– 9.0		2285	8.1
	1630	8.8		2344	– 7.6		2284	17.0
	1631	7.3	Yosida	2343	– 10.5		2283	26.0
	1632	9.3		2342	0.3		2282	19.9
	1633	– 12.6		2341	3.8		2281	19.2
	1634	– 68.6		2340	6.3	Sinzi	J 2269	14.0
	1635	– 29.4		2339	7.5		2270	17.1
Hongo	1636	– 23.9		2338	– 2.0		2271	– 13.5
	1637	– 9.4		2337	2.5		2968	– 0.9
	1638	– 7.9		2336	4.8		2969	– 4.5
	1639	– 9.1		2335	11.2		2970	12.3
	1640	– 10.0		2334	2.8		2971	13.9
	1641	– 11.4		2333	11.8		2972	16.1
	1642	– 20.2		2332	12.5		2973	23.7
	1643	– 20.5		2331	7.0		2974	29.5
	1644	– 25.0	Miyosi	2330	7.7		2975	19.1
Simari	1645	– 24.8		2329	68.4		2976	28.9
	1646	– 27.3		2328	7.0		2977	35.2
	1647	– 31.2		2327	14.1		2978	26.8
	1648	– 27.1		2326	22.5		2979	26.9
	1649	– 39.4		2325	26.8		2980	30.5
	1650	– 36.7		2324	24.3		2981	36.8
	1651	– 44.6		2323	27.6		2982	34.0
	1652	– 39.3		2322	27.8		2983	28.7
	1653	– 40.8		2321	27.1		2984	6.5
	1654	– 33.9		2320	28.1		2985	21.3
	1655	– 33.3		2319	32.7		2986	26.9
Seno	1656	– 35.1	Akaisi	2318	37.9		2987	29.0
	1657	– 36.9		2317	35.6		2988	28.9
	1658	– 32.3		2316	32.8		2989	27.8

(to be continued.)

(continued.)

Locality	B.M.	Displace.	Locality	B.M.	Displace.	Locality	B.M.	Displace.
		mm			mm			mm
	2990	25.0		2192	− 6.0		2252	13.7
	2991	1.9		2193	− 8.7	Yonago	J 2253	15.9
	2992	21.8		2194	− 7.6			
	2993	2.5		2195	− 6.6			
	2994	27.3		2196	− 10.7	Atuta	J 174.1	− 5.2
	2995	27.0		2197	− 14.8		1480	− 70.4
	2996	14.2		2198	− 15.8		1479	− 23.4
	2997	26.7		2199	− 16.2		1478	− 25.8
	2998	27.0		2200	− 19.2		1477	− 33.4
	2999	24.5		2201	− 22.2		1476	− 32.8
	3000	25.1		2202	− 18.5		1475	− 77.6
	3001	24.4		2203	− 20.4		1474	− 62.1
	3002	24.3		2204	− 15.5		1473	− 66.9
	3003	3.9		2205	− 17.7		1472	−223.9
	3004	19.2		2206	− 13.0		1471	−111.4
	3005	4.4		2207	− 8.3		1470	−207.9
	3006	7.5		2208	− 8.4		1469	− 57.6
	3007	13.3		2209	− 8.6		1468	− 47.7
	3008	8.8		2210	− 8.7		1467	− 35.4
	3009	11.9		2211	− 8.9		1466	− 34.8
	3010	14.7		2212	− 9.0		1465	− 22.2
	3011	12.9		2213	− 7.2		1464	− 19.0
	3012	91.6		2214	− 5.5		1463	− 15.1
	3013	− 1.1		2215	− 2.1		1462	− 3.8
	3014	− 0.6		2216	− 1.2		1461	− 20.6
	3015	− 32.2		2217	− 3.9		1460	− 9.9
	3016	4.5		2218	11.3		1459	− 4.0
	3017	− 19.1		2219	15.6		1458	− 5.9
	3018	− 6.5		2220	16.8		1457	3.0
	3019	− 4.5		2221	15.5		1456	3.2
	3020	8.1		2222	16.7		1455	3.3
	3021	9.7		2223	25.7		1454	− 7.2
	3022	2.1		2224	26.3		1453	− 17.9
	3023	− 7.4		2225	27.0		1452	− 1.0
	3024	6.2		2226	27.6		1451	− 18.1
	3025	− 1.6		2227	29.1		1450	− 7.9
	3026	4.3		2228	30.5		1449	− 4.8
	3027	7.0		2229	32.0		1448	− 6.7
	J 3028	− 93.8		2230	30.7		1447	− 8.4
Hamada	6	− 1.1		2231	26.3		1446	− 12.6
				2232	22.7	Issinden	J 1445	− 16.1
				2233	15.8			
Oka-	J 379	− 29.8		2234	7.0			
yama	378	− 24.4		2235	18.6	Atuta	J 174.1	− 5.2
	377	− 19.0		2236	15.3		174	− 8.3
	376	− 19.8		2237	19.9		173.1	4.6
	J 375	− 23.9		2238	10.2		173	− 10.8
	J 1587	− 18.5		2239	9.2		172.1	5.6
	2180	− 22.9		2240	9.6		172	19.8
	2181	− 18.3		2241	9.9		171.1	25.0
	2182	− 23.0		2242	8.0		171	24.6
	2183	− 27.7		2243	6.1		170.1	20.3
	2184	− 16.3		2244	9.3		170	24.4
	2185	− 17.6		2245	9.0		169.1	27.9
	2186	− 14.4		2246	8.6		169	35.6
	2187	− 17.1		2247	10.4		168.1	31.3
	2188	− 12.5		2248	8.5		168	36.3
	2189	− 12.4		2249	6.6		167.1	30.7
	2190	− 12.3		2250	8.9		167	9.1
	2191	− 9.4		2251	11.2		166.1	7.9

(to be continued.)

(continued.)

Locality	B.M.	Displace.	Locality	B.M.	Displace.	Locality	B.M.	Displace.
		mm			mm			mm
	166	28.2		136	−103.2		53	6.3
	165.1	35.9	Simada	135.1	−132.9		52.1	− 28.2
	165	34.7		135	−124.7	Atami	J 52	45.4
	164.1	37.4		134.1	−137.6			
	164	32.5		134	−139.7			
	163.1	38.0		133.1	−158.7	Kake-	J 141	− 34.8
	163	39.9	Huzieda	133	−140.7	gawa	5259	14.1
	162.1	217.3		132.1	−158.9		5260	15.5
	162	38.1		132	−195.7		5261	26.3
	161.1	41.7		131.1	−156.5		5262	25.4
	161	45.3		131	−137.3		5263	60.1
	160.1	50.0		130.1	−145.2		5264	68.9
	160	55.5		130	−153.1		5265	73.6
	159.1	56.0		129.1	−148.9		5266	76.6
	159	53.9		129	−161.7		5267	78.5
	158.1	57.7	Sizuoka	128.1	−155.0		5268	82.6
	158	67.1		128	−165.0		5269	88.2
	157.1	68.1		127.1	−181.2		5270	99.7
	157	73.3		127	−146.1		5271	76.3
	156.1	77.4		126.1	−121.2		5272	107.1
	156	79.1		126	−120.5		5273	48.5
	155.1	74.3		125.1	−114.9		5274	100.0
	155	76.0	Simizu	125	−133.5		5275	95.4
	154.1	72.8		124.1	−126.8		5276	109.1
	154	71.9		124	−123.9		5277	122.8
	153.1	76.3	Okitu	J 70.1	−126.1		5278	126.6
	153	81.0		70	−125.6		5279	129.1
	152.1	78.9		69.1	−136.0		5280	98.5
	152	66.8		69	−122.4		5281	119.5
	151.1	74.5		68.1	−121.1		5282	102.9
	151	74.7		68	−118.7		5283	67.9
	150.1	72.1		67.1	−132.2		5284	6.8
	150	70.1		67	−114.8		5285	49.2
	149.1	57.5		66.1	−109.6		5286	− 18.6
	149	56.4		66	−116.9		5287	194.1
	148.1	43.4		65.1	−116.6		5288	108.4
	148	28.2		65	−113.8		5289	61.2
	147.1	23.1		64.1	−110.8		5290	125.6
	147	19.9		64	−107.7		5291	131.5
	146.1	20.6		63.1	−104.6		5292	126.1
	146	− 1.6		63	− 95.7		5293	121.6
	145.1	16.5		62.1	− 91.0		5294	121.2
	145	12.5		62	− 88.2		5295	124.8
	144.1	− 1.0		61.1	− 85.5		5296	116.0
	144	− 14.5		61	− 85.1		5297	111.8
	143.1	− 27.9		60.1	−115.3		5298	116.0
	143	− 26.8	Numa-	J 60	−100.4		5299	108.6
	142.1	− 23.3	zu	59.1	−101.8		5300	107.2
	142	− 25.4		59	−114.4		5301	103.4
	141.1	− 29.7		58.1	−126.5		5302	98.9
Kake-	J 141	− 34.8		58	−140.0		5303	94.3
gawa	140.1	− 46.5		57.1	−148.2		5304	99.3
	140	− 52.5		57	− 86.0		5305	94.0
	139.1	− 69.3		56.1	−109.8		5306	100.6
	139	− 65.3		56	−145.7		5307	95.3
	138.1	− 58.3		55.1	−202.0		5308	89.3
	138	− 54.3		55	−132.4		5309	100.5
	137.1	− 73.0		54.1	− 62.8		5310	101.5
Kanaya	137	− 82.8		54	− 44.6		5311	101.2
	136.1	− 92.7		53.1	− 26.4		5312	95.9

(to be continued.)

(continued.)

Locality	B.M.	Displace.	Locality	B.M.	Displace.	Locality	B.M.	Displace.
		mm			mm			mm
	5313	592.8		593	75.5		87	− 0.1
	5314	86.8		594	69.6		87.1	− 2.9
	5315	83.9		595	62.6	Kazika-	88	− 7.7
	5316	72.4		596	55.6	zawa	88.1	− 18.6
	5317	176.1		597	51.4		89	− 35.3
	5318	25.5		598	53.2		89.1	− 52.1
	5319	54.9		599	50.1		90	− 34.4
	5320	43.9		600	39.2		90.1	− 30.5
	5321	43.0		601	34.4		91	− 26.5
	5322	20.5		602	27.2		91.1	− 36.3
	5323	31.7		603	24.3		92	− 36.5
	5324	36.9		604	15.9		92.1	− 56.0
	5325	38.8		605	12.1	Kohu	J 93	− 75.6
	5326	36.0		606	8.3		93.1	− 58.8
	5327	39.8		607	4.9		94	− 42.0
	5328	38.1		608	− 0.7		94.1	− 53.6
	5329	26.5		609	− 6.3		95	− 65.3
	5330	24.8		610	− 10.7		95.1	− 77.0
	5331	39.2		611	− 65.6		96	− 88.6
	5332	38.9		612	− 22.5		96.1	−100.3
	5333	46.9		613	− 29.3		B 2	−120.6
	5334	54.9		614	− 31.7		97	−197.4
	5335	26.3		615	− 28.4		97.1	−136.7
	5336	25.3	Kohu	J 93	− 75.6		98	−152.7
	5337	25.6					98.1	−168.7
	5338	30.8					99	−184.7
	5339	11.7	Okitu	J 70.1	−126.1		99.1	−200.7
	5340	28.8		71	−127.0		100	−216.7
	5341	26.7		71.1	−131.6		100.1	−247.4
	5342	24.4		72	−121.9		101	−276.4
	5343	23.7		72.1	−119.4		101.1	−305.4
	5344	24.2		B 1	−113.5		102	−320.8
	5345	5.6		73	−107.5		102.1	−355.6
	5346	31.9		73.1	−102.4		103	−356.9
	5347	40.0		74	− 99.9		103.1	−395.7
	5348	34.3		74.1	−102.4		104	−427.4
	5349	44.4		75	− 98.7		104.1	−442.1
	5350	46.0		75.1	−109.4		105	−488.8
	5351	42.1		76	−110.3		105.1	−545.8
	5352	40.0	Man-	76.1	−104.6		105.2	−570.8
	5353	85.6	zawa	77	− 98.5		105.3	−593.4
	5354	39.4		77.1	− 93.2		105.4	−591.7
	5355	39.0		78	− 87.9		105.5	−595.7
	5356	56.2		78.1	− 71.8		105.6	−581.5
	5357	45.2		79	− 65.2		105.7	−567.2
	5358	46.8		79.1	− 72.1		105.8	−596.0
	5359	38.6		80	− 53.9		105.9	−606.7
Simo-	J 580	52.3		80.1	− 27.9		110	−618.1
suwa	581	22.4		81	− 24.5		110.1	−605.7
	582	36.1		81.1	− 21.0		110.2	−593.3
	583	93.0		82	− 19.8		110.3	−596.7
	584	45.0	Minobu	82.1	− 16.4		110.4	−591.9
	585	44.3		83	− 15.0		110.5	−661.7
	586	59.7		83.1	− 6.7		110.6	−731.5
	587	76.6		84	− 5.1		110.7	−534.0
	588	71.3		84.1	− 1.4		110.8	−515.3
	589	66.2		85	− 5.1		110.9	−480.0
	590	78.8		85.1	− 1.1		B 24	−464.8
	591	81.3		86	− 14.0		110.10	−449.6
	592	86.9		86.1	− 7.0		115	−422.7

(to be continued.)

(continued.)

Locality	B.M.	Displace.	Locality	B.M.	Displace.	Locality	B.M.	Displace.
		mm			mm			mm
	115.1	−387.2		575	27.4		516	− 81.0
	116	−363.1		574	− 6.8		515	− 82.6
	116.1	−348.4		573	− 41.2		514	− 85.7
	117	−322.1		572	6.3		513	− 82.4
	117.1	−312.8		571	8.6		512	− 86.0
	118	−299.2		570	7.6		511	− 83.2
	118.1	−288.8		569	4.3		510	− 90.1
	119	−278.3		568	3.8		509	−132.0
	119.1	−261.4		567	8.6		508	−102.3
	120	−238.4		566	9.6		507	−100.5
	120.1	−225.8		565	11.1		506	−113.2
	121	−211.6		564	9.6		505	−122.7
	121.1	−198.0		563	12.2		504	−126.6
	122	−184.4		562	15.3		503	−130.7
	122.1	−160.5		561	24.1		502	−133.2
	123	−154.0		560	33.0		501	−145.0
	123.1	−137.7		559	17.3		500	−152.3
Yoyo-	J 14	−138.2		558	17.1		499	−218.8
hata	15	−158.3		557	26.9		498	−207.3
	16	−179.4		556	25.5		497	−195.8
	17	−154.4		555	25.1		496	−184.2
	II	−142.2		554	25.9		495	−178.6
	18	−163.5		553	25.2		494	−167.9
	19	−164.5		552	30.6		493	−178.7
	20	−164.2		551	42.7		492	−184.6
	21	−173.1		550	47.1		491	−189.6
	III	−168.0		549	51.7		490	−186.9
Itabasi	J 22	−167.3		548	37.8		489	−192.2
	23	−153.0		547	32.2		488	−189.2
	24	−130.9		546	18.2		487	−198.9
	25	−366.5		545	− 62.7		486	−206.9
	26	−258.1		544	− 2.7		485	−214.9
	3365	−243.5		543	1.7		484	−215.3
Senzyu	J IV	−344.4		542	23.9		B 36	−214.9
	3366	−289.9		541	9.4		483	−214.5
	3367	−189.7		540	7.8		482	−211.9
	3368	−260.6		539	− 20.6		481	−209.3
	0	−255.7		538	− 16.3		480	−206.6
	3369	−161.1		537	− 12.1		479	−203.8
	3370	−207.1		536	− 13.3		478	−208.9
	0	—		535	− 14.7		477	−214.8
	3371	− 98.6		534	− 15.9		476	−215.4
	V	− 93.3		533	− 17.3		475	−223.1
	3372	−100.3		532	− 22.0		474	−223.0
	J 3373	− 94.3		B 3	− 19.5		773	−206.3
	3822	− 82.2		531	− 16.9	Itabasi	J 22	−167.3
	3823	− 46.9		530	− 24.2			
	3824	− 12.7		529	− 27.7			
	3825	7.8		528	− 27.0	Numa-	J 60	−100.4
Huna-	J 3826	21.3		527	− 33.2	zu	9406	−110.9
basi				526	− 37.8		9405	−106.1
				525	− 43.4		9404	−130.9
Simo-	580	52.3		524	− 47.0		9403	−126.2
suwa	579.1	58.3		523	− 54.6		9402	−127.9
	579	36.4	Taka-	J 522	− 57.5		9401	−125.4
	578.1	34.2	saki	521	− 62.2		9400	−113.1
	578	32.2		520	− 67.0		9399	−124.4
	577.1	30.0		519	− 69.4		9398	−134.0
	577	24.8		518	− 73.3		9397	−147.2
	576	77.3		517	− 77.2		9396	−147.5

(to be continued.)

(continued.)

Locality	B.M.	Displace.	Locality	B.M.	Displace.	Locality	B.M.	Displace.
		mm			mm			mm
	9395	−123.5	Ito	9335	63.9		29.1	−157.7
	9394	−121.1		9334	66.3		30	− 59.2
	9393	−137.1		9333	68.8		30.1	− 49.5
	9392	−157.3		9332	78.1		31	− 39.8
	9391	−139.2		9331	66.6		31.1	− 19.1
	9390	−151.0	Aziro	9330	95.4		32	− 15.6
	9389	−128.2		9329	− 61.1		32.1	19.7
	9388	−140.6		9328	− 26.0		33	36.5
	9387	−153.8		9327	2.5		B 25	65.3
	9386	−130.0		52.2	− 44.3		33.1	94.1
	9385	−129.8	Atami	J 52	45.4		34	45.9
	9384	−128.3					34.1	89.0
	9383	−125.8					J 35	236.3
	9382	−114.6	Atami	J 52	45.4		35.1	317.3
	9381	−122.5		51.1	45.8		36	391.8
	9380	−119.7		51	81.2	Huzi-	36.1	495.0
	9379	−111.7		50.1	116.7	sawa	5360	528.7
	9378	−108.9	Yuga-	50	152.0		5360.1	422.1
	9377	−120.4	wara	49.1	487.8		5361	315.4
	9376	−115.1		49	562.3		5361.1	614.8
	9375	−146.2		48.1	624.2		5362	634.3
	9374	−128.7		48	824.9		5362.1	653.9
	9373	−127.6		47.1	1025.7		5363	668.8
	9372	120.6		47	964.3		5363.1	683.7
	9371	−110.3		46.1	903.0		5364	741.3
	9370	−116.8		46	841.7		5364.1	799.0
	9369	−108.0	Oda-	45.1	1035.8		5365	803.6
	9368	−103.8	wara	45	1230.0		5365.1	818.6
	9367	−103.3		44.1	1444.1		5366	891.9
	9366	−102.5		44	1499.4		5366.1	976.7
	9365	−109.3		43.1	1592.9		5367	1052.0
	9364	−103.6		43	1622.0		5367.1	1117.4
	9363	−103.9		42.1	1570.8		5367.2	1154.0
	9362	− 91.6		42	1511.5		B 26	1143.9
	9361	− 90.5		41.1	1460.7	Abura-	2	1133.7
	9360	− 91.4		41	1347.1	tubo		
	9359	− 90.9		40.1	1111.7			
	9358	− 90.2		40	978.6	Huna-	J 3826	21.3
	9357	− 80.6		39.1	669.9	basi	4011	7.4
	9356	− 74.5		39	673.8		4010	3.9
	9355	− 78.2		38.1	677.8		4009	17.9
	9354	− 85.1		38	605.0		4008	21.4
	9353	− 81.0		37.1	576.6		4007	28.2
	9352	− 67.8		37	535.8		4006	30.2
	9351	− 66.1	Huzi-	J 36.1	495.0		4005	33.1
	9350	− 64.5	sawa				4004	26.0
	9349	− 70.6					4003	25.2
	9348	− 76.0	Yoyo-	J 14	−138.2		4002	25.1
	9347	− 73.9	hata	13	−130.3		4001	−288.6
	9346	− 70.8		12	−135.3		4000	21.7
	9345	− 68.9		11	−115.3		3999	25.0
	9344	− 69.2		I	−103.8		3998	27.9
	9343	− 67.4		10	−130.1		3997	30.7
	9342	− 74.2	Taka-	9	−108.8		3996	33.5
	9341	− 68.1	nawa	9.1	−103.3		3995	27.8
	9340	− 54.6		27	−105.1		3994	26.5
	9339	− 38.2		27.1	−110.0		3993	17.8
	9338	16.7		28	− 91.7		3992	23.9
	9337	52.8		28.1	− 97.8		3991	24.1
	9336	73.4		29	−121.5		3990	21.6

(to be continued.)

(continued.)

Locality	B.M.	Displace.	Locality	B.M.	Displace.	Locality	B.M.	Displace.
		mm			mm			mm
	3989	19.5		3875	1290.1		3935	75.9
	3988	15.8		3876	1196.8		3936	66.3
	3987	20.6		3877	1195.8		3937	54.6
	3986	11.3		3378	1213.3		3938	43.7
	3985	6.6		3879	1285.8		3939	41.4
	3984	11.2	Hozyo	3830	1358.4		3940	18.1
	3983	11.0		3881	1331.7		3941	29.3
	3982	12.1		3882	1280.0		3942	33.2
Sawara	J 3981	8.9		3883	1221.8		3943	16.9
				3884	1593.2		3944	24.2
				3885	955.6		3945	22.5
Huna-	J 3826	21.3		3886	916.7		3946	13.8
basi	3527	7.3		3887	858.2		3947	21.6
	3828	11.1		3888	805.9		3948	19.1
	3829	12.2		3889	867.2		3949	12.9
	3830	23.5		3890	821.2		3950	19.3
	3831	32.6		3891	769.7		3951	20.4
	3832	41.8		3892	765.3		3952	19.0
	3833	50.4		3893	735.8		3953	16.2
	3834	43.6		3894	880.7		3954	15.8
	3835	57.4		3895	832.9		3955	14.9
	3836	66.5		3896	728.9		3956	15.2
	3837	73.3		3897	654.1		3957	12.0
	3838	85.2		3898	585.1		3958	20.4
	3839	91.3		3899	491.0		3959	16.2
	3840	87.5		3900	439.2		3960	20.1
	3841	76.0		3901	389.9		3961	21.5
	3842	98.5	Komi-	3902	346.8		3962	6.6
	3843	108.9	nato	3903	292.2		3963	15.3
	3844	105.8		3904	280.4		3964	18.1
	3845	117.2		3905	262.4		3965	18.1
	3846	128.5		3906	230.7		3916	16.4
	3847	118.0		3907	217.9		3967	12.2
	3848	132.8		3908	178.6		3968	16.1
	3849	87.3		3909	182.0		3969	15.7
	3850	165.8		3910	180.9		3970	12.6
	3851	214.5		3911	185.6		3971	12.6
	3852	228.8		3912	176.3		3972	7.3
	3853	274.2		3913	173.9		3973	8.4
	3854	329.9		3914	180.5		3974	1.9
	3855	388.3		3915	175.1		3975	6.1
	3856	553.5		3916	173.8		3976	12.2
	3857	555.8		3917	185.2		3877	10.5
	3858	624.9		3918	172.0		3878	10.5
	3859	670.5		3919	172.1		3979	4.9
	3860	751.8		3920	184.2		3980	9.1
	3861	852.0		3921	181.7	Sawara	J 3981	8.9
	3862	909.7		3922	158.3		4012	5.3
	3863	967.5		3923	169.8		4013	2.6
	3864	978.3		3924	158.2		4014	− 2.7
	3865	1018.8		3925	157.1		4015	− 3.2
	3866	1050.8		3926	166.9		4016	− 5.3
	3867	1091.7		3927	138.4		4017	− 41.9
	3868	1097.6		3928	134.3		4018	− 16.7
	3869	1078.1		3929	125.5		4019	− 6.4
	3870	1022.3		3930	116.2		4020	− 6.7
	3871	1078.3		3931	109.5		4021	− 7.4
	3872	1121.8		3932	99.6		4022	− 15.5
	3873	1186.9		3933	88.9		4023	− 14.9
	3874	1248.5		3934	67.5		4024	− 18.0

(to be continued.)

(continued.)

Locality	B.M.	Displace.	Locality	B.M.	Displace.	Locality	B.M.	Displace.
		mm			mm			mm
	4025	− 16.5		4179	− 60.5		4117	− 74.6
	4026	− 24.3		4180	− 74.6		4116	− 78.5
	4027	− 26.7		4181	− 80.9		4115	− 82.2
	4028	− 29.1		4182	− 84.7		4114	− 86.0
	4029	− 33.6		4183	− 84.5		4113	− 42.3
	4030	− 37.3		4184	− 86.7		4112	− 36.5
	4031	− 38.0		4185	− 93.2		4111	− 34.7
	4032	− 34.1		4186	− 95.4		4110	− 30.7
	4033	− 76.8		4187	− 91.3		4109	− 27.4
	4034	− 42.9		4188	− 92.3		4108	− 27.2
	4035	− 31.1		4189	− 97.2		4107	− 30.3
	4036	− 32.2		4190	− 99.0		4106	− 22.9
	4037	− 46.7		4191	− 98.3		4105	− 27.2
	4038	− 38.0		4192	−111.4		4104	− 15.0
	4039	− 39.6		4193	−111.8		4103	− 2.6
	4040	− 42.8		4194	−139.4		4102	− 19.2
	4041	− 51.0		4195	−143.1		4101	− 21.4
	4042	− 52.0		4196	−143.6		4110	− 18.7
	4043	− 52.3		4197	−157.7		4099	− 13.9
	4044	− 50.3		4198	−192.3		4098	− 26.6
	4045	− 50.6		4199	−647.7		4097	− 28.4
	4046	− 50.7		4200	−183.1		4096	− 28.7
	4047	− 52.6	Taira	J 4201	−246.5		4095	− 43.5
	4048	− 55.8					4094	− 40.3
	4049	− 57.3					4093	− 50.8
	4050	− 58.7	Taka-	J 522	− 57.5		4092	− 53.0
	4051	− 60.6	saki	4151	− 58.0		4091	− 53.7
	4052	− 63.5		4150	− 56.2		4090	− 52.1
	4053	− 62.4		4149	− 52.2		4089	− 52.0
	4054	− 68.1		4148	− 50.6	Utuno-	J 2052	− 58.0
	4055	− 67.9		4147	− 61.4	miya	4088	− 55.9
Mito	J 4056	− 69.4		4146	− 49.3		4087	− 53.6
	4152	− 64.7		4145	− 51.9		4086	− 50.6
	4153	− 90.9		4144	− 46.4		4085	− 50.3
	4154	− 81.2		4143	− 46.3		4084	− 49.3
	4155	−117.0		4142	− 42.2		4083	− 57.6
	4156	− 67.0		4141	− 40.9		4082	− 65.8
	4157	− 55.2		4140	− 33.3		4081	− 53.7
	4158	− 54.7		4139	− 34.5		4080	− 49.9
	4159	− 54.3		4138	− 35.5		4079	− 53.8
	4160	− 54.7		4137	− 28.7		4078	− 64.0
	4161	− 55.7		4136	− 31.9		4077	− 57.8
	4162	− 82.7		4135	− 26.7		4076	− 63.8
	4163	− 59.9		4134	− 26.4		4075	− 66.8
	B 27	− 58.1		4133	− 25.4		4074	− 69.4
	4164	− 56.3		4132	− 24.1		4073	− 67.1
	4165	− 54.7		4131	− 24.5		4072	− 65.8
	4166	− 58.5		4130	− 20.4		4071	− 65.7
	4167	− 57.2		4129	− 20.6		4070	− 71.4
	4168	− 70.8		4128	− 27.8		4069	− 62.7
	4169	− 56.1		4127	− 36.3		4068	− 65.6
	4170	− 52.4		4126	− 31.9		4067	− 72.3
	4171	− 56.4		4125	− 30.7		4066	− 74.4
	4172	− 63.0		4124	− 33.1		4065	− 73.8
	4173	− 59.7		4123	− 39.4		4064	− 77.6
	4174	− 61.3		4122	− 42.1		4063	− 77.3
	4175	− 62.0		4121	− 65.7		4062	− 68.5
	4176	− 60.0		4120	− 72.5		4061	− 67.4
	4177	− 62.9		4119	− 71.6		4060	− 77.9
	4178	− 94.2		4118	− 72.8		4059	− 70.3

(to be continued.)

(continued.)

Locality	B.M.	Displace.	Locality	B.M.	Displace.	Locality	B.M.	Displace.
		mm			mm			mm
	4058	− 74.9	Hukui	J 5258	− 87.4		844	− 33.5
	4057	− 78.5		902	− 91.1		843	− 25.9
Mito	J 4056	− 69.4		901	− 91.0		842	− 20.6
				900	−109.9		841	− 30.0
				899	− 86.0		840	− 32.0
Utuno-	J 2052	− 58.0		898	− 94.1		839	− 49.4
miya	B 4	− 58.1		897	−104.9	Taka-	J 12	− 30.5
	2051	− 58.2		896	−116.0	oka	9326	− 36.5
	2050	− 62.0		895	− 84.7		9325	− 42.6
	2049	− 63.0		894	− 78.9		9324	− 48.6
	2048	− 66.6		893	− 74.1		9323	− 31.9
	2047	− 67.7		892	− 77.0		9322	− 30.7
	2046	− 68.2		891	− 73.7		9321	− 11.2
	2045	− 70.2		890	− 67.4		9320	− 13.9
	2044	− 75.7		889	− 66.9		9319	− 6.9
	2043	− 77.3		888	− 54.3		9318	0.0
	2042	− 79.8		887	− 63.1		9317	− 13.6
	2041	− 82.2		886	− 53.0		9316	− 1.5
	2040	− 87.7		885	− 50.4		9315	0.2
	2039	− 93.0		884	− 52.0		9314	4.2
	2038	−103.4		883	− 61.0		9313	− 7.6
	2037	−113.8		882	− 63.9		9312	− 19.4
	2036	−118.8		881	− 44.7		9311	− 31.1
	2035	−121.8		880	− 42.8		9310	− 23.5
	2034	−138.0		879	− 40.2		3909	− 16.0
	2033	−135.2		878	− 34.9		9308	− 5.5
	2032	−138.3		877	− 36.8		9307	− 11.3
	2031	−141.4		876	− 38.9		9306	− 8.6
	2030	−141.1		875	− 36.9		9305	− 16.1
	2029	−149.7		874	− 39.3		9304	− 11.3
	2028	−158.6		873	− 38.7		9303	− 6.2
	2027	−161.7		872	− 37.5		9302	− 10.6
	2026	−171.7		871	− 27.6		9301	− 3.2
	2025	−197.4		870	− 20.7		9300	− 14.5
	2024	−339.4		869	− 22.8		9299	− 16.7
	2023	−213.2		868	− 24.2		9298	− 12.5
	2022	−501.8		867	− 27.3		9297	− 6.9
	2021	−263.5		866	− 37.8		9296	− 28.1
	2020	−223.4		865	− 27.9		9295	− 4.8
	2019	−219.1		864	− 22.5		9294	− 7.5
	2018	−230.3	Kana-	863	− 22.5		9293	− 10.5
	2017	−228.8	zawa	862	− 35.5		9292	− 2.3
	2016	−226.7		861	− 43.6		9291	0.0
	2015	−233.7		860	− 82.0		9290	− 4.7
	2014	−261.4		859	− 27.8		9289	− 30.3
	2013	−289.2		858	− 29.6		9288	3.6
	2012	−330.9		857	− 34.3		9287	3.7
	2011	−246.0		856	− 30.4		9286	3.8
	2010	−286.5		855	− 28.4		9285	− 2.0
	2009	−256.8	Inoue	J 11	− 28.6		9284	− 0.9
	2008	−246.1		854	− 36.2		9283	− 11.5
	2007	−295.3		853	−107.2		9282	− 9.6
	2006	−258.1		852	− 32.9		9281	− 1.3
	2005	−239.5		851	− 24.7		9280	− 14.8
	2004	−250.7		850	− 22.0		9279	− 6.5
	2003	−252.2		849	− 16.8		9278	− 11.0
	2002	−289.3		848	− 17.6		9277	− 21.3
Senzyu	J IV	−344.4		847	− 42.1		9276	− 17.8
				846	− 27.9	Wazi-	7	− 24.3
				845	− 23.8	ma	9275	− 10.6

(to be continued.)

(continued.)

Locality	B.M.	Diaplace.	Locality	B.M.	Displace.	Locality	B.M.	Displace.
		mm			mm			mm
	9274	– 25.7		835	– 36.7		3715	– 61.1
	9273	– 17.4		834	– 41.2		3716	– 58.0
	9272	– 20.7		833	– 42.9		3717	– 55.0
	9271	– 24.5		832	– 49.8		3718	– 51.8
	9270	– 41.6		831	– 51.2		3719	– 46.5
	9269	– 29.3		830	– 54.2		3720	– 50.9
	9268	– 23.7		829	– 55.3		3721	– 53.4
	9267	– 24.1	J	828	– 58.9		3722	– 55.9
	9266	– 44.2		2967	– 58.5		3723	–110.4
	9265	– 29.7		2966	– 57.7		3724	– 91.6
	9264	– 32.4		2965	– 57.9		3725	–100.5
	9263	– 32.7		2964	– 81.7		3726	– 98.3
	9262	– 25.0		2963	– 75.3		3727	– 60.8
	9261	– 33.5		2962	– 79.4		3728	– 56.2
	9260	– 42.0		2961	– 57.0		3729	– 49.5
	9259	– 18.9		2960	– 65.0		3730	– 40.2
	5258	– 17.5		2959	– 58.0		3731	– 43.6
	9257	– 16.5		2958	– 49.9		3732	– 39.4
	9256	– 19.0		2957	– 50.9		3733	– 33.4
	9255	– 20.2		2956	– 57.6		3734	– 27.0
	9254	– 25.7		2955	– 61.4		3735	– 28.6
	9253	– 23.8		2954	– 56.9		3736	– 24.1
	9252	– 26.6		2953	– 64.2		3737	– 18.2
	9251	– 29.1		2952	– 69.1		3738	– 15.1
	9250	– 12.6		2951	– 64.6		3739	– 12.2
	9249	– 22.3		2950	– 70.4		3740	– 21.1
	9248	– 33.4		2949	– 74.9		3741	– 13.5
	9247	– 21.6		2948	– 76.3		3742	– 13.2
	9246	– 14.7		2947	– 73.4		3743	– 17.6
	9245	– 29.8		2946	– 84.6		3744	– 46.4
	9244	4.5		2945	– 88.4	Nisina-kadori	J 3745	– 55.0
	9243	– 21.4		2944	– 89.0			
	9242	– 22.1		2943	– 92.4			
	9241	– 33.5		2942	– 97.3	Simo-suwa	J 580	– 52.3
	9240	– 19.8		2941	– 99.5		616	35.6
	9239	– 14.7		2940	–112.6		617	43.3
	9238	– 16.3		2939	–100.8		618	62.2
	9237	– 27.8		2938	–104.7		619	47.7
	9236	– 26.0		2937	–102.0		620	58.7
	9235	– 34.7		2936	– 99.3		621	44.6
	9234	– 30.0		2935	–100.3		622	43.3
	9233	– 23.0		2934	– 98.1		623	38.4
	9232	– 26.6		2933	– 89.1		624	41.3
	9231	– 44.1		2932	–282.5		625	40.8
	9230	– 31.2		2931	–109.5		626	39.8
	9229	– 18.1		2930	– 89.5		J 627	42.8
	9228	– 23.4		2929	– 90.9		2866	37.8
	9227	– 33.3	J	2928	– 91.7		2867	36.8
	9226	– 43.2		3703	– 91.7		2868	38.9
	9225	– 46.4		3704	– 91.9		2869	33.2
	9224	– 43.0		3705	–106.4		2870	26.9
	9223	– 32.6		3706	– 86.5		2871	23.6
	9222	– 31.6		3707	– 76.4		2872	12.8
Inoue	J 11	– 28.6		3708	– 79.9		J 2873	– 1.7
				3709	– 84.1		3702	– 28.8
				3710	– 77.0		3761	– 19.2
Taka-oka	J 12	– 30.5		3711	– 74.2		3700	10.1
	838	– 29.9		3712	– 58.2		3699	– 0.7
	837	– 26.2		3713	–238.4		3698	– 1.7
	836	– 41.6		3714	–149.8		3697	– 1.7

(to be continued.)

(continued.)

Locality	B.M.	Displace.	Locality	B.M.	Displace.	Locality	B.M.	Displace.
		mm			mm			mm
	3696	4.8		3636	− 57.2		3750	4.0
	3695	− 3.2		3635	− 67.2		3749	− 16.0
	3694	− 3.2		3634	− 49.7		3748	− 50.0
	3693	0.0		3633	− 43.4		3747	− 76.5
	3692	− 13.1		3632	− 45.0		3746	− 41.0
	3691	3.8		3631	− 21.4	Nisina-	J 3745	− 55.0
	3690	2.5		3630	− 32.5	kadori	4463	− 19.3
	3689	− 31.0		3629	− 21.2		4462	− 37.4
	3688	3.5		3628	− 41.4		4461	− 37.0
	3687	39.5		3627	−218.0		4460	− 31.3
	3686	22.6		3626	− 14.9		4459	− 31.2
	3685	4.9		3625	8.6		4458	− 29.1
	3684	5.0		3624	7.9		4457	− 29.6
	3683	− 71.3		3623	1.1		4456	− 30.3
	3682	5.0		3622	3.8		4455	− 31.3
	3681	− 47.5		3621	0.3		4454	383.8
	3680	11.4		3620	4.6		4453	− 11.2
	3679	14.0		2619	1.1		4452	− 10.8
	3678	8.2		3618	4.1		4451	− 15.0
	3677	13.7		3617	0.8		4450	− 75.9
	3676	40.7		3616	7.7		4449	− 48.4
	3675	48.9		3615	3.3		4448	− 32.6
	3674	46.8		3614	7.6		4447	− 21.3
	3673	47.0		3613	5.2		4446	− 31.3
	3672	53.3		3612	7.0		4445	− 30.4
	3671	53.2		3611	4.9		4444	− 44.9
	3670	39.6		3610	− 20.2		4443	− 30.8
	3669	80.3		3609	− 5.0		4442	− 23.1
	3668	22.4		3608	− 16.8		4441	− 23.0
	3667	19.0		3607	− 1.3		4440	− 21.5
	3666	12.4		3606	3.0		4439	− 18.3
	3665	11.1		3605	4.5		4438	− 25.5
	3664	11.3		3604	0.1		4437	− 31.5
	3663	7.8		3603	13.6		4436	− 37.4
	3662	− 0.3		3602	12.9		4435	− 37.0
	3661	− 8.5		3601	5.7		4434	− 33.0
	3660	− 16.8		3600	13.6		4433	− 43.5
	3659	− 18.7		3599	− 71.4		4432	− 50.4
	3658	− 23.6		3598	21.2		4431	− 74.7
	3657	− 25.1		3597	14.3		4430	−113.8
	3656	− 23.6		3596	0.1		4429	−102.5
	3655	− 37.5		J 3595	0.1		4428	−102.7
	3654	− 34.3		3768	− 7.1		4427	−108.8
	3653	− 35.0		3767	− 14.8		4426	−122.4
	3652	− 5.2		3766	− 20.9		4425	−123.1
	3651	11.7		3765	− 39.0		4424	−135.6
	3650	28.5		3764	− 26.6		4423	−122.7
	3649	− 19.3		3763	− 23.7		4422	− 85.9
	3648	− 6.3		3762	− 35.5		4421	− 85.9
	3647	20.5	Naga-	J 3761	− 37.9		4420	− 86.4
	3646	25.4	oka	3760	− 43.6		4419	− 65.0
	3645	19.6		3759	− 23.0		4418	−111.1
	3644	− 44.7		3758	5.4		4417	− 83.7
	3643	− 21.4		3757	0.6		4416	− 56.3
	3642	− 21.6		3756	− 23.0		4415	− 47.5
	3641	− 29.3		3755	− 22.7		4414	− 34.8
	3640	− 46.0		3754	13.0		4413	− 40.9
	3639	− 38.3		3753	− 15.5		4412	− 19.2
	3638	−101.1		3752	− 24.4		4411	− 32.3
	3637	− 61.8		3751	− 11.2	Sibata	J 4410	− 28.0

(to be continued.)

(continued.)

Locality	B.M.	Displace.	Locality	B.M.	Displace.	Locality	B.M.	Displace.
		mm			mm			mm
Sibata	J 4410	− 28.0		6530	47.5		5799	− 16.8
	6472	− 8.5		6531	3.0		5798	− 11.9
	6473	− 22.9		6532	44.5		5797	− 12.0
	6474	2.6		6533	40.6		5796	− 10.0
	6475	1.0		6534	29.8		5795	− 14.1
	6476	−143.0		6535	34.4		5794	− 13.8
	6477	3.6		6536	36.9		5793	− 6.1
	6478	0.2		6537	39.8		5792	− 21.5
	6479	− 19.8		6538	45.7		5791	− 11.6
	6480	22.3		6539	35.7		5790	− 9.4
	6481	26.9		6540	39.3		5789	− 7.3
	6482	28.6		6541	39.7		5788	− 4.4
	6483	23.9		6542	23.8		5787	6.2
	6484	19.1		6543	19.9		5781	− 0.7
	6485	31.0		6544	25.0		5785	− 49.7
	6486	8.4		6545	26.1	Akita	J 9	8.5
	6487	− 14.3		6546	31.0		5784	− 8.5
	6488	22.7		J 6547	17.6		5783	− 14.8
	6489	− 7.5		6571	33.6		5782	− 14.4
	6490	36.8		6572	10.5		5781	12.0
	6491	30.1		6573	− 58.4		5780	14.1
	6492	32.2		6574	− 50.2		5779	− 1.5
	6493	42.9		6575	− 46.0		5778	− 29.7
	6494	52.1		6576	− 45.9		5777	− 9.2
	6495	52.3		6577	− 49.3		5776	− 5.5
	6496	45.0		6578	−137.8		5775	− 12.7
	6497	54.9		6579	−125.9		5774	− 96.0
	6498	60.8		6580	−148.9		5773	− 10.5
	6499	61.0		6581	− 29.8		5772	− 26.6
	6500	63.6		6582	11.4		5771	− 38.8
	6501	60.5		6583	19.3		5770	− 43.7
	6502	55.6		6584	18.5		5769	− 40.6
	6503	− 21.1		6585	19.4		5768	− 40.6
	6504	49.0		6586	29.0		5767	−205.7
	6505	57.4		6587	23.4		5766	−268.9
	6506	60.0		6588	29.7		5765	− 73.5
	6507	49.7		6589	19.6		5764	− 76.9
	6508	40.5		6590	18.9		5763	− 84.5
	6509	50.1		6591	9.9		5762	−108.3
	6510	45.9		6592	0.8		5761	− 66.0
	6511	46.6		6593	3.1		5760	−120.0
	6512	41.8		6594	2.8		5759	−102.4
	6513	50.3		6595	4.9		5758	−112.8
	6514	47.2		5815	9.4		5757	−131.8
	6515	44.0		5814	6.1		5756	−131.5
	6516	44.9		5813	0.5		5755	−167.9
	6517	43.8		5812	− 5.0		5754	−155.0
	6518	48.4		5811	9.9		5753	−163.7
	6519	45.9		5810	− 3.0		5752	−160.1
	6520	43.5		5809	− 3.5		5751	−167.9
	6521	42.4		5808	−157.2		5750	−151.1
	6522	51.1		5807	− 30.0		5749	−155.9
	6523	44.2		5806	− 0.3		5748	−154.5
	6524	49.1		5805	− 7.5		5747	−153.7
	6525	40.6		5804	1.8		J 8	−153.4
	6526	32.0		5803	− 10.2		5559	−166.0
	6527	23.5		5802	− 13.2		5558	−166.3
	6528	46.0		5801	− 16.2		5557	−165.3
	6529	39.3		5800	− 11.2		5556	−164.3
							5555	−171.3

(to be continued.)

(continued.)

Locality	B.M.	Displace.	Locality	B.M.	Displace.	Locality	B.M.	Displace.
		mm			mm			mm
	5554	−197.6		6824	− 96.1		6063	− 17.4
	5553	−155.3		6823	−101.7		6064	− 17.2
	5552	−153.1		6822	−107.3		6065	− 15.8
	5551	−152.3		6821	−110.1		6066	− 25.4
	5550	−155.4		6820	−119.9		6067	− 25.2
	5549	−178.4		6819	−113.7		6068	− 20.5
	5548	−155.7		6818	−103.6		6069	− 25.5
	5547	−140.3		6817	− 97.2		6070	− 32.0
	5546	−138.9		6816	− 94.7		6071	− 25.1
	5545	−136.7		6815	− 95.8		6072	− 26.9
	5544	−125.2		6814	− 87.1		6073	− 30.3
	5543	−114.6		6813	− 93.3		6074	− 36.0
	5542	−120.5		6812	− 90.5		6075	− 28.3
	5541	−113.2		6811	− 95.0		6076	− 35.1
	5540	−111.6		6810	− 97.2		6077	− 34.0
	5539	−110.1	Kamaisi	J 3	−102.0	Iwasaki	6078	− 27.9
	5538	−114.0					6079	− 26.9
	5537	−113.7					6080	− 34.6
	5536	−119.9	Akita	J 9	8.5		6081	− 30.7
	5535	−114.3		5816	− 3.4		6082	− 37.8
	5534	−112.6		5817	8.5		6083	− 35.1
	5533	−117.1		5818	7.6		6084	− 32.4
	5532	−105.6		5819	6.2		6085	− 37.2
	5531	−102.5		5820	− 5.7		6086	− 38.4
	5530	−102.7		5821	− 13.4		6087	− 61.5
	5529	−101.6		5822	− 4.0		6088	− 66.4
	5528	− 79.8		5823	− 4.6		6089	− 52.1
	J 5466	− 98.3		5824	− 30.7		6090	− 59.2
	6856	−105.0		5825	12.3		6091	− 63.7
	6855	− 99.7		5826	− 28.1		6092	− 68.2
	6854	−101.7		5827	− 60.3		6093	− 72.6
	6853	−115.4		5828	− 19.8		6094	− 69.6
	6852	−106.7		5829	− 16.5		6095	− 59.9
	6851	−107.0		5830	− 10.4		6096	− 68.4
	6850	−105.9		5831	− 22.4		6097	− 64.5
	6849	−103.4		5832	− 12.1		6098	− 90.1
	6848	− 97.0		5833	− 22.6		6099	− 72.0
	6847	− 6.0		5834	− 9.0		6100	− 79.1
	6846	−110.2		5835	− 17.1		6101	− 80.2
	6845	− 89.2		5836	− 14.1		6102	− 71.9
	6844	− 98.2		5837	− 20.1		6103	− 68.1
	6843	−104.6		5838	− 31.1		6104	− 69.6
	6842	−103.5		5839	− 30.3		6105	− 71.0
	6841	−101.5		5840	− 28.4		6106	− 71.7
	6840	−118.6		5841	− 26.0		6107	− 73.5
	6839	−104.6		5842	− 24.1		6108	−101.9
	6838	−101.2		5843	− 26.3		6109	−105.5
	6837	−101.8		5844	− 63.6		6110	−106.7
	6836	− 99.8		5845	− 20.6		6111	−118.3
	6835	− 98.4		J 1	− 12.9		6112	−108.2
	6834	− 93.1		6053	− 10.4		6113	− 98.0
	6833	− 88.9		6054	− 8.0		6114	− 98.7
	6832	− 90.0		6055	− 4.5		6115	− 77.0
	6831	−101.5		6056	− 7.7		6116	−107.9
	6820	− 84.4		6057	− 17.2		6117	− 91.7
	6829	− 86.6		6058	− 13.4		6118	− 86.4
	6828	− 78.6		6059	− 7.9		6119	− 81.1
	6827	− 70.6		6060	− 7.4		J 5	− 75.8
	6826	− 84.9		6061	− 12.7		5959	− 89.4
	6825	− 90.5		6062	− 12.5		5960	−103.1

(to be continued.)

(continued.)

Locality	B.M.	Dispiace.	Locality	B.M.	Displace.	Locality	B.M.	Displace.
		mm			mm			mm
	5961	– 97.3		6959	–134.3		6899	– 81.0
	5962	– 80.6	Hati-	6958	–128.4		6898	– 81.7
	5963	–107.2	nohe	6957	–127.8		6897	– 88.4
	5964	–169.7		6956	–128.7		6896	– 86.0
	5965	– 76.3		6955	–123.2		6895	– 80.5
	5966	– 91.8		6954	– 98.7		6894	– 86.2
Aomori	J 6052	– 97.4		6953	–117.5	Taro	6893	– 77.5
	6051	–127.2		6952	–121.0		6892	– 87.1
	6050	– 87.8		6951	–126.1		6891	– 93.4
	6049	– 78.4		6950	–124.2		6890	– 82.0
	6048	– 81.5		6949	–121.1		6889	– 98.0
	6047	– 79.6		6948	–114.8		6888	– 89.1
	6046	– 82.8		6947	–116.3		6887	– 87.8
	6045	– 89.6		6946	–128.1		6886	– 89.0
	6044	– 97.2		6945	–139.9	Miyako	6885	– 91.8
	6043	– 99.0		6944	–112.8		6884	– 92.2
	6042	–106.1		6943	–106.2		6883	– 89.2
	6041	–106.6		6942	–104.9		6882	– 92.4
	6040	–107.0		6941	–103.2		6881	– 90.7
	6039	–137.9		6940	–101.6		6880	– 94.4
	6038	– 87.3		6939	– 96.4		6879	–100.7
	6037	–110.9		6938	– 95.9		6878	– 96.9
	6036	–121.0		6937	–100.1		6877	– 99.1
	6035	–119.1		6936	– 85.6		6876	–110.4
	6034	–120.3		6935	– 96.3		6875	– 98.5
	6033	–113.4		6934	– 86.9		6874	–103.9
	6032	–117.9		6933	– 85.5		6873	–107.8
Nohezi	6031	–117.4	Kuzi	6932	– 95.4		6872	–116.6
	6030	–112.7		6931	– 92.7		6871	–124.3
	6029	–108.9		6930	– 70.7		6870	–116.6
	6028	–105.3		6929	– 73.9		6869	–103.4
	6027	– 91.4		6928	– 85.2		6868	–118.3
	6026	– 94.6		6927	– 89.8		6867	–109.7
	6025	–102.5		6926	– 81.2		6866	–105.6
	6024	–113.1		6925	– 72.8		6865	–103.9
	6023	–114.3		6924	– 78.8		6864	–109.3
	6022	–115.5		6923	– 71.9		6863	– 98.2
Sitinohe	6021	–112.5		6922	– 79.0		6862	–102.8
	6020	–111.9		6921	– 70.9		6861	– 94.4
	6019	–110.6		6920	– 75.5		6860	– 97.0
	6018	–109.6		6919	– 80.1		6859	– 90.9
	6017	–109.1		6918	– 85.5		6858	– 99.1
	6016	–108.4		6917	– 85.2		6857	– 93.8
Sanbon-	6015	–107.8		6916	– 82.5	Kamaisi	J 3	–102.0
gi	6014	–104.3		6915	– 79.8			
	6013	–108.3		6914	– 87.5			
	6012	–109.3		6913	– 80.2	Sibata	J 4410	– 28.0
	6011	–110.4		6912	– 78.1		4409	– 21.7
	6010	–110.8		6911	– 82.7		4408	– 13.2
	6009	–110.6		6910	– 88.4		4407	– 39.1
	6008	–108.6		6909	– 91.8		4406	– 36.8
	6007	–121.9		6908	– 84.9		4405	– 55.5
	J 6006	–124.5		6907	– 81.1		4404	– 40.6
	6966	–112.3		6906	– 85.4		4403	– 34.1
	6965	–123.6		6905	– 77.3		4402	– 30.9
	6964	–135.1		6904	– 84.7		4401	– 21.3
	6963	–137.2		6903	– 86.5		4400	– 19.0
	6962	–149.1		6902	– 82.4		4399	– 15.3
	6961	–144.6		6901	– 78.2		4398	– 11.9
	6960	–140.2		6900	– 92.9		4397	– 13.8

(to be continned.)

(continued.)

Locality	B.M.	Displace.	Locality	B.M.	Displace.	Locality	B.M.	Displace.
		mm			mm			mm
	4396	− 16.5		4248	− 20.7		5616	− 58.8
	4395	− 25.4		4247	− 6.0		5615	− 68.0
	4394	− 5.4		4246	− 9.3		5614	− 55.2
	4393	− 9.8		4245	− 14.0		5613	− 99.7
	4392	− 4.1		4244	42.7		5612	− 57.7
	4391	− 3.2		4243	85.6		5611	− 70.1
	4390	− 15.7		4242	52.7		5610	− 55.5
	4389	− 2.2		4241	74.1		5609	− 50.8
	4388	9.1		4240	72.8		5608	− 52.8
	4387	9.5		4239	67.0		5607	− 64.9
	4386	9.8		4238	63.9		5606	− 58.0
	4385	6.3		4237	57.0		5605	− 56.9
	4384	12.3		2114	56.1		5604	− 71.8
	4383	3.7		4236	55.2		5603	− 61.7
	4382	16.7		4235	48.6		5602	−102.7
	4381	16.9		4234	52.9		5601	− 73.9
	4380	23.7		4233	44.0		5600	− 79.9
	4379	22.1		4232	47.2		5599	− 65.7
	4378	21.1		4231	42.0		5598	− 64.3
	4377	20.9		4230	48.0		5597	− 22.1
	4376	20.7		4229	45.3		5596	− 60.7
	4375	17.4		4228	39.5		5595	−132.9
	4374	14.6		4227	33.6		5594	− 65.1
	4373	16.1		4226	42.7		5593	− 82.6
	4372	10.6		4225	43.4		5592	− 72.1
	4371	12.1		4224	38.7		5591	− 61.4
	4370	10.8		4223	40.8		5590	− 83.9
	4369	4.7		4222	27.2		5589	− 78.9
	4368	1.4		4221	32.6		5588	− 75.6
	4367	9.1		4220	32.6		5587	− 73.4
	4366	6.4		4219	34.7		5586	− 71.2
	4365	− 0.5		4218	27.0		5585	− 70.7
	4364	3.5		4217	22.6		5584	− 76.3
	4363	− 0.3		4216	22.1		5583	− 73.3
	4362	− 2.8		4215	18.7		5582	− 65.5
	4361	− 5.3		4214	14.9		5581	− 62.0
	4360	− 4.7		4213	7.2		5580	− 75.7
	4359	− 25.5		4212	6.5		5579	− 91.2
	4358	− 18.7		4211	3.5		5578	− 63.6
	4357	− 10.2		4210	1.4		5577	− 63.9
	4356	− 9.0		4209	0.4		5576	− 97.6
	4355	− 10.9		4208	− 11.0		5575	− 91.7
	4354	0.4		4207	− 8.1		5574	− 85.1
	4353	3.0		4206	− 30.7		5573	−109.2
	J 4264	− 5.3		4205	− 48.5		5572	− 67.5
	4263	− 4.6		4204	− 57.7		5571	− 90.0
	4262	0.4		4203	− 81.7		5570	−119.4
	4261	4.7		4202	−167.6		5569	− 74.1
	4260	4.2	Taira	J 4201	−246.5		5568	− 88.7
	4259	6.8		5627	−184.2		5567	− 88.2
	4258	4.1		5626	−124.8		5566	− 90.2
	4257	7.5		5625	−107.8		5565	− 55.0
	4256	8.5		5624	− 79.5		5564	− 55.0
	4255	10.0		5623	− 79.0		5563	− 47.7
	4254	5.9		5622	− 63.9		5562	− 59.5
	4253	− 52.2		5621	− 51.7		5561	− 58.7
	4252	− 0.9		5620	− 62.7		5560	− 68.5
	4251	− 6.1		5619	− 56.3		J 2169	− 52.6
	4250	− 3.7		5618	− 73.2		2170	− 62.8
	4249	− 1.2		5617	− 62.6		2171	−175.7

(to be continued.)

(continued.)

Locality	B.M.	Displace.	Locality	B.M.	Displace.	Locality	B.M.	Displace.
		mm			mm			
	2172	− 64.0		5699	− 45.0		SIKOKU	
	2173	− 66.9		5700	− 49.0			mm
	2174	− 63.8		5701	− 48.2	Konzozi	J 3385	− 10.7
	2175	− 63.1		5702	− 50.2		3386	− 7.3
	2176	− 71.5		5703	− 59.8		3387	− 0.8
	2177	− 63.5		5704	− 45.2		3388	2.3
	2178	− 72.6		5705	− 68.3		3389	1.5
Sendai	J 2179	− 58.0		5706	− 57.4		3390	4.3
	5648	− 61.2		5707	− 56.7	Katuma	3391	0.1
	5649	− 72.7		5708	− 72.5		3392	4.4
	5650	− 66.9		5709	− 57.4		3393	8.8
	5651	− 59.9		5710	− 68.3		3394	13.0
	5652	− 62.2		5711	− 58.6		3395	15.7
	5653	− 59.2		6767	− 54.8		3396	16.5
	5654	− 73.8		6768	− 53.7		3397	17.3
	5655	− 57.6		6769	− 61.4		3398	20.4
	5656	− 56.2		6770	− 64.3		3399	− 11.3
	5657	− 56.9		6771	− 90.1		3400	19.5
	5658	− 53.8		6772	−101.4		3401	21.8
	5659	− 69.3		6773	− 93.8		3402	14.8
	5660	− 56.1		6774	− 69.0		3403	21.3
	5661	− 51.6		6775	− 64.2	Kawa-	3404	15.7
	5662	− 53.4		6776	− 69.3	noe	3405	5.4
	5663	− 83.9		6777	− 70.2		3406	− 5.5
	5664	− 48.4		6778	− 62.1		3407	− 4.9
	5665	− 77.5		6779	− 66.4		3408	− 3.5
	5666	− 50.4		6780	− 52.4		3409	− 5.8
	5667	− 65.6		6781	− 79.4		3410	− 0.6
	5668	− 54.1		6782	− 62.3		3411	− 3.9
	5669	− 29.6		6783	− 65.2		3412	− 5.6
	5670	−112.8		6784	− 65.9		3413	− 1.9
	5671	− 73.7		6785	− 65.9		3414	1.9
Hebita	J 2	− 53.8		6786	− 76.6		3415	− 17.4
	5672	−180.5		6787	− 61.2		3416	− 0.3
	5673	− 45.6		6788	− 80.3		3417	1.7
	5674	− 97.1		6789	− 86.7		3418	− 2.5
	5675	− 55.8		6790	− 83.1		3419	− 26.6
	5676	− 65.6		6791	− 88.2		3420	− 0.3
	5677	− 54.4		6792	− 93.5		3421	− 0.8
	5678	−159.7		6793	− 89.7		3422	− 1.0
	5679	− 70.8		6794	− 99.8	Saizyo	3423	− 1.3
	5680	− 61.4		6795	− 90.1		3424	− 1.6
	5681	− 64.2		6796	− 87.6		3425	− 1.1
	5682	− 45.6		6797	− 75.1		3426	− 0.2
	5683	− 81.4		6798	− 70.7		3427	− 0.4
	5684	− 59.4		6799	− 72.4		3428	− 1.0
	5685	− 57.7		6800	− 86.8		3429	− 9.2
	5686	− 74.3		6801	− 83.7		3430	− 6.7
	5687	− 76.9		6802	− 54.4		3431	− 8.4
	5688	− 70.7		6803	− 82.7		3432	− 12.6
	5689	− 66.3		6804	− 82.9		3433	− 9.5
	5690	− 64.1		6805	− 88.9		3434	− 16.8
	5691	− 61.7		6806	− 97.6		3435	− 18.2
	5692	− 56.4		6807	− 96.0		3436	− 17.3
	5693	− 48.1		6808	− 89.8		3437	− 16.7
	5694	− 47.9		6809	− 94.4		3438	− 34.9
	5695	− 51.8	Kamaisi	J 3	−102.0		3439	− 33.0
	5696	− 66.2				Ima-	J 3440	− 33.1
	5697	− 51.6				baru	3461	− 31.4
	5698	− 48.6					3462	− 33.6

(to be continued.)

(continued.)

Locality	B.M.	Displace.	Locality	B.M.	Displace.	Locality	B.M.	Displace.
		mm			mm			mm
	3463	− 33.4		4574	17.3		4634	66.5
	3464	− 35.2		4575	36.0		4635	62.8
	3465	− 27.6		4576	34.9		4636	60.3
	3466	− 31.2	Uwa	4577	32.4		4637	56.4
	3467	− 34.8		4578	45.9		4638	49.1
	3468	− 42.3		4579	54.6		4639	33.7
	3469	− 42.3		4580	50.1		4640	31.2
Kikuma	3470	− 47.0		4581	30.5		4641	35.4
	3471	− 21.5		4582	10.8		4642	38.2
	3472	− 31.3		4583	17.5		4643	43.5
	3473	− 29.3		4584	23.7		4644	59.8
	3474	− 30.7		4585	24.5		4645	59.2
	3475	− 32.2		4586	25.4		4646	66.4
	3476	− 28.0		4587	15.2		4647	67.0
	3477	− 24.3	Uwa-	4588	4.9		4648	76.3
	3478	− 40.8	zima	4589	18.6		4649	76.3
	3479	− 30.2		4590	24.1		4650	82.4
	3880	− 11.4		4591	12.6		4651	84.9
	3881	− 18.4		4592	22.1		4652	87.4
	3882	− 25.5		4593	25.2		4653	89.7
Matu-	J 3883	− 16.7		4594	24.1	Kubo-	4654	90.8
yama	4535	− 7.9		4595	26.1	kawa	4655	101.7
	4536	− 6.5	Iwa-	4596	22.9		4656	16.0
	4537	− 16.7	matu	4597	19.6		4657	106.5
	4538	− 27.0		4598	23.5		4658	150.5
	4539	− 0.9		4599	27.2		4659	105.4
Guntyu	4540	1.5		4600	34.4		4660	110.6
	4541	4.5		4601	46.9		4661	105.2
	4542	18.8		4602	29.0		4662	106.6
	4543	18.8		4603	30.1		4663	97.9
	4544	26.7		4604	31.2		4664	96.0
	4545	31.9		4605	36.5	Kure	4665	91.4
	4546	32.8	Utumi	4606	42.0		4666	78.3
	4547	38.7		4607	35.9		4667	90.4
	4548	41.8		4608	25.3		4668	95.7
	4549	56.4		4609	65.8		4669	88.2
	4550	17.5		4610	106.4		4670	94.1
	4551	− 28.7		4611	45.7		4671	82.6
	4552	53.9		4612	46.5		4672	85.1
	4553	58.7		4613	47.1	Susaki	4673	72.5
	4554	60.4		4614	50.5		4674	45.4
Naisi	4555	43.0		4615	50.4		4675	69.7
	4556	49.4	Sukumo	4616	52.6		4676	95.9
	4557	43.3		4617	54.9		4677	103.2
	4558	44.2		4618	35.6		4678	108.8
	4559	40.9		4619	51.8		4679	72.7
	4560	24.6		4620	67.9		4680	84.2
Ozu	4561	41.4		4621	17.5		4681	95.8
	4562	36.7		4622	63.7		4682	98.3
	4563	2.0		4623	69.0	Sagawa	4683	99.4
	4564	25.1		4624	71.5		4990	101.4
	4565	48.3		4625	77.4		4991	92.0
	4566	42.0		4626	75.7		4992	82.9
	4567	35.7		4627	68.7		4993	81.1
	4568	29.4		4628	69.2		4994	79.3
Yahata-	J 4569	36.4		4629	72.9		4995	77.5
hama	4570	22.9		4630	57.7		4996	75.6
	4571	22.5	Naka-	4631	54.0	Ino	4997	73.7
	4572	32.3	mura	4632	65.2		4998	71.9
	4573	31.8		4633	66.1		4999	69.9

(to be continued.)

(continued.)

Locality	B.M.	Displace.	Locality	B.M.	Displace.	Locality	B.M.	Displace.
		mm			mm			mm
	5000	67.9		5127	– 5.9		5068	– 24.8
	5001	65.8		5126	3.9		5067	– 33.2
	5002	63.8		5125	10.4		5066	– 30.4
	5003	60.7		5124	16.9		305	– 31.5
Koti	J 5004	78.8	Kan-no-	5123	7.6		306	– 36.3
	5182	79.1	ura	5122	11.4	Bando	307	– 26.0
	5181	77.4		5121	15.0		308	– 25.5
	5180	79.1		5120	18.6		309	– 25.0
	5179	78.2		5119	22.2		310	– 23.6
	5178	79.0		5118	25.8		311	– 21.4
	5177	77.2		5117	29.3		312	– 25.4
Noiti	5176	75.4		5116	25.3		313	– 19.8
	5175	73.6		5115	21.3	Itizyo	314	– 19.5
	5174	68.5		5114	18.8		315	– 12.2
	5173	65.1		5113	16.4		316	– 10.5
	5172	30.9		5112	17.5		317	– 9.1
	5171	66.2		5111	25.9	Hati-	318	– 6.9
	5170	63.9	Muki	5110	27.8	man	319	– 3.8
	5169	56.6		5109	30.1		320	– 6.3
	5168	49.0		5108	32.4		321	– 9.1
	5167	36.0		5107	31.4		322	– 7.3
	5166	31.5		5106	31.9		323	– 5.4
	5165	30.9		5105	29.0		324	– 13.0
Aki	5164	22.2		5104	26.2		325	– 9.4
	5163	17.4		5103	23.9		326	– 12.2
	5162	2.8	Hiwasa	5102	24.2		327	– 9.7
	5161	– 8.1		5101	19.4		328	– 17.8
	5160	– 28.8		5100	19.8		329	– 18.4
	5159	– 35.8		5099	20.1		320	– 19.1
	5158	– 47.3		5098	20.5		331	– 26.7
	5157	– 51.3		5097	22.3		332	– 27.7
	5156	– 53.4		5096	24.1		333	– 30.0
	5155	– 55.4		5095	26.0		334	– 29.5
Nabari	5154	– 72.0		5094	28.5	Nagao	335	– 32.9
	5153	– 88.6		5093	22.6		336	– 29.0
	5152	– 97.3		5092	18.4		337	– 32.4
	5151	– 99.6		5091	17.8		338	– 19.7
	5150	–110.0		5090	16.4		339	– 30.2
	5149	–113.9	Nino	5089	18.1		340	– 30.8
	5148	–126.8		5088	1.0		341	– 39.2
	5147	–114.9		5087	15.7		342	– 42.1
Muroto	5146	–131.7		5086	1.4		343	– 36.5
	5145	–127.0		5085	– 29.4	Taka-	344	– 37.9
	5144	–138.2		5084	– 3.1	matu	B 42	– 38.5
Muroto-	5143	–143.0	Tomi-	0	0.2		345	– 35.7
zaki	5142	–152.8	oka	5083	3.5		346	– 41.6
	5141	–137.4		5082	– 1.3		347	– 31.5
	5140	–162.3		5081	3.7		348	– 29.3
	5139	–153.1		5080	– 6.1		349	– 26.5
	5138	–144.7		5079	4.0		350	– 20.6
	5137	–135.3	Koma-	5078	0.0		351	– 26.6
	5136	–113.2	tusima	5077	2.5		352	– 22.7
	5135	–108.7		5076	2.5		353	– 28.9
Sakino-	5134	– 90.8		5075	– 2.3	Sakaide	3354	– 21.4
hama	5133	– 81.3		5074	– 7.2		J 3380	– 20.0
	5132	– 71.8		5073	– 22.9		3381	– 20.2
	5131	– 61.5	Toku-	5072	– 9.2	Maru-	3382	– 20.8
	5130	– 49.2	sima	5071	– 27.7	game	3383	– 16.3
	5129	– 38.6	Kamo	5070	– 29.7		3284	– 9.6
None	5128	– 21.1		5069	– 26.9	Konzozi	J 3385	– 10.7

(to be continued.)

(continued.)

Locality	B.M.	Displace.	Locality	B.M.	Displace.	Locality	B.M.	Displace.
		mm			mm			mm
Konzozi	J 3385	– 10.7		5006	75.6		2759	95.7
	5065	– 4.8		5005	73.1		2760	92.7
	5064	– 7.6	Koti	J 5004	78.8		2761	89.7
	5063	– 11.2					2762	86.7
	5062	– 11.7					2763	83.4
	5061	– 3.6		KYUSYU			2764	71.2
	5060	1.2					2765	94.4
	5059	– 8.8	Nobe-	J 2635	93.3		2766	89.8
	5058	– 1.2	oka	2708	86.1		2767	91.7
	5057	5.3		2709	89.3		2768	84.7
	5056	18.7		2710	90.5		2769	30.7
	5055	– 5.1		2711	91.7		2770	90.5
	5054	– 39.5		2712	91.0		2671	82.1
	5053	31.1		2713	80.2		2772	77.7
	5052	25.3		2714	87.3		2773	54.7
	5051	36.2		2715	83.8		2774	65.7
	5050	44.6		2716	85.0		2775	109.4
	5049	47.7		2717	81.3		2776	76.3
	5048	36.3		J 2718	84.8		2777	78.8
	5047	28.2		2719	81.0		2778	74.8
	5046	16.4		2720	82.3		2779	72.1
	5045	42.5		2721	81.0		2780	71.3
	5044	40.6		2722	81.2		2781	66.7
	5043	46.8		2723	75.8		2782	69.7
	5042	47.7		2724	82.1		2783	69.6
	5041	52.4		2725	76.2		2784	61.4
	5040	8.5		2726	79.6		2785	50.8
	5039	56.1		2727	64.2		2786	51.7
	5038	63.4		2728	73.5		2787	36.5
	5037	63.7		2729	69.4		2788	34.4
	5036	56.9		2730	68.1		2789	23.1
	5035	37.3		2731	77.9		2790	8.0
	5034	69.0		2732	78.8		2791	– 12.5
	5033	59.5		2733	79.7		2792	– 5.8
	5032	65.1		2734	68.1		2793	– 25.8
	5031	70.4		2735	75.1		2794	– 38.5
	5030	– 73.8		2736	76.1		2795	– 52.1
	5029	– 21.4		2737	78.1		2796	– 86.7
	5028	–136.2		2738	35.1	Sikine	2797	– 98.7
	5027	48.1		2739	79.5		2488	–139.2
	5026	82.5		2740	81.1		2489	–154.6
	5025	84.2		2741	82.8		2486	–123.4
	5024	71.6		2742	79.7		2485	–135.6
	5023	67.7		2743	83.5		2484	–116.3
	5022	68.9		2744	47.2		2483	–104.1
	5021	46.4		2745	77.4		2482	– 97.5
	5020	4.4		2746	83.3		2481	– 16.1
	5019	76.4		2747	76.5		2480	– 16.0
	5018	78.1		2748	88.2		2479	12.6
	5017	82.6		2749	60.9		2478	19.8
	5016	92.9		2750	94.5		2477	– 33.6
	5015	81.2	Miya-	J 2751.1	75.9		2476	– 92.1
	5014	83.8	zaki	2751	96.3		2475	–139.4
	5013	46.6		2752	109.1		2474	–212.8
	5012	92.0		2753	96.3		2473	–177.4
	5011	88.3		2754	98.5		2472	–129.9
	5010	83.3		2755	100.7		2471	–102.5
	5009	93.9		2756	100.2		2470	– 87.5
	5008	65.5		2757	99.6		2469	–125.2
	5007	61.9		2758	98.7		2468	–102.8

(to be continued.)

(continued.)

Locality	B.M.	Displace.	Locality	B.M.	Displace.	Locality	B.M.	Displace.
		mm			mm			mm
	2467	– 80.2		2407	107.5		1957	94.7
	2466	– 57.8		2406	106.5		1856	96.2
	2465	– 52.6		2405	110.3		1855	97.8
	2464	– 60.6		2404	106.2		1854	95.3
	2463	– 54.3		2403	108.0		1853	92.7
	2462	– 22.8		2402	100.8		1852	90.1
	2461	– 57.8		2865	107.4		1851	87.5
	2460	1.7		2401	108.2		1850	83.6
	2459	– 16.5		2400	109.0		1849	83.2
	2458	– 16.8		2399	109.8		1848	76.2
	2457	– 12.7		2398	106.8		1847	69.4
	2456	17.4		2397	116.7		1846	62.4
	2455	– 10.2		2396	–553.2		1845	63.2
	2454	106.4		2395	119.2		1844	64.1
	2453	16.6		2394	77.6		1843	64.9
	2452	47.5		2393	36.0		1842	55.4
	2451	36.1		2392	114.8		1841	62.3
	2450	55.8		2391	120.2		1840	69.3
	2449	46.2		2390	100.5		1839	42.2
	2448	33.4		2389	119.1		1838	15.2
	2447	8.0		2388	109.7		1837	32.3
	2446	34.4		2387	121.6	Kuru-	J 1636	49.5
	2445	53.0		2386	125.9	me	1835	57.5
	2444	66.0		2385	124.1		1834	52.5
	2443	61.6		2384	126.7		1833	53.7
	2442	62.3		2383	126.8		1832	54.9
	2441	70.5		2382	125.2		1831	51.7
	2440	16.0		2381	130.1		1830	40.2
	2439	34.4		2380	125.0		1829	39.3
	2438	41.5		2379	118.1		1828	47.3
	2437	32.1		2378	111.3		1827	40.5
	2436	74.8		2377	104.4		1826	34.3
	2435	111.3		2376	95.0		1825	49.6
	2434	81.2		2375	96.8		1824	46.2
	2433	79.1		2374	133.9		1823	42.5
	2432	85.4		2373	130.9		1822	38.3
	2431	58.1		2372	131.5		1821	36.2
	2430	53.5		2371	128.3		1820	33.7
	2429	60.2		2370	129.1		1819	14.0
	2428	82.2		2369	97.6		1818	20.4
	2427	87.1		2368	76.2		1817	4.9
	2426	92.0		2367	122.8		1816	22.3
	2425	50.1		2366	123.5		1815	24.7
	2424	40.4		2365	130.7		1914	30.3
	2423	– 46.3	Kuma-	J 1873	126.8		1813	26.6
	2422	70.3	moto	1872	122.0		1812	24.3
	2421	69.6		1871	123.3		1811	35.7
	2420	72.2		1870	117.7		1810	31.5
	2419	101.3		1869	114.5		1809	13.5
	2418	84.6		1868	101.3		1808	29.1
	2417	104.0		1867	99.8		1807	30.2
	2416	104.1		1866	94.5		1806	28.5
	2415	55.2		1865	100.3		1805	28.7
	2414	8.6		1864	83.8		1804	26.7
	2413	92.7		1863	104.4		1803	29.7
	2412	89.4		1862	95.8		1802	21.0
	2411	101.6		1861	87.2		1801	17.5
	2410	105.9		1860	91.6		1800	– 28.1
	2409	110.3		1859	96.0		1799	10.2
	2408	109.6		1858	93.2		1798	31.2

(to be continued.)

(continued.)

Locality	B.M.	Displace.	Locality	B.M.	Displace.	Locality	B.M.	Displace.
		mm			mm			mm
	1797	28.6		1959	82.9		2604	95.2
	1796	28.2		1958	95.5		2603	123.2
	1795	35.4		1957	75.0		2602	113.0
	1794	30.4		1956	73.9		2601	112.7
	1793	34.8		1955	104.6		2600	112.3
	1792	35.1		1954	114.0		2599	119.0
	1791	42.8		1953	116.7		2598	122.0
	1790	16.8		1952	122.3		2597	127.3
	1789	34.3		1951	125.5		2596	130.8
	1788	36.5		1950	128.6		2595	131.3
	1787	36.3		1949	129.9		2594	129.2
	1786	36.1		1948	135.8		2593	127.0
	1785	21.4		1947	134.3		2592	123.8
	1784	23.1		1946	127.6		2591	100.3
	1783	39.0		1945	120.8		2590	113.4
	1782	34.5		1944	118.8		2589	121.5
	1781	40.3		1943	118.9		2588	107.4
	1780	23.7		1942	111.3		2587	146.1
	J 1779	37.6		1941	103.1		2586	41.8
	2000	38.7		1940	111.3		2585	104.5
	1999	43.1		1939	119.5		2584	89.6
	1998	43.9		1938	117.4		2583	50.7
	1997	48.3		1937	117.1		2582	98.8
	1996	41.9		1936	112.3		2581	95.4
	1995	36.2		J 1935	111.9	Nobe-	J 2635	93.3
	1994	32.0		5372	102.1	oka		
	1993	48.4		5371	123.0			
	1992	202.7		5370	127.2	Nobe-	J 2635	93.3
	1991	47.8		5369	130.5	oka	2636	93.2
	1990	47.7		5368	133.0		2637	89.5
	1989	36.7		2634	125.3		2638	92.7
	1988	52.7	Saka-	J 2633	135.4		2639	89.4
	1987	59.0	noiti	2632	127.2		2640	92.3
	1986	59.2		2631	131.1		2641	96.6
	1985	56.3		2630	139.4		2642	106.8
	1984	37.3		2629	138.0		2643	105.9
	1983	63.5		2628	140.4		2644	105.4
	1982	60.7		2627	145.9		2645	102.9
	1981	62.6		2626	146.1		2646	105.9
	1980	66.0		2625	135.7		2647	94.8
	1979	63.7		2624	148.2		2648	103.0
	1978	99.8		2623	147.6		2649	104.8
	1977	58.3		2622	147.2		2650	108.2
	1976	55.8		2621	145.2		2651	107.2
	1975	66.6		2620	288.7		2652	108.3
	1974	71.4		2619	152.1		2653	107.0
	1973	65.7		2618	156.2		2654	110.7
	1972	72.1		2617	164.6		2655	111.9
	1971	75.1		2616	153.3		2656	111.7
	1970	79.8		2615	155.0		2657	113.5
	1969	75.0		2614	151.3		2658	111.5
	1968	70.2		2613	154.4		2659	118.2
	1967	78.2		2612	150.1		2660	114.0
	1966	81.6		2611	139.6		2661	116.5
	1965	97.5		2610	140.1		2662	118.3
	1964	91.3		2609	129.7		2663	116.7
	1963	83.1		2608	140.5		2664	119.9
	1962	58.2		2607	139.1		2665	121.9
	1961	92.3		2606	134.5		2666	119.2
	1960	101.8		2605	78.2		2667	119.8

(to be continued.)

(continued.)

Locality	B.M.	Displace.	Locality	B.M.	Displace.	Locality	B.M.	Displace.
		mm			mm			mm
	2668	97.2		9180	83.3		9133	121.1
	2669	111.2		9179	69.5		9132	118.2
	2670	108.1		9178	− 97.1		9131	111.7
	2671	108.6		9177	96.1		9130	105.5
	2672	108.2		9176	66.0		9129	119.7
	2673	111.1		9175	51.7		9128	109.9
	2674	108.4		9174	62.3		9127	25.5
	2675	110.4		9173	13.0		9126	132.4
	2676	101.0		9172	72.5		9125	125.9
	2677	107.7		9171	57.3		9124	119.9
	2678	108.7		9170	8.0		9123	114.3
	2678	111.0		9169	69.0		9122	122.4
	2680	100.2		9168	− 29.6		9121	116.2
	2681	112.1		9167	39.0		9120	109.9
	2682	111.1		9166	125.5		9119	102.6
	2683	118.0		9165	−218.7		2518	95.3
	2684	109.6		9164	141.8		2517	87.4
	2685	113.3		9163	149.9		2516	92.6
	2686	68.7		9162	146.2		2515	87.4
	2687	116.4		9161	128.4		2514	82.2
	2688	116.9		9160	87.1		2513	70.4
	2689	117.0		9159	131.0	Hana-	2512	54.9
	2690	105.0		9158	118.4	oka	2511	56.5
	2691	101.5		9157	117.5		2510	58.2
	2692	119.6		9156	115.7		2509	25.7
	2693	124.8		9155	111.5		2508	33.7
	2694	124.0		9154	107.2		2507	28.6
	2695	129.7		9153	121.7		2506	5.9
	2696	126.3		9152	46.5		2505	11.5
	2697	122.9		9151	97.4		2504	− 10.8
	2698	108.8		9150	109.1		2503	− 24.0
	2690	94.6		9149	117.2		2502	− 52.3
	2700	111.9		9148	116.7		2501	− 76.7
	2701	100.0		9147	110.8		2500	−117.1
	2702	87.9		9146	121.4		2499	−157.5
	2703	113.2		9145	− 8.6		2498	− 82.8
	2704	111.4		9144	92.1		2497	− 84.0
	2705	115.6		9143	118.9		2496	− 58.9
	2706	117.1		9142	90.0		2495	− 65.4
	2707	128.5		9141	118.8		2494	−118.4
Kuma-	J 1873	126.8		9140	107.7		2493	− 97.4
moto				9139	114.9		2492	−103.7
				9138	35.6		2491	− 50.5
Miya-	J 2751.1	75.9		9137	119.0		2490	− 64.3
zaki	9183	100.5		9136	116.9		2489	− 86.2
	9182	99.1		9135	116.9	Sikine	J 2797	− 98.7
	9181	96.0		9134	118.3			

3. The vertical displacements, deduced as above, of the bench-marks situated near the mareograph stations of Hamada (Tonoura), Wazima and Aburatubo are respectively −1.1 mm., −14.3 mm, and 1132.7 mm., which differ slightly from the vertical displacements estimated from the mareogram data at respective mareograph stations, i.e., −4 mm. at Hamada, −40 mm. at Wazima and 1166 mm. at Aburatubo. These differences in the values of the vertical displacements deduced from

different sources are thought as not exceeding greatly the permissible limit of fluctuations in the values of vertical displacements deduced from the mareogram data.

It is worthy of remark however that the vertical displacements thus worked out of the bench-marks may still be questionable as to whether they show the real mode of the deformation of the earth's surface, for the reason that these values are based on such assumptions as mentioned above.

On the other hand, the data of the vertical displacements of the bench-marks hitherto obtained are those due to various epochs of time. Hence, if we wish to get a general view of the distribution of the vertical earth movement in Japan, some method or procedure similar to that employed in the present study should be applied to deduce the values of vertical displacements of bench-marks distributed along various lines of levels.

In conclusion, the present writer wishes to express his sincere thanks to the Ministry of Education for the Science Research Fund granted to the writer when he was engaged in the research work in Tokyo University and in Nagoya University, by the aid of which the present work was carried out. The writers thanks are also due to Miss Fumiko Abiko, Miss Fumiko Maeda, Miss Harue Kuroki and Miss Yosiko Imai for their assistances in executing the numerical calculations and preparing the figures and tables in the present work.

---

14. 水準改測の結果から見た日本の陸地變動

建設省地理調査所　宮部直巳

日本各地にある水準点の改測は屢々行なわれて，局部的な土地の變動はよく知られているが，これらをつぎあわせて，日本全體の變動を一眸におさめようという場合には，若干の問題がある．それは主として，各水準線路に沿うて測量の行われた時期が區々であるという点に存する．そこで本文では，これらの資料を統一して，全國的な土地の變動を知ろうと試みた．

多数の水準線路のうち，2 回以上測量の行なわれた線路をとり，まず，測量の時期を調べてみると，大部分の線路につき，その測量の時期は，1900 年前後及びその以前と，1928 年前後とその以後であることが多い．そこで，各水準線路に沿い，隣接水準点の高さの差の変動量を，按分的にこの期間の変動量に改算した．この結果には，色々な意味で誤差を含むことが豫想されるが，それらの誤差を解析的にとり除くことは殆ど不可能であると思われるので，次のような考えで之を調整した．それは，これらの変動量は一つの水準線の環について加え合せた場合には 0 になるべきであるという考えをもととする．この場合，この変動には地下の質量の著しい変化，即ち重力場の変化は伴わないと假定する．多數の水準環線について上に述べたような考え方が同時に適用されるとすることによつて，隣接水準点の間の高さの差の変化量を一應調整することが出來る．

上述の調整値を用い，ある特定水準点の變動量を與えることによつてすべての水準点の 1900-1928 の間の變動量を求めることが出來る．例えば，本州にある水準点の變動量を求めるに際しては，串本にある B.M. 3 の變動量を -188.0 mm. として計算した．この値は，串本の驗潮記錄における年平均潮位の永年變化から推定したものである．これによつて，濱田，輪島，油壺などにある水準点の變動量を求めると夫々，-1.1 mm. (濱田)，-14.3 mm. (輪島)，1132.7 mm. (油壺) となる．これらの場所には驗潮場があるので，夫々年平均潮位の永年變化から同じ期間の變動量を求めることが出來る．その値は，夫々，-4 mm. (濱田)，-40 mm. (輪島)，1166 mm. (油壺) であつて，驗潮記錄から求められる年平均潮位の値の誤差は略々 20-30 mm. であるから，比較的よく一致した値が得られたというべきである．

本文には上述の如くして推定された各水準点の 1900-1928 の間の變動量を表示してある．

15. 褶曲運動による地表の變形について*

地質学教室　杉　村　　新

(昭和 27 年 2 月 19 日発表——昭和 27 年 3 月 20 日受理)

§1. これまでのこと

1942 年に主として大塚弥之助[1)~3)]が言いだした“活動している褶曲構造”は，水準点の変位および河岸段丘の高さが，褶曲構造と同じ傾向の分布を示すと云うことであつた．そのうちの水準点の方に関しては，その後宮村摂三ら[4)]によつて検討され，この関係がうたがわれはじめているが，河岸段丘の方に関しては，その再検討あるいはさらにつつこんだ調査がまだ行われていなかつた．

大塚が河岸段丘と褶曲構造と関係している例に挙げたのは，主として最上川の支流小国川にそうものであつた．この例では，河岸段丘の高さを 5 万分の 1 の地形図“新庄”に記入された等高線に求めている．その等高線から，段丘の縦断面を画く場合に，大塚は別の面とおもわれる 2 つの高さを結んで面が傾いているように表現したりしているので，野外の観察とこれとを照し合せたかぎりでは，示されたグラフ[5)]の一部はこじつけとうたがうこともできた．さらに，この地形図の等高線は，場所によつては画きかたがあらく，河岸段丘の高さについては，利用にたえられない 2~3 の場所のあることが分つた．

これらの理由から，段丘面の高さをじつさいに測つてみる必要を感じた．

§2. フィールドのえらびかた

大塚[6)]の述べているように，現在までひきつづいて造構造運動の継続している地域が，日本列島(臺湾をのぞく)のなかで，かれの言うミズホ(瑞穂)フオツサマグナ褶曲帯にかぎられるかどうかは問題であるとしても，すくなくとも褶曲のていど[7)]が大きくなくては，

---

* 宮村摂三紹介

この論文を心から，亡き大塚彌之助先生にさゝげる．

1) Y. Otuka, *Proc. Imp. Acad., Japan*, **17** (1942), 518-522.

2) 大塚彌之助　地震 (*Zisin*) **14** (1942), 46.

3) 池辺展生　石油技術協会誌 (*Jour. Jap. Assoc. Petr. Techn.*), **10** (1942), 184.
大塚彌之助　“日本の地質構造”, 東京 (1942), 181-182 ; 184.
A. Imamura and Y. Otuka, *Proc. Imp. Acad. Japan*, **18** (1943), 662-665.

4) 宮村摂三　地震研究所彙報 (*Bull. Earthq. Res. Inst.*) **21** (1943), 197.
宮村摂三・岡田惇　地震研究所彙報 (*Bull. Earthq. Res. Inst.*) **27** (1949), 141.

5) Y. Otuka, 前出 1) fig. 1 ; 2) 第 2 図.

6) Y. Otuka, 前出 1).

7) Y. Otuka, *Bull. Earthq. Res. Inst.* **11** (1933), 723-731.

それが継続しているかどうかをたしかめることがむずかしくなるので，筆者は褶曲度の大きいミズホ・フオツサマグナ褶曲帯について，まずしらべてみることにした．それで，この地帯にふくまれる河岸段丘[8]のうち5万分の1の地形図によくあらわれているもの（川の数で約 90）を全部ぬきだし，そのなかから

（1） 新第三紀層または洪積層が露出し且褶曲している．

（2） 変位のていどの分らない断層が走つていない．

（3） 火山物質に被われていない[9]．

（4） 褶曲軸にほぼ直角に川が流れている．

（5） 段丘面が何段もあつて，発達がよい．

の条件に適するところ3か所をえらんだ．それは北より，米代川の支流阿仁川，雄物川の支流岩見川，最上川の支流小国川である（第1図）．さいごの場所は §1 で述べた古典的な例のところである．

これらはどれも，大きな川の支流であり，支流のなかでも大きなものに属する．これは偶然に一致したのではなくて，なにかわけがありそうにおもえる．

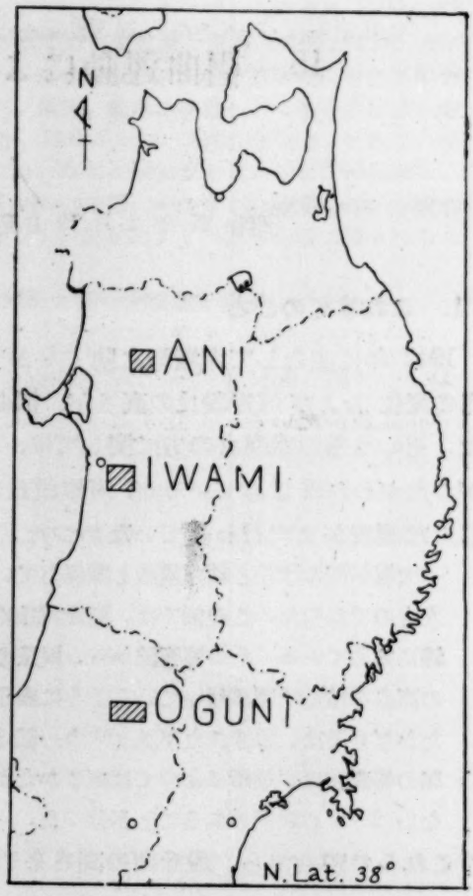

Fig. 1. Disposition of the localities mentioned.

§3. 氣壓計のつかいかた

1. 気圧計をつかつたわけ．

段丘面は，できはじめから多少の凹凸があり，のちの侵蝕などによつて変化を蒙つているから，精度の高い測量をしてもそれだけの精度で対象を論ずることはできない．このいみからも，費用・労力・時間などの点からも，気圧計を用いるのがてきとうと考えた．

筆者は 1949 年以来，地形や地質の調査には気圧計をつかつており，比較的使いなれていたと云うこともある．

この場合，以下に示すような若干のくふうをしたが，これは手軽に高さを知る方法の1つにすることができると考えている．

---

8) 海岸段丘では，岬と湾奥とではじめからすでに多少の高低ができている可能性があるので，河岸段丘をえらぶことにした．

9) かたい熔岩などのため，縦断曲線がスムーズにならなくなるからである．

2. 気圧計により高さを知る方法のあらすじ.

筆者のとつた高さを知る2つの方法のうち, A 法とここで仮に呼ぶものは, つぎのようなやりかたである. (A 法は小国川についてだけ用いた).

(1) 基地に自記気圧計を置いておき, その高さをトランシットによつて測つた. (一等水準点までの距離は約 300 m で, 往復閉塞差は 20 cm であつた.)

(2) 水準点など高さのすでに分つている地点と, 測定すべき地点とで, 携帯気圧計を読み, 同じ時刻の自記気圧計の読みとの差を求めた. この場合, 高さの既知な点の測定と, 未知な点の測定との条件があまりちがわないように計画した. すなわち, 場所の条件については第2図に示すように, また測定日の条件については第1表に示すように, 両者の分布範囲がだいたい一致するようにした.

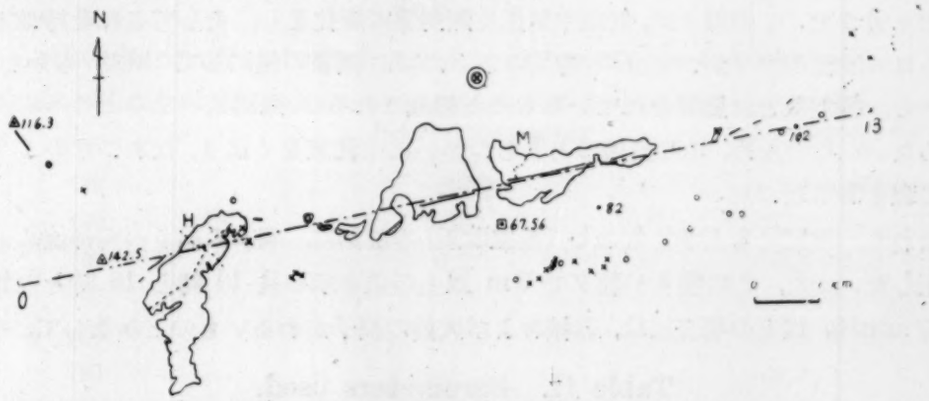

Fig. 2. Profile line, measuring routes and altitude-known points along the River Ogu n i
—·—·: profile line Closed lines: the fifth (V) plain
——○: routes and points measured by A-method
- - -×: ,, ,, ,, B- or C-method
Numbers: already-known altitudes
⊛: the locality of self-registering barometer
H: Hukuzyuno, M: Murasakiyama

Table I. The numbers of times of measurement.

Date	1951									
	October								November	
	16	17	18	19	20	22	25	26	22	24
△ 116.3					1				1	
△ 142.5				1		1				
⊡ 67.56		1				1				
· 82		1	1							
· 102								1		1
Measurement by A-method	5	30			4	55	4	5	4	12

(3) 高さの既知な地点に関する (2) の読みの差が，(1) からみちびかれる比高の値に対して，どのような分散を示すかを計算して，これをだいたい同じ条件におかれた未知の地点に関する読みの分散にほゞ等しいと考えた．

もう1つの，仮にここで B 法と呼ぶものは，A 法に似ているのであるが，自記計の高さを測るのに携帯計を何回もつかうと云う方法をとつたものである．但し，この場合は，精度を求めることはできない．

3. 器械およびその読みについて．

検定の成績などを第 II～IV 表に示す[10]．調査中，毎日朝夕 2 回これらの同時同所の読みをつづけたところ，自記計と携帯計との読みの差が，時がたつとともに少しづつ変化した．自記計は 2 臺並べているので，この変化のほとんど全部が携帯計の値のかたよるためだと分つた．この偏りは，気温や気圧と無関係に変化をし，そしてこれを持つて走つた或る日に変化が大きかつた (15 時間のあいだに，高さの値にして 10 m もかわつた) ことから，衝撃などに影響されているものと想像されるが，原因はいまのところにつきりは分らない．このため，この器械のとりあつかいには注意をくばり，なおつぎのような資料の処理をおこなつた．

すなわち，検定にもとずくなおし (器差改正) のほかに，朝夕の偏りの内挿値によつても補正した．また，この偏りが朝夕で 3 m 以上の差を示し且 10 時と 16 時との気圧の差が 2 mmHg 以上の場合には，器械および天候の調子がわるいものとみなして，その資

Table II. Barometers used.

Kind		self-registering (weekly turning)		portable (1 gradation 10 m with vernier and magnifying glass)
Maker		OGASAWARA, Tokyo	ÔTA, Tokyo	SHORT and MASON, London
Number		241092	851	2052
Attached to		Geological Institute, Tokyo University	Section of Meteorological Observation, Central Meteorological Observatory	Earthquake Research Institute, Tokyo University
Class of official approval	Before the survey	1st class	—	2nd class
	After the survey	1st clase	2nd class	2nd class
Result of official approval		table III	—	table IV

10) 携帯計は，ヴアーニアの位置を慎重にきめて，0.5 m の単位で読んだ．

Table III.

Result of official approval for the self-registering barometer.

	Before the survey	After the survey
780 mmHg	+0.1 mmHg	−0.2 mmHg
760	0.0	0.0
740	0.0	+0.1
710	+0.1	+0.2
Correction for temperature	0.00 mm/°C	0.00 mm/°C

Table IV.

Result of official approval for the portable barometer.

	Before the survey	After the survey
780 mmHg	−0.7 mmHg	−0.5 mmHg
770		−0.2
760	0.0	0.0
750		−0.6
740	−0.2	−0.6
730		−0.7
720		−0.6
710	0.0	−0.5
Correction for temperature	−0.02 mm/°C	−0.04 mm/°C

料を A 法からとりのぞいた．これらのとりのぞかれた資料を便宜上，C 法による測定と呼んでおく．

4. A 法の測定の精度について．

高さ既知の諸点（第 2 図）における，気圧計で求めた高さ（2 回づつ測つた）と地形図に記入されている高さとの差は第 V 表のようになる．これらの試料の母集団が正規であ

Table V. Differences between the measured altitudes and the real altitudes

(unit: meter)

△ 116.3	−1.3,	−2.8
△ 142.5	+1.5,	+1.0
⊡ 67.56	−0.1,	−1.1
· 82	−1.0,	+1.0
· 102	+1.0,	−1.5

るとして，まずその平均値が 0 であつてもよいかどうかを検定する．$Pr\{|Z|>\lambda\}=0.05$ (但し，Z は自由度 9 の t 分布をする函数) であるような λ は 2.262 であり，この試料の Student の t は -0.717 なので，$|t|<\lambda$ となるから，平均値は 0 であつてもよい．つぎに，平均値を 0 にさだめて分散を推定すると，$\hat{\sigma}^2=2.016$，これより気圧計で求めた高さの誤差は，95% の信頼度で ±2.8 m 以内であると云うことができる．

§4, 測定の結果に対する註

1. 段丘の縦断面について．

前§に述べた精度は，もちろんそのまま，のちの変形の量に対するそれにはならない．すなわち，

(1) 段丘面は最初からデコボコをもつており，面の山がわのへりと川がわのへりとで高さの差が数 m に達するところもある．

Table VI. Terrace Deposits.

Along	Number of Terrace	Thickness of Volcanic Ash	Thickness of Sand and Gravel	Thickness of Both Added	Maximum Grain of Gravel
the R. Oguni	II	1 m	2-5 m		cobble
	III	1-4 m			cobble
	IV	4-7 m			—
	V	0.3 m-1 m	2-13 m		boulder or cobble
	V′	—	2 m		boulder
the R. Ani	III	2 m	1-7 m		cobble or pebble
the R. Iwami	III	10 m			—

(2) ここで扱つている段丘面はすべて火山灰土をかぶつていて，その厚さは 0.3～2m である (第 VI 表)．このため，現在の高さは 2m 以下のていどでもとの面よりかたよつているとおもわれる．

(3) のちの侵蝕のためもとの面の跡をのこしていないところは，小さな谷をつくつていて，面ののこつているところとの区別はわりにはつきりしており，のちの侵蝕で低まつたところを測つている心配はそれほど大きくない．しかし，これを考えにいれないわけにいかない．

それで測定のルートをどのようにえらぶか，およびルートのえらびかたによつて結果がどのようにちがつてくるかが問題になる[11]．ここで扱つている多くの段丘は模式的に第3図のようになつていて，“川がわのへり”とした部分は“山がわのへり”にくらべて狭く，且 A 点の位置は

11) この点については，坂本峻雄・河角広両先生の御指摘をいただいた．

ぼんやりしていてどことはつきりはきめられないが，B 点の位置はだいたいはつきりしている．だから C と云う範囲にルートを求めるのがのぞましいと考えた．これを第1の条件とし，第2，段丘面の分布方向になるべく平行に近くルートをとる，第3，前ページ(3)にしるしたようなところの疑いのある場所をさける，第4，作図上の便利のため部分的にはルートを直線にとる，第5，

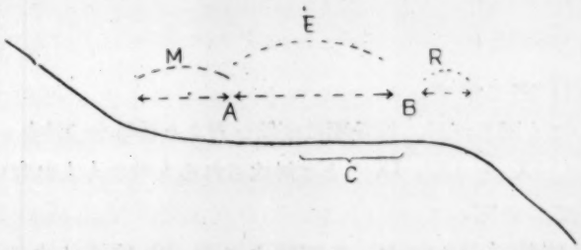

Fig. 3. Schema of transversal profile of river terrace.
M : mountainside border, E : even part, R : riverside border

なるべく人工を加えていない道路にする，などの条件を考えると，ほとんど迷うことなく一意的にルートがきまつた．すなわち筆者は段丘面のひとつゞきの部分として最もプロバブルで且能率的なものをルートにえらんだのである．しかし，画かれた縦断曲線に対しては前ページ(1)~(3)の理由から多少ぼんやりした見かたをしなければならないし，またルートのえらびかたについてもまだ検討すべき問題はのこつている．(なお §5 の 2 でもういちどふれる．)

気圧計を読んだ位置の間の距離は，歩巾または，自転車の車の回転数によつて測つた．

2. 地層の褶曲構造について．

段丘面の高さと褶曲構造とを比べるときは，極大点と背斜軸とが一致するかどうかと云うことよりも，両者の曲率が相関しているかどうかが問題だと考えて，褶曲構造の方は，だいたいの断面図を画いてみた．これらの断面図のかくじつさは key beds のあるなしによつて，またくわしさは層位 (attitude，地層の走向傾斜) を測つた点の密度によつて見当をつけることができよう．

3. 段丘面と地質構造との比較について[12]．

この論文では，段丘面も地層も或る測定地以内での変形だけを考えているのであり，測定地全体にわたる傾動はさしあたり問題にしない．と云うのは，段丘面のできはじめに，それがどんな傾斜をもつていたかを知る手がかりがないからである．このことは土地全体の昇降についても同じである．地層については，たとえば単斜構造のように全体として或る方向への傾きが卓越しているときには，傾きの平均をステレオグラフによつて求め，それからの差を，段丘面のと比べなければならない．この論文で扱つている地域では，いずれも層位の平均はほゞ水平になるので，断面図をそのまゝ用いてよい．

したがつて残された疑念は，段丘面や地層がはじめから曲つていたかどうかと云う点である．前者は基盤の岩質などに影響されるものであるが，小国川の場合における舟形層群と長沢累層とのちがいをのぞいては，これを支配するほどの岩質の差はみとめられない．たとえあつたとしても，地層が或ていど傾いている以上，現在の川の縦断曲線 (のちに述べる各々の I 面) と比べる

12) この項の一部は坪井忠二先生の御指摘にこたえて，つけくわえたものである．

ことによつてこの疑念を回避することができよう．後者については，こゝの場合は地層の厚さの地域的な変化がそれほど甚しくないので，大たいにおいて現在の層位が堆積后の変形を示すと考えられ，やはり断面図そのまゝを使うことができる．

§5. 小国川にそう例

1. 段丘面の分布．

第5図および第 VII 表に示す．

他の川の例についても同じだが，段丘面には低い方より番号をつけた．これらのうち IV と IV′, V と V′, V″, IX と IX′, IX″ とは対比されるものかもしれない．

2. 段丘面の高さについて．

第 4 図の上半に，縦断面[13]を示す．たてはよこの 10 倍にひきのばされている．地形図に記入された標高点などで，段丘面上にあるものは，その高さを，A 法による測定値と同じ○で示した．これは他の川の例でも同様である．II キヨウダンバラ面の高さは，現在の川の水面（平水のとき）から，ハンドレベルをつかつて測り，やはり○で示した．

Table VII. Classification of Terrace Plains along the R. Oguni.

Number of terrace	Name of terrace	Sign of clossification used by Y. Otuka in 1942
I	Recent Flood Plain of the R. Oguni	g
II	Kyôdanbara (経壇原) Plain	f
III	Haba (幅) Plain	
IV	Noda Plain	a part of e
IV′	"No" (野) Plain	
V	Lower Hukuzyuno Plain	e
V′	Nagasawa Plain (provisional name)	a part of e
V″	Nagao Plain (provisional name)	
VI	Middle Hukuzyuno Plain	a part of d
VII	Upper Hukuzyuno Plain	a part of d
VIII	Ôkurayamabara Plain	c and a part of d
IX	Uranoyama Plain	b
IX′	Kidomo Plain (provisional name)	a part of a
IX″	Lower Takakurayama Plain	a part of b
X	Sabane (猿羽根) Group of Plains	a and the others

V 低位福寿野面においては，横断面が第6図のようになる．これより縦断面を測るルートの位置が左右にかわつても，その結果はそれほど甚しくはかわらないことが分る．

この研究で重要な役目を果している紫山（第4図 M）附近の V 面において，横断方向の傾斜

13) I は地形図上の等高線をもとにして画かれた．II の上下 2 段は山がわのへりと川がわのへりとを示す．

(第6図) より縦断方向の傾斜 (第4図) の方が大きいことは，東への急な傾斜を確認させるよりどころを与える．じつさいこの部分では，面上の田を流れる水は，南へではなく東へ流れている．

IX ウラノヤマ面は，高さを測つた地点が少いけれども，保存のいい面で，ずつとつゞきになつている．こゝでは，段丘面のはじめからのデコボコを考える必要のないほどに大きくなみうつていていて[14]，ルートのえらびかたは問題にならないとおもわれる．

3. 地質構造について．

大塚[15]が 1941 年に調査したときからいままでの 10 年以上のあいだに，この地域の地質調査はいちゞるしくはかどつている．その主なものは，地質調査所石炭課·帝国石油 K. K.·仙臺通産局によるものである．筆者は調査所の徳永重元ら[16]の調査結果をつかつて，第 4 図下半の断面図を画いた．

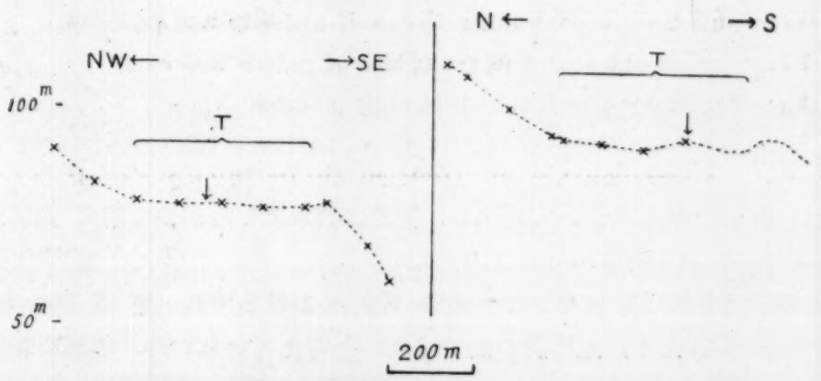

Fig. 6. Transversal profiles of the fifth (V) terrace and the position (↓) of measuring route along the river.
The left: in the neighborhood of Hukuzyuno (H in fig. 5)
The right: in the neighborhood of Murasakiyama (M in fig. 5)
T: terrace plain

層序を第 VIII 表に示す．K_1～K_4 は key beds であつて，これらの岩質は第 IX 表に示すように，だいたい火山抛出物からなり，堆積の同時面と考えられる．したがつて，この断面図には大きなあやまりはないはずである．地層の年代は，現在諸論があつて定説がなく，化石からは舟形層群は中新世中期乃至洪積世初期と考えられているが，鮮新世またはそれ以后の可能性がつよい．

4. 段丘の高さと地層の傾きとの関係．

少くともこの地域では，両者に相関があるようである．とくに V 低位福寿野面の一部 (M·Ky 間) のもり上りに対応して，それより古い IX ウラノヤマ面がもり上つており V 面より変形が進んでいるとおもわれることは注目すべきことである．最も新しい II キョウダンバラ面では，はじめからのデコボコのため，そのわずかな変形が分解能以下にぼけてしまつているのであろう．

14) 第5図で分るように，第4図に示す傾斜に consequent な沢によつて刻まれている．

15) 大塚彌之助 石油技術協会誌 (*Jour. Jap. Assoc. Petr. Techn.*) **10** (1942) 22-29.

16) 徳永重元 未発表資料．

Table VIII.

Stratigraphic column along the lower part of the R. Oguni.

Sign	Name	Defined by	Geological age	
—	Hunagata Group	Y. OTUKA in 1942	Pliocene or Pleistocene	contains the key beds K_1-K_4
N	Nagasawa Superformation	S. TOKUNAGA (MS)	Miocene	contains the so-called "green tuff"

Table IX. Rock Names of Key Beds.

(after S. TOKUNAGA)

K_1: turff-breccia containing blocks of andesite and pumices
K_2: pumice-tuff with the grain size of pebble and sand
K_3: pebble-conglomerate containing pumices
K_4: tuff-breccia containing pumices (maximum thickness: 12 m)

なおつぎに 2 つの断層について述べる．位置は徳永にしたがつて第 5 図に示す．

(1) キヨウダンバラ断層

第 4 図に示すように IX ウラノヤマ面の Ky におけるずれ（第 5 図から推定されるように，ずれの両がわは，互に別の面ではないと考えている）は，地層において key beds の分布から推定されているキヨウダンバラ断層の運動と同じ方向に行われたと考えられるし，この断層の北方のつゞきは舟山裕士・北村信によつて追跡されているが，8 km 北で村田貞蔵[17]の指摘している大森山のケルンバットの附近を通つている．これらのことからこの断層は少くとも休断層とみなすことができる．

(2) 松山断層

徳永によれば，この断層の西がわの地層が，東がわのそれより古いにもかゝわらず，断層面の東への傾き (30~40°) が，地層の同じ方向への傾き (40°~80°) に比べてゆるいので，西おちの逆断層と結論されている．5 万分の 1 の地形図 "清川" をみると，断層の位置をさかいにして東がわの方が地形は急峻である．これは，岩石のかたさがちがうためか近い時代に西おち・東あがりの断層運動の行われたためか，いずれかであるとおもわれ，休断層の可能性がある．

この 2 つの断層にはさまれた地域の褶曲，とくに紫山 (図の M) 附近のものは，非対称的で，W. SCHMIDT 流の考えかたをすれば西おち東あがりのすべり (shear) が狭い局部に行われたような形をしており，ちようど 2 つの断層と同じ方向の運動を考えることもできる．

§6. 阿仁川にそう例

段丘面の分布を第 7 図，その高さの分布を第 8 図上半に示す．后者では，たてがよこ

17) 村田貞蔵 地理学評論 (*Geogr. Rev. Jap.*) **17** (1941), 464.

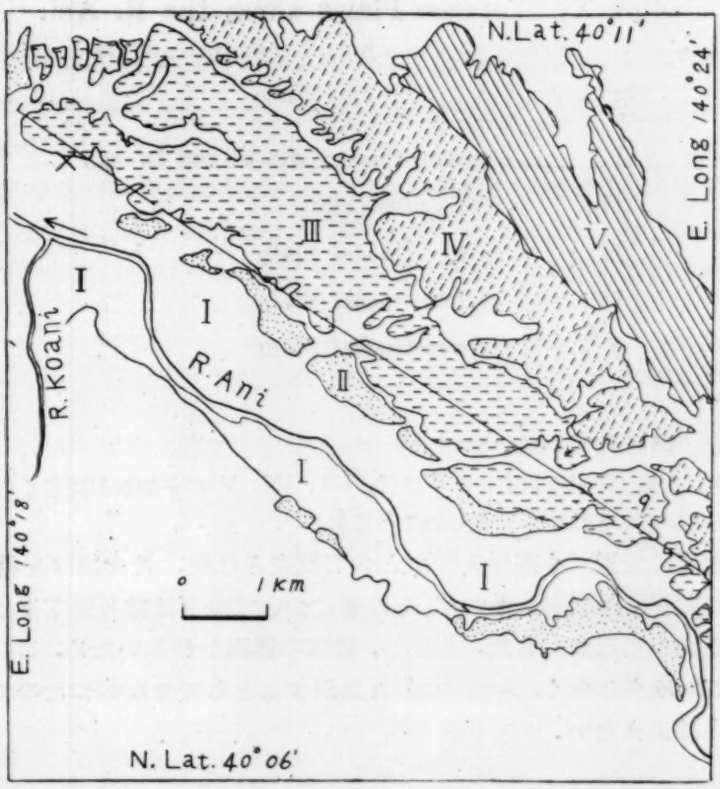

Fig. 7. Distribution of terraces along the River Ani and position of profile line.
× : outcrop of a group of small faults

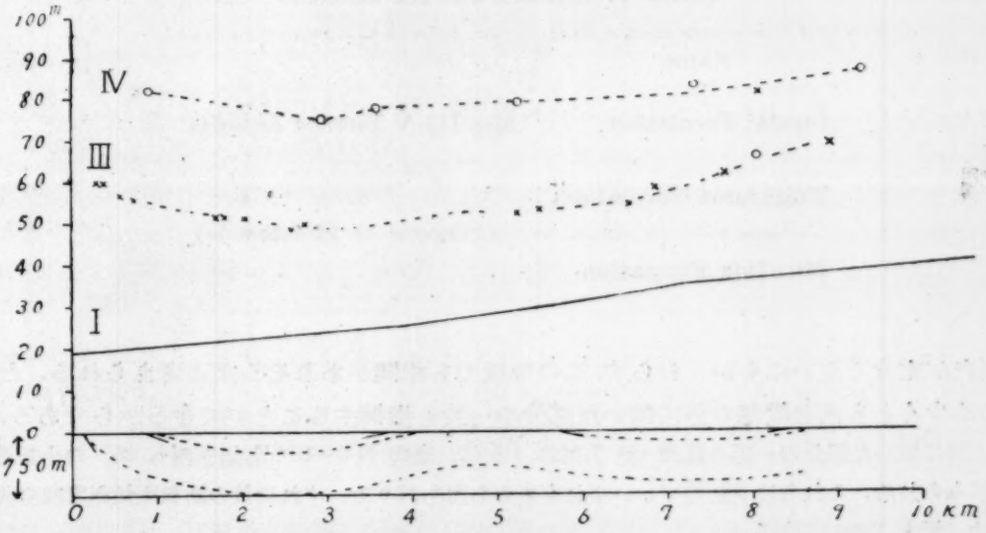

Fig. 8. Distribution of altitudes of terraces and geologic profile along the River Ani.
----: therrace plains continuing
/: apparent dips of strata (points of measurement)

Table X. Terrace Plains along the R. Ani.

Number	Name
I	Recent Flood Plain of the R. Ani
II	Yonaizawa Plain
III	Lower Ônodai Plain
IV	Middle Ônodai Plain
V	Upper Ônodai Plain

の 50 倍にひきのばされている.

段丘の名まえを第 X 表に示す. とくに I, III, IV, V の平面形が同じくらいの巾の短冊形に平行に並んでいることはいちじるしいことである.

この地域の地質は最近, 小高民夫[18]によつて調査された. その層序を第 XI 表に示すが, 段丘地域の基盤は湯車層であつて, その層について筆者は第 8 図下半に断面の示されるような傾きを測ることができた. しかし, 層理の露出がわるいため, この図に明かなように層位を測つた地点が少く, key bed を見出すこともできなかつたので, この断面図は確実なものとは云えない.

Table XI. The younger formations along the R. Ani.

(after T. KOTAKA and the author)

Name	
Ônodai Formation	the III-V terrace deposits
Yuguruma Formation	(Pliocene or Pleistocene)
Mitukida Formation	

調査が充分でないにもかゝわらず, この地域でも相関がありそうだと考えられる. と云うのは少くとも西北端部の急に傾いた部分の一致を指摘することができるからである.

急に傾いた部分の一部の露頭 (第 7 図の ×) に, 走向 N 5~10° E, 傾き西へ 25° の小断層群がみられる. これらは逆断層で, いずれも東おち西あがりで, ずれの量の断層面傾斜方向の成分は, 最大 2 cm である.

18) 小高民夫 "鷹巣盆地南縁部地質調査報告書", 秋田県地下資源開発委員会 (MS), (1950).

§7. 岩見川にそう例

第 9 図に段丘の分布，第 XII 表にその名まえを示す．阿仁川とともに，一方のかわにだけ段丘が残つている例である．その高さの分布を第 10 図上半に示す．この図のたてはよこの 10 倍にひきのばされている．

地質は，1948 年に河井興三によつてこの地域の東北半が調査され，西南半は 1927 年に村山賢一によつて作られた和田油田図の範囲に属している[19]．第 10 図下半の断面図は，右半分が河井の画いたの[20]を借用したもので，左半分が和田図巾にもとずいて筆者

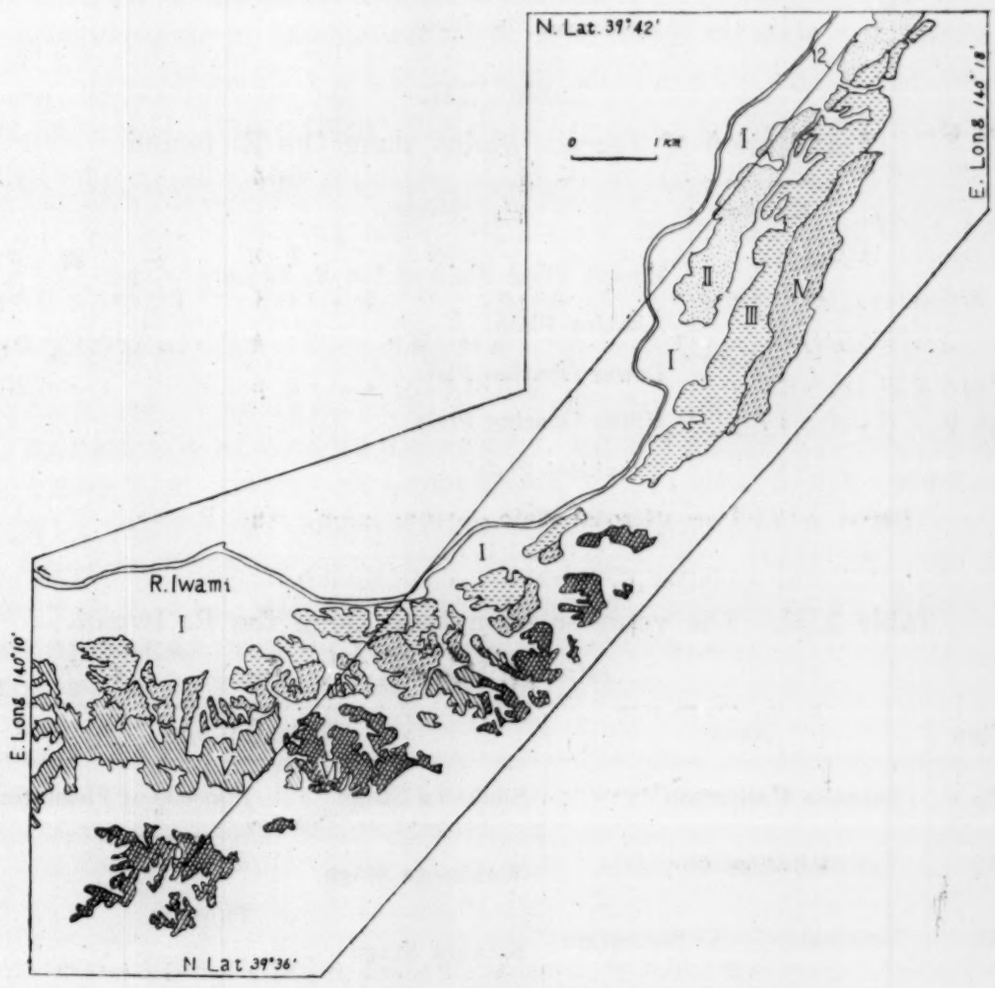

Fig. 9. Distribution of terraces along the River Iwami and position of profile line.

19) 河井興三 石油技術協会誌 (*Jour. Jap. Assoc. Petr. Techn.*) **15** (1950), 33-38.
村山賢一 "油田第 23 区和田油田地質図" (1927).

20) 河井興三 "秋田県太平山南西麓地域地質調査報告", PEAC (MS), (1948).

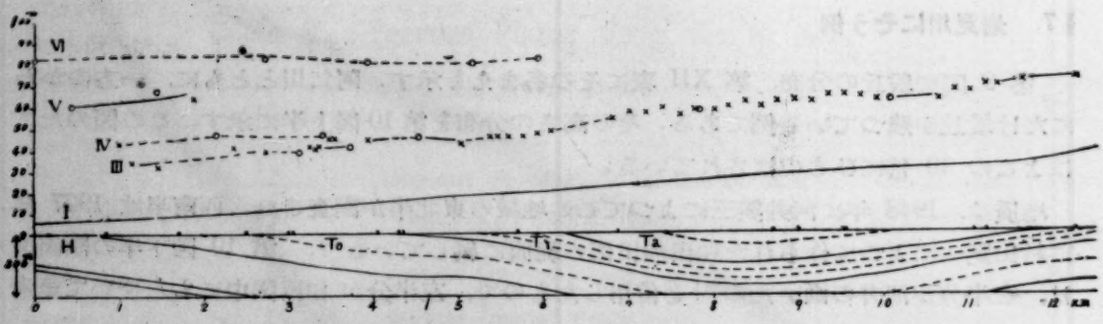

Fig. 10. Distribution of altitudes of terraces and geologic profile along the River Iwami.

Table XII.
Classification of Terrace Plains along the R. Iwami.

Number	Name
I	Recent Flood Plain of the R. Iwami
II	Akabira Plain
III	Lower Ôbarino Plain
IV	Upper Ôbarino Plain
V	Tubakidai Plain
VI	Ninodai Plain

Table XIII. The younger formations along the R. Iwami.

(after K. KAWAI)

Sign	Name	Geological age	
Ta	Takaoka Formation	Sibikawa Stage	Pliocene or Pleistocene
Ty	Tyôkai Formation	Wakimoto Stage	Pliocene
To	Tosantai (十三岱) Formation	Kitaura Stage	
H	Higasi Formation	Hunagawa Stage	Later Miocene

の画いたものである．層位のほかに，岩質の分布も考えにいれてあるから，この図に大きなまちがいはないであろう．第 XIII 表に年代を示す．

21) この面のデコボコは，段丘面のできはじめからのものかもしれない．

この地域の例では，III 低位大張野面が[21]，褶曲と相関をもつた変形をしたとは考えられないが，VI 二ノ台面はほゞ水平で，現在の川床にくらべて，西南が高まつており，地層の傾きとおなじ傾向である．しかし，これはこの地域全体の傾動によるものかもしれないし，もとの流れがゆるやかだつたためかもしれない．

§8. ま と め

筆者は，いわゆる“活動している褶曲構造”の河岸段丘の方に関する検討をおこなつた．その方法および結果はつぎのとおりである．

（1） 大塚弥之助の言う“ミズホ・フオツサマグナ褶曲帯”に分布する河岸段丘のすべてのなかから，この研究に適しているとおもわれるところ 3 か所をえらび出した．それは米代川の支流阿仁川，雄物川の支流岩見川，最上川の支流小国川にそう 3 か所である．

（2） 段丘面の高さを，2 臺の気圧計を同時に用いて測定した．その精度は，小国川V面の測定に当つて，95%の信頼度で誤差が ±2.8 m 以内と考えられるていどであつた．

（3） 測定の結果から第 4，8，10 図を画いた．

（4） これらより，少くとも小国川と阿仁川とでは，段丘面が褶曲と同じ傾向へ変形したらしいと推定できる．

§9. あ と が き

この研究には多くの人のおせわになつた．とくに徳永重元氏は，地質調査結果をことごとく提供され，且野外調査上のいろいろの便宜をはかつて下さり，現地では，中山炭鉱 K.K. の中山啓氏に全面的な援助をうけた．この研究における地質学的資料については，大橋良一・大橋加一・河井興三の諸氏に負うところが多い．また，村井勇・今村学郎の両氏には，段丘面の測定について議論していたゞき，図版の作製は久我正弘氏をわずらわした．そして，宮村摂三・森本良平の兩氏は種々の点で後援・討論してくれた．さらに，地震研究所および中央気象台測候課からは器械をお借りし，費用はすべて文部省の科学研究費をつかつた．これらの関係者にあつく感謝する．

なお，野外調査は1950 年 9 月と 1951 年 10～11 月に行つた．

15. *On the Deformation of the Earth's Surface Owing to the Rock Folding in Japan.*

By Arata SUGIMURA,
Geological Institute, Faculty of Science, Tokyo University.

The late Professor Y. OTUKA showed in his treatise[1)2)] in 1942 examples where rock folding is still in progress. His argument has two different foundations: (1) that which is concerned with the movement of the leveling points and (2) that which is concerned with the distribution of altitudes of river terraces. The first problem has lately been re-examined by S. MIYAMURA and A. OKADA and the given relation has been found to be doubtful[4)]. But the second problem has not yet been re-examined or surveyed in detail. The author tried this survey by the following method and obtained the following results.

1. It seems that the Mizuho-Fossa Magna Folded Zone proposed by Y. OTUKA is a zone where the folding movement has continued up to the most recent time[1)]. Among the river terraces existing within the area, the author picked up three localities which would serve his purpose. These are the terraces along (1) the River Ani, a branch of the River Yonesiro, (2) the River Iwami, a branch of the River Omono and (3) the River Oguni, a branch of the River Mogami.

2. Distribution of altitudes of the terrace plains was measured by using simultaneously two barometers. The measure of precision proved that the error is less than ± 2.8 m with the confidence coefficient of 95%, in the measurement of the fifth (V) plain of the R. Oguni.

3. Based on the results of these measurements, the Fig. 4 (the R. Oguni), 8 (the R. Ani) and 10 (the R. Iwami) were drawn.

4. Then, we can infer that at least along the R. Oguni and the R. Ani, the terrace plains deformed with the same tendency as the rock folding.

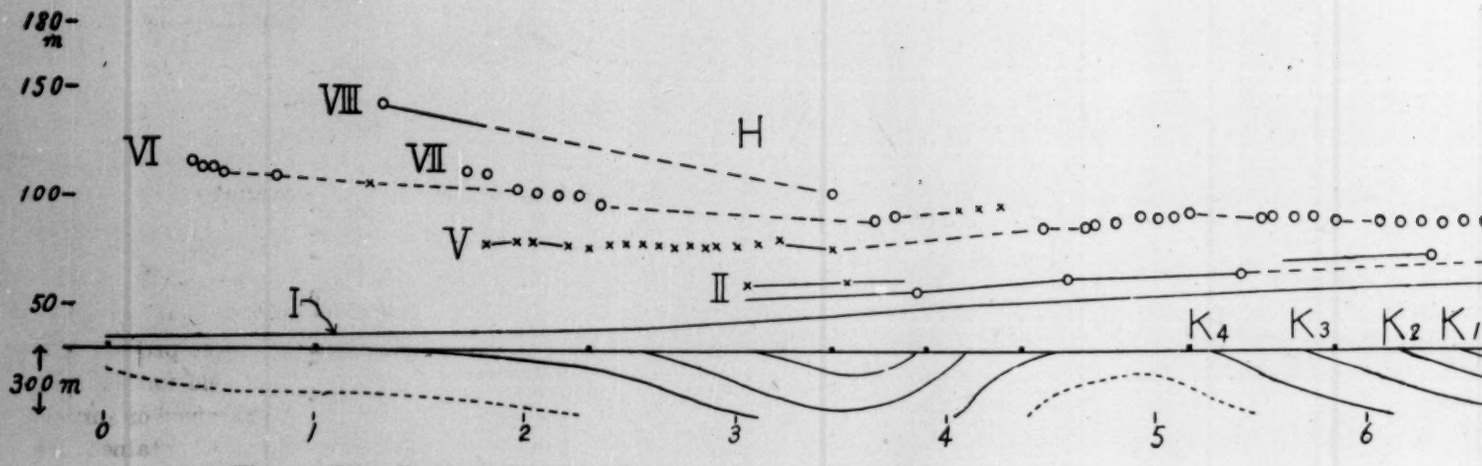

Fig. 4. Distribution of altitudes of terraces and geologic structure along the River Oguni.

○: points measured by A-method
×: ,, ,, ,, B- or C-method
——: terrace plains continuing
- - -: terrace plains intermitted
■: points where the dips of the strata were measured
~~~: unconformity
K_1-K_4: key beds
N: Nagasawa superformation
H: Hukuzyuno, M: Murasakiyama
Ky: Kyôdanbara fault

Fig. 5.
~~~

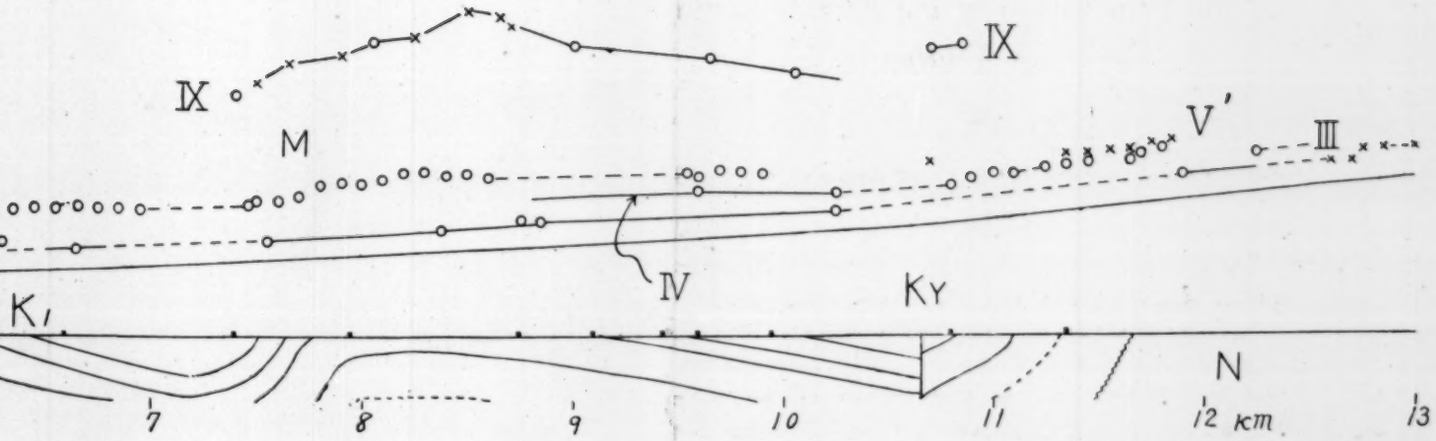

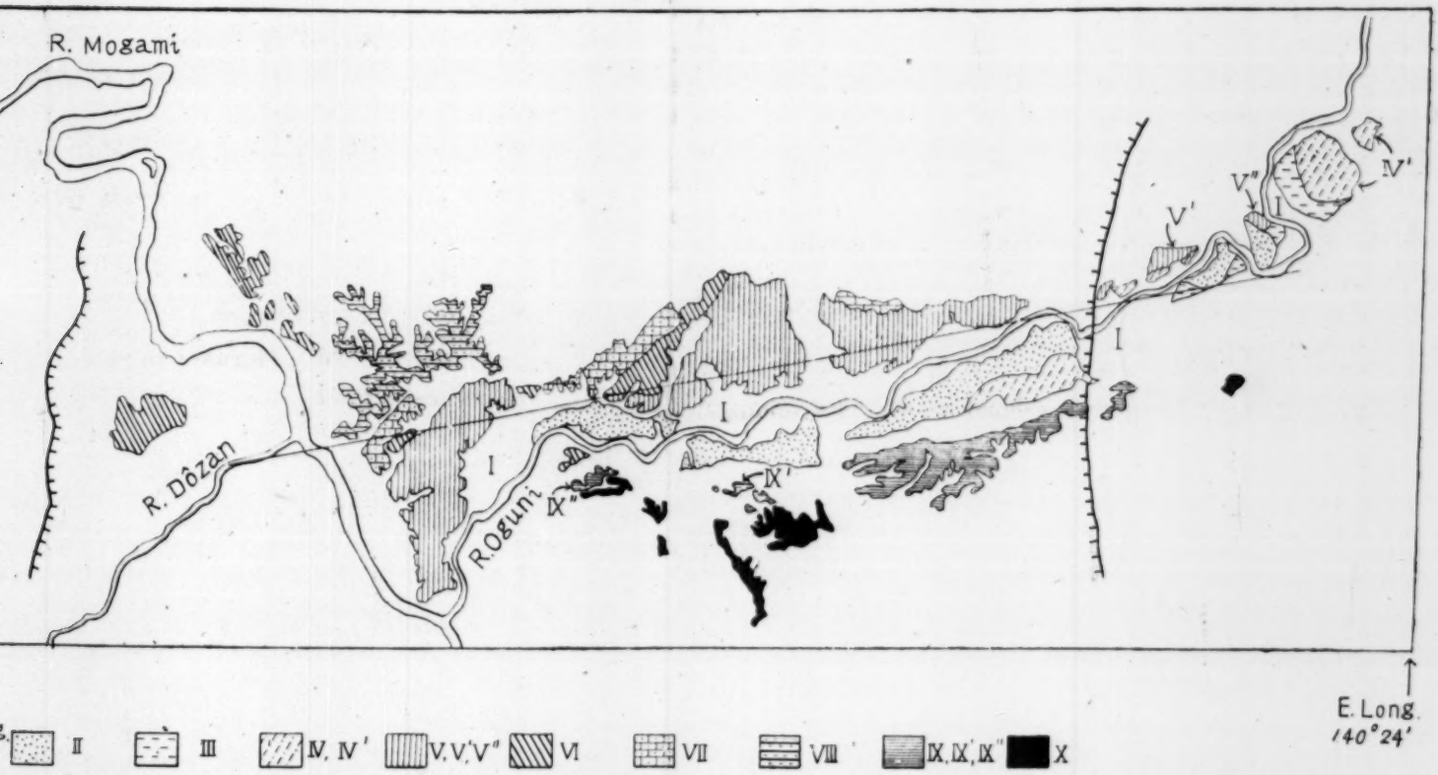

II III IV, IV' V, V', V" VI VII VIII IX, IX', IX" X

5. **Distribution of river terraces along the River Oguni, and localities of Matuyama and Kyôdanbara faults.**

所　報

◎談話会記事

第284回談話會（昭和26年12月18日）

1. 東京，横濱における加速度地震計記象の解析結果（第1報）　鈴木正治・金井清
2. 地表層の性質と地震動振幅との關係　金井清
3. 保土ケ谷で行つた爆破による地震動の研究　爆破地震動研究グループ代表 松澤武雄
4. 近畿二上火山の地質（序報）
   （所謂瀬戸内火山帶の火山活動と地史の總合的研究）　森本良平
5. 日本の古期岩群について　坪井誠太郎

第285回談話會（昭和27年1月22日）

1. 南海地震に伴つた津浪の一反射位相に就いて　下鶴大輔・秋間哲夫
2. 表面波の研究（7）
   ラブ波の速度を求める圖表　佐藤泰夫
3. 東京都江東區における地盤沈下の測定　岸上冬彦
4. 川崎市に於ける地盤沈下の狀況　那須信治・岸上冬彦

第286回談話會（昭和27年2月19日）

1. 褶曲運動による地表の變形について　杉村新（森本所員紹介）
2. 新潟市附近一等水準測量結果報告　橋山甲三（萩原所員紹介）
3. 第二回石淵爆破震動觀測　爆破地震動研究グループ
4. 多孔性媒質を傳わる彈性波の速さ　佐藤泰夫
5. 地震記象の最大動の走時曲線　表俊一郎
6. 本州西部における重力測定　坪井忠二・貫川顯・岡田惇一・田島廣

第287回談話會（昭和27年3月18日）

1. 淺間火山の活動とそれに伴つた微小地震　水上武・内堀貞雄
2. 淺間火山の地形變動　水上武・岡田惇
3. 三原山1951年噴出熔岩の化學成分　津屋弘達・森本良平・小坂丈予

4. その後の本學構内深井の水位　佐藤泰夫
5. 潮汐荷重による土地變形と地殻比抵抗の變化（第1報）　横山泉
6. 湖氷中に發生する自然震動の研究（序報）　表俊一郎・山崎良雄・小林直吉・村内必典・荻原輝一
7. 建物の振動減衰性について　金井清・吉澤靜代

第288回談話會（昭和27年4月15日）

1. 高温での岩石の力學的性質（序報）　佐久間修三
2. 地球内部の電氣的性質（其の12）—地球核の電氣傳導度—　力武常次
3. 衝撃法に依る彈性波速度の測定（其の1）　表俊一郎・山崎良雄
4. 彈性波の發生機構に關する實驗（續報）　笠原慶一
5. 十勝沖地震通信調査報告　佐藤泰夫・佐山守・柴野睦夫郎
6. 十勝沖地震踏査速報　河角廣・佐久間修三・嶋悦三
7. 十勝沖地震に依る三陸沿岸の津浪調査報告　岸上冬彦・平能金太郎・下鶴大輔
8. 十勝沖地震に依る釧路港内外の津浪の高さに就いて　高橋龍太郎・下鶴大輔

第289回談話會（昭和27年5月20日）

1. 三原山活動中のガス噴出量について　村内必典（津屋所員紹介）
2. 日本に於ける地磁氣短周期變化の異狀と地下構造（序報）　力武常次・横山泉・麥山よね子
3. 表面波の研究（8）ラブ波の走時　佐藤泰夫
4. 昭和27年3月7日北陸の地震の通信調査　佐藤泰夫・柴野睦夫
5. 和歌山県御坊町における微小地震の觀測　宮村攝三・辻浦賢
6. 日立鑛山における地震動の觀測結果　第2報（P波，S波の周期の問題）　金井清・田中貞二

昭和27年6月15日印刷
昭和27年6月20日發行

東京都文京區本富士町一番地
東京大學構內
編纂兼發行者 東京大學地震研究所

東京都千代田區富士見町一丁目十番地
印刷者 笠井康賴

東京都千代田區富士見町一丁目十番地
印刷所 株式會社國際文献印刷社

賣捌所 東京都千代田區神田一ツ橋通
岩波書店

東京都中央區日本橋通二丁目六番地
丸善株式會社

Sold by

Iwanami Shoten,

Hitotsubashi dôri, Chiyoda-ku, Tôkyô,

and

Maruzen Co., Ltd.,

Nihonbashi dôri, Chûô-ku, Tôkyô.

Price of this copy: 320 Yen. (Postage exclusive.)

BULLETIN OF

THE EARTHQUAKE RESEARCH INSTITUTE

TOKYO UNIVERSITY

Vol. XXX, Part 2. June, 1952.

Contents.

Papers and Reports.

Page

12. Y. SATÔ, Study on Surface Waves VI. Generation of Love- and Other Type of SH-Waves. (in English)..... 101

13. K. KANAI and S. YOSHIZAWA, On the Damping of Vibration of Actual Buildings. I. (in English)..... 121

14. N. MIYABE, Vertical Earth Movements in Japan as Deduced from the Results of Rerunning the Precise Levels. (in English)..... 127

15. A. SUGIMURA, On the Deformation of the Earth's Surface Owing to the Rock Folding in Japan. (in Japanese)..... 163

Institute Notes.

(For the papers written in Japanese or in occidental languages, the abstracts are given in occidental languages or in Japanese respectively.)

BULLETIN OF THE EARTHQUAKE RESEARCH INSTITUTE,
TOKYO UNIVERSITY. Vol. XXX, Part 3. September, 1952.

東京大學
地震研究所彙報

第 30 號　第 3 冊

昭和 27 年 9 月

目　次

論文及報告

			頁
16.	小さな穴のあいた媒質内を傳はる彈性波の速さ (英文).....	佐藤泰夫	179
17.	地球核の電気傳導度 (英文).....	力武常次	191
18.	日本に於ける地磁気短周期変化の異常と地下構造 (序報) (英文).....	力武常次 横山泉 菱山よね子	207
19.	南海地震に伴つた津浪の反射 (英文).....	下鶴大輔 秋間哲夫	223
20.	伊豆大島三原山 1951 年熔岩の化学成分 (英文).....	津屋弘逵 森本良平 小坂丈予	231
21.	1950年8月15日のアッサム大地震の表面波の分散曲線について (英文)	秋間哲夫	237
22.	彈性波の発生機構に関する実驗 (第1報) (英文).....	笠原慶一	259
23.	高温に於ける火山岩の粘性及び彈性 第1報 (英文).....	佐久間修三	269
24.	東北日本における第2回爆破地震動観測 (英文).....	爆破地震動研究グループ	279

(The titles in occidental languages are given on the back cover.)

本彙報ハ年4回 (但シ第1號ヨリ第6號マデハ不定期ニ, 第7號ハ3冊トシテ發行セリ), 彙報別冊ハ不定期ニ發行ス.

本彙報掲載ノ論文及ビ報告ノ内容ニ關シテハ著者ノミニ其責任アルモノトス.

本彙報ニ關スル照會通信ハ東京大學地震研究所長ヘ宛テラレタシ.

The Bulletin is published quarterly. (Vols. I–VI were published at irregular intervals and Vol. VII consisted of three parts.)
Supplementary Volume is published at irregular interval.

The authors of the papers alone are responsible for the statements and opinions contained in their respective papers.

All communications relating to this Bulletin should be addressed to the Director of the Earthquake Research Institute, Tokyo University.

16. *Velocity of Elastic Waves Propagated in Media with Small Holes.*

By Yasuo SATÔ,

Earthquake Research Institute.

(Read Feb. 19, 1952.—Received April 28, 1952.)

1. Introduction.

Today, the theory of elastic waves is generally discussed under the assumption of isotropy and homogeneity. However, the actual material which we ordinarily observe or treat at the field or observatory has rarely such simple properties. For example, it commonly contains small obstacles or holes which are sometimes empty, but more often filled with water. These obstacles or holes exist scattered randomly throughout the material and after all it shows apparent isotropic and homogeneous property. Thus the theory treating such heterogeneous medium becomes necessary, and one attempt was skillfully performed by J. K. Mackenzie[1] concerning a solid containing spherical empty holes. In this paper, we will introduce his theory briefly, and after that adapt it to the case when the holes are filled up with liquid.

As our purpose exists in the application to the theory of elastic waves, mere calculations of apparent statical elastic properties would be insufficient. Fortunately, however, the waves we observe have far longer wave-lengths compared with the radii of holes or the intervals of them. Consequently we may neglect the effect of reflection or diffraction and apply the quasi-static theory in calculating the propagation velocity of waves by means of bulk modulus and rigidity deduced from statical treatment. In fact the observed velocity of seismic waves is not that of real material with neither crevice nor obstacle, but that of a medium porous and heterogeneous.

2. Notations used in this paper.

In this section we will give some notations and fundamental quantities used in the following articles.

ρ Relative density of actual material (when holes are empty).

1) J. K. MACKENZIE, "The Elastic Constants of a Solid Containing Spherical Holes," *Proc. Phys. Soc.*, **B 63** (1950), 2.

The porosity is expressed by $1-\rho$.

a Radius of a hole.

r_0 Every hole of radius a is surrounded by a spherical shell of real material out to the radius r_0.

Therefore $n\cdot\left(\frac{4}{3}\pi r_0^3\right)=\frac{1}{\rho}$ (n is defined below.)

$\delta, \delta_0, \delta_1$ Density of actual material, real material and of the liquid fulfilling holes respectively.

$\lambda, \mu; \lambda_0, \mu_0$ Lamé's constants of actual material which are to be calculated, and those of real material.

k, k_0, k_1 Bulk modulus of actual material, real material and of the liquid filling holes respectively.

σ, σ_0 Poissin's ratio of actual and real material respectively.

V_S, V_{S0} Velocity of S-waves propagated in actual and real material respectively.

V_P, V_{P0} Velocity of P-waves propagated in actual and real material respectively.

n Number of holes per unit volume of real material.

νn Number of holes filled up with liquid per unit volume of real material.

K Ratio of the bulk modulus of the liquid k_1 to that of the real material k_0. $(=k_1/k_0)$

D Ratio of the density of the liquid δ_1 to that of the real material δ_0. $(=\delta_1/\delta_0)$

The next relations are easily obtained from the above definition.

when holes are empty $\delta=\rho\delta_0$ .....(2.1)

$$\frac{1}{\rho}=1+(1-\rho) \quad \text{.....(2.2)}$$

In the following calculations we will always neglect the square term of $(1-\rho)^2$.

3. Mackenzie's theory concerning a medium with spherical holes.[2)]

J. K. Mackenzie discusses briefly the problem of finding the elastic constants of a solid containing spherical holes as follows. He assumes that a hole of radius a is surrounded by a spherical shell of real material out to radius r, and these in turn are surrounded by a

2) This method seems to be first indicated by FRÖHLICH and SACK (*Proc. Roy. Soc.*, A. **185** (1946), 415), but unfortunately the author cannot read this paper in his country.

spherical shell of equivalent homogeneous material out to some large radius R. A particular stress is applied to this outer spherical boundary and the displacements of the outer surface are calculated. Finally, the resulting displacement is equated to the displancement which would have resulted had the sphere of radius R been completely filled with equivalent homogeneous material. (cf. Fig. 1)[3]

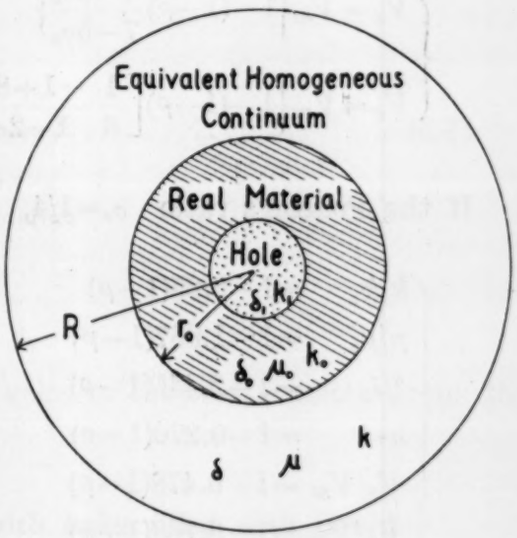

Fig. 1.

Although his method is neat he assumes that the holes are all empty. This assumption is not sufficient for us who want to apply the results to the problem of propagation of waves in rock or soil which is often moist or contains large number of small obstacles.

His results calculated under the said assumptions are[4]

$$\begin{cases} \dfrac{1}{k}=\dfrac{1}{k_0\rho}+\dfrac{3(1-\rho)}{4\mu_0\rho}+0[(1-\rho)^3], \\ \dfrac{\mu_0-\mu}{\mu_0}=5(1-\rho)\dfrac{3k_0+4\mu_0}{9k_0+8\mu_0}+0[(1-\rho)^2] \end{cases} \qquad \cdots\cdots\cdots\cdots\cdots\cdots(3.1)$$

from which we can deduce other elastic constants and the velocity of waves propagated in this medium.

Introducing a non-dimensional quantity $\sigma_0\equiv\lambda_0/2(\mu_0+\mu_0)$, which is known as Poisson's ratio, we have easily obtained the following formulae.

$$\begin{cases} k=k_0\left\{1-(1-\rho)\dfrac{3}{2}\dfrac{1-\sigma_0}{1-2\sigma_0}\right\} \\ \mu=\mu_0\left\{1-(1-\rho)15\dfrac{1-\sigma_0}{7-5\sigma_0}\right\} \\ \lambda=\lambda_0\left\{1-(1-\rho)\dfrac{1-\sigma_0}{\sigma_0}\left[\dfrac{1}{2}\dfrac{1+\sigma_0}{1-2\sigma_0}-5\dfrac{1-2\sigma_0}{7-5\sigma_0}\right]\right\} \\ \sigma=\sigma_0\left\{1-(1-\rho)\dfrac{(1-2\sigma_0)(1-\sigma_0^2)}{\sigma_0}\left[\dfrac{1}{2(1-2\sigma_0)}-\dfrac{5}{7-5\sigma_0}\right]\right\} \end{cases} \qquad \cdots\cdots(3.2)$$

3) This figure is same with that of Mackenzie.
4) *loc. cit.*, 1). Expressions (7) and (19).

Substituting (2.2),

$$\begin{cases} V_S = V_{S0}\left\{1-(1-\rho)\dfrac{4-5\sigma_0}{7-5\sigma_0}\right\} \\ V_P = V_{P0}\left\{1-(1-\rho)\left[\dfrac{1}{6}\dfrac{-1+8\sigma_0}{1-2\sigma_0}+5\dfrac{1-2\sigma_0}{7-5\sigma_0}\right]\right\} \end{cases} \quad \cdots\cdots\cdots(3.3)$$

If the Poisson's ratio $\sigma_0=1/4$, or $\lambda_0=\mu_0$

$$\begin{cases} k/k_0 = 1-2.25(1-\rho) \\ \mu/\mu_0 = 1-1.957(1-\rho) \\ \lambda/\lambda_0 = 1-2.445(1-\rho) \\ \sigma\cdot 4 = 1-0.270(1-\rho) \\ V_S/V_{S0} = 1-0.478(1-\rho) \\ V_P/V_{P0} = 1-0.768(1-\rho) \end{cases} \quad \cdots\cdots\cdots(3.4)$$

and if $\sigma_0=1/3$, or $\lambda_0=2\mu_0$

$$\begin{cases} k/k_0 = 1-3(1-\rho) \\ \mu/\mu_0 = 1-1.875(1-\rho) \\ \lambda/\lambda_0 = 1-3.375(1-\rho) \\ \sigma\cdot 3 = 1-0.333(1-\rho) \\ V_S/V_{S0} = 1-0.4375(1-\rho) \\ V_P/V_{P0} = 1-0.865(1-\rho) \end{cases} \quad \cdots\cdots\cdots(3.5)$$

When the real material is incompressible, or $\sigma_0=1/2$, the process of deducing the expressions (3.4) and (3.5) from (3.2) fails to be correct and some of the results do not hold, so we will start from the expression (3.1).

Substituting $\sigma_0=1/2$, or $k_0=\infty$

$$\begin{cases} \dfrac{1}{k} = \dfrac{3(1-\rho)}{4\mu_0\rho} \\ \dfrac{\mu_0-\mu}{\mu_0} = \dfrac{5}{3}(1-\rho) \end{cases} \quad \cdots\cdots\cdots(3.6)$$

from which we have

$$\begin{cases} k = \dfrac{4}{3}\mu_0 \dfrac{\rho}{1-\rho} \\ \mu = \mu_0\left[1-\dfrac{5}{3}(1-\rho)\right] \\ \sigma = \dfrac{1}{2}\left[1-\dfrac{3}{4}(1-\rho)\right] \\ V_S = V_{S0}\left[1-\dfrac{1}{3}(1-\rho)\right] \\ V_P = V_{P0}\sqrt{\dfrac{4}{3(1-\rho)}} \end{cases} \qquad \cdots\cdots\cdots\cdots\cdots\cdots\cdots\cdots\cdots\cdots(3.7)$$

In every case, the propagation velocity becomes smaller from the effect of holes.

4. Theory on the media with holes filled with liquid.

Now, we will calculate the elastic constants and the velocity of waves in the substance with holes filled with liquid.

The structure of the model used for the calculation of this case is same with that of Mackenzie's except the fact that the inner hole is filled with a liquid of density δ_1 and bulk modulus k_1. (cf. Fig. 1)

Thus the method by which the formulae (3.1) were obtained is applicable to this case also. Moreover, the rigidity of the medium is not affected by the existence of liquid in the holes. Therefore, it is sufficient for us to obtain the apparent decrease of the volume of the actual substance when the hydrostatic pressure is applied to the outer spherical boundary.

Conditions which must hold at the boundary surfaces are:

$$\begin{cases} r=R; & [\widehat{rr}]_R = -P \\ r=r_0; & [\widehat{rr}]_{r_0+0} = [\widehat{rr}]_{r_0-0},\ [u]_{r_0+0} = [u]_{r_0-0} \\ r=a; & [\widehat{rr}]_{a+0} = [\widehat{rr}]_{a-0},\ [u]_{a+0} = [u]_{a-0} \end{cases} \qquad \cdots\cdots\cdots(4.1)$$

On the other hand, the general solutions of the three parts are—in equivalent homogeneous continum;

$$\begin{cases} u = Ar + Ar^{-2} \\ \widehat{rr} = 3kA - 4\mu Br^{-3} \end{cases} \qquad \cdots\cdots\cdots\cdots\cdots(4.2)$$

in real material;

$$\begin{cases} u = A_0 r + B_0 r^{-2} \\ \widehat{rr} = 3k_0 A_0 - 4\mu_0 B_0 r^{-3} \end{cases} \qquad \cdots\cdots\cdots\cdots\cdots\cdots(4.3)$$

in liquid; $\begin{cases} u=A_1 r \\ \widehat{rr}=3k_1 A_1 \end{cases}$ .....(4.4)

Therefore from (4.1) we have

$$\begin{pmatrix} 3k & -4\mu R^{-3} & 0 & 0 & 0 \\ 3k & -4\mu r_0^{-3} & -3k_0 & 4\mu_0 r_0^{-3} & 0 \\ r_0 & r_0^{-2} & -r_0 & -r_0^{-2} & 0 \\ 0 & 0 & 3k_0 & -4\mu_0 a^{-3} & -3k_1 \\ 0 & 0 & a & a^{-2} & -a \end{pmatrix} \begin{pmatrix} A \\ B \\ A_0 \\ B_0 \\ A_1 \end{pmatrix} = \begin{pmatrix} -P \\ 0 \\ 0 \\ 0 \\ 0 \end{pmatrix} \quad \ldots(4.5)$$

Solving these equations with respect to A, B; A_0, B_0 and A_1 and putting them into the expression (4.2), we can easily calculate the amount of displacement at the surface $r=R$, namely

$$[u]_R=(-P/3k)\cdot R + \{-(k-k_0)(3k_1+4\mu_0)-(k_0-k_1)(3k+4\mu_0)(1-\rho)\} \quad \ldots\ldots(4.6)$$

which must be equal to the displacement in case the same pressure had been applied to the sphere of radius R filled with equaivalent homogeneous substance with a bulk modulus k.

Therefore

$$[u]_R=-(P/3k)R \quad \ldots\ldots\ldots\ldots(4.7)$$

Combining (4.6) and (4.7) we get

$$k=k_0-(k_0-k_1)\frac{3k_0+4\mu_0}{3k_1+4\mu_0}(1-\rho) \quad \ldots\ldots\ldots\ldots(4.8)$$

This is the very formula which we have intended to obtain in this calculation.

(4.8) can be expressed in the following form using Poisson's ratio σ_0 of the real material and $K=k_1/k_0$.

$$k=k_0\left[1-(1-\rho)\frac{3(1-K)(1-\sigma_0)}{2(1-2\sigma_0)+K(1+\sigma_0)}\right] \quad \ldots\ldots\ldots(4.9)$$

Since the rigidity suffers no effect by the existence of the liquid (3.2) holds in this case, too. Combining these two formulae we have

$$\begin{cases} \lambda = \lambda_0 \left\{1-(1-\rho)\dfrac{1-\sigma_0}{\sigma_0}\left[\dfrac{(1+\sigma_0)(1-K)}{2(1-2\sigma_0)+K(1+\sigma_0)}-5\dfrac{1-2\sigma_0}{7-5\sigma_0}\right]\right\} \\ \sigma = \sigma_0 \left\{1-(1-\rho)\dfrac{(1-2\sigma_0)(1-\sigma_0^2)}{\sigma_0}\left[\dfrac{1-K}{2(1-2\sigma_0)+K(1+\sigma_0)}-\dfrac{5}{7-5\sigma_0}\right]\right\} \\ V_S = V_{S0}\left\{1-(1-\rho)\dfrac{1}{2}\left[15\dfrac{1-\sigma_0}{7-5\sigma_0}-(1-D)\right]\right\} \qquad \text{.....(4.10)} \\ V_P = V_{P0}\left\{1-(1-\rho)\dfrac{1}{2}\left[\dfrac{(1-K)(1+\sigma_0)}{2(1-2\sigma_0)+K(1+\sigma_0)}+10\dfrac{1-2\sigma_0}{7-5\sigma_0}-(1-D)\right]\right\} \\ \delta = \delta_0\{1-(1-\rho)(1-D)\} \end{cases}$$

If we put $K=0$ and $D=0$ in the above formulae, we obtain expressions equivalent to (3.2) and (3.3) which are the case of empty holes.

5. General considerations concerning the velocity in heterogeneous medium.

First let us assume a medium composed of two kinds of substances denoted by A and B. If these two substances are mixed by the ratio $\rho_A:\rho_B$ in a volume, an arbitrary straight line taken in this medium will be occupied by A and B at the same ratio $\rho_A:\rho_B$. For, in an

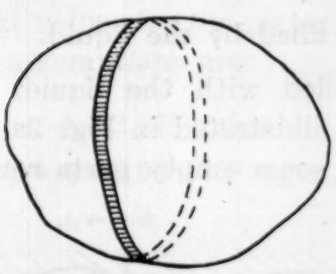

Fig. 2a.

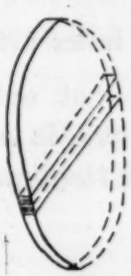

Fig. 2b.

Fig. 2c.

arbitrary sheet cut out of this mixture (cf. Figs. 2a and 2b) A and B are involved by the ratio $\rho_A:\rho_B$. Further, if a thin rod is again cut out of the said sheet, in this rod also A and B are mixed by the ratio $\rho_A:\rho_B$. If we denote the propagation velocity in A and B by V_A and V_B, the next doubt naturally arises. Can the mean velocity $\overline{V}$ in this mixed substance be expressed by the following formula?

$$\frac{1}{\overline{V}}=\frac{\rho_A}{\rho_A+\rho_B}\frac{1}{V_A}+\frac{\rho_B}{\rho_A+\rho_B}\frac{1}{V_B} \qquad \text{.....(5.1)}$$

This relation may hold if the wave-length is far smaller compared with the dimension of the mass of A or B. However, it is not certain whether the same relation holds or not when the wave-length is extremely large. Now that we have solved the problem under the latter assumption in the previous section, we can easily examine the validity of the above formula in this case.

We assume the substance A to be an elastic medium with Lamé's constants λ_0 and μ_0, and B a liquid with the bulk modulus k_1. Further we put

$$\begin{cases} V_A = V_{P0}, & V_B = V_{P1}, \\ \rho_A = \rho, & \rho_B = 1-\rho, \end{cases} \quad \cdots\cdots\cdots\cdots (5.2)$$

then the right hand member of (5.1) becomes

$$\frac{\rho}{V_{P0}} + \frac{1-\rho}{V_{P1}} = \frac{1}{V_{P0}} \left\{ 1 + (1-\rho) \left[-1 + 1 \Big/ V\left(\frac{K}{D} \frac{1}{3} \frac{\sigma_0}{1-\sigma_0} \right) \right] \right. \cdots (5.3)$$

which differs clearly from the value expected from the expression of V_P in (4.10), namely

$$\frac{1}{V_{P0}} \left\{ 1 + (1-\rho) \left[\frac{1}{6} \frac{-1+8\sigma_0}{1-2\sigma_0} + 5 \frac{1-2\sigma_0}{7-5\sigma_0} \right] \right\} \quad \cdots\cdots (5.4)$$

Therefore the above doubt has been negatively cleared up.

6. When the holes are partly filled by the liquid.

When the holes are not entirely filled with the liquid, we can suppose two cases. One case is when, as illustrated in Fig. 3a, all the holes are partly filled with the liquid with some empty parts remaining,

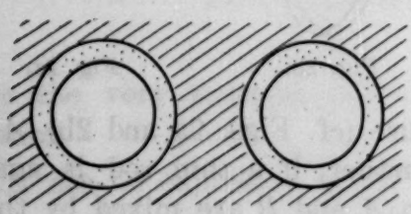

Fig. 3a.

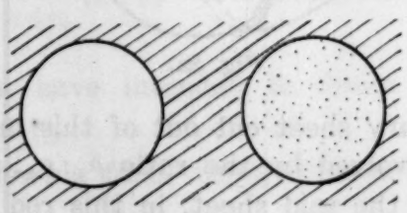

Fig. 3b.

and the other when some of the holes are entirely filled up with the liquid, with the rest remaining empty (cf. Fig. 3b). Of course, we cannot decide which of these two cases really exists in natural conditions.

If there remains some empty part, as in the first model, the existence of the liquid does not affect the amount of the bulk modulus, the only effect being to increase the density.

In the second model, the effect due to empty holes (—the theory of this case was developed by Mackenzie)—and that due to holes filled up with some liquid, must be summed up.

Fortunately all the equations in this calculation are linear, hence we can simply superpose both the effects and obtain the final results. Of the n holes existing in an unit volume of real material, we assume that νn holes are filled up with liquid and the others are empty. Thus any material constant such as the density or the bulk modulus may be expressed as the weighted mean of the values corresponding to perfectly empty and perfectly wet cases. Therefore

$$\begin{aligned} k \text{ (partly filled with the liquid)} \\ =(1-\nu)\cdot k \text{ (empty)} \\ +\nu\cdot k \text{ (entirely filled up with the liquid)} \end{aligned} \qquad \ldots\ldots\ldots(6.1)$$

etc.

7. Numerical examples.

To illustrate the above theory we will assume some adequate numerical values for the material constants and will perform calculations.

Our assumptions are:

$$\left\{\begin{array}{ll} \delta_0=2.778\ \text{gr/cm}^3, & \delta_1=1.000\ \text{gr/cm}^3 \\ \lambda_0=\mu_0=3.90\times10^{11}\ \text{c.g.s.}, & k_1=2.10\times10^{10}\ \text{c.g.s.} \\ \sigma_0=1/4 & \end{array}\right. \qquad \ldots\ldots\ldots(7.1)$$

from which we have

$$\begin{aligned} k_0 &= 6.50\times10^{11}\ \text{c.g.s.} \\ V_{S0} &= 3.75 \quad \text{km/sec} \\ V_{P0} &= 6.49 \quad \text{km/sec.} \end{aligned}$$

and

$$\begin{aligned} K&=k_1/k_0=0.0323. \\ D&=\delta_1/\delta_0=0.36. \end{aligned} \qquad \ldots\ldots\ldots(7.2)$$

Introducing these values into the formula (4.10), we have

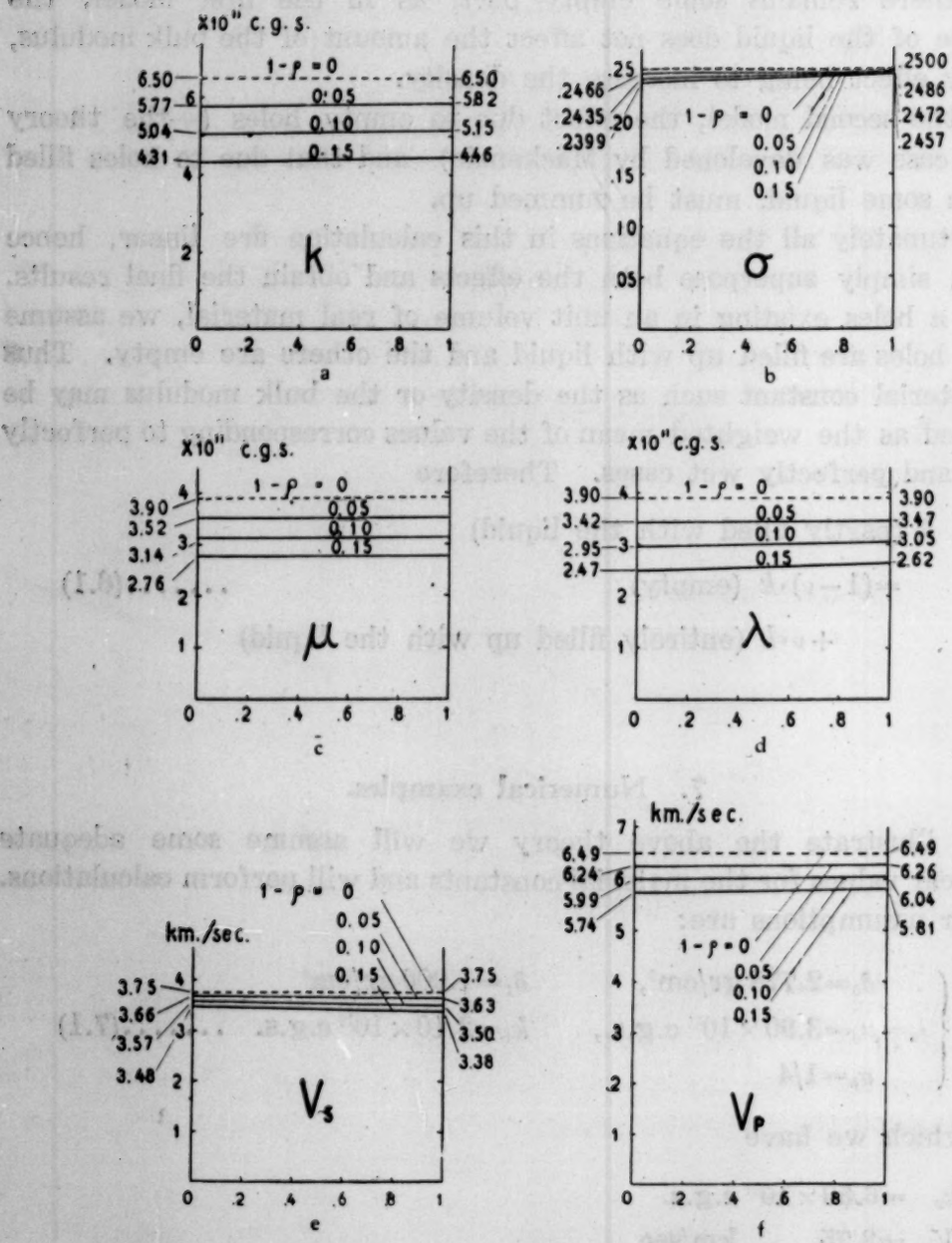

Fig. 4. Numerical values of the elastic constants k, σ, λ, μ and the propagation velocity V_s and V_p, assuming the material constants

$\delta_0 = 2.778$ gr/cm^3, $\quad \delta_1 = 1.000$ gr/cm^3

$\lambda_0 = \mu_0 = 3.90 \times 10^{11}$ c.g.s., $\quad k_1 = 2.10 \times 10^{10}$ c.g.s.

$\sigma_0 = 1/4$

Parameter is the porosity $1-\rho$, and the abscissa is ν, or the proportion of the number of holes filled with the liquid.

$$\begin{cases} k = 6.50\times10^{11}\cdot\{1-(1-\rho)\ 2.092\} & \text{c.g.s.} \\ \mu = 3.90\times10^{11}\cdot\{1-(1-\rho)\ 1.957\} & \text{c.g.s.} \\ \lambda = 3.90\times10^{11}\cdot\{1-(1-\rho)\ 2.184\} & \text{c.g.s.} \\ \sigma = 0.25\ \cdot\{1-(1-\rho)\ 0.1134\} & \\ \delta = 2.778\ \cdot\{1-(1-\rho)\ 0.64\} & \text{gr/cm}^3 \\ V_S = 3.75\ \cdot\{1-(1-\rho)\ 0.6582\} & \text{km/sec.} \\ V_P = 6.49\ \cdot\{1-(1-\rho)\ 0.6960\} & \text{km/sec.} \end{cases} \quad \cdots\cdots\cdots\cdots(7.3)$$

Combining these expressions with (3.4) we can arrive at the final results, which are illustrated in

Fig. 4a.—Bulk modulus k,
Fig. 4b.—Poisson's ratio σ,
Fig. 4c.—Rigidity μ,
Fig. 4d.—Lamé's constant λ,
Fig. 4e.—Velocity of S-waves V_S,
and Fig. 4f.—Velocity of P-waves V_P,

where the abscissa is ν and the parameter is the porosity $(1-\rho)$. When the material is perfectly dense, or the porosity is zero, the variation of ν is meaningless. However, for comparison with other cases, we have written it in a broken line.

8. Summary and conclusion.

Under the assumptions cited in § 1, we have calculated the elastic constants and propagation velocity in media with small holes, following the way of investigation of J.K. Mackenzie.

When the holes are empty, Mackenzie's results are used unconditionally, and the convenient expressions for practical use are shown in § 3.

When the holes are filled with some liquid we cannot apply the above formula. Hence we calculated anew the volume change of the equivalent homogeneous sphere with a single hole applying hydrostatic pressure to the outer boundary. In this way we got the bulk modulus k of such a medium. Rigidity remains unaltered even if a hole is filled up with liquid, therefore combining it with the former formula we have the elastic constants λ, σ and the velocity of P and S waves.

Next we discussed whether the next relation can hold in this medium.

$$\frac{1}{V_P}=\frac{\rho}{V_{P0}}+\frac{1-\rho}{V_{P1}}$$

The answer is negative; we cannot deduce the propagation velocity in heterogeneous medium from the weighted harmonic mean of the velocity of two component substances.

When the holes are partly filled with liquid we can use a simple formula of weighted mean such as (6.1).

Numerical examples are shown in (7.3) and Figs. 4a–4f.

---

16. 小さな穴のあいた媒質内を傳はる彈性波の速さ

地震研究所 佐 藤 泰 夫

J.K. Mackenzie は，小さな穴のあいた彈性體の，體積彈性率及び剛性率を，equivalent homogeneous continuum の考へを用ゐて，極めてたくみに導き出した．彼のとつた方法は靜力學的なものであるから，その結果をそのまま應用して，彈性波が傳はる場合の速さを求めることは，嚴密には正しくない．しかし，波長が十分に長い場合には，準靜的な取扱ひが許されるであらうから，第一近似としては，上にえられた k と μ とから，波の傳播速度を出してもさしつかへないであらう．

このような考へに從つて，空隙率 $(1-\rho)$ の二乘以上を省略して得られた公式が (3.2)～(3.5) および (3.7) である．

次に我我は，Mackenzie と全く同樣な考へに從つて，穴を液體が滿してゐる場合を調べた．この時剛性率には變化のないこと勿論である．結果は (4.8) または (4.9) であるが，これと前の (3.2) の第 2 式を組み合せて，λ その他を求めたものが (4.10) にあげてある．

二種類の物質 A, B が體積で ρ_A と ρ_B の割合で混合してゐる時，この中を傳はる彈性波の速さ $\overline{V}$ が，weight をつけた簡單な調和平均の式

$$\frac{1}{\overline{V}}=\frac{\rho_A}{\rho_A+\rho_B}\frac{1}{V_A}+\frac{\rho_B}{\rho_A+\rho_B}\frac{1}{V_B}$$

で與へられるかもしれない，といふ事は誰にも考へられる事であるが，§4 にえられた公式を適用して，その當否をしらべて見た．結果は否定的である．

液體がすべてのすき間を滿してゐない時にも，Fig. 3a のやうな狀態でなく，Fig. 3b のやうになつてゐるとするならば，穴全體の中で，液體が充滿してゐるものが占める割合 ν を用ゐて，簡單に彈性常數や速度を求めることができる．すべての式は $(1-\rho)$ の一次式であるから，(6.1) の形の公式が成立つわけである．

最後に適當な數値 (7.1) を代入して計算を行つた．結果は (7.3) と Figs. 4a～4f に示してある．普通の岩石と，水との組合せでは，全然水がない場合とあまり大きなちがいはない．この事は圖から一目で知ることができる．圖の橫軸は ν であり，$(1-\rho)$ が 0 の時には，ν をかへて考へるといふ事は意味を持たないが，他との比較のために破線で示した．

17. *On the Electrical Conductivity in the Earth's Core.*

By Tsuneji RIKITAKE,

Earthquake Research Institute.

(Read April 15, 1952.—Received June 20, 1952.)

1. Introduction.

The origin of the earth's main magnetic field which has long been a mystery in geophysics seems to be successfully explained by the coupling of magnetic field and fluid motion in the earth's core, the theory being developed by W. M. Elsasser[1] and E. C. Bullard[2]. Since the possibility of existence of a self-exciting dynamo was recently proved by H. Takeuchi and Y. Shimazu[3], the Elsasser-Bullards' theory is thought to be the most reliable one. According to the theory, the electrical conductivity in the core (σ_c) is assumed to amount to the order of 10^{-6} *emu*. Though the said order of σ_c is adopted from a physical consideration of metallic iron under high pressure and temperature, it would be of importance to criticize the value more precisely from the standpoints of both physics and geophysics as briefly stated by the writer in his former paper[4].

Geophysically speaking, the electrical state of the earth's interior can be inferred from the studies of electromagnetic induction into the earth by transient geomagnetic variations, and the theory has been developed by S. Chapman[5], A. T. Price[6], B. N. Lahiri[7] and the writer[8]. From these studies, we have an approximate knowledge about the electrical conductivity down to a depth of about 1500 *km*. The writer[9] also studied the length of the period of geomagnetic variation required to infer the electrical conductivity in the core. The conclusion was as follows: We should analyse geomagnetic variations having periods

1) W. M. ELSASSER, *Phys. Rev.*, **69** (1946), 106, **70** (1946), 202.
2) E. C. BULLARD, *Proc. Roy. Soc. London A*, **197** (1949), 433, **199** (1949), 413.
3) H. TAKEUCHI and Y. SHIMAZU, *Journ. Phys. Earth.*, **1** (1952), 1.
4) T. RIKITAKE, *Geofisica pura e applicata*, **22** (1952), 37.
5) S. CHAPMAN, *Phil. Trans. Roy. Soc. London A*, **218** (1919), 1.
6) S. CHAPMAN and A. T. PRICE, *Phil. Trans. Roy. Soc. London A*, **229** (1930), 427.
7) B. N. LAHIRI and A. T. PRICE, *Phil. Trans. Roy. Soc. London A*, **227** (1939), 509.
8) T. RIKITAKE, *Bull. Earthq. Res. Inst.*, **28** (1950), 45, 219, 263, **29** (1951), 61.
9) T. RIKITAKE, *Bull. Earthq. Res. Inst.*, **29** (1951), 539.

longer than 10 *years* in order to determine σ_c, but an analysis of such a long period variation would be almost impossible judging from the accuracy of geomagnetic observation to-day.

Though we failed to tackle the problem by geophysical method, some researchers studied the problem from physical standpoint. Elsasser made an estimate of σ_c as the electrical conductivity of metallic iron under high pressure and temperature. He assumes the relation

$$\sigma = c\theta^2/T ,$$

which is valid for ordinary iron at high temperature, where σ, θ and T denote respectively the electrical conductivity, Debye temperature and absolute temperature. In the earth's core, the factor c is assumed to remain constant and T is taken to be 9000°. It becomes then

$$\sigma_c = 1.3 \times 10^{-5}\ emu.$$

Meanwhile, Bullard[2] has obtained $\sigma_c = 1 \times 10^{-6}\ emu$ by using empirically determined pressure and temperature variations.

According to Elsasser[11], we have powerful evidences for iron-nickel core as revealed by the relation between density and pressure in the earth. He shows that the density-pressure curve determined by K. E. Bullen[12] seems to continue to those of silicate group at low pressure and to those of substance having Z (atomic number)$\fallingdotseq$30 at high pressure, the former being based on laboratory experiments and the latter on a quantum-theoretical estimate for Thomas-Fermi-Dirac model.

A direct estimate[13] of σ_c based on Thomas-Fermi-Dirac model which is valid under enormous pressure also leads to the conclusion: $\sigma_c \simeq 10^{-4}$ *emu*.

As stated above, we may expect that σ_c amounts to the order of 10^{-5} *emu* or more from physical viewpoint. But it should be borne in mind that these estimates still include some unknown factors.

The writer, intending to obtain the possible range of σ_c, will make an estimate of σ_c from some geophysical standpoints which are quite different from those mentioned before.

---

10) W. M. ELSASSER, *Rev. Mod. Phys.*, **22** (1950), 1.
11) W. M. ELSASSER, *Science*, **113** (1951), 105.
12) K. E. BULLEN, *Introduction to the theory of seismology*. Cambridge (1947).
13) H. MIKI, *Kagaku*, **21** (1951), 468.

2. Possibility of the existence of magneto-hydrodynamic waves in the earth's core.

As has been suggested first by H. Alfvén[14], there is a type of wave-motion, called magneto-hydrodynamic waves, in an electrically conducting fluid placed in a magnetic field. The magneto-hydrodynamic waves play an important rôle in solar physics such as the origin of sunspots, the heating of solar corona, and the generation of cosmic radiation. The existence of the magneto-hydrodynamic waves is experimentally observed[15] as the coupling between a magnetic field and sound waves in mercury.

In the earth's core which is thought to be more or less electrically conducting and to have a magnetic field, a kind of magneto-hydrodynamic waves would be excited if the boundary of the core is stimulated by seismic waves which come from the earth's mantle. The magneto-hydrodynamic waves thus produced, which are essentially transverse waves, would be propagated along the magnetic lines of force as fully studied by Alfvén[16] and would appear again at the surface of the core if the waves had sufficient intensity. The velocity of the waves which is proportional to the intensity of the magnetic field would be very small in case of non-extraordinary magnetic field. Thus we could observe seismic waves which pass through the core as the magneto-hydrodynamic waves, the damping effect in the core being assumed to be small. We should further pay attention to the fact that the seismic waves reflected at the surface of the core, such as ScS waves, would be much affected if the magneto-hydrodynamic waves of appreciable intensity are generated in the core.

According to the results of seismic observations, we cannot find phases of seismic waves which come through the core as the magneto-hydrodynamic waves and ScS waves, one of the most distinct phases of the waves reflected at the surface of the core, do not seem to be affected by the reaction of the hypothetical magneto-hydrodynamic waves. Hence the electrical property and magnetic field in the core should be within limits in which no magneto-hydrodynamic waves of appreciable intensity would be generated.

The writer would here like to determine the possible range of σ_c

14) H. ALFVÉN, *Ark. f. Mat. Astr. o. Fys.*, **29B** (1942), No. 2.
15) S. LUNDQUIST, *Phys. Rev.* **76** (1949), 1805.
16) H. ALFVÉN, *Cosmical Electrodynamics* (1950), Oxford.

which does not contradict with the seismic observation mentioned above.

Combining the fundamental equations of electromagnetism with those of hydrodynamics, we have the next equations in the electrically conducting fluid.

$$\frac{\partial \vec{v}}{\partial t} = -\frac{1}{\rho}\,\mathrm{grad}\,p - \lambda[\vec{B}\,\mathrm{rot}\,\vec{B}], \tag{1}$$

$$\frac{\partial \vec{B}}{\partial t} = \mathrm{rot}\,[\vec{v}\;\vec{B}] + \nu_m \nabla^2 \vec{B}, \tag{2}$$

where $\vec{v}$, $\vec{B}$, p and ρ denote respectively velocity, magnetic induction, pressure and density and λ and ν_m are defined by

$$\lambda = \frac{1}{4\pi\mu\rho}, \quad \nu_m = \frac{1}{4\pi\mu\sigma}, \tag{3}$$

where μ and σ denote magnetic permeability and electrical conductivity, ν_m being called magnetic viscosity. In the above expressions, we have neglected the displacement current, the inertia term of fluid-motion and fluidal viscosity.

Now let us consider plane waves propagated along z-direction, while the initial magnetic field is also parallel to the z-direction. We have, then,

$$\vec{B} = \vec{B}_0 + \vec{b}$$

in which $\vec{B}_0$ and $\vec{b}$ correspond respectively to the initial magnetic field and the field due to the electric current. In such a simple case, the equations are reduced to

$$v_z = \text{const.}, \tag{4}$$

$$\partial v_y/\partial t = \lambda B_0 \partial b_y/\partial z \tag{5}$$

$$\partial v_z/\partial t = -\rho^{-1}\partial p/\partial z - (\lambda/z)\partial(b_y^2)/\partial z, \tag{6}$$

$$\partial b_y/\partial t = -B_0 \partial v_y/\partial z - \partial(v_z b_y)/\partial z + \nu_m \partial^2 b_y/\partial z^2. \tag{7}$$

Neglecting, for the first time, the second term of the righthand-side of (7) and combining it with (5), we get a wave equation of the type

$$\partial^2 b_y/\partial t^2 = \lambda B_0^2 \partial^2 b_y/\partial z^2 + \nu_m \partial^3 b_y/\partial^2 z \partial t, \tag{8}$$

from which we get a typical solution

$$b_y = A e^{i\alpha\left(t + \frac{z}{\sqrt{\lambda B_0^2 + i\nu_m \alpha}}\right)}, \tag{9}$$

the solution being correct for $|B_0| \gg |b|$.

Putting (9) into (5) and integrating with respect to t, we obtain the velocity

$$v_y = \frac{A\lambda B_0}{\sqrt{\lambda B_0^2 + i\nu_m \alpha}} e^{i\alpha\left(t + \frac{z}{\sqrt{\lambda B_0^2 + i\nu_m \alpha}}\right)}, \tag{10}$$

and the displacement

$$u_y = \frac{A\lambda B_0}{i\alpha\sqrt{\lambda B_0^2 + i\nu_m \alpha}} e^{i\alpha\left(t + \frac{z}{\sqrt{\lambda B_0^2 + i\nu_m \alpha}}\right)}, \tag{11}$$

while v_z denotes the longitudinal wave of usual sense slightly modified by the magneto-hydrodynamic waves. v_z is not important in the following discussions.

Let us next consider a transverse wave expressed by

$$u_y = ae^{i\alpha\left(t + \frac{z}{c}\right)} \tag{12}$$

which comes from the mantle with null incident angle to the surface of the core, c denoting the velocity of the wave. We denote the reflected wave which is also a transverse one by

$$u_y = de^{i\alpha\left(t - \frac{z}{c}\right)}. \tag{13}$$

From the continuity of tangential displacement and stress at the boundary, we have

$$\begin{aligned} a + d &= \frac{A\lambda B_0}{i\alpha\sqrt{\lambda B_0^2 + i\nu_m \alpha}}, \\ a - d &= \frac{A\lambda B_0 \rho}{ic\alpha\rho_c}, \end{aligned} \tag{14}$$

from which we get

$$\frac{d}{a} = \frac{1-x}{1+x} \tag{15}$$

where

$$x = \frac{\rho}{\rho_c} \frac{\sqrt{\lambda B_0^2 + i\nu_m \alpha}}{c}, \tag{16}$$

and where ρ_c denotes the density in the core.

Taking $\rho_c = 9.4$, $\rho = 5.7$ and $c = 7.3\ km/sec$, *mod.* $\frac{d}{a}$ can be calculated for various combinations of σ and B_0, where μ is assumed as unity. As the period of ScS waves is usually observed to be several

seconds, $\alpha=\frac{2\pi}{5}$ is adopted here. *mod.* $\frac{d}{a}$ (the ratio of the amplitude of the reflected wave to that of incident one) thus calculated is shown in Fig. 1 in which we see that *mod.* $\frac{d}{a}$ is scarcely affected by B_0 except the case of very large intensity such as $10^5\ emu<B_0$. *mod.* $\frac{d}{a}$ becomes small when σ_c approaches $10^{-12}\ emu$ where the phase change becomes also remarkable. Taking into consideration the fact that we have no reliable evidence for $d<a$ and phase difference as shown, for example, by H. Honda[17] we could tentatively adopt $B_0<10^4\ emu$ and $\sigma_c>10^{-8}$ *emu* from the consideration stated above.

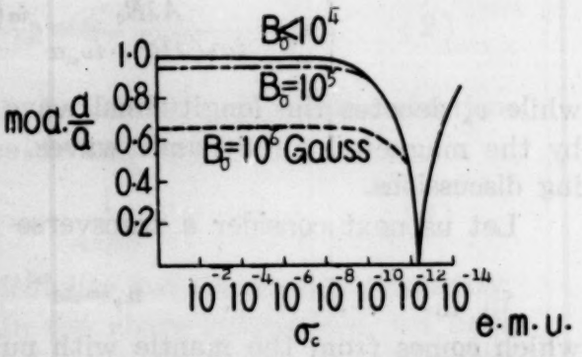

Fig. 1. The relation between the ratio of the amplitude of the reflected waves to that of the incident ones and the electrical conductivity in the core.

From (11), we can estimate the distance z_0 in which the amplitude of the magnetohydrodynamic waves reduced to $1/e$. z_0 is tabulated in Table I in *cm* unit.

In a favorable case of distribution of magnetic lines of force and of high conductivity, we might observe the waves which come through the core. We tentatively assume here that the wave might be observed for $z_0>100\ km$ which corresponds to $\sigma_c>10^2$ for $B_0=10^2$, $\sigma_c>1$ for $B_0=10^3$, and $\sigma_c>10^{-3}$ for $B_0=10^4$ all in electromagnetic unit. However, we have

Table I

z_0 in *cm* unit.

$B_0(emu)$ / $\sigma_c(emu)$	10	10^2	10^3	10^4
10^{-8}	3.6×10^3	3.6×10^3	3.6×10^3	3.8×10^3
10^{-6}	3.6×10^2	3.6×10^2	3.8×10^2	1.2×10^4
10^{-4}	3.6×10	3.8×10	1.2×10^3	1.2×10^6
10^{-2}	3.8	1.2×10^2	1.2×10^5	1.2×10^8
1	1.2×10	1.2×10^4	1.2×10^7	1.2×10^{10}
10^2	1.2×10^3	1.2×10^6	1.2×10^9	1.2×10^{12}

17) H. HONDA, *Geophys. Mag.*, **8** (1934), 161.

no evidence in seismology for such a wave. From this seismological evidence, we presume $\sigma_c<10^3$, $\sigma_c<1$, and $\sigma_c<10^{-3}$ respectively for $B_0=10^2$, $B_0=10^3$ and $B_0=10^4$. Since the magnetic field is not well known in the core, we cannot make any accurate estimate for σ_c, but if we take the view of Elsasser-Bullards' theory in which B_0 amounts to scores of *gauss*, we get $\sigma_c<10^3$ *emu*.

Combining the simple consideration on ScS waves with those of the damping of magneto-hydrodynamic waves in the core, we arrive at a conclusion $10^3>\sigma_c>10^{-8}$ in electromagnetic unit. Though the conclusion is rather incomplete, it is impossible to determine the possible range of σ_c accurately by the method studied above.

3. Some considerations on the shielding and cancelling effect of geomagnetic secular variation.

In his previous paper[18], the writer studied the electromagnetic shielding within the earth and its relation to the geomagnetic secular variation. Though only the case for the first degree component of spherical harmonic was discussed in that paper, it was made clear that the time-dependent part of geomagnetic secular variation due to electric currents flowing on the surface of the core would be fairly shielded by the mantle and cancelled by the electric currents induced in the conducting core.

In so far as we take a view that the geomagnetic secular variation is caused by the time-varying electric currents flowing near the surface of the core, the fact that we observe secular variation notwithstanding the above-mentioned shielding and cancelling effect would give some clue to the electrical conductivity in the core.

As has been pointed out by H. G. Macht[19] and as will be also shown in the following section, the second degree potential constituent would be more important for the actual secular variations than the first degree one. The writer will calculate here the shielding and cancelling effect for the second degree potential constituent together with the first degree one. As already shown in the writer's previous paper, the coefficient i_n of magnetic potential due to a time-dependent current-sheet on the surface of the core is given by

18) T. RIKITAKE, *Bull. Earthq. Res. Inst.*, **29** (1951), 263.
19) H. G. MACHT, Personal communication.

$$-(4\pi/a)K_n^m=q_1^{-n-1}\frac{2n+1}{n}z_1\left\{\frac{z_2}{2\nu}\left(I_{\nu+1}(z_2)K_{\nu+1}(z_1)-K_{\nu+1}(z_2)I_{\nu+1}(z_1)\right)\right.$$
$$\left.+\frac{F_{n-1}(q_2)}{F_n(q_2)}\left(I_\nu(z_2)K_{\nu+1}(z_1)+K_\nu(z_2)I_{\nu+1}(z_1)\right)\right\}i_n, \tag{17}$$

the current-function being defined by

$$J_n^m=K_n^mS_n^m. \tag{18}$$

z_1 and z_2 respectively denote $z_{\rho=q_1}$ and $z_{\rho=q_2}$, q_1 and q_2 mean the values of ρ at the upper and lower boundaries of the conducting mantle respectively, ρ denoting the ratio of the radial distance r to the radius of the earth a, z and ν are defined by

$$\rho^{1-l/2}=(l-2)z/(2\zeta),\quad \nu=(2n+1)/(l-2),\quad \zeta^2=4\pi a^2\sigma_0 p \tag{19}$$

where the conductivity in the mantle is assumed to be expressed by $\sigma=\sigma_0\rho^{-l}$ as determined by the writer. The operator p should be replaced by ia in case of periodic variation having a period $2\pi/a$.

If we neglect the shielding and cancelling effect wholly the coefficient $i_{n,0}$ of the magnetic potential at the earth's surface is given by

$$-(4\pi/a)K_n^m=q_2^{-n-1}\frac{2n+1}{n}i_{n,0}.$$

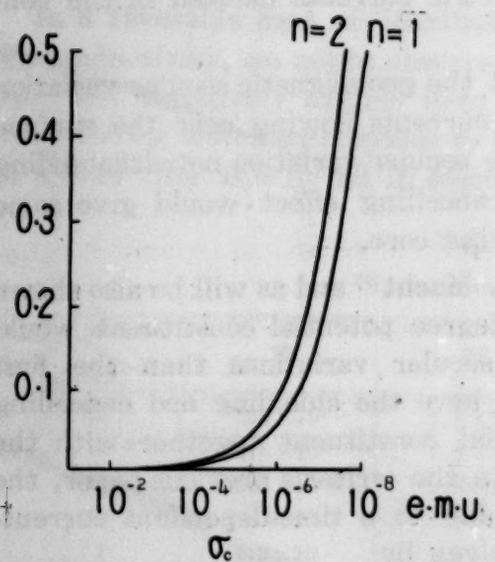

Fig. 2. The shielding and cancelling effect (*mod.* $i_2/i_{2,0}$ and *mod.* $i_1/i_{1,0}$) for various conductivity in the core.

By taking *mod.* $i_n/i_{n,0}$, we can estimate the shielding and cancelling effect as in the writer's previous paper. By taking into consideration the fact that the secular variations of regional character have apparent periods or duration-time of the order of 100 *years*, *mod.* $i_2/i_{2,0}$ and *mod.*

Table II

σ_c (*e.m.u*)	*mod.* $i_1/i_{1,0}$	*mod.* $i_2/i_{2,0}$
10^{-8}	0.477	0.737
10^{-7}	0.166	0.265
10^{-6}	0.0536	0.0880
10^{-5}	0.0172	0.0287
10^{-4}	0.00543	0.00900
10^{-3}	0.00172	0.00287
10^{-2}	0.000543	0.000900

$i_1/i_{1,0}$ are calculated for variation having 100-*year* period as shown in Table II and Fig. 2 in which σ_c is taken as abscissa. The functions K_ν, I_ν and F_n, which are essentially Bessel functions, are numerically calculated with the aid of ascending and descending power series.

As may be clearly seen in the figure, the shielding and cancelling effect become considerable as σ_c takes a high value. Hence the amplitude of the time-dependent electric currents, which correspond to the primary origin of the secular variation flowing near the surface of the core, would become enormously large in case of high conductivity.

But it seems unlikely that the current density is much larger than that required to produce the main dipole field. If we assume that the main dipole field is produced by the current flowing on the surface of the core, the current density amounts to 0.5 *emu/cm*. As for the secular variation, it amounts to as much as 100γ/*year* in South Africa. Adopting this value as a maximum of changing rate, the amplitude of the secular variation amounts to 1.6×10^{-2} *emu* for 100 *year* period variation. The amplitude of the electric currents on the surface of the core or K_n^m in (18) can be obtained by taking into account the shielding and cancelling effect. The current density for the second degree constituent thus calculated is tabulated in Table III.

Table III

σ_c	Amplitude of current density
10^{-8} *emu*	0.047 *emu*
10^{-7}	0.14
10^{-6}	0.41
10^{-5}	1.2
10^{-4}	4.0
10^{-3}	12
10^{-2}	40

Comparing the amplitude of the current density with that of the main magnetic field, we arrive at a conclusion $\sigma_c<10^{-5}$ *emu*. Though it is a matter of common sense to assume that the current density required to produce the secular variation should not be much larger than that required to produce the main field, we may tentatively presume that σ_c is not much larger than 10^{-5} *emu* from the geophysical consideration discussed in this section.

4. Mathematical studies on the magnetic dipole that corresponds to the regional secular variation.

F. J. Lowes and S. K. Runcorn[20] showed that the geomagnetic secular variation for the epoch 1922.5 can be expressed fairly well by

20) F. J. Lowes and S. L. Runcorn, *Phil. Trans. Roy. Soc. London A*, **243** (1951). 525.

the field of 13 magnetic dipoles situated at depths of $(0.6\pm0.1)a$, the directions of these dipoles being all radial. Their conclusions seem to be interesting and suggestive together with similar conclusion reached by Elsasser[21] and A. G. McNish[22] concerning the non-dipole part of the main field. However, the said dipoles are under the influence of the shielding and cancelling effect in the earth, the effect being of some importance in estimating the strength and position of the primary origin of the dipole. From this viewpoint a mathematical study on the time-dependent magnetic dipole will be carried out here in detail.

Let us consider a magnetic dipole situated at the surface of the core, the direction of which is vertical to the surface and coincides with $\theta=0$ axis. If the distance between the dipole and the earth's centre is denoted by d, the magnetic potential due to this dipole can be written as

$$W_d=M\frac{r\cos\theta-d}{R^3}, \quad (R^2=r^2+d^2-2rd\cos\theta) \tag{21}$$

where M denotes the magnetic moment of the dipole. The right-hand-side of (21) is readily expanded into a series of zonal harmonics such as

$$W_d=\begin{cases} M\dfrac{1}{r}\sum_{n=0}^{\infty} n\dfrac{d^{n-1}}{r^n}P_n(\cos\theta) & \text{for } r>d, \\ -M\dfrac{1}{d^2}\sum_{n=0}^{\infty}(n+1)\dfrac{r^n}{d^n}P_n(\cos\theta) & \text{for } r>d, \end{cases} \tag{22}$$

whence we can replace the dipole by a magnetized shell or electric current sheet whose potential are expressed by (22).

Taking an earth-model, as shown in Fig. 3 in which the distribution of the electrical conductivity ($\sigma'=10^{-15}$ *emu*, $\sigma_0=1.0\times10^{-12}$ *emu*, $l=11$, $q_1=0.94$, $q_2=0.545$) is the same with the one adopted in the writer's preliminary study on the electromagnetic shielding in the earth, the typical term of the magnetic potential can be expressed as

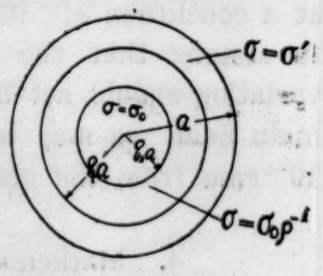

Fig. 3.

$$W_n^m=ai_n(t)\rho^{-n-1}S_n^m, \tag{23}$$

where the external origin part is not taken into account since the secular variation originates only inside the earth. The magnetic permeability is assumed as unity everywhere. S_n^m denotes

21) W. M. ELSASSER, *Phys. Rev.*, **60** (1941), 876.
22) A. G. MCNISH, *Trans. A.G.U. 21st Annual Meeting*, **II** (1940), 287.

spherical surface harmonic. The components of the magnetic field become

$$\left.\begin{aligned} H_r &= (n+1)\rho^{-n-2} i_n S_n^m, \\ H_\theta &= -\rho^{-n-2} i_n \partial S_n^m/\partial\theta, \\ H_\phi &= -\rho^{-n-2} i_n \partial S_n^m/(\sin\theta\partial\phi). \end{aligned}\right\} \tag{24}$$

We have in the conducting medium vector potential $\vec{A}$ which satisfies the relation

$$\nabla^2\vec{A} = 4\pi\sigma(\rho)\partial\vec{A}/\partial t \tag{25}$$

for slow variations. The typical term of the solutions of (25) becomes

$$\vec{A}_n^m = a f_n(t, \rho)[r \operatorname{grad} S_n^m], \tag{26}$$

where f_n satisfies the differential equation

$$\partial(\rho^2\partial f_n/\partial\rho)/\partial\rho = \{n(n+1) + 4\pi a^2\sigma\rho^2\partial/\partial t\} f_n . \tag{27}$$

The components of the magnetic field are given as

$$\left.\begin{aligned} H_r &= -n(n+1)\rho^{-1} f_n S_n^m \\ H_\theta &= -\rho^{-1}\frac{\partial}{\partial\rho}(\rho f_n)\partial S_n^m/\partial\theta, \\ H_\phi &= -\rho^{-1}\frac{\partial}{\partial\rho}(\rho f_n)\partial S_n^m/(\sin\theta\partial\phi). \end{aligned}\right\} \tag{28}$$

The function f_n becomes respectively for the regions 2 and 3 as follows:

$$f_{n,2} = \rho^{-1/2}\{C_2 K_\nu(z) + D_2 I_\nu(z)\} \qquad \text{for region 2,} \tag{29}$$

where C_2 and D_2 are both functions of time, K_ν and I_ν denote modified Bessel functions, while ν and z are defined by (19), and

$$f_{n,3} = C_3\rho^n F_n(\rho) \qquad \text{for region 3,} \tag{30}$$

where C_3 also denotes a function of time. F_n was fully studied in the theory of electromagnetic induction within the earth as given in the well-known book "*Geomagnetism*"[23]. In the above treatment, $\partial/\partial t$ is replaced by p as is usual in operational calculus.

Now we get the next relation from the continuity at the boundary of the core or at $\rho = q_2$

$$\{\partial(\rho f_{n,2})/\partial\rho\}_{\rho=q_2} - \{\partial(\rho f_{n,3})/\partial\rho\}_{\rho=q_2} = Ma^{-3} q_2^{-2}(2n+1), \tag{31}$$

$$(f_{n,2})_{\rho=q_2} = (f_{n,3})_{\rho=q_2} . \tag{32}$$

23) S. CHAPMAN and J. BARTELS, *Geomagnetism* (1940), p. 738.

We have also

$$n(f_{n,2})_{\rho=q_1}=-i_n q_1^{-n-1} \tag{33}$$

$$\{\partial(\rho f_{n,2})/\partial\rho\}_{\rho=q_1}=i_n q_1^{-n-1} \tag{34}$$

from the boundary conditions at $\rho=q_1$.

Then, solving the simultaneous equations (31), (32), (33), and (34), we get, with the aid of recurrence formula, the relation

$$Ma^{-3}q_2^{-2}=q_1^{-n-1}z_1\left[\frac{z_2}{2\nu}\left(I_{\nu+1}(z_2)K_{\nu+1}(z_1)-K_{\nu+1}(z_2)I_{\nu+1}(z_1)\right)\right.$$
$$\left.+\frac{F_{n-1}(q_2)}{F_n(q_2)}\left(I_\nu(z_2)\,K_{\nu+1}(z_1)+K_\nu(z_2)\,I_{\nu+1}(z_1)\right)\right]i_n \tag{35}$$

where z_1 and z_2 denote respectively $z_{\rho=q_1}$ and $z_{\rho=q_2}$ as before. In the case of periodic variation having a period $2\pi/a$, the operator p is replaced by ia in the above expressions. When $|z|\ll 1$, that is, for variations having period longer than about 10 *years*, we obtain i_n approximately as follows;

$$i_n=\frac{Ma^{-3}q_2^n}{\dfrac{F_{n-1}(q_2)}{F_n(q_2)}+\dfrac{i}{\nu(\nu+1)}\left\{\left(\dfrac{x_2}{2}\right)^2+\left(\dfrac{q_2}{q_1}\right)^{2n+1}\left(\dfrac{F_{n-1}(q_2)}{F_n(q_2)}-1\right)\left(\dfrac{x_1}{2}\right)^2\right\}}, \qquad (z=x\sqrt{i}) \tag{36}$$

Table IV

(Unit: $Ma^{-3}q_2{}^n$)

n	$i_{n,0}$	*mod.* i_n	Phase dif.	n	$i_{n,0}$	*mod.* i_n	Phase dif.
1	0.162	0.0^2867	44.°5	16	0.0^3288	0.0^3141	35.°2
2	0.176	0.0155	43.7	17	0.0^3168	0.0^4865	34.7
3	0.144	0.0176	42.9	18	0.0^4965	0.0^4518	34.3
4	0.105	0.0162	42.2	19	0.0^4553	0.0^4308	33.8
5	0.0715	0.0133	41.8	20	0.0^4319	0.0^4185	33.4
6	0.0468	0.0102	41.1	21	0.0^4182	0.0^4109	33.0
7	0.0298	0.0^2742	40.3	22	0.0^4103	0.0^5638	32.6
8	0.0186	0.0^2516	39.8	23	0.0^5588	0.0^5377	32.2
9	0.0113	0.0^2347	39.2	24	0.0^5334	0.0^5220	31.7
10	0.0^2687	0.0^2230	38.5	25	0.0^5189	0.0^5128	31.3
11	0.0^2413	0.0^2150	38.0	26	0.0^5108	0.0^6752	30.9
12	0.0^2245	0.0^3957	37.4	27	0.0^6608	0.0^6437	30.5
13	0.0^2144	0.0^3598	36.9	28	0.0^6344	0.0^6254	30.2
14	0.0^3850	0.0^3374	36.4	29	0.0^6194	0.0^6146	29.9
15	0.0^3495	0.0^3230	35.9	30	0.0^6109	0.0^7837	29.6

while the coefficient $i_{n,0}$ for the earth, in which we neglect all the shielding and cancelling effect, is readily obtained from (22) or from the limiting case of (36) for $\sigma_c \to 0$. It becomes

$$i_{n,0}=Ma^{-3}q_2^n n. \tag{37}$$

By adopting $\sigma_c=10^{-6}$ *emu*, the writer calculated here $i_{n,0}$ and i_n for 100-*year* period variation. The amplitude and phase difference of i_n are shown together with $i_{n,0}$ in Table IV. Owing to the slowness of convergence of the series, high degree terms such as $n=30$ are needed in order to calculate the magnetic field at the earth's surface. The behaviors of the magnetic field thus calculated are shown in Figs. 4 and 5

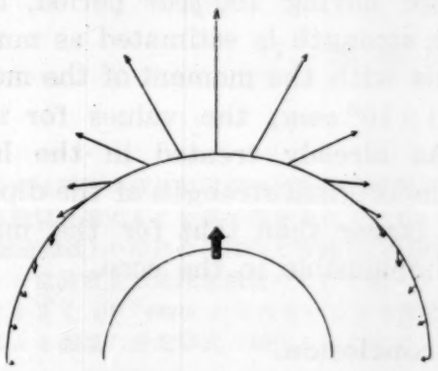

Fig. 4. The distribution of the magnetic force in a meridional section of the non-conducting earth. The primary magnetic dipole is shown with a thick arrow.

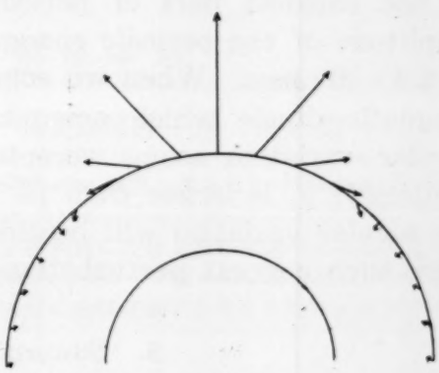

Fig. 5. The magnetic force for conducting earth. The magnitude is multiplied 5.86 times.

respectively for non-conducting and conducting earth where the phase differences for different harmonics are neglected because of the small differences for main harmonics. In the figures, we must pay attention to the fact that the field for conducting earth is multiplied 5.86 times in order to make the field at the pole agree with that of the non-conducting earth.

Looking at Fig. 5, we find that the distribution of the magnetic field on the earth's surface is fairly modified in case of conducting earth though the general character of it remains unchanged. If we approximate this distribution with a dipole, the position of it will become slightly shallower than that of non-conducting earth. Taking into account the accuracy of determination for actual secular variation, however, we may obtain a dipole whose position falls within a range as determined by Lowes and Runcorn if the secular variation is produced

by a time-dependent dipole situated near the surface of the core. Hence, the assumption that σ_c takes a value of order of 10^{-6} *emu* seems to be consistent with the analysis of the actual secular variation.

An important fact, which is deduced from the calculus for $\sigma_c=10^{-6}$ *emu*, is that the changing rate of the magnetic moment of the primary dipole becomes several times larger than the one directly obtained from the analysis of the actual secular variation. As was pointed out by Lowes and Runcorn, a surface field of $100\gamma/year$ implies a dipole at depth $0.6a$ of strength 2.78×10^{22} *emu/year*. By taking into account the shielding and cancelling, the strength of the primary dipole will amount to 1.5×10^{23} *emu/year*. Even when we assume that this value corresponds to the rapidest part of periodic change having 100-*year* period, the amplitude of the periodic change in the strength is estimated as much as 2.4×10^{24} *emu*. When we compare this with the moment of the main magnetic dipole which amounts to 8.1×10^{25} *emu*, the values for the secular variation seems acceptable. As already treated in the last section, if σ_c is larger than 10^{-5} *emu*, the original strength of the dipole for secular variation will become much larger than that for the main field, such a great perturbation being implausible in the core.

5. Summary and conclusion.

In order to investigate the electrical conductivity in the earth's core, the writer studied the possibility of the magneto-hydrodynamic waves in the core and the shielding and cancelling effect in the earth together with the behavior of time-dependent dipole situated at the surface of the core. From the observational results in seismology that ScS waves are not likely affected by the magneto-hydrodynamic waves and we find no waves which come through the core as the magneto-hydrodynamic waves, it may be roughly concluded that $10^3>\sigma_c>10^{-8}$ *emu* while the intensity of magnetic field should be less than 10^4 *emu*.

After taking into account the shielding and cancelling effect for geomagnetic secular variation which is produced by the time-dependent electric currents flowing near the surface of the core, $\sigma_c>10^{-5}$ *emu* is tentatively concluded by adopting the criterion that the electric current density for the primary origin of secular variation will not be much larger than the one for the main dipole field, the study being done for a variation having a 100-*year* period. A similar conclusion is obtained from the study concerning the modification of the magnetic field of a time-dependent dipole situated at the surface of the core.

Although the estimate of σ_c mentioned in this paper is crude, it is of interest that the possible range of σ_c, say $10^{-5} > \sigma_c > 10^{-8}$ *emu*, fairly agrees with those obtained before from a quite different standpoint such as physics of metallic iron at high temperature and pressure. The writer is of opinion that Elsasser-Bullards' consideration that σ_c amounts to the order of 10^{-6} *emu* is fairly right judging from both physical and geophysical viewpoints.

---

17. 地球核の電氣傳導度

地震研究所　力　武　常　次

従來地球核の電氣傳導度は物性論的考察より 10^{-5}～10^{-6} *emu* 程度と考えられ，Elsasser-Bullard の地磁氣理論にもこの値が採用されている．筆者は核内に於ける Magneto-hydrodynamic wave（電磁流體波）の存在の可能性を吟味し，地磁氣永年變化が核表面に於ける變化電流によると考える時にその電流密度が地球主磁場のそれを越えないという常識的見解より，核の電氣傳導度は 10^{-5} *emu* より小さく 10^{-8} *emu* より大きいことを推論した．核表面に磁氣双極子を考えた時のシールディングによる磁場の分布形式の變化もあわせてしらべてある．

---

18. A Preliminary Study on the Anomalous Behavior of Geomagnetic Variations of Short Period in Japan and Its Relation to the Subterranean Structure.

By Tsuneji RIKITAKE, Izumi YOKOYAMA
and Yoneko HISHIYAMA,

Earthquake Research Institute.

(Read May 20, 1952.—Received June 20, 1952.)

1. Introduction.

A recording of changes in the three geomagnetic components has been carried on at Aburatsubo (35°09′ N, 139°37′ E) by the Earthquake Research Institute since September, 1951. The magnetograms show strong parallelism between short period changes in horizontal (H) and vertical (Z) components. The writers also find out that changes in Z-component (ΔZ) are anomalously large there, usually amounting to as much as 60 per cent of changes in H-component (ΔH). Since similar tendencies at Kakioka Magnetic Observatory has been already pointed out by T. Nagata[1], the said parallelism and anomalously large amplitude of ΔZ may be regarded as the characteristics peculiar to the central part of Japan.

In order to bring out the peculiarity more clearly, the writers analysed the geomagnetic data at the occassion of the 32nd cooperative observation of the Ionosphere Research Committee, Japan. The geomagnetic data[2] related to a solar eclipse that occurred near Japan on June 19, 1936 were also analysed, the data at that occasion being the best for the purpose because of the proper distribution of temporary stations in Japan and her vicinity.

Although the writers arrived at no decisive conclusion concerning the detailed nature and origin of the anomalous behavior of geomagnetic variations in Japan, it may be of some use to report here the results of the analysis, referring especially to the special conditions in the earth's interior below Japan.

---

1) T. NAGATA, *Rep. Ionos. Res. Japan*, **5** (1951), 134.

2) A. TANAKADATE and others, *Japanese Journ. Astro. Geophys.*, **14** (1938), 85.

2. Geomagnetic observation at Aburatsubo.

(1) *Outline of the observation.*

It was already reported by T. Hagiwara[3] and others that a geophysical station for observing the deformation of the earth's surface was set up at Aburatsubo (35°09′ *N*, 139°37′ *E*), near the southern extremity of the Miura Peninsula. A continuous observation of the three geomagnetic components were added there for the purpose of finding out changes in the earth's magnetic field that might occur at the time of an earthquake and also of recording geomagnetic variations of short period.

The magnetic variometers are installed in a cave drilled in the Tartiary sandstone, the cave being just adjacent to the gallery for the

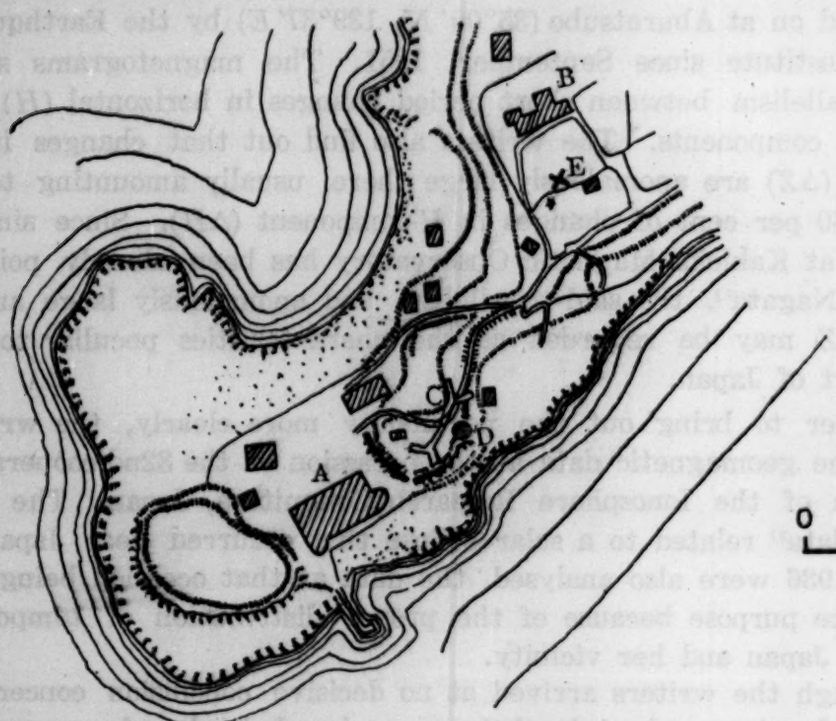

Fig. 1. The sketch map near the magnetometer room. A: Marine Biological Station, B: Dormitory, C: Gallery for the observation of crustal deformation, D: Magnetometer room, E: The place on which the absolute measurements had been made.

3) T. HAGIWARA, T. RIKITAKE and J. YAMADA, *Bull. Earthq. Res. Inst.*, **26** (1948), 23.

observation of crustal deformation. The topography near the magnetometer-room is shown in Fig. 1. The arrangement of the magnetometers are shown in Fig. 2 and Plate I. The sensibility of the D (declination)-variometer is $0.648'/mm$ with $2.7\,m$ optical lever, a M.K. magnet being suspended by a fine phosphorbronze wire.

The suspending wire of H (horizontal intensity)-variometer is a quartz fibre of $60\,\mu$, the sensibility being usually $1.5\gamma/mm$. A Z (vertical intensity)-variometer of Watson type with a sensibility-range $2\sim5\,\gamma/mm$ is also used. An example of the record is shown in Fig. 3 in which we find small fluctuations probably due to the stray electric currents from an electric railway at a distance of about $10\,km$.

Absolute measurements of the three components were carried out with a G.S.I. type magnetometer on April 27 and 28, 1951 in the garden of the dormitory of the Marine Biological Station, the place on which the measurements were made being also shown in Fig. 1. The results

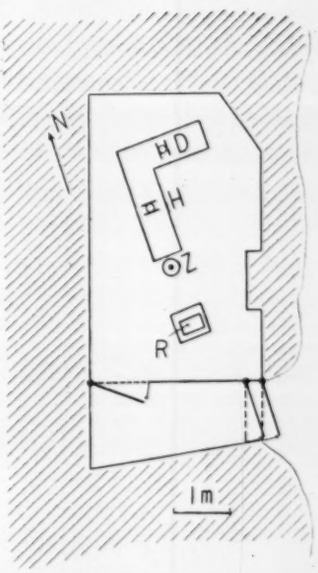

Fig. 2. The arrangement of the D (declination)-, H (horizontal-intensity)-, and Z (vertical intensity)-magnetometers and R (recording drum) in the magnetometer room.

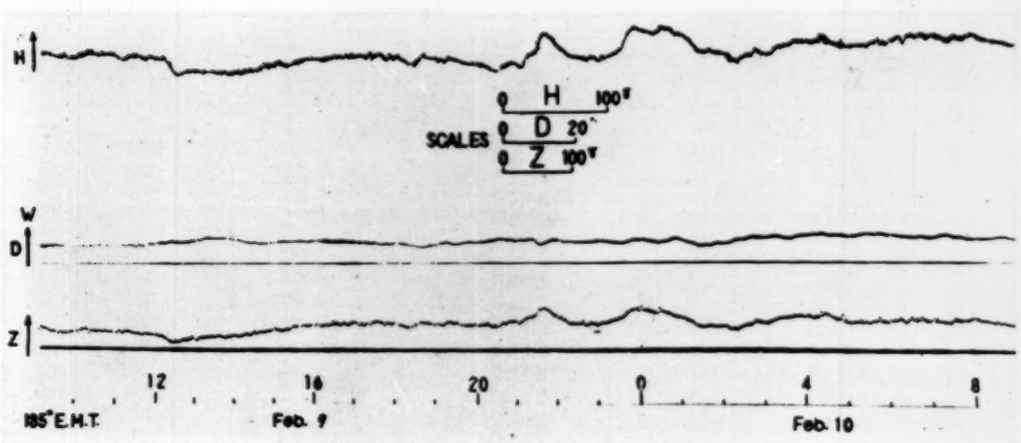

Fig. 3. An example of the record. (Feb. 9 and 10, 1952)

are given in the footnote[4] for future use.

(2) *Characteristics of short period variation.*

As early as in the year 1909, T. Terada[5] carried out an observation of the three geomagnetic components at almost the same place with the present one. He studied in great detail the behavior of rapid periodic variations and concluded that the vertical component of the waves is a reduced reproduction of the *NS*-component though some

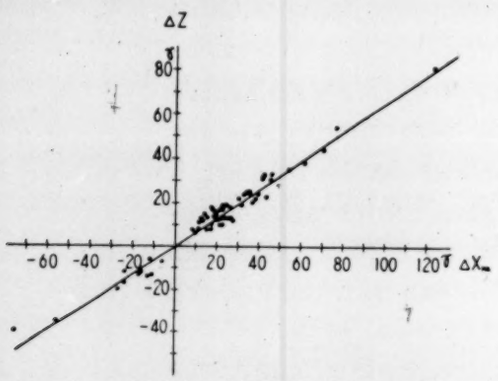

Fig. 4. The relations between ΔX_m and ΔZ for short period variations during the period from Sept. 9 to Oct. 14, 1951.

phase retardation could be found, especially with regards to rapid variations having period of several *minutes*. In Fig. 4, ΔZ is plotted against ΔX_m (change in magnetic north component) for variations having duration-time of scores of *minutes*, the phase difference being almost

4) The results of the absolute measurements are as follows:

Declination and Dip

Time	*D*	*I*
April 27th		
19h14m	6°35′.3	48°23′.4
20 20	34 .6	23 .1
22 32	34 .4	23 .3
23 52	32 .8	22 .0
28th		
9 34	30 .7	21 .0
10 44	34 .0	21 .6
11 35	34 .8	21 .7
12 30	35 .8	21 .2
13 28	35 .7	20 .6
14 27	34 .8	20 .8
15 46	34 .2	20 .9
17 00	32 .7	21 .0

Horizontal Intensity

Time	*H*
April 27th	
19h26m	30371γ
20 30	374
22 44	365
28th	
0 02	384
9 44	370
10 50	361
11 42	367
12 36	384
13 34	390
14 32	397
16 00	402
17 20	395

5) T. TERADA, *Journ. Coll. Sci. Tokyo Imp. Univ.* **37** (1917) Article 9.

negligibly small for these variations. The mean value of $\Delta Z/\Delta X_m$ is estimated at 0.62 that seems to harmonize well with Terada's results.

3. Study on the remarkable geomagnetic variation on Sept. 27, 1951.

At about 7 *h* 30 *m* *GMT* on Sept. 27, 1951, we had a rapid change in the earth's magnetic field. Since the 32nd cooperative observation of the Ionosphere Research Committee was under way at that date, the writers could collect copies of magnetograms from Wakkanai (45.4 *N*, 141.7 *E*), Kakioka (36.2 *N*, 140.2 *E*), and Aso (32.9 *N*, 131.0 *E*) Observatories together with that from Aburatsubo.

In order to pick up variations of short duration-time, the writers made running averages by averaging 13 readings of every 5 *minutes* of the magnetograms. Subtracting the running averages thus calculated from the original curves, we got the short period variations as shown in Fig. 5 for each observatory. The figures show a remarkable parallelism between ΔH and ΔZ at both Kakioka and Aburatsubo. And we

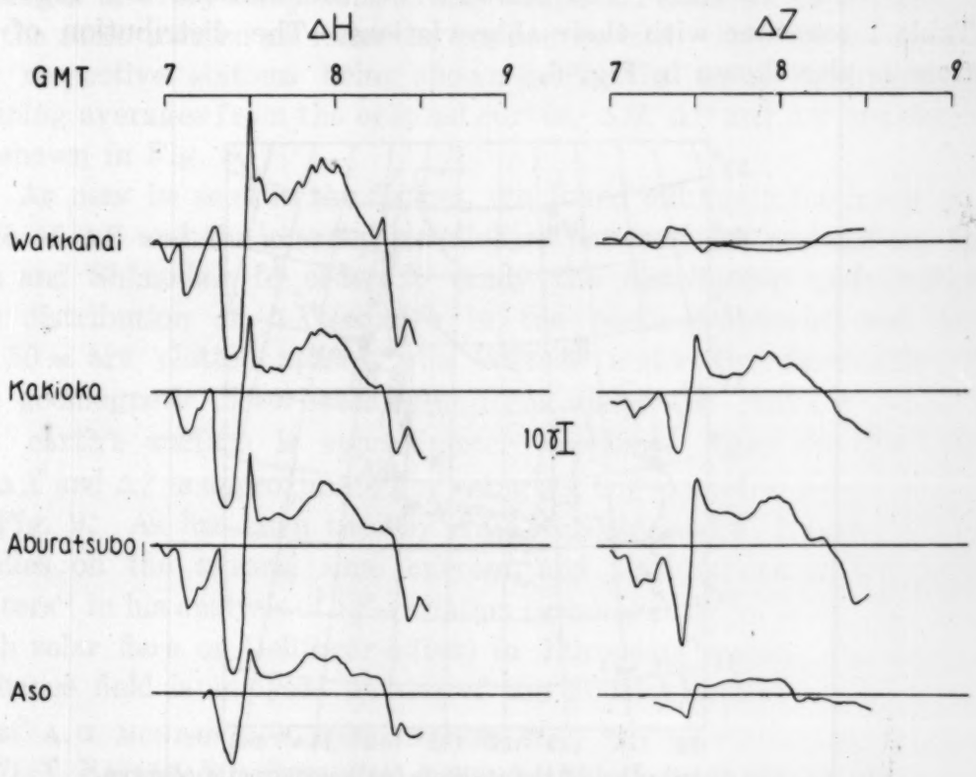

Fig. 5. The short period variations at respective stations on Sept. 27, 1951.

found out also the anomalously large amplitude of ΔZ at these stations. Though the forms of ΔH seem to be almost the same throughout the four observatories, ΔZ becomes small in its amplitude and also the parallelism becomes less at the northern and southern parts of Japan. Even the direction of ΔZ reverses at Wakkanai. As was manifested in Fig. 5, the curious distributions of geomagnetic variations, especially in Z-component, should be examined in fuller detail though the geomagnetic data cited here are unsatisfactory for that purpose.

4. Study on the geomagnetic variation at the time of the solar eclipse on June 19, 1936.

A total solar eclipse[2] occurred in the vicinity of Japan on June 19, 1936. In order to detect the influence of a solar eclipse on geomagnetic variation, many temporary stations were prepared in Japan, Manchuria, North China and Saghalien. Since a magnetic storm began at $9h\ 41m$ *GMT* on June 18, we could investigate in detail the behavior of geomagnetic variations of short period with the magnetograms from these well-distributed stations. The positions of the stations are tabulated in Table I together with their abbreviations. The distribution of the stations is also shown in Fig. 6.

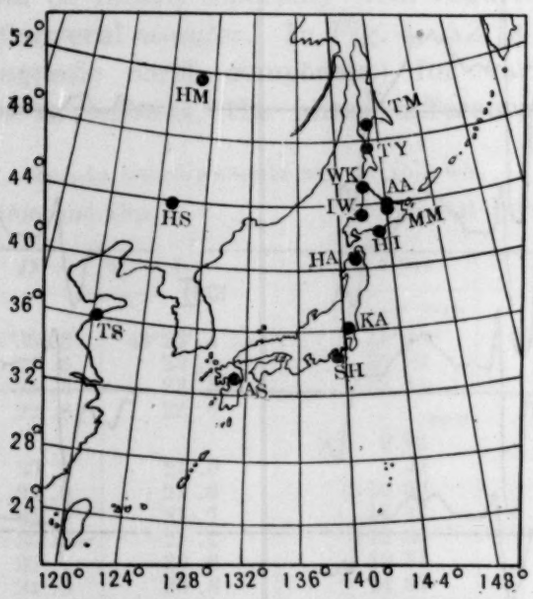

Fig. 6. The distribution of the stations for geomagnetic observation at the time of the solar eclipse on June 19, 1936.

Table I. The position and abbreviation of the stations.

Station	Abbreviation	Latitude	Longitude
Huma	HM	51.°7 N	126.°7 E
Tomarigishi	TM	49.0	142.9
Toyohara	TY	47.0	142.8
Wakkanai	WK	45.4	141.7
Abashiri	AA	44.0	144.3
Hsingking	HS	43.9	125.3
Memanbetsu	MM	43.9	144.4
Iwamizawa	IW	43.2	141.8
Hiroo	HI	42.3	143.3
Hirosaki	HA	40.6	140.5
Kakioka	KA	36.2	140.2
Tsingtau	TS	36.1	120.3
Shimoda	SH	34.7	138.9
Aso	AS	32.9	131.0

A very rapid change that occurred at about $5h\ 50m$ *GMT* was investigated in the main. For that purpose, the writers made running averages of every component during the period from $4h$ to $8h$ by means of the same method as stated in the last section, the original variations for respective stations being shown in Fig. 7. After subtracting the running averages from the original curves, ΔH, ΔD and ΔZ are obtained as shown in Fig. 8.

As may be seen in the figures, we found out again the large amplitude of ΔZ and the marked parallelism between ΔH and ΔZ at Kakioka and Shimoda. In order to study the distribution quantitatively, the distribution of ΔX (change in the north-component) and ΔZ at $5h\ 50m$ are plotted against the latitude under the assumption that the geomagnetic disturbance is uniform along the latitude circle and the earth's surface is approximately a plane. Then the distribution of ΔX and ΔZ is approximated by using six trigonometric terms as shown in Fig. 9. As has been used by A.G. McNish[6] and T. Nagata[7] in their studies on the auroral zone current and also by one of the present writers[8] in his analysis of SF-variation (geomagnetic variation associated with solar flare or Dellinger-effect) in European region, the said disturbance field is analysed by use of the Fourier series.

6) A. G. McNish, *Terr. Mag.*, **43** (1938), 67.
7) T. Nagata, *Rep. Ionos. Res. Japan.* **4** (1950), 87.
8) T. Rikitake, *Bull. Earthq. Res. Inst.*, **28** (1950), 219.

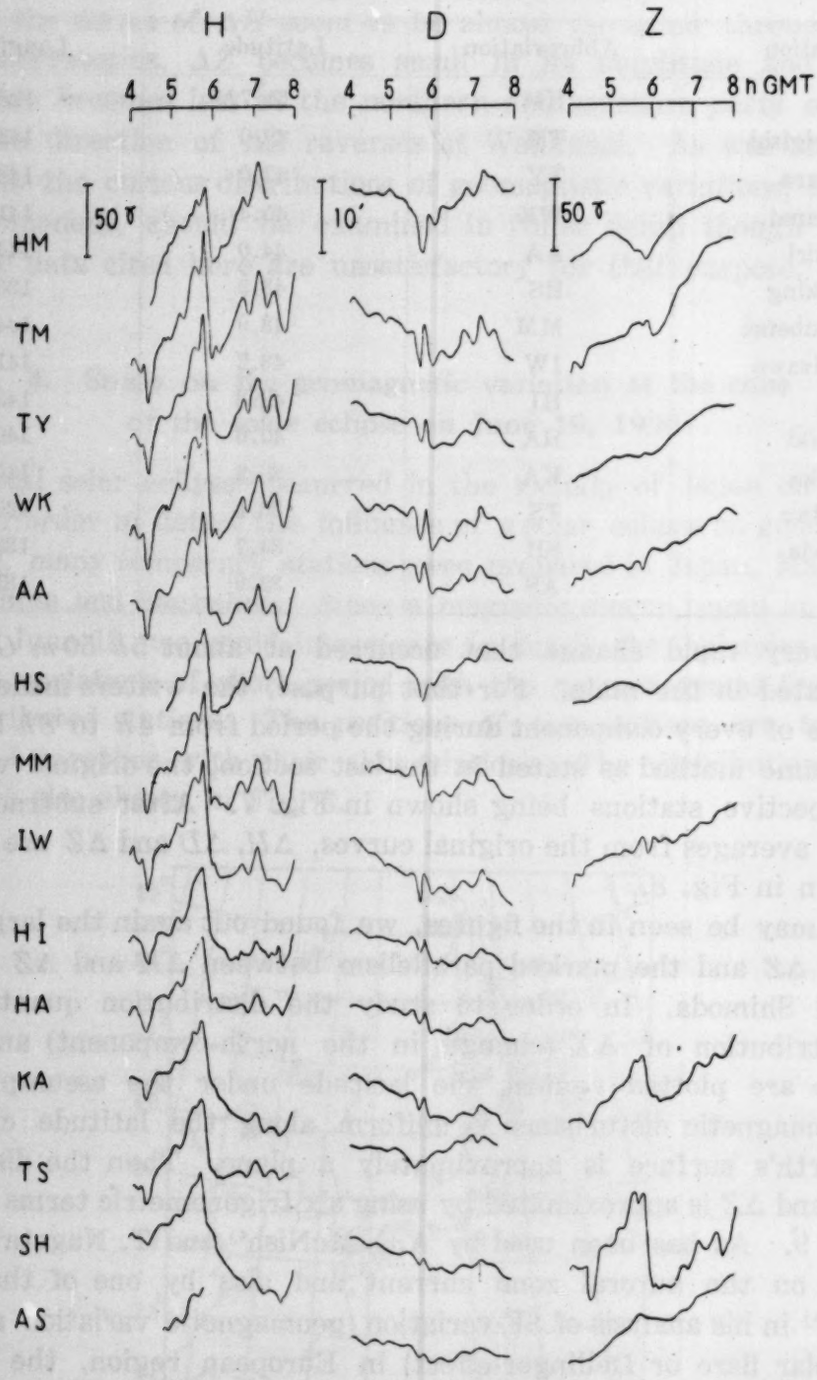

Fig. 7. The magnetograms for respective stations from 4 to 8 *h GMT* on June 19, 1936.

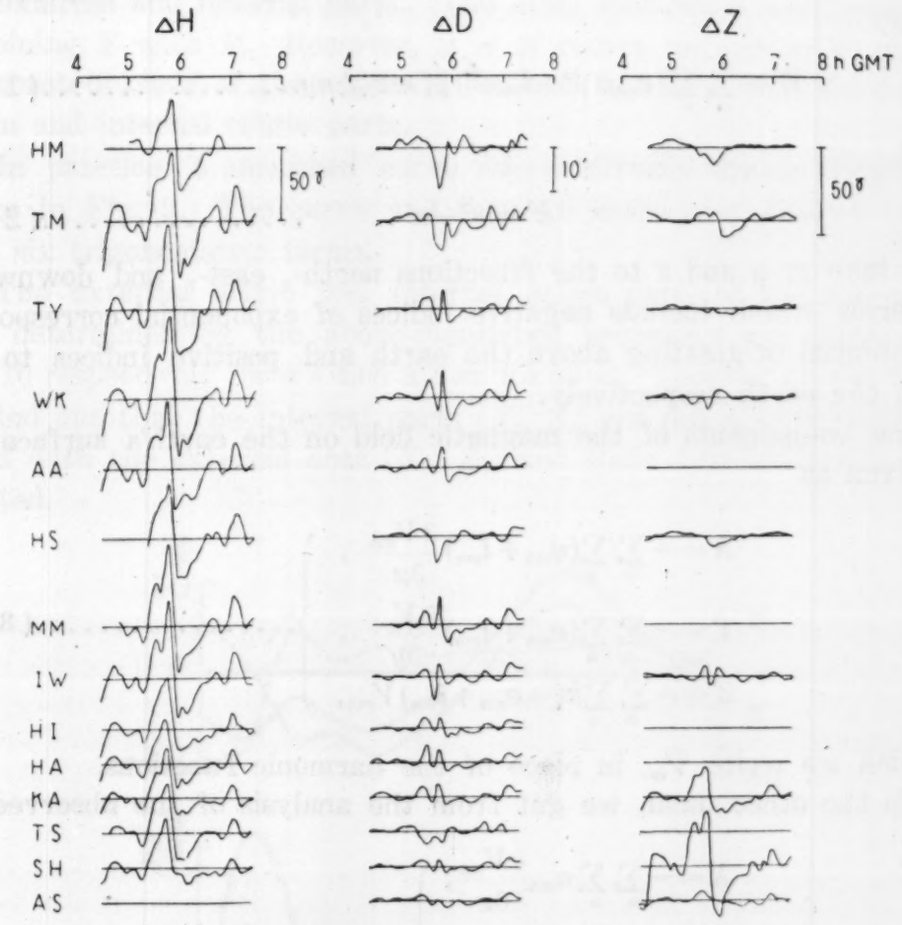

Fig. 8. The short period variations obtained from the original curves as shown in Fig. 7.

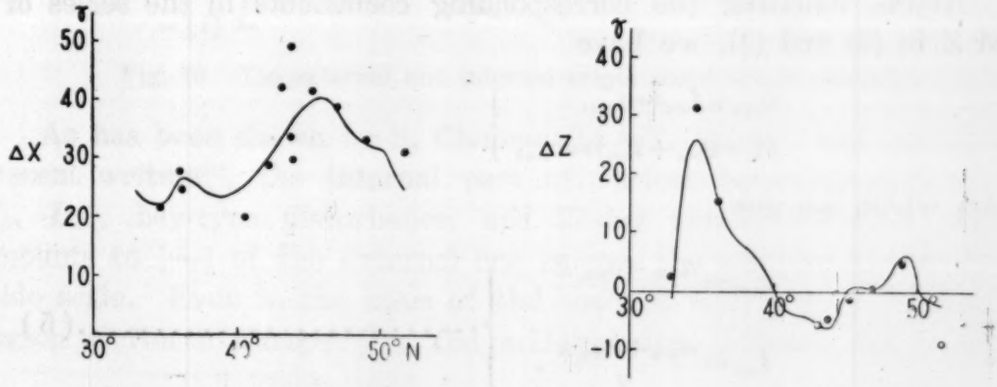

Fig. 9. The distribution of ΔX and ΔZ. The curves are the approximations with six trigonometric terms. (5 *h* 50 *m* *GMT*, June 19, 1936.)

The magnetic potential of the variation is generally expressed as follows,

$$W=\sum_m \sum_n (e_{mn}e^{-kz}+i_{mn}e^{kz}) \begin{matrix}\cos\\ \sin\end{matrix} mx \begin{matrix}\cos\\ \sin\end{matrix} ny \quad \cdots\cdots\cdots\cdots\cdots\cdots (1)$$

where

$$k^2=m^2+n^2 . \quad \cdots\cdots\cdots\cdots\cdots\cdots (2)$$

If we take x, y and z to the directions north-, east-, and downwards, the terms which include negative indices of exponential correspond to the potential originating above the earth and positive indices to that within the earth respectively.

The components of the magnetic field on the earth's surface $z=0$ are given as

$$\left.\begin{aligned} X&=-\sum_m \sum_n (e_{mn}+i_{mn})\frac{\partial V_{mn}}{\partial x} ,\\ Y&=-\sum_m \sum_n (e_{mn}+i_{mn})\frac{\partial V_{mn}}{\partial y} ,\\ Z&=-\sum_m \sum_n k(-e_{mn}+i_{mn})V_{mn}, \end{aligned}\right\} \cdots\cdots\cdots\cdots\cdots\cdots (3)$$

in which we write V_{mn} in place of the harmonic functions.

On the other hand, we get from the analysis of the observed data

$$\left.\begin{aligned} X&=-\sum_m \sum_n a_{mn}\frac{\partial V_{mn}}{\partial x},\\ Y&=-\sum_m \sum_n b_{mn}\frac{\partial V_{mn}}{\partial y},\\ Z&=-\sum_m \sum_n c_{mn}V_{mn} . \end{aligned}\right\} \cdots\cdots\cdots\cdots\cdots\cdots\cdots\cdots (4)$$

Hence, equating the corresponding coefficients in the series of X and Z in (3) and (4), we have

$$\left.\begin{aligned} e_{mn}+i_{mn}&=a_{mn},\\ k(-e_{mn}+i_{mn})&=c_{mn}, \end{aligned}\right\}$$

from which we get

$$\left.\begin{aligned} e_{mn}&=\frac{a_{mn}-c_{mn}/k}{2},\\ i_{mn}&=\frac{a_{mn}+c_{mn}/k}{2} . \end{aligned}\right\} \cdots\cdots\cdots\cdots\cdots\cdots\cdots\cdots (5)$$

Thus we can separate the coefficients of the magnetic potential into

the external and internal parts. The same solution is also possible by combining Y with Z. However, it is of course impossible to separate the constant parts of the magnetic potential and force into the external origin and internal origin parts.

In practice, a smoothed curve was arbitrarily drawn through the points in Fig. 9. The curve was then subjected to a Fourier analysis with six trigonometric terms.

The external origin and internal origin parts of the non-uniform field determined by the above-mentioned procedure are illustrated in Fig. 10 respectively for ΔX and ΔZ at $5h\ 50m$. Looking at the figures, we find out that the internal parts (X_i, Z_i) are not always small compared with the external ones (X_e, Z_e) and their distributions are complicated.

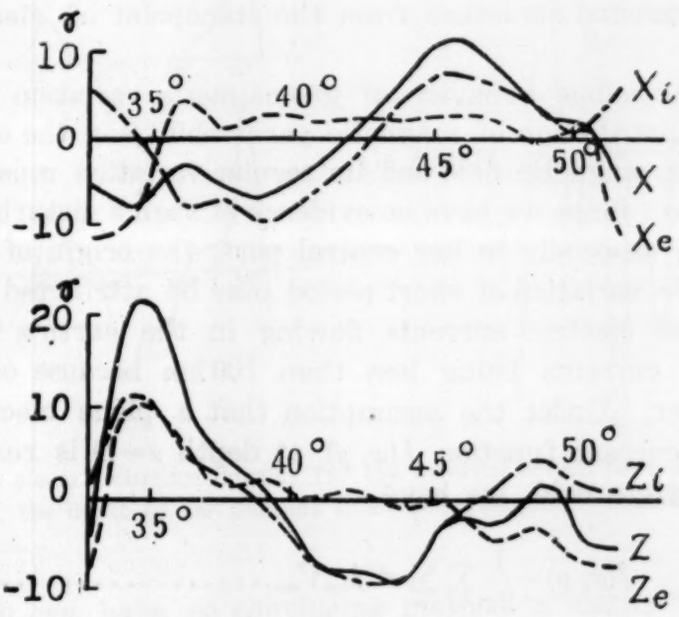

Fig. 10. The external and internal origin parts of ΔX and ΔZ.

As has been shown by S. Chapman[9], A.T. Price,[10] and one of the present writers[11], the internal part of various variations such as S_q, S_D, D_{st}, bay-type disturbance, and 27-day period variation usually amounts to $\frac{1}{4}\sim\frac{1}{3}$ of the external one in case the analyses are of world-wide scale. Even in the cases of the analyses with respect to a limited region of North Europe[6),7),8)], the said relation between the external

9) S. Chapman, *Phil. Trans. Roy. Soc. London A*, **218** (1919), 1.
10) S. Chapman and A. T. Price, *Phil. Trans. Roy. Soc. London A*, **229** (1930), 427.
11) T. Rikitake, *Bull. Earthq. Res. Inst.*, **28** (1950), 45, 219, **29** (1951), 61.

and internal parts seems to hold true. Hence, the curious distribution of both parts of geomagnetic variation in the vicinity of Japan as revealed in Fig. 10 can hardly be explained from the viewpoint of the electromagnetic induction theory within a homogeneous earth notwithstanding the success of the theory in the explanation of geomagnetic changes of world-wide scale. We, therefore, suspect the existence of some peculiar conditions in the earth's interior under Japan.

5. The electrical condition in the earth's interior below Japan and her vicinity.

Although the analysis of the geomagnetic variation treated in the last section is one-dimensional and not sufficient for studying the source of the peculiarity, we shall make a preliminary investigation concerning the underground structure from the standpoint of electromagnetic induction.

If the anomalous behavior of geomagnetic variation is caused by an abnormal distribution of magnetic permeability in the earth's crust, the permanent magnetic field and its secular variation must be greatly disturbed there. Since we have no evidence of such a disturbed magnetic field in Japan, especially in her central part, the origin of the anomaly of geomagnetic variation of short period may be attributed in the main to the induced electric currents flowing in the earth's interior, the depth of the currents being less than $100\,km$ because of the reason mentioned later. Under the assumption that a plane electric current sheet having current function $J(x, y)$ at depth $z=D$ is responsible for the internal origin field, we have

$$J(x, y)=\frac{1}{2\pi}\sum_m\sum_n e^{kD}\boldsymbol{i}_{mn}V_{mn}, \quad \cdots\cdots(6)$$

from which we can get the current intensity by the following relations

$$I_x=\frac{\partial J}{\partial x}, \quad I_y=-\frac{\partial J}{\partial y}. \quad \cdots\cdots(7)$$

With these relations, the current density by which the internal origin field at $5h\,50\,m$ would be produced is calculated for $D=0$, 50, 100 and $200\,km$ as illustrated in Fig. 11. As may be seen in the figures, the distribution of the current density becomes more complicated according as the depth of the current sheet becomes great. The distribution for $D=200\,km$ seems to be too much oscillatory to be adopted

as a real distribution, while that for $D=100\,km$ seems to be fairly convergent. Hence, we may tentatively assume that the main part of the electric currents, which produce the anomalous geomagnetic variation in Japan, are flowing in the earth's interior at a depth less than about $100\,km$.

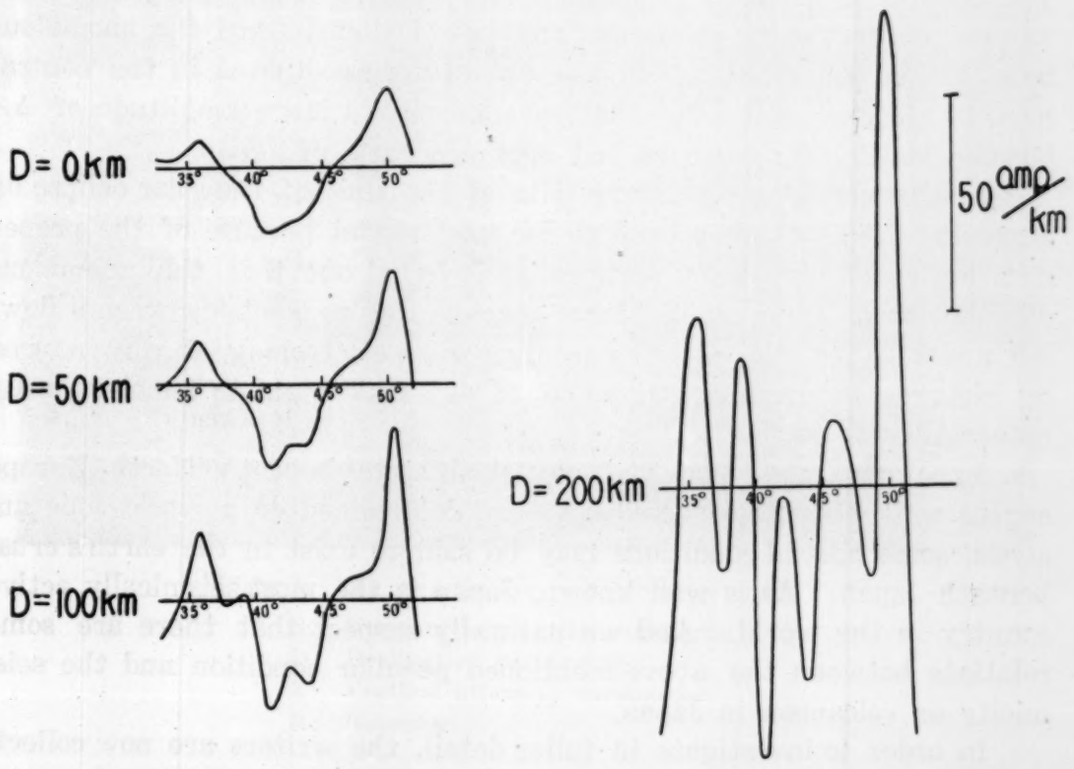

Fig. 11. The electric current density for the internal origin part of the geomagnetic variation, the depth of the current sheet being assumed respectively to be 0,50,100 and 200 *km*.

Though we have no convincing method to clarify the reason why the abnormal distribution of electric currents occur at the time of short period variation in the earth's magnetic field, it may be naturally regarded as the electric current induced by changes in the magnetic field of external origin, the special distribution of the currents being ascribed to a heterogeneous distribution of the electrical conductivity in the earth. The constant part of external origin field, which can not be analysed on a plane earth, would of course play an important rôle in the case of a heterogeneous distribution of the electrical conductivity.

6. Summary and conclusion.

A brief outline of geomagnetic observation at Aburatsubo is described. The anomalously large amplitude of ΔZ and the strong parallelism between ΔH and ΔZ are found on the magnetograms there. The anomalous behavior is studied with the aid of magnetograms from various observatories in Japan and her vicinity. And the anomalous behavior is confirmed at all the observatories situated in the central part of Japan, while the said parallelism and large amplitude of ΔZ become less in the southern and northern parts of Japan.

Analysing the geomagnetic data at the time of the solar eclipse on June 19, 1936, which proved to be most useful because of the proper distribution of temporary stations, it is found out that the anomalous distribution of geomagnetic force may be due to electric currents flowing under Japan, the currents seeming to be electromagnetically induced by changes in geomagnetic force of external origin in an electrically heterogeneous earth.

Since we know that the electrical state beneath North Europe agrees well with the electrical states determined on a world-wide analysis, some special conditions may be said to exist in the earth's crust beneath Japan. As is well known, Japan is the most seismically active country in the world. And we naturally suspect that there are some relations between the above-mentioned peculiar condition and the seismicity or volcanism in Japan.

In order to investigate in fuller detail, the writers are now collecting copies of magnetograms on June 19, 1936 from foreign observatories all over the world. A more complete analysis concerning the anomalous behavior of geomagnetic variations of short period in Japan will be made in the near future.

In conclusion, the writers are grateful to the Ionosphere Research Committee of Japan with whose data a part of the present study was carried out. Especially the writers wish to express their thanks to the Wakkanai, the Kakioka and the Aso Magnetic Observatories. The writers are also indebted to Professor T. Nagata and Mr. N. Fukushima for their helpful discussions.

[Bull. Earthq. Res. Inst., Vol. XXX, Pl. V.]

（震研彙報　第三十號　圖版　力武・横山・菱山）

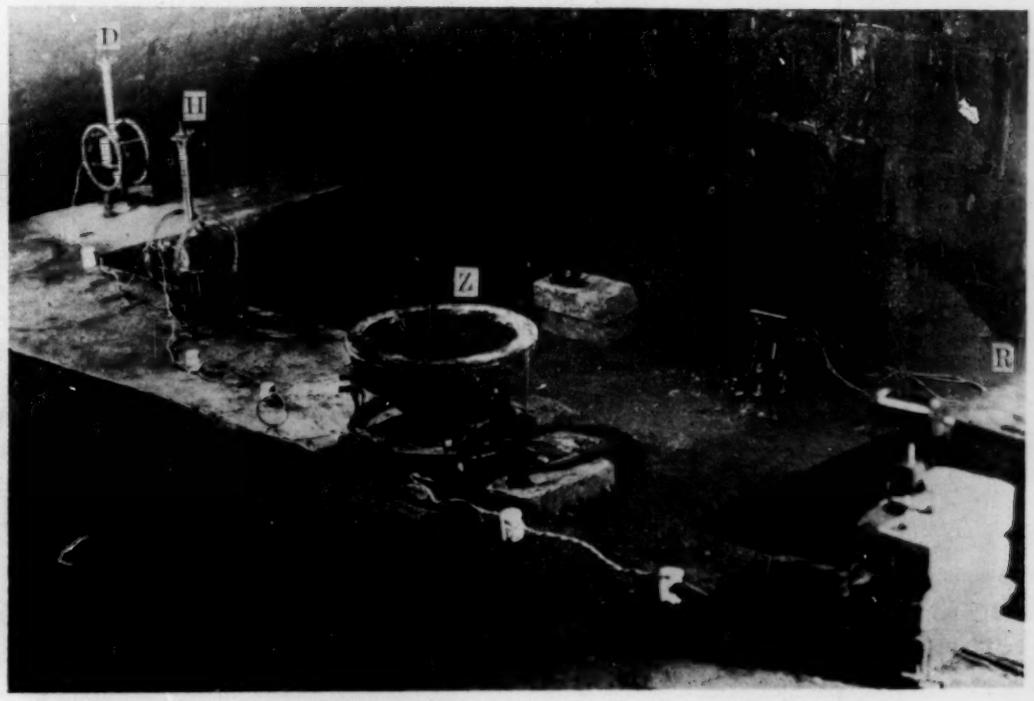

Plate I. The view in the magnetometer room.

H: Horizontal intensity variometer
D: Declination variometer
Z: Vertical intensity variometer
R: Recorder

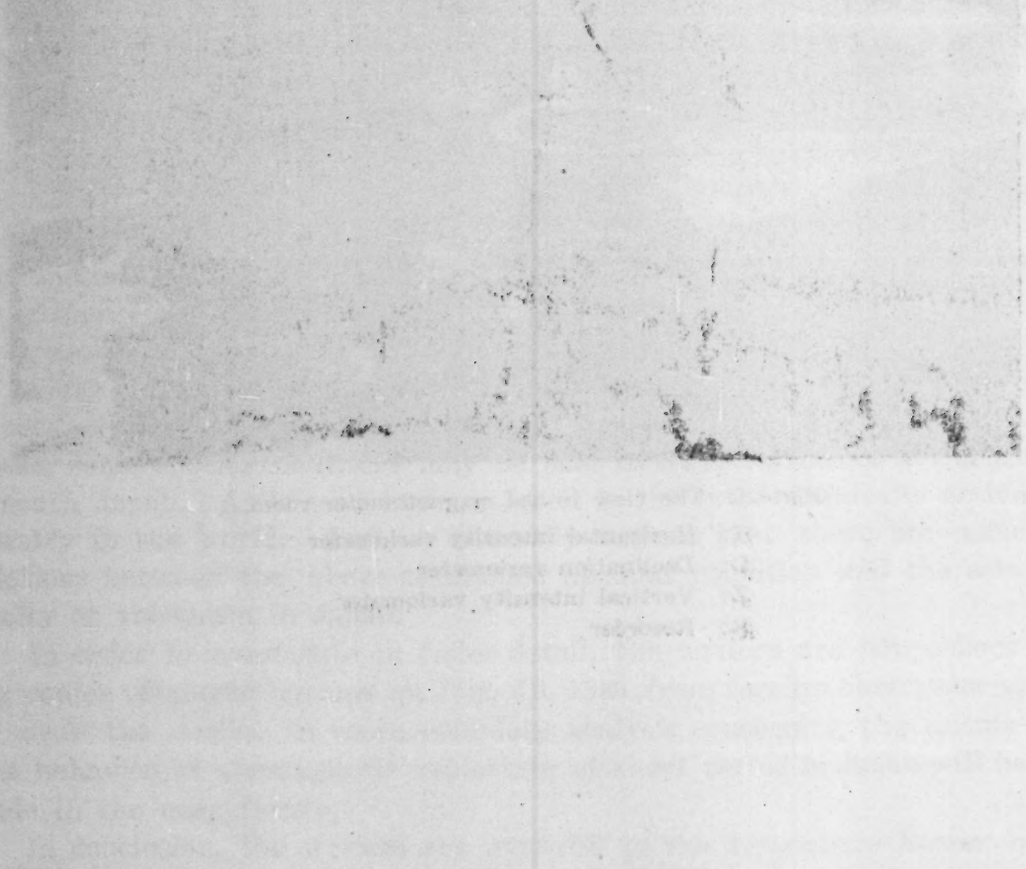

18. 日本に於ける地磁氣短周期變化の異常と地下構造 (序報)

地震研究所 { 力武常次 / 横山泉 / 菱山よね子

1951 年 9 月より神奈川縣油壺に於いて，地磁氣 3 成分の連續觀測が開始されたが，短周期變化に於いて水平分力と鉛直分力の著しい平行性が見出された．また鉛直分力の振幅がいちじるしく大きく水平分力の 60% に達する事實も見出された．このような事情はすでに柿岡に於ける地磁氣變化にも見られるところである．筆者等は電離層總合研究委員會の第 32 回協同觀測期間および 1936 年 6 月 19 日の日食時の地磁氣資料について檢討したところ，上記の短周期變化の異常は主として日本中部にのみ見られることを確認した．

この變化の分布を Fourier 級數の方法を用いて，地球内および外に原因をもつ部分にわける時は，その相互の關係は一樣な地球内への電磁感應として說明することは出來ず，日本の地下に異常な電氣傳導度の分布を考えなければならないことになつた．

19. *Reflections on the Tsunami of December 21, 1946.*

By Daisuke SHIMOZURU and Tetsuo AKIMA,

Earthquake Research Institute.

(Read Jan. 22, 1952.—Received June 20, 1952.)

1. Synopsis.

It is well known that, in the case of a tsunami, tide gauges show disturbances of sea surface for two days or more. These disturbances are not caused only by the waves which were propagated directly from the origin, but, with the exception of their initial part, also by such waves as are reflected from far distant continents or shallow water waves transmitted along the sea coast. They may include also secondary waves produced in the neighbourhood of tidal stations. The fact that the analysis of mareogram is far behind that of seismogram, is mainly due to the irregularities of the sea coast or to the great varieties of the boundary of reflection.

The authors have ascertained the existence of long-period waves in the tsunami which accompanied the Nankai Earthquake of 1946, and have detected a phase in them which seems to be due to the reflected waves from Guam Island.

2. Existence of Tsunami Waves having Long Periods.

The Nankai Earthquake of Dec. 21, 1946 (Origin time : 04 : 19. J.S.T. Epicentre: $\varphi=33°.0$ N, $\lambda=134°.8$ E, M=8.1[1]) inflicted much damage on the southern coast of Shikoku Island not only through the shock itself, but also through the accompanying tsunami.

Among the tide gauge records of this tsunami, those of Hachinohe, Mera, Itô and Uchiura were available. These records are shown in Fig. 1. They seem to have waves of long period superposed by the short period waves. At the oceanic trench or continental shelves, waves of large wave-length are more easily reflected and suffer less dissipation than waves of short wave-length. Therefore, the phases of reflection are, if there are any, more likely to be detected in the long period waves. In order to separate the waves of very long period from tide

1) H. KAWASUMI, *Bull. Earthq. Res. Inst.* **29** (1951), 481.

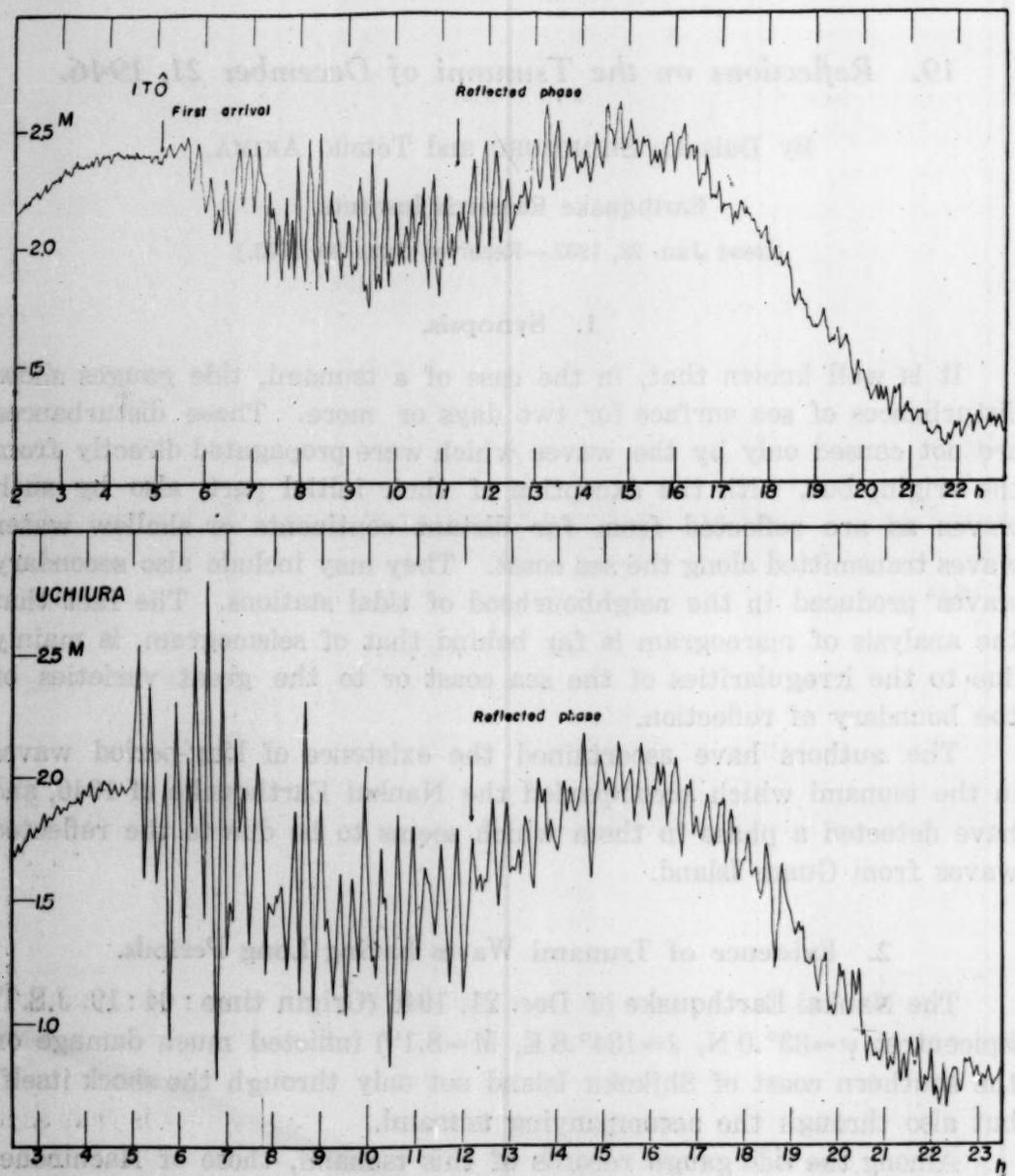

Fig. 1a.

and short period waves in the mareogram of four stations cited above, the tidal variation was at first eliminated by means of the tide curves predicted for the respective stations. Then by means of mechanical low-pass filter of torsion pendulum type[2], which was constructed by one of the authors for seismogram analyses, short period waves were taken away completely after repeating the filtration two or three times.

2) T. AKIMA, *Bull. Earthq. Res. Inst.* **30** (1952), 53.

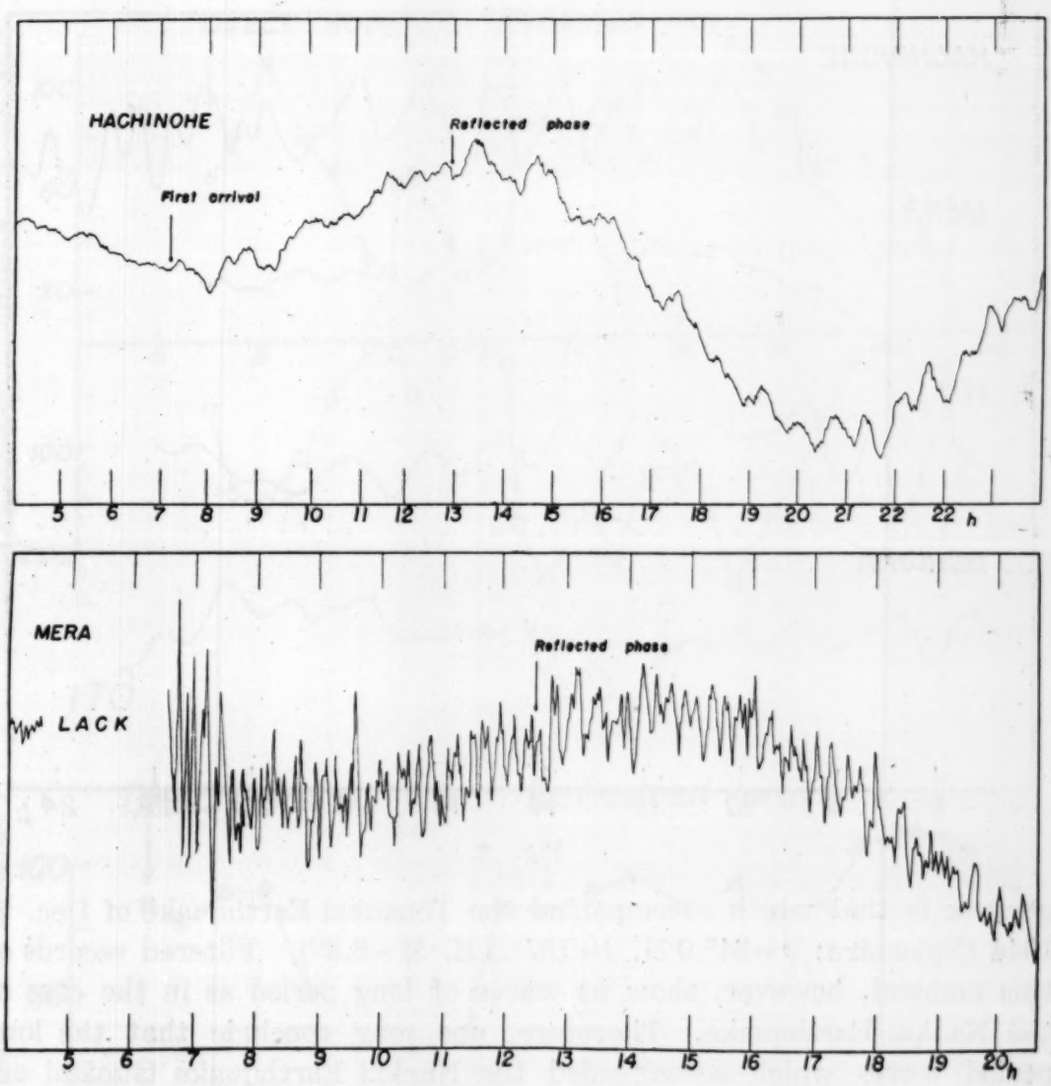

Fig. 1 b.

Fig. 2 shows the results of filtration. The obvious fact is that each record has waves of considerably long period, 80 minutes on the average, which appear as early as in the initial phase of the disturbances. A question is raised, however, whether these are propagated really from the origin or whether they are produced secondarily in the neighbourhood of the stations, i.e., in the bay in which the station lies, or at the continental shelves. To answer this question, an attempt was made to collate the records of two different tsunamis, of which the origins are near enough to each other so that the wave paths to a tidal station can be considered almost identical. The tsunami adopted here for this

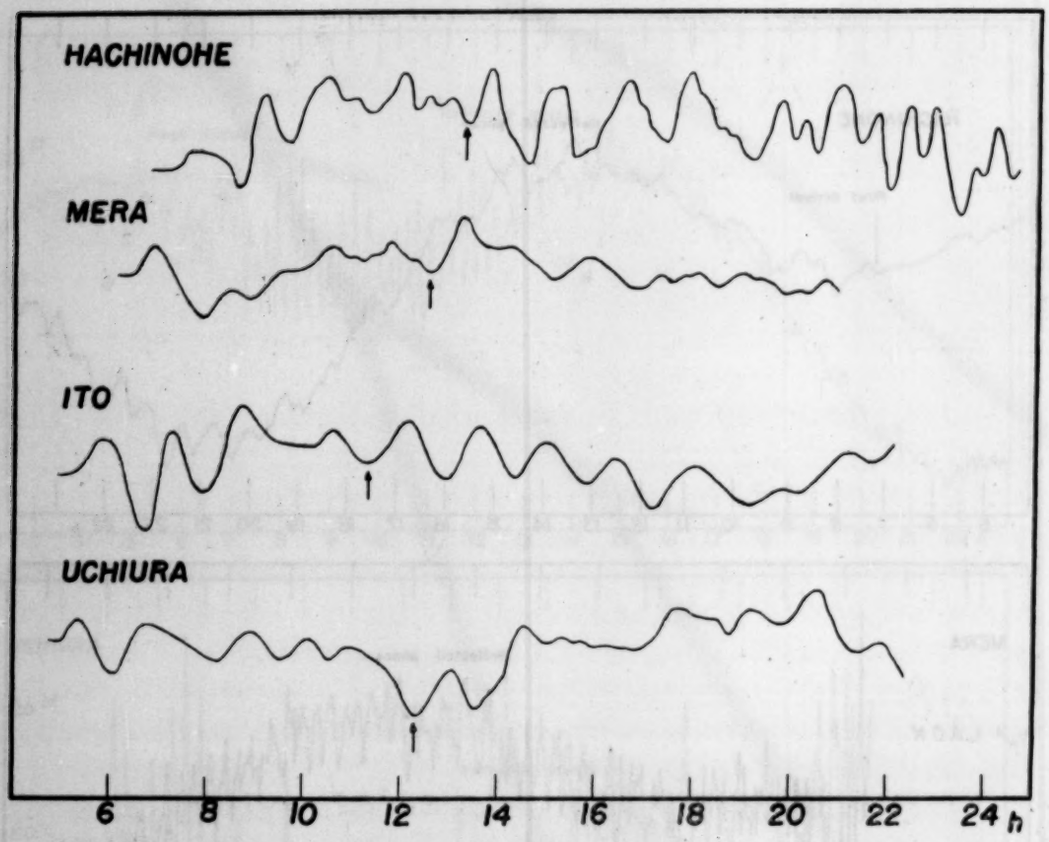

Fig. 2.

purpose is that which accompanied the Tônankai Earthquake of Dec. 7, 1944 (Epicentre: $\varphi=34°.0$ N, $\lambda=137°.1$ E, M=8.3[1]). Filtered records of this tsunami, however, show no waves of long period as in the case of the Nankai Earthquake. Therefore, one may conclude that the long period waves which accompanied the Nankai Earthquake tsunami are not of a local character, but generated at the origin of the tsunami.

3. On the Phase of Reflection.

The resemblance of the shape of filtered records shown in Fig. 2 is very conspicuous. Fig. 3. is the time-period and time-amplitude[2] curves for Itô and Hachinohe. The ordinates indicate the period of each wave (upward) and amplitude[2] (downward) respectively, while the abscissa is J.S.T. The wave periods were first measured from trough to trough and then, from crest to crest and so on. Usually near the origin of tsunami, the first wave is the largest of the train of disturbances, but at a considerable distance, it becomes smaller than the immediately succeeding waves.

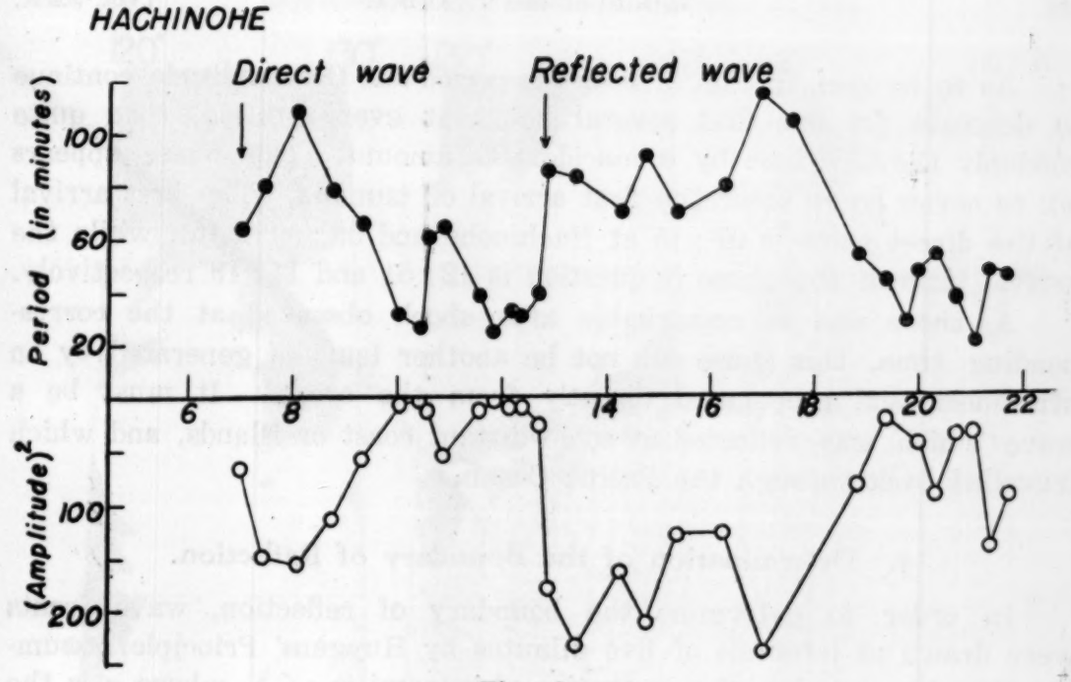
HACHINOHE
Direct wave
Reflected wave
Period (in minutes)
100
60
20
6
8
14
16
18
20
22
(Amplitude)²
100
200

Fig. 3a.

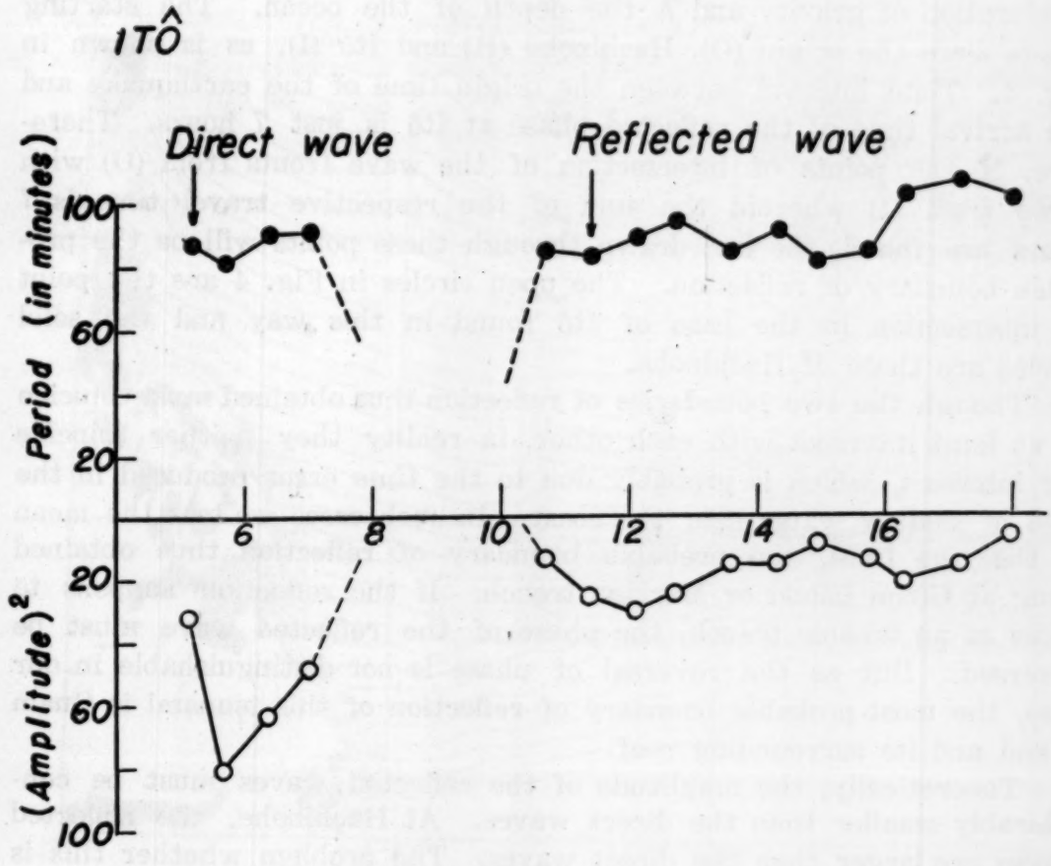
ITÔ
Direct wave
Reflected wave
Period (in minutes)
100
60
20
6
8
10
12
14
16
(Amplitude)²
20
60
100

Fig. 3b.

As to be seen in Fig. 3, both the period and the amplitude continue to decrease for the first several hours at every station, then quite suddenly they increase by a conciderable amount. This phase appears six or seven hours after the first arrival of tsunami. The first arrival of the direct wave is 07 : 15 at Hachinohe and 05 : 09 at Itô, while the arrival time of the phase in question is 12 : 51 and 11 : 19 respectively.

As there was no remarkable after-shock observed at the corresponding time, this phase can not be another tsunami generated by an aftershock and propagated directly from the origin. It must be a wave which was reflected at some distant coast or islands, and which travelled back through the Pacific Ocean.

4. Determination of the Boundary of Reflection.

In order to determine the boundary of reflection, wave fronts were drawn at intervals of five minutes by Huygens' Principle, assuming that the velocity of propagation of tsunami is $\sqrt{gh}$, where g is the accelaration of gravity and h the depth of the ocean. The starting points were the origin (O), Hachinohe (H) and Itô (I), as is shown in Fig. 4. Time interval between the origin time of the earthquake and the arrival time of the reflected phase at Itô is just 7 hours. Therefore, if the points of intersection of the wave fronts from (O) with those from (I) wherein the sum of the respective travel time is 7 hours are found, the line drawn through these points will be the probable boundary of reflection. The open circles in Fig. 4 are the point of intersection in the case of Itô found in this way and the solid circles are those of Hachinohe.

Though the two boundaries of reflection thus obtained must coincide or at least intersect with each other, in reality they neither coincide nor intersect, which is probably due to the time error produced in the area of shallow water near the coast. In such cases we took the mean of the two lines, the probable boundary of reflection thus obtained lying at Guam Island or Mariana trench. If the reflection happens to occur at an oceanic trench, the phase of the reflected wave must be reversed. But as the reversal of phase is not distinguishable in our case, the most probable boundary of reflection of this tsunami is Guam Island and its surrounding reef.

Theoretically, the amplitude of the reflected waves must be considerably smaller than the direct waves. At Hachinohe, the reflected waves are larger than the direct waves. The problem whether this is

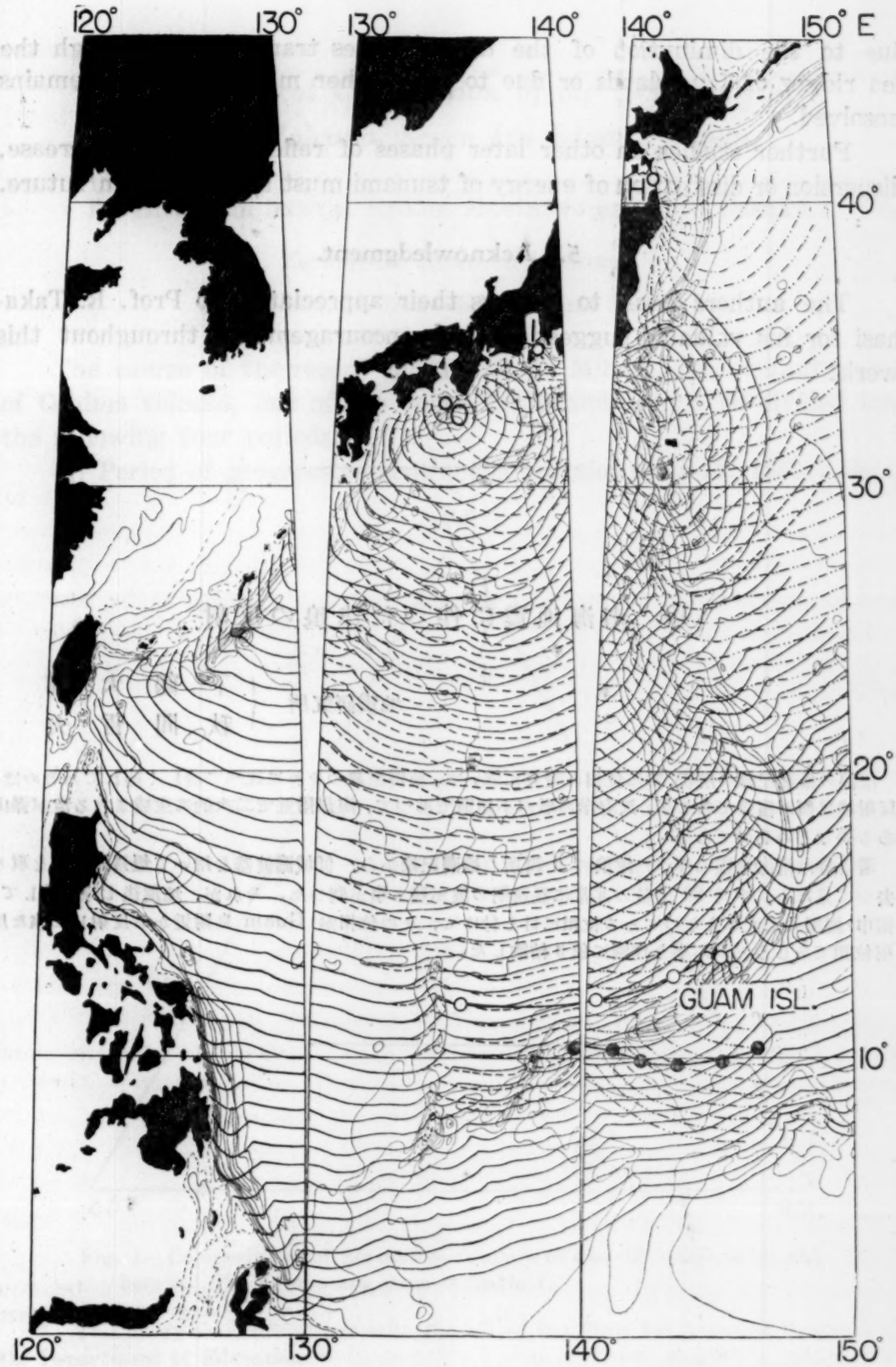

Fig. 4. Path of the tsunami waves of the Nankai Earthquake, Dec. 21, 1946.

due to the diminution of the direct waves transmitting through the sea ridges of Izu Islands or due to some other mechanism still remains unsolved.

Further studies on other later phases of reflection, period increase, dispersion or dissipation of energy of tsunami must be pursued in future.

5. Acknowledgment.

The authors wish to express their appreciation to Prof. R. Takahasi for his valuable suggestions and encouragements throughout this work.

---

19. 南海地震に伴つた津浪の反射

地震研究所 { 下鶴大輔 / 秋間哲夫 }

津浪の檢潮記錄の解析，特に位相の發見に就いて，地震記象のそれに比べて著しく遲れてゐるのは，反射境界面が複雜である事，又海岸の形が不規則であつて，海岸附近で二次的に生成される波が澤山ある事などの爲めである．

著者等は南海地震に伴つた津浪の 4 箇所の檢潮記錄から，低域濾波器を用いて短週期の波を取り去つて見たら，平均 80 分位の非常に長週期の波が殘る事が判つた．それが，地震後七時間位して，振巾・週期共に大きくなつてゐる位相に目を付けて，その位相が Guam 島附近から反射して來た反射位相であらうと云ふ事を作圖に依り結論した．

---

20. *Chemical Composition of the 1951-lavas of Oshima Volcano, Seven Izu Islands, Japan.**

By Hiromichi TSUYA, Ryōhei MORIMOTO and Joyo OSSAKA,

Earthquake Research Institute.

(Read March 18, 1952.—Received June 20, 1952.)

The course of the recent activity of Mt. Mihara, the summit crater of Oshima volcano, one of the Seven Izu Islands, may be divided into the following four periods:

(1) Period of progressive continuous eruption (July 16, 1950...Sept.

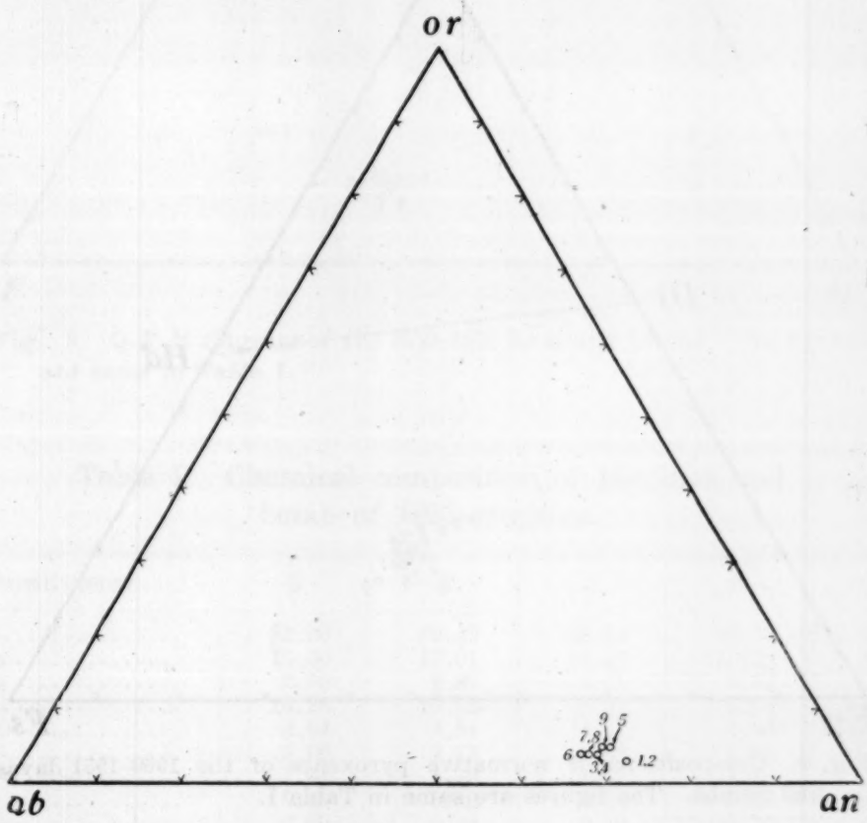

Fig. 1. Compositions of normative felspars of the 1950-1951 lavas and bombs. The figures are same in Table I.

* This study was carried out with the aid of the Fund for Scientific Research of the Department of Education,

23, 1950.), (2) period of climax of the continuous eruption of larger scale (Feb. 4, 1951...Apr. 1, 1951.), (3) period of intermittent eruption (Apr. 16–19, 20–21, 29, May 1, 3, 6–7, 1951.), and (4) period of explosive eruption (June 9–11, 14–15, 17–18, 19, 27, 1951.).

Petrographic features of the 1951-lavas are quite similar to those of the 1950-lavas which was described in the previous paper[1]. Fixed constituents of the lavas and the fragmental ejecta in 1950–1951 eruption are same during these changing phases of the activity[2]. The results of chemical analyses of the representative specimens of the 1951-lavas and bombs are shown in the following table and plotted in or-ab-an, wo-en-fs, and Q-F-M diagrams (Fig. 1–3).

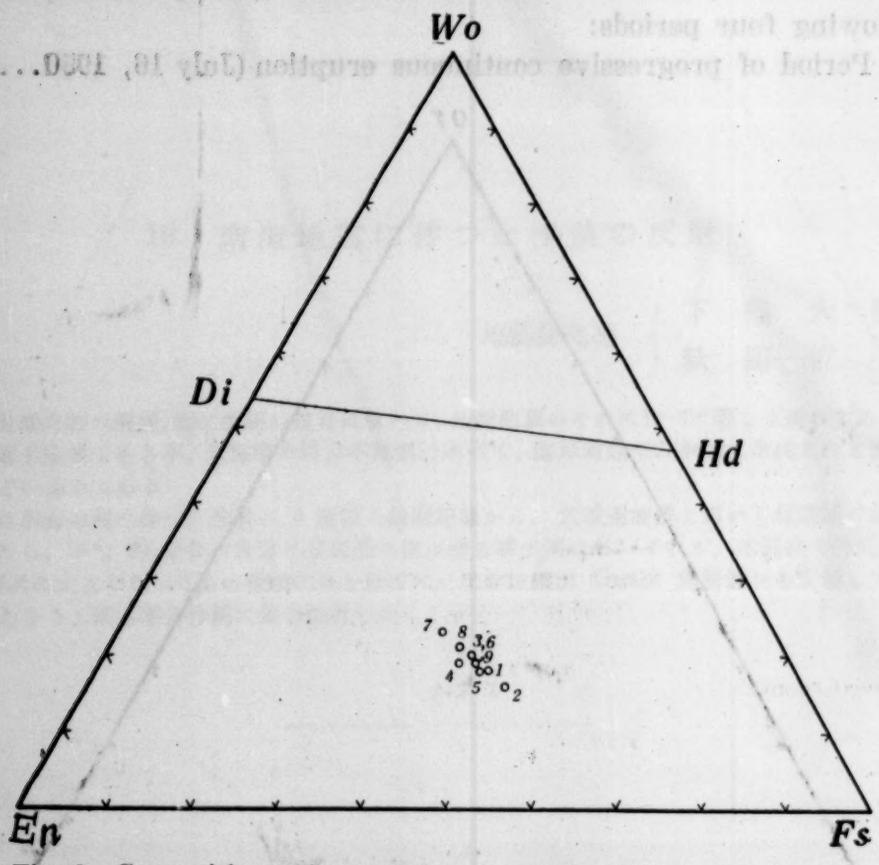

Fig. 2. Compositions of normative pyroxenes of the 1950-1951 lavas and bombs. The figures are same in Table I.

1) H. TSUYA and R. MORIMOTO, *Bull. Earthq. Res. Inst.*, **29** (1951), 563-570.
R. MORIMOTO and J. OSSAKA, *Jour. Geography*, **60** (1951), 136-140 (in Japanese).

2) The pigeonites separated by Dr. H. KUNO from the 1778-lava and from the 1950-lava were analyzed by one of the writers (J. O.). The groundmass pigeonites in both lavas are quite similar in its mean chemical compositions. The results of the analyses will be reported in the other day.

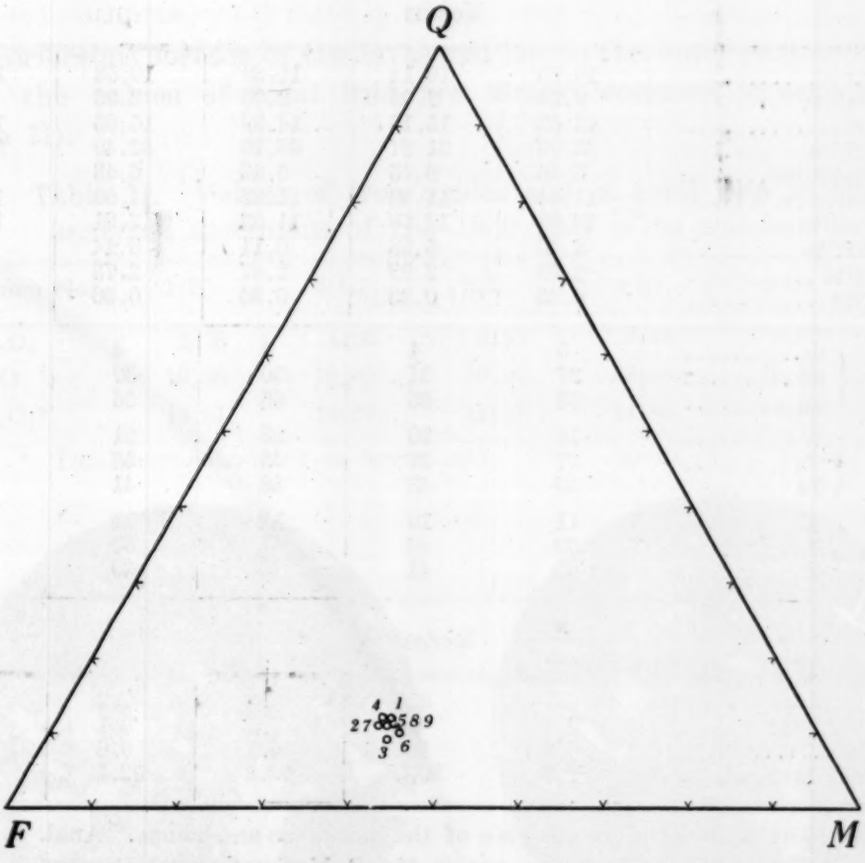

Fig. 3. Q-F-M diagram of the 1950-1951 lavas and bombs. The figures are same in Table I.

Table I. Chemical composition of the lava and bomb of 1951-eruption.

Constituents	5	6	7	8	9
SiO_2	52.30	52.43	52.24	52.34	52.44
Al_2O_3	15.50	15.01	15.41	15.21	15.44
Fe_2O_3	2.96	2.87	4.21	3.54	3.16
FeO	10.26	10.52	8.97	9.75	10.11
MgO	4.64	4.81	4.51	4.66	4.66
CaO	9.65	9.73	9.98	9.86	9.74
Na_2O	1.61	1.79	1.77	1.78	1.66
K_2O	0.33	0.35	0.34	0.35	0.33
H_2O+	0.70	0.28	0.42	0.35	0.59
H_2O-	0.21	0.08	0.11	0.10	0.17
TiO_2	1.49	1.57	1.30	1.44	1.47
P_2O_5	0.09	0.14	0.16	0.15	0.12
MnO	0.10	0.12	0.10	0.11	0.10
	99.84	99.70	99.52	99.64	99.99

Norms

Quartz	10.75	10.14	11.29	10.53	10.78
Orthoclase	2.23	2.06	2.00	2.06	1.95
Albite	13.63	15.15	14.99	15.05	14.05
Anorthite	33.93	31.87	33.10	32.49	33.71
Wollastonite	5.46	6.46	6.42	6.43	5.80
Enstatite	11.54	11.98	11.22	11.60	11.60
Ferrosilite	13.98	13.78	11.03	12.81	13.71
Magnetite	4.40	5.53	6.11	5.14	4.58
Ilmenite	2.88	2.99	2.47	2.73	2.79
Apatite	0.33	0.33	0.36	0.36	0.26
NF or	5	4	4	4	5
NF ab	27	31	30	30	28
NF an	68	65	66	66	67
NPy Wo	18	20	23	21	19
NPy En	37	37	39	38	37
NPy Fs	45	43	38	41	44
QFM Q	11	10	11	11	11
QFM F	50	49	51	50	50
QFM M	39	41	38	39	39

Modes*

Plagioclase	6.7	8.0	6.3	7.2	6.9
Hypersthene	0.4	tr.	0.2	0.1	0.3
Augite	0.2	1.1	0.1	0.6	0.4
Groundmass	92.6	90.9	93.4	92.1	92.4

5. Mean of four chemical analyses of the 1951-lavas and bombs. Anal. J. Ossaka. (Cf. H. Tsuya and R. Morimoto, *op. cit.* 564. R. Morimoto and J. Ossaka, *op. cit.* 137.)
6. The basalt solidified on March 22, 1951 at the front of lava flow approaching to the inner wall of the somma near Goshinkachaya (SO 51032201). The temperature and the viscosity of the lava were measured by Dr. Minakami and his collaborater (Cf. T. Minakami, *Bull. Earthq. Res. Inst.* **29**(1951), 487-498). The writers thank Mr. S. Ohya, a student of the Geological Institute of the university for his offer of the specimen. (Cf. Fig. 4 a-b.) Anal. J. Ossaka.
7. The bomb ejected on Kengamine June 14, 1951 (HT 51081601). Thin film of iron oxides coats the surface of the tabular ellipsoidal bomb. The result shows the mean composition of the bomb. Anal. J. Ossaka. (Cf. Fig. 5 a-b.) The writers owe much to Miss. F. Toraiwa for her assistance in chemical analyses of the rock.
8. Mean of 6 and 7.
9. Mean of 1, 2, 3, 4, 6, and 7. (Cf. Table I of the previous paper. H. Tsuya and R. Morimoto, *op. cit.* 564.)

* Percentage in volume.

As revealed in Table I, the chemical composition of these specimens are quite the same, within the experimental errors to be expected during the procedures of the silicate analyses, except for iron oxides. The values of ferrous iron oxide and of ferric iron oxide are different in each analyzed specimen; the latter is always high in bombs or in

the scoriaceous surface of the lavas and low in the inner part of the lavas; while the values of total iron are almost constant in each specimen (Table II).

Table II. Values of iron oxides and of total iron in the analyzed specimens of the 1950–1951 lavas and bombs.

Specimen Nos.	1(B)	2(L)	3(L)	4(B)	6(L)	7(B)
Fe_2O_3	2.78	2.28	2.92	3.84	2.87	4.21
FeO	10.56	10.80	10.22	99.46	10.52	8.97
Fe_2O_3*	14.51	14.28	14.27	14.35	14.56	14.18

* Total iron calculated as ferric oxide. (B)....bomb, (L)....lava.

a. Polarizer only b. With analyzer inserted

Fig. 4. Photomicrographs of the 1951-lava. (× ca. 40).

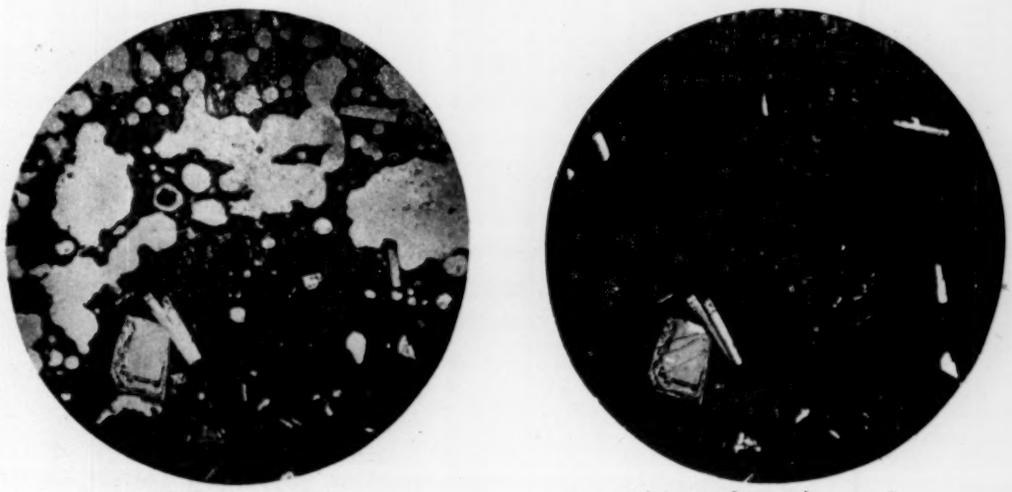

a. Polarizer only b. With analyzer inserted

Fig. 5. Photomicrographs of the 1951-bomb. (×ca. 40)

It may be allowed to say that the distribution areas of the small circles plotted on the diagrams (Fig. 1–3) will afford a clue finding out practically an appropriate diameter of circle, by which the results of bulk analyses of lavas of geological age may be expressed on some given diagrams.

---

20. 伊豆大島三原山 1951 年熔岩の化学成分

地震研究所 津屋弘達・森本良平・小坂丈予

伊豆大島三原山の 1951 年の活動中に噴出した熔岩及び火山彈の代表的な標本についての化學分析結果を，すでに報告した 1950 年噴出の熔岩及び火山彈の分析値とあわせて記載した．

---

21. On Dispersion Curves of Surface Waves from the Great Assam Earthquake of September 15, 1950.

By Tetsuo AKIMA,

Earthquake Research Institute.

(Read June 17, 1952.—Received June 20, 1952.)

1. Introduction.

Many authors have already studied the propagation of seismic surface waves[1]. The dispersion curves for Love-type or Rayleigh-type waves along various paths of propagation, such as the Pacific, the Atlantic, the Indian Oceans, or the continents of Eurasia and America etc., have separately been obtained by them. None has, however, succeeded in obtaining the dispersion curves of both Love and Rayleigh waves with respect to one and the same earthquake.

On September 15, 1950, a great earthquake took place in Assam district in India. The epicenter of the earthquake was located at $\lambda=28°.6\text{N}$, $\varphi=96°.5\text{E}$. The seismic waves of this earthquake were reported to have been well recorded by almost all the seismographs in the world. Records of the seismic waves of this earthquake were also obtained by Wiechert-type seismographs working at a number of Meteorological Observatories in Japan.

This great earthquake gave the writer a good opportunity to obtain both of these two dispersion curves. Since, as is seen in Fig. 1, the paths of seismic waves from the origin to the observatories in Japan have

1) For instance,
G. ANGENHEISTER, *Nachr. d. Kgl. Ges. d. Wiss. Gött., Heft* **1** (1906).
F. ROESENER, *Gerl. Beitr. Geophys.*, **12** (1913).
B. GUTENBERG, *Phys. Zeit.*, **25** (1924), 377.
T. MATUZAWA, *Bull. Earthq. Res. Inst.*, **6** (1929), 214.
P. BYERLY, *Gerl. Beitr. Geophys.*, **26** (1930).
W. ROHRBACH, *Zeit. für Geophys.*, **8** (1932), 113.
W. MÜHLEN, *Zeit. für Geophys.*, **8** (1932).
D. S. CARDER, *Bull. Seis. Soc. Amer.*, **24** (1934), 231.
J. T. WILSON, *Bull. Seis. Soc. Amer.*, **30** (1940), 273.
J. F. De LISTLE, *Bull. Seis. Soc. Amer.*, (1941), 303.
J. T. WILSON and O. BAYKAL, *Bull. Seis. Soc. Amer.*, (1948), 41.

almost E–W direction, Love and Rayleigh waves are expected to be separately recorded on seismograms of N–S and W–E or U–D components at each observatory respectively.

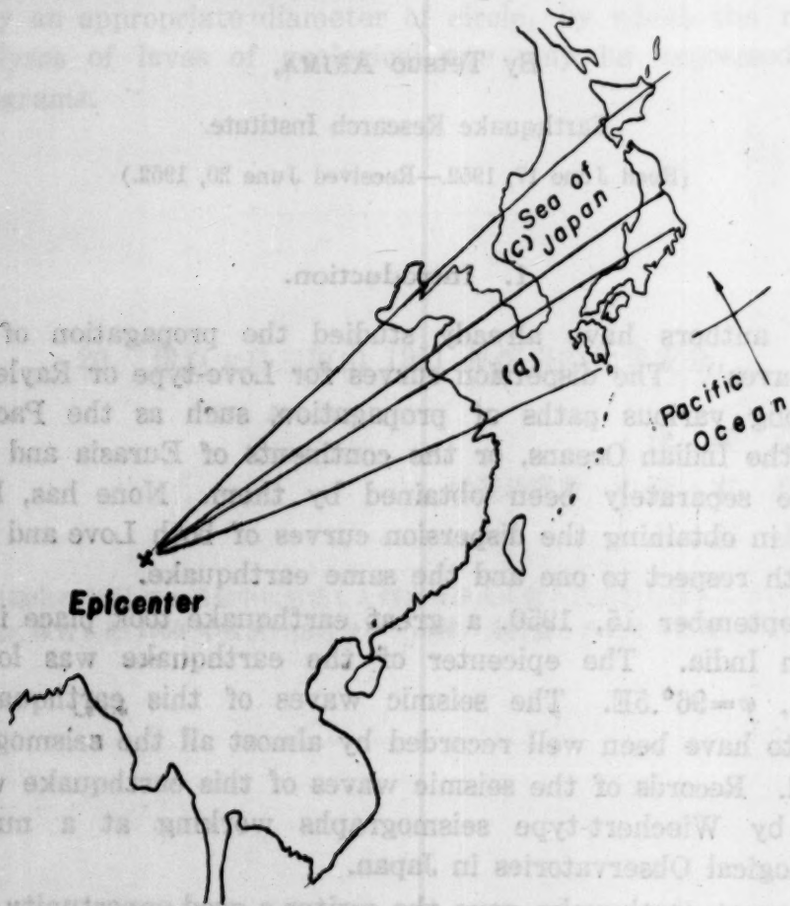

Fig. 1. The paths of wave propagation from the epicenter to the observatories in Japan.

2. Filtering of seismorgrams.

Short period waves recorded on seismograms make it pretty difficult to study the surface waves alone. Fig. 2 shows examples of such seismograms. Though a few series of long waves are recognizable on these seismograms, the onsets or the latter parts of the series are very obscure, being largely effaced by short period waves.

In order to observe clearly the long period waves involved in these seismograms by eliminating the short period waves, a torsion pendulum low-pass filter which was constructed by the writer was used[2]. Several

2) T. AKIMA, *Bull. Earthq. Res. Inst.*, **30** (1952), 53.

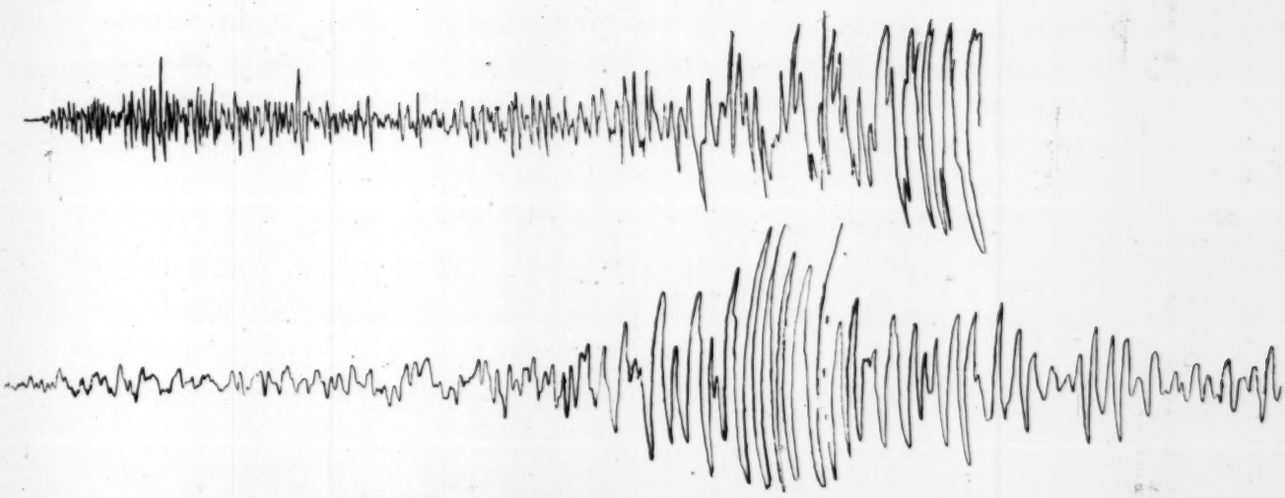

Fig. 2. Examples of seismograms.

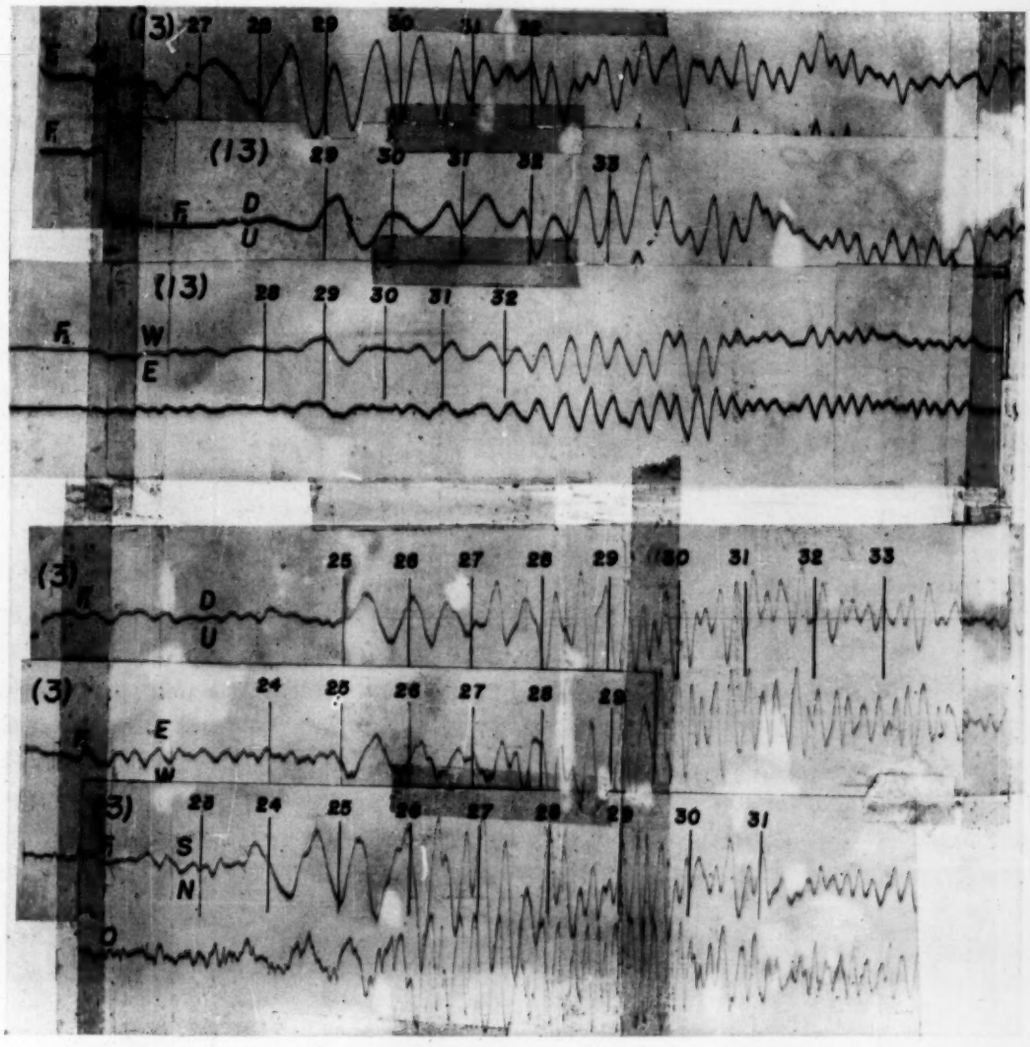

Fig. 3. Examples of the filtered record representing the separated Love and Rayleigh waves.

examples of the records after filtration are shown in Fig. 3, in which O, F_1, F_2 and F_3 denote the original, once-, twice- and thrice- filtered waves respectively. The times indicated in this figure are minutes in G.M.T.

3. Confirmations of Love and Rayleigh waves.

In these long period waves which remain after filtration, the arrival times and the periods of the first waves were measured at first. In measuring the arrival times of waves, the time lags of the motion of the torsion pendulum were of course taken into account and were reduced to the original times. The time intervals between the onset times and the times of the next occurrence of the same phases were taken as the periods of these waves. The results of readings are given in Table I. From this Table and Fig. 3, the arrival times of long period waves of E–W components are evidently almost the same as those of U–D

Table I.

	Δ in km	P	L			T_L			$\frac{T_{EW}}{T_{NS}}$	$\frac{T_{UP}}{T_{NS}}$
		(G.M.T.)	EW	NS	UD	EW	NS	UD		
1. Nagasaki	3220	h m s 14 15 27.3		m s 23 20			s 51			
2. Yakusima	3293	〃 34.5	m s 24 50	23 25	m s 24 55	s 46	52	s 46	0.89	0.89
3. Hukuoka	3280	〃 36.3	24 50	23 42	24 50	47	52.5	47	0.90	0.90
5. Ôita	3285	〃 47.1	25 41	24 12			54			
6. Simizu	3500	〃 56.4			26 17			42		
7. Hamada	3450	〃 48.9	25 25	24 05		50	53		0.94	
8. Kôti	3560	〃 48.2	25 30			49				
9. Sumoto	3700	16 08.9			26 30			50		
10. Ôsaka	3760	〃 13.5	26 25	24 25	26 42	48	55	54	0.87	0.98
11. Gihu	3865	〃 21.8	27 25	26 00		51	57		0.90	
12. Tôkyô	4080	〃 41.5		27 30	28 45		57	52		0.91
13. Tukubasan	4080	〃 43.8	28 30	27 25	28 50	57	56	52	1.02	0.93
14. Morioka	4275	〃 54.2	29 00	27 35	29 05	52	57	51	0.91	0.90
15. Sendai	4250	〃 49.1	29 00	27 30	29 05	51	60	52	0.85	0.87
16. Sapporo	4330	〃			28 25			53		
17. Nemuro	4670	17 20.5	31 30	29 05		50	58		0.86	

P: Arrival times of P waves.
L: Arrival times of surface waves in each component.
T_L: Periods of surface waves in each component.
T_{EW}/T_{NS}: Ratios of period of Rayleigh and Love waves in E-W and N-S component.

components, while they are considerably later than those of N–S components. This fact suggests that the long waves which are seen in the filtered records of N–S and E–W or U–D components correspond to Love and Rayleigh waves respectively. In order to make sure of this supposition, the dispersive character of these long period waves was investigated. The arrival times and periods of the waves which followed were measured on each filtered record. The method of measuring is illustrated schematically in Fig. 4, in which the times of a_1, b_1, a_2, b_2, etc. were taken as the arrival times of waves with the periods corresponding to the time differences of a_2-a_1, b_2-b_1, a_3-a_2, b_3-b_2, etc. respectively.

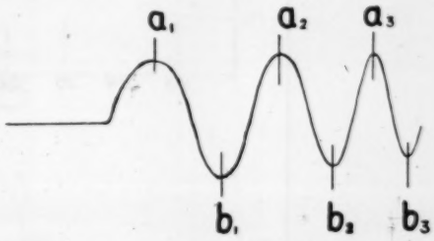

Fig. 4.

Figs. 5–a, –b, –c represent the relations between the periods and the arrival times of the filtered long waves in each component. The numbers given on both ends of each curve indicate the position numbers of the observatories whereby the curves were obtained. (cf. Fig. 8). Though the examples given here are limited in number, they clearly show the dispersive character of the waves; i. e. the longer period waves have greater velocities. In these figures, it can be seen that some points, marked by hollow circles, do not lie on the smooth trend of the curves. The discussion for these points will be given later.

The orbits of the ground motions due to the long period waves recorded as E–W and U–D components at each observational position were next calculated in order to see whether the waves appeared in these components are Rayleigh-type waves or not. Fig. 6 shows the results for the observatories Nos. 2, 3, 10, 13, 14 and 15. The double-feathered arrows show the directions of wave propagation and the numbers given on each curve denote the times in minutes reckoned from the beginings of the long period waves. Except for the earlier part of the orbit at the station No. 10 (Ôsaka), all show the retrograde nature of the motions, which makes it certain that the filtered long period waves on E–W and U–D components are Rayleigh waves.

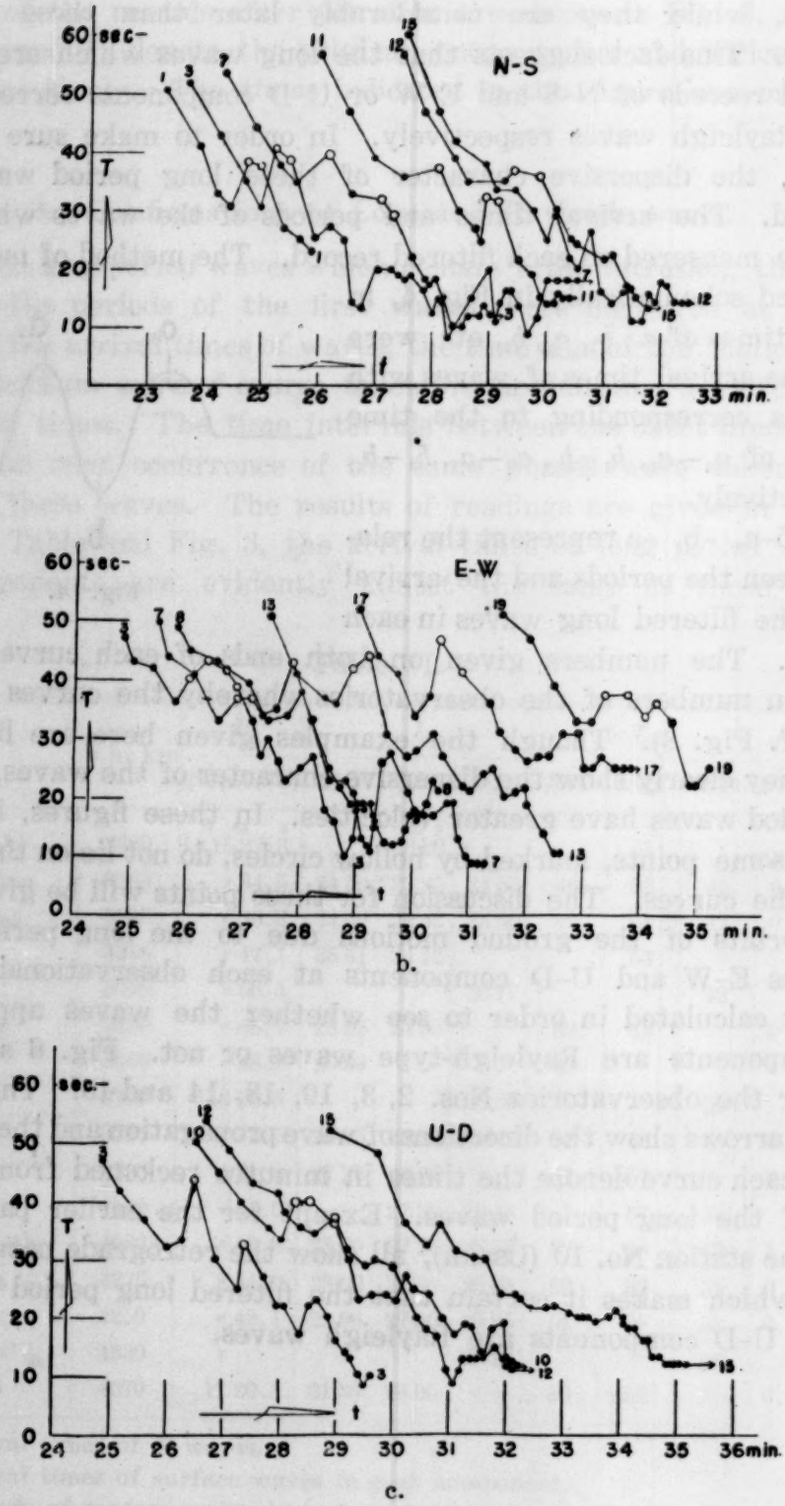

b.

c.

Fig. 5. Relations between the arrival times and the periods of the filtered waves. a. N-S, b. E-W, c. U-D

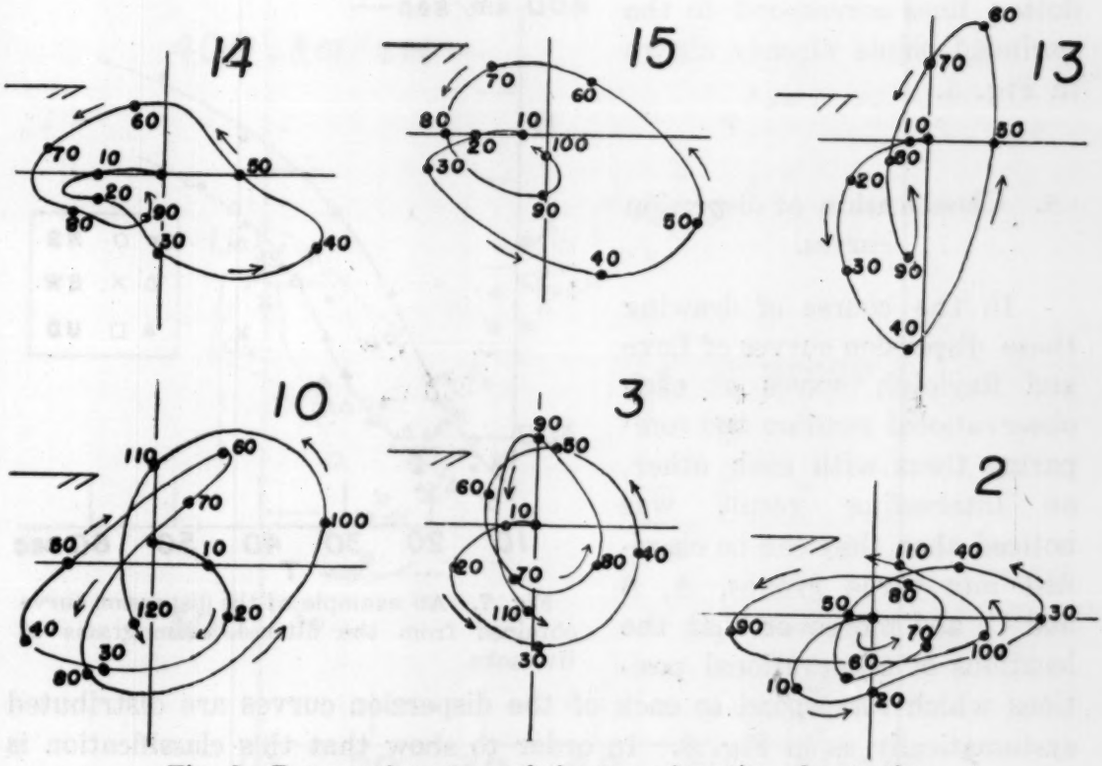

Fig. 6. Retrograde nature of the ground motions due to the filtered long period waves.

4. Dispersion curves.

Owing to the favourable positions of observatories in Japan with respect to the direction of wave propagation of this great earthquake and with the aid of the torsion pendulum low-pass filter, two kinds of surface waves, Love and Rayleigh waves, have clearly appeared on the filtered records of N–S and E–W or U–D components separately. The dispersion curves of these two kinds of surface waves could be obtained from the filtered records at each observatory.

The velocities of successive waves were calculated according to $\Delta/(t_{ai}-t_0)$, or $\Delta/(t_{bj}-t_0)$, $(i, j=0, 1, 2, 3, \ldots)$ where t_{ai} and t_{bj} are the times of a_i and b_j as shown in Fig. 4 and t_0, Δ are the origin times and travel distances from the epicenter to each observational position measured along the great circles. The velocities thus obtained are the group velocities. An example of the dispersion curve is shown in Fig. 7, in which the upper and the lower curves correspond to the dispersion curves concerning the group velocities of Love and Rayleigh waves respectively. In this figure, several points enclosed by

dotted lines correspond to the excluded points already shown in Fig. 5.

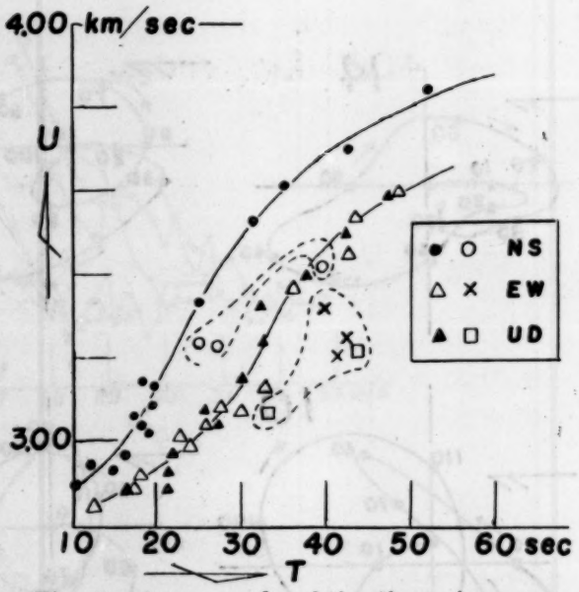

Fig. 7. An example of the dispersion curve obtained from the filtered seismograms of Hukuoka.

5. Classification of dispersion curves.

In the course of drawing these dispersion curves of Love and Rayleigh waves at each observational position and comparing them with each other, an interesting result was noticed that they can be classified into three groups, A, B and C, and moreover that the locations of observational positions which correspond to each of the dispersion curves are distributed systematically as in Fig. 8. In order to show that this classification is

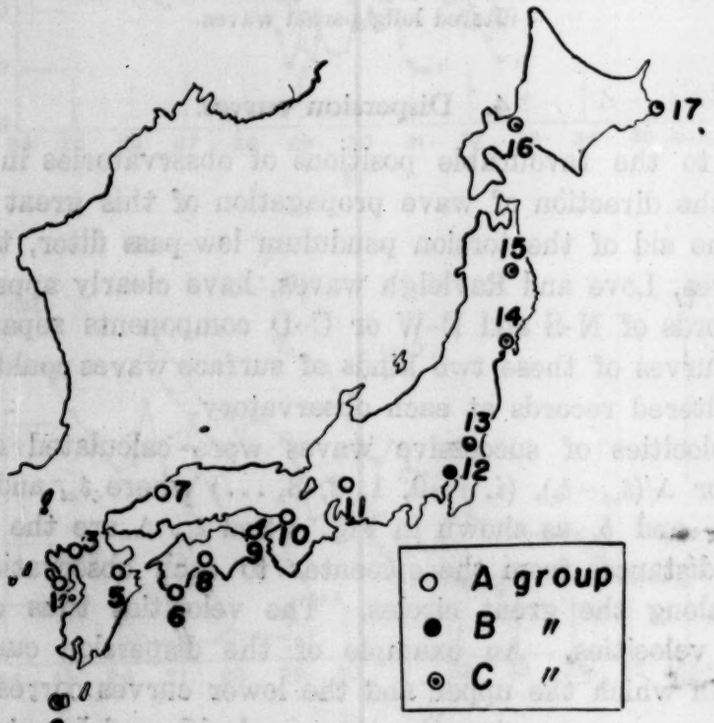

Fig. 8. The distribution of the observatories of three groups.

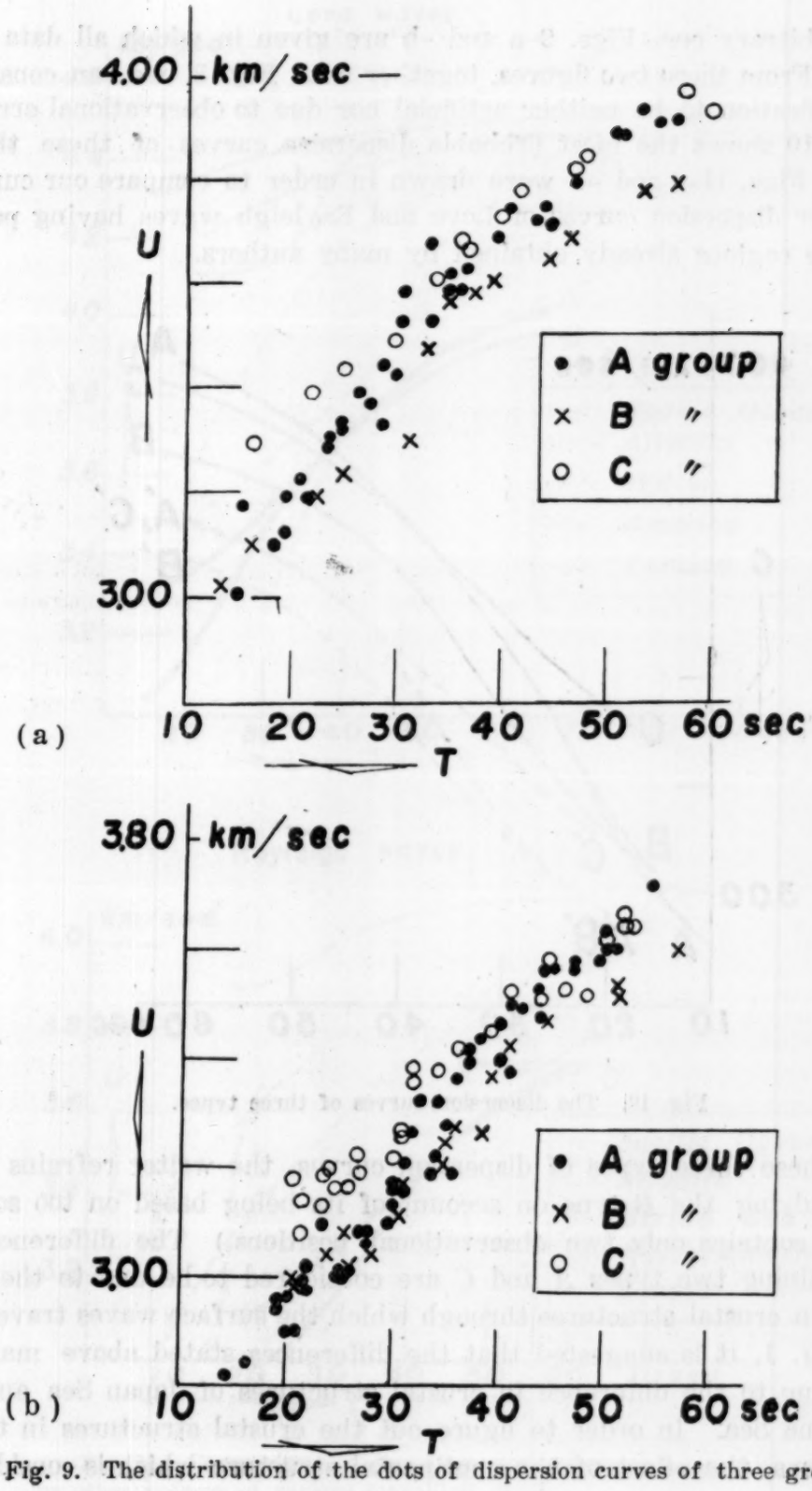

Fig. 9. The distribution of the dots of dispersion curves of three groups.

not an arbitrary one, Figs. 9-a and -b are given in which all data are plotted. From these two figures, together with Fig. 8, we can consider the classification to be neither artificial nor due to observational errors.

Fig. 10 shows the most probable dispersion curves of these three types and Figs. 11-a and -b were drawn in order to compare our curves with other dispersion curves of Love and Rayleigh waves having paths of various regions already obtained by many authors.

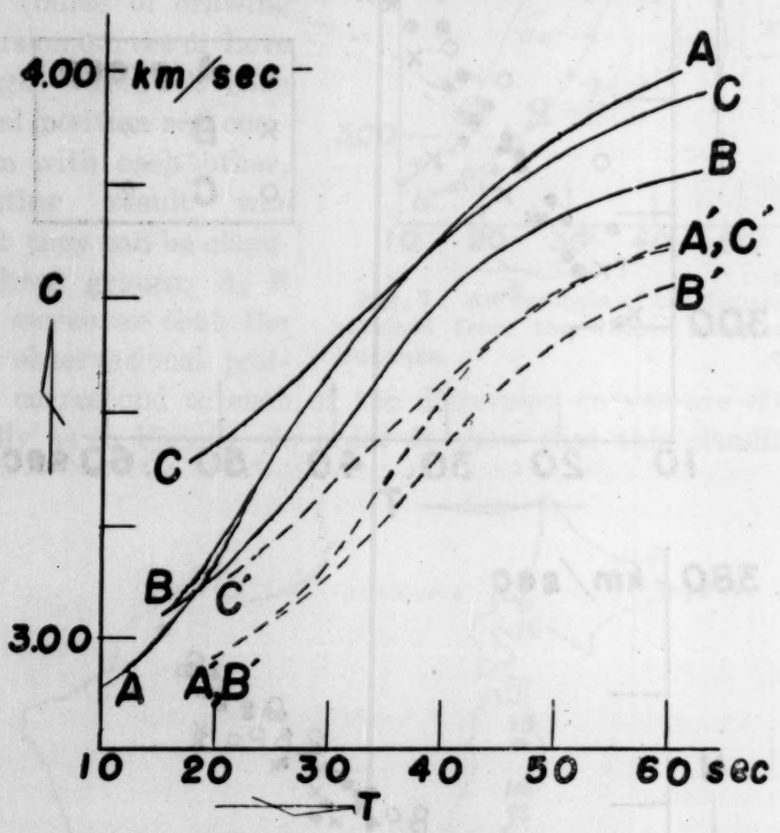

Fig. 10. The dispersion curves of three types.

Of these three types of dispersion curves, the writer refrains here from studying the *B* type on account of its being based on too scarce data. (It contains only two observational positions.) The difference of the remaining two types *A* and *C* are considered to be due to the difference in crustal structures through which the surface waves travelled. From Fig. 1, it is suggested that the differences stated above may be mainly due to the difference in crustal structures of Japan Sea and of East China Sea. In order to figure out the crustal structures in these two regions, the effect of the continental structure which is considered

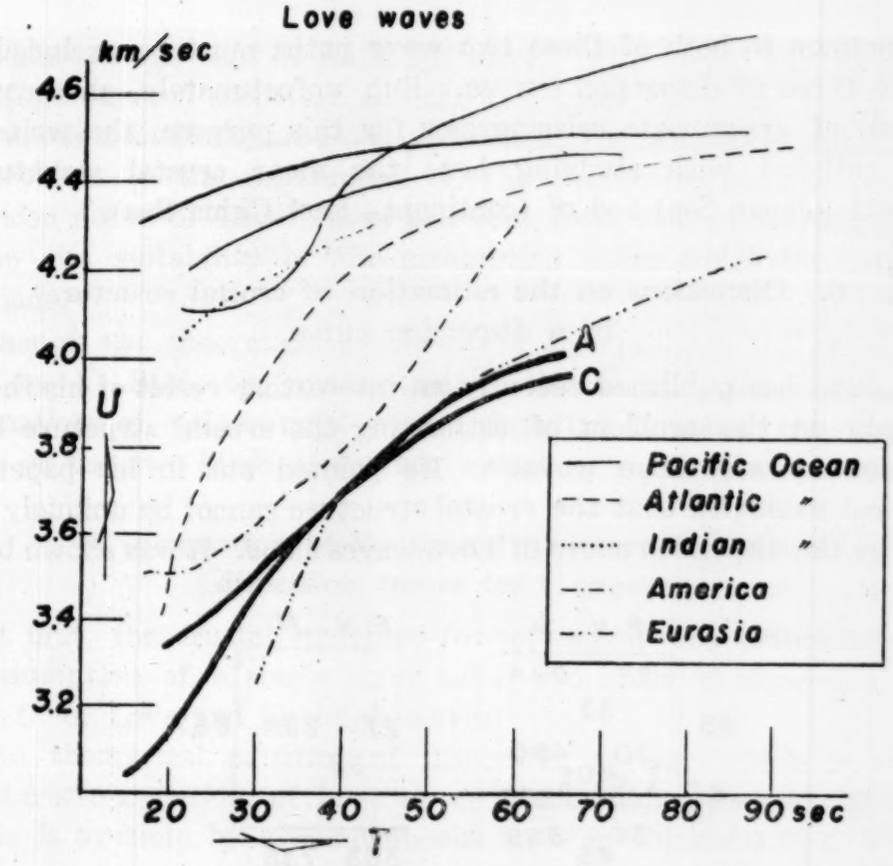

a.

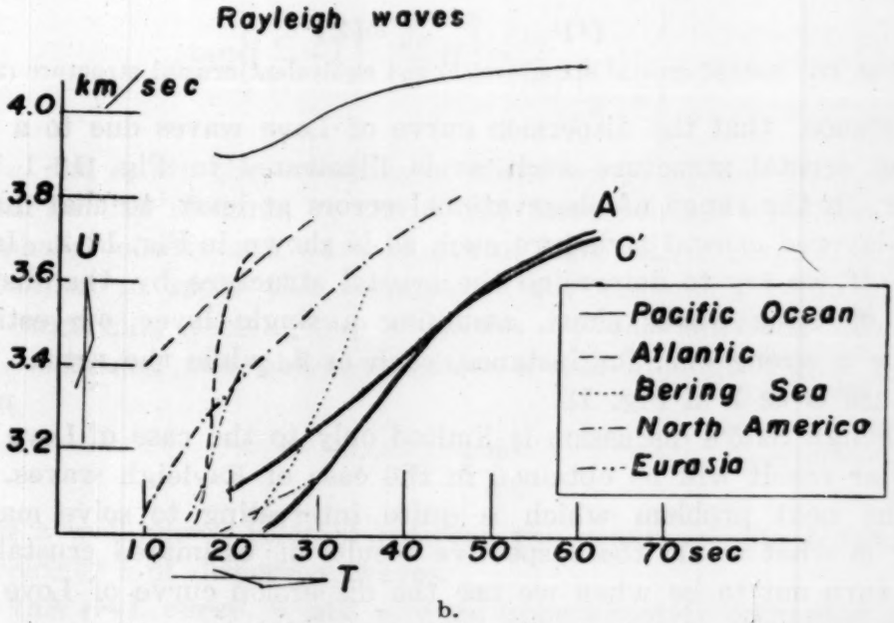

b.

Fig. 11. Comparison of the dispersion curves obtained with those by other authors of various travelling paths.

to be common to both of these two wave paths must be excluded from our two types of dispersion curves. But, unfortunately, on account of the lack of appropriate seismograms for this purpose, the writer had to be satisfied with studying here the mean crustal structure of (continent+Japan Sea) and of (continent+East China Sea).

6. Discussions on the estimation of crustal structure by a dispersion curve.

Y. Satô has published recently an interesting result of his theoretical study on the problem of estimating the crustal structure by the dispersion curve of Love waves[3]. He pointed out in his paper with numerical examples that the crustal structure cannot be uniquely determined by the dispersion curve of Love waves alone. It was shown by him,

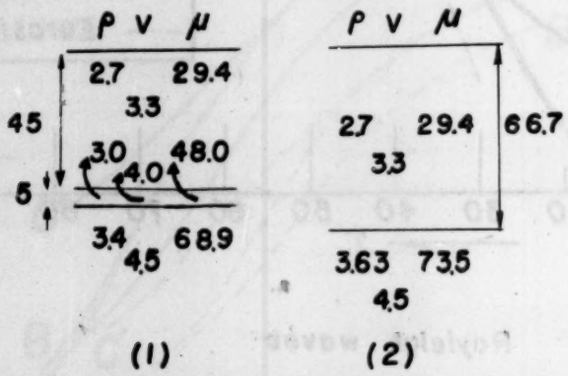

Fig. 12. Actual crustal structure (1) and equivalent crustal structure (2).

for instance, that the dispersion curve of Love waves due to a doubly layered crustal structure such as is illustrated in Fig. 12–1 is very similar, in the range of observational errors at least, to that due to a single-layered crustal structure such as is shown in Fig. 12–2. In other words, if we try to determine the crustal structure by the dispersion curve of Love waves alone, assuming a single layer, our estimation may be a wrong one, for instance, such as 2, while the actual crustal structure is as 1 in Fig. 12.

Though Satô's discussion is limited only to the case of Love waves, a similar result will be obtained in the case of Rayleigh waves.

The next problem which is quite interesting to solve mathematically is what would the respective results of estimated crustal structures turn out to be when we use the dispersion curve of Love waves

3) Y. SATÔ, *Bull. Earthq. Res. Inst.*, **29** (1951), 519.

and when we use that of Rayleigh waves both under the assumption of a single-layered structure for the two cases when the actual crustal structure is a single-layered one and when it is not; or in other words, the problem if the agreement of the respective results from the dispersion curve of Love waves and that from that of Rayleigh waves confirm the suitability of the assumption under which the estimation was made.

Though the theoretical conclusion of this problem will presently be given by Y. Satô, the writer would like to give the results of his examinations of estimating a crustal structure by using the dispersion curves of the two kinds of surface waves.

7. Estimation of the crustal structures using two dispersion curves for C groups.

At first, the crustal structure for (*c*) region was estimated under the assumption of a single layer using two kinds of dispersion curves C and C' of Love and Rayleigh waves.

The theoretical equation of dispersion curves, which is called a characteristic equation, of Love waves when a homogeneous semi-infinite medium is overlain by a homogeneous layer of thickness H is given as follows:

$$\tan\left\{\left(\frac{c^2}{v_1^2}-1\right)^{1/2}\frac{2\pi}{L}H\right\}=\frac{\mu_2}{\mu_1}\frac{\left(1-\frac{c^2}{v_2^2}\right)^{1/2}}{\left(\frac{c^2}{v_1^2}-1\right)^{1/2}} \quad \cdots\cdots\cdots (1),$$

where v_1 and v_2 are the velocities of shear waves in the layer and in the semi-infinite medium, μ_1 and μ_2 the corresponding rigidities, c and L the phase velocity and wave length of Love waves respectively.

In order to apply this formula to our dispersion curve of Love waves concerning their group velocities U, the observed dispersion curve concerning the phase velocities c was at first drawn by the formula

$$U=c-L\frac{dc}{dL}$$

which is a well-known relation between the group velocity U and the phase velocity c of dispersive waves.

By this $c\sim L$ curve, v_1 and v_2 were approximately estimated as 3.4 km/sec and 4.2 km/sec respectively as are seen from the trends of the

curves in Fig. 13. Then, a suitable pair of two parameters μ_2/μ_1 and H, by which the numerical relations between c and L obtained from the equation (1) agree with the observed curve of $c\sim L$, can be obtained from the same equation. Practically, however, not only one but a few suitable pairs of μ_2/μ_1, and H are found. In our case, (1.6, 25 km); (1.8, 26 km); (1.9, 27 km) all seemed to be suitable for observational curve within observational errors at least. (See Table II).

Table II.

C	($\mu_2/\mu_1=1.6$, $H=24$ km)		($\mu_2/\mu_1=1.8$, $H=26$ km)		($\mu_2/\mu_1=1.9$, $H=27$ km)	
	L/H	L	L/H	L	L/H	L
4.1 km/sec	10.0	240 km	9.08	236 km	8.67	234.0 km
4.0 〃	5.76	138 〃	5.31	138 〃	5.12	139.0 〃
3.9 〃	4.35	105 〃	4.07	106 〃	3.96	107.0 〃
3.8 〃	3.30	79 〃	3.10	81 〃	3.05	82.5 〃
3.7 〃	2.54	61 〃	2.42	63 〃	2.38	64.4 〃
3.5 〃	1.18	28 〃	1.16	32 〃	1.15	31.0 〃

On the other hand, the same estimation can be done using the dispersion curve of Rayleigh waves with the same single-layered assumption.

The characteristic equation in this case is somewhat cumbersome, being as follows:

$$\begin{vmatrix}
-\frac{f^2-s_2^2}{k_1^2}Y_2, & 2\frac{\mu_2}{\mu_1}\frac{ifs_2}{k_2^2}Y_1, & 0, & -2\frac{\mu_2}{\mu_1}\frac{ifs_2}{k_2^2}, & 0, & \frac{s_2 f}{k_2^2} \\
-\frac{f^2-s_2^2}{k_2^2}Y_1, & -2\frac{\mu_2}{\mu_1}\frac{ifs_2}{k_2^2}Y_2, & \frac{\mu_2}{\mu_1}\frac{f^2-s_2^2}{k_2^2}, & 0, & -\frac{if_1^2}{k_2^2}, & 0 \\
2\frac{ifr_2}{h_2^2}X_1, & \left(2\frac{\mu_2}{\mu_1}\frac{r_2^2}{h_1^2}-\frac{\lambda_2}{\mu_1}\right)X_2, & -\frac{\mu_2}{\mu_1}\frac{2ifr_2}{h_2^2}, & 0, & \frac{r_2 f}{k_2^2}, & 0 \\
2\frac{ifr_2}{h_2^2}X_2, & \left(2\frac{\mu_2}{\mu_1}\frac{r_2^2}{h_2^2}-\frac{\lambda_2}{\mu_1}\right)X_1, & 0, & \frac{\lambda_2}{\mu_1}-2\frac{\mu_2}{\mu_1}\frac{r_2^2}{h_2^2}, & 0, & -\frac{if^2}{h_2^2} \\
0, & 0, & -\frac{f^2+s_1^2}{k_1^2}, & 2\frac{ifs_1}{k_1^2}, & \frac{if^2}{k_1^2}, & -\frac{sf^2}{k_1^2} \\
0, & 0, & \frac{2ifr_1}{h_1^2}, & 2\frac{r_1^2}{h_1^2}-\frac{\lambda_1}{\mu_1}, & -\frac{r_1 f}{h_1^2}, & \frac{if^2}{h_1^2}
\end{vmatrix} = 0 \quad (2),$$

where $r^2=f^2-h^2$, $s^2=f^2-k^2$, $h^2=\rho p^2/(\lambda+2\mu)$, $k^2=\rho p^2/\mu$, in which

λ, μ, ρ= Lamés elastic constant and density,

$p=2\pi/T$,
$f=2\pi/L$,
T, L=period and wave length of Rayleigh waves,

and $X_1=\cosh r_1H$, $X_2=\sinh r_2H$, $Y_1=\cos s_2H$, $Y_2=\sin s_2H$. Suffix 1, 2, except those of X and Y, correspond to that of superficial layer and of semi-infinite medium respectively[4].

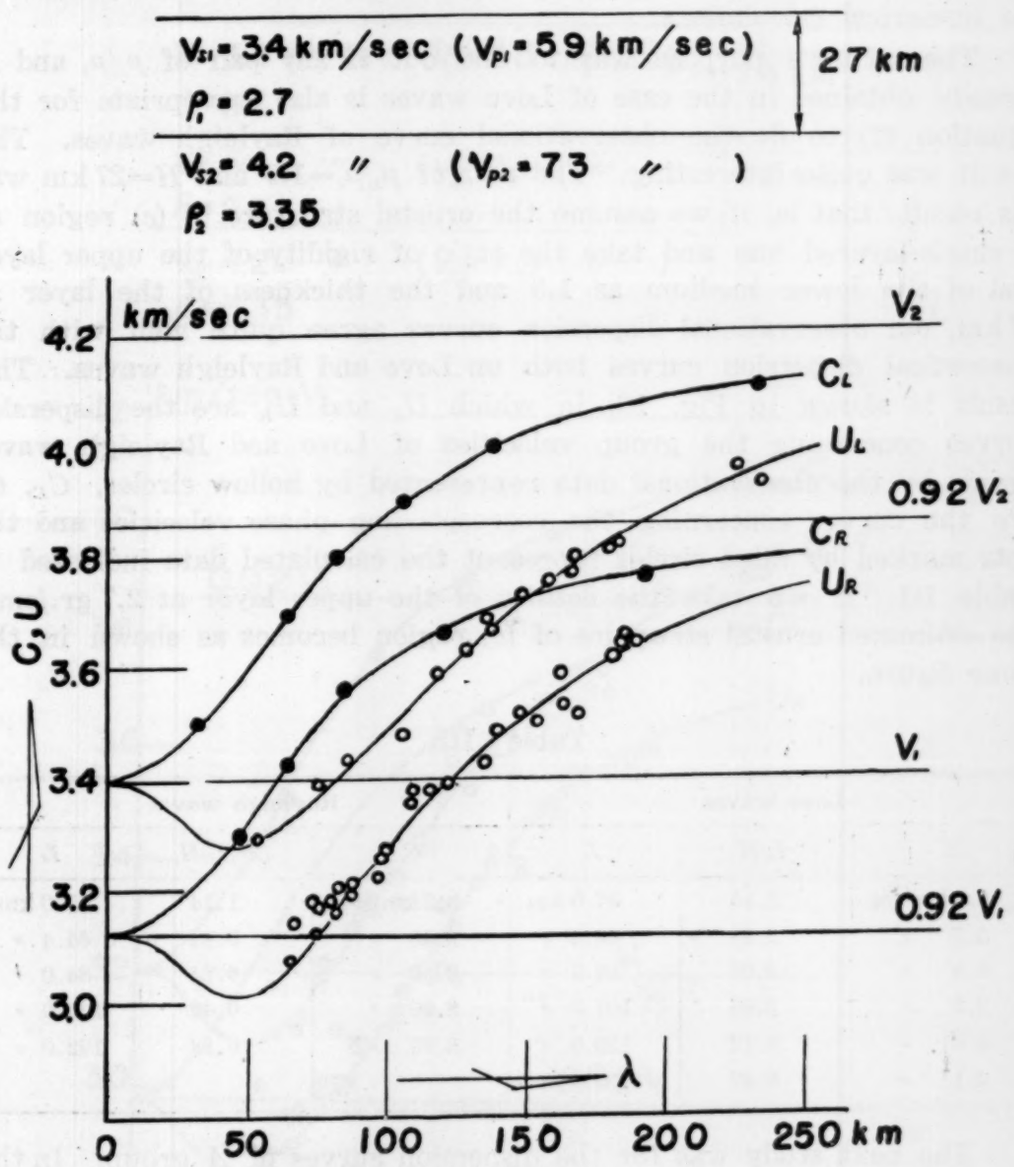

Fig. 13. The estimated crustal structure of (c) ragion and the results of theoretical calculations (filled circle).

4) K. SEZAWA. *Bull. Earthq. Res. Inst.*, **3** (1927), 1.

Putting $\lambda_1=\mu_1$, $\lambda_2=\mu_2$ and substituting u (the velocity of P-waves) and v (the velocity of S-waves) for λs considering that $u^2=(\lambda+2\mu)/\rho$, $v^2=\mu/\rho$, the theoretical curves between the phase velocity c and the wave length L of Rayleigh waves can be obtained with parameters μ_2/μ_1 and H from the equation (2). The practical calculations were performed transforming the equation (2) into a form more convenient for numerical calculations.

The writer's purpose was to find out if any pair of μ_2/μ_1 and H already obtained in the case of Love waves is also appropriate for the equation (2) to fit the observational curve of Rayleigh waves. The result was quite interesting. The pair of $\mu_2/\mu_1=1.9$ and $H=27$ km was his result, that is, if we assume the crustal structure of (*c*) region as a single-layered one and take the ratio of rigidity of the upper layer and of the lower medium as 1.9 and the thickness of the layer as 27 km, our observational dispersion curves agree quite well with the theoretical dispersion curves both on Love and Rayleigh waves. This result is shown in Fig. 13, in which U_L and U_R are the dispersion curves concerning the group velocities of Love and Rayleigh waves drawn by the observational data represented by hollow circles, C_L, C_R are the curves concerning the corresponding phase velocities and the dots marked by filled circles represent the calculated data indicated in Table III. If we take the density of the upper layer at 2.7 gr./cm^3, the estimated crustal structure of (*c*) region becomes as shown in the same figure.

Table III.

Love waves			Rayleigh waves		
C	L/H	L	C	$(2\pi/L)H$	L
3.5 km/sec	1.15	47.0 km	3.3 km/sec	1.14	47.0 km
3.7 〃	2.38	64.4 〃	3.43 〃	0.84	64.4 〃
3.8 〃	3.05	82.5 〃	3.56 〃	0.64	84.0 〃
3.9 〃	3.96	107.0 〃	3.66 〃	0.45	120.0 〃
4.0 〃	5.12	139.0 〃	3.76 〃	0.28	192.0 〃
4.1 〃	8.67	234.0 〃			

The next study was for the dispersion curves of *A* group. In this case, the velocities of shear waves in the upper layer and in the lower medium were approximately estimated at 3.2 km/sec and 4.2 km/sec from C_L and C_R curves in Fig. 14. Considering that the velocity of

shear waves in the upper layer 3.2 km/sec in this case is smaller than that in *C* group, while that in the lower medium is the same, it seems rather natural to consider that in (*a*) region another superficial layer exists over the upper layer in (*c*) region, which means the crustal structure is a double-layered one. But, in order to see if there is a

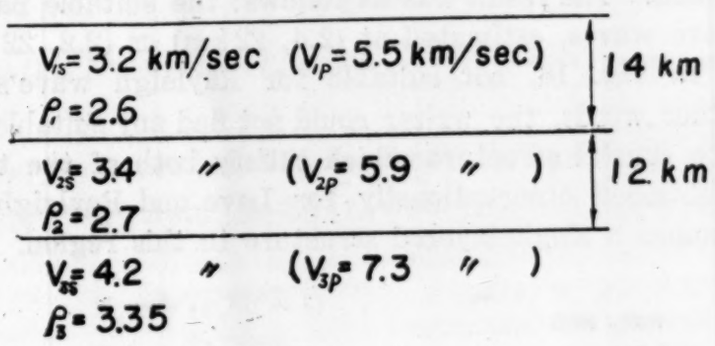

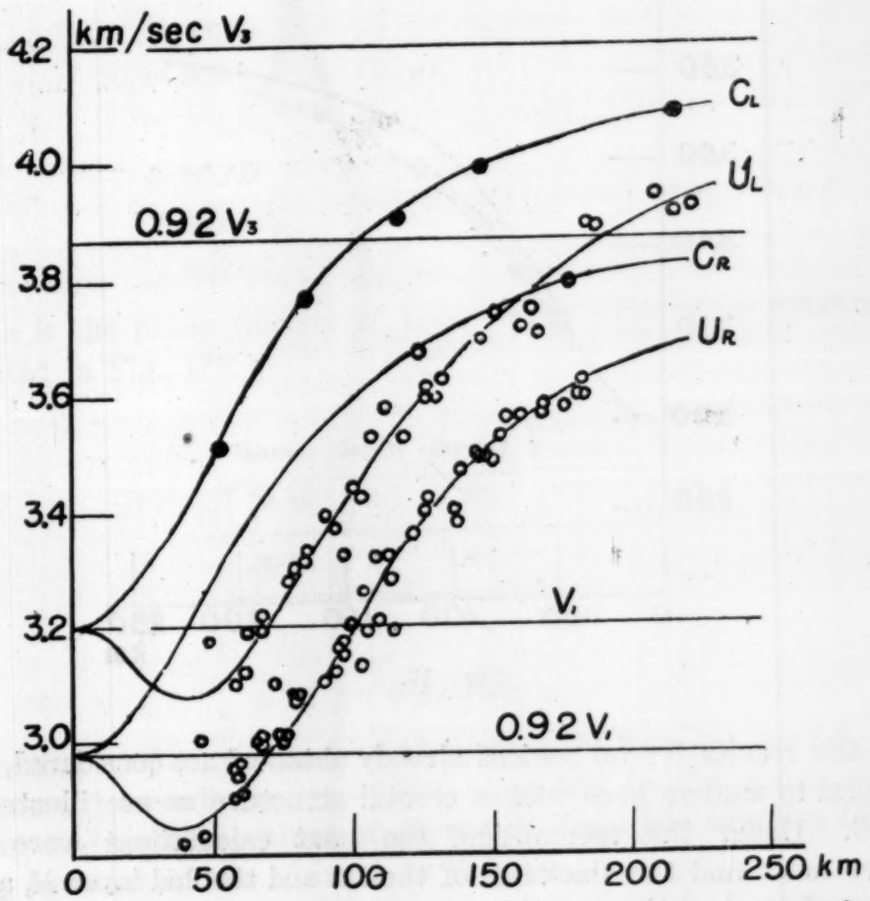

Fig. 14. The estimated crustal structure of (a) region and the results of theoretical calculations (filled circle).

case when the suitable values of μ_2/μ_1 and H for Love waves dispersion curve are not suitable for Rayleigh waves dispersion curve when we assume a single-layered structure, the writer tried at first to estimate the crustal structure of this region also under the assumption of a single layer. The method is quite the same as for the case of C group already described. The result was as follows: the suitable pairs of μ_2/μ_1 and H for Love waves, estimated at (2.4, 22 km) or (2.2, 22 km), were, as is shown in Fig. 15, not suitable for Rayleigh wave's dispersion curve. In other words, the writer could not find any suitable quantities concerning the crustal structure which satisfy both of the two dispersion curves obtained observationally for Love and Rayleigh waves, so far as he assumes a single-layered structure in this region.

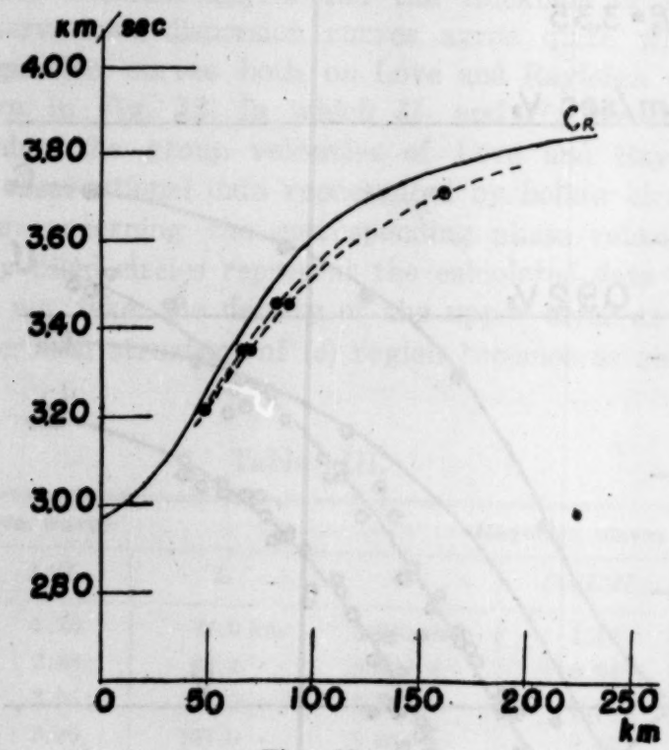

Fig. 15.

If the results for (*c*) regions already obtained are considered, it may be natural to assume here such a crustal structure as are illustrated in Fig. 16. Under this assumption, the next calculations were made. Now we must find the thickness of the 1st and the 2nd layer H_1 and H_2.

The characteristic equation of Love waves for doubly stratified medium is as follows:

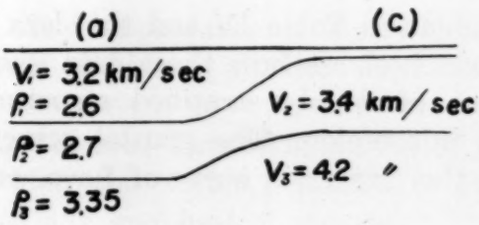

Fig. 16.

$$D \equiv D^c + D^s = 0 \qquad (3)$$

where

$$D^c/\mu_2^2 f^2 \equiv \mathfrak{A}_2 \cos\{\xi h_1 \mathfrak{A}\}\,[-\chi_{32}\mathfrak{A}\cos\{\xi h_2 \mathfrak{A}_2\} + \mathfrak{A}_2 \sin\{\xi h_2 \mathfrak{A}_2\}]$$

$$D^s/\mu_2^2 f^2 \equiv \chi_{12}\mathfrak{A}\sin\{\xi h_1 \mathfrak{A}_1\}\,[\chi_{32}\mathfrak{A}\sin\{\xi h_2 \mathfrak{A}_2\} + \mathfrak{A}_2 \cos\{\xi h_2 \mathfrak{A}_2\}]$$

in which

$$\mathfrak{A}_k \equiv \sqrt{(r_k^2 \mathfrak{B}^2 - 1)}\ , \qquad k=1,\ 2,\ 3$$

$$\mathfrak{A} \equiv \sqrt{(1-\mathfrak{B}^2)}\ ,$$

$$\mathfrak{B}_k \equiv c/v_k\ , \qquad k=1,\ 2,\ 3$$

$$v \equiv v_3\ ,$$

$$r_k \equiv v_3/v_k\ , \qquad k=1,\ 2$$

$$\xi \equiv fH\ ,$$

$$\chi_{jk} \equiv \mu_j/\mu_k\ ,$$

$$f \equiv 2\pi/L\ ,$$

where c is the phase velocity of Love waves while other notations are illustrated in Fig. 17[5].

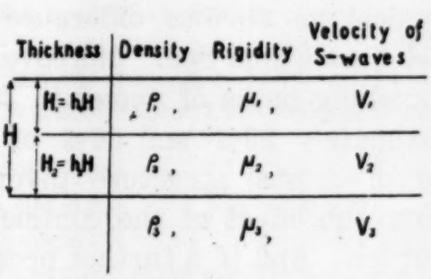

Fig. 17.

Putting $v_1=3.2$ km/sec, $v_2=3.4$ km/sec, $v_3=4.2$ km/sec, $\rho_1=2.6$, $\rho_2=2.7$, $\rho_3=3.35$, and accordingly, $\chi_{12}=0.852$, $\chi_{32}=1.888$ in the above equation, we can find suitable values of H_1 and H_2 from the equation (3) which fit the equation to the C curve in Fig. 14.

5) Y. SATÔ. *loc. cit.*

The results are given in Table IV and the data are shown in Fig. 14 by filled circles, which shows how these data given above obtained under the assumption of doubly stratified structure agree with the observational data in this region. The crustal structure of (*a*) region thus estimated from the dispersion curve of Love waves are illustrated in the same figure.

Table IV.

C	$L(H_1=14\,\text{km},\ H_2=12\,\text{km})$
3.52 km/sec	52.5 km
3.76 〃	89.0 〃
3.90 〃	117.0 〃
3.98 〃	147.0 〃
4.01 〃	198.0 〃

There remains the next work to be done. That is to see if these values of $H_1=14\,\text{km}$ and $H_2=12\,\text{km}$ obtained from the Love waves dispersion curve are also suitable for that of Rayleigh waves. But numerical calculations of theoretical dispersion curve of Rayleigh waves in the case of double layers are so cumbersome that the writer has not yet completed this work.

8. Conclusions.

Though a few theoretical studies must be completed before the writer gives any conclusion from his study given above, it may be said at least that there exists an obvious difference of crustal structure between Japan Sea and East China Sea. Moreover, if we consider that the length of the travelling paths of waves in Japan Sea and in East China Sea was approximately 25% and 35% of the whole travelling length, the difference of crustal structure given above will become ever more larger when the effect of the continental path is excluded from the dispersion curves. And if a further presumption is permitted, we may imagine the following figure on the crustal structure of our regions, that is, the crustal structure of both continents and East China Sea is a double-layered one while in Japan Sea regions, the structure is a single-layered one and in which the middle layer appears at the surface, or if the uppermost layer exists, it is quite thin.

There remain two points to be considered in this investigation, that is,

1) What does the reappearance of somewhat longer period waves in the filtered records of almost all the observational position mean? (See Fig. 5)

2) Has the difference of dispersion curves of *B* group from those of *A* and *C* on which the writer hesitated to consider on account of their too scarce data any geophysical meaning?

Of these two points the writer will treat in the next opportunity.

In conclusion, the writer wishes to express his sincere thanks to S. Miyamura who gave him many advices and encouragements in the course of his works and to Y. Satô who gave him kindly instructions in numerical calculations.

The expense of the present study was partly defrayed from the Fund of the Scientific Research from the Ministry of Education.

---

21. 1950年8月15日のアッサム大地震の表面波の分散曲線について

地震研究所　秋　間　哲　夫

1950年8月15日にインドのアッサム地方で起つた大地震の國内における地震記象の中から20点ばかりをえらんで，それを各成分毎に振り振子を利用した低域濾波器にかけて長周期の波だけにして調べて見ると，極めて明瞭にラヴ波とレーリー波とが夫々南北成分，及び東西，上下成分に分離して観測出來た．そこで，各点毎にラヴ波，レーリー波に關する分散曲線を作つて見ると，之等の分散曲線が東北日本のものと西南日本のものとで之またかなり明瞭に相異していることが認められた．そこでこの二つの型の分散曲線から，震源から大陸を渡り，日本海を通つて東北日本に達する部分と同じく大陸を通り，東支那海を通つて西南日本に達する部分との地殻構造を求めて見ると，前者に於ては厚さ 27 km の單一戸，後者に於ては，厚さ 14 km と 12 km より成る二重戸を考えると，共にラブ波とレーリー波の分散曲線の何れにも夫々の分散曲線の理論式がよくあてはまることが分つた．

從來から表面波を用いて地下構造を求めることは，多くの人達によつてしばしばやられているけれ共，殆んどすべてのものが，ラヴ波乃至はレーリー波の分散曲線の一方だけから求めており，しかも單一戸と云う假定のもとに構造が求められている．しかしそうすると，佐藤泰夫氏の理論的研究でも分る樣に，もし實際の地下構造が例えば二重戸だつたとすると，實際とは大分異つた物理常數と厚さとをもつた單一戸の地下構造が求められてしまう危險が生ずる．

筆者の場合には幸いにしてラヴ波とレーリー波の兩方の分散曲線が得られたので，その兩者から地下構造をきめた．その点ではこゝにえられた結果は，少くとも從來のこの種の試みよりは高い信用度がおけるのではないかと思う．

---

22. *Experimental Studies on the Mechanism of Generation of Elastic Waves I.*

By Keichi KASAHARA,

Earthquake Research Institute.

(Read Nov. 20, 1951, Apr. 15, 1952.—Received June 20, 1952.)

1. Introduction.

It is one of the fundamental objects in seismology to obtain an accurate knowledge of the mechanism of generation and propagation of elastic waves. Since the earthquake phenomena came to be studied physically, serious efforts have been continued in this direction. The problem has attracted notice of mathematical physicists in the beginning and has been studied elaborately by them for many years. The results are so valuable and so enormous that we owe a considerable part of our knowledge of seismology to them. We cannot, however, always apply the results directly to the case of actual earthquakes, because their mathematical works are usually carried out under idealized assumptions, and their knowledge concerning the phenomena occurring in the vicinity of the energy source is rather meagre.

Recently, as the technique of seismic prospecting advances and spreads, the elastic wave phenomena have come to be studied under considerably simple conditions utilizing energy sources controlled artificially. Such experiments, called "field tests", apparently bid fair to clarify the present object, and in fact, they have already brought out many valuable results. But in spite of the advantages which the methods obviously possess, we can not fail to realize their faults, when we undertake more fundamental investigations on the phenomena. For example, we can scarcely find a test field of ideally simple conditions, and furthermore, it is impossible to control the conditions in the course of experiment. These circumstances must introduce into the results some uncertainties, which are most undesirable for the present purpose.

It is considered that the methods of model experiment can offset these disadvantages only when operated in a proper way. Formerly, Terada and Tsuboi had attempted these kind of laboratory work[1] and

1) T. TERADA and C. TSUBOI, *Bull. Earthq. Res. Inst.*, **3** (1927), 55; C. TSUBOI, *Bull. Earthq. Res. Inst.*, **4** (1928), 9.

found out some practical characters of surface waves. Their study was, however, limited to the case of stationary problems and no further investigation has been undertaken since.

Recently Kaufman and Roever performed a laboratory study on the transient phenomena of elastic waves.[2] Although their interest lies mainly in the phenomena encountered during the seismic prospecting of subsurface structures, the work is related, in principle, with that undertaken in the present paper.

2. Properties of the material.

In the case of model experiment, selection of the material for the elastic medium requires careful consideration. In general, the material should have properties suitable for generating and observing the disturbance in it, that is to say, velocities of the propagated disturbances should not be too high, so that the times of arrival may lie within the measurable range and the wave lengths may be considerably shorter than the dimensions of the medium. The material should also present high uniformity as well as stability in its properties. High viscosity, good electrical conductivity, and low cost are also desirable in the present stage of experiment.

From the above-mentioned standpoint, a block of agar-agar was adopted as the medium. This material has been used in testing the elastic deformation of various kind of structures under stress and, were also adopted by Terada and Tsuboi in their studies on the stationary surface waves. The elastic property of the material has attracted the notice of rheologists in this country and it is being investigated in detail from their standpoint.[3]

The water gel adopted in the present study contains a few percents of agar-agar, which is boiled in a pot and then cast into the wooden vessel to solidify. Test pieces are prepared at that time for the purpose of estimating elastic constants of the material. In the course of experiment, Young's modulus and rigidity are measured statically. The former is measured adopting a tension stress to the test piece floating in water (Fig. 13), while the latter by the method devised by Schwedoff.[4] The elastic medium used in the present study shows the following properties:

2) S. KAUFMAN and W. L. ROEVER, *Proc. 3rd World Petr. Congr., Sec.* **1** (1951),537.
3) T. NAKAGAWA, *Kagaku*, **20** (1950), 130. (in Japanese).
4) Th. SCHWEDOFF, *J. de Phys.*, (2), **8** (1889), 341. T. NAKAGAWA, *loc. cit.*

Young's modulus $E=1.7\times10^5$ c.g.s.
Rigidity $G=0.61\times10^5$ c.g.s.
Density $\rho=1.0$

In the same way as the measurement of rigidity, the viscosity of the medium could be estimated, which proved to be high enough for the present purpose.

3. Apparatuses and observation.

The system of the experiment is shown schematically in Fig. 1.

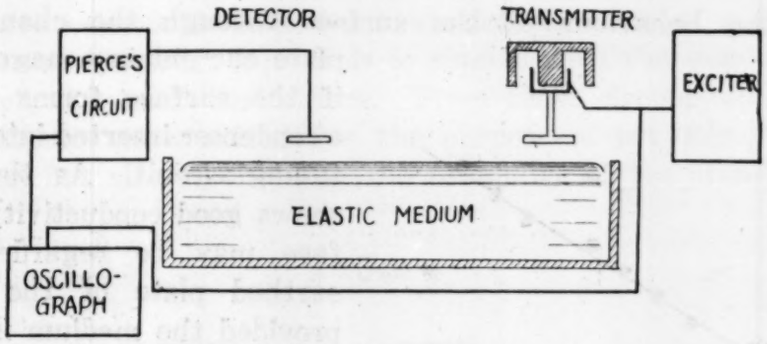

Fig. 1.

The material solidified in the vessel ($72\times33\times13$ cm) forms the elastic medium in which the disturbances propagate. At the sides of the vessel, pads of cotton wool is spread for the purpose of diminishing reflected waves whose existence brings trouble into the observation. As it is difficult to keep this material unchanged for long[5], one series of experiments should be carried out as rapidly as possible.

The wave transmitter is constructed from parts of a dynamic loud speaker and provides a long and light bar, which touches the surface of the medium and transmits elastic disturbances. This source is

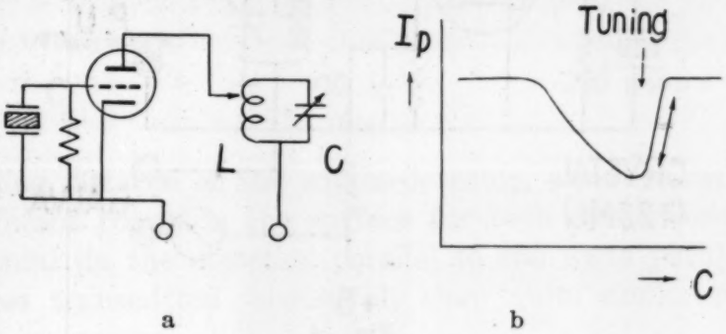

a b

Fig. 2.

5) Unstability is considered to originate from evaporation of water contents and other causes.

excited with electric current controlled by the exciter.

Disturbances propagated along the surface are detected with a variable capacity-type detector, which is inserted in an electric circuit containing Pierce's crystal oscillator. As can be seen in Fig. 2a, the circuit consists of a crystal-controlled grid circuit and a LC-tuning element forming the plate tank circuit coupling with the former through *g-p* capacity of the tube. Plate current comes to a minimum when the circuit falls into tuning (f=7.22 MC in the present case), and increases abruptly with the cessation of tuning (Fig. 2b). We can, therefore, observe the behaviour of the surface through the change of DC plate current in a magnified scale, if the surface forms a part of a condenser inserted into the plate-tuning circuit. As the material shows good conductivity, the surface may be regarded as the earthed plate of the condenser provided the medium is grounded at the bottom. Close to the surface, a small piece of metal plate is set, which forms the opposite plate of the condenser and picks up the displacement of the surface. This pick-up instrument provides a micrometer for calibration.[6]

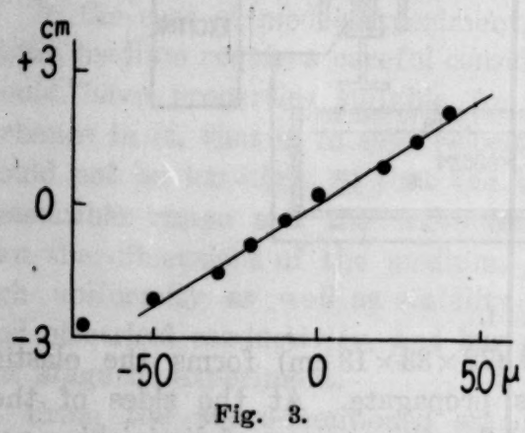

Fig. 3.

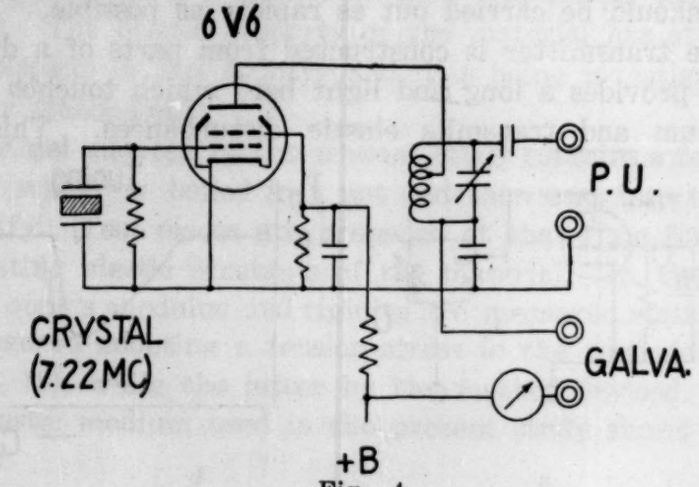

Fig. 4.

6) Under actual conditions, the observation is made with an area of 3-4 mm width regarded as a point, which is quite smaller compared with the wave lengths.

Fig. 3 is the circuit diagram in practical use, and an example of sensitivity calibration of the detector is illustrated in Fig. 4. An electro-magnetic type oscillograph is employed to record the motion of the surface, the figure of exciting current, and time marks. Experimental errors are estimated in reading of arrival times at 10^{-3} sec, and those in recording of amplitudes of the displacement at less than 10%, taking into consideration the effect of the stray capacity.

The main object to be studied in this paper is the behaviour of the surface of a homogeneous semi-infinite elastic body under the effect of impulsive external force acting in vertical direction at a certain point on the surface (see Fig. 5a). This is similar with the case investigated theoretically by Lamb and others. From these circumstances, the present conditions seem suited for the purpose of not only studying the phenomena but also of checking the reliability of the present method.

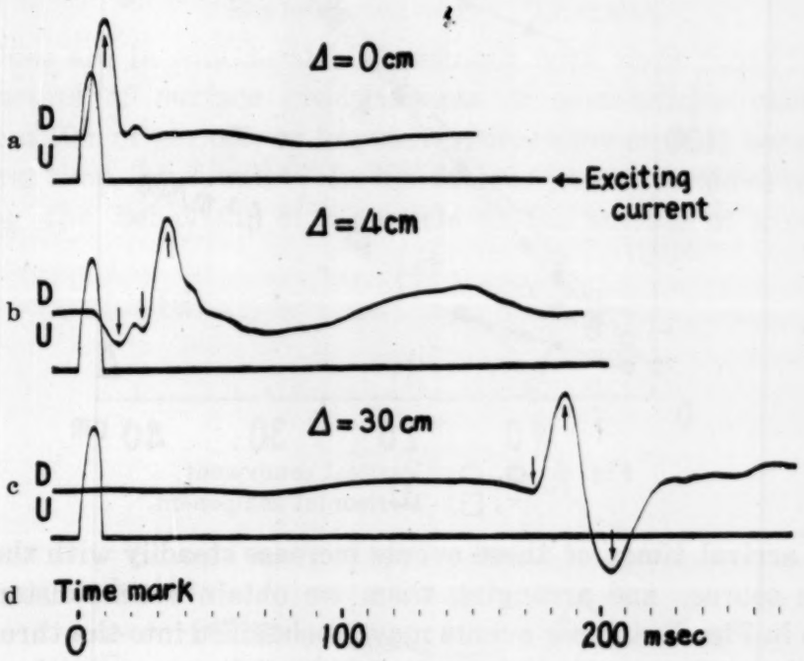

Fig. 5.

Changing distance of the source-detector, observations were carried out at different points on the surface for both components of vertical and horizontal (in the direction parallel to the wave path).[7] Since the disturbances transmitted successively show quite similar results at the

7) When the horizontal component is observed, a little trench is scooped at the observing point. In this case, its dimensions should be decided not to disturb the phenomena under observation and to keep the effect of stray capacity possibly slight.

same point, the collection of records obtained at different point may be considered as representing the general behaviour caused by an action of force. Fig. 5 illustrates representative records obtained at the points $\Delta=0$, 4, and 30 cm. Several kinds of remarkable events are shown in the figure.

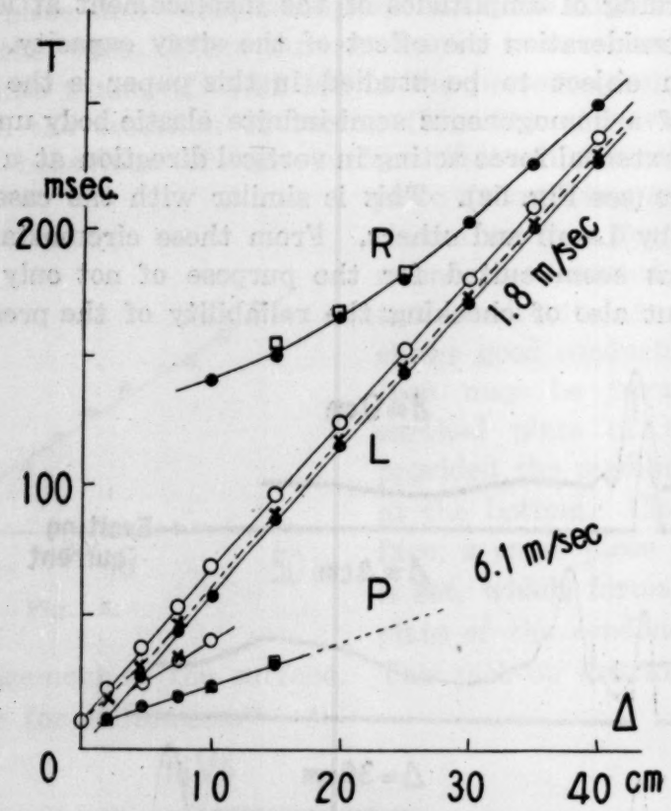

Fig. 6. ●, ○: Vertical component,
×, □: Horizontal component.

The arrival times of these events increase steadily with the distance from the source, and arranging them we obtain a time-distance curve as shown in Fig. 6. These events may be classified into the three phases, P, L, and R. The former two of which indicate velocities 6.1 m/sec and 1.8 m/sec, respectively.

4. Discussions.

The phase P forms the initial motion and is supposed to represent the dilatational wave propagating directly through the medium. Though the phase shows a distinct figure near the source, it becomes dimmer as the distance increases and is to be observed no more beyond the distance of 15 cm. The second phase L represents the main part of

disturbances which looks like a kind of surface waves. Its character will be investigated in detail in the following part of the paper where it is considered a Rayleigh-type wave. The third and the last phase R, expressing the peculiar feature of curve, is considered as a reflected wave. A simple calculation made under this assumption indicates the depth of reflecting plane and the velocity of propagation to be 13.0 cm and 2.0 m/sec, respectively. The former corresponds exactly to the thickness of the present medium. Though the phase representing the direct transversal wave cannot be found in the figure,[8] the velocity of phase R seems to correspond to that of the transversal wave in the medium. Velocities of these phases can be estimated from elastic constants as follows:

velocity of	longitudinal wave:	6.1 m/sec
"	transversal wave:	2.4 m/sec
"	Rayleigh wave :	2.2 m/sec.

These values are in considerable agreement with those found in Fig. 6.

Characters of surface displacements of semi-infinite elastic body under the action of periodic or impulsive force were studied theoretically for the first time, by Lamb.[9] In his famous paper, he gave the figure illustrating the behaviour of a particle on the surface at a great dis-

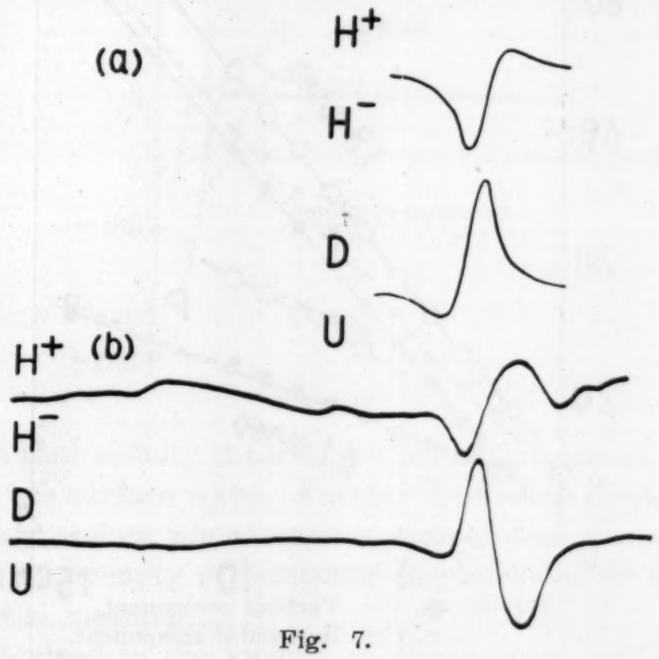

Fig. 7.

8) The similar phenomena has been pointed out with some discussions by Kaufman and Roever.

9) H. LAMB, *Phil. Trans. Roy. Soc., A*, **203** (1904), 1.

tance from the source, which can be observed when an impulsive force acts vertically at a point on the surface (Fig. 7). Records obtained at the point $\Delta=30$ cm are drawn in the same figure, for the sake of comparison. Considering the conditions under which the studies were pursued,[10] a considerable degree of agreement can be expected between both results, and, in fact, the figure indicates a satisfying agreement,

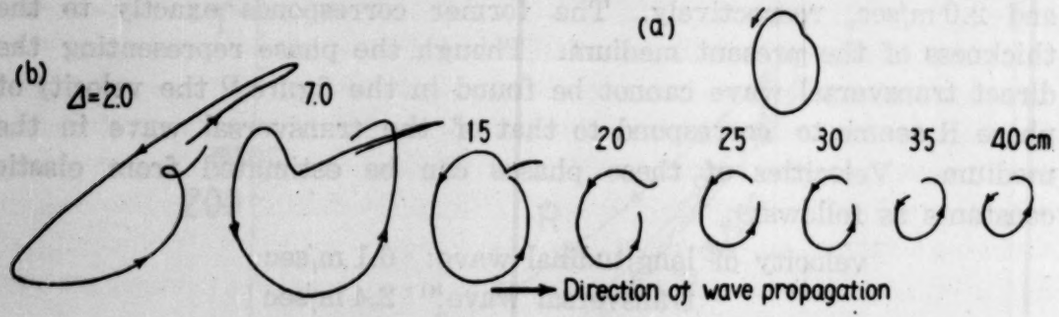

Fig. 8. Locuses in (b) except that of $\Delta=2.0$ cm are drawn in the same scale.

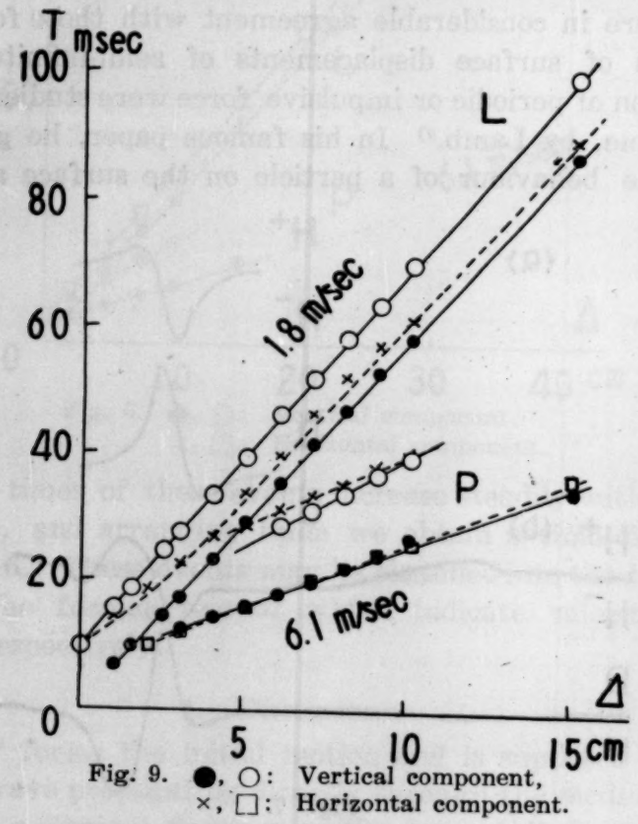

Fig. 9. ●, ○: Vertical component,
×, □: Horizontal component.

10) The source cannot be regarded as a point source in the present experiment, because it has a considerable length amounting to 15 cm. To make the comparison more strict, experiments should be repeated with an exact point source.

particularly in the part of the main disturbance. Kaufman and Roever attempted a similar comparison in their laboratory study undertaken in the vertical component of motion. Another comparison is attempted in Fig. 8, which show the locus of a particle motion in the case of a main shock. Those obtained at distances beyond 7 cm are identical with those predicted theoretically in their shape, but, in the vicinity of the source, they appears in a more complicated form. We may, therefore, consider that the surface wave is to be observed in complete form at points more than 7 cm away from the source, while at nearer points no complete surface wave is to be observed. Although the critical distance corresponds to the wave length of surface wave in this case, their general meaning remains unexplained. Process of development of the surface wave can be seen more clearly in Fig. 9, where events of extreme displacements are plotted successively. According to the figure, extremities in vertical component travel from the origin separately into two series and the velocities correspond to those of dilatational and surface wave, respectively. Extremity in horizontal component, however, travels in one series of events to the critical

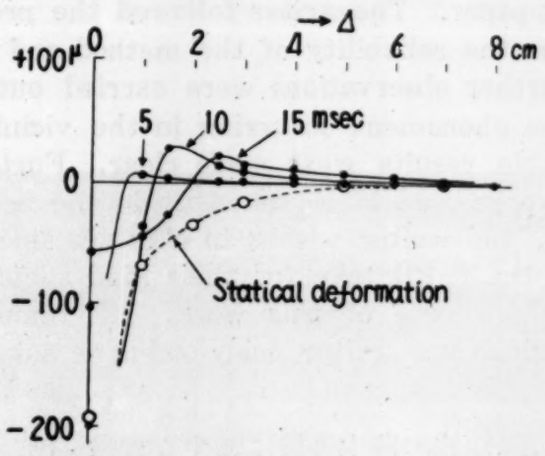

Fig. 10.

distance and in that vicinity it parts into two series, one of which travels away forming the surface wave. Further discussions must be postponed, because in those regions where various sorts of disturbances exist closely together, an extremity of compound displacement do not necessarily have an essential meaning.

Records obtained in the vicinity of origin show another noticeable feature, that is, the surface is displaced upwards initially. In Fig. 10, illustrating the shape of surface observed at successive instances, we

see a distinct swelling-up propagating at the head of disturbances. The broken line in the figure represents the deformation of the surface when the statical force acts vertically at the origin, where no swell is to be seen. This fact seems quite curious from the standpoint of statical theory of elasticity, because throughout the course of experiment, the impulse of force acts downwards at the origin.

A similar phenomenon has been observed in the field. According to the paper of Inouye[11], he found that the surface of the ground is displaced upwards initially in the vicinity of the origin where a weight is dropped down. To interpret this fact, he suggested the swelling-up of ground surface near the origin as one of the probable causes. The present result therefore requires further investigation in laboratory as well as in the field.

5. Concluding remarks.

A series of model experiments were undertaken adopting a block of agar-agar as the elastic medium to investigate the mechanism of generation of elastic waves. An approach to the subject is reported in the present paper. The writer followed the prediction in Lamb's theory to examine the reliability of the method and obtained a satisfying result. Further observations were carried out to obtain fuller information of the phenomena occurring in the vicinity of the source, and some noticeable results were made clear. Further discussions on the results were postponed to be taken up in the near future.

In conclusion, the writer wishes to offer his sincere thanks to Dr. T. Hagiwara and Dr. T. Rikitake for their kind advices and encouragement given in the course of this work. His thanks are also due to those who have given the writer many valuable suggestions.

22. 彈性波の發生機構に關する實驗 (第 1 報)

地震研究所 笠 原 慶 一

寒天溶液を媒質に用いて彈性波の發生機構を模型實驗的に研究する試みを行つた．種々の事情から理論的にも，野外實驗的にも取扱い難い對象がこの分野に存在するけれども，その幾分かは模型實驗的手段で取扱えるように思われる．

こゝでは模型媒質の表面に局所的な垂直衝撃力を作用させた場合の現象を取扱つた．表面の呈する垂直・水平方向の變位は可變容量型の檢出裝置によつて觀測する事が出來る．波動源から離れた場所での變位は，理論的に豫想されるものと質的に一致する事が認められた．更に波動源近傍の運動を觀察することにより表面波の發生過程及び初動の方向に關して興味深い現象が知られた．

11) W. INOUYE, *Bull. Earthq. Res. Inst.*, **13** (1935), 194.

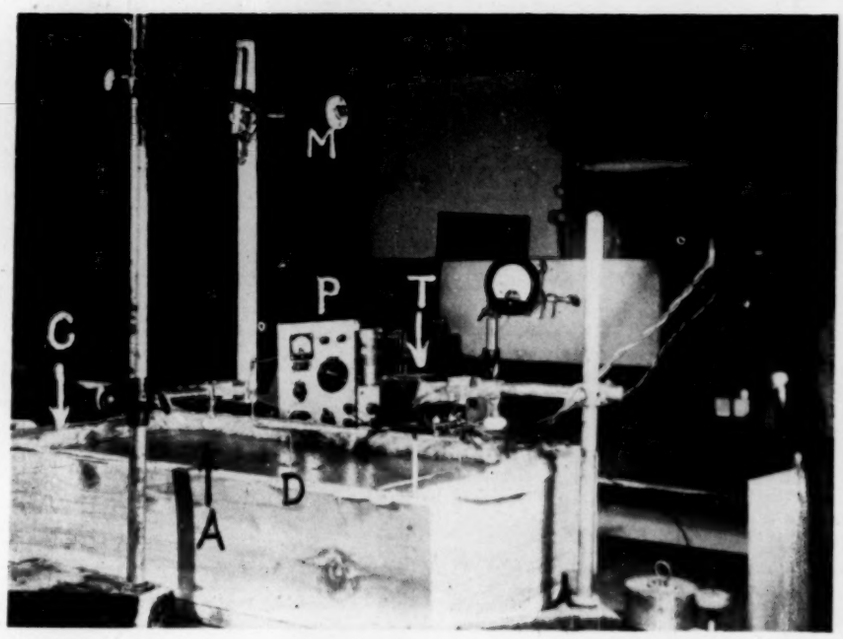

Fig. 11. General view of the experiment.

A: Elastic medium, C: Cotton wool, D: Detector,
M: Micrometer, P: Pierce's oscillator, T: Wave transmitter.

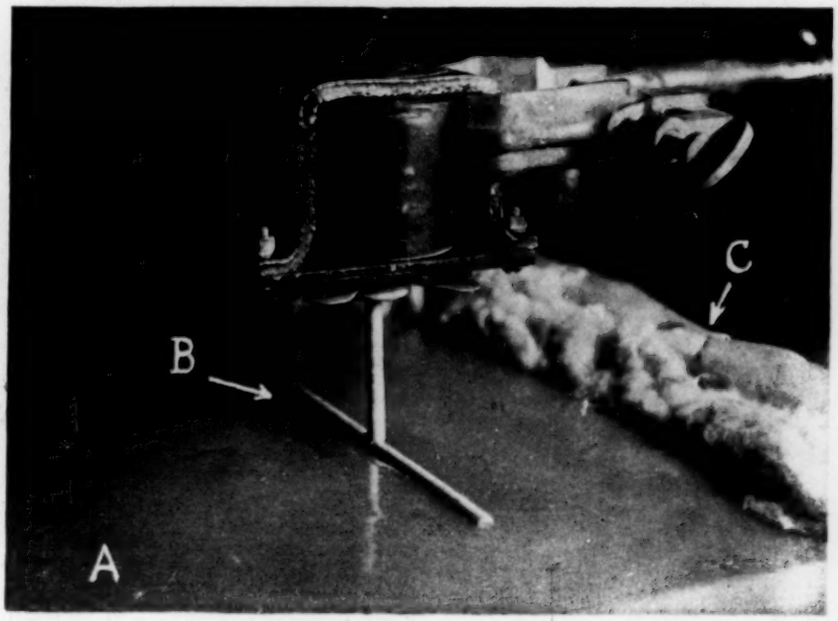

Fig. 12. The wave transmitter.

A: Elastic medium, B: Transmitting bar, C: Cotton wool.

（震研彙報 第三十號 圖版 笠原）

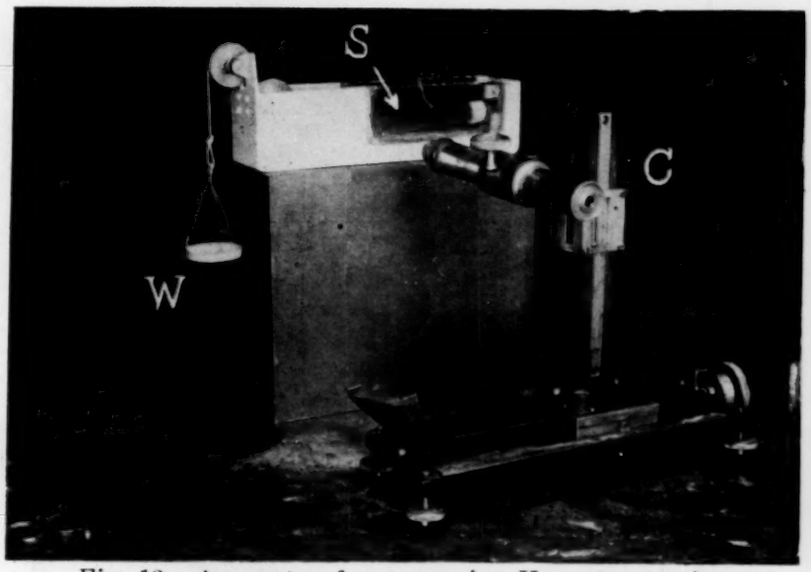

Fig. 13. Apparatus for measuring Young's modulus.
C: Comparator, S: Specimen, W: Weight.

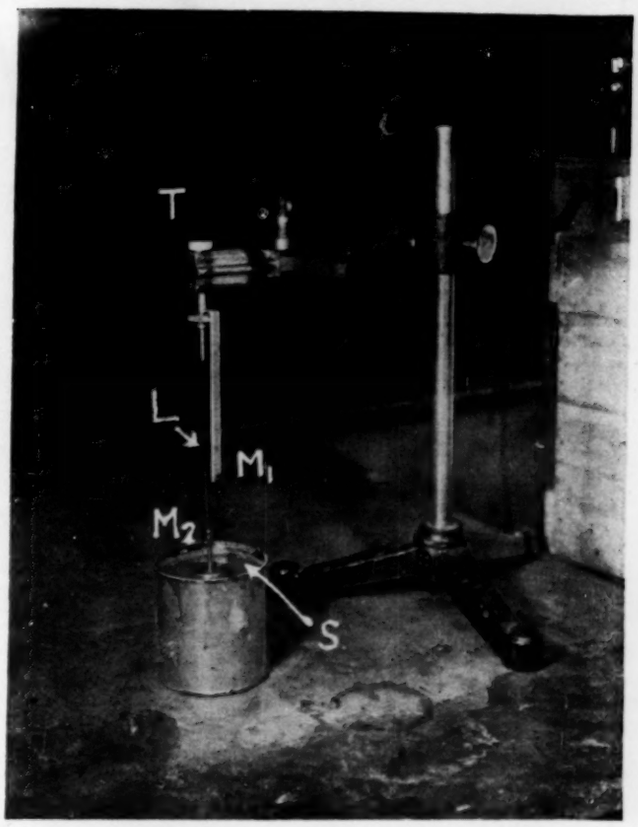

(震研彙報 第三十號 圖版 笠原)

Fig. 14. Apparatus for measuring rigidity.
L: Torsion wire, M_1, M_2: Mirror, S: Specimen, T: Torsion head.

23. *Elastic and Viscous Properties of Volcanic Rocks at Elevated Temperature. Part 1.*

By Shūzō SAKUMA,

Earthquake Research Institute.

(Read June 17, 1952.—Received June 20, 1952.)

1. Introduction.

In recent years, remarkable developments have been achieved in the field of elasticity and plasticity of rocks[1]. The most eminent and leading among them were the works done by D. Griggs and F. Birch. Especially, their studies on the physical behaviours of the materials which compose the earth's crust were full of instructions for solving difficult geological and geophysical problems. Their researches, however, were concentrated mainly on crystalline rocks, such as granite and marble which are the commonly accepted components of the crust in its deeper part. The earth's surface is composed not only of them but also of glassy rocks such as basalt and obsidian. On the other hand, the recent progress in the physics of volcanoes, partly advanced in Japan, calls for a more detailed knowledge on the physical properties of volcanic rocks and the parent magma. In this connection, the experimental studies by K. Kani, K. Iida and M. Ide and others are also to be remembered[2]. The present writer also planned to investigate the elasticity and viscosity of glassy rocks at elevated temperature and to throw some light on the difficult problem concerning the relation of the structure and history of rocks to their mechanical properties.

---

1) F. ADAMS and E. COKER, *Am. J. Sci.*, **29** (1910), 489.
L. ADAMS and R. GIBSON, *Proc. Nat. Akad. Sci.*, **15** (1929), 713.
F. BIRCH and D. BANCROFT, *J. Geol.*, **46** (1938), 59; **48** (1940), 752; *Am. J. Sci.*, **240** (1942), 457.
F. BIRCH, *Bull. Geol. Soc. Amer.*, **54** (1943), 263.
D. GRIGGS and others, *J. Geol.*, **44** (1936), 541; **47** (1939), 225; *Bull. Geol. Soc. Amer.*, **62** (1951) 853, 1385.

2) K. KANI, *Proc. Imp. Acad. Japan* **10** (1934), 29 and 79; **11** (1935), 334, 383.
K. IIDA, *Bull. Earthq. Res. Inst.*, **17** (1939), 59, 79.
M. IDE, *J. Geol.*, **15** (1937), 689.

2. Method and Instrument.

The ordinary bending or sagging method of measuring elasticity and slow viscous flow was adopted. Instead of measuring the subsidence of the centre of the beam, the change in curvature of the beam caused by the applied load was observed by the double reflection through the two rectangular prisms which were set face to face on the ends of the beam of the specimen. The knife-edges for supporting the specimen and applying the load, the two prisms and the framework for suspending the load were all made of fused silica, because the fused silica not only remains rigid and free from oxidation at high temperatures but is also easy of shaping. (Fig. 1 & 10).

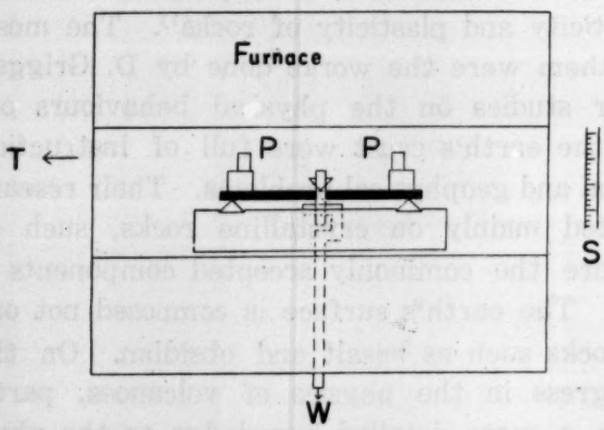

Fig. 1. Apparatus, P: prisms, T: telescope, S: scale, W: weight.

The two prisms, the specimen, the knife-edges and the suspender were mounted on a block of hard porcelain, which was reported to remain rigid up to 1300°C. The whole contrivance was inserted horizontally into a doubly wound Nichrome electric furnace. The incident and reflected light was allowed to enter and go out through the holes on the lids at both sides of the furnace. The load to bend the specimen with was suspended in the air by a suspender through a tiny hole in the furnace, right beneath the centre of the specimen. Though such holes disturbed the uniformity of temperature in both radial and axial direction in the furnace, the actual difference in temperature was found to be less than ±5°C within the space which was to be occupied by the specimen itself.

The temperature of the specimen was measured with the aid of a Pt-PtRh thermo-couple which was inserted in the furnace close to the

specimen. The temperature was raised and lowered at the rate of about 200°C in one hour and the temperature was kept constant from ten minutes before and during a series of measurement. The load was applied and removed, and thus the difference in the image of the scale was read with the telescope. The flow of the specimen under load at constant temperatures was also observed.

In computing the material constants from the observed results, the writer adopted a formula which is availed of sometimes in the field of rheology. The time-derivatives of stress-components could be reckoned at zero in our experiment. Accordingly, the stress-strain equations became as follows, where z-axis is taken upward and x-axis perpendicular to the axis of the bending moment.

$$P_{yy}=P_{zz}=P_{zx}=P_{xy}=P_{yz}=0$$

$$\frac{P_{xx}}{\tau}=E(\dot{e}_{xx}+\tau'\ddot{e}_{xx})\,.$$

Put $P_{xx}=E\varphi z\,,$

$$e_{xx}=\frac{\varphi z}{\tau}t-\frac{\varphi z\tau'}{\tau}+C+C'e^{-\frac{t}{\tau'}}\,.$$

If perfectly elastic, ($\tau\to\infty$ and $\tau'\to 0$)

$$e_{xx}=\varphi z.$$

$$\therefore\quad e_{xx}=\varphi z\left\{\frac{t}{\tau}+\left(1-\frac{\tau'}{\tau}\right)\right\}+C'e^{-\frac{t}{\tau'}}\,.$$

Put $C'=\varphi' z$, we obtain

$$\begin{cases} e_{xx}=z\phi(t) \\ \phi(t)=\varphi\left\{\dfrac{t}{\tau}+\left(1-\dfrac{\tau'}{\tau}\right)\right\}+\varphi' e^{\frac{t}{\tau'}}\,. \end{cases}$$

The quantity of subsidence ζ is given by ordinary integrations,

$$\zeta=K\left\{\left(1-\frac{\tau'}{\tau}\right)+\frac{t}{\tau}\right\}+Ge^{-\frac{t}{\tau'}}\,,$$

where G and K are constants, and

$$\begin{cases} K=\dfrac{5wl^4g}{384EI}+\dfrac{Wl^3g}{48EI}\,, \\ I=\dfrac{1}{12}bd^3\,. \end{cases}$$

where
- b and d : breadth and thickness of specimen,
- w : weight of the specimen per unit length,
- W : applied load,
- l : distance between the supporting knife-edges.

ζ is connected to the observed scale-reading X through the equation

$$\zeta=\frac{l}{6(2D+a+2A)}X,$$

where
- D : distance between the scale and a prism,
- a : distance between the prisms,
- A : length of the sides of prisms.

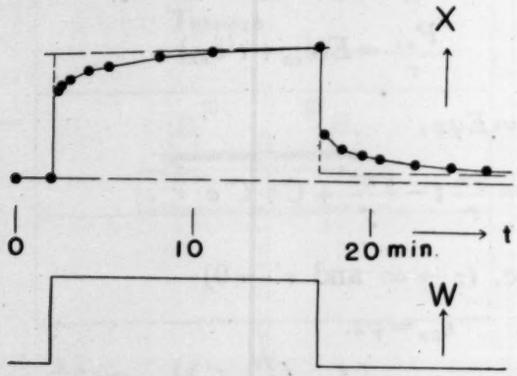

Fig. 2. An example of observations under constant load.

The material constants used here are those which were defined by M. Toda[3]. E is Young's modulus, and τ, τ' are the relaxation times for shear and voluminal change respectively. The coefficient of viscosity (η) can also be derived from the following formula

$$\eta=\frac{\tau E}{3}.$$

Fig. 2 illustrates an actually observed curve.

At first, a copper-plate was tested in the furnace up to 900°C and the result was satisfactory. The method proved to be also adequate for the purpose of measuring elasticity and viscosity of metals and alloys near their melting points, where the vibration method fails because of high attenuation.

3) M. TODA, 'Structure of liquids' (1947), Tokyo. (in Japanese)

3. Specimen.

The present specimens were cut out of a piece from the 1950 lava-flow of Volcano Oo-sima and were ground smoothly to the size of ca. $1.0 \times 0.3 \times 8.0\,cm^3$ (Fig. 10–A). The chemical and petrographical studies were already carried out by H. Tsuya and R. Morimoto[4] of our Institute. According to their studies, the 1950 lava of Oo-sima is identified as an augite-hypersthene-bytownite-basalt (SiO_2 52.25 in wt %). The groundmass, which occupies about 90% in volume, is composed of bytownite, pigeonite, iron ores, cristobalite and glass.

4. Results of Experiment.

Young's moduli of specimens, even when taken from one piece of lava, did not give the same value, but differed in accordance with their porosity (Fig. 3).

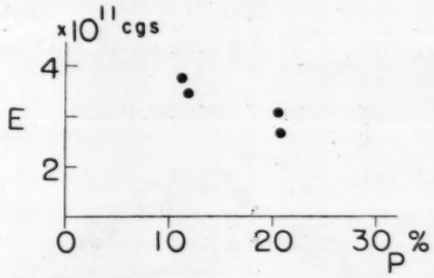

Fig. 3. Effect of porosity (P) on Young's modulus at room temperature.

It should be stated here that the present specimens followed Hooke's law fairly well even at elevated temperatures.

Young's modulus of the rock increased surprisingly with the rise in temperature until it began to show a decrease at nearly 700°C–800°C, where the viscous flow under the applied load also began to appear. The specimen behaved as a visco-elastic body at higher temperature than that up to 1100°C. We can determine the quantities of E, τ and τ' from the observed deformation and the rate of their change with time.

This tendency of elasticity to vary with the rise in temperature is similar to the results concerning amorphous silica[5]. However, this

4) H. Tsuya and R. Morimoto, *Bull. Earthq. Res. Inst.*, **29** (1951), 563.
5) R. Sosman, 'The Properties of Silica' (1927), New York.
K. Iida, *Bull. Earthq. Res. Inst.*, **13** (1935), 665.

tendency differs from that of common materials, such as metals and most of natural rocks[6].

At the cooling stage, more extraordinary and characteristic phenomena took place. The values of Young's modulus were estimated at higher values than those in the heating process. The modulus attained to its maximum at about 650°C and then decreased.

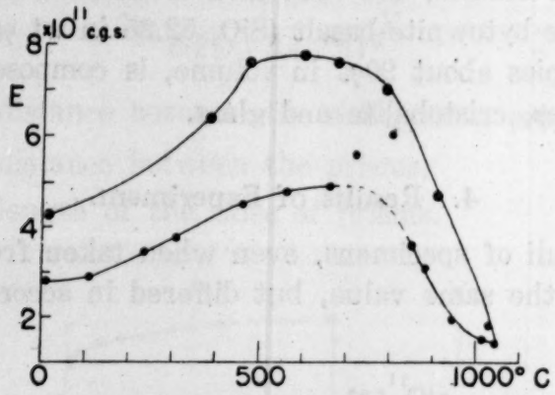

Fig. 4. Variation of Young's modulus with temperature.
Specimen No. 4.
larger circle: cooling stage.

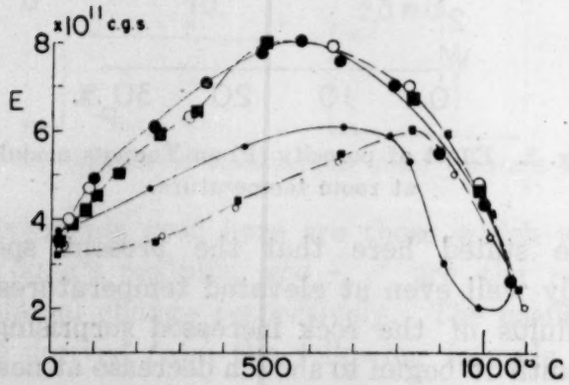

Fig. 5. Variation of Young's modulus with temperature.
Specimen No. 1.
larger marks: cooling stage,
closed circle : 1st run,
square : 2nd run,
open circle : 3rd run.

If the same specimen was heated and cooled again, the modulus showed less gradient of increase in the heating process, and the elasticity was observed to decrease at a higher temperature than before. In the

6) F. BIRCH, *loc. cit.*, p. 269.

cooling process, the modulus changed with temperature along the same curve of the first run of cooling. The *E-T* relation at the third run was almost the same as that of the above described second run. (Fig. 5)

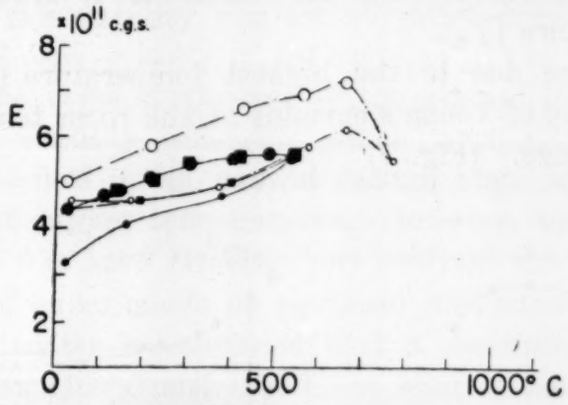

6-a. 1st~3rd run.
larger marks: cooling stage,
closed circle : 1st run up to 540°C,
square : 2nd run " ,
open circle : 3rd run up to 770°C,

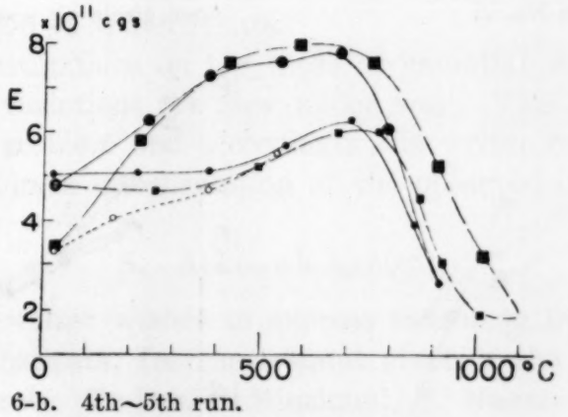

6-b. 4th~5th run.
larger marks: cooling stage,
closed circle : 4th run up to 910°C,
square : 5th run up to 1100°C,
open circle : 1st run (for reference).

Fig. 6a, b. Variation of Young's modulus with temperature, for successively elevated highest temeratnres (T_M). Specimen No. 2.

In addition, the 'hysteresis' phenomena are concerned with the highest temperature (T_M) which the specimen has experienced in the laboratory. When we stopped heating and began cooling at a definite temperature, the above-described transition was repeated. However, when the turning temperature (T_M) was once raised, the matter became

somewhat different. A series of experiments was carried out for a single specimen in this connection, as will be seen in Fig. 6. It is also to be remarked that, though the heating curves differ in general between the first and the second run, the values of E always agree at the highest temperature (T_M).

The difference due to the highest temperature (T_M) was also reflected in the value of Young's modulus at the room temperature at the end of cooling stage. (Fig. 7)

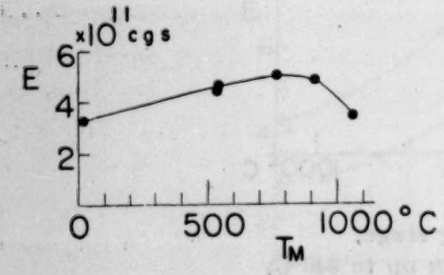

Fig. 7. Young's modulus at the room temperature after cooling from the highest temperature (T_M). (Specimen No. 2)

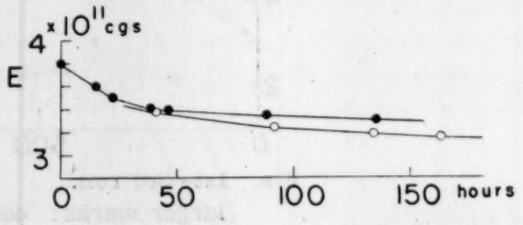

Fig. 8. Variation of Young's modulus at room temperature with time elapsed after cooling from above 1000°C.
closed circle : specimen No. 1,
open circle : specimen No. 2.

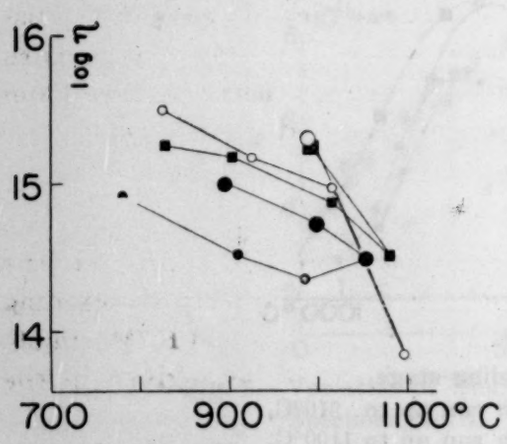

9-a. Specimen No. 1.
closed circle : 1st run,
square : 2nd run,
open circle : 3rd run.

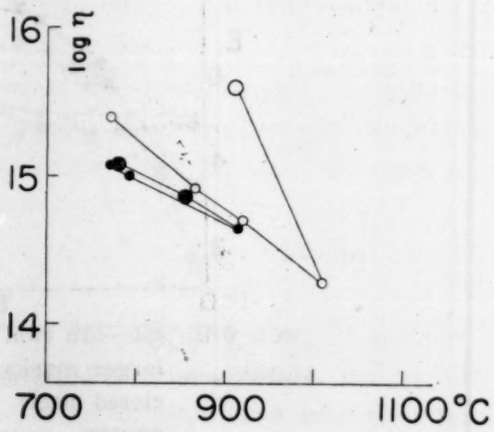

9-b. Specimen No. 2.
closed circle : 3rd and 4th runs,
open circle : 5th run.

Fig. 9. Variation of viscosity coefficient (η) with temperature.
larger marks : cooling stage.

The value of E at the end of cooling process, however, varies slightly in course of time as will be seen in Fig. 8. This and other facts mentioned above lead us to assume the existence of some kind of

change of internal structure of the specimen of rather slow velocity, such as crystallization or decomposition.

The relaxation time, or viscosity, was determined from the terminal velocity of deformation under a constant load at a constant temperature. The accuracy of this quantity was not so satisfactory because of the high viscosity and slow velocity of deformation in the present range of temperature. The value of viscosity of the order of 10^{11} poise at 1050°C far exceeds the viscosity cofficients which were obtained both by T. Minakami[7] in the field in its natural molten state and by K. Kani[8] experimentally at higher temperatures. However, by the experiences of those chemists who have remolten and analysed the lava of Oo-sima, and the results of experiments on electrical conductivity of the lava by T. Nagata[9], the writer is convinced that a discontinuity of viscosity does exist between 1100°C and 1150°C, at least in the remelting treatment. One of the causes of this high viscosity can be ascrided to the possible escape of volatile constituents and to the possible changes in crystalline structure. In fact, even in our experiments, the values of relaxation time (τ) increased not only in the cooling stages when compared with those in the preceding heating stages, but also increased with the repetition of experiments.

Further investigations on the mode of causation of elasticity, viscosity and their variations are now under way. This report is a mere approach to the problem and accordingly the writer refrains here from proposing any definite interpretation of the observed phenomena.

5. Acknowledgement.

The present writer wishes to express thanks to Dr. H. Tsuya, the director of our Institute, for the consent given to the writer regarding the present research. To Drs. T. Minakami, T. Nagata and R. Morimoto his cordial thanks are also due for their kind advices given in the course of the experiments.

---

7) T. MINAKAMI, *Bull. Earthq. Res. Inst.*, **29** (1951), 437.
8) K. KANI, *loc. cit.*, p. 269.
9) T. NAGATA, *Bull. Earthq. Res. Inst.*, **15** (1937), 663.

23. 高溫に於ける火山岩の粘性及び彈性 第1報

地震研究所 佐久間修三

火山物理學の最近の進歩に伴つて，火山岩の粘性，彈性に關する實驗的知識の必要が痛感されるので，高溫域に於けるこれらの性質を，まづ靜的に，撓みの方法によつて測定した．

1950 年に噴出した大島熔岩のヤング率は，溫度上昇に伴つて增加し，700°C～800°C に至つて急に減少し始める．粘性流動が觀測されるのも 700°C 以上の高溫域に於てであり，粘性は 1050°C で約 10^{14} poise であつた．ヤング率は冷却の過程では加熱の過程に於けるよりも一般に大きい値を示し，又この傾向は，試料が嘗て實驗室内で処理された最高の溫度にも關係するやうである．

これらの，異常な性質の原因については，火山岩中の揮發性成分の逸出，或は微細な結晶の析出などの可能性が考えられるが，尙今後の檢討を要する．

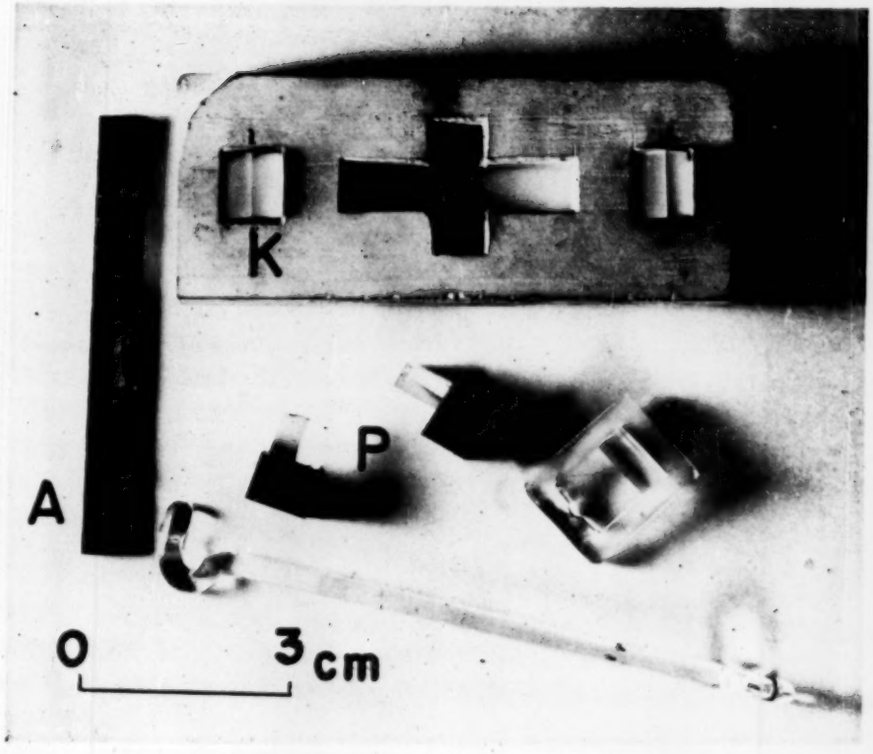

(震研彙報 第三十號 圖版 佐久間)

Fig. 10. A specimen and a part of the instrument.
A: specimen, K: knife-edge, P: prism.

24. *The Second Explosion-Seismic Observations in North-Eastern Japan.*

By The Research Group for Explosion Seismology,*

Earthquake Research Institute, Tokyo University,
Geophysical Institute, Faculty of Science, Tokyo University,
Seismological Section, Central Meteorological Observatory,
Section of Geophysical Exploration, Geological Survey,
Geophysical Institute, Faculty of Science, Tohoku University,
Faculty of Mining, Akita University.
National Science Museum,
Geophysical Institute, Faculty of Science, Kyoto University,
International Latitude Observatory of Mizusawa.

(Read Feb. 19, 1952.—Received June 20, 1952.)

1. Preface.

Seismic prospecting on a large scale, using a large amount of explosives is highly effective in studying the propagation of seismic waves as well as in mapping earth crust structures of geologic interest. In Japan such an experiment was first made on October 25th, 1950 when a large amount of explosives was exploded for engineering purposes in Iwate-ken. In spite of the short time of preparation, the experiment went unexpectedly well as has already been reported.[1)]

---

* Members of the group, who participated in the project are as follows (in alphabetic order).

AKIMA T., HORI M., HAGIWARA Terukazu, HIRAGA S., KAWASUMI H., KASAHARA K., KOBAYASI Naoyosi., MATUMOTO T., MATUMOTO H., MIYAMURA S., MIYAZAKI T., OMOTE S., SAKUMA S., SAWAKURI T., SHIMA E., SHIBANO M., TUZIURA M., YAMAZAKI Y., YANAGISAWA M. (E.R.I.)

ASADA T., DEN N., HAYATU A., KOBAYASHI Naota, MATUZAWA T., MOGI K., SATO R., SHIMIZU Y. (Geophys. Inst., Tokyo Univ.)

AIHARA K., INOUYE W., ICHIKAWA M., OGAWA T., SUYEHIRO S., UTSU T. (C.M.O.)

HURUYA S., KANEKO T., KOJIMA S., TATEISHI T., UZIIE A. (Geol. Surv.)

KATO Y., MINE N., NORITOMI K., OSSAKA G., SUZUKI Z., TAKAGI A. (Geophys. Inst., Tohoku Univ.)

TAZIME K. (Akita Univ.) HONDA T., MURAUCHI S. (Nat. Sci. Mus.)

KOZUKI A., OKANO K., TAMAKI H. (Geophys. Inst., Kyoto Univ.)

MURAKAMI G., SUKAWA T. TAKAHASI T., (Mizusawa Lat. Obs.)

1) La Groupe pour Recherches de Séismologie par Explosion, Tokio, Observation Sismique par Explosion d'Isibuti., ZISIN Ser. II, **3** (1951), 77-82.

The Research Group for Explosion Seismology, Tokyo, Explosion Seismic Observations in North-eastern Japan, Bull. E.R.I. **29** (1951), 97-106.

Table I. Second Isibuti
(1951-XII-27, $12^h\,06^m$,

	Observation point	Location	Elevation	Distance from shot	Seismographs
			m	km	
Nearby region	2. Tunnel	Near the explosion point	340	0.22 0.32	Electromag. (20 c/s Vert.)
	1. Orose	140°52′57″E 39 04 38 N	340	1.08	Mechanical (1 c/s Hor. $V_G=400$)
	3. Isibuti	140 54 43 E 39 06 51 N	300	1.69	Mechanical (1 c/s Hor. $V_G=400$)
	4. Umadome	140 56 32 E 39 07 05 N	195	4.31 4.40	Electromag. (10 c/s Hor. Ver.)
Eastern profile	5. Atago	140 59 31 E 39 07 26 N	150	8.65	Electromag. (10 c/s Ver.)
	6. Dobasi	141 01 58 E 39 07 31 N	100	12.09	Electromag. (3 c/s Hor. Ver.)
	7. Wakayanagi	141 03 41 E 39 07 43 N	100	14.62	Electromag. (3 c/s Hor. Ver.)
	8. Mizusawa	141 08 13 E 39 07 54 N	50	21.10	Mechano-optical (1 c/s, Hor. $V_G=4000$)
	9. Ide	141 17 30 E 39 10 30 N	150	30.00	Electromag. (10 c/s Hor. Ver.)
	10. Setamai	141 32 27 E 39 08 57 N	100	55.90	Electromag. (3 c/s Hor. Ver.)
	11. Kamaisi	141 53 31 E 39 15 36 N	10	87.54	Electromag. (3 c/s Hor. Ver.)
Southern profile	12. Hondera	140 56 29 E 38 58 24 N	206	15.29	Electromag. (3 c/s Hor. Ver.)
	13. Kurikoma	140 54 35 E 38 54 13 N	200	22.52	Electromag. (3 c/s Hor. Ver.)
	14. Hosokura	140 54 33 E 38 48 13 N	140	33.03	Electromag. (5 c/s Ver.)
	15. Kawatabi	140 45 31 E 38 44 38 N	220	41.92	Electromag. (3 c/s Hor. Ver.)
	16. Nakaniida	140 51 30 E 38 34 00 N	50	60.00	Electromag. (3 c/s Hor. Ver.)
	17. Matusima	141 04 31 E 38 23 05 N	10	81.60	Electromag. (3 c/s Hor. Ver.)
	18. Sinobu	140 30 31 E 37 41 39 N	180	159.92	Electromag. (3 c/s Hor. Ver. 1c/s Hor.)

explosion-seismic observations.
$\varphi=39°06'22''N$, $\lambda=140°53'39''E$, h=300 m)

Electronic amplifier	Electro-magnetic oscillographs (type of vibrator)	Observers
None	6-elements Haeno (Haeno-type vibr.)	Kojima, Huruya, Sakuma
None	None	Ichikawa, Takahashi
None	None	Suyehiro, Kobayashi, Sukawa, Murakami
None	6-elements YEW (YEW-D-type vibr.)	Matumoto, Aihara, Hayatu
1 for H-vibr.	2-elements (YEW-H-type vibr.)	Tuziura, Mogi
2 for D-vibr.	3-elements YEW (YEW-H-type vibr.)	Noritomi, Ossaka, Takagi
3 for D-vibr.	4-elements (YEW-D-type vibr.)	Utsu, Ogawa
None	None	Miyazaki, Hiraga
1 for H-vibr. 2 for D-vibr.	4-elements (YEW-H&D-type vibr.)	Akima, Sawakuri
3 for D-vibr.	6-elements Haeno-type	Tateishi, Ujiie
3 for H-vibr.	4-elements (YEW-H-type vibr.)	Kasahara, Sato
3 for H-vibr.	7-elements (YEW-H-type vibr.)	Hori, Den, Shimizu
3 for D-vibr.	4-elements (YEW-D-type vibr.)	Murauchi, Honda
		Tamaki, Okano, Kozuki
4 for D-vibr.	7-elements (YEW-D-type vibr.)	Tazime, Kobayashi
3 for D-vibr.	5-elements (YEW-D-type vibr.)	Shima, Shibano, Yanagisawa
3 for D-vibr.	7-elements (YEW-H-type vibr.)	Yamazaki, Kobayasi, Hagiwara
3 for H-vibr.	4-elements (YEW-H-type vibr.)	Suzuki, Mine, Oowaki

After that our group awaited for the second opportunity, which came on December, 27th, 1951. In this paper, the second explosion-seismic observation will be reported.

2. Preparation of observation.

With the experience of the first experiment as a guide, every phase of the instruments was much improved both in quality and quantity as compared with the first experiment. Vertical and horizontal electromagnetic seismographs of 3 cycles in natural frequency, high-gain electronic amplifiers and electromagnetic oscillographs were prepared in a large number. Most of them were designed on almost the same standard so as we could register seismic motions of the ground far from the explosion point and compare seismograms with sufficient accuracy. In addition to the seismographs of 3 cycles, electromagnetic

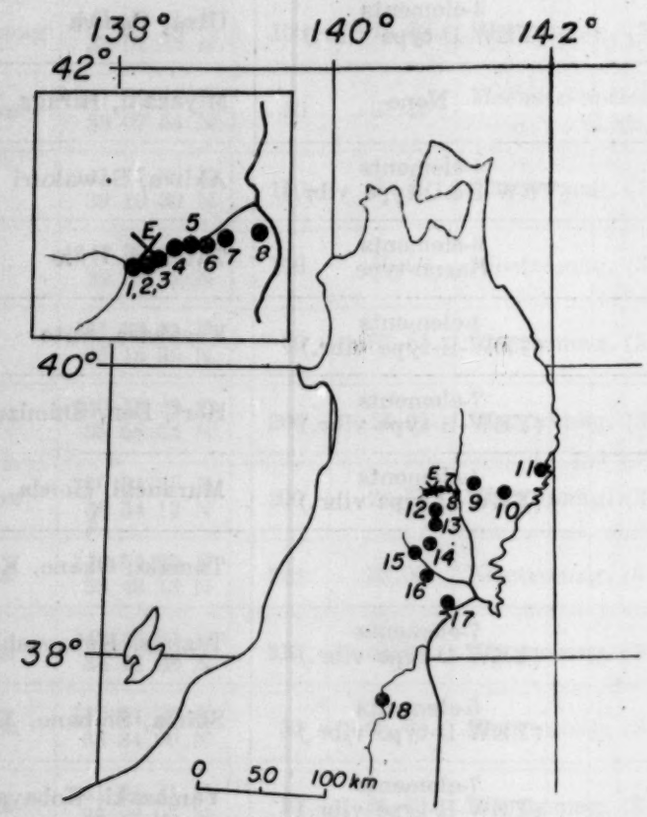

Fig. 1. Seismic observation stations for the second Isibuti explosion.
(Letter E indicates the place of shot and the numbers correspond to those in Table I.)

seismographs of 10 cycles and 1 cycle, mechanical seismographs and mechano-optical seismographs of 1 cycle were also employed.

As for the time-marking system, a similar method to that used in the previous case was adopted, whereby the time signals of the standard radio wave, JJY were received by a special receiver and put directly on the seismograms. Chronometers and other clocks were also prepared to cover unfavourable conditions of radio receiving.

Thus equipped, 18 temporary observation points were established as shown in Fig. 1 and Table I. Generally speaking, observations in only one direction are insufficient for mapping earth crust structures, and this is especially the case in the Tohoku District (North-eastern part of Honsyu) according to our geophysical knowledge. From the above point of view, the observation points were lined up in two directions, eastwards and southwards from the explosion point.

The amount of explosives used in the present explosion was one seventh of that of the first explosion, but the observation points could be extended as long as 160 km owing to the high quality of instruments.

The communication among these observation points was made by the government telephone network, the special telephone network of Tohoku Electric Company and the radio broadcast of NHK.

3. Explosion point.

7.8 tons of carlit were exploded at Isibuti (in Wakayanagi-mura, Isawa-gun, Iwate-ken) adjacent to the site of the first experiment ($\lambda=140°53'39''$E, $\varphi=39°06'22''$N) in order to loosen 36,000 cubic meters of rock for the construction of a dam (cf. Fig. 4). The explosives were charged in 9 chambers and were fired simultaneously by electric detonator and fuse (cf. Fig. 2). In one of the 9 chambers an electric circuit was put in to mark the time of explosion.

The explosion came off at 12h 06m, 27th of December, 1951.

4. Observation and results.

Unfortunately a strong wind and rain or snow due to a barometric depression which was passing over the Tohoku District from the day before and the bad condition in radio receiving affected the observation to some extent, but generally the observation went on successfully.

It would have been desirable to make an observation of three components in every observation point for the analysis of seismic waves, but it was practically impossible to make such observations. However,

in order to analyse the local state of propagation of seismic waves, several seismographs were lined up some hundred meters apart at several observation points[2].

The epicentral distances were calculated through spherical trigonometry (the radius of the earth: 6367.7 km), the longitude and the latitude of the observation points being determined from the ordnance map (scale: 1/50,000). However, the epicentral distances of the observation points in the neighbourhood of the explosion point were measured horizontally on a 1/5,000 map. In this case, an epicentral distance means the distance from an observation point to the nearest explosive chamber among the nine, and the error is supposed to be less than 30 meters.

In determining the arrival time of the phases, more stress was laid on the seismograms of vertical component, and other components were referred to only when necessary. The seismograms obtained are shown in photographic copies (Figs. 5~9), where the arrows show the commencements of the phases adopted.

As described previously, the time accuracy reaches about a hundredth of a second, favoured by the direct mark of the radio time signal. The time determination of the initial phase is comparatively easy, and its error is supposed to be less than several hundredths of a second, even when every source of error is taken into consideration. In fact, the arrival time of the initial motion was determined twice, once by the observer himself and then by another, and the personal error was only two or three hundredths of a second. On the other hand, the determination of other phases is largely affected by personal judgement, and the accuracy in this case is poorer.

In Table II. the arrival time of every phase is shown and arrival times which are supposed to belong to the same phase are shown in the same column. Numerical values written besides are deviations from the value which is computed by the least square method (cf. eqs. (1)-(5)). The travel-time curves from the data are shown in Fig. 3, where (a) is the travel-time curve consisting of the nearby points to the explosion point, while (b) consists of more distant points. In the diagram (b), it is an outstanding fact that travel times in eastern direction and those in southern direction show different features. For example, at Wakayanagi and Hondera, and at Mizusawa and Kurikoma, in each pair two points being at almost the same epicentral distance

2) At Umadome, Hondera, Kawatabi and Kamaisi were made these arrangements of seismographs.

Table II. Arrival times of the second Isibuti explosion tremors observed at the temporary stations of the group.

Observation point		Epi-central distance	Time of phase commencement (12 h 06 m+)							
			1		2		3		4	
			Time of commence-ment	Deviation	Time of commence-ment	Deviation	Time of commence-ment	Deviation	Time of commence-ment	Deviation
		km	sec.	sec.						
Nearby region	Tunnel I	0.22	−0.095*)	+0.0020	—	—	—	—	—	—
	Tunnel II	0.32	−0.056*)	−0.0020	—	—	—	—	—	—
	Orose	1.08	0.25	+0.0001	—	—	—	—	—	—
	Isibuti	1.69	0.50	−0.0002	—	—	—	—	—	—
	Umadome I	4.31	—	—	sec. 1.18	sec. −0.0754	—	—	—	—
	Umadome II	4.40	1.56	+0.0001	—	—	—	—	sec. 1.56	sec. −0.136
Eastern profile	Atago	8.65	—	—	2.26	+0.0742	sec. 2.20	sec. +0.175	2.97	+0.015
	Dobasi	12.09	—	—	2.90	−0.0644	2.52	+0.022	3.93	−0.044
	Wakayanagi	14.62	—	—	3.53	−0.0232	3.03	−0.072	—	—
	Mizusawa	21.10	—	—	4.82	−0.0348	3.93	−0.144	6.67	+0.028
	Setamai	55.90	—	—	12.31	−0.0052	9.79	−0.012	—	—
	Kamaisi	87.54	—	—	—	—	15.04	+0.031	26.44	+0.121
Southern profile	Hondera	15.29	—	—	3.44	—	2.78	−0.040	5.08	+0.159
	Kurikoma	22.52	—	—	—	—	3.99	−0.054	7.08	+0.017
	Kawatabi	41.92	—	—	—	—	7.43	+0.102	—	—
	Matusima	81.60	—	—	—	—	14.06	+0.015	24.4	−0.160
	Sinobu	159.92	—	—	—	—	I: 26.57 II: 27.28	−0.023	46.3	—

* Shot time is calculated from the least squares as 12 h 05 m 59.84s. (cf. eq. (1)).

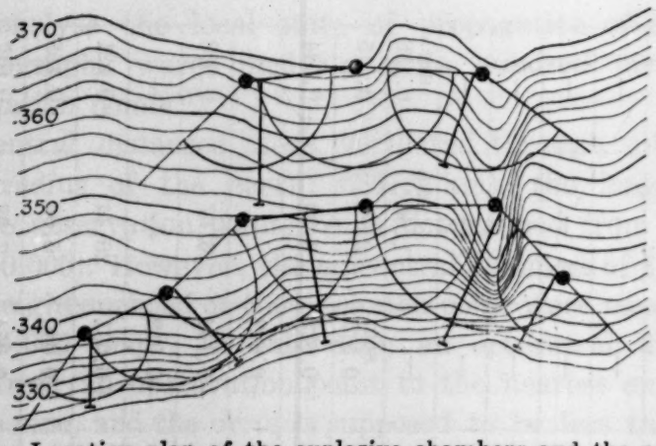

Fig. 2. Location plan of the explosive chambers and the area to be loosened by each chamber charge.

but not the same in direction, a difference is obviously greater than an error seen in the arrival time of the initial motion. From this fact, it is reasonable to discuss the results of the two directions separately.

Observation points, "Inside of tunnel", Orose, Isibuti, and Umadome are located in different directions from the explosion point. Therefore, the results from the observations at these points are treated separately from those of the above two profiles. As seen in Fig. 3 (a), the travel-time of these points are on a straight line, and by the method of the least squares, the line is given by the following equation, (Δ being measured in kilometers.)

$$t_1 = 12\text{h}06\text{m} + (-0.1617 \pm 0.0022)\text{s} + (0.3910 \pm 0.0008)\Delta.\text{s} \quad \ldots(1)$$

Consequently, the velocity corresponding to the equation (1) is

$$V_1 = (2.56 \pm 0.005)\ \text{km/sec.}$$

As shown in Fig. 3 (b), the travel-time curve of the initial motion in the eastern direction consists of a combination of two straight lines of different tangents showing different velocities. If number 2 is put to the line of lower velocity and 3 to the line of higher velocity, line 2 and line 3 are expressed by the following equations respectively,

$$t_2 = 12\text{h}06\text{m} + (0.331 \pm 0.040)\text{s} + (0.2144 \pm 0.0016)\Delta.\text{s}, \quad \ldots\ldots(2)$$

$$t_3 = 12\text{h}06\text{m} + (0.602 \pm 0.076)\text{s} + (0.1646 \pm 0.0017)\Delta.\text{s}. \quad \ldots\ldots(3)$$

Then the velocities are

$$V_2 = (4.67 \pm 0.034)\ \text{km/sec}, \qquad V_3 = (6.08 \pm 0.063)\ \text{km/sec.}$$

In the seismograms in the southern direction no phase corrosponding to phase (2) can be found, therefore the initial motion may be

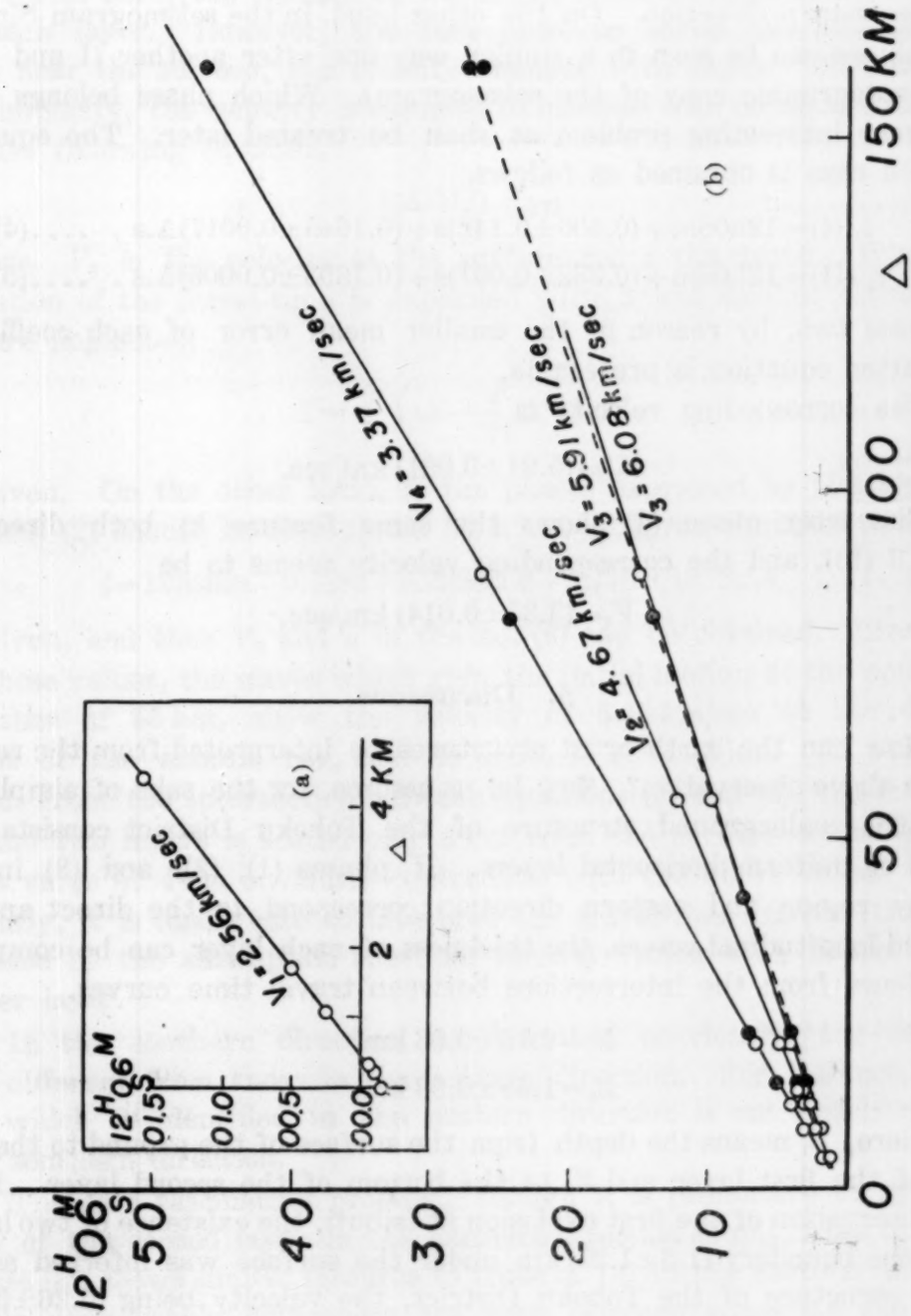

Fig. 3. Travel-time curves from the second Isibuti explosion data.

considered to correspond to phase (3). If this phase is on a straight line (let this be called 3′.), the line shows a larger tangent than that in the eastern direction. On the other hand, in the seismogram Sinobu, two phases can be seen in a similar way one after another (I and II in the photographic copy of the seismogram). Which phase belongs to 3′ is a very interesting problem as shall be treated later. The equation in each case is obtained as follows,

$$t_3'(\mathrm{I}) = 12\mathrm{h}06\mathrm{m} + (0.400 \pm 0.142)\mathrm{s} + (0.1645 \pm 0.0017)\Delta.\mathrm{s}\ , \quad \ldots.(4)$$

$$t_3'(\mathrm{II}) = 12\mathrm{h}06\mathrm{m} + (0.232 \pm 0.051)\mathrm{s} + (0.1693 \pm 0.0006)\Delta.\mathrm{s}\ . \quad \ldots.(5)$$

Of these two, by reason of the smaller mean error of each coefficent, the latter equation is preferable.

The correspoding velocity is

$$V_3' = (5.91 \pm 0.021)\ \mathrm{km/sec.}$$

The later phase (4) shows the same feature in both directions (Fig. 3 (b)), and the corresponding velocity seems to be

$$V_4 = (3.37 \pm 0.014)\ \mathrm{km/sec.}$$

5. Discussions.

How can the earth crust structures be interpreted from the results of the above observation? Now let us assume, for the sake of simplicity, that the underground structure of the Tohoku District consists of a series of uniform horizontal layers. If phases (1), (2), and (3) in the nearby region and eastern direction correspond to the direct and refracted longitudinal waves, the thickness of each layer can be computed as follows from the intersections between travel time curves.

$$Z_1 = 0.75 \pm 0.06\ \mathrm{km},$$

$$Z_2 = 1.59 \pm 0.33\ \mathrm{km}.$$

Here, Z_1 means the depth from the surface of the ground to the bottom of the first layer and Z_2 to the bottom of the second layer. From the observation of the first explosion at Isibuti, the existence of two layers with the boundary (1.3 ± 1.27) km under the surface was inferred as the mean structure of the Tohoku District, the velocity being (5.26 ± 0.007) km/sec in the upper layer and (6.13 ± 0.017) km/sec in the lower. Z_2, V_2 and V_3 seem to correspond to the above values, respectively. Z_2 and V_3 coincide well with the values in the previous case, while V_2 does not. Further discussion will be necessary on this difference.

Up to here, the velocity of waves has been assumed to be uniform in each layer. However, the fact must be taken into consideration that near the surface, the velocity changes with depth. For the sake of simplicity, the velocity is assumed to increase with depth as expressed by the following equation,

$$V=V_0(1+\alpha z) \qquad \cdots\cdots\cdots(6)$$

where, V_0 is the velocity at the surface and z the depth. When the equation of the travel-time is expanded with Δ and smaller terms than Δ^5 are neglected,

$$T=\frac{1}{V_0}\left(\Delta-\frac{\alpha^2}{24}\Delta^3\right)+\cdots\cdots \qquad \cdots\cdots\cdots(7)$$

is given. On the other hand, if the phases expressed by the two lines (1) and (2) should be formulated by a third degree equation with Δ,

$$t=12\text{h}06\text{m}+0.128\text{s}+0.2296\Delta.\text{s}-3.776\times10^{-6}\Delta^3.\text{s} \qquad \cdots\cdots(8)$$

is given, and thus V_0 and α in the eq. (6) can be obtained. According to these values, the waves which give the initial motion at the epicentral distance of 55 km, show the velocity of 5.15 km/sec at the deepest point of the seismic ray, and its depth is about 9 km. On the other hand, from the intersection between equations (3) and (8), the boundary of the two layers is seated only 4 km from the surface of the ground. This value of 4 km obviously contradicts with the above value. Consequently, it is inadequate to interpret the travel-time curves (1) and (2) en bloc by the assumption that the velocity varies with depth in the upper layer.

In the southern direction, as described previously, the features are different from those in the eastern direction. For instance, phase (2) which is identified in the eastern direction is not clearly seen in the southern direction.

This is a fascinating problem, though it is premature to infer the lack of the second layer in the southern direction simply from this fact. Phase (3′) shows similar features to those of (3) in the eastern direction, while considerable differences are seen between times at the origin and velocities. So far as uniform and horizontal layers are assumed, the heterogeneity of seismic velocity in the third layer seems to be beyond dispute. However, owing to some uncertainty in the assumption, no decisive conclusion can be obtained in this stage. If the travel times of the nearby region and in the southern direction are considered en

bloc, the thickness of the first layer turns to be (0.55 ± 0.08) km. But this value is the result of mere assumption.

From the standpoint of lessening the mean error in the travel-time equation, phase II of Sinobu was considered to belong to phase (3′). If this be true, initial motion I of Sinobu must be given by the waves which are propagated through a layer beneath the third layer with a higher velocity. The velocity of phase (3) or (3′) coincides with that of the so-called P^*, and therefore it gives rise to a possibility of correspondence between initial motion I at Sinobu and so-called P_n. Then, if this assumption is reasonable and if the velocity of P_n be 7.5 km/sec (which has been obtained from the observations of natural earthquakes in Japan), the depth of the layer of P_n is computed at about 24 km, and this value does not seem to be unreasonable. However, this conclusion is too premature, and further investigations, such as observations in the coming third large explosion, are desirable to give us a definite answer to this problem.

The phase with the velocity of $V_1 = 3.37$ km/sec observed in both directions is the same phase as was observed in the previous experiment and temporarily called S_1. Though little is known about this phase, it may be a kind of surface waves. Anyhow, further investigations are also requested in this matter. In the previous experiment, the peculiar phenomenon was seen that phase S_2 showing the same velocity as that of S_1 appeared 1 second after S_1. But this phenomenon was not seen in the present case. If such a phenomenon depends on the way the explosives are charged and exploded as was alluded to in the previous reports, the lack of the phenomenon in the present case may be understandable, because the conditions of explosion were different from those in the previous case. (cf. Figs. 4, 5 of the previous paper and Fig. 4 of the present paper.)

6. Conclusions.

More facts about the propagation of seismic waves in Tohoku District have been revealed by the seismic observations of the present explosion. The most outstanding fact is that the propagation of seismic waves in the eastern direction differs from that in the southern direction. In the eastern direction, at least three layers are expected on the assumption that the underground structure consists of uniform and horizontal layers. The depths from the surface to the two boundaries are 0.75 km and 1.59 km and the velocities of the seismic waves which give the initial

motion are 2.56, 4.67 and 6.08 km/sec, respectively. Different features are seen in the southern direction, that is, no effect of the second layer can be recognized, and the velocity in the lower layer is about 5.91 km/sec. At the observation point where the epicentral distance is 160 km, a phase is seen, which may correspond to the so-called P_n. Also, a phase with the velocity of 3.37 km/sec is seen in both directions. Though it corresponds to the phase which was supposed to be S wave in the previous experiment, no phase of the same velocity is found this time about 1 sec before or after.

After all, the present results have clarified that the phenomenon which we observed and tried to interpret by means of experiment is not so simple. Further development covering this complicacy and giving a clear interpretation about the earth crust structures of Tohoku District calls for a third explosion seismic observation in the same area.

7. Acknowledgements.

Finally, many thanks go to the agencies and persons under whose helpful cooperation this experiment has been successfully done. They are Tohoku District Construction Bureau of Ministry of Construction, Nisimatu-gumi Construction Company, Tohoku Electric Company, Sendai Broadcasting Station of Nippon Hoso Kyokai (NHK), Broadcasting Station of Standard Wave JJY, Prefectural Authorities of Iwate, Miyagi and Hukusima-ken and Mizusawa Forestry Bureau.

We also acknowledge the help given by the Geophysical Committee of the National Council of Japan, the Director of the Central Meteorological Observatory and the Director of the Earthquake Research Institute, in preparing the experiment.

---

24. 東北日本における第2回爆破地震動観測

爆破地震動研究グループ

東大地震研究所，東大地球物理学教室，中央気象臺地震課，
地質調査所物理探鉱部，東北大地球物理学教室，秋田大学，
科学博物館，京大地球物理学教室，水沢緯度観測所．

1950 年 10 月 25 日岩手縣膽澤郡若柳村石淵（水澤西方約 20 km）で東北地方建設局が堰堤工事のために行つた 57 トンの大爆破による地震動を觀測した結果はすでに報告した．1951 年 12 月 27 日ふたゝび同所において 7.8 トンの工事用爆破が行われることになつたので，われわれは前回にくらべ相当向上した裝備と組織とをもつてその地震動觀測をおこない，東北地方の地殻構造についての

よりすゝんだ知見をうることができた.

今回は第 I 表および第 1 圖にしめすように爆破点近傍，東方測線，南方測線にわけて合計 18 点の觀測点をもうけ，その大部分はあらたに準備された電磁型地震計をもちい，またおゝむね增巾器を使用した．爆破方法は前回と大差なく，第 2 図にしめすような藥室配置で一斉爆破をおこなつた．今回は特に發破時刻を記錄するため，藥室に導線をひきいれたが，別の故障のためこの發火記錄は解析には利用できなかつた.

低氣壓通過のため当日は風雨，風雪のところがおゝく，電波天候もわるく無線分秒報時 (JJY) の受信も困難であつたが，2～3 の点をのぞいて觀測に成功した．圖版 II～VI は各点の記錄寫眞である.

初動および若干の位相についてのよみとりは第 II 表に示すとおりであり，これを圖示した走時圖は第 3 圖である．東方測線と南方測線とは別々にとりあつかう方が適当であることは疑をいれない．結果を簡單にまとめればつぎのとおりになる．すなわち，各測線別の走時を最小自乘法によりもとめると，Δ を km でとつて，

爆破点附近：　$t_1=12^h06^m+(-0.^s1617\pm0.^s0022)+(0.3910\pm0.0008)\Delta^s$,

$V_1=2.56\pm0.005$ km/s.

東方測線：　$t_2=12^h06^m+(0.^s331\pm0.^s040)+(0.2144\pm0.0016)\Delta^s$,

$t_3=12^h06^m+(0.^s602\pm0.^s076)+(0.1646\pm0.0017)\Delta^s$,

$V_2=4.67\pm0.034$ km/s,　$V_3=6.08\pm0.063$ km/s.

南方測線：　$t_3'(\mathrm{II})=12^h06^m+(0.^s232\pm0.^s051)+(0.1693\pm0.0006)\Delta^s$,

$V_3'=5.91\pm0.021$ km/s.

($t_3'(\mathrm{I})=12^h06^m+(0.^s400\pm0.^s142)+(0.1645\pm0.0017)\Delta^s$ は南方最遠点信夫の初動をとつた場合で，第 2 動をとつた $t_3'(\mathrm{II})$ にくらべ誤差が大きいのですてた．初動はより深い層に對應する屈折波と考えられるからである.)

これより，東北地方のこの部分の水平成層構造は，東方測線ではつぎのとおりになる.

第 1 層 (P 波速度 2.56 km/s)

境界面の深さ $Z_1=0.75\pm0.06$ km

第 2 層 (P 波速度 4.67 km/s)

境界面の深さ $Z_2=1.59\pm0.33$ km

第 3 層 (P 波速度 6.08 km/s)

南方測線では第 2 層に對應する走時がえられてないが，適当な震央距離に觀測点がないので，第 2 層が南方でかけているということはできない．たゞ $t_3'(\mathrm{II})$ の震央時刻 τ (intercept time) は t_3 のそれとかなりちがつており，むしろ t_2 のものに近い．そこで一應第 2 層をなしと考えれば爆破点附近の走時と組合わせて，

第 1 層 (P 波速度 2.56 km/s)

境界面の深さ 0.55±0.08 km

第 3 層 (P 波速度 5.91 km/s)

なる構造がえられる.

信夫の第 1 動 I をより深い層 (第 4 層) からの屈折波と考えるとき，かりにそれを自然地震の P_n にあたるとし，速度を 7.5 km/s と假定すれば，この層までの深さは約 24 km になる.

第 1 回の石淵爆破の結果では觀測点が震央に近い方は東方，遠い方ほど南方になつていて，えられた平均的構造に疑問がのこつたが，その点は今回でやゝ明確になつたと考えてよい．第 1 回の結果では，平均として地表から 1.3±1.27 km まで第 1 層で 5.26±0.007 km/s の速度の層があり，その下第 2 層の速度は 6.13±0.017 km/s であつた.

なお，東方，南方兩測線とも $V_4=3.37$ km/s の波がえられ，これは前回一應 S_1 波となづけたものに對應している．これが S 波かどうかは疑問もあるが，速度は前回の S_1 と全く同じ値である．なお前回は S_1 に約 1 秒おくれ S_1 と同じ速度でつたわる S_2 が大きく記錄されたが，今回はこのような位相はみられなかつた．爆破條件のちがいによるのかも知れない.

最後に今回の觀測について，多大の後援をあたえられた東北地方建設局，西松組，東北電力株式會社，日本放送協會仙臺放送局，電波廳標準電波發射所，水沢營林署，岩手・宮城・福島各縣警察当局，各觀測点所在官民各機關及び各觀測班所屬機關關係者各位にあつく御禮申し上げる次第である.

なお本研究の經費の一部は文部省科學研究費によるものである．附記して謝意を表する.

A

B

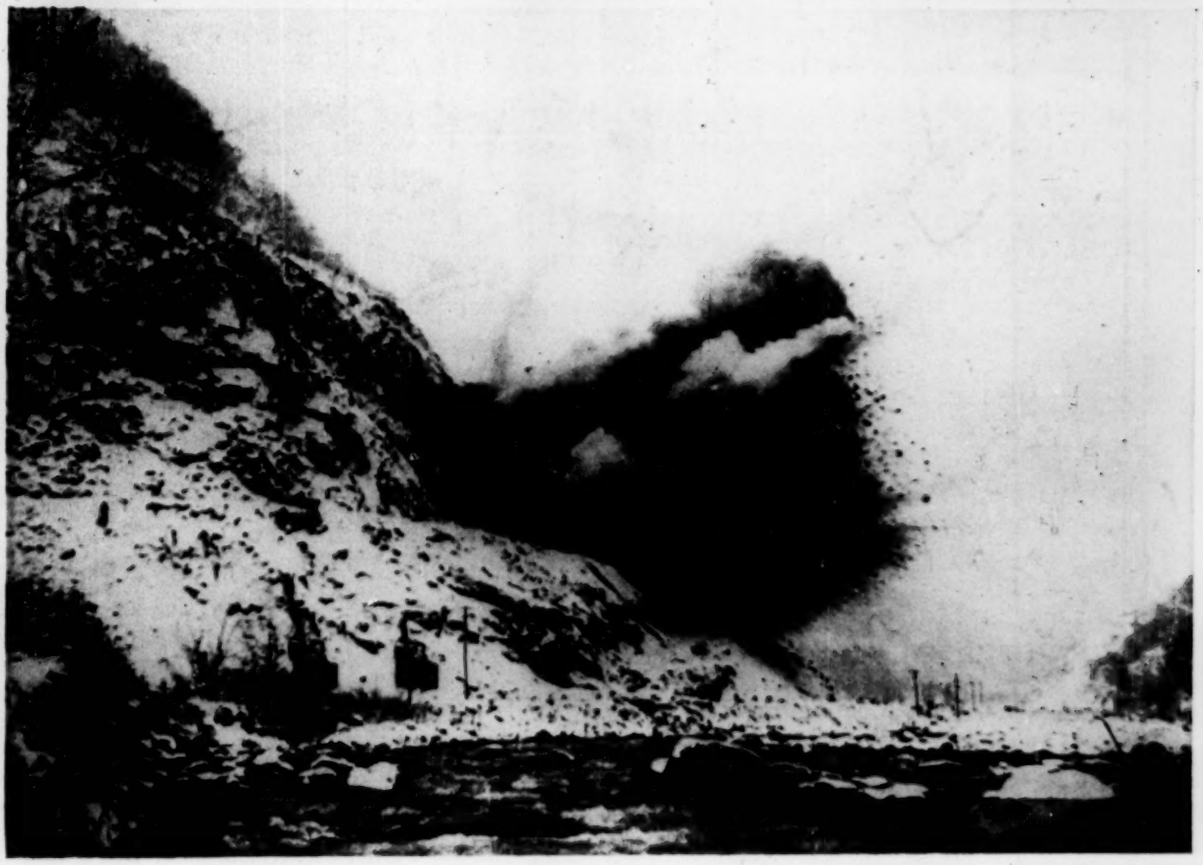

Fig. 4. The second large explosion at Isibuti, Iwate-ken, on December 27th, 1951.
A. Broken line indicates the area to be loosened.
B. Instant of explosion.

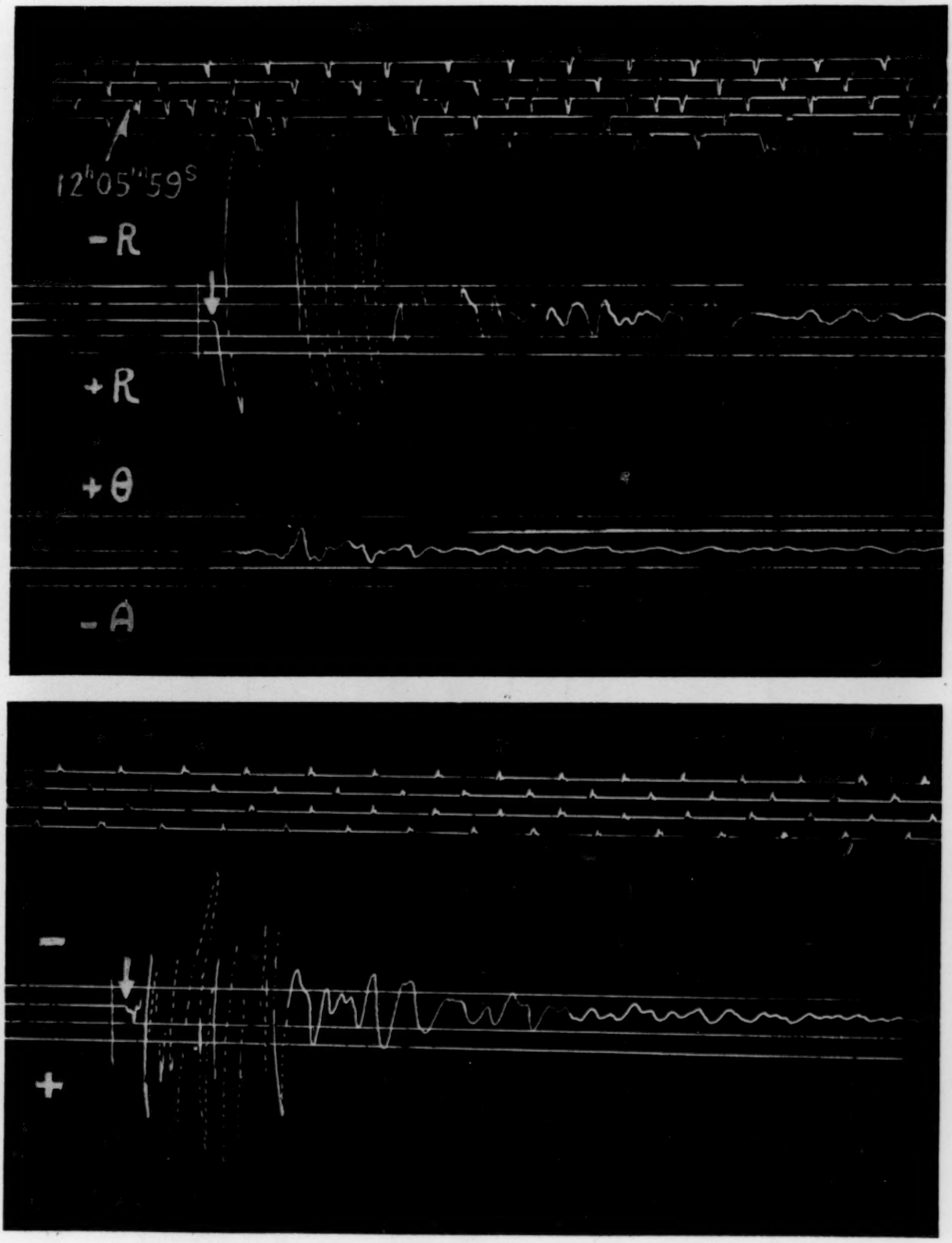

Fig. 5. Seismograms obtained at the second Isibuti explosion of 1951 at Isibuti (A) and Orose (B).

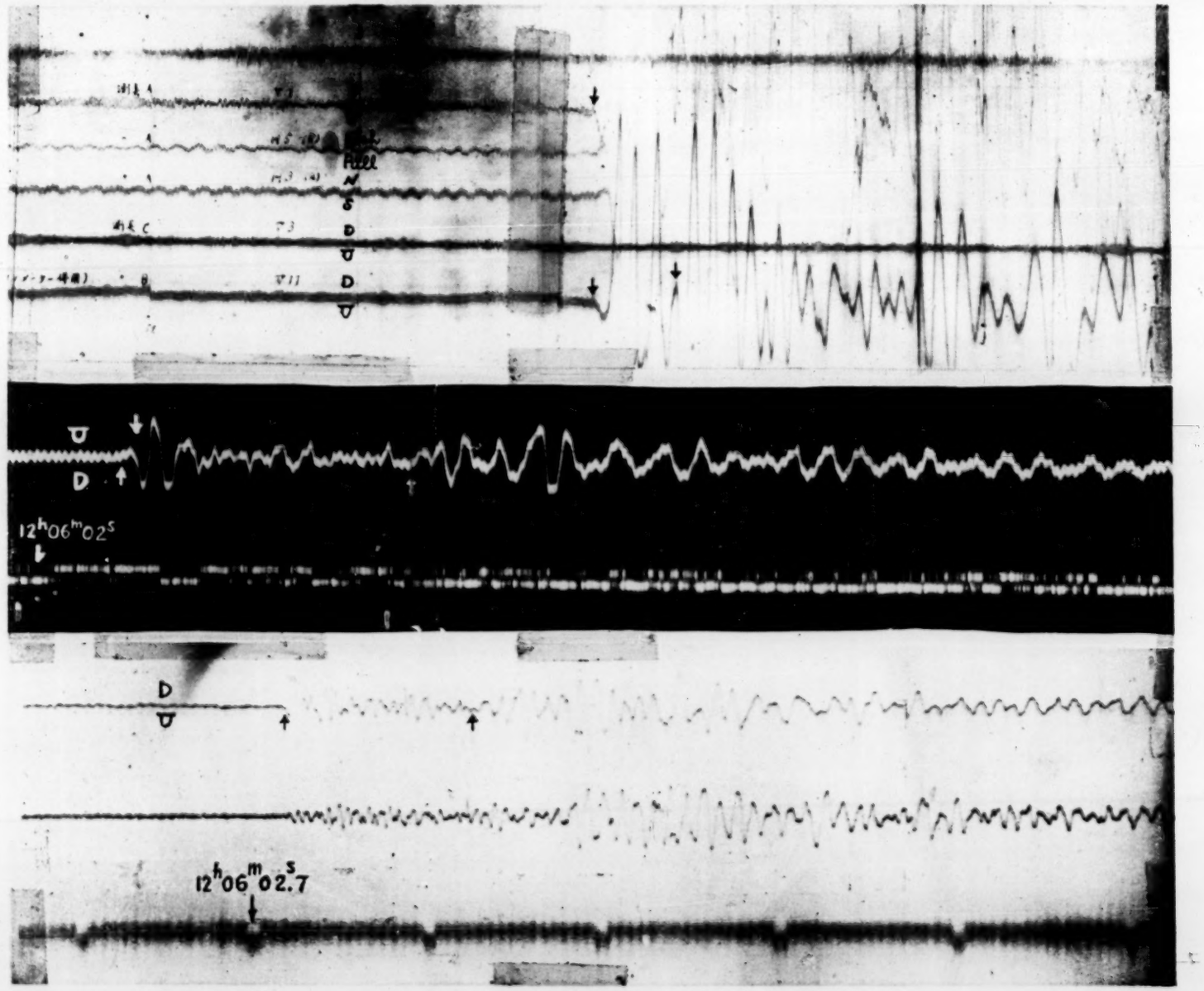

Fig. 6. Seismograms obtained at the second Isibuti explosion of 1951 on the eastern profile at Umadome (A), Atago (B) and Dobasi (C).

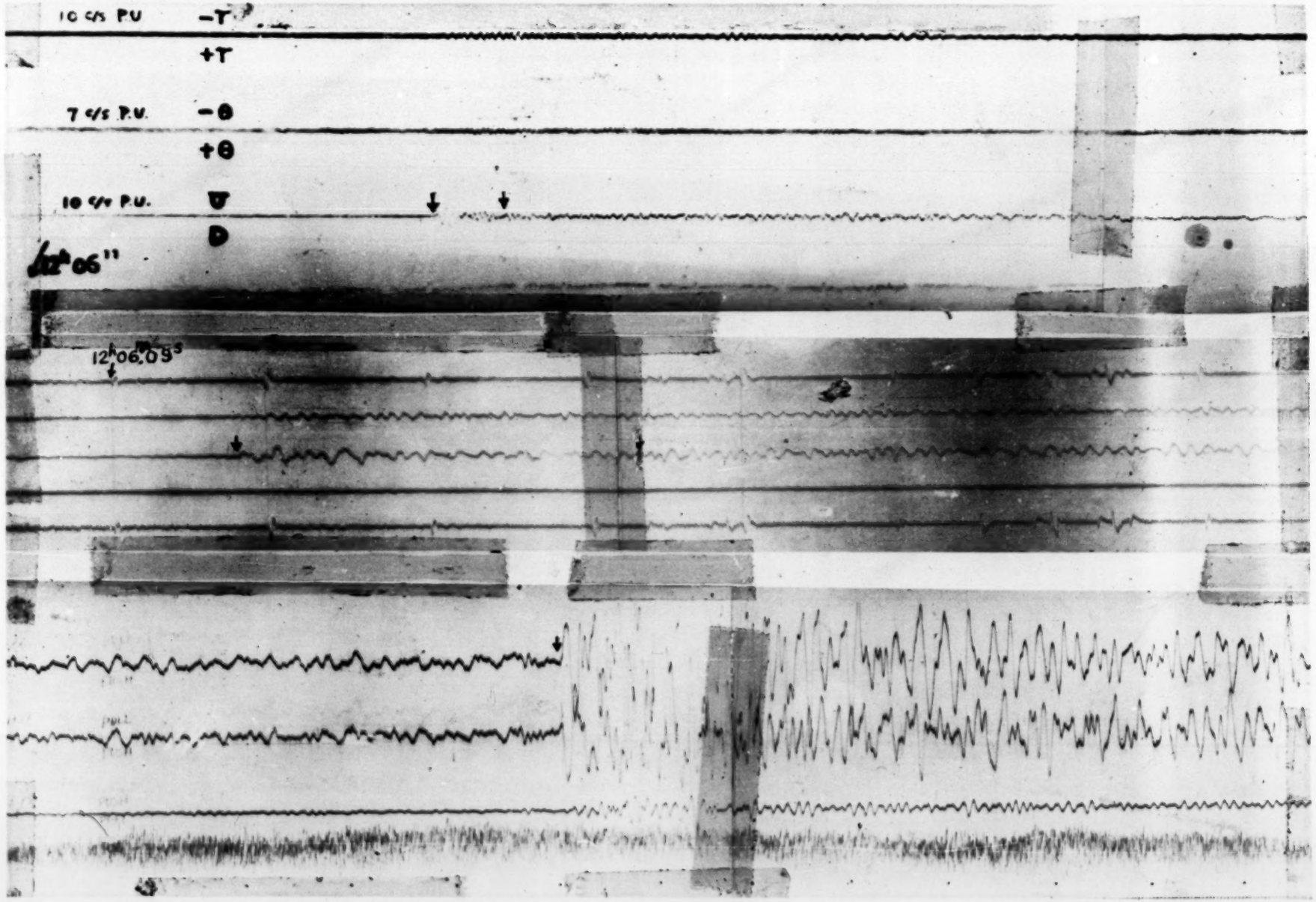

Fig. 7. Seismogrms obtained at the second Isibuti explosion of 1951 on the eastern profile at Wakayanagi (A) Setamai (B) and Kamaisi (C).

(震研彙報 第三十號 圖版 爆破地震動研究グループ)

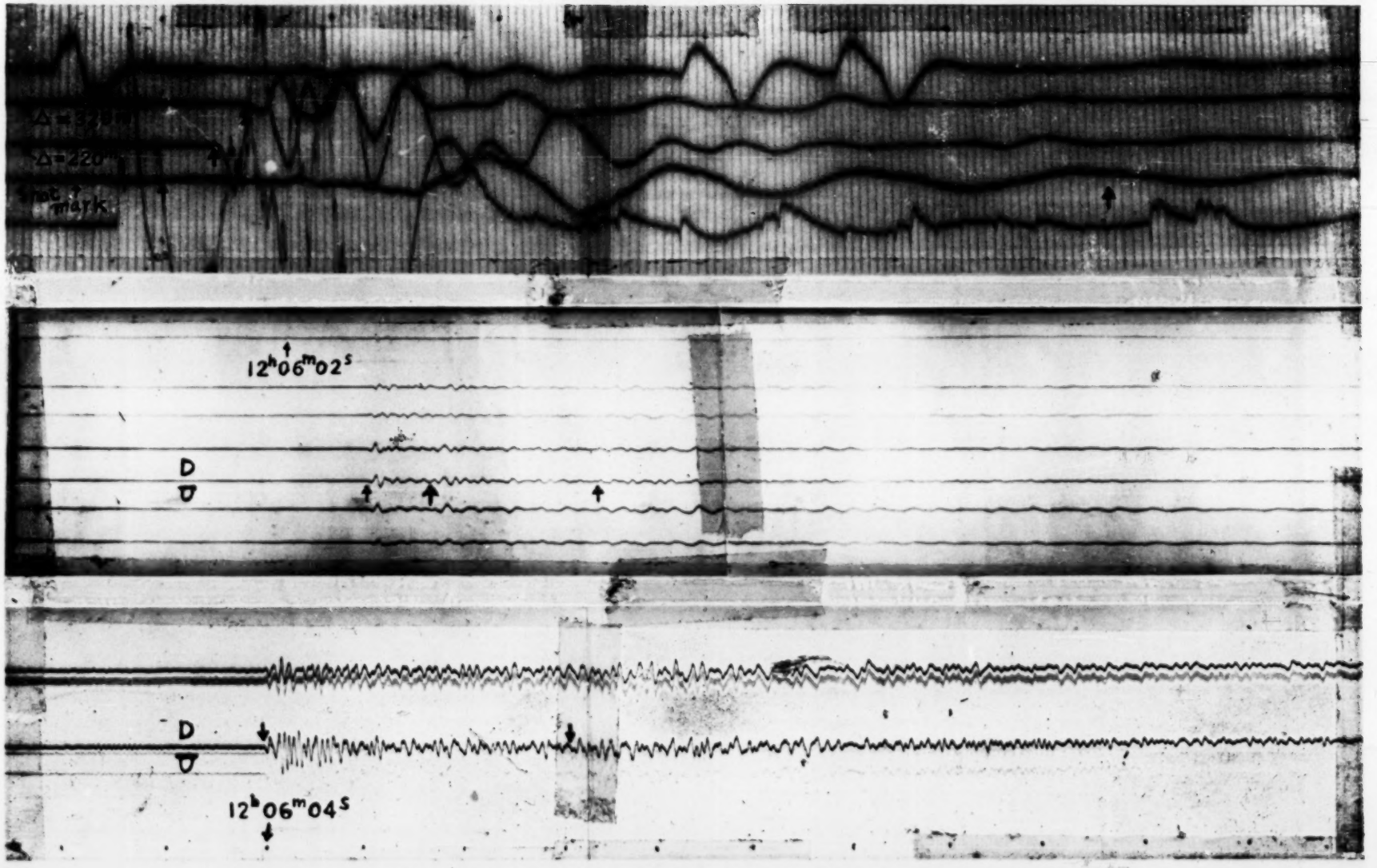

Fig. 8. Seismograms obtained at the second Isibuti explosion of 1951 on the southern profile near the explosion point (A) and at Hondera (B) and Kurikoma (C)

(震研彙報 第三十號 圖版 爆破地震動研究グループ)

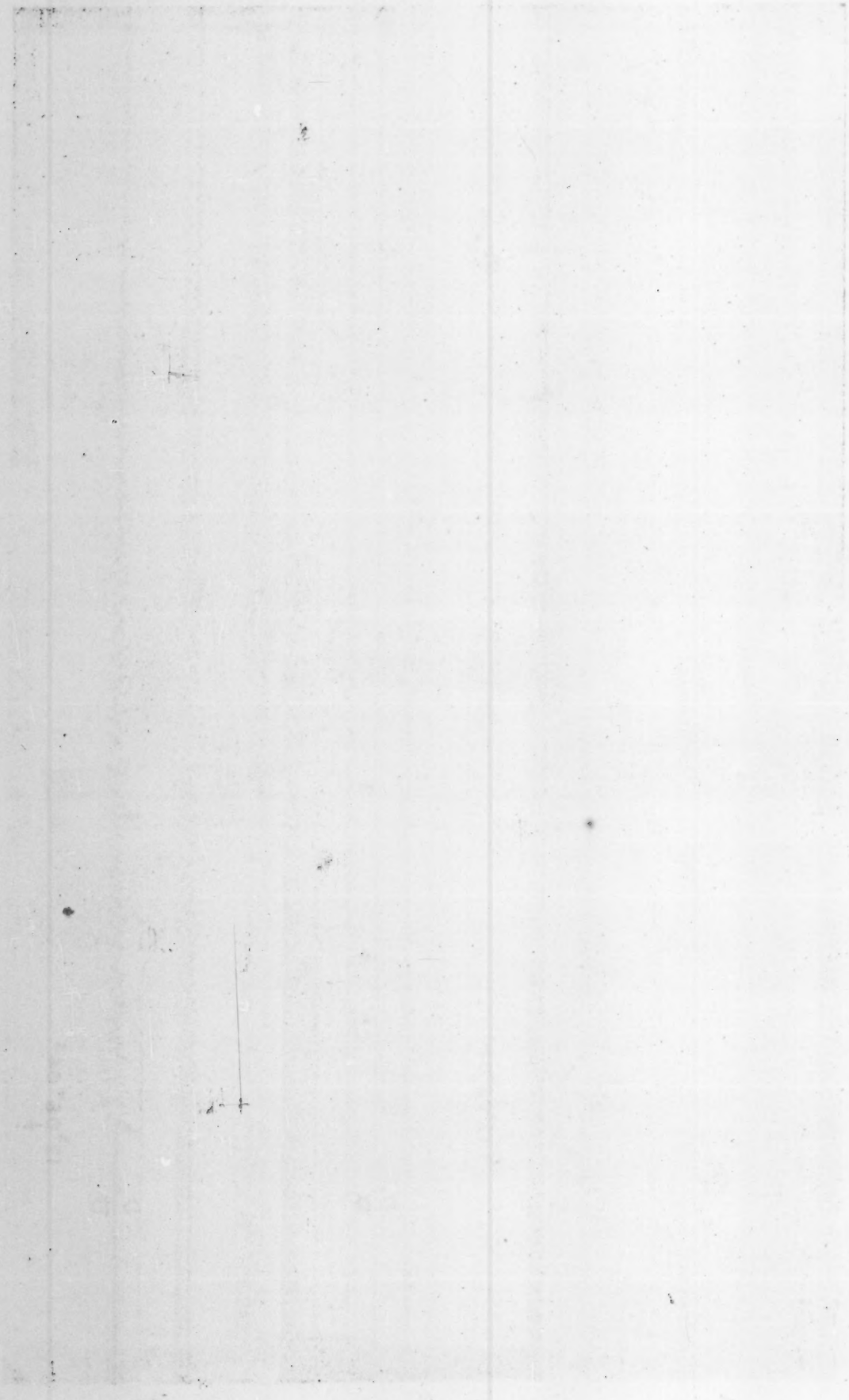

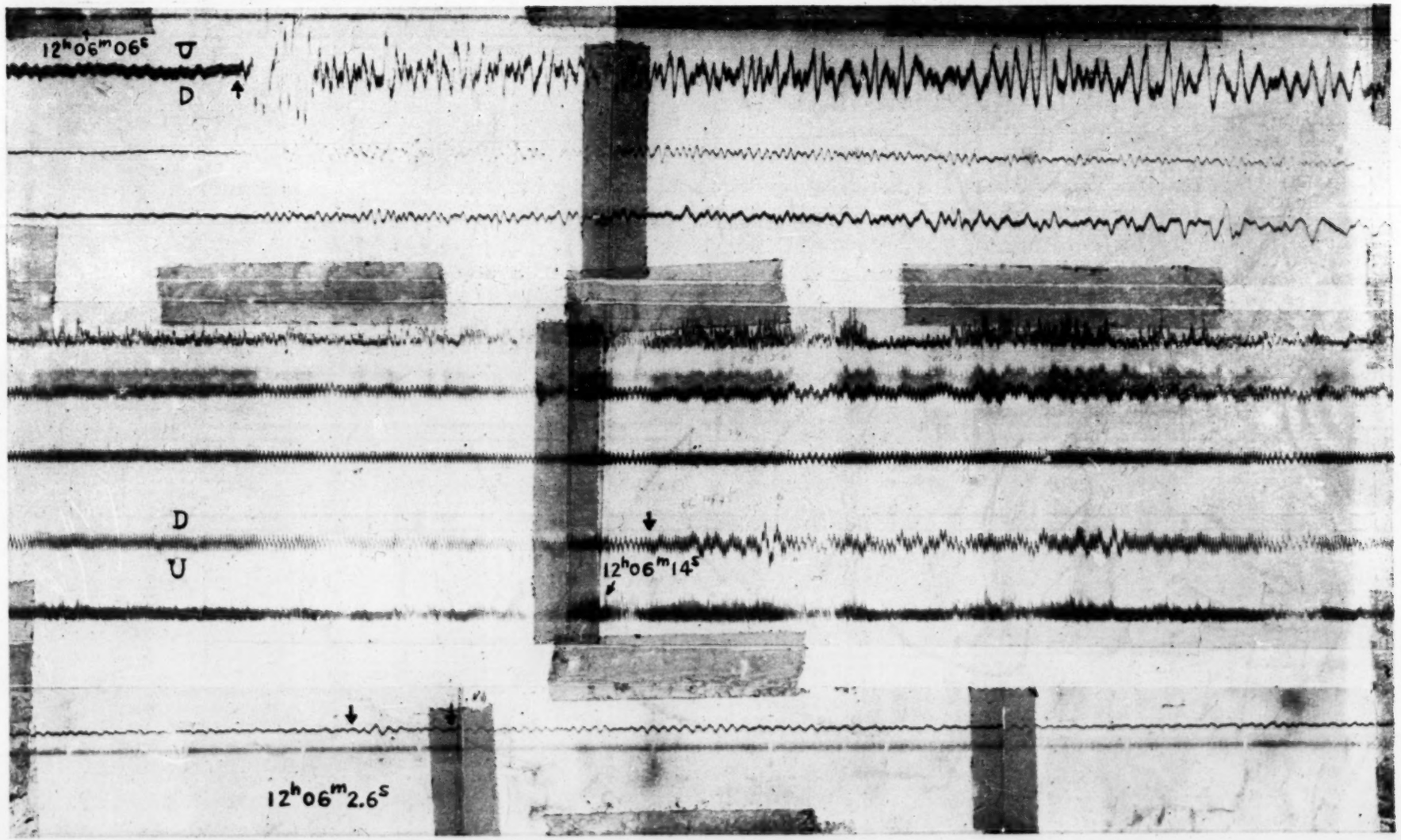

（震研彙報 第三十號 圖版 爆破地震動研究グループ）

Fig. 9. Seismograms obtained at the second Isibuti explosion of 1951 on the southern profile at Kawatabi (A), Matusima (B) and Sinobu (C).

昭和27年9月15日印刷
昭和27年9月20日發行

東京都文京區本富士町一番地
東京大學構內
編纂兼發行者 東京大學地震研究所

東京都千代田區富士見町一丁目十番地
印刷者 笠井康賴

東京都千代田區富士見町一丁目十番地
印刷所 株式會社 國際文献印刷社

賣捌所 東京都千代田區神田一ツ橋通
岩波書店

東京都中央區日本橋通二丁目六番地
丸善株式會社

Sold by
Iwanami Shoten,
Hitotsubashi dôri, Chiyoda-ku, Tôkyô,
and
Maruzen Co., Ltd.,
Nihonbashi dôri, Chûô-ku, Tôkyô.
Price of this copy: 489 Yen. (Postage exclusive.)

BULLETIN OF

THE EARTHQUAKE RESEARCH INSTITUTE

TOKYO UNIVERSITY

Vol. XXX, Part 3. September, 1952.

Contents.

Papers and Reports.

Page

16. Y. SATÔ, Velocity of Elastic Waves Propagated in Media with Small Holes. (in English)..... 179

17. T. RIKITAKE, On the Electrical Conductivity in the Earth's Core. (in English)..... 191

18. T. RIKITAKE, I. YOKOYAMA and Y. HISHIYAMA, A Preliminary Study on the Anomalous Behavior of Geomagnetic Variations of Short Period in Japan and Its Relation to the Subterranean Structure. (in English).... 207

19. D. SHIMOZURU and T. AKIMA, Reflections on the Tsunami of December 21, 1946. (in English)..... 223

20. H. TSUYA, R. MORIMOTO and J. OSSAKA, Chemical Composition of the 1951-lavas of Oshima Volcano, Seven Izu Islands, Japan. (in English)... 231

21. T. AKIMA, On Dispersion Curves of Surface Waves from the Great Assam Earthquake of September 15, 1950. (in English)..... 237

22. K. KASAHARA, Experimental Studies on the Mechanism of Generation of Elastic Waves I. (in English)..... 259

23. S. SAKUMA, Elastic and Viscous Properties of Volcanic Rocks at Elevated Temperature. Part 1. (in English)..... 269

24. The Research Group for Explosion Seismology, The Second Explosion-Seismic Observations in North-Eastern Japan. (in English)..... 297

(For the papers written in Japanese or in occidental languages, the abstracts are given in occidental languages or in Japanese respectively.)

BULLETIN OF THE EARTHQUAKE RESEARCH INSTITUTE,
TOKYO UNIVERSITY. Vol. XXX, Part 4. December, 1952.

東京大學
地震研究所彙報

第 30 號　第 4 册

昭和 27 年12月

目　次

論文及報告

頁

25. エルミツト函數による地磁氣の解析（英文）…… 力武常次 293

26. 表面波の研究 Ⅶ ラブ波の走時（英文）…… 佐藤泰夫 305

27. 日本に起る地震のエネルギー法則（英文）…… 河角廣 319

28. 東京附近に起る地震のエネルギー法則（英文）…… 河角廣 325

所報

索引

(The titles in occidental languages are given on the back cover.)

本彙報ハ年4回（但シ第1號ヨリ第6號マデハ不定期ニ，第7號ハ3冊トシテ發行セリ），彙報別冊ハ不定期ニ發行ス．

本彙報掲載ノ論文及ビ報告ノ内容ニ關シテハ著者ノミニ其責任アルモノトス．

本彙報ニ關スル照會通信ハ東京大學地震研究所長ヘ宛テラレタシ．

The Bulletin is published quarterly. (Vols. I–VI were published at irregular intervals and Vol. VII consisted of three parts.)
Supplementary Volume is published at irregular interval.

The authors of the papers alone are responsible for the statements and opinions contained in their respective papers.

All communications relating to this Bulletin should be addressed to the Director of the Earthquake Research Institute, Tokyo University.

25. *Analyses of Geomagnetic Field by Use of Hermite Functions.*

By Tsuneji RIKITAKE,

Earthquake Research Institute.

(Read Sept. 16, 1952.—Received Sept. 20, 1952.)

1. Introduction.

It is of much importance and interest to interpret geomagnetic anomalies in both pure and applied geophysics. As has been summarized by E. H. Vestine and N. Davids[1], we have a good number of methods for analyzing and interpreting geomagnetic anomalies. Among these methods, the method of Fourier series developed by T. Nagata[2] seems to be one of the most convenient owing to the ease with which it can be applied in practice. The idea of the method by which the subterranean mass distribution may be obtained directly from the anomaly observed on the earth's surface was first adopted tentatively by C. Tsuboi and T. Fuchida[3] for finding out the density distribution concentrated on a subterranean plane directly from the gravity values observed on the earth's surface.

According to the T-N (Tsuboi-Nagata) method, we take a certain region in which the anomalies are predominant and then the anomalies are subjected to a Fourier analysis. Hence we are obliged to assume that the same anomalies are repeated periodically outside the said region, the distribution of anomaly then being different from the actual one. In so far as we discuss the anomaly and the corresponding subterranean structure within the limited region taken above, the result of the method seems to be approximately correct as already shown by Tsuboi and Nagata for various examples.

We, however, have sought after a more rigorous method by which we could treat not the limited are aalone but the whole area in question. Such a method of analysis would be particularly useful for studying an isolated anomaly and the corresponding underground structure. From

1) E. H. VESTINE and N. DAVIDS, *Terr. Mag.*, **50** (1945), 1.
2) T. NAGATA, *Bull. Earthq. Res. Inst.*, **16** (1938), 550.
3) C. TSUBOI and T. FUCHIDA, *Bull. Earthq. Res. Inst.*, **15** (1937), 636.

this viewpoint, the writer would like to propose here a method with the aid of Hermite functions. This method is to be applied in studying an anomaly together with the corresponding magnetization concentrated on a subterranean plane. The validity of the result will be under no spatial restrictions.

2. Theory for the two dimensional analysis.

It is well known that any function of x defined in a region from $x=-\infty$ to $x=+\infty$ can be expressed with a series of Hermite polinominals multiplied by $e^{-\frac{x^2}{2}}$. We shall, in the first place, express the geomagnetic anomaly, for instance the anomaly in the vertical component $\Delta Z(x)$ which is observed on the earth's surface, with a series as

$$\Delta Z(x)=\sum_{n=0}^{\infty} K_n H_n(x) e^{-\frac{x^2}{2}}, \tag{1}$$

where $H_n(x)$ is a Hermite polinominal defined by

$$\left.\begin{aligned} H_{2m}(x)&=\sum_{s=0}^{m}(-1)^s\frac{(2m)!}{(2m-2s)!s!}(2x)^{2m-2s},\\ H_{2m+1}(x)&=\sum_{s=0}^{m}(-1)^s\frac{(2m+1)!}{(2m-2s+1)!s!}(2x)^{2m-2s+1},\end{aligned}\right\} \tag{2}$$

respectively for even and odd degrees. The first several polinominals become as follows;

$$\left.\begin{aligned} &H_0=1,\\ &H_1=2x,\\ &H_2=4x^2-2,\\ &H_3=8x^3-12x,\\ &H_4=16x^4-48x^2+12,\\ &H_5=32x^5-160x^3+120x,\\ &H_6=64x^6-480x^4+720x^2-120,\\ &H_7=128x^7-1344x^5+3360x^3-1680x,\\ &H_8=256x^8-3584x^6+13440x^4-13440x^2+1680,\\ &H_9=512x^9-9216x^7+48384x^5-80640x^3+30240x,\\ &\cdots\cdots\cdots\cdots\cdots\cdots\cdots\cdots\cdots\cdots\end{aligned}\right\} \tag{3}$$

If we define $\phi_n(x)$ by

$$\phi_n(x)=H_n(x)e^{-\frac{x^2}{2}}, \tag{4}$$

$\phi_n(x)$'s form a system of orthogonal functions in a region from $x=-\infty$ to $x=+\infty$ as easily proved. The values of $\phi_n(x)$ for various x will be given in Table I.

We have from (1)

$$K_n=\frac{1}{2^n n!\sqrt{\pi}}\int_{-\infty}^{\infty}\Delta Z(\xi)\phi_n(\xi)d\xi, \tag{5}$$

because we know that

$$\int_{-\infty}^{\infty}\{\phi_n(\xi)\}^2 d\xi=\int_{-\infty}^{\infty}\{H_n(\xi)\}^2 e^{-\xi^2}d\xi=2^n n!\sqrt{\pi}. \tag{6}$$

Taking next the typical term $\phi_n(x)$ we shall apply a Fourier integral to it. If we assume that $\phi_n(x)$ can be expressed as

$$\phi_n(x)=\int_0^{\infty}A_n(u)\cos uxdu+\int_0^{\infty}B_n(u)\sin uxdu, \tag{7}$$

we readily obtain

$$\left.\begin{aligned} &A_{2m}(u)=\frac{2}{\pi}\int_0^{\infty}\phi_{2m}(\xi)\cos u\xi d\xi, \qquad B_{2m}(u)=0,\\ &A_{2m+1}(u)=0, \quad B_{2m+1}(u)=\frac{2}{\pi}\int_0^{\infty}\phi_{2m+1}(\xi)\sin u\xi d\xi, \end{aligned}\right\} \tag{8}$$

by taking into consideration that $\phi_n(x)$ is an even or an odd function corresponding to even or odd n's.

To calculate the integrals in (8), we should take into account (2), whence we get

$$A_{2m}(u)=\frac{2}{\pi}\sum_{s=0}^{m}(-1)^s\frac{2^{2m-2s}(2m)!}{(2m-2s)!s!}\int_0^{\infty}\xi^{2m-2s}e^{-\frac{\xi^2}{2}}\cos u\xi d\xi. \tag{9}$$

On the other hand, it is proved that

$$\left.\begin{aligned} &\int_0^{\infty}e^{-\frac{t^2}{2}}\cos ut\,dt=\sqrt{\frac{\pi}{2}}e^{-\frac{u^2}{2}},\\ &\int_0^{\infty}te^{-\frac{t^2}{2}}\sin ut\,dt=\sqrt{\frac{\pi}{2}}ue^{-\frac{u^2}{2}},\\ &\int_0^{\infty}t^2e^{-\frac{t^2}{2}}\cos ut\,dt=\sqrt{\frac{\pi}{2}}(1-u^2)^{-\frac{u^2}{2}}, \end{aligned}\right\} \tag{10}$$

Table I. Table for Hermite Functions.

x	ϕ_0	ϕ_1	ϕ_2	ϕ_3	ϕ_4	ϕ_5	ϕ_6	ϕ_7	ϕ_8	ϕ_9
0.0	1.000	0	-2.000	0	12.00	0	-120.0	0	1680	0
0.2	0.9802	0.3921	-1.830	-2.290	9.906	22.28	-90.14	-303.4	1141	5311
0.4	0.9231	0.7385	-1.255	-3.958	4.366	35.16	-15.53	-434.3	-196.5	6845
0.6	0.8353	1.002	-0.4678	-4.571	-2.678	33.35	66.81	-320.3	-1320	3538
0.8	0.7262	1.162	0.4067	-3.997	-8.835	17.84	116.9	-26.25	-1680	-2300
1.0	0.6065	1.213	1.213	-2.426	-12.13	-4.852	111.6	281.4	-1001	-6502
1.2	0.4868	1.168	1.830	-0.2804	-11.66	-25.73	54.80	440.3	289.4	-6350
1.4	0.3753	1.051	2.192	1.934	-7.748	-37.13	-26.60	371.1	1411	-1982
1.6	0.2780	0.8896	2.291	3.772	-1.674	-35.53	-91.40	116.1	1729	3398
1.8	0.1979	0.7124	2.167	4.959	4.837	-22.26	-128.5	-195.5	1095	6872
2.0	0.1353	0.5412	1.894	5.412	10.23	-2.165	-111.5	-420.0	-123.9	6243
2.2	0.08892	0.3912	1.543	5.227	13.74	18.63	-55.17	-466.3	-1290	1787
2.4	0.05614	0.2695	1.181	4.592	14.95	35.04	18.25	-388.9	-1837	-5119
2.6	0.03405	0.1771	0.8526	3.725	14.26	44.33	88.26	-73.02	-1628	-7332
2.8	0.01984	0.1111	0.5825	2.818	12.28	46.25	136.0	206.8	-741.5	-7462
3.0	0.01111	0.06666	0.3777	2.000	9.732	42.40	157.1	433.6	402.6	-4516
3.2	$0.0^2$5864	0.03753	0.2285	1.312	7.026	34.47	150.4	548.9	1405	21.19
3.4	$0.0^2$3091	0.02102	0.1367	0.8458	4.931	26.76	132.6	580.6	2095	4952
3.6	$0.0^2$1535	0.01105	0.07650	0.5066	3.189	18.91	104.3	523.9	2311	8254
3.8	$0.0^3$7319	$0.0^2$5396	0.03959	0.2793	1.885	12.09	76.00	410.1	2082	9354
4.0	$0.0^3$3355	$0.0^2$2684	0.02080	0.1557	1.121	7.719	50.55	312.1	1786	9303
4.2	$0.0^3$1478	$0.0^2$1241	0.01013	0.08013	0.6108	4.502	31.70	212.2	1367	7851
4.4	$0.0^4$6252	$0.0^3$5502	$0.0^2$4717	0.03931	0.3170	3.665	18.65	134.4	921.3	5957
4.6	$0.0^4$2542	$0.0^3$2339	$0.0^3$2101	0.01839	0.1563	1.802	10.33	79.55	587.2	4129
4.8	$0.0^5$9930	$0.0^4$9532	$0.0^3$8953	$0.0^2$8213	0.07338	0.8382	5.406	44.22	348.8	2641
5.0	$0.0^5$3725	$0.0^4$3725	$0.0^3$3651	$0.0^3$3502	0.03279	0.3747	2.674	23.14	193.9	1569
5.2	$0.0^5$1344	$0.0^4$1398	$0.0^3$1427	$0.0^2$1428	0.01532	0.1610	1.255	11.44	101.4	871.6
5.4	$0.0^6$4656	$0.0^5$5028	$0.0^4$5337	$0.0^3$5563	$0.0^2$6149	0.06629	0.5586	5.343	49.94	453.8
5.6	$0.0^6$1550	$0.0^5$1736	$0.0^4$1913	$0.0^3$2073	$0.0^2$2361	0.02632	0.2362	2.369	23.22	218.8
5.8	$0.0^7$4956	$0.0^6$5749	$0.0^5$6570	$0.0^4$7391	$0.0^3$8175	$0.0^2$9938	0.09503	0.9955	10.22	102.6
6.0	$0.0^7$1522	$0.0^6$1826	$0.0^7$2161	$0.0^4$2520	$0.0^3$2892	$0.0^3$3591	0.03636	0.3971	4.256	42.33
6.2	$0.0^8$4496	$0.0^7$5576	$0.0^6$6824	$0.0^5$8238	$0.0^4$9802	$0.0^2$1246	0.01328	0.1509	1.685	17.70
6.4	$0.0^8$1275	$0.0^7$1633	$0.0^6$2064	$0.0^5$2577	$0.0^4$3173	$0.0^3$4125	$0.0^2$4620	0.05450	0.6330	6.987
6.6	$0.0^9$3476	$0.0^8$4588	$0.0^7$5987	$0.0^6$7719	$0.0^5$9827	$0.0^3$1309	$0.0^2$1533	0.01875	0.2261	2.684
6.8	0.0^{10}9102	$0.0^8$1238	$0.0^7$1667	$0.0^6$2215	$0.0^5$2912	$0.0^4$3975	$0.0^3$4855	$0.0^2$6149	0.07683	0.9465
7.0	0.0^{10}2290	$0.0^9$3206	$0.0^8$4442	$0.0^7$6091	$0.0^6$8258	$0.0^4$1108	$0.0^3$1468	$0.0^2$1923	0.02486	0.3173
7.2	0.0^{11}5535	0.0^{10}7970	$0.0^8$1137	$0.0^7$1605	$0.0^6$2242	$0.0^5$3101	$0.0^4$4241	$0.0^3$5735	$0.0^2$7665	0.1012
7.4	0.0^{11}1285	0.0^{10}1902	$0.0^9$2790	$0.0^8$4053	$0.0^7$5830	$0.0^6$8306	$0.0^4$1171	$0.0^3$1633	$0.0^2$2253	0.03074
7.6	0.0^{12}2868	0.0^{11}4359	0.0^{10}6569	$0.0^9$9810	$0.0^7$1452	$0.0^6$2128	$0.0^5$3090	$0.0^4$4441	$0.0^3$6318	$0.0^2$8892
7.8	0.0^{13}6148	0.0^{12}9592	0.0^{10}1484	$0.0^9$2277	$0.0^8$3462	$0.0^7$5220	$0.0^6$7802	$0.0^4$1154	$0.0^3$1690	$0.0^2$2452
8.0	0.0^{13}1265	0.0^{12}2024	0.0^{11}3214	0.0^{10}5061	$0.0^9$7903	$0.0^7$1224	$0.0^6$1880	$0.0^5$2862	$0.0^4$4314	$0.0^3$6445

$$\left.\begin{aligned}
&\int_0^\infty t^3 e^{-\frac{t^2}{2}} \sin ut\, dt = \sqrt{\frac{\pi}{2}}(3u-u^3)e^{-\frac{u^2}{2}},\\
&\cdots\cdots\cdots\cdots\cdots\cdots\cdots\cdots\cdots\cdots\cdots\cdots\cdots\cdots\cdots\cdots\\
&\cdots\cdots\cdots\cdots\cdots\cdots\cdots\cdots\cdots\cdots\cdots\cdots\cdots\cdots\cdots\cdots\\
&\int_0^\infty t^{2k} e^{-\frac{t^2}{2}} \cos ut\, dt = \frac{(-1)^k}{2^k}\sqrt{\frac{\pi}{2}}\, H_{2k}\left(\frac{u}{\sqrt{2}}\right)e^{-\frac{u^2}{2}},\\
&\int_0^\infty t^{2k+1} e^{-\frac{t^2}{2}} \sin ut\, dt = \frac{(-1)^k}{2^{k+1/2}}\sqrt{\frac{\pi}{2}}\, H_{2k+1}\left(\frac{u}{\sqrt{2}}\right)e^{-\frac{u^2}{2}}.
\end{aligned}\right\}$$

With the aid of (10), (9) becomes

$$A_{2m}(u) = \sqrt{\frac{2}{\pi}}\sum_{s=0}^{m}(-1)^m \frac{2^{m-s}(2m)!}{(2m-2s)!\,s!} H_{2m-2s}\left(\frac{u}{\sqrt{2}}\right)e^{-\frac{u^2}{2}}. \tag{11}$$

Meanwhile we have the relations

$$\left.\begin{aligned}
&\sum_{s=0}^{m}\frac{2^{m-s}(2m)!}{(2m-2s)!s!} H_{2m-2s}\left(\frac{u}{\sqrt{2}}\right) = H_{2m}(u),\\
&\sum_{s=0}^{m}\frac{2^{m-s+1/2}(2m)!}{(2m-2s+1)!s!} H_{2m-2s+1}\left(\frac{u}{\sqrt{2}}\right) = H_{2m+1}(u),
\end{aligned}\right\} \tag{12}$$

which are easily proved. Substituting (12) into (11), we get finally

$$A_{2m}(u) = (-1)^m\sqrt{\frac{2}{\pi}}\phi_{2m}(u). \tag{13}$$

And in a similar way, we have also

$$B_{2m+1}(u) = (-1)^m\sqrt{\frac{2}{\pi}}\phi_{2m+1}(u). \tag{14}$$

Assuming that the anomaly is caused by a magnetization concentrated on an underground plane at a depth of D with the direction of magnetization inclining θ from the horizontal plane, Nagata[2] has shown that the Fourier coefficients of the magnetization are given as

$$\left.\begin{aligned}
a_n(u) &= \frac{e^{uD}}{2\pi u}\{A_n(u)\sin\theta - B_n(u)\cos\theta\},\\
b_n(u) &= \frac{e^{uD}}{2\pi u}\{A_n(u)\cos\theta + B_n(u)\sin\theta\},
\end{aligned}\right\} \tag{15}$$

respectively for harmonics $\cos ux$ and $\sin ux$. Applying (15) to the

present problem and summing up with respect to n or m, the magnetization corresponding to the anomaly is formally expressed as

$$J(x)=\frac{1}{2^{1/2}\pi^{3/2}}\sum_{m=0}^{\infty}(-1)^m K_{2m}\int_0^{\infty}\frac{e^{uD}}{u}\phi_{2m}(u)\sin(ux+\theta)du$$

$$-\frac{1}{2^{1/2}\pi^{3/2}}\sum_{m=0}^{\infty}(-1)^m K_{2m+1}\int_0^{\infty}\frac{e^{uD}}{u}\phi_{2m+1}(u)\cos(ux+\theta)du. \quad (16)$$

In an actual analysis, K_n would be easily obtained by numerical integrations in (5) because, in so far as we treat an isolated anomaly, ΔZ becomes fairly small for large values of $|x|$. And moreover since the integrals in (16) contain the factor $e^{-\frac{u^2}{2}}$ which becomes fairly small for large u, the integrals can be calculated by means of the same method for an assumed value of D.

The Hermite function method stated here will be applied not only to an anomaly in vertical geomagnetic force but also to that in horizontal force as well.

We should pay attention, however, to the fact that the integral $\int_0^{\infty}\frac{e^{uD}}{u}\phi_{2m}(u)\cos ux\,du$ that is included in (16) does not generally converge because the integrand reaches infinity at $u=0$. In that case, the difficulty can be avoided by analyzing magnetic potential which may be obtained by

$$\Delta W(x)=\frac{2}{\pi}\int_{-\infty}^{\infty}\Delta Z(x')\log|x-x'|\,dx', \quad (17)$$

where the integral can be calculated numerically. After that the magnetic potential is expanded into a series of Hermite functions as before. If we denote the coefficient by K'_n, the corresponding magnetization is expressed as

$$J(x)=-\frac{1}{2^{1/2}\pi^{3/2}}\sum_{m=0}^{\infty}K'_{2m}\int_0^{\infty}e^{uD}\phi_{2m}(u)\sin(ux+\theta)du \quad (18)$$

$$+\frac{1}{2^{1/2}\pi^{3/2}}\sum_{m=0}^{\infty}K'_{2m+1}\int_0^{\infty}e^{uD}\phi_{2m+1}(u)\cos(ux+\theta)du,$$

where the integrals included are all convergent.

3. A special case.

In order to examine the relation between the present method and the T-N method, we shall study a special and simple case in which the anomaly is given as

$$\Delta W=\cos \alpha x \qquad \text{for} \quad -\infty<x<\infty, \tag{19}$$

and the direction of magnetization is taken downwards or $\theta=\pi/2$ for the sake of simplicity.

In that case, we have

$$K'_{2m}=\frac{1}{2^{2m-1}(2m)!\sqrt{\pi}}\int_0^\infty \phi_{2m}(t)\cos \alpha t\,dt,\ K_{2m+1}=0 \tag{20}$$

from (5) and

$$J(x)=\frac{1}{2^{1/2}\pi^{3/2}}\sum_{m=0}^{\infty}(-1)^m K'_{2m}\int_0^\infty e^{uD}\phi_{2m}(u)\cos uxdu. \tag{21}$$

As proved in the last section, we get

$$\int_0^\infty \phi_{2m}(t)\cos \alpha t\,dt=(-1)^m\sqrt{\frac{\pi}{2}}\phi_{2m}(\alpha), \tag{22}$$

and hence

$$K'_{2m}=\frac{(-1)^m}{2^{2m-1/2}(2m)!}\phi_{2m}(\alpha). \tag{23}$$

Substituting (23) into (21), we obtain

$$J(x)=\frac{-1}{2\pi^{3/2}}\sum_{m=0}^{\infty}\frac{\phi_{2m}(\alpha)}{2^{2m-1}(2m)!}\int_0^\infty e^{uD}\phi_{2m}(u)\cos uxdu. \tag{24}$$

Since the right-hand side of (24) is identical with the expansion of $-\frac{e^{\alpha D}\cos \alpha x}{2\pi}$ in a series of Hermite functions whose variable is α, it follows that

$$J(x)=-\frac{e^{\alpha D}\cos \alpha x}{2\pi}, \tag{25}$$

which agrees exactly with the result obtained by the T-N method. Thus it is made clear that if the harmonics such as $\cos \alpha x$ and $\sin \alpha x$

are defined throughout the whole space both mothods give the same result.

4. A typical example for an isolated anomaly.

Now we are going to study an example in order to compare the writer's method to T-N one in case of an isolated anomaly. We shall consider an anomaly in the vertical geomagnetic component which is given as

$$\Delta Z=\begin{cases} 0 & \text{for} \quad x<-\pi, \\ \sin x & \text{for} \quad -\pi<x<\pi, \\ 0 & \text{for} \quad \pi<x. \end{cases} \tag{26}$$

According to the T-N method of Fourier series, we obviously find only one harmonic $\sin x$ by taking the region from $x=-\pi$ to $x=\pi$. And so the magnetization concentrated on an underground plane at a depth D with an assumed downward direction is immediately obtained as

$$J=\frac{e^{D}\sin x}{2\pi} \tag{27}$$

On the other hand, ΔZ given by (26) is expressed fairly well with five odd terms of Hermite functions. That is

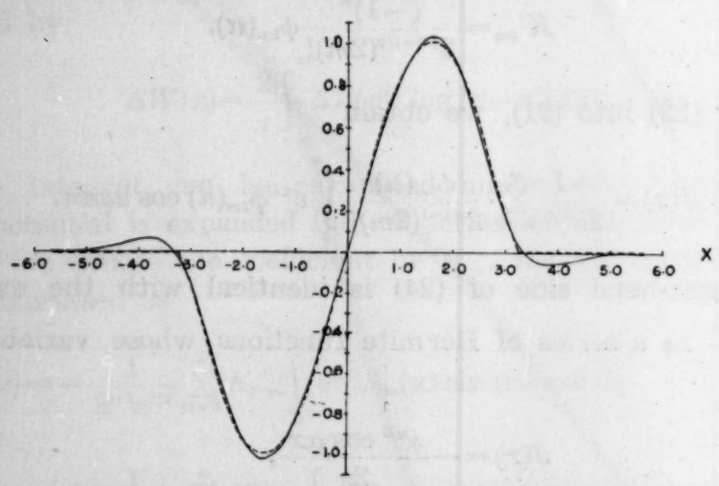

Fig. 1. The approximation of the curves defined by 0 for $x<-\pi$, $\sin x$ for $-\pi<x<\pi$ and 0 for $\pi<x$ (broken line) with five Hermite functions (full line).

$$\Delta Z = \sum_{m=0}^{4} K_{2m+1}\phi_{2m+1}(x), \tag{28}$$

where

$$K_1 = 0.8601, \quad K_3 = 0.0760, \quad K_5 = -0.000154,$$
$$K_7 = -0.000140, \quad K_9 = -0.00000278. \tag{29}$$

The approximations of this series seems to be good as shown in Fig. 1, the error being within a few per cent. With the aid of the values of K_1, K_3, ..., we can calculate the magnetization by (16), for example when D is assumed as 0 and 1. The results are shown in Figs. 2 and 3 respectively together with the calculated results obtained by the T-N method.

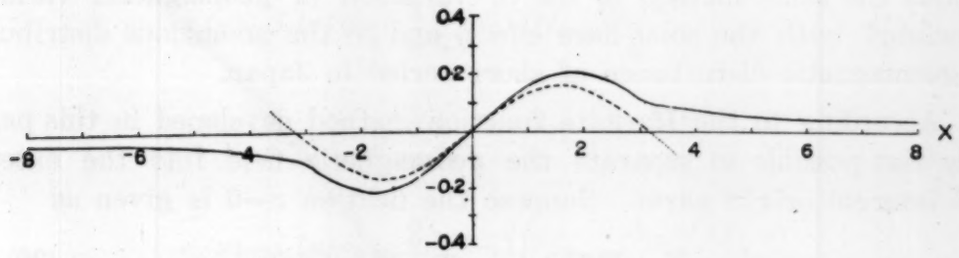

Fig. 2. The magnetization obtained by T-N method (broken line) and by the Hermite function method (full line) for $D=0$.

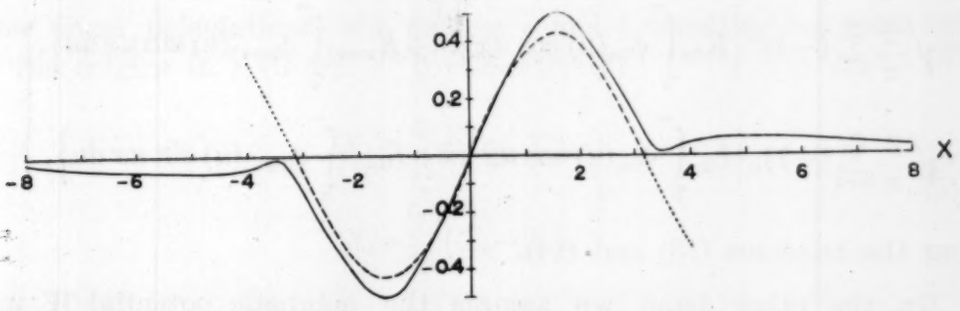

Fig. 3. The magnetization obtained by T-N method (broken line) and by the Hermite function method (full line) for $D=1$.

As clearly shown in these figures, the discrepancies between the results obtained by the T-N method and those by the Hermite function method become fairly large at the ends of the anomaly distribution. However, we find no serious difference in the central part of the distribution as may be naturally expected. Hence the T-N method may be applied if one does not wish to keep rigorousness near the ends of the anomaly distribution.

5. Separation of geomagnetic field into external and internal origin parts.

When the X- and Z- components of a geomagnetic field are given over a plane surface $z=0$, it is obvious that the field can be separated into two parts originating from above and below $z=0$ respectively. Such a separation has already been discussed by Vestine[1] by use of Fourier series and surface integrals. Meanwhile the Fourier series method has been applied to some actual problems concerning the field under the auroral zone by A. G. McNish[4] and Nagata[5], while the writer[6],[7] applied the same method to the SF-variation (a geomagnetic variation associated with the solar-flare effect) and to the anomalous distribution of geomagnetic disturbance of short period in Japan.

According to the Hermite function method developed in this paper, it is also possible to separate the geomagnetic field into the external and internal origin parts. Suppose the field on $z=0$ is given as

$$X_0=\sum_n K_n\phi_n(x),\quad Z_0=\sum_n L_n\phi_n(x), \tag{30}$$

these components can be written in the next forms;

$$\left.\begin{aligned} X_0&=\sqrt{\frac{2}{\pi}}\sum_{m=0}^{\infty}(-1)^m\left\{K_{2m}\int_0^{\infty}\phi_{2m}(u)\cos ux\,dn+K_{2m+1}\int_0^{\infty}\phi_{2m+1}(u)\sin ux\,du\right\},\\ Z_0&=\sqrt{\frac{2}{\pi}}\sum_{m=0}^{\infty}(-1)_m\left\{L_{2m}\int_0^{\infty}\phi_{2m}(u)\cos ux\,du+L_{2m+1}\int_0^{\infty}\phi_{2m+1}(u)\sin ux\,du\right\},\end{aligned}\right\} \tag{31}$$

using the relations (13) and (14).

On the other hand we assume the magnetic potential W which satisfies $\nabla^2W=0$. It is given as

$$W=\int_0^{\infty}[\{e_c(u)e^{-uz}+i_c(u)e^{uz}\}\cos ux+\{e_s(u)e^{-uz}+i_s(u)e^{uz}\}\sin ux]\,du. \tag{32}$$

---

4) A. G. MCNISH, *Terr. Mag.*, **43** (1938), 67.
5) T. NAGATA, *Rep. Ionos. Res. Japan*, **4** (1950), 87.
6) T. RIKITAKE, *Bull. Earthq. Res. Inst.*, **28** (1950), 219.
7) T. RIKITAKE, I. YOKOYAMA and Y. HISHIYAMA, *Bull. Earthq. Res. Inst.*, **30** (1952), 207.

Then we get X_0 and Z_0 from (32) as follows;

$$\left.\begin{aligned} X_0&=\int_0^\infty [\{e_c(u)+i_c(u)\}u\sin ux-\{e_s(u)+i_s(u)\}u\cos ux]\,du,\\ Z_0&=\int_0^\infty [\{e_c(u)-i_c(u)\}u\cos ux+\{e_s(u)-i_s(u)\}u\sin ux]\,du. \end{aligned}\right\} \quad (33)$$

Comparing (31) with (33), we have the next simultaneous equations

$$\left.\begin{aligned} e_c(u)+i_c(u)&=\sqrt{\frac{2}{\pi}}\sum_m(-1)^m K_{2m+1}\frac{\phi_{2m+1}(u)}{u},\\ e_c(u)-i_c(u)&=\sqrt{\frac{2}{\pi}}\sum_m(-1)^m L_{2m}\frac{\phi_{2m}(u)}{u},\\ -e_s(u)-i_s(u)&=\sqrt{\frac{2}{\pi}}\sum_m(-1)^m K_{2m}\frac{\phi_{2m}(u)}{u},\\ e_s(u)-i_s(u)&=\sqrt{\frac{2}{\pi}}\sum_m(-1)^m L_{2m+1}\frac{\phi_{2m+1}(u)}{u}. \end{aligned}\right\} \quad (34)$$

from which we can obtain e_c, i_c, e_s and i_s. With these coefficients we have the external and internal parts of X on $z=0$ as written below after some calculations, the suffices e and i denoting the parts caused by the origins in $z>0$ and $z<0$ respectively;

$$\left.\begin{aligned} X_e&=\frac{1}{2}(X_0+X'),\\ X_i&=\frac{1}{2}(X_0-X'), \end{aligned}\right\} \quad (35)$$

where

$$X'=\sqrt{\frac{2}{\pi}}\sum_{m=0}^{\infty}(-1)^m\left\{L_{2m}\int_0^\infty\phi_{2m}(u)\sin ux\,du-L_{2m+1}\int_0^\infty\phi_{2m+1}(u)\cos ux\,du\right\}. \quad (36)$$

And we have also

$$\left.\begin{aligned} Z_e&=\frac{1}{2}(Z_0-Z'),\\ Z_i&=\frac{1}{2}(Z_0+Z'), \end{aligned}\right\} \quad (37)$$

where

$$Z'=\sqrt{\frac{2}{\pi}}\sum_{m=0}^{\infty}(-1)^m\left\{K_{2m}\int_0^{\infty}\phi_{2m}(u)\sin ux\,du-K_{2m+1}\int_0^{\infty}\phi_{2m+1}(u)\cos uxdu\right\}. \quad (38)$$

6. Conclusions.

By using Hermite functions, the writer proposed a rigorous method of obtaining subterranean magnetization by which the geomagnetic anomaly on the earth's surface is caused. As shown in the example, the present method is more accurate than the one based on Fourier series which has been developed by Tsuboi and Nagata. Though the Hermite function method seems to be rather complicated, the writer is now arranging the tables of integrals such as $\int_0^{\infty}e^{uD}\phi_n(x)\begin{matrix}\cos\\ \sin\end{matrix}ux\,du$ for various D and x, which will be useful for actual analyses. The theory of separation of geomagnetic field into external and internal origin parts is also discussed in this paper.

In conclusion the writer is grateful to Miss Y. Hishiyama and Miss Y. Naito who assisted the writer in the course of the numerical work. A part of this study was conducted with the financial aid of research grant from the Department of Education and the writer's sincere thanks are also due to the Department.

---

25. エルミット函数による地磁気の解析

地震研究所　力　武　常　次

エルミット函数の直交性を利用して，地表で觀測された磁場分布より地下の1平面上の帶磁分布を直接求める方法を考案した．この方法によれば，孤立した地磁気異常を解析する場合に正確な結果を與える．フーリエ級数による坪井—永田の方法とくらべる時，異常の中央部附近ではほとんど一致するが，末端ではいちじるしい喰違いが見られ，嚴密を要する場合はエルミット函数法によるべきであると考えられる．地表の磁場を外部および内部に原因を有する部分に分ける方法も述べてある．

---

26. *Study on Surface Waves VII. Travel-Time of Love-Waves.*

By Yasuo SATÔ,

Earthquake Research Institute.

(Read May 20, 1952.—Received Sept. 20, 1952.)

1. Introduction.

Among the properties of seismic waves, the travel-time is perhaps about the most important, and is known fairly well with respect to the bodily waves, especially the dilatational waves. In regard to the surface waves, however, we have less knowledge than in regard to *P*-waves. If we confine our attention to the theoretical side of investigation, we have only a few papers published in Japan; viz. the famous study of H. Nakano[1] treating the two-dimensional problem, and the complicated mathematical studies of T. Sakai[2] and S. Syôno[3] treating the three dimensional problem. However, these three papers are all concerned with Rayleigh-waves, and not a single paper has been published concerning the travel-time of Love-waves. This fact is rather strange, for if we compare Love- and Rayleigh-waves, the chance of observing the former is not smaller than the chance of observing the latter. Moreover, the mathematical treatment is easier in Love-waves. (But this circumstance might not have affected positively the advancement of investigation[4].)

In our calculations, we will pay little attention to the amplitude, and confine ourcelves to the retardation of phases in Love-waves. Integral representations of displacements has been given already[5], and the

1) H. NAKANO, "On Rayleigh Waves", *Jap. Journ. Astro. and Geophy.*, **2** (1925), 233.

2) T. SAKAI, "On the Propagation of Tremors over Plane Surface of an Elastic Solid produced by an Internal Source," *Geophys. Mag.*, **8** (1934), 1.

3) S. Syôno, "On the Propagation of Tremors over the Plane Surface of a Semi-infinite Perfect Elastic Solid I," *Geophys. Mag.*, **12** (1938), 67.

4) K. SEZAWA, "Propagation of Love-waves on a Spherical Surface and Allied Problems." *Bull. Earthq. Res. Inst.*, **7** (1926), 437. Summary written in Japanese.

5) K. SEZAWA, "Love-waves Generated from a Source of a certain Depth," *Bull Earthq. Res. Inst.*, **13** (1935), 1. Y. SATÔ, "Study on Surface Waves VI," *ibid.*, **30** (1952), 101.

integration path was shown to be not of a single way[6], therefore the results are easity obtained as follows.

2. When the origin resides in the superficial layer.

If the origin is situated at a point $Q(O, E)$ in the superficial layer (cf. Fig. 1), and the displacement is expressed by the equation

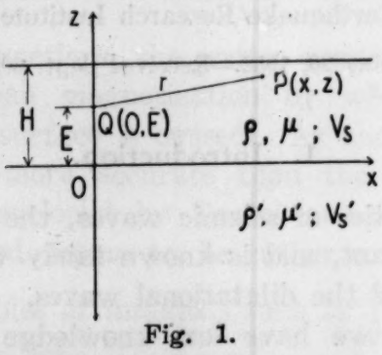

Fig. 1.

$$v_0=H_0^{(2)}(kr)\exp(ipt) \tag{2.1}$$

the relevant solution in this case is, as is well known[7],

in the layer;

$$\begin{cases} v=\dfrac{i}{\pi}\displaystyle\int_{-\infty}^{\infty}\frac{(\beta+\chi\beta')e^{\beta H}+(\beta-\chi\beta')e^{-\beta H}}{(\beta+\chi\beta')e^{\beta H}-(\beta-\chi\beta')e^{-\beta H}}\{e^{\beta(H-z)}+e^{-\beta(H-z)}\}e^{ifx}\frac{df}{\beta}\ldots Z>E \\ v=\dfrac{i}{\pi}\displaystyle\int_{-\infty}^{\infty}\frac{(\beta+\chi\beta')e^{\beta z}+(\beta-\chi\beta')e^{-\beta z}}{(\beta+\chi\beta')e^{\beta H}-(\beta-\chi\beta')e^{-\beta H}}\{e^{\beta(H-E)}+e^{-\beta(H-E)}\}e^{ifx}\frac{df}{\beta}\ldots Z<E \end{cases} \tag{2.2}$$

in the substratum;

$$v'=\frac{i}{\pi}\int_{-\infty}^{\infty}2\frac{e^{\beta(H-E)}+e^{-\beta(H-E)}}{(\beta+\chi\beta')e^{\beta H}-(\beta-\chi\beta')e^{-\beta H}}e^{\beta z}\cdot e^{ifx}df\ldots \qquad Z<0$$
$$\chi=\mu'/\mu \tag{2.3}$$

As we are mainly interested with the displacement along the surface, we put $z=H$ into the upper expression of (2.2), then we have

$$\begin{aligned} v&=\frac{i}{\pi}\int_{-\infty}^{\infty}\frac{2}{\beta}\frac{1}{C(f)}e^{-\beta(H-E)}\{1+qe^{-2\beta E}\}e^{ifx}df \\ &=\frac{i}{\pi}\int_{-\infty}^{\infty}\frac{2}{\beta}\{\exp[-\beta(H-E)] \\ &\quad+\frac{q}{C(f)}\exp[-\beta(H+E)]+\frac{q}{C(f)}\exp[-\beta(3H-E)]\}\exp(ifx)df \\ C(f)&\equiv 1-q\exp[-2\beta H], \qquad q\equiv(\beta-\chi\beta')/(\beta+\chi\beta') \end{aligned} \tag{2.4}$$

6) H. NAKANO, *loc. cit.*, 1) § 6. Y. SATÔ, "Transformation of Wave-functions Related to the Transformation of Coordinates Systems. I," *Bull. Earthq. Res. Inst.*, **28** (1950), 1. § 2.

7) *loc. cit.*, 5). Time factor is omitted for brevity.

Now, we will examine the three terms in the bracket { } of the expression (2.4).

The first term is obviously the direct waves radiated from the origin $Q(O, E)$.

Of the second term, the main factor which determines the path of steepest descent is

$$\exp[-\beta(H+E)+ifx].$$

By this function the travel-time is determined, while the other factors, which do not affect the travel-time relation, determine the amplitude.

Similarly, of the third term

$$\exp[-\beta(3H-E)+ifx]$$

is the most important.

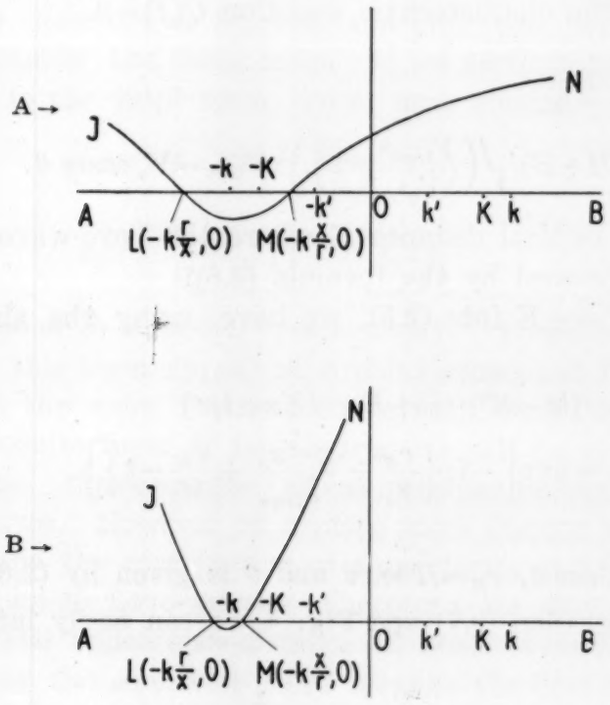

Fig. 2. A, B.

In our previous paper[8] we have touched on the nature of direct and refracted waves, so here, we will only treat the appearance-distance and travel-time of Love-waves.

Employing H. Nakano's way of calculation, we will at first calculate the second term of (2.4);

8) *loc. cit.*, 5). Latter paper, §§ 4 and 5.

$$\int_{-\infty}^{\infty} \frac{2}{\beta} \frac{q}{C(f)} \exp\left[-\beta(H+E)+ifx\right]df.$$

Deform the integration path $\int_{-\infty}^{\infty}$ into that which passes the saddle point (cf. Figs. 2a and b), then the real coordinates of L and M, on which point the integration path of steepest descent crosses the real axis, will be $-kr/x$ and $-kx/r$ respectively. Here

$$r^2=(H+E)^2+x^2.$$

Thus from Fig. 3

$$-kr/x=-k\operatorname{cosec}\theta, \quad -kx/r=-k\sin\theta.$$

As the epicentral distance becomes larger θ increases monotonously; consequently the point M moves to the left until it reaches $-K$, which is the solution of the characteristic equation $C(f)=0$.
In this case

$$-k\sin\theta=-K$$

or
$$x=x_c'\equiv(H+E)/\sqrt{\left(\frac{V_{\text{Love}}^2}{V_s^2}-1\right)}, \quad V_{\text{Love}}=V_s\operatorname{cosec}\theta. \tag{2.6}$$

Therefore the critical distance x_c' where the Love-waves can be observed may be expressed by the formula (2.6).

Substituting $f=-K$ into (2.5), we have, using the above-obtained relation

$$\exp\left[-i\sqrt{(k^2-K^2)}\cdot(H+E)-iKx+ipt\right]$$
$$=\exp\left[-ip\left\{\frac{r_E}{V_s}+\frac{x-x_c}{V_{\text{Love}}}+\frac{r_H}{V_s}-t\right\}\right] \tag{2.7}$$

in which

$r_E=E\sec\theta$, $r_H=H\sec\theta$ and θ is given by (2.6).

From the expression (2.7) and Fig. 4 we can easily infer that;

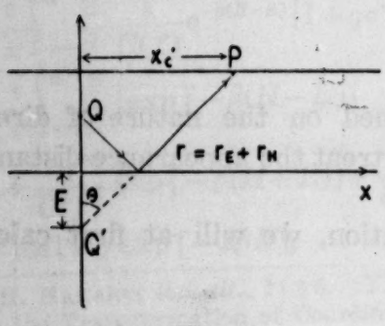

Fig. 3.

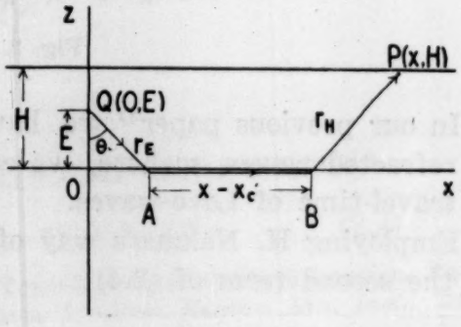

Fig. 4.

1) The Love-waves observed at $P(x, H)$ are the waves which started at $Q(O, E)$ and travelled QA at the velocity V_s, $AB(=x-x_c')$ at the velocity V_{Love} and again BP at V_s.

2) These waves can appear only from the distance x_c', defined by (2.6), as will be clarly seen in Fig. 3. x_c' is also the distance where the travel-time curve of reflected waves touches the line (cf. Fig. 5)

$$t=\frac{r_E+r_H}{V_s}+\frac{x-x_c'}{V_{\text{Love}}} \tag{2.8}$$

3) The intercept-time t_0' of these waves is, putting $x=0$ into (2.7),

$$t_0'=\frac{H+E}{V_s}\sqrt{\left(1-\frac{V_s^2}{V_{\text{Love}}^2}\right)} \tag{2.9}$$

4) Hence the travel-time of Love-waves takes the from of Fig. 5.

We have examined so far only the first two terms of (2.4). We must next consider the third term. If we perform a similar calculation with regard to the third term, we at once obtain

$$\begin{cases} x_c\equiv(3H-E)/\sqrt{\left(\dfrac{V_{\text{Love}}^2}{V_s^2}-1\right)} \\ t_0\equiv\dfrac{3H-E}{V_s}\sqrt{\left(1-\dfrac{V_s^2}{V_{\text{Love}}^2}\right)} \end{cases} \tag{2.10}$$

which correspond to x_c' and t_0' respectively. Therefore, the wave represented by this term appear at a point somewhat farther than x_c'.

Although the wave discussed above both show the velocity of Love-waves, the definite form of Love-waves can not be given by one kind of waves alone. Consequently we can consider neither term to be complete Love-waves. However at a place more distant than x_c two terms both appear and the combination of these terms with the direct waves gives the grown-up Love-waves. Therefore, we may safely assert that x_c is the critical appearance-distance of Love-waves. We will call the waves given by the second or third term as the first or second "complementary Love-waves". The relation between x_c', x_c and the depth of focus is illustrated in Fig. 6.

So long as we are dealing with waves of harmonic origin the above theory seems to be complete. If, however, the origin is of the aperiodic type, the situation becomes different. In this case, the travel-time of the three kinds of waves represented by the three terms in the expression (2.4) are all different. Waves of the second term arrives first, then those of the third term, and the direct waves are the slowest. The time lag of the two complementary Love-waves never becomes large

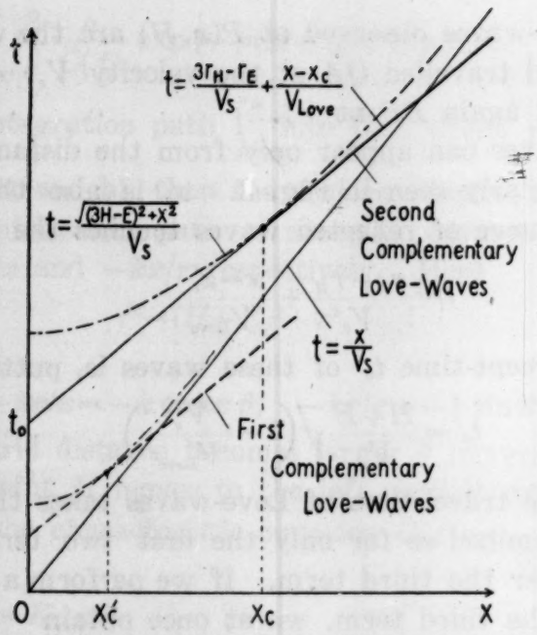

Fig. 5. Critical appearance distance x_c', x_c, intercept time t_0', t_0 and the travel-time of Love-waves when the origin is situated at the point $Q\ (O,\ E)$ in the superficial layer.

With regard to the first complementary Love-waves,

$$x_c'=(H+E)/\sqrt{\left(\frac{V_{Love}^2}{V_s^2}-1\right)}$$

$$t_0'=\frac{H+E}{V_s}\sqrt{\left(1-\frac{V_s^2}{V_{Love}^2}\right)}$$

$$t=\frac{r_E+r_H}{V_s}+\frac{x-x_c'}{V_{Love}}$$

$$r_E=E\sec\theta,\qquad r_H=H\sec\theta,$$

$$V_{Love}=V_s\ \mathrm{cosec}\ \theta.$$

x_c and t_0 are the corresponding values in the second complementary Love-waves, viz.,

$$x_c=(3H-E)/\sqrt{\left(\frac{V_{Love}^2}{V_s^2}-1\right)}$$

$$t_0=\frac{3H-E}{Vs}\sqrt{\left(1-\frac{V_s^2}{V_{Love}^2}\right)}$$

and the travel time is

$$t=\frac{3r_H-r_E}{V_s}+\frac{x-x_c}{V_{Love}}$$

Combination of the first and second complementary waves and the direct waves constitute Love-waves.

$t=\sqrt{(3H-E)^2+x^2}/V_s$ shows the reflected wave at the free and the boundary surfaces.

When the origin resides in the semi-infinite part, E should be taken zero in the expressions of x_c' and t_0' even if the depth of the focus is finite. In this case the complementary Love-waves do not exist.

(cf. Fig. 5), while the direct waves are considerably slow compared with the former two. Therefore, as a matter of fact, we observe only the two kinds of complementary Love-waves for a while, until by the arrival of the direct waves the wave forms are somewhat disturbed. These circumstances are partly described by H. Jeffeys[9], and observational facts also seem to confirm the above theory[10].

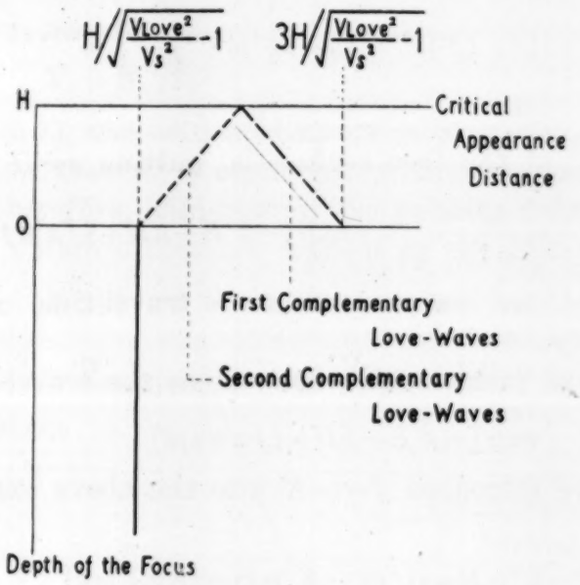

Fig. 6.

3. When the origin is in a lower medium.

When an origin of the type

$$v' = H_0^{(2)}(k'r)\exp(ipt) \tag{3.1}$$

is at the point $Q(O, -E)$ in the lower semi-infinite elastic medium, a relevant solution satisfying the boundary conditions is[11]

in the layer;

$$v = \frac{i}{\pi}\int_{-\infty}^{\infty} \frac{2\chi\{e^{\beta(H-z)} + e^{-\beta(H-z)}\}}{(\beta+\chi\beta')e^{\beta H} - (\beta-\chi\beta')e^{-\beta H}} e^{-\beta' E + ifx} df \tag{3.2}$$

9) H. Jeffreys, "The Formation of Love Waves in a Two-Layer Crust." *Beitr. z. Geophys.*, **30** (1931), 336.

10) T. Akima, "On Dispersion Curves of Surface Waves of the Great Assam Earthquake of September 15, 1950." *Bull. Earthq. Res. Inst.*, **30** (1952), 237. See Fig. 5a.

11) *loc. cit.*, 5).

in the lower medium

$$\begin{cases} v'=\dfrac{i}{\pi}\displaystyle\int_{-\infty}^{\infty}[(\beta+\chi\beta')\{e^{\beta H-\beta' z}+e^{-(\beta H-\beta' z)}\}-(\beta-\chi\beta')\{e^{\beta H+\beta' z}+e^{-(\beta H+\beta' z)}\}] \\ \qquad\qquad \div\{(\beta+\chi\beta')e^{\beta H}-(\beta-\chi\beta')e^{-\beta H}\}\cdot\dfrac{1}{\beta'}e^{ifx-\beta' E}df\ldots.Z>-E \\ v'=\dfrac{i}{\pi}\displaystyle\int_{-\infty}^{\infty}[(\beta+\chi\beta')\{e^{\beta H+\beta' E}+e^{-(\beta H+\beta' E)}\}-(\beta-\chi\beta')\{e^{\beta H-\beta' E}+e^{-(\beta H-\beta' E)}\}] \\ \qquad\qquad \div\{(\beta+\chi\beta')e^{\beta H}-(\beta-\chi\beta')e^{-\beta H}\}\cdot\dfrac{1}{\beta'}e^{ifx+\beta' z}\,df\ldots.Z<-E \end{cases} \tag{3.3}$$

Displacement at the free surface is, putting $z=H$ into (3.2),

$$v=\frac{i}{\pi}\int_{-\infty}^{\infty}\frac{4\chi}{\beta+\chi\beta'}\frac{1}{C(f)}\exp[-\beta' E-\beta H+ifx]df \tag{3.4}$$

As in the former case we can obtain the travel-time of Love-waves in this case similarly.

The important factor which determines the travel-time is

$$\exp[-\beta' E-\beta H+ifx+ipt] \tag{(3.5)}$$

As before we introduce $f=-K$ into the above expression, then we have

$$\begin{aligned}&\exp[-\sqrt{(K^2-k'^2)}\cdot E-i\sqrt{(k^2-K^2)}\cdot H-iKx+ipt] \\ &\quad=\exp[-\sqrt{(K^2-k'^2)}\cdot E]\cdot\exp\left[-ip\left\{\frac{r_H}{V_s}+\frac{x_c}{V_{\text{Love}}}-t\right\}\right]\end{aligned} \tag{3.6}$$

in which $r_H=H\sec\theta$, θ is given by (2.6)

and $$x_c=H/\sqrt{\left(\frac{V_{\text{Love}}^2}{V_s^2}-1\right)} \tag{3.7}$$

The critical distance x_c where the Love-waves can first be observed is given by (3.7), and the depth of focus E has nothing to do with the travel-fime. Similar phenomenon was discovered by H. Nakano in the problem of generation of Rayleigh-waves[12]. The intercept-time t_0 is always given by the expression

$$t_0=\frac{H}{V_s}\sqrt{\left(1-\frac{V_s^2}{V_{\text{Love}}^2}\right)} \tag{3.8}$$

which is equivalent to the expression obtained by putting $E=0$ into the formula (2.9).

12) *loc. cit.*, 1). Figs. 10, 15 and 18.

4. Numerical calculation.

Through two numerical exmples, we will explain the above theory here.

I. At first we will employ the model which we have used in our previous paper, i.e.:

$$\left.\begin{aligned} &\rho=\rho' \\ &\mu=\mu'/8 \\ &V_s=V_s'/2\sqrt{2} \end{aligned}\right\} \qquad (4.1)$$

By (2.6) or (3.7), the critical distance is expressed as a function of velocity, while the velocity is connected with the period by the dispersion curve; therefore, eliminating the velocity from the above two relations we can obtain a formula connecting the critical distance and the period. The constant factor is understood and the relation between

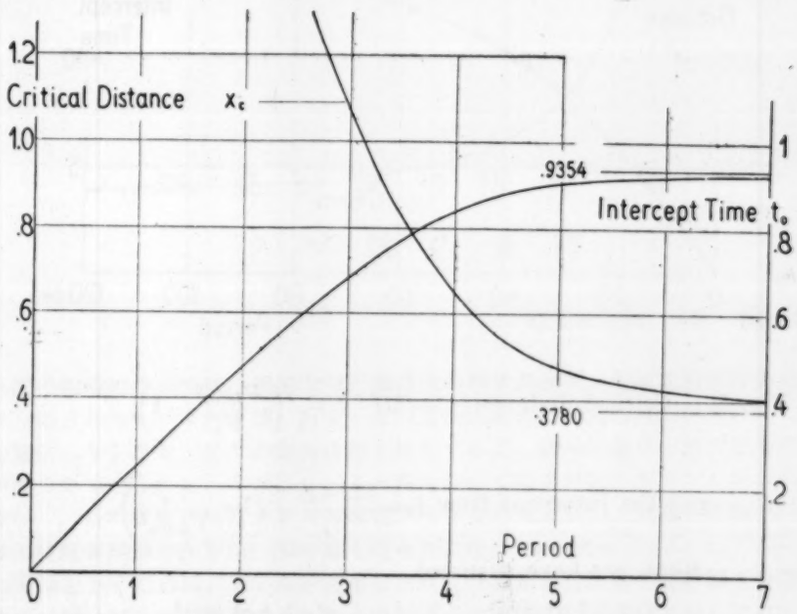

Fig. 7. Critical distance $x_c=H\Big/\sqrt{\left(\frac{V_{\text{Love}}^2}{V_s^2}-1\right)}$,

and the intercept time $t_0=\frac{H}{V_s}\sqrt{\left(1-\frac{V_s^2}{V_{\text{Love}}^2}\right)}$,

when $\rho=\rho'$

$\chi=\mu'/\mu=8$.

(Unit of distance is H and that of time is H/V_s.)

13) *loc. cit.*, 5). § 6, Table III and Figs. 9, 10, 11a and 11b.

period (unit; H/V_s) and $x_c/(3H-E \text{ or } H)=1/\sqrt{\left(\frac{V_{\text{Love}}^2}{V_s^2}-1\right)}$ is shown in Fig. 7. The intercept-time $t_0=\sqrt{\left(1-\frac{V_s^2}{V_{\text{Love}}^2}\right)}$ is also plotted in the same figure with the factor $(3H-E)/V_s$ or H/V_s omitted.

II. Next, we will present a more practical case. In Japan, the crustal structure was determined by T. Matuzawa and others, and of the many results proposed, we will employ the constants[14]

$$\begin{cases}\rho=2.7\ \text{gr/cm}^3, & \mu=29.4\ \text{km. gr. sec.}, & V_s=3.3\ \text{km/sec},\\ \rho'=3.4\ \text{gr/cm}^3, & \mu'=68.9\ \text{km. gr. sec.}, & V_s'=4.5\ \text{km/sec}.\end{cases} \tag{4.5}$$

These values were already used in our preceding paper as a model

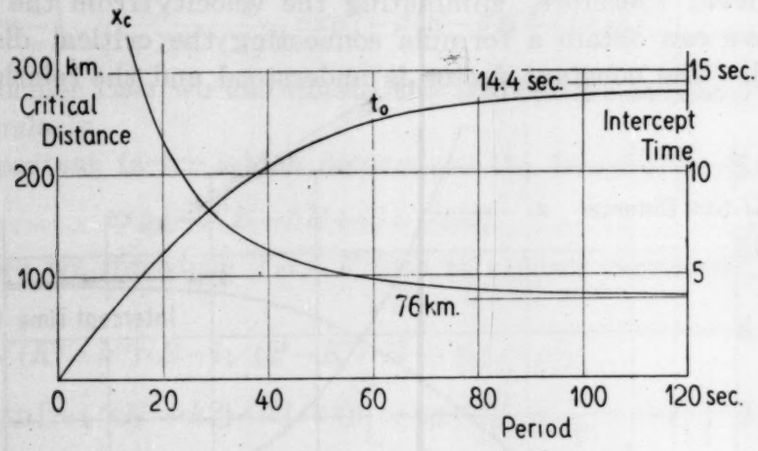

Fig. 8. Critical distance $x_c=(3H-E)/\sqrt{\left(\frac{V_{\text{Love}}^2}{V_s^2}-1\right)}$,

and the intercept time $t_0=\frac{3H-E}{V_s}\sqrt{\left(1-\frac{V_s^2}{V_{\text{Love}}^2}\right)}$.

Here, we have assumed

$\rho=2.7\ \text{gr/cm}^3$, $\rho'=3.4\ \text{gr/cm}^3$

$\mu=29.4\ \text{km. gr. sec.}$, $\mu'=68.9\ \text{km. gr. sec.}$

$V_s=3.3\ \text{km/sec.}$, $V_s'=4.5\ \text{km/sec.}$

and $H=30\ \text{km}$, $E=20\ \text{km}$.

---

14) *e.g.* T. MATUZAWA, *Bull. Earthq. Res. Inst.*, **5** (1928), 1; **6** (1929), 177; **7** (1929), 241. K. WADATI, *Journ. Met. Soc., Japan*, **[ii], 3** (1925). See also, H. KAWASUMI, *Bull. Earthq. Res. Inst.*, **10** (1932), 94. Foot note 2). T. MATUZAWA, "Propagation of Love Waves along a Doubly Stratified Layer". *Proc. Phys.-Math. Soc. Jap.* **[iii], 10** (1928), 25.

structure of equivalent single layer.[15] Assuming the thickness of the layer and the depth of the focus to be

$$H=30\,\text{km.}, \qquad E=20\,\text{km.}$$

we have calculated x_c and t_0 as the functions of the period (cf. Fig. 8).

The intercept-time of a wave with a period of half a minute is about ten seconds, and the critical appearance-distance is about two hundred kilometers. This theoretical result agrees with the observational facts ascertained by T. Akima using his low-pass filter.[16]

Though, in this paper, a structure with a single superficial layer has been treated, we must proceed, in the next step, to the problem of a doubly-stratified medium in order to explain the observation more fully.

The author wishes to express sincere thanks to Prof. H. Kawasumi for his kind encouragement.

---

26. 表 面 波 の 研 究 Ⅶ
ラ ブ 波 の 走 時

地震研究所 佐 藤 泰 夫

レーリー波の走時については，有名な中野實博士の研究があり，半無限彈性体内で有限の深さにある震源から起されたレーリー波は，ある一定の震央距離の所ではじめて現われ，これより遠くにおいてのみ觀測しうること，又その走時曲線を延長すれば，震央距離0の所では走時も亦0となるべき事等が明らかにせられた．その後レーリー波について研究が進んだにもかかわらず，ラブ波關係の論文はなく，走時曲線の延長が原点を通過すべきものであるか，又震央距離がいかほどの所から，ラブ波の發現が期待されるか，等の事も明らかになつていない．

これらの問題をとくために，ラブ波の発生しうるような簡單な媒質と振動源とを考へ，從來得られている變位の積分表示式を用いて，これに中野博士の流儀による積分方法を適用した．計算は極めて簡單であり，得られた主な結果は次の通りである．

1) 震央距離 x が

$$x=x_c'\equiv(H+E)/\sqrt{\left(\frac{V_{\text{Love}}^2}{V_s^2}-1\right)} \qquad \cdots\cdots\cdots\cdots \quad (2,6)$$

で表わされる所で，ラブ波ははじめて出現する．

15) Y. Satô, "Study on Surface Waves IV. Equivalent Single Layer to Double Superficial Layer." *Bull. Earthq. Res. Inst.*, **30** (1952), 519.

16) *cf.* T. Akima, *Bull. Earthq. Res. Inst.* **27** (1949), 69. His recent study is not yet published.

2) 走時曲線を延長しても原点は通過せず $x=0$ をきるのは

$$t=t_0'\equiv\frac{H+E}{V_s}\sqrt{\left(1-\frac{V_s^2}{V_{\text{Love}}}\right)} \qquad \cdots\cdots\cdots (2.8)$$

の點である.

3) 走時は

$$t=\frac{r_E}{V_s}+\frac{x-x_c'}{V_{\text{Love}}}+\frac{r_H}{V_s} \qquad \cdots\cdots\cdots (2.8)$$

$$r_E=E\sec\theta,\quad r_H=H\sec\theta$$

$$V_{\text{Love}}=V_s\operatorname{cosec}\theta$$

で與えられるが,この式から,"ラブ波は(第4図において) $QA=r_E$ を V_s の速さで, $AB=x-x_c'$ を V_{Love} の速さで,さらに $BP=r_H$ を V_s で傳わつた波" と解釋することが可能であろう.

4) もつとも,上にあげた波は,いわば最初に表われる補足的な波であり,走時のみからみると完全なラブ波の如く見えるが,実は完成したラブ波ではなく,上式の中の $H+E$ の代りに, $3H-E$ を代入してえられる x_3, t_0 等をもつ第二の補足的な波と,震源からつたわつた直接波とが加わつて,はじめてラブ波の成長した形をととのへるものと考えられる.ただし,二つの補足的な波の所要時間は大差ないが,直接波はかなりおそいから,最初はこの波の加わらないものを觀測し,これが到達すると波の狀態に變化のおこることが予想される.

5) 以上の議論は,震源が表面層内にあるものとして行つたが,震源が半無限体内にある時には震源の深さは関係を持たず,(2.6),(2.8),(2.9)で $E=0$ とおいたのと同じことが成立つ.この事は,レーリー波の時に,震源の深さにかかわらず.走時曲線が原點を通過したことに対應しよう.(この場合表面で觀測するラブ波は二つの補足的な波に分れない.)

震源の深さとラブ波の発現距離の關係は第6図に,走時曲線は第5図に示してある.

最後に上の議論を適用した実例を数値計算によつて示した.

終始御指導を給わつた河角教授に厚く御禮を申し上げる.

Supplementary Notes.

In my former paper "Study on Surface Waves III", I have wrongly written that H. Menzel had asserted that the group velocity of Love-waves becomes infinity at the point $V=V_2$ (V and V_2 being the phase velocity of Love-waves and that of S-waves in the intermediate layer respectively). It is not H. Menzel, but von zur Mühlen[17] who asserted the said wrong property. I apologize to Mr. H. Menzel and thank him for his kind notice to my mistake. I take with regret this opportunity to make clear another property of the dispersion curve in question. Mr. Menzel asserted that the tangent of the curve of the group velocity versus the period becomes vertical at the point $V=V_2$, but it seems also erroneous. We can easily prove using our former calculation.

Employing the same notation with the former paper.

17) *Zeitschrift der Deutschen Geologischen Gesellschaft*, **88** (1936), 341.

$$\frac{dU}{dT}=\frac{1}{2\pi}p^2U^2\frac{d}{dp}\left(\frac{1}{U}\right) \qquad \text{(T; period)}$$

$$=\frac{1}{2\pi}p^2U^2\left[-\frac{1}{V^2}\frac{dV}{dp}\left(1+\frac{pD_p}{-2eD_e}\right)+\frac{1}{V}\frac{d}{dp}\left(\frac{pD_p}{-2eD_e}\right)\right]$$

Now, p, e, U, $1/V$, dV/dp and $(pD_p)/(-2eD_e)$ are all finite at $V=V_2$. Therefore in order that $dU/dT\to\infty$ (when $V\to V_2$),

$$\frac{d}{dp}\left(\frac{pD_p}{-2eD_e}\right)\to\infty$$

must necessarily hold.

As we have proved formerly, $(pD_p)/(-2eD_e)$ can be expanded as a power series of $s_2^2=f^2\{(V^2/V_2^2)-1\}$ near the point $V=V_2$. In such a case we can show without difficulty that the function cannot have a derivative which becomes infinity at this point. Therefore,

when $V\to V_2$

$dU/dT\to$finite,

or the tangent of the curve (group velocity vs. period) does not become vertical.

附　　記

「表面波の研究 III」において，二つの表面層がある時，ラブ波の群速度は位相速度が中間層のそれと等しくなる點で無限大になる，ということを H. Menzel が言つたように書いた事は，筆者のあやまりであり，この主張をしたのは von zur Mühlen であります．ここに訂正し，筆者の誤りを指摘された Menzel 氏におわびとお禮とを致します．

但し，この點（$V=V_2$）で接線が横軸（周期）に垂直になる，という同氏の主張も正しくない事は，前の計算から容易に証明する事ができます．

前と同じ記號を用い，

$$\frac{dU}{dT}=\frac{1}{2\pi}p^2U^2\frac{d}{dp}\left(\frac{1}{U}\right)$$

$$=\frac{1}{2\pi}p^2U^2\left[-\frac{1}{V^2}\frac{dV}{dp}\left(1+\frac{pD_p}{-2eD_e}\right)+\frac{1}{V}\frac{d}{dp}\left(\frac{pD_p}{-2eD_e}\right)\right]$$

所が，p，U，$1/V$，dV/dp，$(pD_p)/(-2eD_e)$ は有限であるから

$V\to V_2$ の時　$dU/dT\to\infty$ ならば $\dfrac{d}{dp}\left(\dfrac{pD_p}{-2eD_e}\right)\to\infty$

前に示したように$(pD_p)/(-2eD_e)$は$V=V_2$の近くで $s_2^2=f^2(\{V^2/V_2^2\}-1\}$ のべき級数に展開することが可能であり，このような函数の導函数が無限大になることはあり得ない．從つて，

$V\to v_2$ の時　dU/dT　有限．

27. *On the Energy Law of Occurrence of Japanese Earthquakes.*

By Hirosi KAWASUMI,

Earthquake Research Institute.

(Read Nov. 20, 1942.—Received Sept. 20, 1952.)

As far back as in 1862 R. Mallet estimated the *vis viva* of the Neapolitan earthquake of 1857, and T. C. Mendenhall proposed a method of estimating the energy of earthquakes, and applied it to the Charleston earthquake of 1886, although his assumption was in no wise perfect. O. Enya later discussed the same problem from a broader point of view. H. F. Reid calculated the energy released from the fault in the California earthquake of 1906, and B. Galitzin estimated the energy of the Pamir earthquake from the seismogram observed at a single station Pulkovo. Navarro-Neumann also determined the energy of a number of earthquakes by his own and Galitzin's formula. Recently in Japan, K. Wadati inferred relative magnitudes (not energy) of earthquakes by means of intensity-distance ($I-\Delta$) curve. More recently C. F. Richter and B. Gutenberg made a thorough investigation on the problem based on the observed maximun amplitude by means of the Wood-Anderson torsion seismometer. The writer also made a magnitude scale and calculated the energy for each magnitude, and determined the magnitudes of Japanese earthquakes from 1885 to 1943. The résumé of the study is given here.

The writer first determined the $I-\Delta$ and $A-\Delta$ curves for normal earthquakes using the data of some hundred earthquakes in Japan. The result is

$$e^I=\left(\frac{100}{\Delta}\right)^2 e^{M_K-0.00183(\Delta-100)}, \qquad (1)$$

$$A=\left(\frac{100}{\Delta}\right)^{1/2} e^{m-0.00305(\Delta-100)} \quad \text{for } 100\leqq\Delta\leqq700 \qquad (2)$$

$$=\left(\frac{100}{\Delta}\right)^2 e^{m+1.21-0.00041(\Delta-600)} \quad \text{for } 700\leqq\Delta\leqq2000 \qquad (2')$$

This paper was presented to the Pan-Pacific Science Congress held in 1949 at Wellington, New Zealand. Owing to the delay of publication in New Zealand it is submitted here for publication.

where A is the maximum amplitude in μ at epicentral distance Δ measured in km, while M_k and m are I and $\log_e A$ at $\Delta=100$ km respectively. Between M_k and m the following relation was found to exist

$$m=3.4+1.2M_k \quad \text{or} \quad \log_{10} A_{100}\fallingdotseq 1.5+0.5M_k. \tag{3}$$

By means of these formula we can infer the magnitude M_k of any earthquake from the $I-\Delta$ or $A-\Delta$ curve observed.

The energy of earthquake as sent out from the origin may be calculated by the formula

$$4\pi r^2 vt\tfrac{1}{2}\sigma(2\pi A/T)^2 \tag{4}$$

where v and σ are the velocity in and the density of the earth's crust and A, T and t are the amplitude, period and duration of earthquake motion at distance r respectively. Since energy is proportinal to the square of amplitude, the energy is concentrated to the maximum phase so that we may use for A the maximum amplitude and its equivalent duration for t.

From the observations at Tokyo the writer obtained the relation

$$\overline{\alpha}=(2\pi/T)^2\overline{A}=0.412(3.266)^I\fallingdotseq 0.45\times 10^{0.5I} \text{ gals} \tag{5}$$

for the mean acceleration $\overline{\alpha}$ of earthquakes of intensity I in Japanese scale. Introducing this into the equation (4) we have

$$\frac{\overline{dE}}{dt}=3\times 10^{17+M_k} \quad \text{ergs/sec.} \tag{6}$$

since M_k is the intensity at $r\fallingdotseq\Delta=100$ km.

In the above calculation we have assumed A to be the mean value of A on the sphere $r=r_0$. From observations in Japan we see that earthquakes are in no wise of uniform amplitude in all azimuths. The writer has proved the existence of such earthquakes of which the displacement may be expressed as

$$\begin{aligned} u\fallingdotseq & \mathbf{i}_1\frac{\mathfrak{A}}{r}\cos(pt-hr)P_n^m(\cos\theta)\sin m\varphi \\ & +\mathbf{i}_2\frac{\mathfrak{B}}{r}\cos(pt-kr)\frac{dP_n^m(\cos\theta)}{d\theta}\sin m\varphi \\ & +\mathbf{i}_3\frac{m\mathfrak{B}}{r}\cos(pt-kr)\frac{P_n^m(\cos\theta)}{\sin\theta}\cos m\varphi, \end{aligned} \tag{7}$$

where $n=2$ and $m=0$, 1, or 2. In these cases the time mean of the total energy flux calculated as usual is

$$\overline{\frac{dE}{dt}}=\frac{\pi(n+m)!}{(2n+1)(n-m)!}\sigma p^2\{\mathfrak{A}^2V+n(n+1)\mathfrak{B}^2\mathfrak{V}\}=4\pi r^2\tfrac{1}{2}\sigma p^2\overline{\mathfrak{B}}^2\mathfrak{V}C \quad (8)$$

in which V and $\mathfrak{V}$ are the velocities of P- and S-waves respectively, and $\overline{\mathfrak{B}}$ is the mean amplitude at $r=r_0$ of S-wave for all azimuths. The constant C is about 1.5 for $n=2$, $m=0$; or 2.2 for $n=2$ and $n=1$ or 2, provided that Poisson's ratio of the crust is $\frac{1}{4}$ and $\mathfrak{A}/\mathfrak{B}=\frac{1}{2}\sim\frac{1}{4}$ as is usually the case with deep earthquakes hitherto observed in this country.

Thus we find that the usual formula (4) should be multiplied by ca. 2 if we consider the mechanism of occurrence and use the mean amplitude, an effect rather unimportant compared with the case when the amplitude observed at a single station (7) is used, since the latter is subjected to a wide variation owing to instruments and underground-conditions. It is also to be remarked that the amplitude observed on the earth's surface is about twice that of the incident wave owing to the effect of reflection, so that the energy calculated by (8) from observed maximum amplitude should be divided by 4. We may therefore roughly substitute 1 for the coefficient 3 in the right hand side of the equation (6). It must also be added that the writer's later investigation showed that the attenuation of amplitude even to such small distance as $r=100$ km. is not negligible. If this result of the Tokyo observation is to be adopted, the energy passing the sphere $r=100$ km. is about one thirtieth of the energy emitted from the hypocentre. This is a grave ploblem for future investigation.

The $I-\Delta$ or $A-\Delta$ curve expressed in (1) or (2) was applied to the observations of all normal earthquakes which took place from 1885 to 1943, and their magnitudes were determined. The magnitudes of the earthquakes in recent 40 years of which the epicentres were more accurately determined are represented on the map in Fig. 1 with the magnitudes of the circles denoting the meizoseismic area (in which the demolition of houses is to be seen, i. e. $I=6$).

The statistics of the number N of earthquakes of magnitude M_k in the same 40 years from 1904 to 1943 shows

M_k	4	5	6	7	8
N	275	84	21	1	2

which is expressed by the least square solution

$$N=273\times10^{-0.537(M_k-4)}. \quad (9)$$

The statistics of smaller earthquakes seems imperfect from two reasons, that is (1) the records of smaller earthquakes in this country

were not kept regularly, and (2), as is evident from Fig. 1, most of the earthquakes occur under the ocean bed off the Pacific coast of NE Japan and smaller earthquakes were liable to be omitted from previous observations. The energy law of smaller earthquakes is therefore examined from a different viewpoint by making use of observations at Tokyo the result of which is reported in next paper. The result also proves the energy law

$$N \propto 10^{-0.556 M_K}. \tag{10}$$

The difference of the index 0.556 from the above 0.537 is not significant from the statistical point of view. So it may be concluded that the number of Japanese earthquakes diminishes inversely to power equal to half the magnitude of 10, that is

$$N \propto 10^{-0.5 M_K} \tag{11}$$

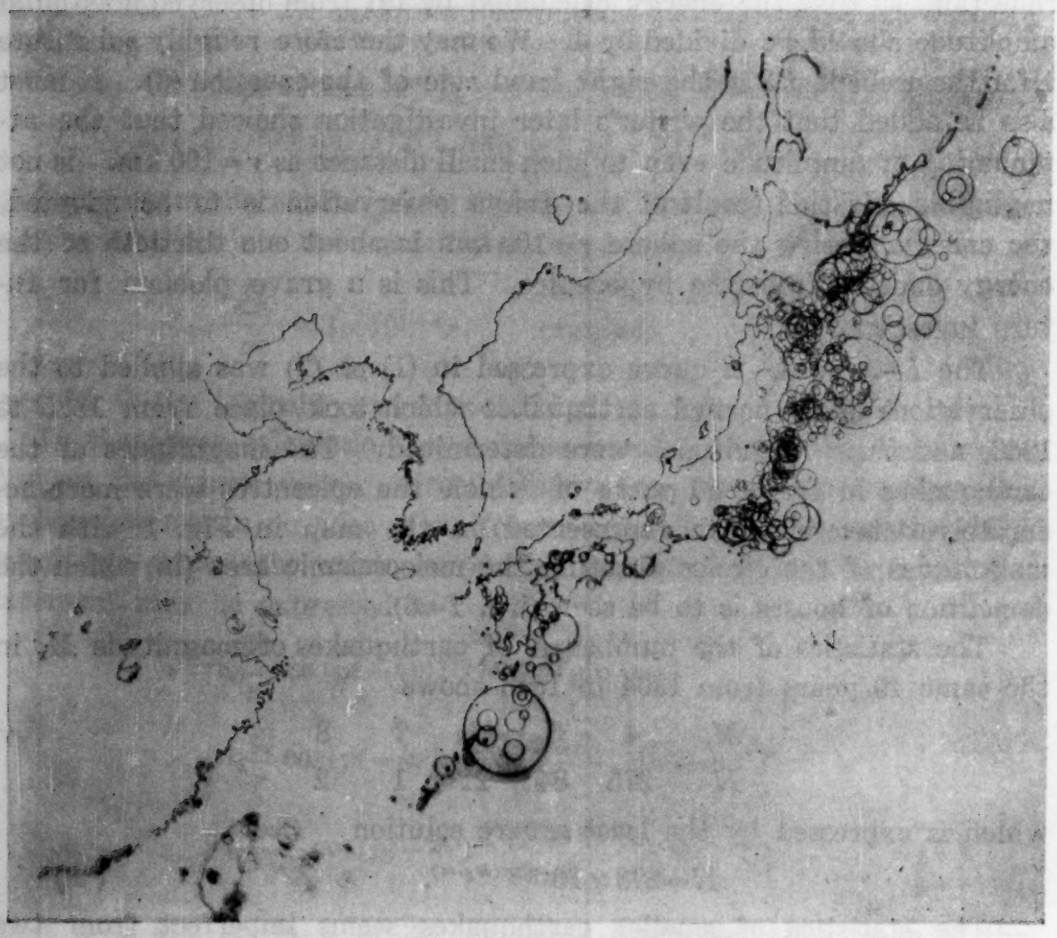

Fig. 1. Map of the meizoseismic Area of Large Earthquakes in Japan during 1904—1943

27. 日本に起る地震のエネルギー法則

地震研究所 河 角 広

地震のエネルギーは R. Mallet が 1857 年のナポリ地震について計算したのが始りで，T. C. Mendenhall, Galitzin, Navarro-Neuman, Jeffreys 等の計算があり，最近では C.F. Richter, B. Guteberg 等が特殊の地震計により観測した最大振幅からその地震のエネルギーを計算する方式を確立した．筆者も日本に於ける地震観測結果を用いて同様な事を行つた．

それは標準の $I(\triangle)$ 及び $A(\triangle)$ 曲線（1）及び（2）を定めそれを用いて震央距離 $\triangle=100$km の所に於ける震度 $I\equiv M_k$ 及び，最大振幅 A_{100}（單位 μ）を用いるもので

$$A_{100}\fallingdotseq 10^{1.5+0.5M_k}$$

の關係があり，最大動の継続時間を t とすればエネルギー E は

$$E\fallingdotseq t\cdot 10^{17+M_k}\quad \text{エルグ}$$

である．

この様にして筆者は日本古來の地震の大きさ M_k を定めたが，それ等の頻度を統計して見ると 1911～1940 の間の比較的大きな地震については

$$N(M_k)=273\times 10^{-0.537\,(M_k-4)}$$

の關係が得られた．

統計の精度から見て

$$N(M_k)\ \infty\ 10^{-0.5M_k}$$

と見て差支へないであろう．即ち地震の頻度はその大きさ M_k が二階級昇るごとに10分の一に減少することになる．

28. *Energy Law of Earthquake Occurrence in the Vicinity of Tokyo.*

By Hirosi KAWASUMI,

Earthquake Research Institute.

(Read Nov. 20, 1942.—Received Sept. 20, 1952.)

In the former paper on Japanese earthquakes, the writer obtained a conspicuous energy law on the occurrence of larger earthquakes. An extension of the law so as to include smaller earthquakes will be made in this paper. Investigations related to the present problem have hitherto been made by senior authorities such as Prof. Terada, Prof. Ishimoto, Prof. Matuzawa and Prof. Gutenberg as well as Dr. Wadati and Dr. Iida. Further studies including some theoretical improvements and the actual examinations which support the present theory have here been made by the writer.

The energy of an earthquake sent out from the hypocentre is transmitted as elastic bodily and surface waves, diminishing their amplitudes with the hypocentral distance owing to the spreading of wave-fronts, reflection, refraction and absorption. The amplitude observed at a single station therefore depends firstly upon the magnitude of the energy sent out from the origin, and secondly upon the focal distance and thirdly upon the structure of the medium through which it is propagated. But, for simplicities' sake, the last item is here neglected, and the effects of reflection and refraction are not taken into consideration.

The amplitude is thus assumed to vary only with the focal distance. The effect of absorption is assumed to be proportional to e^{-kr}. Thus we put

$$A=A_0R(r)e^{-kr} \qquad (1)$$

where A_0 is the amplitude at distance $r=r_0$, so that

$$R(r_0)e^{-kr_0}=1$$

Let us now consider the frequency of the maximum amplitude of earthquakes observed at a station. If we denote by FdA_0 the frequency of earthquakes having amplitude A_0 at r_0 and occurring in unit volume

This paper was presented to the Pan-Pacific Science Congress held in 1949 at Wellington, New Zealand. Owing to the delay of publication in New Zealand it is submitted here for publication.

per unit time, then F is generally a function of position (x, y, z), time, and amplitude A_0. But as we are here dealing with the statistical mean value, we will assume that F is independent of time, whereupon

$$F=\varphi(x, y, z)f(A_0) \tag{2}$$

Then the frequency $\delta n(A)dA$ of A between A and $A+dA$ observed at a station at (0, 0, 0) is

$$\delta n(A)dA=\varphi(x, y, z)f(AR^{-1}e^{kr})d(AR^{-1}e^{kr})dx\,dy\,dz. \tag{3}$$

As already stated, we are dealing with the mean value of seismic activities, so we will assume φ to be constant in the domain $-\infty\leqq x\leqq\infty$, $-\infty\leqq y\leqq\infty$ and $z_1\leqq z\leqq z_2$ and to be 0 outside the domain. *This is approximately true* in the region concerned. By integrating (3) with respect to polar coordinates we obtain the frequency of earthquakes occurring at a distance between r and $r+dr$ from the station and having amplitude between A and $A+dA$ at the station. When r is sufficintly large it results in

$$\delta n_r(A)drdA=2\pi\varphi hrR^{-1}e^{kr}drf(AR^{-1}e^{kr})dA, \tag{4}$$

where h denotes (z_2-z_1).

Next comes the determination of φ, h, k and the functional form of f. Empirically we know already that $f(\infty)=0$, so we will introduce Laurent's series

$$f=\sum_{i=1}^{\infty}a_i/A_0^i$$

into (4). Then integrating with respect to A within the variable interval $A_I=A_1\kappa^{I-1}$ and $A_{I+1}=A_1\kappa^I$, and denoting the result by $n_r(I)dr$, we have

$$n_r(I)=2\pi\varphi hrR^{-1}e^{kr}\left[a_1Re^{-kr}\log\kappa+\sum_{i=2}^{\infty}a_iR^ie^{-ikr}\frac{1}{(i-1)A_I^{i-1}}\{1-\kappa^{1-i}\}\right]. \tag{6}$$

We know also from actual observations that $\lim_{I=\infty}n_r(I)=0$, and thus $a_1=0$. For convenience' sake we will integrate this equation from r to $r+\rho$, for finite interval ρ, then

$$N(I, r, \rho)=2\pi\varphi h\sum_{i=2}^{\infty}\frac{a_i(1-\kappa^{1-i})}{(i-1)A_I^{i-1}}\int_r^{r+\rho}rR^{i-1}e^{-(i-1)kr}dr. \tag{7}$$

Observations at Tokyo show that $N(I, r, \rho)$ is invariably proportional to $e^{-\lambda r}$. This leads to the conclusion that rR^{i-1} is *constant* for only one admissible integer i greater than 1.

In addition to this, the observations at Tokyo show that

$$N(I, r, \rho) \propto 1/A_I \tag{8}$$

indicating that $i=2$, so that

$$R=r_0 e^{kr_0}/r, \tag{9}$$

and

$$f=a_2/A_0^2. \tag{10}$$

Thus we have

$$F(A_0)=\varphi a_2/A_0^2. \tag{11}$$

Since the energy of seismic waves is proportional to the square of amplitude, the energy of all earthquakes with amplitude between A_0 and A_0+dA_0 is proportional to $F(A_0)A_0^2dA_0=\varphi a_2 dA_0$ which is a constant, that is to say, the law of equipartition of energy holds true here.

Now we have

$$N(I, r, \rho)=2\pi\varphi h a_2 r_0(1-\kappa^{-1})(1-e^{-k\rho})(kA_I)^{-1}e^{-k(r-r_0)}. \tag{12}$$

Assuming that r′ is the minimum distance for the equation (12) to hold, we will sum up all the earthquakes with I and occurring at all distances. The result is equivalent to the limit of (12) when $\rho\to\infty$, at r'.

$$N(I)=N(I, r', \rho\to\infty)=2\pi\varphi h a_2 r_0(1-\kappa^{-1})(\kappa A_I)^{-1}e^{-k(r'-r_0)}. \tag{13}$$

Similarly if we take the limit of (12) for $I=1$, when $\kappa\to\infty$, the result is equivalent to the sum $N'(r, \rho)$ of all the earthquakes occurring at distances between r and $r+\rho$.

$$N'(r, \rho)=2\pi\varphi h a_2 r_0(1-e^{-k\rho})(kA_1)^{-1}e^{-k(r-r_0)}. \tag{14}$$

From (13) or (14) we obtain the total number $\bar{N}$ of earthquakes observed at a station

$$\bar{N}=2\pi\varphi h a_2 r_0(kA_1)^{-1}e^{-k(r'-r_0)}. \tag{15}$$

Introducting $\bar{N}$ into (12), (13) and (14) we have

$$N(I, r, \rho)=\bar{N}(\kappa-1)(1-e^{-k\rho})\kappa^{-I}e^{-k(r-r')}, \tag{16}$$

$$N(I)=\bar{N}(\kappa-1)\kappa^{-I}, \tag{17}$$

$$N'(r, \rho)=\bar{N}(1-e^{-k\rho})e^{-k(r-r')}=\bar{N}(1-e^{-k\rho})e^{-nk\rho} \tag{18}$$

provided $r=r'+n\rho$.

Now let us calculate the energy emitted from a unit volume in the layer considered. As we have seen, the number of earthquakes occurring in the same volume in unit time is $F(A_0)dA_0$. And the energy emitted in time t (duration of maximum amplitude) from the hypocentre of an earthquake having amplitude A_0 at r_0 is $4\pi r_0^2 v t \frac{1}{2}\sigma(2\pi A_0 e^{kr_0}/T)^2$. The total energy of all the earthquakes having amplitudes between A

and A_0+dA_0 from unit volume per unit time is thus obtained from the product of these two values. If we multiply this by the thickness of the layer, h, we have a measure of seismicity:

$$S=(2\pi/T)^2A_1\bar{N}kr_0e^{k(r'+r_0)}\sigma vtdA_0, \tag{19}$$

which is a constant independent of A_0 and r_0, since $A_0r_0e^{kr_0}$ is invariant owing to (1) and (9). From a practical point of view it will be convenient to use the energy per 100 km. square and per 100 years. If we integrate (19) with respect to A_0 from its minimum to maximum value, we may have a better measure of seismicity, but still simpler and more direct is the number of earthquakes of magnitude M_k per unit area in unit time, that is

$$N(M_k)=\int_{A_{0I}}^{\kappa A_{0I}}hF(A_0)dA_0=\varphi ha_2(\kappa-1)A_{0I}^{-1}\kappa^{-1}. \tag{20}$$

Let us now compare the above theory with actual observations, and determine the constants $\bar{N}$, φa_2, κ, and k. As already pointed out by the late Prof. Ishimoto, Weber-Fechner's law holds true in the Japanese intensity scale and earthquake acceleration. The writer's later determination with ampler materials of the relation is

$$\bar{\alpha}=0\cdot422(3.266)^I\fallingdotseq0.45\times10^{0.5I} \tag{21}$$

for the mean acceleration corresponding to I, while the lower limit $\alpha_l=0.25\times10^{0.5I}$. And since the periods of earthquake motion manifesting maximum acceleration at Hongō (Tokyo) is invariably 0.3 sec., the acceleration and amplitude there may be assumed to be proportional. The writer therefore took the statistics of the earthquake observations at Tokyo in the 30 years from 1911 to 1940 with intensity I, and the result is shown in Table 1.

From this table we see that r' is the distance where the duration of preliminary tremor $(S-P)$ is ca. 5 sec. and $\bar{N}=1847$. From the values of $N(I)$ and $N'(r,\rho)$ in the last row and column of the table, we have by the method of least squares

$$\bar{N}=1785,\ \kappa=3.602;\ \text{and}\ \bar{N}=1730,\ kv=0.1467,$$

where v is the virtual velocity of $(S-P)$ wave for which the value satisfying $12v=100$ km is adopted here.

Using the observed $\bar{N}=1847$, κ and kv determined above, we have

$$N(I,r,\rho)=2499\times10^{-0.556I}e^{-0.734\rho},$$

in 30 years, and the values calculated by this formula are tabulated in Table 1. Comparing the calculated values with those observed we find a fairly good conformity.

Table 1. Statistics of earthquakes with intensity I and duration of preliminary tremor $(S-P)$ observed at Hongō, Tokyo during 1911–1940. The number without bracket is the observed frequency, $N(I, r, \rho)$, while those in bracket are the values calculated from the above theory.

I / $(S-P)$	n	1	2	3	4	5	6	$N'(r,\rho)$
sec.		[29]	[3]	[1]	[0]	[0]	[0]	[33]
		(0)	(0)	(0)	(0)	(0)	(0)	(0)
5	0	810	208	55	9	5	1	1088
		(694)	(193)	(54)	(15)	(4.1)	(1.1)	(960)
10	1	303	62	27	12	3	0	407
		(333)	(92)	(27)	(7.1)	(2.0)	(0.5)	(461)
15	2	136	34	8	4	0	0	182
		(160)	(44)	(12)	(3.4)	(0.9)	(0.3)	(221)
20	3	71	13	2	0	0	0	86
		(77)	(21)	(5.9)	(1.6)	(0.5)	(0.1)	(106)
25	4	34	8	3	1	0	0	46
		(37)	(10)	(2.8)	(0.8)	(0.2)		(51)
30	5	22	3	2	0	0	0	27
		(18)	(4.9)	(1.4)	(0.4)	(0.1)		(24)
35	6	4	5	1	1	0	0	11
		(8.5)	(2.4)	(0.7)	(0.2)			(12)
$N(I)$		1380	333	98	27	8	1	1847
		(1334)	(370)	(103)	(29)	(7.9)	(2.2)	

The seismicity S calculated by (19) thus becomes

$$S=0.9\times10^{25}tdA_0 \text{ ergs/(100 km)}^2 \text{ 100 years},$$

and from (21)

$$N(M_k)=1.5\times10^{3-0.556M_k}/(100\text{ km})^2 \text{ 100 years},$$

while the number of all earthquakes occurring at any distance and manifesting intensity I at Tokyo in 100 years is, by (17)

$$N(I)=1.6\times10^{4-0.556I}$$

The index 0.556 may be approximately replaced for the present by $\frac{1}{2}$ so long as the present statistical accuracy is concerned. Then a notably simple law $N(M_k)=C\times10^{-0.5M_k}$ will be found to exist in the occurrence of earthquakes in the vicinity of Tokyo, and this law is by no means a peculiarity conbined to this region, since, it is nearly the same as the law for Japanese earthquakes already mentioned.

28. 東京附近に起る地震のエネルギー法則

地震研究所 河 角 広

前論文に於て日本に起る比較的大きな地震の頻度が $10^{-0.5M_k}$ に比例して，M_k が大きくなると小くなる事を示したが，本論文に於てはもつと小さい地震の発生頻度にも同様な關係のあることを東京に於ける三十年間の地震の震度別並びに距離別回数の統計とその理論的考察から確めた．

東京に於て距離 r と $r+\rho$ の間の所で起り，震度が I である地震の回数 $N(I, r, \rho)$ は

$$N(I, r, \rho)=N(\kappa-1)(1-e^{-k\rho})\ \kappa^{-I}e^{-\kappa(r-r')}$$

なる理論的関係でよく表わされる．ここに κ は震度階級の差に対する加速度の倍數で k は地殻表層に於ける吸收係數であり r' は上の公式が成り立つ最小距離である． この式は地下或る深さにある一定の厚さの層の中だけに地震が振幅の二乘に逆比例した頻度で起る事を意味し，実際の觀測からは $\kappa=10^{0.556}$ で前論文に得た日本に起る大きな地震の発生法則の常数 $10^{0.537}$ と極めて近く，実際の震度と加速度の関係を示す式の常數 $10^{0.514}$ とかなり近い事は偶然とは思われない．これ等は何れも現在の觀測精度から $10^{0.5}$ と見てよかろう．

之が正しいとすれば，日本に起る地震は少くとも有感地震以上ではその発生頻度は，今地震動の周期を別問題にすれば，最大振幅の2乘に逆比例する．換言すればエネルギーの等配則が成り立つと云う事が出来る．

因みに上の結果から最大動は吸收作用で 100km の間で 0.17 に減じ，從つてエネルギーは約 1/30 に減ずる事になり，地震のエネルギーを論ずる時決して無視出来ない．之の點は將來他の方面から大いに確めなければならない問題であろう．

——所　　報——

◎談話会記事

第290回談話会（昭和27年6月17日）

1. 高温での岩石の力学的性質（第2報）　佐久間修三
2. 伊豆大島の地質についての2，3の觀察　森本良平・小坂丈予
3. 所謂瀬戸内地域の火山地形に関する一考察　森本良平
4. 東京青森間を往復した重力測定　坪井忠二・実川顯一・田島廣
5. 高倍率電磁式微動計による十勝沖地震の余震觀測結果について　松本利松・田望・浅田敏
6. 1950年のアッサム地震の表面波について（追補）　秋間哲夫
7. 異種地盤上の壁式鐵筋コンクリート造建物の振動的性質　金井清・鈴木富三郎

第291回談話会（昭和27年7月15日）

1. 小さな異物を含む媒質内を傳わる彈性波の速さ　佐藤泰夫
2. 浅間山の活動とそれに伴う微小地震（続報）　水上武・内堀貞雄・高橋智子

第292回談話会（昭和27年9月16日）

1. 不連続層によるP波の透過及び反射について　松本利松
2. 「ラブ波の走時」に関する訂正　佐藤泰夫
3. 昭和18年鳥取地震余震觀測（第2報）　表俊一郎
4. エルミット函数による地磁氣の解析　力武常次
5. 和歌山，宇治山田間の重力再測　坪井忠二・実川顯一・田島廣
6. 吉野地震現地調査略報　森本良平
7. 日立鑛山における地震動の觀測結果　第3報（周期と振幅との關係）　金井清・長田甲斐男・吉澤靜代
8. 水中に立てられた円筒の内外にはたらく地震時の動水圧について　河角廣
9. 東京都内地盤調査結果と地盤調査の方法について　（附）地盤の振動特性　地震研究所地盤調査班

第293回談話会（昭和27年10月21日）

1. 明神礁の噴火について（予報）　津屋弘逵・森本良平・小坂文予
2. 彈性波の発生機構に関する実験（第3報）　笠原慶一

3. 小さな異物を含む媒質内を傳わる彈性波の速さ（2） 佐藤泰夫
4. 第3回石淵爆破地震動觀測 爆破地震動研究グループ
5. 日立鑛山における地震動の觀測結果（第3報補遺） 金井清・長田甲斐男・吉澤靜代

第294回談話会（昭和27年11月18日）

1. 榛名火山の磁気異常 横山泉
2. 日本における地磁気短周期変化の異常と地下構造（第2報） 力武常次・横山泉・菱山よね子
3. 津浪に対する防波堤の効果 高橋龍太郎・平館金太郎・相田勇・羽鳥徳太郎

第295回談話会（昭和27年12月16日）

1. 表面波の研究(9) 表面波の分類と新らしい型 佐藤泰夫
2. 湖氷中に発生する自然震動 表俊一郎・山崎良雄・村内必典
3. 泥炭地における彈性波試験結果 金井清・田中貞二
4. 高温での岩石の力学的性質（第3報） 佐久間修三
5. 藏王火山の地質学的研究（第2報）青麻火山 市村毅
6. 燒山火山產硫黄結晶の形態 市村毅・津屋弘遠雄・湊秀雄
7. 四國地方の地盤變動と潮位變化 河角廣
8. 油壺(神奈川縣)・松山(愛媛縣)・間瀬(新潟縣)における地殻變動の觀測 萩原尊禮・山田重平・岡田惇夫・齋藤貞

Index to Vol. XXX.

Page

AKIMA, T., (6) A New Mechanical Low-pass Filter for Seismogram Analyses. (in English) 53

AKIMA, T., (21) On Dispersion Curves of Surface Waves from the Great Assam Earthquake of September 15, 1950. (in English). 237

AKIMA, T. and SHIMOZURU, D., (19) Reflections on the Tsunami of December 21, 1946. (in English)..... 223

HISHIYAMA, Y., RIKITAKE, R. and YOKOYAMA, I., (18) A Preliminary Study on the Anomalous Behavior of Geomagnetic Variations of Short Period in Japan and Its Relation to the Subterranean Structure. (in English)..... 207

KANAI, K., (4) Relation between the Nature of Surface Layer and the Amplitudes of Earthquake Motions. (in English)..... 31

KANAI, K., (5) Examinations of the Assumption concerning Mechanism of Earthquake Origin through Seismograms. (in English)..... 39

KANAI, K. and YOSHIZAWA, S., (13) On the Damping of Vibration of Actual Buildings. I. (in English)..... 131

KASAHARA, K., (22) Experimental Studies on the Mechanism of Generation of Elastic Waves I. (in English)..... 259

KAWASUMI, H., (27) On the Energy Law of Occurrence of Japanese Earthquakes. (in English)..... 319

KAWASUMI, H., (28) Energy Law of Earthquake Occurrence in the Vicinity of Tokyo. (in English)..... 325

KISHINOUYE, F., (7) Earth-vibrations on Soft Ground caused by Fallen Body. (in English)..... 59

MIYABE, N., (14) Vertical Earth Movements in Japan as Deduced from the Results of Rerunning the Precise Levels. (in English)... 127

MORIMOTO, R., TSUYA, H. and OSSAKA, J., (20) Chemical Composition of the 1951-lavas of Oshima Volcano, Seven Izu Islands, Japan. (in English)..... 231

OSSAKA, J., TSUYA, H. and MORIMOTO, R., (20) Chemical Composition of the 1951-lavas of Oshima Volcano, Seven Izu Islands, Japan. (in English)..... 231

RIKITAKE, T., (2) Electrical Conductivity and Temperature in the Earth. (in English)..... 13

RIKITAKE, T., (9) On Magnetization of Volcanoes. (in English)..... 71

RIKITAKE, T., (17) On the Electrical Conductivity in the Earth's Core. (in English)..... 191

RIKITAKE, T., (25) Analyses of Geomagnetic Field by Use of Hermite Functions. (in English)..... 293

RIKITAKE, T., YOKOYAMA, I. and HISHIYAMA, Y., (18) A Preliminary Study on the Anomalous Behavior of Geomagnetic Variations of Short Period in Japan and Its Relation to the Subterranean Structure. (in English)..... 207

SAKUMA, S., (3) Earth-current Potentials near Boundaries of Various Geological Formations. (in English)..... 25

SAKUMA, S., (23) Elastic and Viscous Properties of Volcanic Rocks at Elevated Temperature. Part 1. (in English)..... 269

SATÔ, Y., (1) Study on Surface Waves V. Love-Waves Propagated upon Heterogeneous Medium. (in English)..... 1

SATÔ, Y., (11) Determination of Epicentre by means of the Directions of Overturning. (in Japanese)..... 93

SATÔ, Y., (12) Study on Surface Waves VI. Generation of Love- and Other Type of SH-Waves. (in English)..... 101

SATÔ, Y., (16) Velocity of Elastic Waves Propagated in Media with Small Holes. (in English)..... 179

SATÔ, Y., (26) Study on Surface Waves VII. Travel-Time of Love-Waves. (in English)..... 305

SHIMOZURU, D., (8) Dynamical Measurements of the Elastic Constants of Rocks subjected to Initial Stresses. 1. Measurement of Young's Modulus under Uniaxial Compression. (in English)..... 63

SHIMOZURU, D. and AKIMA, T., (19) Reflections on the Tsunami of December 21, 1946. (in English)..... 223

SUGIMURA, A., (15) On the Deformation of the Earth's Surface Owing to the Rock Folding in Japan. (in Japanese)..... 163

TSUYA, H., MORIMOTO, R. and OSSAKA, J., (20) Chemical Composition of the 1951-lavas of Oshima Volcano, Seven Izu Islands, Japan. (in English)..... 231

YOKOYAMA, I., (10) Magnetization of the Gabbro from Mt. Tsukuba with Special Relation to the Geomagnetic Anomalies. (in English). 83

YOKOYAMA, I., RIKITAKE, T. and HISHIYAMA, Y., (18) A Preliminary Study on the Anomalous Behavior of Geomagnetic Variations of Short Period in Japan and Its Relation to the Subterranean Structure. (in English) 207

YOSHIZAWA, S. and KANAI, K., (13) On the Damping of Vibration of Actual Buildings. I. (in English) 121

The Research Group for Explosion Seismology, (24) The Second Explosion-Seismic Observations in North-Eastern Japan. (in English) 279

索引第30號

頁

秋間哲夫 (6) 電磁制振式新低域濾波器について (英文) …… 53

秋間哲夫 (21) 1950年8月15日のアツサム大地震の表面波の分散曲線について (英文) …… 237

秋間哲夫・下鶴大輔 (19) 南海地震に伴つた津浪の反射 (英文) …… 223

菱山よね子・力武常次・横山 泉 (18) 日本に於ける地磁気短周期変化の異常と地下構造 (序報) (英文) …… 207

金井 清 (4) 地表層の性質と地震動振幅との関係 (英文) …… 31

金井 清 (5) 地震計記象による発震機構の仮定の吟味 (英文) …… 39

金井 清・吉沢静代 (13) 実在建物の振動減衰性について 第1報 (英文) … 121

笠原慶一 (22) 彈性波の発生機構に関する実験 (第1報) (英文) …… 259

河角 広 (27) 日本に起る地震のエネルギー法則 (英文) …… 319

河角 広 (28) 東京附近に起る地震のエネルギー法則 (英文) …… 325

岸上冬彦 (7) 軟弱地盤の上に落された物体によつて起された土地の振動 (英文) …… 59

宮部直巳 (14) 水準改測の結果から見た日本の陸地変動 (英文) …… 127

森本良平・津屋弘逵・小坂丈予 (20) 伊豆大島三原山1951年熔岩の化学成分 (英文) …… 231

小坂丈予・津屋弘逵・森本良平 (20) 伊豆大島三原山1951年熔岩の化学成分 (英文) …… 231

力武常次 (2) 地球内の電気伝導度と温度 (英文) …… 13

力武常次 (9) 火山の帯磁 (英文) …… 71

力武常次 (17) 地球核の電気伝導度 (英文) …… 191

力武常次 (25) エルミツト函数による地磁気の解析 (英文) …… 293

力武常次・横山 泉・菱山よね子 (18) 日本に於ける地磁気短周期変化の異常と地下構造 (序報) (英文) …… 207

佐久間修三 (3) 各種の地質境界線の近くの地電位差 (英文) …… 25

佐久間修三 (23) 高温に於ける火山岩の粘性及び彈性 第1報 (英文) …… 269

佐藤泰夫 (1) 表面波の研究 V 不均質媒質を伝はるラブ波 (英文) …… 1

佐藤泰夫 (11) 物の倒れた方向から震央を求めること (邦文) …… 93

佐藤泰夫 (12) 表面波の研究 VI ラブ波及びその他の SH 波の発生 (英文) 101

佐藤泰夫 (16) 小さな穴のあいた媒質内を伝はる彈性波の速さ (英文) …… 179

佐藤泰夫 (26) 表面波の研究 VII ラブ波の走時 (英文) …… 305

下鶴大輔 (8) 応力がかゝつた状態に於ける岩石彈性率の動力学的研究

1. 軸圧のかゝつた状態に於けるヤング率の測定 (英文) … 63

下鶴大輔・秋間哲夫　(19) 南海地震に伴つた津浪の反射 (英文)…… 223
杉村　新　(15) 褶曲運動による地表の変形について (邦文)…… 163
津屋弘逵・森本良平・小坂丈予　(20) 伊豆大島三原山1951年熔岩の化学成分 (英文)…… 231
横山　泉　(10) 筑波山斑糲岩の帯磁と地磁気異常 (英文)…… 83
横山　泉・力武常次・菱山よね子　(18) 日本に於ける地磁気短周期変化の異常と地下構造 (序報) (英文)…… 207
吉沢静代・金井　清　(13) 実在建物の振動減衰性について　第1報 (英文) 121
爆破地震動研究グループ　(24) 東北日本における第2回爆破地震動観測 (英文)…… 279

BULLETIN

OF THE

EARTHQUAKE RESEARCH INSTITUTE

TOKYO UNIVERSITY

VOL. XXX

1952

東京大學

地震研究所彙報

第 30 号

昭和 27 年

BULLETIN

OF THE

EARTHQUAKE RESEARCH INSTITUTE

TOKYO UNIVERSITY

VOL. XXX

1952

東京大學

地震研究所彙報

第 30 号

昭和 27 年

CONTENTS.

Vol. XXX.

Part 1. March, 1952.

Papers and Reports.

Page

1. Y. SATÔ, Study on Surface Waves V. Love-Waves Propagated upon Heterogeneous Medium. (in English) 1
2. T. RIKITAKE, Electrical Conductivity and Temperature in the Earth. (in English) 13
3. S. SAKUMA, Earth-current Potentials near Boundaries of Various Geological Formations. (in English)..... 25
4. K. KANAI, Relation between the Nature of Surface Layer and the Amplitudes of Earthquake Motions. (in English)..... 31
5. K. KANAI, Examinations of the Assumption concerning Mechanism of Earthquake Origin through Seismograms. (in English). 39
6. T. AKIMA, A New Mechanical Low-pass Filter for Seismogram Analyses. (in English)..... 53
7. F. KISHINOUYE, Earth-vibrations on Soft Ground caused by Fallen Body. (in English)..... 59
8. D. SHIMOZURU, Dynamical Measurements of the Elastic Constants of Rocks subjected to Initial Stresses. 1. Measurement of Young's Modulus under Uniaxial Compression (in English). 63
9. T. RIKITAKE, On Magnetization of Volcanoes. (in English).... 71
10. I. YOKOYAMA, Magnetization of the Gabbro from Mt. Tsukuba with Special Relation to the Geomagnetic Anomalies. (in English)..... 83
11. Y. SATÔ, Determination of Epicentre by means of the Directions of Overturning. (in Japanese)..... 93

Part 2. June, 1952.

12. Y. SATÔ, Study on Surface Waves VI. Generation of Love- and Other Type of SH-Waves. (in English)..... 101
13. K. KANAI and S. YOSHIZAWA, On the Damping of Vibration of Actual Buildings. I. (in English)..... 121

14. N. MIYABE, Vertical Earth Movements in Japan as Deduced from the Results of Rerunning the Precise Levels. (in English). 127
15. A. SUGIMURA, On the Deformation of the Earth's Surface Owing to the Rock Folding in Japan. (in Japanese)..... 163

Part 3. September, 1952.

16. Y. SATÔ, Velocity of Elastic Waves Propagated in Media with Small Holes. (in English)..... 179
17. T. RIKITAKE, On the Electrical Conductivity in the Earth's Core. (in English)..... 191
18. T. RIKITAKE, I. YOKOYAMA and Y. HISHIYAMA, A Preliminary Study on the Anomalous Behavior of Geomagnetic Variations of Short Period in Japan and Its Relation to the Subterranean Structure. (in English)..... 207
19. D. SHIMOZURU and T. AKIMA, Reflections on the Tsunami of December 21, 1946. (in English)..... 223
20. H. TSUYA, R. MORIMOTO and J. OSSAKA, Chemical Composition of the 1951-lavas of Oshima Volcano, Seven Izu Islands, Japan. (in English) 231
21. T. AKIMA, On Dispersion Curves of Surface Waves from the Great Assam Earthquake of September 15, 1950. (in English). 237
22. K. KASAHARA, Experimental Studies on the Mechanism of Generation of Elastic Waves I. (in English)..... 259
23. S. SAKUMA, Elastic and Viscous Properties of Volcanic Rocks at Elevated Temperature. Part 1. (in English)..... 269
24. The Research Group for Explosion Seismology, The Second Explosion-Seismic Observations in North-Eastern Japan. (in English)..... 279

Part 4. December, 1952.

25. T. RIKITAKE, Analyses of Geomagnetic Field by Use of Hermite Functions. (in English)..... 293
26. Y. SATÔ, Study on Surface Waves VII. Travel-Time of Love-Waves. (in English)..... 305
27. H. KAWASUMI, On the Energy Law of Occurrence of Japanese Earthquakes. (in English)..... 319
28. H. KAWASUMI, Energy Law of Earthquake Occurrence in the Vicinity of Tokyo. (in English)..... 325

目　次

第 30 號

第 1 冊　　昭和 27 年 3 月

論文及報告

		頁
1.	表面波の研究　V．不均質媒質を伝はるラブ波（英文）……佐藤泰夫	1
2.	地球内の電気伝導度と温度（英文）……力武常次	13
3.	各種の地質境界線の近くの地電位差（英文）……佐久間修三	25
4.	地表層の性質と地震動振幅との関係（英文）……金井清	31
5.	地震計記象による発震機構の仮定の吟味（英文）……金井清	39
6.	電磁制振式新低域濾波器について（英文）……秋間哲夫	53
7.	軟弱地盤の上に落された物体によつて起された土地の振動（英文）……岸上冬彦	59
8.	応力がかゝつた状態に於ける岩石弾性率の動力学的研究	
	1. 軸圧のかゝつた状態に於けるヤング率の測定（英文）…下鶴大輔	63
9.	火山の帯磁（英文）……力武常次	71
10.	筑波山斑糲岩の帯磁と地磁気異常（英文）……横山泉	83
11.	物の倒れた方向から震央を求めること（邦文）……佐藤泰夫	93

第 2 冊　　昭和 27 年 6 月

12.	表面波の研究　VI　ラブ波及びその他の SH 波の発生（英文）佐藤泰夫	101
13.	実在建物の振動減衰性について　第1報（英文）……{金井清／吉沢静代}	121
14.	水準改測の結果から見た日本の陸地変動（英文）……宮部直巳	127
15.	褶曲運動による地表の変形について（邦文）……杉村新	163

第 3 冊　　昭 和 27 年 9 月

16. 小さな穴のあいた媒質内を伝はる弾性波の速さ（英文）……佐 藤 泰 夫　179

17. 地球核の電気伝導度（英文）……力 武 常 次　191

18. 日本に於ける地磁気短周期変化の異常と地下構造（序報）（英文）……力 武 常 次・横 山 泉・菱 山 よ ね 子　207

19. 南海地震に伴つた津浪の反射（英文）……下 鶴 大 輔・秋 間 哲 夫　223

20. 伊豆大島三原山1951年熔岩の化学成分（英文）……津 屋 弘 逵・森 本 良 平・小 坂 丈 予　231

21. 1950年 8 月15日のアツサム大地震の表面波の分散曲線について（英文）……秋 間 哲 夫　237

22. 弾性波の発生機構に関する実験　第 1 報（英文）……笠 原 慶 一　259

23. 高温に於ける火山岩の粘性及び弾性　第 1 報（英文）……佐 久 間 修 三　269

24. 東北日本における第 2 回爆破地震動観測（英文）……爆破地震動研究グループ　279

第 4 冊　　昭 和 27 年 12 月

25. エルミツト函数による地磁気の解析（英文）……力 武 常 次　293

26. 表面波の研究　Ⅶ　ラブ波の走時（英文）……佐 藤 泰 夫　305

27. 日本に起る地震のエネルギー法則（英文）……河 角 広　319

28. 東京附近に起る地震のエネルギー法則（英文）……河 角 広　325

昭和28年1月25日印刷
昭和28年1月30日發行

東京都文京區本富士町一番地
東京大學構内
編纂兼發行者 東京大學地震研究所

東京都千代田區富士見町一丁目十番地
印刷者 笠井康賴

東京都千代田區富士見町一丁目十番地
印刷所 株式會社 國際文献印刷社

賣捌所 東京都千代田區神田一ツ橋通
岩波書店

東京都中央區日本橋通二丁目六番地
丸善株式會社

Sold by
Iwanami Shoten,
Hitotsubashi dôri, Chiyoda-ku, Tôkyô,
and
Maruzen Co., Ltd.,
Nihonbashi dôri, Chûô-ku, Tôkyô.
Price of this copy: 193 Yen. (Postage exclusive.)

BULLETIN OF

THE EARTHQUAKE RESEARCH INSTITUTE

TOKYO UNIVERSITY

Vol. XXX, Part 4. December, 1952.

Contents.

Papers and Reports.

Page

25. T. RIKITAKE, Analyses of Geomagnetic Field by Use of Hermite Functions. (in English) 293

26. Y. SATÔ, Study on Surface Waves VII. Travel-Time of Love-Waves. (in English) 305

27. H. KAWASUMI, On the Energy Law of Occurrence of Japanese Earthquakes. (in English) 319

28. H. KAWASUMI, Energy Law of Earthquake Occurrence in the Vicinity of Tokyo. (in English) 325

Institute Notes.

Index.

(For the papers written in Japanese or in occidental languages, the abstracts are given in occidental languages or in Japanese respectively.)